Titre: Title:	The use of waste rock inclusions to control the effects of liquefaction in tailings impoundments
Auteur: Author:	Michael James
Date:	2009
Type:	Mémoire ou thèse / Dissertation or Thesis
Référence: Citation:	James, M. (2009). The use of waste rock inclusions to control the effects of liquefaction in tailings impoundments [Thèse de doctorat, École Polytechnique de Montréal]. PolyPublie. https://publications.polymtl.ca/8284/

UNIVERSITÉ DE MONTRÉAL

THE USE OF WASTE ROCK INCLUSIONS TO CONTROL THE EFFECTS OF LIQUEFACTION IN TAILINGS IMPOUNDMENTS

MICHAEL JAMES
DÉPARTEMENT DES GÉNIES CIVIL, GÉOLOGIQUE ET DES MINES
ÉCOLE POLYTECHNIQUE DE MONTRÉAL

THÈSE PRÉSENTÉE EN VUE DE L'OBTENTION
DU DIPLÔME DE PHILOSOPHIAE DOCTOR (Ph.D.)
(GÉNIE MINÉRAL)

MARS 2009

UNIVERSITÉ DE MONTRÉAL

ÉCOLE POLYTECHNIQUE DE MONTRÉAL

Cette thèse intitulée :

THE USE OF WASTE ROCK INCLUSIONS TO CONTROL THE EFFECTS OF LIQUEFACTION IN TAILINGS IMPOUNDMENTS

présentée par : JAMES Michael
en vue de l'obtention du diplôme de : Philosophiae Doctor
a été dûment acceptée par le jury d'examen constitué de :

M. BUSSIÈRE Bruno, Ph.D., président
M. AUBERTIN Michel, Ph.D., membre et directeur de recherche
M. TINAWI René, Ph.D., membre
M. GRABINSKY Murray, Ph.D., membre

ACKNOWLEDGEMENTS

There are many people to whom I'm grateful for their support and assistance during the course of this research, particularly Professor Michel Aubertin, whose insight, guidance, assistance, and patience made this project possible. Professor Aubertin developed the idea of using waste rock inclusions to increase the seismic stability of tailings impoundments and this research has allowed me to bring his concept a few steps forward.

Sincerest thanks are also extended to the following individuals whose assistance, advice and encouragement contributed to my efforts:

Jean-Baptiste Drommer,
Dr. Bassam El Husseini
of McGill University
Gilles Labranche,
Vincent Martin,
Nicolas Pepin,
Domenic Tremblay,
Dr. Dharma Wijewickreme
of The University of British Columbia,
and
Dr. G. Ward Wilson
of The University of British Columbia.

I also very much appreciate my family and friends for their love, support, kindness and patience while I've been occupied with this project.

RÉSUMÉ

Plusieurs ruptures de digues de parcs à résidus miniers on été causées par la liquéfaction des résidus au cours des dernières décennies. Les déversements des résidus ont causé des pertes de vie ainsi que des dommages significatifs. Une technique de contrôle consistant à disposer de la roche stérile dans les parcs à résidus miniers a été proposée par Aubertin et al. (2002). La roche stérile pourrait alors être disposée de façon à créer des structures continues ou des amoncèlements isolés, de façon à et limiter les effets de la liquéfaction et aussi pour accélérer la consolidation des résidus. Les objectifs premiers de cette étude étaient : a) évaluer l'utilisation d'inclusions de roches stériles pour contrer les effets de la liquéfaction dans les parcs à résidus miniers; b) présenter des conclusions et des recommandations reliées à l'utilisation des inclusions de roche stérile.

Une revue des connaissances et des pratiques relatives à l'évaluation du comportement dynamique des résidus indique que les méthodes existantes développées surtout pour analyses les sols sableux (tel la méthode Simplifiée pour évaluer le potentiel de liquéfaction ou la méthode pseudo-statique pour évaluer la stabilité des digues) pourraient ne pas être applicable.

L'état des connaissances et de la pratique indiquent que :

- Les résidus miniers peuvent être sujets à la liquéfaction causée par les séismes. Cependant, l'application des méthodes actuelles d'évaluation du potentiel de liquéfaction est incertaine.
- La technique des colonnes de roche à été utilisée avec succès pour contrôler les effets de la liquéfaction de sols naturels.
- Les modèles d'analyse numériques constituent la meilleure façon d'évaluer l'utilisation d'inclusion de roches stériles dans les parcs à résidus miniers.

Une étude géotechnique a été effectuée sur un parc à résidus miniers représentatif situé en Abitibi, dans l'ouest du Québec. Cette étude comprenait des puits d'exploration, des

essais au piezocone (CPT), des essais conventionnels et dynamiques en laboratoire, la caractérisation du site et des résidus miniers non-consolidés et normalement consolidés, ainsi que des analyses sure la liquéfaction des résidus et la stabilité de la digue ceinturant le parc (en utilisant des méthodes analytiques). Des différences significatives ont été observées au niveau de la réponse des résidus en place et de leur résistance à la liquéfaction, selon que les résidus étaient non-consolidés ou normalement consolidés. Néanmoins, dans les deux cas, les résidus étaient fortement susceptibles à liquéfaction lorsque soumis à des charges causées par des tremblements de terre de magnitude 6.5 à 7.5 (en supposant une rupture de faille située à 30 km du site). Les analyses pseudo-statiques ont démontré un potentiel de d'instabilité et ont indiqué que la liquéfaction d'un parc à résidus miniers pourrais avoir un impact négatif sur la stabilité sismique de la digue.

Une modélisation numérique dynamique à été réalisée en utilisant le logiciel de différences finies « FLAC » avec le modèle « UBC Sand » (de University of British-Columbia) pour simuler les résidus miniers. Une modélisation préliminaire fut effectuée afin de calibrer le modèle selon les résultats d'essais cycliques de cisaillement simple (CDSS) afin d'obtenir des comparaisons avec les analyses de liquéfaction utilisant la méthode Simplifiée. Cette modélisation a permis de conclure que les paramètres du model 'UBC Sand' de résidus normalement consolidés peuvent relis a l'indicé de pénétration standard corrigé, $(N_1)_{60}$, qui prend une valeur de 11 (coups/300 mm), angle de friction à volume constant, ψ_{cv}, devient alors 35.6°. Les facteurs de sécurité, estimés lors de l'évaluation numérique de la liquéfaction, sont assez similaires à ceux calculés en utilisant la méthode analytique, malgré les différences significatives du comportement in situ selon les deux méthodes.

Des analyses numériques dynamiques d'un parc à résidus miniers de référence one ensuite été réalisées avec et sans inclusions de roches stériles pour le cas d'un tremblement de terre de magnitude 7.5. La présence des inclusions a eu pour effet d'améliorer la performance sismique du parc, en réduisent les déformations au niveau de

la digue. Malgré le fait que les analyses pseudo-statiques indiquaient un potentiel de rupture de la digue (FS=0,88), aucun signe de comportement défavorable n'a été observé selon l'analyse numérique.

L'utilisation d'inclusions de roches stériles pour contrôler les effets de la liquéfaction sur les parcs à résidus miniers fut évaluée de façon plus approfondie à l'aide d'analyses numériques dynamiques sur un parc à résidus miniers conceptuel, avec des digues construites selon la méthode amont (avec et sans inclusions), soumis à des chargements sismiques équivalents à des événements de magnitudes 6.5 à 7.5 (à 30 km de la faille). Les analyses ont été réalisées en trois étapes : état statique, condition dynamique et comportement post-séisme (avec dissipation des pressions interstitielles en excès). La présence d'inclusions de roches stériles améliore considérablement le comportement dynamique du parc conceptuel : on ainsi observe que: a) la réponse du site avec inclusions était plus raide; b) la zone de liquéfaction des résidus miniers a été réduite ; c) les déformations et le déplacement des résidus ont été réduits (par un ordre de grandeur) ; et d) la taille des zones de rupture potentielle à l'intérieur du parc à résidus miniers a été réduite de façon significative. Les évaluations paramétriques du comportement du parc à résidus miniers conceptuel ont ainsi révélé que le nombre, la taille ou la conductivité hydraulique des inclusions affectaient peu leur performance pour les cas étudiés. Cependant, la position et l'espacement des inclusions peuvent avoir une influence significative.

L'utilisation d'inclusions de roches stériles devrait être considérée dans les projets de parcs à résidus miniers où il existe un risque de déformation excessive ou de rupture due aux charges sismiques. Cependant, plusieurs facteurs devront être analysés davantage afin de poursuivre le développement du concept, mentionnons entre autres : a) une évaluation plus complète du comportement dynamique et de la liquéfaction potentielle de résidus miniers; b) l'effet des inclusions de roche stérile sur la déposition et la consolidation des résidus ; c) les propriétés dynamiques des roches stériles ; et d)

l’utilisation des inclusions de roches stériles dans des parcs ayant différentes tailles, formes, et inclinaisons.

ABSTRACT

There have been several failures of tailings impoundments in the last few decades due to liquefaction of the retained tailings or of the tailings used to construct the retention structures. The resulting flows of liquefied material have resulted in significant loss of life as well as environmental and economic damage. A co-disposal technique consisting of placing waste rock in tailings impoundments prior to and during tailings deposition was proposed by Aubertin et al. in 2002. The waste rock would be placed to create continuous inclusions or isolated heaps within the impoundment that would counteract the effects of liquefaction of the tailings and accelerate the consolidation of the tailings. The primary objectives of this research were to: a) evaluate the use of waste rock inclusions to control the effects of liquefaction in tailings impoundments; and b) develop conclusions and recommendations regarding the use of waste rock inclusions.

A review of the current state of the knowledge and practice with respect to various aspects involved in evaluating the dynamic behavior of tailings and tailings impoundments indicates that existing analytical methods (e.g. the use of the Simplified method to evaluate the liquefaction potential or the application of the pseudo-static method to evaluate the stability of slopes) may not be applicable due to the differences in the characteristics of tailings and the effect of the liquefied tailings on the seismic behavior of impoundments.

The current state of the knowledge and practice indicate that:

- Tailings can be subjected to seismically-induced liquefaction. However, the applicability of existing liquefaction evaluation methods is uncertain, particularly correlations based on in situ testing and gradation.
- Stone columns have been successfully used to control the effects of liquefaction in naturally-occurring soils.
- Currently, dynamic numerical modeling offers the best means for evaluating the use of waste rock inclusions in tailings impoundments.

A geotechnical study was conducted at a representative tailings impoundment located in Abitibi in the western part of Quebec. The study consisted of test pits, cone penetration testing, conventional and dynamic laboratory testing, characterization of site and subsurface conditions, of the tailings when under-consolidated (active sites) and normally consolidated (closed sites), as well as liquefaction evaluation of the tailings and stability evaluation of the zoned earthfill dike forming the impoundment (using analytical methods). Significant differences were found with the site response and liquefaction resistance of the tailings when under-consolidated or normally consolidated. However, in both cases, the tailings were highly susceptible to liquefaction due to the loadings of moment magnitude 6.5, 7 and 7.5 earthquakes (for an assumed fault rupture to site distance of 30 km). Pseudo-static stability analysis indicated the potential for failure and that the liquefaction of the impounded tailings had a detrimental impact on the seismic stability of the dike.

Dynamic numerical modeling was conducted using the FLAC finite difference computer program with the "UBC Sand" model (from the University of British Columbia) used to simulate the tailings. Preliminary modeling was conducted to calibrate the UBC Sand model based on the results of cyclic direct simple shear (CDSS) testing to provide comparisons with the "level ground" liquefaction analysis completed using analytical methods. The UBC Sand parameters of the normally consolidated tailings were found to correspond to a corrected standard penetration test blow count, $(N_1)_{60}$, of 11 (blows/300 mm) and a constant volume friction angle, ψ_{cv}, of 35.6°. The factors of safety of the numerical liquefaction evaluation were in reasonable agreement with those calculated using analytical methods, despite significant differences in the site responses estimated by the two methods.

Dynamic numerical analyses of the representative tailings impoundment with and without waste rock inclusions and subjected to the magnitude 7.5 earthquake loading were conducted. The presence of the inclusions resulted in improved seismic performance of the impoundment, as indicated by a reduction in the deformation of the dike. Although

the pseudo-static analysis indicated a potential for failure of the dike (FS=0.88), there were no indications of unacceptable behavior in the numerical analysis.

The use of waste rock inclusions to control the effects of liquefaction in tailings impoundments was further evaluated through dynamic numerical analyses of a conceptual upstream-raised tailings impoundment (with and without inclusions) that was subject to earthquake loadings equivalent to magnitude 6.5 through 7.5 events at a fault rupture to site distance of 30 km. The analyses were conducted in three phases: static, dynamic (shaking) and post-shaking (excess porewater pressure dissipation). The horizontal accelerations, cyclic stress ratios, porewater pressure, and displacements at critical locations in the model were recorded during the shaking and post-shaking phases. The presence of waste rock inclusions significantly improved the dynamic behavior of the conceptual impoundment in four major ways: a) the site response of the impoundment with inclusions was stiffer; b) the zone of liquefaction of the tailings was somewhat reduced; c) the deformations and displacements of the impoundment were reduced by as much as an order of magnitude; and d) the size of potential failure zones in the impoundment were significantly reduced. Parametric evaluations of the conceptual impoundment revealed that the number, size, or hydraulic conductivity of the inclusions was not a significant factor in their performance, for the cases investigated. However, the spacing of the inclusions did make a significant difference.

The use of waste rock inclusions should be considered in proposed tailings impoundments where the risk of excessive deformation or failure due to seismic loading and liquefaction is a concern. However, there are several areas where additional research is required for further development of this concept, most importantly: a) a more complete evaluation of the dynamic behavior and liquefaction potential of unconsolidated and normally consolidated tailings based on in situ testing; b) the effect of waste rock inclusions on the deposition and consolidation of tailings; c) the dynamic properties of waste rock; and d) the use of waste rock inclusions in impoundments of various sizes and shapes and in impoundments located on sloped ground.

CONDENSÉ EN FRANÇAIS

Introduction

L'augmentation du nombre de parcs à résidus miniers et de leur taille, ainsi que leur susceptibilité à des ruptures dues aux effets des tremblements de terre, constituent des facteurs d'inquiétude. Ces facteurs mettant en évidence le besoin de mieux comprendre le potentiel de liquéfaction des résidus miniers et la stabilité des parcs à résidus, ainsi que le besoin de développer des techniques pour contrôler les effets de la liquéfaction.

L'utilisation de colonnes de sable et gravier peu s'avérer efficace pour contrôler les effets de la liquéfaction dan les sols naturels, en permettant la dissipation rapide des pressions interstitielles et en renforçant le sol durant le tremblement de terre. Par analogie, on peut postuler que l'ajout d'inclusions de roches stériles avant et pendant la déposition des résidus miniers, ou encore l'ajout de colonnes de roches stériles dans des résidus existants pourrait également permettre de contrôler les effets de la liquéfaction sur les parcs à résidus miniers. La présence d'inclusions de roches stériles pourrait aussi faciliter la consolidation des résidus, tout comme les drains verticaux le font pour les sols argileux.

Les objectifs principaux de cette étude thèse de : a) évaluer l'utilisation d'inclusions de roches stériles afin de contrôler les effets de la liquéfaction des résidus miniers en des analyses numériques; et b) développer des conclusions et des recommandations reliées à l'utilisation d'inclusions de roches stériles.

Revue des connaissances et des pratiques usuelles

Les résidus miniers utilisés dans cette recherche provenaient d'une exploitation de roches dures. Ce type de résidus souvent résulte de l'exploitation de métaux tels que le plomb, le nickel, le cuivre, l'argent, l'or et le molybdène. La granulométrie de ces résidus varie entre la taille des colloïdes (moins de 0.001 mm) et la taille de grains de sable moyen (1 mm). La fraction fine, qui représente la fraction inférieure à 0.075 mm de diamètre, représente typiquement entre 40 à 90% de masse totale de des rejets. Les résidus

provenant des mines en roches montrent peu ou pas de plasticité et ils sont généralement classifiés comme des silts sableux ou des sables silteaux.

Pour leur part, les roches stériles représentent la portion non-économique de la roche encaissante excavée pour obtenant le minérales durant l'exploitation minière. La granulométrie des roches stériles varie généralement entre le sable et des blocs de tailles variées. Les roches stériles décrites dans cette recherche sont comme étant durables, chimiquement stables et angulaires.

L'information présentée au Chapitre 2 de la thèse montre que la liquéfaction engendrée par les séismes est causée par l'augmentation des pressions interstitielles dans un matériaux contractant et sans cohésion. L'augmentation des pressions interstitielles est alors due au chargement sismique et la liquéfaction se produit lorsque ce chargement est suffisant pour que le matériau atteigne un état critique ou que les contraintes effectives soient suffisamment faibles pour entraîner une déformation excessive sous l'effet de la gravité ou des charges externes. La susceptibilité des résidus miniers à la liquéfaction ou aux déformations excessives a été confirmée par divers observations sur le terrain et par des essais en laboratoire.

La méthode d'évaluation du potentiel de liquéfaction la plus courante est la méthode Simplifiée proposée par Seed et Idriss (1982). Typiquement, la stabilité sismique des parcs à résidus miniers est évaluée selon à deux méthodes : la méthode simplifiée pour statuer sur le potentiel de liquéfaction des résidus miniers ; et l'analyse par équilibre limite avec la méthode pseudo-statique pour évaluer le potentiel de rupture des pentes. Toutefois, l'application de ces méthodes, qui furent développées pour des sols naturels et pour des digues de rétention d'eau conventionnelles, au cas des résidus miniers et des parcs à résidus miniers n'a pas encore été analysée en détail.

Analyse géotechnique d'un parc à résidus miniers

Une étude géotechnique a été effectuée sur un parc à résidus miniers jugé représentatif, soit le parc formé par la digue No. 1 à la mine Laronde située près de Pressiac en Abitibi, dans l'ouest du Québec. Il s'agit d'un parc à résidus miniers actif où les résidus sont sous-consolidés par rapport aux charges existantes. L'étude présentée au Chapitré 3 comprenait le travail sur le terrain ainsi que des essais et des analyses en laboratoire. Le travail sur le terrain consistait en une reconnaissance du site, l'excavation de puits d'exploration et la réalisation d'essais de piezocone (CPT) ; cette étude été complémentée avec des résultants de mesures forages fournis par des tiers. Des essais conventionnels en laboratoire et des essais cycliques de cisaillement simple (CDSS) furent effectués sur des échantillons de résidus miniers prélevés à même les puits d'exploration.

Les données de terrain et les essais de laboratoire furent utilisés pour caractériser respectivement les résidus sous-consolidés (CPT) et normalement consolidés (tests de laboratoire). La valeur corrige de l'indice de pénétration standard $(N_1)_{60}$ pour les résidus in situ (sous-consolidés) est de 3.5 en moyenne selon des résultats CPT, alors que les valeurs de (N1)60 est de 11 pour les résidus consolidés (voir plus bas).

Cinq scénarios furent développés à des fins d'évaluation sismique comparative. Les données utilisées simulent des séismes de magnitudes entre 6.5 et 7.5, pour une faille située à 30 km du site. Les mouvements du sol rattachés à ces séismes furent développés à partir de modifications apportées au registre S16T du séisme de 1988 au Saguenay (magnitude 5.9).

Le potentiel de liquéfaction des résidus miniers à été évalué en utilisant la méthode Simplifiée. Les résidus étudiés étaient considérés sous-consolidés ou normalement consolidés. L'analyse Þ4 montre que le potentiel de liquéfaction était très élevé pour les séismes considérés, pour les deux niveaux de consolidation des résidus. Toutefois, les facteurs de sécurité face la liquéfaction étaient plus élevés pour les résidus sous-consolidés que pour les résidus consolidés. Ce résultant un peu surprenant est attribuable

à l'augmentation de la rigidité des résidus miniers causée par la consolidation, ce qui entraîne moins d'amortissement des mouvements du matériau.

L'évaluation de la stabilité sismique du parc à résidus miniers, effectuée en utilisant la méthode d'analyse pseudo-statique, a permis de conclure qu'il existe un potentiel de rupture du parc lorsque celui-ci est soumis à un séisme de magnitude 7.5 et que les résidus contenus dans le parc sont liquéfiés. Ces derniers représentent d'ailleurs la cause principale de la rupture.

Analyse numérique préliminaire du comportement sismique des résidus

Des analyses numérique préliminaires ont été effectués afin de : a) valider l'approchée utilisée pour l'analyse numérique dynamique (avec la version 5.00.346 du logiciel de différences finies « FLAC » et du modèle de comportement « UBC Sand ») ; b) déterminer les paramètres à utiliser pour le modèle « UBC Sand » dans le cadre de la modélisation numérique dynamique des résidus miniers ; c) comparer l'analyse numérique dynamique de la liquéfaction avec la méthode Simplifiée.

Les résultats présentée au Chapitre 4 montre que les outils utilisée d'analyse (FLAC et UBC Sand) permettant de simuler le comportement dynamique des résidus pour l'ensemble des données de séismes considéré. Ainsi, un modèle à 2 dimensions d'un essai CDSS a permis d'obtenir des résultats assez similaires aux résultats réels obtenus en laboratoire. Les paramètres du modèle « UBC Sand » découlant de les analyses correspondent à un indice de pénétration $(N_1)_{60}$ de 11 (coups par 300 mm) et un angle de friction à volume constant, ψ_{cv} , de 35.6º pour les résidus normalement consolidés.

Les facteurs de sécurités déterminés par les évaluations numérique et analytique du potentiel de liquéfaction des résidus miniers sous-consolidés et normalement consolidés étaient relativement similaires, malgré des différences significatives au niveau de la réponse du site telles que déterminée selon les facteurs d'amplification. Ces différences sont attribuées au développement de surpressions interstitielles, lesquelles étaient prises en compte dans les évaluations numériques mais pas dans les évaluations analytiques.

Analyse numérique du parc à résidus miniers de référence

Les objectifs principaux de l'analyse numérique du parc à résidus miniers de référence étaient: a) d'obtenir des évaluations comparatives du comportement dynamique du parc avec et sans inclusions de roches stériles ; b) évaluer la réponse dynamique des résidus miniers en comparaison avec les évaluations selon de méthode Simplifiée; et c) comparer le comportement dynamique du parc à résidus miniers avec les résultats des analyses pseudo-statique.

La digue modélisée au Chapitre 5 est formée d'un remblai rocheux de 21 m de hauteur la digue du parc à résidus on été construite en trois étapes. La première étape, de 11 m de hauteur, comportait un rideau d'argile compactée en amont. Les deux étapes subséquentes comportant des digues de 5 m hauteur construites par la méthode amont. Ces digues comportent un noyau d'argile compacté raccordé au rideau de la première phase. La hauteur maximale des résidus dans le parc est d'environ 20 m.

Les inclusions de roches stériles ont été simulées avec une largeur de 8 m de, sur toute la hauteur des résidus, avec un espacement de 20 m de centre à centre.

L'analyse numérique dynamique du parc à résidus miniers à été effectuée en utilisant des données modifiées du signal sismique (accélérations horizontales) équivalent à un séisme de magnitude 7.5 pour une faille située à une distance de 30 km. L'analyse fut effectuée en deux phases : a) une analyse statique afin de déterminer les contraintes, les déformations et les pressions interstitielles dans le parc avant les secousses ; b) une analyse dynamique simulant le séisme. Les données principales furent enregistrées à des endroits critiques du modèle pendant l'analyse dynamique.

Dans les calculs, nous avons considéré que les résidus étaient sous-consolidés. Leurs propriétés furent établies à partir des essais au piézomètre et des essais de laboratoire. Les valeurs de $(N_1)_{60}$ ont été appliquées en utilisant la fonction « rdev » dans FLAC, créant ainsi une distribution normale (gaussienne). Une valeur moyenne $(N_1)_{60}$ de 3.5 avec un écart-type de 0.5 fut utilisée pour les résidus. La distribution de la valeur $(N_1)_{60}$

représente une hétérogénéité typique des résidus miniers. Les propriétés des autres matériaux furent basées sur des valeurs représentatives publiées.

Les résultats des évaluations du comportement du parc à résidus minier modélisé, avec et sans inclusions de roches stériles, mènent aux observations suivants :

a) Il y a un l'amortissement très élevé du signal sismique à l'intérieur du parc sans inclusions; la présence des inclusions réduisit modérément l'amortissement ;
b) Sur la base des rapports de contrainte cyclique développés dans les résidus et les inclusions, a notre que les derrières ont subit des contraintes de cisaillement élevé et ont bien résisté aux mouvements du parc pendant les secousses ;
c) La présence des inclusions a réduit la génération des pressions interstitielles excédentaires dans les résidus adjacents ;
d) La présence des inclusions a réduit le déplacement horizontal de la crête de la digue (de 0.95 m à 0.61 m) et le déplacement vertical (de 0.30 m à 0.25 m).
e) Globalement, la présence des quelque inclusions a eu pour résultat d'améliorer légèrement la performance sismique du parc à résidus de référence.

Certaines différences importantes ont surgit entre l'analyse numérique et les analyses de liquéfaction selon la méthode Simplifiée. Par exemple, la réponse du site est plus rigide dans les analyses sur le liquéfaction du terrain que dans les analyses numériques du parc. Ces différences sont attribuées à la présence de la digue dans l'analyse due parc de référence, qui constituait la principale différence entre les deux types d'analyses.

Les résultats de l'analyse numérique n'ont pas indiqué de risque de rupture du parc. Tel qu'indiqué précédemment, l'analyse pseudo-statique a quant à elle indiqué l'existence d'un potentiel de rupture le parc.

Évaluation de l'utilisation d'inclusions de roche stérile

L'utilisation d'inclusions de roches stériles pour contrôler les effets de la liquéfaction de parcs à résidus miniers à été évaluée à l'aide d'analyses numériques dynamiques pour le cas d'un parc à résidus miniers conceptuel, avec et sans inclusions. Les objectifs principaux du Chapitre 6 consistaient à : a) analyser et évaluer le comportement d'un parc conceptuel sous différentes charges sismiques ; et b) déterminer l'influence des inclusions sur le comportement dynamique du parc et leur capacité à contrôler les effets de la liquéfaction.

Le parc conceptuel a une hauteur de 21 m et la digue est construite par la méthode amont en cinq étapes (soit une digue de départ en de moraine glaciaire compactée et quatre rehaussements construits à partir de résidus miniers grossiers) avec une pente aval de 2 : 1 (H : V). Le niveau de la nappe phréatique concordait avec la surface des résidus.

Les cinq inclusions de roches stériles ont 5 m de largeur et elles sont placées parallèlement à la digue à une distance nominale centre-à-centre de 20 m, sur toute la hauteur des résidus.

Les propriétés des résidus ont été obtenues à partir des mesures in situ et des essais en laboratoire. Les propriétés des autres matériaux étaient basées sur des données publiées pour des matériaux similaires. Les roches stériles ont les mêmes propriétés que le remblai rocheux de la digue, à l'exception de sa conductivité hydraulique qui est plus faible due à la présence de particules fines. Les résidus à l'intérieur du parc avaient une hauteur de 20 m et étaient sous-consolidés. Une valeur moyenne $(N_1)_{60}$ de 3.5 (avec un écart-type de 0.5) fut utilisée. Les résidus grossiers pour chaque phase de rehaussement de la digue étaient représentés par une valeur moyenne $(N_1)_{60}$ de 11 (avec un écart-type de 0.5). Un amortissement dynamique fut simulé en assignant une courbe de réduction du module de cisaillement aux différents matériaux et en appliquant un facteur d'amortissement de la rigidité de Rayleigh de 0.005 au modèle.

Les analyses ont été effectuées en trois phases ; condition statique, cas dynamique et condition post-séisme. Cette dernière phase pour effet de dissiper la pression interstitielle excédentaire générée durant le tremblement de terre et le retour à l'équilibre de la pression d'eau dans le parc. Afin d'augmenter la vitesse de calcul pour la phase post-séisme, la conductivité hydraulique de tous les matériaux à été augmentée par deux ordres de grandeur. Les résultats préliminaires indiquent que ces changements n'ont pas eu d'effet significatif sur les tendances obtenues.

Les performances dynamiques et post-séisme du parc furent évaluées sur la base de la réponse du site, du rapport des contrainte cycliques, de la pression interstitielle excédentaire et de sa dissipation, ainsi que selon les déformations et des déplacements de la crête de la digue.

Les effets des inclusions de roches stériles sur le parc se résument comme suit :

a) La présence d'inclusions cause une réponse plus rigide aux charges sismiques (moins d'amortissement).
b) Les inclusions réduisent la production de pression interstitielle dans les résidus adjacents et au fonds du parc (proche du tapis drainant).
c) Les déplacements du parc avec inclusions de roches stériles furent substantiellement plus faibles que ceux parc sans inclusions; dans certains cas la différence atteint jusqu'à un ordre de grandeur.
d) L'ampleur de la déformation à été réduite significativement par la présence des inclusions, avec pour effet que moins de résidus seraient relâchés lors d'une rupture de la digue.
e) Globalement l'utilisation d'inclusions de roches stériles peuvent de réduire significativement la déformation du parc pour les charges sismiques utilisées.

Évaluations paramétriques et discussion

Plusieurs évaluations complémentaires furent effectuées afin de déterminer l'influence de différents paramètres sur la performance dynamique du parc avec des inclusions de roches stériles. Les résultats présentés au Chapitre 7 se résument ainsi :

a) Le degré de consolidation des résidus a un effet mineur sur le comportement dynamique du parc conventionnel.
b) Le compactage des résidus grossiers utilisés dans la construction des digues n'a pas eu d'effet sur le comportement dynamique du parc.
c) La conductivité hydraulique des roches stériles (inclusions) n'a pas eu d'effet significatif sur le comportement dynamique du parc.
d) La largeur des inclusions de roches stériles (4, 6 ou 8 m) n'a pas eu d'impact significatif sur le comportement dynamique du parc ;
e) Le nombre d'inclusions de roches stériles (2, 3, 4 ou 5) n'a pas eu d'impact significatif sur le comportement dynamique du parc ; et
f) L'augmentation de l'espacement entre les inclusions (de 20 m à 24 m) a eu un impact défavorable sur le comportement dynamique du parc et a résulté en une déformation excessive.

Conclusions et recommandations

De manière générale, l'utilisation d'inclusions de roches stériles a eu comme effet d'améliorer significativement la réponse dynamique du parc conceptuel soumis aux charges sismiques considérées. Les travaux futurs devraient porter sur une analyse plus élaborée des divers composantes du concept d'inclusions de roches stériles afin d'avantage le mode d'utilisation pratique.

TABLE OF CONTENTS

LIST OF TABLES

LIST OF FIGURES

LIST OF SYMBOLS AND ABBREVIATIONS

Symbols

a_{max}	peak horizontal ground acceleration.
$a_x(t)$	horizontal component of acceleration at a given time, t.
$a_y(t)$	vertical component of acceleration at a given time, t.
B^e	elastic bulk modulus.
B_f	fluid bulk modulus.
c	cohesion.
c_v	coefficient of consolidation.
C_c	compression index.
C_r	recompression index.
CSR	cyclic stress ratio.
C_c	coefficient of curvature.
C_u	coefficient of uniformity.
C_N	Standard penetration test blow count correction factor for the effective overburden stress.
C_E	Standard penetration test blow count correction factor for the hammer energy (efficiency).
C_B	standard penetration test blow count correction factor for the diameter of the borehole.

C_R	standard penetration test blow count correction factor for the length of rods (depth of the borehole).
C_S	standard penetration test blow count correction factor for the sampling method.
CDSS	cyclic direct simple shear testing.
CRR	cyclic resistance ratio.
CSR_{CSS}	cyclic stress ratio causing liquefaction in cyclic simple shear testing.
CSR_{TRX}	cyclic stress ratio causing liquefaction in cyclic triaxial testing.
[D']	constitutive model matrix.
$[D_f]$	equivalent fluid stiffness matrix.
D	diameter.
D_e	diameter of the tributary area of the drains.
D_r	relative density (see also G_s, specific gravity, and I_D, density index).
D_x	grain size equivalent to x% passing a specific sieve size (by weight or mass).
e	void ratio.
e_c	void ratio at the end of consolidation.
e_0	initial void ratio.
E	Young's modulus; elastic modulus.

$\overline{E}_r$	rebound modulus.
FS	factor of safety.
f	factor (generic); yield function.
f_{ani}	anisotropic factor.
F_a	amplification factor.
g	acceleration due to gravity; plastic potential function.
G_{MAX}	low strain shear modulus (maximum shear modulus).
G_s	specific gravity (see also D_r, relative density).
G^e	elastic shear modulus.
G*	normalized plastic shear modulus.
h	height.
I_D	density index.
I_h	Arias Intensity.
I_p	plasticity index (see also PI).
I_{xx}	Horizontal component of the Arias intensity.
I_{yy}	Vertical component of the Arias intensity.
k	pseudo-static coefficient.
k_B^e	elastic bulk modulus number.
k_G^e	elastic shear modulus number.
k_G^p	plastic shear modulus number.

k_H	horizontal saturated hydraulic conductivity.
k_r	horizontal hydraulic conductivity.
k_{sat}	saturated hydraulic conductivity.
k_v	vertical saturated hydraulic conductivity.
k_{wr}	hydraulic conductivity of waste rock.
K_α	initial static shear stress correction factor.
K_σ	overburden stress correction factor.
K_o	Coefficient of earth pressure at-rest (at-rest coefficient); principal stress ratio.
LL	liquid limit.
me	elastic bulk modulus factor.
m_{v3}	compressibility.
M_L	Richter magnitude.
MSF	magnitude scaling factor.
M_w	moment magnitude.
m_{v3}	coefficient of compressibility.
n	porosity.
N	standard penetration test blow count; number of loading cycles.
$(N_1)_{60\text{-}cs}$	equivalent clean sand, corrected standard penetration test blow count.
$(N_1)_{60}$	corrected standard penetration blow count.

N_{EQ}	number of equivalent cycles.
N_{LIQ}	number of cycles to trigger liquefaction.
n_d	developed stress ratio.
n_f	stress ratio at failure.
n_p	plastic shear modulus exponent.
n_{ult}	ultimate strength from the best fit hyperbola.
ne	elastic shear modulus factor.
p’	mean effective stress; effective confining stress.
Δp’	mean effective stress increment.
P_a	atmospheric pressure.
PGA	peak (horizontal) ground acceleration (see also PHA and amax).
PGA_x	peak (horizontal) ground acceleration at some reference point (e.g. the ground surface).
PGA_{BR}	peak (horizontal) ground acceleration on the top of bedrock.
PI	plasticity index (see also IP).
q	shear stress; maximum shear stress.
Δq	shear stress increment.
q_c	cone penetration test (CPT) tip resistance.
q_{c1}	normalized cone penetration test (CPT) tip resistance.
q_{c1N}	corrected cone penetration test (CPT) tip resistance.

q_{ss}	shear strength in the steady state condition.
r	porewater pressure ratio.
r_u	excess porewater pressure ratio.
r_d	stress reduction coefficient.
R_F	failure ratio.
S_r	degree of saturation.
S_u	liquefied shear strength.
t	time.
t_d	earthquake duration.
T_{ad}	dimensionless time coefficient.
t_d	earthquake duration (duration of shaking).
u	porewater pressure.
Δu	change in porewater pressure; porewater pressure increment.
U_{excess}	change in porewater pressure, see Δu.
w	natural water content; water content (moisture content).
x	a cardinal direction perpendicular to y.
y	a cardinal direction perpendicular to x.
z	depth below the ground surface.
α	factor for calculation of fine content correction coefficient.
β	factor for calculation of fine content correction coefficient.

γ	shear strain.
γ_{TOTAL}	total unit weight.
γ_w	unit weight of water.
γ_{pc}	peak post-cyclic shear strain.
$\{\Delta\sigma'\}$	vector of effective stress increments.
$\{\Delta\varepsilon\}$	vector of total strain increments.
Δe_{rd}	change in void ratio.
$\Delta\varepsilon_{rd}$	volumetric strain under drained conditions.
$\Delta\varepsilon^e$	elastic strain increment.
$\Delta\varepsilon_v^p$	plastic shear strain increment.
$\Delta\varepsilon_v^p$	plastic volumetric strain increment.
$\Delta\varepsilon_v^f$	equivalent fluid volumetric strain.
Δn_d	developed stress ratio increment.
$\Delta\sigma$	cyclic deviatoric stress.
$\Delta\sigma$’	effective stress increment.
$\Delta\gamma^p$	plastic shear strain increment.
λ	constant of proportionality.
ν	Poisson’s ratio.
ρ_{TOTAL}	total mass density.
σ_1	major principal stress.

σ_3	isotropic effective confining stress; minor principal stress.
σ_{vo}	initial total vertical stress.
σ'	effective stress.
σ'_o	initial effective overburden stress.
σ'_{3c}	effective minor confining stress.
σ'_v	effective overburden stress; vertical effective stress.
σ'_{vo}	initial effective overburden stress; initial vertical effective stress.
σ'_{vc}	effective vertical consolidation stress.
σ_d	deviatoric stress.
σ_{DEV}	cyclic deviatoric stress.
τ	shear stress.
τ_{av}	average shear stress.
τ_{max}	maximum shear stress.
$\tau_{max\text{-}pc}$	maximum post-cyclic shear stress (peak post-cyclic shear strength).
$\tau_{max\text{-}pc}/\sigma'_{v,c}$	liquefied strength ratio.
ϕ'	effective internal angle of internal friction; effective friction angle.
ϕ_{cv}	constant volume friction angle.
ϕ_d	developed friction angle.
ϕ_f	peak friction angle; friction angle at failure.

ψ	dilation angle; constant volume friction angle; state parameter.
ψ'	limiting state of stress or ultimate failure surface in p'-q space.
ψ_L	angle defining the initiation of liquefaction.

Abbreviations

ASCE	American Society of Civil Engineers
ASTM	American Society for Testing Materials.
BPT	Becker penetration test.
CPT	cone penetration test.
CPTu	cone penetration test with porewater pressure measurements.
CRR	cyclic resistance ratio.
CSR	cyclic stress ratio.
FLS	flow liquefaction surface.
FS	factor of safety (also F.S.).
H	horizontal.
ICOLD	International Commission on Large Dams.
ML	silt of no or low plasticity (USCS).
MSF	magnitude scaling factor.
NGI	Norwegian Geotechnical Institute.
PGA	peak horizontal ground acceleration (see also PHA and a_{max}).
PHA	peak horizontal ground acceleration (see also PGA).

SM-ML	silty sand (USCS).
SPT	standard penetration test.
UNEP	United Nations Environmental Program.
US EPA	United States Environmental Protection Agency.
USCS	Unified Soil Classification System.
V	vertical.

LIST OF APPENDICES

(On CD-ROM)

CHAPTER 1. INTRODUCTION

The increasing size and number of tailings impoundments and the relatively recent awareness of the seismicity of large areas of the province of Quebec, and eastern North America in general are a cause for concern. Combined, they highlight the need for a better understanding of the liquefaction potential of tailings and the seismic stability of tailings impoundments, and for the development of means of controlling the effects of liquefaction in tailings impoundments.

In recent decades there have been several failures of tailings impoundments due to liquefaction of the impounded tailings or of tailings used to construct the retaining structures (dams and dikes) forming the impoundments. Some of these failures have resulted in considerable loss of life and they have all caused significant environmental damage and economic loss. For instance, on March 28, 1965 central Chile was struck by an earthquake with a Richter magnitude of about 7. The region is a major copper production center and had over 10 active mining sites with more than 20 active and inactive tailings impoundments at the time. All of the tailings impoundments were formed from incrementally raised, hydraulically placed tailings and most of them failed as a result of seismically-induced liquefaction of the tailings. The failure of the three El Cobre tailings dams resulted in a flow of liquefied tailings that traveled 20 km and killed over 200 people while destroying part of the town of El Cobre (Dolbry & Alvarez, 1967).

Stone columns have been shown to be a very effective means of controlling the effects of liquefaction in natural soils by providing for the rapid dissipation of excess porewater pressure and by reinforcing the soil mass during earthquake shaking (Ledbetter, 1985; Sonu, 1993). By analogy, it was assumed by Aubertin et al. (2002) that the placement of waste rock inclusions before and during tailings deposition or the placement of waste rock columns in existing tailings deposits could similarly act to control the effects of liquefaction in tailings impoundments. The presence of waste rock inclusions would also facilitate consolidation of the tailings as stone columns or wick drains do clayey soils.

Figure 1-1 schematically illustrates the placement of waste rock inclusions prior to tailings deposition and Figure 1-2 illustrates the placement of waste rock columns after tailings deposition. The inclusions shown on Figure 1-1 need not be continuous, they could be placed a heaps within the impoundment.

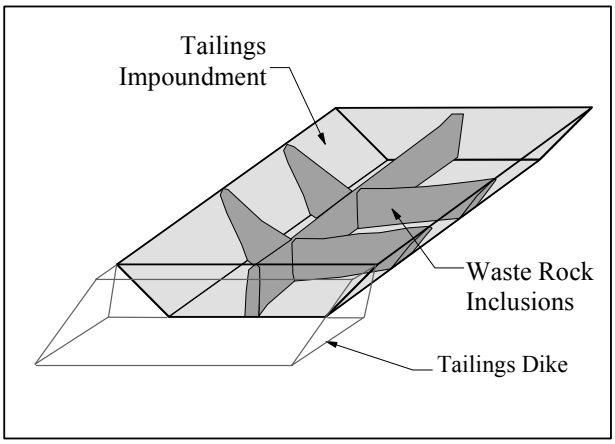

Figure 1-1 – Schematic illustration of a tailings impoundment with waste rock inclusions placed prior to tailings deposition. (adapted from Aubertin et al. 2002).

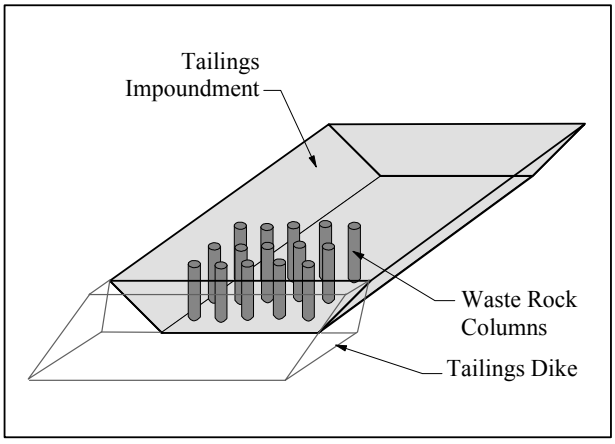

Figure 1-2 – Schematic illustration of a tailings impoundment with waste rock columns constructed after tailings deposition.

1.1 OBJECTIVES

The primary objectives of this research were: a) to evaluate the use of waste rock inclusions to control the effects of liquefaction in tailings impoundments (numerical analysis of various scenarios); and b) develop conclusions and recommendations regarding the use of waste rock inclusions.

To attain these primary objectives, there were several secondary, or intermediate, objectives that had to be completed in the course of the research. These included:

- A study of the liquefaction potential and dynamic behavior of hard rock tailings based on situ testing and laboratory testing;
- The applicability of existing methods for liquefaction evaluation to tailings;
- Selection, verification and calibration of an existing numerical model for soil liquefaction based on published results and dynamic laboratory testing of tailings;
- Development of a numerical procedure for the analysis and evaluation of the dynamic stability of tailings impoundments through preliminary modeling of an example tailings impoundment;
- Development of a conceptual tailings impoundment and numerical analysis and evaluation of the dynamic behavior of the conceptual tailings impoundment under a range of seismic loadings, with and without waste rock inclusions;
- Parametric evaluation of the use of waste rock inclusions; and
- Formulation of conclusions and recommendations regarding the use of waste rock inclusions to control the effects of liquefaction in tailings impoundments.

1.2 SCOPE AND CONTENT OF THIS THESIS

Although the objectives of this research are relatively narrow, the scope was relatively broad due to the number and complex nature of the phenomena involved.

This research included a review of the state of knowledge and practice with respect to:

- The typical properties and characteristics of tailings, specifically hard rock tailings;
- The causes, mechanisms, effects, and control of liquefaction as well as methods of evaluating the potential for liquefaction;
- The dynamic behavior and liquefaction potential of hard rock tailings;
- The seismic behavior of tailings impoundments and means of evaluating their dynamic stability; and
- Numerical modeling of liquefaction, liquefaction control measures and of the dynamic response of tailings impoundments.

The review of the state of knowledge and practice (literature review) is presented in Chapter 2 of this thesis.

A geotechnical study was completed at the active tailings impoundment of a representative hard rock mine to evaluate the properties and characteristics of the tailings and determine surface and subsurface conditions. The study included a review of documents (geologic reports, design and construction documents, aerial photographs, topographic maps, and geotechnical reports by others), field exploration (site reconnaissance, cone penetration test and test pits), conventional and dynamic laboratory testing, and an evaluation of the liquefaction potential of the tailings deposit based on conventional analytical methods and on the dynamic laboratory testing, assuming “level ground” conditions. The study also contains an evaluation of the static and seismic stability of the impoundment based on limit equilibrium methods. The geotechnical study is presented in Chapter 3.

Chapter 4 presents preliminary numerical analyses which included modeling of the cyclic direct simple shear testing conducted on tailings from the representative impoundment for validation and calibration of the numerical model and "level ground" dynamic numerical liquefaction analysis of the tailings deposit for comparison with analytical results presented in Chapter 3. Numerical analyses were conducted using version 5.00.377 of the FLAC (Fast Lagrangian Analysis Continua) software program by the Itasca Consulting Group (2005) and the UBC Sand Model (Byrne et al., 1995, 2003, 2004; Puebla et al., 1997; Beatty & Byrne, 1998; Puebla, 1999; Park & Byrne, 2003).

Dynamic numerical analyses of the tailings impoundment of the representative mine, as constructed and with waste rock inclusions, are presented in Chapter 5. Material properties were derived from the geotechnical study and published sources. The results of the numerical analyses are compared with the analytical results of Chapter 3.

The use of waste rock inclusions to control the effects of liquefaction in tailings impoundments was evaluated using dynamic numerical methods and is presented in Chapter 6. The model was a conceptual upstream-raised tailings impoundment based on typical dimensions. The material properties were based on the findings of Chapters 3 and 4 as well as published sources. The conceptual impoundment, with and without waste rock inclusions, was subjected to dynamic loads equivalent to moment magnitude 6.5 to 7.5 events with a fault rupture to site distance of 30 km.

Chapter 7 presents parametric modeling of the conceptual impoundment that considers:

- The degree of consolidation of the impounded tailings;
- The compaction of the tailings used to construct the dike;
- The hydraulic conductivity of the waste rock inclusions;
- The size, number and spacing of the waste rock inclusions; and
- Waste rock inclusions placed adjacent to the dike or constructed as columns in the impounded tailings.

A general discussion on the findings of the research and on the interaction between the various elements of the research is also presented in Chapter 7.

Conclusions and recommendations are presented in Chapter 8.

This thesis also contains an extensive list of references and appendices that provide additional details and information on the various elements of the research. A bibliography of documents that were consulted but not cited in text is also provided.

CHAPTER 2. THE STATE OF THE KNOWLEDGE AND PRACTICE

This literature review is based on available information on the current state of the practice and research concerning the various phenomena associated with the objectives and scope of this research as described in Chapter 1, specifically:

- The properties and characteristics of tailings and waste rock from hard rock mines, common types of tailings impoundments, and stability considerations for tailings impoundments (Section 2.1);
- Liquefaction – the mechanics, causes, and effects (Section 2.2);
- Methods of evaluating the potential for liquefaction (Section 2.3);
- Observations and research on the liquefaction resistance of hard rock tailings (Section 2.4);
- Methods of controlling liquefaction and its effects, including the use of gravel columns (Section 2.5);
- A general description of the proposed use of waste rock inclusions to control the effects of liquefaction in tailings impoundments (Section 2.6);
- Numerical modeling of dynamic behavior (Section 2.7); and
- Methods of evaluating the stability of tailings impoundments (Section 2.8).

Remarks on the literature review are presented in Section 2.9.

2.1 HARD ROCK MINE WASTE AND TAILINGS IMPOUNDMENTS

2.1.1 Hard Rock Tailings

2.1.1.1 Hard Rock Tailings Defined

The geotechnical characteristics of tailings are determined by the properties of the parent rock, particularly the mineral composition, by the processing of the ore for mineral extraction and the method of deposition. Typically, tailings are classified into one of four categories that are primarily based on the properties of the parent rock (Vick, 1990): soft rock tailings, fine tailings, coarse tailings, and hard rock tailings.

Hard rock tailings are typically produced from the mining of lead, zinc, copper, gold, silver, molybdenum, and nickel, but may also be produced from uranium, cobalt, tin, platinum-palladium, tungsten, chromium, titanium, and mercury. These tailings typically vary in size from colloids to sands with the colloidal fraction being inactive (nonplastic) and the behavior of the tailings is thus governed by inter-particle friction (Vick, 1990). For purposes of this research, this definition of hard rock tailings will apply.

2.1.1.2 Typical Properties of Hard Rock Tailings

The density and heterogeneity of tailings deposits are significantly influenced by the method of placement, age and height of the deposit. Typically, hard rock tailings are placed in tailings impoundments and allowed to consolidate under their own weight. The placement method, usually by slurry pumped from pipes along the perimeters of impoundments, results in varying degrees of segregation of the particles based on grain size and variation of the specific gravity (Vick, 1990; Aubertin et al., 2002; Bussière, 2007). Other types of tailings disposal methods include the backfilling of open pits and stopes, subaqueous disposal, and surface disposal of densified tailings. The tailings described in this thesis are assumed to have been placed as slurry within a tailings impoundment.

Segregation of tailings due to placement results in a heterogeneous structure consisting of interbedded layers and lenses of silt, sandy silt, silty sand, and sand and is caused by the grain size distribution of the tailings, the velocity of flow at the outlets, the positions of the outlets, the slope onto which the tailings slurry is deposited, and the presence of flowing or standing water. Typically, beaches of coarser material are formed near the outlets of the slurry pipes and finer material travels further into the impoundment (Vick, 1990).

Upon placement, tailings are at very low relative densities. Self-weight and the pressure applied by subsequent layers causes tailings to consolidate and become denser with depth and time. Consolidation can be relatively rapid in the absence of fines (colloid to silt sized particles passing a 0.075 mm sieve) or can be relatively slow when the fines content is significant.

The properties of hard rock tailings have been investigated by several researchers. Vick (1990) provides comprehensive data on the properties of tailings from a wide range of sources. Aubertin et al. (1996) conducted research on the properties of tailings from four hard rock mines in the Abitibi region of the province of Quebec. Qui & Sego (2001) present geotechnical laboratory results for tailings from four mines in western Canada that include two hard rock mines (a gold mine and a copper mine). Data from geotechnical laboratory testing of copper-gold and copper-gold-zinc tailings from mines in western Canada is provided in Wijewickreme et al. (2005a). Bussière (2007) summarizes the properties of hard rock tailings as reported from various research and engineering activities. The typical properties measured for hard rock tailings from these sources are described below.

Specific Gravity –The specific gravity, G_s (relative density, D_r, in Canadian Geotechnical Society terminology) of tailings is determined by the mineralogical composition of the parent rock. Vick (1990) gives typical values for the specific gravity of hard rock tailings

that vary from 2.6 to 2.9. The specific gravity of the samples tested by Aubertin et al. (1996) ranged from 2.78 to 2.87. Qiu & Sego (2001) give values of 2.75 and 3.17 for copper and gold tailings, respectively. The average G_s of copper-gold tailings reported by Wijewickreme et al. (2005a) was 2.78 for four samples. For 20 samples of copper-gold-zinc tailings from the same mine, Wijewickreme et al. (2005) give low and high values of 3.36 and 4.42, respectively, with an average value of 3.73. Due to their mineral composition, the G_s values for hard rock tailings are typically much greater than those for naturally-occurring soils.

Gradation – The grain size distribution of hard rock mine tailings is determined by the methods used to process the ore and generally produces particles varying from colloidal to sand-sized (passing a 4.75 mm sieve). The grain size distributions of hard rock mine tailings generally fall within the shaded area shown on Figure 2.1 which was compiled from information in Vick (1990), Aubertin et al. (1996), Qui & Sego (2001), Wijewickreme et al. (2005a), and Bussière (2007).

As shown on Figure 2-1, hard rock mine tailings typically consist of 5 to 60 percent fine to medium-grained sand-sized particles by weight with the remainder consisting of silt to colloid sized particles. In some instances the sand fraction of tailings is removed, typically by cycloning, for use as a construction material, and the resulting finer materials are referred to as “slimes” (Vick, 1990).

Plasticity – As measured by the plasticity index, hard rock mine tailings are commonly nonplastic or of very low plasticity (Vick, 1990). The tailings studied by Aubertin et al. (1996) exhibited slight plasticity with plastic indices close to zero. The copper and gold tailings tested by Qiu & Sego (2001) were nonplastic. Wijewickreme et al. (2005a) reported that the copper-gold tailings they tested were nonplastic and that the copper-gold-zinc tailings had a plasticity index of 2. Bussière (2007) indicates that the liquid

limit of hard rock tailings is generally less than 40 and that the plastic limit is generally less than 15, if present.

Classification – Applying the Unified Soil Classification System (Holtz & Kovacs, 1981) to the typical gradations and plasticity of hard rock mine tailings as described above, the tailings are classified as silts of no or low plasticity (ML) or sandy silts/silty sands (SM-ML).

Shear Strength Parameters – As they are nonplastic or of very low plasticity, the shear strength of hard rock mine tailings is derived from internal friction with no significant contribution from cohesion, c. The effective angle of internal friction, ϕ', of hard rock tailings is estimated to vary between 30° and 41° depending on the density, grain size distribution, angularity of the grains, and confining pressure (Vick, 1990).

Chen and van Zyl (1988) conducted 73 isotropically-consolidated, drained and undrained triaxial compression tests on compacted, back-pressure-saturated samples of copper tailings. The tailings consisted of well-graded silty sand with 37 percent fines and a specific gravity of 2.74. The effective friction angle of the tailings was found to decrease with increasing effective consolidation (confining) stress, varying from 48° at 48 kPa to 34° at 883 kPa. This variation was assumed to be due to strong dilation of the tailings under low confining stresses and particle breakage under high confining stresses.

The drained friction angle of dense silt is typically 33° to 37°. This indicates that despite their high fines content, hard rock tailings have drained strengths more similar to sands than naturally-occurring silts. Mittal & Morgenstern (1977) and Vick (1990) indicate that the effective internal friction angle of hard rock tailings is typically about 6° higher than that of naturally occurring soils of similar gradation because of grain angularity and particle strength.

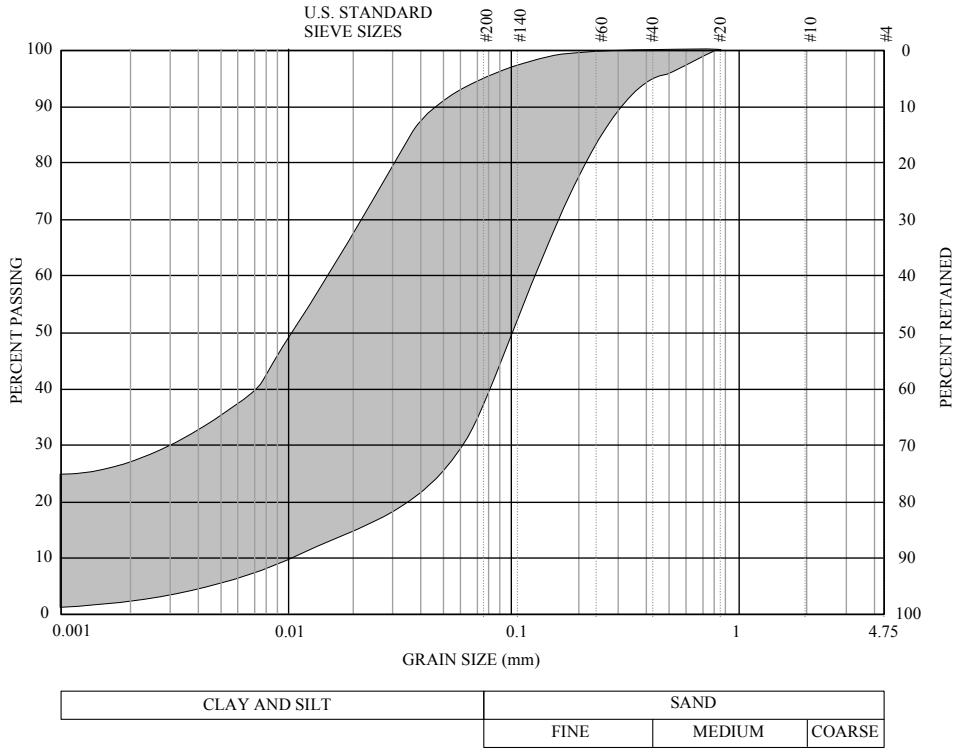

Figure 2-1 – General range of grain size distributions for hard rock tailings from Vick (1990), Aubertin et al. (1996), Qiu & Sego (2001), Wijewickreme (2005a) & Bussière (2007).

Chen & Van Zyl (1988) reported that the volumetric behavior of the tailings in undrained loading was comparable to that reported by Castro (1969) for similar tests on contractive sands. Typically, the porewater pressure increased rapidly until a maximum deviatoric stress and then declined to a steady state condition.

Void Ratio and Density – The in-place void ratio of hard rock tailings, excluding slimes, typically varies between 0.6 and 0.9 with the void ratio decreasing with increasing depth and confining stress (Vick, 1990). The dry density of tailings exhibits significant variation due to the effects of variation of the void ratio, specific gravity and gradation

within a deposit (Aubertin et al., 2002). Given the range of specific gravities and typical void ratios of hard rock tailings, the in-place dry densities are expected to vary from 16 to 27 kN/m^3.

Saturated Hydraulic Conductivity – Vick (1990) presents a typical range for the saturated hydraulic conductivity, k_{sat}, of hard rock tailings of $5.0x10^{-7}$ cm/s for slimes of little or no plasticity to $1.0x10^{-4}$ cm/s for sands with up to 30 percent fines by weight.

Bussière (2007) presents a compilation of hydraulic conductivity test results on remolded and undisturbed samples of hard rock mine tailings. The hydraulic conductivities vary from $3x10^{-7}$ to $1x10^{-2}$ cm/s, yet are within the expected range for naturally occurring soils of similar classification as presented in Freeze & Cherry (1979). There is no appreciable difference between the tests results of remolded samples and undisturbed samples of similar classification. It can be inferred that at the test scale, the method of deposition, or sample preparation, did not significantly affect the saturated hydraulic conductivity in the direction of measurement.

Aubertin et al. (1996) and Mbonimpa et al. (2002) demonstrated that conventional predictive equations to estimate the saturated hydraulic conductivity of soils are not directly applicable to tailings and provided new equations to estimate the saturated hydraulic conductivity of tailings that are in better agreement with measured values.

Vick (1990) reports that the ratio of horizontal to vertical saturated hydraulic conductivity, k_H/k_v, within tailings deposits is generally 2 to 10 but can be in excess of 100 where the methods of discharge have resulted in extensive inter-layering of finer and coarser materials.

Consolidation Properties – Typical values of the compression index, C_c, provided by Vick (1990) for hard rock tailings vary from 0.05 to 0.28. Typical values of the

coefficient of consolidation, c_v, for hard rock tailings vary from 10^{-2} to 10^{-4} cm^2/s for slimes and from 0.5 to 100 cm^2/s for the coarse fraction of the tailings (Vick, 1990).

Bussière (2007) contains a compilation of consolidation test results on undisturbed and remolded samples of hard rock tailings,. The compression indices, C_c, vary from 0.05 to 0.54 and the values of recompression indices, C_r, were typically 5 to 20% of the compression indices, which is the approximate range for naturally occurring soils given by Holtz & Kovacs (1981). The coefficients of consolidation, c_v, vary from $4.3x10^{-3}$ to $3.7x10^{-1}$ cm^2/s with no significant difference between the results from undisturbed and remolded samples.

The ranges of compression indices from both sources are well below that normally associated with fine soils of very low plasticity and the range of the coefficient of consolidation is significantly higher than that typical of fine soils of low plasticity based on typical values provided in Holtz & Kovacs (1981). This indicates that the amount of consolidation of tailings is expected to be less than that of naturally occurring silts (ML) over a similar range of stresses, while the rate of consolidation would be greater.

Stone et al. (1994) used field measurements, laboratory testing, centrifuge modeling, and numerical analysis to evaluate the consolidation behavior of tailings at a gold mine in Australia. They found that for an active impoundment, the coefficient of consolidation, c_v, of the tailings as measured using a conventional one-dimensional Rowe consolidation test device was about half that determined from field measurements, centrifuge testing, and numerical modeling. However, after the end of deposition, the results of centrifuge testing and numerical analyses appeared to converge with the results of conventional consolidation testing. The disparity was attributed to the effect of the deposition of the tailings into interbedded layers of variable gradation and degrees of consolidation.

2.1.2 Waste Rock

Waste rock is material excavated from a mine to reach the ore-bearing rock or to construct underground openings necessary for mine operation, e.g. ventilation shafts and access tunnels.

The characteristics of waste rock are determined by the properties of the parent rock, specifically its hardness, brittleness, and type and frequencies of discontinuities, and the excavation method (usually by drilling and blasting). The vast majority of rock excavated from hard rock mines consists of sand to boulder sized fragments. In some mines, particularly underground mines, the waste rock size is reduced for transport. Waste rock from hard rock mining tends to be strong, durable and angular. A distinction is sometimes made between waste rock and low-grade ore, which is rock that contains an insufficient percentage of the desired minerals to be processed and may be chemically unstable.

Waste rock is classified as reactive or nonreactive with respect to it tendency to produce acid when exposed to air and moisture. The acid produced by reactive waste rock can contribute to acid mine drainage and thereby create a serious environmental hazard that requires containment or collection and treatment.

Mining operations usually possess facilities for breaking and separating waste rock into any desired size so that it might be used for the construction of roadways, dikes, berms and other earthworks required at the mine, provided the waste rock is nonreactive or is adequately contained.

The quantity of waste rock produced from hard rock mining varies depending on site specifics, but typically exceeds the volume and weight of tailings produced from ore-bearing rock, particularly for open pit mines. Within the province of Quebec, the ratios of the weight of waste rock to the weight of tailings produced are typically 10:1 for open pit mining and 3:1 for underground mines (Aubertin et al., 2002).

Typical grain size distribution curves for waste rock from hard rock mines are presented on Figure 2-2.

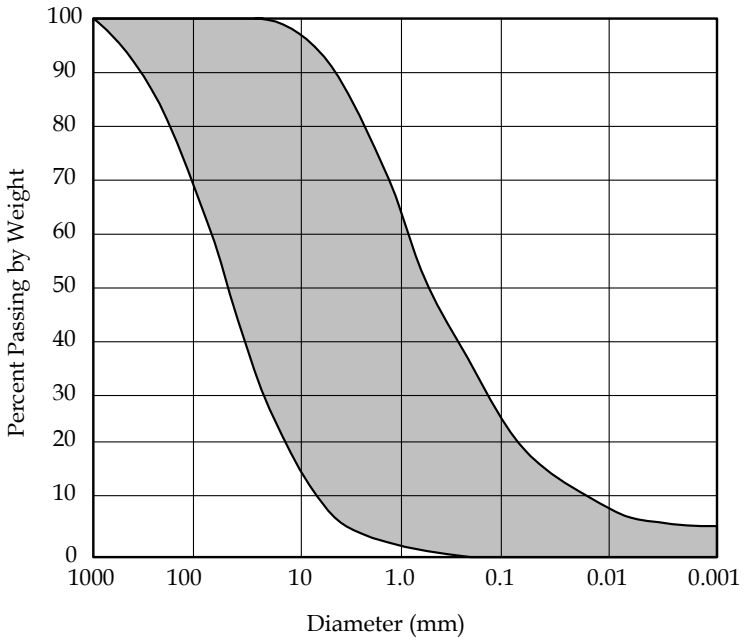

Figure 2-2 – Range of grain size distribution curves of waste rock from hard rock mining (adapted from Gamache-Rochette (2004).

Sherard et al. (1963) indicates that the angle of internal friction of "loosely dumped" varies from 40º to 45º and that the internal friction angle of compacted rockfill is "much higher." Leps (1970) used large-scale triaxial testing to evaluate the shear strength of rockfill from various sources and found that the average friction angle varied from 55° at low effective normal stresses to 37° at high effective normal stresses (3,500 kPa). The strength of dense, well-graded rockfill composed of strong particles was 5° higher than

the average and the strength of loose, poorly graded rockfill composed of weak particles was 5° lower than the average.

The hydraulic conductivity of waste rock is a function of the grain size distribution, particularly that of the finer fraction. In the absence of a significant fraction of fines, the hydraulic conductivity of waste rock is generally at least 2 to 3 orders of magnitude greater than that of hard rock tailings (Aubertin et al., 2002).

2.1.3 Tailings Impoundments

Worldwide, there are approximately 3,500 tailings impoundments of appreciable size (Davies, 2002). Tailings impoundments have been constructed to heights of hundreds of meters and covering many square kilometers (US EPA, 1994). Volumetrically, the largest impoundments are the largest human-made structures ever created (Davies, 2002). For example, the Tranque Talabre tailings impoundment at the Chuquicamata Mine in northern Chile has an estimated volume to 1,250 million m^3 and a surface area of approximately 5,000 hectares and is still in operation (SNC Lavalin, 2008).

The volume of mine tailings produced annually exceeds that of all other types of solid waste combined (UNEP, 1996). Due to increased demand for metals, many existing tailings impoundments will be enlarged and new tailings impoundments will be created on a continuing basis for the foreseeable future.

Vick (1990) divides surface impoundment into two types; “raised embankments” and “water-retention dam-type”. The vast majority of surface tailings impoundments consist of raised embankments.

Raised embankment impoundments are essentially dikes constructed to contain a quantity of tailings and wastewater expected to be produced over a given period, a year or two for example. The dike is then raised incrementally as necessary to contain the tailings and wastewater produced subsequently. The initial dike of a raised embankment (known as

the starter dike) typically consists of local borrow material, such as glacial till, and the subsequent raises generally consist of tailings.

Raised embankment impoundments are constructed in stages using the upstream, downstream or centerline methods shown schematically on Figure 2-3. The unusual geometries and composition of raised embankment impoundments and important differences between the behavior of tailings and naturally occurring soils (Vick, 1990) create conditions that are outside the standard practice for the design and analysis of conventional water-retention dams (Vick, 1990; Aubertin et al., 2002).

Due to the relatively low hydraulic conductivity of tailings, runoff and rainfall into the impoundments, and the need to maintain a water cover on the tailings to prevent aerial pollution (dust) and inhibit the generation of acid in some types of tailings, the groundwater level within tailings impoundments is usually at or above the surface of the tailings while the impoundment is in active use. After closure the surface of impoundments may be covered with soil and vegetated and the groundwater level within the impoundment is allowed to equilibrate with respect to the hydrogeologic conditions, infiltration, evapo-transpiration, and seepage from the impoundment. Alternatively, the groundwater level in the impoundment may be kept at or above the surface of the tailings to reduce acid generation.

Between 1917 and 2002, there were 215 known incidents involving the unacceptable behavior of tailings dams. The primary causes of these failures were slope stability, overtopping due to flooding, and seismic activity. Approximately 26 of the 215 known incidents were due to seismic activity and many of the seismically-induced incidents were triggered or exacerbated by liquefaction of the impounded tailings or of tailings used to construct the impoundment (ICOLD, 2001; WISE, 2009).

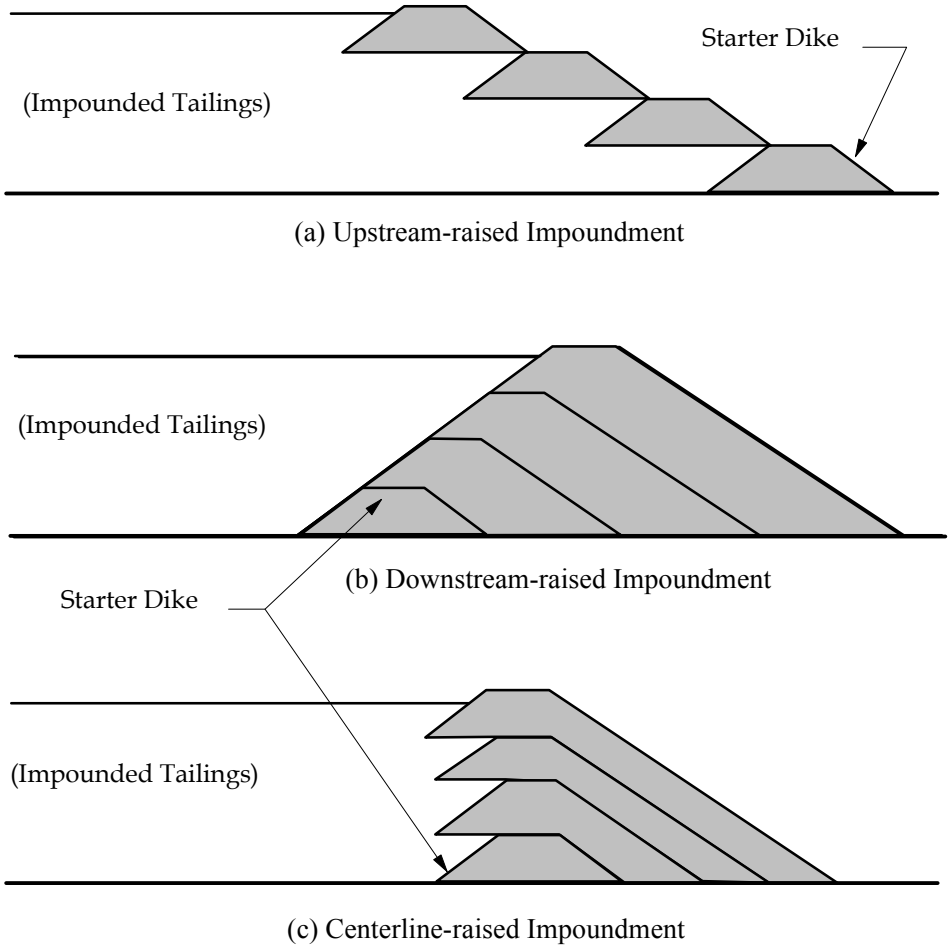

Figure 2-3 – Common types of raised embankments (from Vick, 1990).

Some of the notable incidences of tailings impoundment failure involving seismically-induced liquefaction are briefly described below.

- The Barahona tailings dam, located at the El Teniente copper mine in Chile, was a 61-meter-high dam constructed using the upstream method. On October 1, 1928 a portion of the dam failed, apparently due to liquefaction of the

retained tailings during an earthquake. The failure resulted in the release of an estimated 4 million tons of tailings (Ishihara et al., 1980; ICOLD, 2001).

- On March 28, 1965 northern Chile was struck by an earthquake which resulted in multiple failures of tailings dams, most of which were attributed to liquefaction of the impounded tailings. The failure of the El Cobre tailings dam resulted in the release of over 2 million tons of tailings which extensively damaged a nearby town and caused approximately 200 deaths (Dobry & Alvarez, 1967; Davies & Lighthall, 2001; WISE, 2009).

- On January 14-15, 1978 Mochikoshi, Japan multiple failures of tailings dikes occurred as a result of liquefaction of the impounded tailings during an earthquake. The released tailings caused significant environmental damage to downstream areas (Ishihara, 1984).

- More recently, failure of the Tapo Canyon tailings dam in southern California on January 17, 1994 was attributed to liquefaction of the impounded tailings, and possibly of portions of the dam which were constructed of tailings, induced by the Northridge earthquake (Harder & Stewart, 1996).

To some extent, the static and dynamic stability of tailings impoundments can be analyzed in much the same way as conventional earth dams. Important issues concerning the static stability of tailings impoundments include (ICOLD, 1989 & 1995; Lo & Klohn, 1995; Finn, 1993 & 1998; Vick, 1990):

- Slope stability;
- Foundation bearing capacity;
- Internal erosion (piping);
- Slope erosion; and

- Overtopping due to excessive rainfall or runoff, outlet failure, material inflow (e.g. landslide) or excessive settlement of compressible foundation materials.

Dynamic stability evaluation of tailings impoundments should also address:

- Slope stability under seismic conditions;
- Increased lateral loads on the dike or dam due to the dynamic response of the tailings;
- Deformation of the embankment sufficient to cause overtopping;
- Seismically induced densification of the foundation soils, dam or dike and possible lowering of the crest below acceptable levels;
- The potential for excess porewater generation or liquefaction in the embankment material;
- The potential for excess porewater pressure generation or liquefaction in the foundation materials;
- The potential for liquefaction of the retained tailings; and
- The post-earthquake stability of an impoundment may be affected by the dissipation of excess porewater pressures and strength loss caused by shaking.

All of the issues listed above, except for liquefaction, can typically be analyzed using conventional geotechnical engineering techniques supplemented with advanced numerical methods (e.g. finite elements or finite differences). There has been relatively little research done on the dynamic behavior of mine tailings with respect to the dynamic stability of impoundments. Additional research on tailings liquefaction within the overall context of the dynamic stability of tailings impoundments is required.

Mittal & Morgenstern (1977) reviewed aspects of the design and construction of tailings impoundments with respect to static and dynamic loads. Their primary findings and conclusions were as follows:

- Relative to natural soils of similar gradation, tailings sands tend to be less compressible and have higher shear strength;
- The average downstream slopes of tailings dams in Canada was 36° (1.38 H : 1 V) at the time of the study;
- The relatively poor behavior of upstream-raised tailings dams at that time was mainly attributed to: a) downstream slopes that were too steep; b) high phreatic surfaces within impoundments near the near the dikes resulting in seepage through the downstream slope; and c) weak foundation soils;
- In upstream-raised impoundments, there were often lenses of soft slimes within the coarse tailings of the dike due to the construction method; and
- The hydraulic conductivity of the coarse tailings used to construct dams should be sufficiently greater than that of the slimes such that the phreatic surface is not near the downstream (external) slope.

Although tailings impoundments constructed by the upstream-raised method are known to be particularly vulnerable to seismically-induced failure, the stability of this type and other types of raised impoundments tends to increase after closure due to a lowering of the phreatic surface within the impoundment (depending on the water balance) and consolidation and ageing of the tailings (Vick et al., 1993).

Conlin (1987) conducted a preliminary assessment of the performance of raised tailings impoundments in Chile and Japan constructed of tailings which had been subjected to seismic activity on the basis of the earthquake magnitude and epicentral distance. This work was subsequently expanded by Lo & Klohn (1995). The impoundments were classified as operational or non-operational (closed) and their performance was classified

as “have undergone no damage”, “minor damage” or “significant damage” as a result of the seismic activity. The local or Richter magnitude, M_L, was used to quantify the seismic activity. For operational and non-operational impoundments, Colin (1987) plotted epicentral distance versus earthquake magnitude and observed that there was a boundary between impoundments that had performed satisfactorily and those that had experienced problems. Figure 2-4 presents the results of the work of Conlin (1987) and Lo & Klohn (1995).

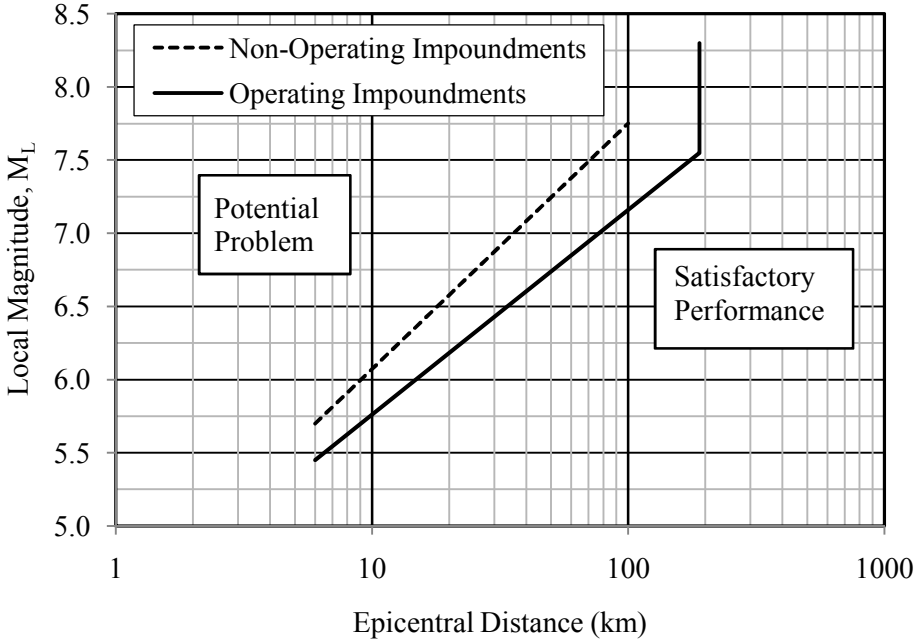

Figure 2-4 – Empirical relationship between earthquake magnitude and epicentral distance for tailings impoundments based on seismic performance (adapted from Conlin, 1987 & Lo & Klohn, 1995).

The figure indicates an exponential relationship between the earthquake magnitude and epicentral distance as they are related to the potential for problems with respect to tailings impoundments and that the stability of impoundments increases significantly after closure. The earthquake magnitude causing a potential stability problem increased with the epicentral distance.

2.2 LIQUEFACTION

2.2.1 An Overview

It has long been recognized that local subsurface conditions significantly influence the effects of earthquakes on the ground surface and on structures. On June 16, 1819, an earthquake with an estimated moment magnitude of 7.7 struck northwest India, in the region between Karachi and Bombay. In the aftermath of the earthquake, James MacMurdo, a British representative in the region, took note of the effects of the earthquake in numerous dispatches and personal papers. MacMurdo's writings contain some of the earliest known realization of the influence of subsurface conditions on the effects of earthquakes (Seed & Idriss, 1982; Bilham 2003). His descriptions of water and sand being ejected from the ground and of ground subsidence are the earliest known accounts of a phenomenon now recognized as liquefaction.

Terzaghi and Peck (1948) used the term "spontaneous liquefaction" in their landmark text *Soil Mechanics in Engineering Practice*. In this text "spontaneous liquefaction" referred to the sudden change of a loose deposit of sand upon disturbance into a material capable of fluid-like flow (Terzaghi and Peck, 1967; Ishihara, 1993). The term "liquefaction" was also used by Mogami and Kubo (1953) in a paper titled "The Behavior of Sand During Vibration" which was presented at the Third International Conference on Soil Mechanics and Foundation Engineering in Zurich (Kramer, 1996). Despite these observations, very little research was conducted on liquefaction per se until 1964.

On March 28, 1964, a magnitude 9.2 earthquake struck the region of Anchorage, Alaska causing extensive damage, a considerable amount of which was due to liquefaction, including the massive Turnagain Heights landslide (Seed & Idriss, 1982). Less than 3 months later, on June 16, 1964, a magnitude 7.5 earthquake resulted in widespread liquefaction which caused significant damage in the region of Niigata, Japan (Seed & Idriss, 1982). These events provided a considerable amount of data on liquefaction and led to extensive research of the phenomenon (Seed & Idriss, 1982; Ishihara, 1993; Kramer, 1996).

Over the last 40 years, hundreds of researchers have investigated the phenomenon known as liquefaction - its causes, mechanisms, and effects, as well as methods of prevention or of limiting its effects. To this date, the definitions of liquefaction and of a related phenomenon, cyclic mobility, vary widely, and no consistent set of definitions has been established throughout engineering practice and research.

In general, liquefaction can be defined as:

- The generation of excess porewater pressure within saturated, contractive, cohesionless soil due to static or dynamic loading, sufficient to bring the soil to the steady state condition or a condition of zero (or very low) effective stress that could result in excessive deformation under gravity or external loading.

This definition of liquefaction encompasses most existing definitions of liquefaction including those of Holtz & Kovacs (1981), Seed & Idriss (1982), and Youd et al. (2001). It is also comparable to what Kramer (1996) refers to as “flow liquefaction.”

Cyclic mobility can be defined as:

- The generation of excess porewater pressure and limited deformation within a saturated, dilative, cohesionless soil caused by dynamic loading.

The term "soil" is used in this thesis in a general manner that includes naturally occurring deposits as well as similar particulate media such as artificial fills and tailings.

The primary differences between liquefaction and cyclic mobility are that liquefaction is associated with the steady state condition and can result in excessive deformation, while cyclic mobility is not associated with the steady state condition and deformation is severely restricted by the dilative nature of the soil. The steady state (or critical state) condition is described in Appendix A.

In geotechnical engineering practice liquefaction and cyclic mobility are usually collectively referred to as "liquefaction." The reason for this is that they can have similar causes and can produce similar effects at the ground surface, particularly deformation and sand boils. Sand boils are mounds of sand transported and deposited by water ejected from the subsurface as excess porewater pressures generated during dynamic loading are relieved at the ground surface.

2.2.2 The Mechanics of Liquefaction

2.2.2.1 Porewater Pressure Generation

The behavior of cohesionless soils, such as sand or hard rock tailings, is significantly influenced by the "state" of the material with respect to a steady state condition which is unique for each material at a given void ratio (or effective confining stress). The state of a material indicates its tendency to contract or dilate upon loading. This tendency directly effects the generation of excess porewater pressure and the stress path of the material in response to loading. Discussions of volumetric behavior and steady state concepts are presented in Appendix A.

Under undrained, deviatoric, monotonic loading, contractive (loose) soils generate positive porewater pressure changes, decreasing the effective stress at constant volume until the steady state condition is reached. Under undrained, deviatoric, monotonic loading, dilative (dense) soils generate negative porewater pressure changes, increasing the effective stress at constant volume until the steady state condition is reached (Holtz & Kovacs, 1981).

Under the action of undrained, cyclic loading, both contractive and dilative materials can generate positive porewater pressure changes (Castro, 1975; Holtz & Kovacs, 1981).

Typical cyclic triaxial compression test results for a contractive sand (relative density, D_r, of 38%, isotropic effective confining stress, σ_3, of 100 kPa, and cyclic deviatoric stress, $\Delta\sigma$, of 39 kPa) are shown on Figure 2-5; (a) presents the number of load cycles versus the axial strain and (b) presents the number of cycles versus the change in porewater pressure, Δu. Note the cyclic, but ever increasing, trend in the porewater pressure in response to the cyclic loading and that at the 10^{th} cycle, Δu reaches a maximum value corresponding to the initial effective confining pressure. Also note that the axial strain of the material is minimal until the 10 cycle where it dramatically increases to over 20%. The cyclic loading led to a transient condition where the effective stress within the sample was completely negated. Referring to the steady state concepts discussed in Appendix A, the sample had to have passed through the steady state condition to reach the condition of zero effective stress (Δu=100 kPa).

Typical cyclic triaxial compression test results for a dilative sand (relative density of 78%, isotropic effective confining stress, σ_3, of 100 kPa, and cyclic deviatoric stress, $\Delta\sigma$, of 70 kPa) are shown on Figure 2-6; (a) presents the number of cycles versus the axial strain and (b) presents the number of cycles versus the change in porewater pressure, Δu. Similarly to the loose sample, the porewater pressure increased cyclically in response to the loading and at the 13^{th} cycle, Δu reached a maximum value corresponding to the

initial effective confining pressure. The axial strain of the material was minimal until the 10th cycle and then gradually increased to about 10% at the 40^{th} cycle. The cyclic loading led to a transient condition where the effective stress within the sample was completely negated. Referring to the steady state concepts discussed in Appendix A, the sample did not pass through the steady state condition to reach the condition of zero effective stress (Δu=100 kPa). Note that a greater deviatoric load (about twice as much) was applied to the dilative sample to get a porewater pressure response similar to that of the contractive sample.

The primary difference in the behavior of the contractive and dilative samples was that as the contractive sample approached zero effective stress, the axial strain increased dramatically, while those of the dilative sample increased more gradually, despite the samples having similar porewater pressure responses.

Figure 2-7 is schematic example of a steady state line (see Appendix A) and the behavior of contractive and dilative cohesionless soils under undrained monotonic and cyclic loadings. Under monotonic loading, the state of a contractive material at an initial effective stress, σ', and void ratio, e, represented by "A" moves towards "B" on the steady state line. The sample then transforms to the steady state at "B" and undergoes excessive deformation at constant stress and volume. If loaded cyclically, the material may move beyond "B" to "C", a state of zero effective stress, for transient periods and will undergo excessive deformation at constant volume.

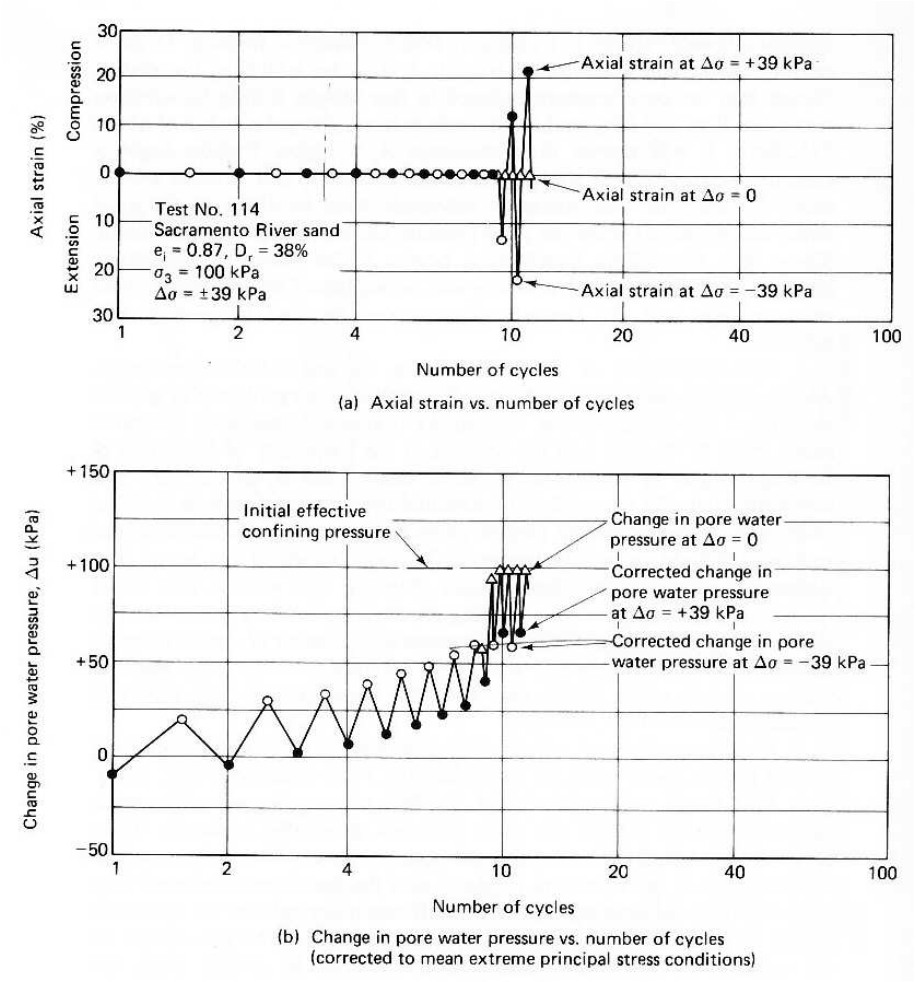

Figure 2-5 - Typical cyclic triaxial compression test results on a sample of contractive sand (from Holtz & Kovacs, 1981).

On Figure 2-7 the initial state of a dilative material is labeled “D”. Under monotonic loading the material experiences a decrease in porewater pressure (an increase in effective stress) until the steady state condition, “E”, is reached and the material undergoes excessive deformation at constant stress and volume. Under cyclic loading, the dilative material experiences an increase in porewater pressure, decreasing the effective

stress, leading towards “F”, where the material may experience transient moments of zero effective stress, but will not transit or approach the steady state and will not undergo excessive deformation.

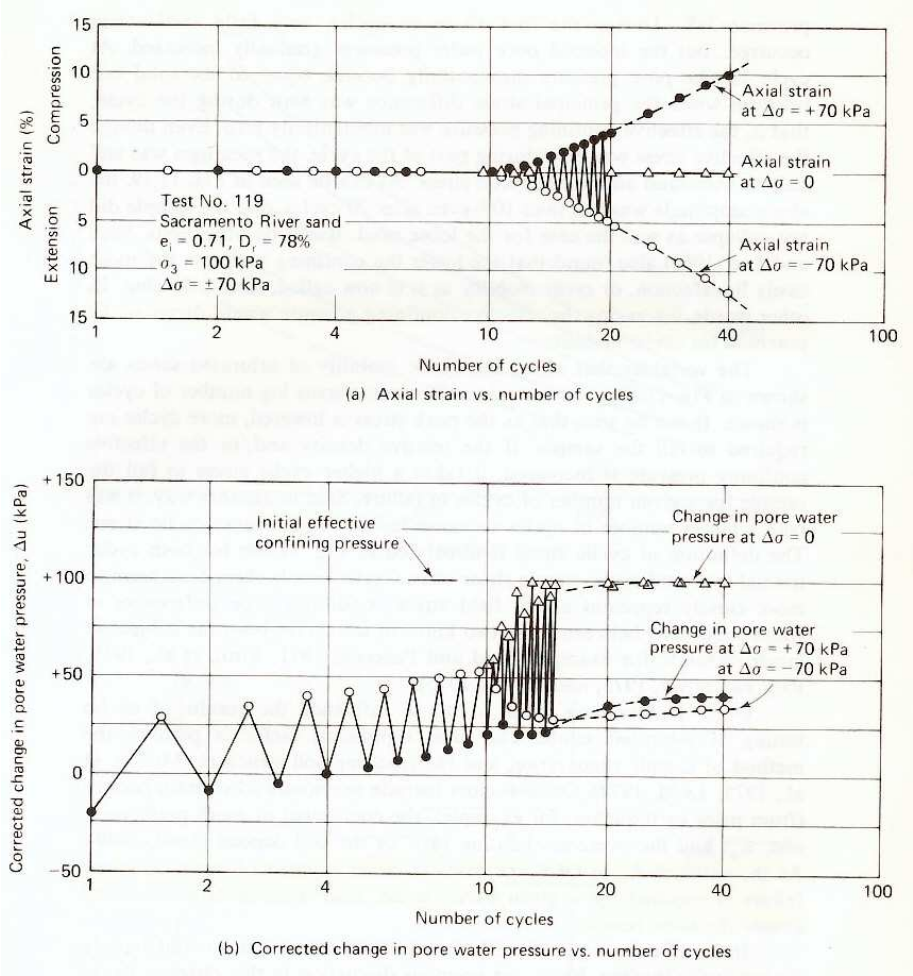

Figure 2-6 - Typical cyclic triaxial compression test results on a sample of dilative sand (from Holtz & Kovacs, 1981).

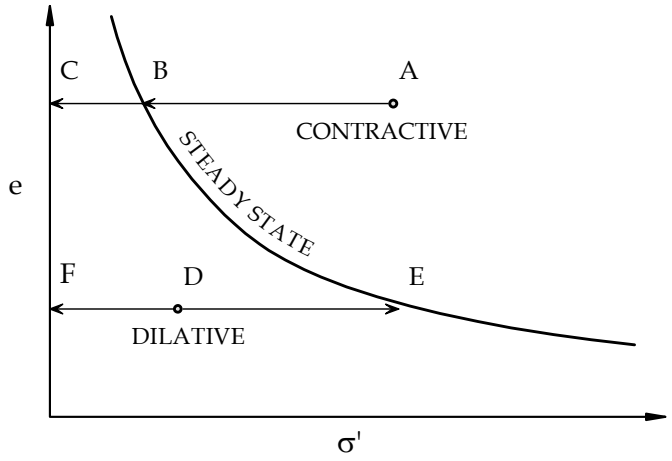

Note: Under static loads the contractive soil moves from (A) towards (B); under cyclic loads it may move as far as (C), zero effective stress. Under static loads the dilative soil moves from (D) towards (E); under cyclic loads it moves from (D) towards (F), zero effective stress.

Figure 2-7 - Undrained behavior of contractive (loose) soil and dilative (dense) soil (adapted from Kramer, 1996).

The mechanism responsible for the generation of additional positive porewater pressure during cyclic loading in contractive soils is well understood and has been elaborated by Seed & Idriss (1982) and Mitchell & Soga (2005) as follows. A schematic compression curve with rebound for sand is presented on Figure 2-8. Point (A) on the figure represents the initial condition of an element of soil which is subjected to the first impulse of a cyclic load under drained or undrained conditions. In response to this impulse, the soil element, if drained, would tend towards point (B) at a lower void ratio and higher effective stress than point (A) and the change in void ratio would be Δe_{rd}. However, since no drainage can take place, the tendency to contract towards point (B) instead results in the generation of additional positive pore pressure, Δu. It has been theorized and

experimentally verified, that the magnitude of the additional positive pore pressure is dependent on the slope of the rebound curve and the expected change in void ratio under drained conditions. Point (C) represents the state of the soil after the generation of the additional porewater pressure, where the void ratio is constant and a line through (B) and (C) is parallel to the rebound curve.

Martin et al. (1975) provide the following formula for the determination of the induced porewater pressure, Δu:

$$\Delta u = \overline{E}_r \cdot \Delta \varepsilon_{rd} \tag{2-1}$$

where:

$\overline{E}_r$ is the rebound modulus determined from laboratory testing; and

$\Delta\varepsilon_{rd}$ is the volumetric strain under drained conditions and can be measured from laboratory testing.

The mechanisms that result in the generation of positive additional excess porewater pressure in dilative soils under cyclic loading are not well understood. Mitchell and Soga (2005) theorize that the development of positive additional porewater pressure in dilative soil under cyclic loading is due to breakdown of the soil structure caused by cyclic strains and that this breakdown leads to contractive behavior in otherwise dilative soils. However, observations of the cyclic triaxial test results shown on Figures 2.5 and 2.6 indicate that the porewater pressure responses of contractive and dilative soils are similar; there seems to be no dilative reaction on the part of the dilative sample. Dilative cohesionless soils develop excess porewater pressures in response to dynamic loading, apparently due to a tendency for all cohesionless soils, contractive and dilative, to contract under dynamic loads.

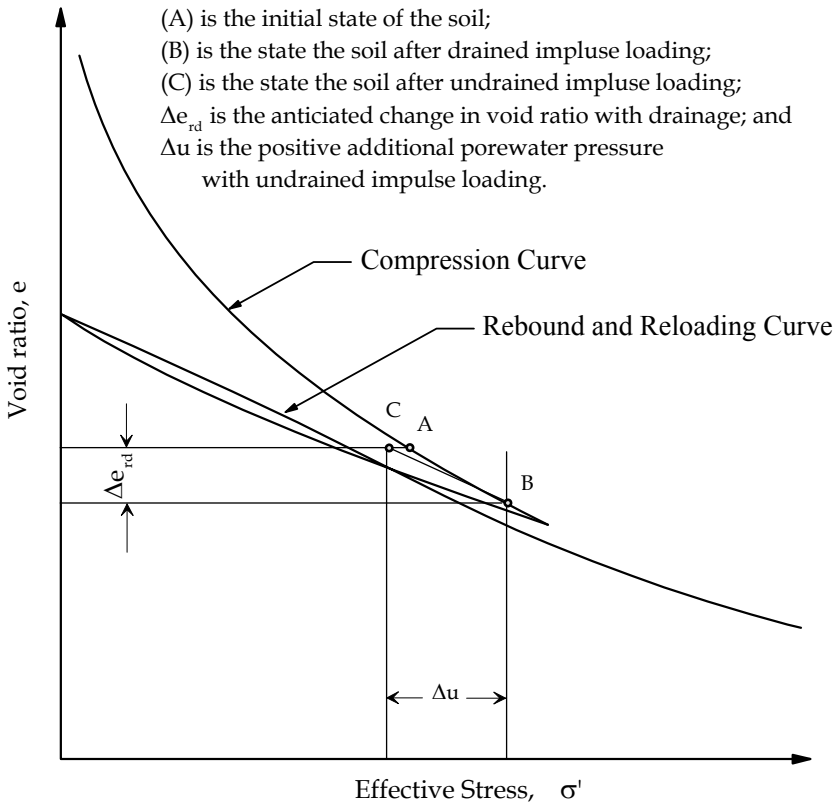

Figure 2-8 – Schematic compression curve of sand to illustrate the mechanism of porewater pressure generation in contractive soils during cyclic loading (modified from Seed & Idriss, 1982).

There is a threshold level of cycling loading necessary to initiate the generation of the excess porewater pressure in cohesionless soil. Through laboratory testing on a variety of types of sand it has been shown that the value of the threshold loading is the loading required to produce shear strains of approximately 0.01 percent (NRC, 1985).

2.2.2.2 The Initiation of Liquefaction

Figure 2-9 presents data from undrained, monotonic loading of a typical specimen of contractive sand. The stress-strain curve (a) shows the characteristic peak stress at relatively low strain (point B) followed by a decline to the steady state condition (point C) where the sand deforms excessively at constant effective stress and constant volume. At point B the excess porewater pressure ratio, $r_u = \Delta u/\sigma'_{3c}$, is well below 1.0. However, at this point the structure of the soil is unstable and the shear stress cannot be maintained. Between points B and C, the structure of the soil rearranges to the most deformable configuration possible and the excess porewater pressure increases resulting in corresponding decreases in the effective stress until the steady state condition is attained, as shown on the steady state diagram (d). At point C, the soil is in a condition of liquefaction as described earlier. At point B on the figure, the rearrangement of the soil structure becomes irreversible. Point B is considered the initiation of liquefaction (Kramer, 1996).

The steady state point for a cohesionless soil at a given void ratio and confining stress is a unique point regardless of the initial state of stress of the soil (Been et al., 1991). On Figure 2-10 the effective stress paths for five samples of a cohesionless soil at the same void ratio but at different confining stresses under monotonic loading are shown. The paths of all five samples, two of which were dilative (A and B) and three of which were contractive (C, D and E), all meet at the steady state point on a "p'-q" diagram. A p'-q diagram is a commonly used method of representing the stress path of a soil element, where p' is the average of the major and minor principal effective stresses, $p'=0.5\cdot(\sigma'_1+\sigma'_3)$, and q is the shear stress, $q= 0.5\cdot(\sigma'_1-\sigma'_3)$, (Holtz & Kovacs, 1981).

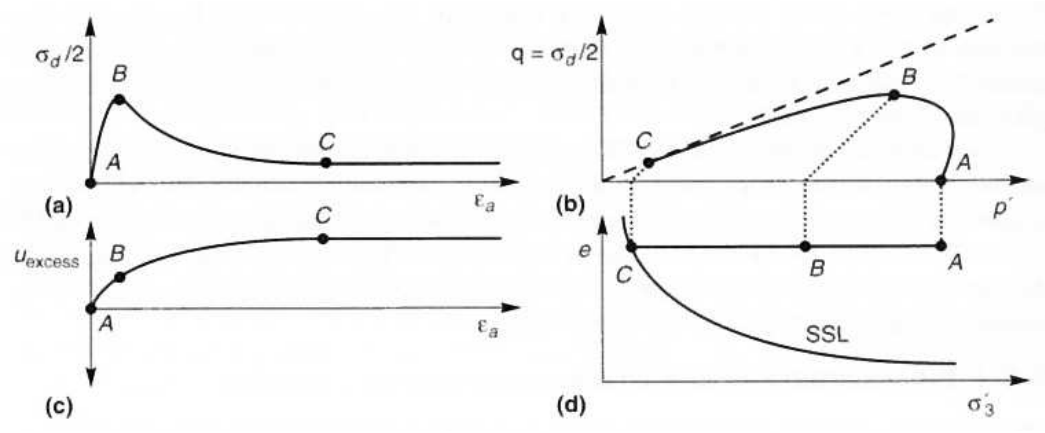

Figure 2-9 - Response of a contractive sand to undrained, monotonic triaxial testing: (a) stress-strain curve[1]; (b) effective stress path; (c) excess porewater pressure[2]; and (d) steady state diagram (from Kramer, 1996).

[1] σ_d is the deviatoric stress (σ_1-σ_3).

[2] U_{excess} is the change in porewater pressure, Δu.

The angle ψ' defines the line from the origin through the steady state point. In stress path space, this line represents a limiting state of stress (or ultimate failure surface) of the soil.

For the contractive soils, the locus of points defining the initiation of liquefaction on the stress paths (marked with 'x'es on Figure 2-10 and analogous to point (B) on Figure 2-9) forms a straight line through the origin which is defined by an angle ψ_L (see Figure 2-11). This line defines the initiation of liquefaction according to Kramer (1996).

Projecting a line horizontally from the steady state point to the line defining the initiation of liquefaction forms a surface called the flow liquefaction surface, as shown on Figure 2-11. Theoretically, the stress path of an undrained element of soil reaching the flow liquefaction surface (FLS) would automatically migrate to the steady state point via porewater pressure generation and changes in the soil structure at constant volume. On

Figure 2-10 the contractive samples (C, D and E) become irreversibly unstable once their stress paths reach the FLS. The dilative samples reached the steady state point via stress paths that remained stable until the steady state point was reached. In monotonic loading, this is a fundamental difference between dilative and contractive behavior.

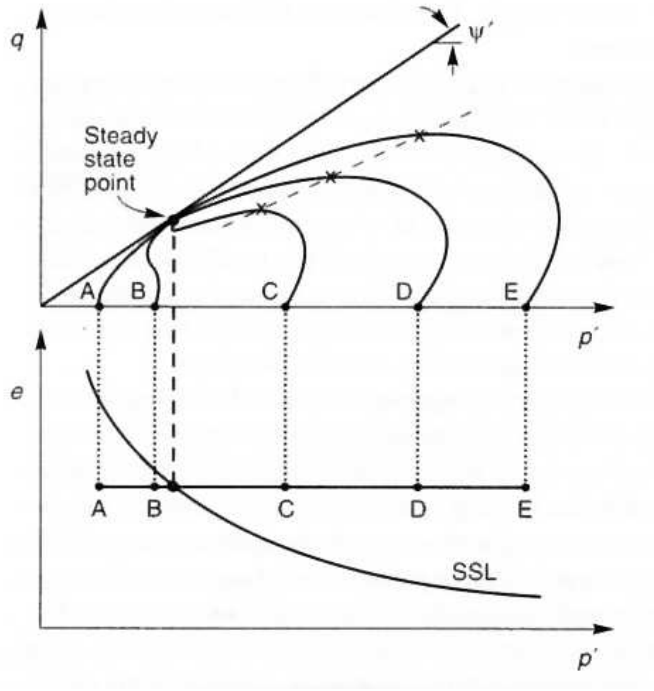

Figure 2-10 - Response of sand samples at the same void ratio and different confining stresses to undrained monotonic triaxial testing in compression (from Kramer, 1996).

The loading which causes an undrained element of contractive soil to reach the flow liquefaction surface and hence the steady state point can be either monotonic or cyclic. The responses of such a soil element subjected to monotonic and cyclic loads are shown on Figure 2-12.

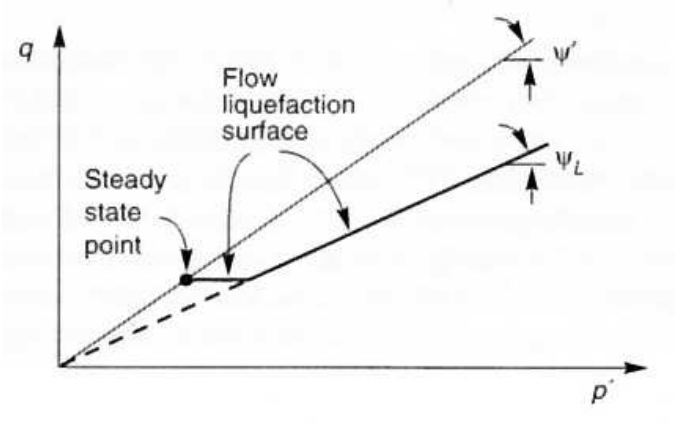

Figure 2-11 - The flow liquefaction surface (FLS) in p'-q space (from Kramer, 1996).

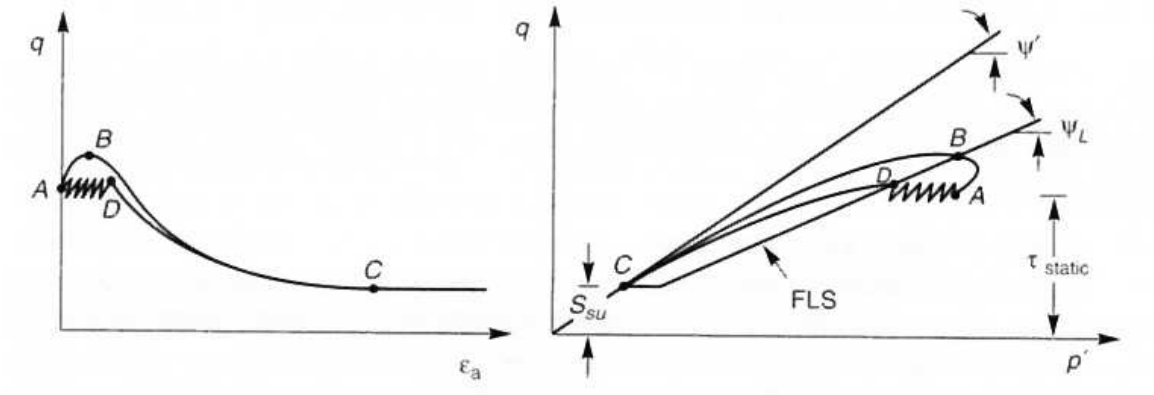

Note: S_{SU} represents the steady state shear strength of the soil.

Figure 2-12 - Stress-strain and stress path responses of an undrained, contractive soil element to monotonic and cyclic loads (from Kramer, 1996).

Point A on Figure 2-12 represents an undrained contractive soil element in a state of static equilibrium. The path A-B represents the effect of monotonic loading sufficient to bring the soil element to the flow liquefaction surface and the path A-D represents the effect of cyclic loading sufficient to bring the soil element to the flow liquefaction surface. From points B and D the state of the soil element migrates to the steady state point where excessive deformation can occur without additional loading (Kramer, 1996). If cyclic loading continues after the soil element is in the steady state condition, additional porewater pressures can continue to develop until the effective confining stress within the soil element is completely nullified for transient periods.

2.2.3 Causes of Liquefaction

Earthquakes are by far the primary causes of liquefaction. Other causes of liquefaction include dynamic loads, such as vibrations from pile driving, railroad and truck traffic, and blasting. However, dynamic loads generated by sources besides earthquakes are very unlikely to cause widespread liquefaction of a tailings impoundment due to the limited area in which their effects are significant (Jedele, 2005).

Liquefaction may also be induced by static loads, such as foundation movement, river bank erosion, and slope excavation (Holtz & Kovacs, 1981).

Although earthquake ground motions consist of a variety of wave motions (p-waves, s-waves, Rayleigh waves, and Love waves), the shear stresses induced by ground motion are due primarily to the upward propagation of horizontal shear waves (s-waves) through the ground (Seed & Idriss, 1982; Kramer, 1996). As shown on Figure 2-13, these shear waves generate cyclic shear stresses in soil elements. In both contractive and dilative soils, these shear stresses will result in the generation of excess porewater pressures which may cause liquefaction (or cyclic mobility). The vertical component of the ground motion is dominated by P-waves (compression waves) that do not cause significant

changes in the effective stress or porewater pressures as they transit soil deposits (Seed & Idriss, 1982; Kramer, 1996; Kayen & Mitchell, 1997).

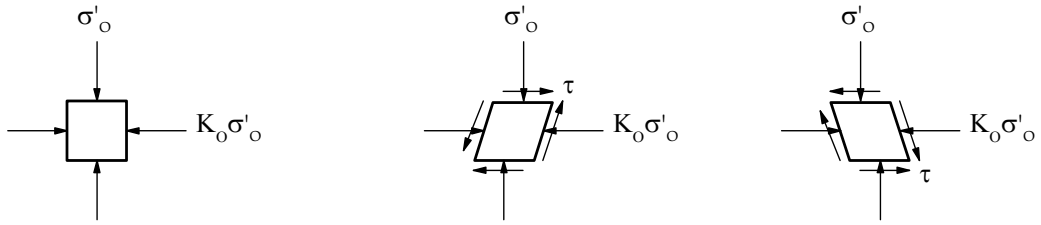

a) INIITIAL STRESSES b) ALTERNATING CYCLIC SHEAR STRESSES

Figure 2-13 - Idealized earthquake loading conditions (from Seed & Idriss, 1982).

The parameters generally used to characterize the dynamic loading of an earthquake are the intensity and frequency characteristics. The intensity is inferred from the magnitude and the peak horizontal ground acceleration (PGA or PHA). The magnitude of an earthquake is a function of the energy released by the fault movement/rupture, while the PGA is the maximum horizontal acceleration measured on a ground motion record and is usually measured on rock. Earthquake ground motions are altered by the dynamic response of the Earth's crust as they travel from the source zone to a specific site. Most importantly the ground motion attenuates with distance from the source zone, leading to a decrease in the PGA. The frequency characteristics of the ground motion can also be significantly influenced by regional bedrock conditions; for example, the harder crystalline bedrock of central and eastern North American generally produce earthquakes of higher intensity and frequency than the softer, sedimentary bedrock of western North America for similar magnitude events (Arango, 1994; Kramer, 1996; Bolt 2004).

There is significant interaction between the frequency characteristics of an earthquake and local subsurface conditions. The frequency characteristics of the ground motion at bedrock influence the response of the overburden, while the response of the overburden influences the frequency characteristics of the ground motion as it approaches the ground surface (Seed & Idriss, 1982; Kramer, 1996; Finn & Wightman 2003).

With respect to liquefaction, the magnitude, peak ground acceleration and frequency characteristics of an earthquake typically have the following effects (Seed & Idriss, 1982):

- The duration of the earthquake, and thus the number of significant cycles of shear stress imposed on a site, generally increases with the magnitude;
- The magnitude of the shear stresses imposed on a site increases with the peak ground acceleration;
- The frequency characteristics of the ground motion influence the response of the site; and
- Generally, amplification of the ground motion increases with softer/looser soils.

Riemer et al. (1994) used stress and strain-controlled cyclic triaxial testing to study the effect of frequency on the liquefaction resistance of fine-grained sand. The samples were prepared by moist tamping to relative densities of 40, 50 and 60%, isotropically consolidated to 100 kPa, and saturated using the backpressure method. In the stress-controlled tests, the CSR varied from 0.21 to 0.35 and in strain-controlled tests, the shear strain varied from 0.0008 to 0.0026. For both types of tests, the loading frequencies were 0.1, 1, 10 and 20 Hz. The study concluded “that within the range of predominant frequencies commonly observed in earthquakes, the specific frequency of loading will

not substantially alter the number of significant cycles required to reach liquefaction of clean sand." Thus, it can be assumed from this study that the liquefaction resistance of a soil is not affected by the frequency of the loading.

The topography of a site also affects the ground motion. Topographic projections, such as ridges, mountains and dams, amplify ground motions while valleys can amplify or dampen ground motions (Kramer, 1996; Bourdeau, 2006; Sigaran-Loria & Hack, 2006; Psarropoulos et al., 2007).

Earthquakes with moment magnitudes as low as 5 have produced liquefaction at sites in proximity to the zone of rupture (Kramer, 1996). Large magnitude earthquakes producing maximum horizontal ground accelerations (PGA) as low as 0.05g may be capable of inducing liquefaction in very loose, cohesionless soil (Carter & Seed, 1985). Typically, a PGA of at least 0.10g is required to induce liquefaction, except in highly susceptible soils subject to large magnitude earthquakes (NRC, 1985).

A more comprehensive, but rarely used measure of the potential for an earthquake to induce liquefaction is the Arias Intensity method (Kayen & Mitchell, 1997). The Arias intensity is a qualitative measure of the energy content of a given ground motion record and represents the energy per unit weight absorbed by a soil element represented by a set of simple oscillators. Since the Arias intensity is not significantly affected by damping within intact (non-liquefied) soil deposits and scalar energy measures are additive, the Arias intensity, I_h, can be calculated from the two horizontal components of a ground motion record, a_x and a_y, using:

$$I_h = I_{xx} + I_{yy} = \frac{\pi}{2g}\int a_x^{\,2}(t)dt + \frac{\pi}{2g}\int a_y^{\,2}(t)dt \qquad (2\text{-}2)$$

where:

I_{xx} and I_{yy} are horizontal, orthogonal components of the Arias intensity, I_h;

$a_x(t)$ and $a_y(t)$ are the horizontal components of acceleration in the x and y directions at a given time;

g is the acceleration due to gravity; and

t is time.

The disadvantage of the magnitude-PGA method of characterizing the intensity or energy of an earthquake is that the PGA is a single point on a ground motion that is somewhat random in nature and is often not representative of the energy content of the ground motion. The Arias intensity method provides a direct measure of the energy content of a ground motion. However, the magnitude-PGA method has become standard worldwide and is widely used in evaluating the potential for liquefaction (Seed & Idriss, 1982; Kayen & Mitchell, 1997).

2.2.4 Factors Influencing the Liquefaction Resistance of Soils

There are many environmental and physical factors that affect the liquefaction resistance of soil to a greater or lesser extent. These factors include the relative density, state of stress, state with respect to the steady state condition as expressed by the state parameter, ψ (see Appendix A), degree of saturation, grain size distribution, plasticity (as measured by the plasticity index, PI), shape of the grains, fines content (where fines are material passing a 0.075 mm sieve), soil structure, layering and anisotropy, age of the deposit, cementation, and loading history. The saturated hydraulic conductivity, k_{sat}, may also influence the liquefaction resistance of soil, depending on the drainage conditions.

Relative Density - Generally, the liquefaction resistance of a soil increases with increasing relative density because the loading (amplitude or number of cycles) required to generate a given amount of excess porewater pressure increases with increasing

relative density. However, as the relative density of a contractive (loose) soil approaches the steady state condition, less excess porewater pressure is required to initiate liquefaction although an increased loading is required to generate an incremental increase in the porewater pressure.

State of Stress - The state of stress can be considered in two ways: the effective confining stress and the static deviatoric shear stress.

The liquefaction resistance of soil increases considerably at effective vertical confining stresses over 100 kPa (Hynes & Olsen, 1999; Youd et al., 2001). Based on the results of dynamic centrifuge testing, Steedman et al. (2000) indicate that there is an upper bound effective confining stress above which liquefaction may not occur, about 300 kPa, due to the limitation of the excess porewater pressure to a value less than the effective confining stress. However, additional centrifuge testing by Gonzalez et al. (2002) found that liquefaction can occur at effective confining stresses in excess of 300 kPa. The differences in the test results were attributed to the differences in the testing equipment, fluid properties, saturation, and particularly stress densification (Byrne et al., 2004). Numerical modeling by Byrne et al. (2004) for comparison with the testing by Gonzalez et al. (2002) confirmed that stress densification increases the liquefaction resistance of sand at high effective confining stresses. In the field, ground surface observations of liquefaction to-date have been limited to depths of about 15 m as liquefaction at greater depths is unlikely to produce evidence at the ground surface. Conventional liquefaction evaluation methods typically assume that liquefaction can occur to depths of 50 m (NRC, 1985; Byrne et al., 2004).

Vaid et al. (1985) used cyclic simple shear testing to investigate the effects of confining pressure and angularity on the liquefaction resistance of an angular tailings sand and a rounded naturally-occurring sand of similar gradation. Testing was conducted at effective confining stresses varying from 200 to 2500 kPa and at relative densities ranging from 40

to 90%. The cyclic resistance of both types of samples increased rapidly with increasing relative density up to a confining stress of about 800 kPa. Beyond this stress level, the liquefaction resistance of the rounded sand increased rapidly while that of the angular tailings increased at a lower rate. At relative densities below 50 to 55%, the liquefaction resistance of both types of samples was equivalent. However, at higher relative densities, liquefaction resistance of the rounded sand tended to be slightly higher than that of the angular tailings. This implies that the effect of confining stress on the liquefaction resistance may not be significant below relative densities of 50 to 55%.

The presence of static deviatoric shear stresses, such as those under embankments, also affects the liquefaction resistance. The liquefaction resistance of dilative soils increases with static shear stresses while that of contractive soils decreases with static shear stresses (Harder & Boulanger, 1997). Based on the research of Vaid et al. (2001), it is theorized that the effect of static deviatoric shear stresses during cyclic loading is to facilitate shear stress reversals in contractive materials and inhibit shear stress reversals in dilative soils. Shear stress reversals during cyclic loading are necessary if transient periods of zero effective stress are to occur (Vaid et al., 2001).

State Parameter - The state of a soil, in terms of its position relative to the steady state line on a graph of void ratio versus effective confining stress, is a significant factor in its liquefaction resistance. For contractive soils, the amount of excess porewater pressure required to advance a soil element to the liquefaction flow surface (the initiation of liquefaction) is directly related to the state parameter, ψ , of the material, defined as the void ratio minus the critical state void ratio at a given effective stress. Thus, positive state parameters indicate contractive conditions, negative state parameters indicate dilative conditions and the value of the state parameter approaches zero as the material approaches the steady state. For contractive materials the magnitude of the state parameter, ψ, is an issue because low values indicate proximity to the steady state so that

relatively small changes in the porewater pressure can initiate liquefaction. Generally, for dilative soils the proximity to the steady state condition is not important since changes in porewater pressures result in stress paths leading away from the steady state condition.

Degree of Saturation - Soils do not need to be fully saturated to be susceptible to liquefaction. However, the degree of saturation has a significant impact on the liquefaction resistance. Research by Xia & Hu (1991) indicates that a reduction in the degree of saturation from 100.0% to 99.5% resulted in a significant increase in the liquefaction resistance during cyclic triaxial testing of sand. In their research the liquefaction resistance increased by 15 to 20 percent with this very slight decrease in saturation. The increase in liquefaction resistance may be due to an increase in suction with a decrease in the degree of saturation. The findings of Bouferra et al. (2007) are in agreement with those of Xi & Hu (1991).

A number of other researchers have studied the effect of saturation on the liquefaction resistance of soils, including, Sherif et al. (1977), Chaney (1978), Yoshimi et al. (1989), and Ishihara et al. (2001). Yang et al. (2004) analyzed the data from these researchers and found that there was a very significant increase in the liquefaction resistance of soil with decreasing saturation as measured by Skempton's B-value. The relationships between the liquefaction resistance and the B-value varied with the type of sand. Yang et al. (2004) developed an equation to correlate the liquefaction resistance of partially saturated soil to that of saturated soil based on the measured velocities of shear waves and compression waves in the soil. The shear wave velocity correlates to the liquefaction resistance of the soil and the compression wave velocity correlates to the degree of saturation.

Plasticity - Research on the effect of the plasticity, as measured by the plasticity index, PI, on the liquefaction resistance has produced seemingly inconclusive results. However, it is known that soils of moderate to high plasticity are not subject liquefaction (Kramer, 1996; Perlea, 2000). From testing of silts of very low plasticity ($PI \leq 3.4$), Prakash &

Sandoval (1992) concluded that the liquefaction resistance decreased with increasing plasticity. Guo & Prakash (1999) tested samples of silts and silt/clay mixes and determined that at plasticity indices between 10 and 15, the liquefaction resistance increased with plasticity. Research by Koester (1994) indicates that at similar void ratios, the plasticity index of the fine fraction of a sandy soil had less of an effect on the cyclic resistance than the size of the fine fraction.

Grain Size Distribution - The effect of the grain size distribution is significant. Well-graded (poorly sorted) soils are more resistant to liquefaction than poorly-graded (well sorted) soils, because well-graded soils are more likely to form stable structures during deposition with the smaller grains occupying spaces between larger grains. Also the development of shear zones in well-graded soils tends to require dilation rather than contraction (Terzaghi et al. 1996). Vaid et al. (1990) conducted cyclic simple shear tests on samples of three sands with subangular particles, identical D_{50} values, linear grain-size distribution curves, and the same mineralogy. The sands had different gradations with coefficient of curvature, C_u, values of 1.5, 3 and 6. At low relative densities ($D_r < 45\%$), the poorly-graded samples had lower liquefaction resistance and were more contractive than the other two types of samples. At higher relative densities ($D_r > 60\%$) the well-graded samples appeared to have lower liquefaction resistance than the other types of samples. Additional research is required for a better understanding of the effect of gradation on the liquefaction resistance.

Particle Shape - The effect of the shape of the soil particles is that the more angular particles can form interlocks which require either particle breakage or dilation for shear zones to form (Kokusho & Hara, 2004). This increases the resistance to liquefaction in soils with angular particles as opposed to rounded particles, provided the particles are hard and durable to resist crushing and breaking at low to moderate stresses (Kokusho & Hara, 2004). The research by Vaid et al. (1990), referenced above with respect to state of

stress, also considered the effect of angularity of the grains. It was found that the liquefaction resistance of the angular sand at relatively low effective confining stresses (less than 200 kPa) was greater than that of the rounded sand at the same relative densities. However, at higher confining stresses, the resistance of the angular sand was greater or lesser than that of the rounded sand depending on relative density. Under higher confining stresses (greater than 800 kPa) the angular sand was less resistant to liquefaction than the rounded sand and was susceptible to liquefaction at relative densities in excess of 80%, while the rounded sand was unlikely to liquefy at this level of relative density.

Fines Content - There has been extensive research on the influence of the fines content, specifically nonplastic fines, on the liquefaction resistance of soil. However, this research has produced seemingly contradictory results (Kuerbis et al., 1988; Koester, 1994; Thevanayagam & Mohan, 1998; Thevanayagam, et al. 2000; Naeini & Baziar, 2004; Chien et al., 2002). The apparent reasons for the contradictions are the various benchmarks used to characterize the soil: void ratio, relative density, penetration resistance, and sand skeleton void ratio (Polito & Martin, 2001) and the effect that the fines content has on the steady state relationships of sand (Bouckovalas, et al. 2003). The sand skeleton void ratio is the void ratio of silty sand that neglects the mass of the silt particles. Bouckovalas et al. (2003) found that with increasing percentages of silt the critical state line of sand (plotted as void ratio versus logarithm of effective stress space) rotated clockwise about an effective confining stress of about 60 kPa. This phenomenon, if applicable to silty sands in general, would indicate that the effect of fines on the liquefaction resistance is to some extent dependent on the effective confining stress and void ratio of the soil.

Polito (1999) and Polito & Martin (2001) conducted a series of about 300 undrained, cyclic triaxial tests on samples of two types of sand, sand and nonplastic silt mixtures,

and nonplastic silt and correlated the results based on relative density, void ratio and sand skeleton void ratio. The sand used in the testing consisted of "Monterey No. 0/30" sand with subrounded to subangular particles, over 98% retained between 0.15 and 0.84 mm sieves, and a D_{50} value of 0.43 mm, and "Yatesville" sand with subrounded to subangular particles, 99% retained between 0.15 and 0.84 mm sieves, and a D_{50} value of 0.18 mm.

Polito (1999) found that for different types of sand, there are critical silt contents where the behavior of the sand changes from being dominated by sand-to-sand particle interaction to being dominated by silt-to-silt particle interaction and that the behavior of soil in monotonic and cycling loading changed dramatically when this threshold was exceeded. In general the limiting value of silt content was 25% to 50%, but in about 20% of the samples tested the limiting value was over 50%.

Polito & Martin (2001) found that there was no apparent relationship between the void ratio and the liquefaction resistance for sand-silt mixtures with void ratios ranging from 0.4 to 0.9. However, the liquefaction resistance at a given void ratio was found to decrease with increasing silt content to a minimum value, hold relatively steady, then increase as the silt content approached 100%.

The liquefaction resistance of sand-silt mixtures was relatively constant for a given sand skeleton void ratio (at values from 0.65 to 2.1), regardless of silt content, for both types of sand tested. Below the limiting silt content, the liquefaction resistance decreased with increasing sand skeleton void ratio, while above this limit the liquefaction resistance was relatively constant and not significantly affected by silt content (Polito & Martin, 2001).

Polito & Martin (2001) indicate that the liquefaction resistance of sand-silt mixtures increased linearly with increasing relative density below the limiting silt content. The liquefaction resistance above the limiting silt content was significantly lower than that

below the limit. However, it increased with relative density, albeit at a lower rate than below the limit.

The testing by Polito & Martin (2001) included a series of tests done on moist-tamped samples with various proportions of sand and silt at a relative density of 30%. These resulted in a relatively constant liquefaction resistance of approximately 0.23. The liquefaction resistance was measured by the cyclic resistance (cyclic resistance ratio, CRR) as defined in Section 2.3.1.2 of this report. Above the critical silt content the liquefaction resistance fell by about 55% and remained relatively constant up to 100% silt. This series of tests is illustrated on Figure 2-14.

A similar series of tests on slurry deposited samples with various proportions of sand and silt at a relative density of 60% resulted in a relatively constant liquefaction resistance of approximately 0.14, as shown on Figure 2-15.

Undrained, cyclic triaxial testing by Naeini & Baziar (2004) on 12 samples of sand and nonplastic silty sand (D_{50} values from 0.08 to 0.19 mm) with void ratios varying from 0.7 to 1.0 provided results that are in good agreement with the results of Polito & Martin (2001).

Soil Structure - Studies on the influence of the soil structure (soil fabric) show that the method of deposition of natural soils and the method of preparation of laboratory samples both have a significant impact on the liquefaction resistance due to the influence of the soil structure on the steady state relationship as some soil structures may be more prone to contraction or dilation than others (Miura & Toki, 1982; Vaid & Sivathalayan, 1999; Thevanayagam et al., 2000). Hydraulically-deposited cohesionless soils are particularly susceptible to liquefaction (Been et al., 1988; McNeilman et al., 1998).

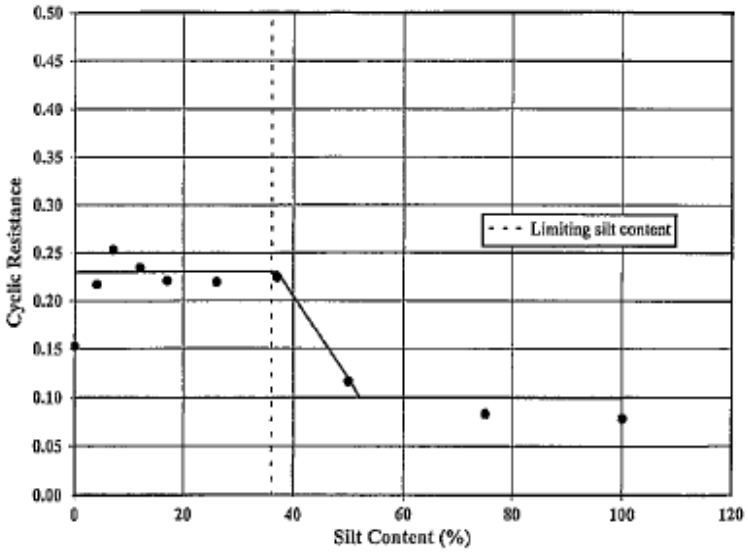

Figure 2-14 – Variation in cyclic resistance with silt content for Yatesville sand specimens prepared by moist tamping to 30% relative density (from Polito & Martin, 2001).

Layering - Some research results on the liquefaction resistance of layers of silt and sand indicate that it is not particularly affected by this type of heterogeneity (Marcuson et al., 1990; Amini & Qi, 2000; Naeini & Baziar, 2004). However, other research (Evans and Zhou 1994; Thevanayagam et al., 2000) suggests that heterogeneity and layering may have a significant impact on the resistance depending on the soil structure. Hence, this aspect requires further study.

A known consequence of horizontal layering of silt and sand, such as occurs in hydraulically placed tailings deposits, is that the horizontal permeability of the deposit is greater than the vertical permeability and that during liquefaction and cyclic mobility, water interlayers can develop at the interface between layers and overlying less

permeable layers (Amini & Qui, 2000; Kokusho & Kojima, 2002; Brennan & Madabhushi, 2005).

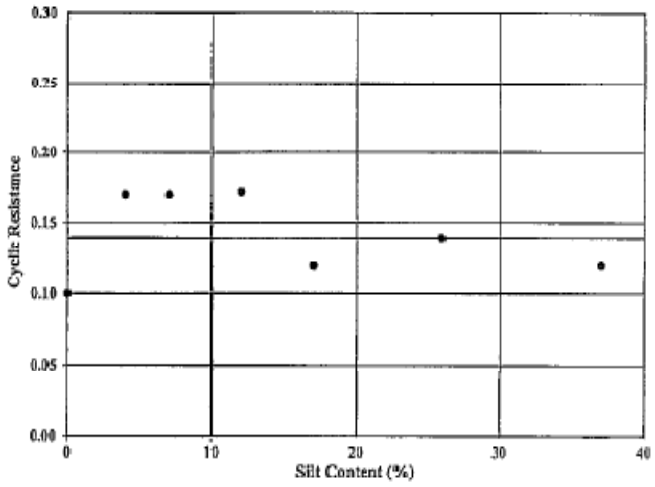

Figure 2-15 – Variation in cyclic resistance with silt content for Yatesville sand specimens prepared by slurry deposition adjusted to 60% relative density (from Polito & Martin 2001).

Amini & Qi (2000) researched the dynamic behavior of stratified silty sands. The research consisted of the undrained, stress-controlled cyclic triaxial testing of 150 samples of homogeneous silt/sand and of stratified silt/sand mixtures at various confining stresses (50 kPa to 250 kPa). The samples were composed of "Ottawa 20-30" sands and 10 to 50 percent low plasticity silt (PI = 3 and LL = 20) by weight. All of the samples were prepared to relative densities between 34 and 44% with void ratios ranging from 0.68 to 0.70. Homogeneous samples were prepared by moist-tamping and stratified samples were prepared by intervals of wet pluviation which allowed the silt/sand mixture to segregate as through sedimentation. The results of the research were:

- There was no significant difference in the liquefaction potential of the stratified samples as compared to the homogeneous samples, despite the different sample preparation methods;
- As the confining pressure increased, the liquefaction resistance of both types of samples decreased; and
- Increasing silt content resulted in increased liquefaction resistance in both types of samples.

Amini & Qi (2000) noted that other research (Fiegel & Kutter, 1992) on the liquefaction of stratified soils found that a water-interlayer of saturated, very loose soil develops at the interface between a sand and overlying silt due to the difference in hydraulic conductivities between the layers. Amini & Qi (2000) also noted that the test results may have been affected by boundary conditions in triaxial testing which are markedly different from what could be expected in the field. The development of a water-interlayer in stratified samples was also identified by Kokusho & Kojima (2002) and Brennan & Madabhushi (2005). Given that the referenced research on the liquefaction of layered soils was conducted using relatively small sample sizes, the sample size may also have significantly affected the results.

The significance of the development of water inter-lenses is that they represent weaker planes that may promote movement or deformation of overlying masses (Seid-Karbasi & Byrne, 2004).

Oka et al. (1981) researched the liquefaction of horizontally layered sand deposits using dynamic numerical analyses and found that the hydraulic conductivity of the layers has a significant impact on the distribution of the excess porewater pressures due to dynamic loading.

Ageing - The liquefaction resistance of soil deposit increases with age (Youd et al., 2001). This has been observed in artificial deposits, e.g. hydraulic fills and tailings (Troncoso & Carcés, 2000) and natural deposits (Leon et al., 2006). The increase in resistance is caused by particle cementation, rearrangement of the particles into denser configuration and interlocking of the particles (Leon et al., 2006).

James et al. (2007) presented corrected standard penetration test data taken over a period of 30 years from two tailings impoundments at a copper mine in the province of Quebec that showed a significant increase in the penetration resistance, and the associated liquefaction resistance of the tailings with time. The increase in the penetration resistance was more pronounced above the groundwater level than below and was attributed to ageing of the tailings as well as cementation, probably due to chemical precipitation, above the groundwater level.

Loading History – Through analytical and laboratory study, Seed et al. (1975) found that sand subject to levels of seismic activity insufficient to cause liquefaction developed an increased resistance to liquefaction due to an increase in the effective lateral pressure or a change in the soil structure with no significant increase in the density.

Ishihara et al. (1978) conducted cyclic triaxial testing on normally consolidated and over-consolidated samples of sand with various fines content. They found that the liquefaction resistance of the overconsolidated samples was significantly higher than that of the normally consolidated samples. However, the magnitude of the increase decreased with increasing fines content. The effect of previous cyclic loading is that the liquefaction resistance of the soil is typically increased due to densification of the soil, although strong seismic loadings can result in uneven densification that results in decreased liquefaction resistance near the ground surface (NRC, 1985).

Saturated Hydraulic Conductivity – The liquefaction resistance is affected by the saturated hydraulic conductivity, k_{sat}, in two primary ways:

a) If the saturated hydraulic conductivity is sufficiently high and the soil drained, liquefaction may not occur because excess porewater pressures will be dissipated as they develop. The relatively high permeability of gravels (typically greater than 0.1 cm/s) is the primary reason that there have been very few instances of the liquefaction of gravelly soils (Wong et al., 1974). The common use of closely-spaced gravel drains in sand deposits to prevent liquefaction is evidence of the significance of drainage and hydraulic conductivity in the occurrence of liquefaction (Ledbetter, 1985; Sonu et al., 1993).

b) As mentioned earlier with regard to the effects of layering, variation of the hydraulic conductivity within a soil mass can have a significant impact on the distribution of excess porewater pressure generation during cyclic loading and cause the development of water inter-layers that may facilitate deformation and failure of the soil mass (Oka et al., 1981; Amini & Qi, 2000; Seid-Karbasi & Byrne, 2004).

Summary - Table 2-1 contains a summary of the general influence of various factors on the liquefaction resistance of soils. There is considerable interaction between the factors that affect the liquefaction resistance and additional research on this interaction is required. Most of the findings discussed above are based on laboratory testing of a particular soil and the findings may or may not be applicable to other types of soil or to field conditions. Therefore, caution should be used in applying these findings.

Table 2-1 – General influence of various factors on the liquefaction resistance.

FACTOR	INFLUENCE ON LIQUEFACTION RESISTANCE
Relative Density, D_r (or I_D) or Void Ratio, e.	The resistance increases with density. Contractive soils may experience liquefaction and possible flow failure while dilative soils may undergo cyclic mobility and limited strains.
Effective Confining Stress	The resistance increases with effective confining stress, particularly at values over 100 kPa.
Static Shear Stress	The presence of static shear stresses decreases the resistance of contractive soils and increases the resistance of dilative soils.
State Parameter, ψ	The resistance of liquefaction of contractive soils decreases with proximity to the steady state line.
Degree of Saturation, S_r	Complete or nearly complete saturation is required for liquefaction. The resistance decreases significantly with slight decreases in saturation below 100%.
Plasticity Index, PI (or I_p)	Generally, the resistance increases with plasticity index of the fine fraction. Moderately to highly plastic soils will not liquefy.
Gradation	Well graded soils are more resistant to liquefaction than poorly graded soils.
Shape of the Grains	Soils consisting of angular grains are more resistant to liquefaction than those consisting of rounded grains at lower confining stresses. At higher confining stresses the resistance of rounded sands is greater than that of angular sands.
Fines Content (<0.075 mm)	The liquefaction resistance is significantly influenced by the fines content. Each soil has a unique limiting silt content value below which the resistance decreases with increasing sand skeleton void ratio and above which the resistance is relatively constant.
Soil Structure	The soil structure has a significant impact on liquefaction resistance with hydraulically deposited soils be more susceptible to liquefaction than other types.
Layering	The effects of layering on the liquefaction resistance appear to be minor. However, layering can result in water inter-lenses that reduces the stability of a soil mass.
Age of the Deposit	The liquefaction resistance increases with the age of the deposit.
Loading History	The resistance increases with over-consolidation, but the rate of increase decreases with fines content. Prior dynamic loading generally increases the resistance due to densification, increase in lateral effective stress or change in soil structure.
Saturated Hydraulic Conductivity, k_{sat}	Drained soils with sufficient saturated hydraulic conductivity may not liquefy. Variations in the hydraulic conductivity may lead to the development of water inter-layers that will promote failure.

Table 2-1 – General influence of various factors on the liquefaction resistance (continued)

FACTOR	INFLUENCE ON LIQUEFACTION RESISTANCE
Layering	The effects of layering on the liquefaction resistance appear to be minor. However, layering can result in water inter-lenses that reduce the stability of a soil mass.
Age of the Deposit	The liquefaction resistance increases with the age of the deposit.
Loading History	The liquefaction resistance increases with the over-consolidation ratio, but the rate of increase decreases with fines content. Prior dynamic loading generally increases the liquefaction resistance due to densification, increase in lateral effective stress or change in soil structure.
Saturated Hydraulic Conductivity, k_{sat}	Well-drained soils with sufficient saturated hydraulic conductivity (gravels) may not liquefy. Variations in the hydraulic conductivity may lead to the development of water inter-layers that will promote deformation and failure.

2.2.5 Strength Loss, Deformation and Flow due to Liquefaction

2.2.5.1 Strength Loss

A soil mass may appear to deform in a fluid-like manner upon liquefaction. This gives the impression that the soil mass has no shear strength. In fact, liquefied soil masses possess some shear strength although they may experience transient periods of zero effective stress during earthquake shaking. There are three basic approaches to determining the shear strength of a liquefied soil mass, also known as the liquefied shear strength, the residual strength, or the post-liquefaction strength.

The first approach was developed by Poulos et al. (1985) and is based on the assumption that the shear strength of a liquefied soil is the same as the steady state strength at the same void ratio. This approach consists of estimation of the void ratio profile of the soil deposit, laboratory testing of undisturbed or reconstituted soil samples to approximate the steady state relationship of the soil (as effective confining stress versus void ratio) and estimating the steady state strength from the void ratio profile.

Given the difficulties involved in obtaining undisturbed samples or reconstituting samples to the same density and structure as encountered in the field, this approach is not practical. Numerous authors, including Alarcon-Guzman et al. (1988) and DeAlba et al. (1975) have commented on the shortcomings of this method that include its failure to consider such phenomena as the dependence of the shape of the steady state curve on the soil structure, partial drainage or flow from underlying soil layers during liquefaction, and the development of large strains in thin zones (or water inter-layers) rather than uniformly throughout the deposit.

A second approach developed by Seed & Harder (1990) is based on the correlation of the standard penetration blow count (prior to liquefaction) with the liquefied shear strength of the soil as back-calculated from observations of liquefaction-induced flow failures. This approach has led to the development of charts such as that in Figure 2-16 and is the most commonly used approach. The "equivalent clean sand SPT blow count, $(N_1)_{60\text{-}cs}$" referenced in the figure is the standard penetration test (SPT) blow count corrected for effective overburden stress, equipment efficiency, and fines content.

A third approach was also developed from back-calculation of liquefaction-induced failures and is known as the normalized strength approach Olson & Stark (2002). It is predicated on the assumption that the liquefied shear strength is influenced by the same factors that determine the penetration resistance. The ratio of the liquefied shear strength, S_u, to the initial effective overburden stress, σ'_{vo}, may be estimated from the standard penetration resistance using:

$$\frac{S_u}{\sigma'_{vo}} = 0.03 + 0.0075(N_1)_{60-cs} \pm 0.03 \qquad (2\text{-}3)$$

where:

$(N_1)_{60\text{-}cs}$ is the standard penetration test (SPT) blow count corrected for overburden stress, equipment efficiency, and fines content.

The liquefied strength ratio may also be estimated from the cone penetration test (CPT) tip resistance using:

$$\frac{S_u}{\sigma'_{vo}} = 0.03 + 0.0143(q_{c1}) \pm 0.03 \quad (2\text{-}4)$$

where:

(q_{c1}) is the CPT tip resistance normalized based on an effective overburden stress of 100 kPa.

Olson & Stark (2002) indicate that residual strengths calculated using this third approach are comparable to those estimated from the approach of Seed & Harder (1990).

Laboratory shear tests on liquefied soils often indicate dilation of the sample and liquefied shear strengths greater than those back-calculated from case histories. Yoshimine et al. (1999) noted that the difference may be due to the difference between dynamic loading conditions in the field and laboratory.

Stark et al. (1998) is a comprehensive report on the shear strength of liquefied soils and describes the methods of evaluating the strength of liquefied soil as well as their development, application and limitations in detail. However, the report indicates the need for additional research in this area.

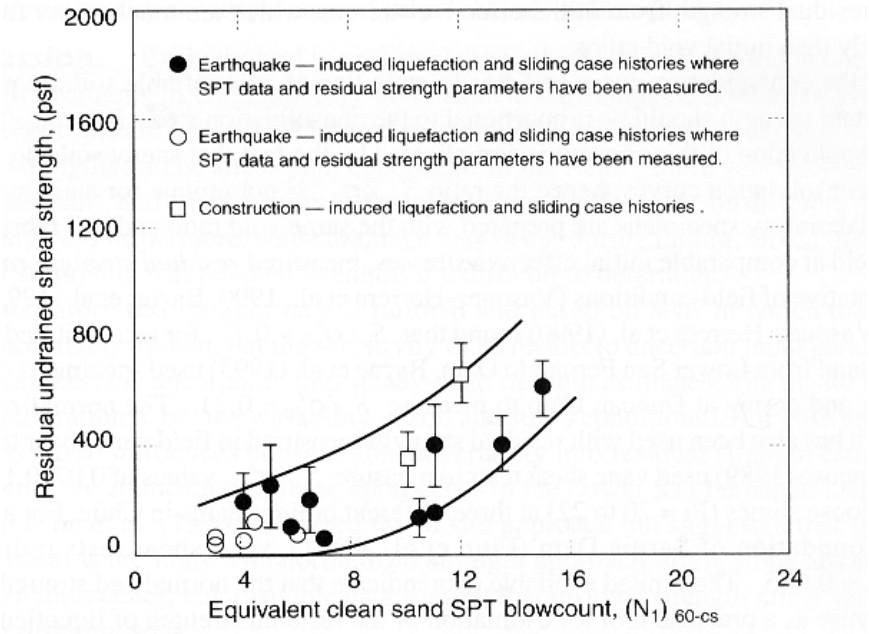

Figure 2-16 – Relationship between residual strength (liquefied shear strength) and corrected SPT resistance (from Seed and Harder 1990).

2.2.5.2 Methods of Evaluating Deformation Prior to Liquefaction

The deformation of a soil mass during earthquake shaking prior to liquefaction is a very complicated phenomenon that involves interaction between several aspects:

- The intensity, duration and frequency characteristics of the ground motion (Kramer, 1996);
- Dissipation of the energy of the ground motion through friction and heat generation within the soil mass, referred to as damping (Kramer, 1996);
- The reduction in the shear moduli of the soil mass with shear strain (Seed & Idriss, 1982; Kramer, 1996; Cundall, 2006);

- The influence of the geometry of lenses and layers in the soil mass with differing dynamic properties (Seed & Idriss, 1982; Kramer, 1996; Cundall, 2006);
- The influence of the topography on the response of the soil mass (Kramer, 1996; Cundall, 2006); and
- Changes in the dynamic properties caused by the generation of excess porewater pressures in some soils (NRC, 1985; Kramer, 1996).

The deformation of a soil mass is evaluated on the basis of the response of the site to earthquake loading. Site response analyses (also known as ground response analyses) are conducted using analytical or numerical methods.

Analytical methods generally use equivalent linear models of soil behavior that assume the soil remains elastic during the dynamic loading. The soil does not undergo permanent deformation or failure. These methods do not consider the effect of excess porewater pressure generation and are limited to one-dimensional site response analyses and specialized applications, such as the Makdisi & Seed (1977, 1978 & 1979) method for estimation the earthquake-induced deformation of embankments (NRC, 1985; Kramer, 1996). SHAKE (Schnabel et al., 1972) is the most widely used computer program for one-dimensional site response analyses. It uses the equivalent linear method but accounts for the non-linearity of the soil response by adjusting the dynamic moduli and damping iteratively so that they are in agreement with the estimated shear strains at the end of shaking (NRC, 1985). The dynamic moduli, damping, and shear strains are thus assumed to be constant throughout shaking.

Several numerical models for site response analysis have been developed over the last 25 year or so. These models simulate the nonlinear behavior of soil masses in response to earthquake loadings on the basis of elasto-plastic behavior that can incorporate

permanent deformation, the non-linearity of the soil moduli and damping with shear strain, the effects of porewater pressure generation, as well as the influence of subsurface geometry and surface topography (NRC, 1985; Kramer, 1996).

Sigaran-Loria and Hack (2006) and Bourdeau (2006) used FLAC (Itasca 2005) for two-dimensional site response analyses of earthquakes in areas of prominent topography and found good agreement between the site response estimated by FLAC and measured ground motions. The ability of FLAC to incorporate the effects of excess porewater pressure generation in dynamic numerical analysis was confirmed by Puebla et al. (1997), Byrne et al. (2004), James et al. (2006), and Seid-Karbasi and Byrne (2007).

2.2.5.3 Post-liquefaction Deformation and Flow

The deformation of a soil mass due to liquefaction depends on the magnitude of driving forces (exterior or gravitational loadings) with respect to the liquefied strength of the soil. These driving forces may consist of initial static shear stresses or shear stresses developed during earthquake loading. Post-liquefaction deformation can be divided into two classes; level ground deformation where there are no significant loadings on the soil mass, and flow deformations where the loadings are sufficient to cause excessive deformation of the soil mass.

Level Ground Deformations - De Alba et al. (1975), through research using large-scale shaking table testing on "Monterey No. 0" sand (a uniform sand with a D_{50} value of 0.34 mm), demonstrated that the deformations on the surface of a liquefied sand layer are a function of the relative density and have a limited shear strain. The limiting shear strain was shown to decrease significantly with increasing relative density, varying from about 40% at a relative density of 50% to 0 at a relative density of 100%. Shear strains were estimated by dividing half the amplitude of the horizontal movement of the surface of the samples by the height of the sample. In De Alba et al. (1975), the definition of

liquefaction (r_u=1.0) was extended to include cyclic mobility, thus dilative samples which underwent cyclic mobility were included in the evaluation.

Flow Deformations - When the driving shear stresses exceed the liquefied shear strength, flow failure of the soil mass can be initiated (Seed & Idriss, 1981; Kramer, 1996). This phenomenon can be triggered or exacerbated by the development of water inter-lenses in layered soil deposits (Kokusho & Kojima, 2002; Sento et al., 2004). Post-liquefaction flows tend to behave as either the movement of granular material of low shear strength until an equilibrium condition is reached (e.g. the Tapo Canyon Tailings Dam failure) or flow in a fluid-like manner for considerable distance (e.g. the Aznalcollar Tailings Dam failure). The difference between the two types of flow appears to be due to a combination of the moisture content of the liquefied material, the liquefied shear strength of the material and the magnitude of the driving shear stress (e.g. inclination of the flow path).

The extent of granular flow can be estimated from the liquefied shear strength and geometric and topographic conditions at a site, as was done afterwards for the 1964 Turnagain Heights (Alaska) liquefaction-induced landslide by Seed & Idriss (1982).

Lucia et al. (1981) researched flow failures of tailings impoundments and developed a method for predicting the flow distance. These researchers studied case histories from 17 tailings impoundment and embankment flow liquefaction failures where the materials were composed of hard rock (4 cases), coal (3 cases), or fine tailings (6 cases), or of sandy fill (4 cases). The probable cause of the failure was listed as seismically-induced liquefaction in 12 of the cases and seepage or statically induced liquefaction in the remainder. These researchers found the following:

a) The saturated liquefied material came to rest at surface inclinations of 1° to 4°;

b) The distance of the flow was related to downstream geometry as well as the volume of material available; and

c) The liquefied material came to rest after flowing onto ground with topographic inclinations of less than 4°.

The flow distances of the failures evaluated in Lucia et al. (1981) typically varied from a few 100 meters to 2 kilometers.

Jeyapalan (1982) & Jeyapalan et al. (1983) investigated flow failures of tailings dams and found that, in general, the liquefied tailings flowed in a laminar manner and behaved as a Bingham plastic fluid. A method for predicting the flow characteristics of liquefied tailings was developed by extending the inviscid (very low viscosity) solutions for the flow of water from failed dams to include laminar viscous resistance to simulate the liquefied strength of the tailings. Flow slides were modeled numerically and the results were found to be comparable to actual flow slides. However, the materials investigated by these researchers consisted of gypsum, coal and phosphate tailings and the results may not be applicable to hard rock tailings.

2.2.6 Effects of Liquefaction

The effects of liquefaction can be catastrophic. The most obvious effects of liquefaction are a loss of shear strength and excessive deformation which can lead to the settlement or displacement of overlying structures and the failure of slopes and embankments. Other significant effects are the loss of strength or liquefaction of adjacent or overlying layers caused by the transmission of excess porewater from liquefied or cyclically mobilized lenses or layers of soil and the development of thin lenses of water under pressures greater than hydrostatic levels between a liquefied or mobilized layer and an overlying less permeable layer. These water inter-layers can create zones of very low shear strength

and lead to the development of slope failures or of sand boils as flow paths are established through the overlying layer (Kramer, 1996; Amini & Qi, 2000).

A comprehensive study by Schneider & Mayne (1999) revealed that extensive liquefaction occurred as a result of the three New Madrid (Missouri) earthquakes of December 16, 1811, January 23, 1812 and February 7, 1812 (moment magnitudes 7.8 to 8.1) and as a result of the moment magnitude 7.3 Charleston (South Carolina) earthquake of August 13, 1886.

In the province of Quebec, the November 25, 1988 Saguenay earthquake had a moment magnitude of 5.9 and produced a peak horizontal ground acceleration of 0.13 g at a distance of 43 km from the epicenter. Extensive liquefaction-induced damage was observed in two small communities 25 km from the epicenter (Tuttle et al., 1989, 1990a & 1990b). Additionally, although there was only limited engineering reconnaissance following the 1935 Temiscamingue earthquake (moment magnitude 6.2), there was inferential evidence of liquefaction (sand boils) in the area effected by the earthquake (Lamontagne & Bruneau, 1990).

2.2.7 The Liquefaction Resistance of Silt and Gravel

Although liquefaction research has focused on sands and silty sands, soils composed of silt (nonplastic material less than 0.075 in maximum grain size) or gravel (material with a gradation between 4.75 mm and 75 mm) are also susceptible to earthquake-induced liquefaction (Youd et al., 2001). There is an increasing amount of research on the liquefaction resistance of silty soils (i.e.: Sangrey et al., 1978; Zhaoji, 1987; Zhu & Law, 1988; Finn et al., 1994; Singh, 1994; Vaid, 1994; Zhou et al., 1995; Singh, 1996; Erten & Maher, 1995; Guo & Prakash, 1999; Thevanayagam et al., 2000; Polito & Martin, 2001; Hyde et al., 2006). However, most of this research has focused on silty sand rather than silt. Very little research has focused on the liquefaction potential of gravel.

Generally, the liquefaction resistance of non-plastic silt is lower than that of sand at the same relative density and the rates of shear strain and excess porewater pressure development in silt are more rapid than those of sand (Singh, 1996; Polito & Martin, 2001).

There are very few known instances of gravel liquefaction due to the capacity for gravel to dissipate excess porewater pressure during earthquake shaking and the fact that gravel has a greater liquefaction resistance than sand (Wong et al., 1975; Evans & Zhou, 1995). Yasuda et al. (1997) conducted undrained cyclic triaxial and torsional simple shear tests on compacted rockfill and found that the dynamic response of rockfill was similar to that of sand, but that the cyclic resistance was substantially higher and shear strains were limited, indicating a condition of cyclic mobility rather than liquefaction.

2.3 EVALUATION OF THE POTENTIAL FOR LIQUEFACTION

The primary issues in the evaluation of the potential for seismically-induced liquefaction of a soil could be summarized as:

a) Is the region subject to earthquakes of sufficient magnitude to cause liquefaction; and

b) Is the soil susceptible to liquefaction as a result of earthquake ground motions;

c) Will liquefaction occur;

d) Is the potential for danger to life and the environment and to structures acceptable; and

e) What can be done to reduce the potential for damage (Kramer, 1996).

This section addresses methods of evaluating the potential for liquefaction (item c).

2.3.1 The Simplified Method of Seed & Idriss (Youd et al., 2001)

The most widely used analytical liquefaction evaluation procedure was initially developed by Professors H. Bolton Seed and I. M. Idriss of the University of California, Berkeley, based on observations and research following devastating earthquakes in Alaska and Japan in 1964. This method is known as the "Simplified method" or the "cyclic stress method" and is described in Seed & Idriss (1970 & 1982) and Seed (1979). It has been subject to extensive review and was most recently updated following workshops sponsored by the U. S. National Science Foundation and the National Center for Earthquake Engineering Research in 1996 and 1998, respectively, (Youd et al., 2001). This updated version of the procedure is described below. It is noted that this approach does not differentiate between liquefaction and cyclic mobility. In the Simplified Method, liquefaction is defined as the development of a porewater pressure ratio, r_u, of 1.0, which is equivalent to an effective confining stress of zero.

The basis of the Simplified Method is to compare the average cyclic shear loading of a given earthquake on an element of soil to the ability of that element to resist the loading.

2.3.1.1 Applicability

Seed & Idriss (1982) state that the applicability of the Simplified method is limited to level or gently sloping ground and alluvial and fluvial deposits of the Holocene epoch. However, the Simplified method is used worldwide for the evaluation of the liquefaction potential of natural and artificial deposits of cohesionless soils, including tailings.

Although the method was developed based on observations and research involving earthquakes along the west coast of North America and the western Pacific rim, Youd et al. (2001) indicate that the method is applicable to the eastern North America as well. This is supported by the research of Arango (1994) that included comprehensive cyclic laboratory testing at frequencies typical of earthquakes on the west and east coasts of

North America, numerical modeling and analyses of the ground motions produced by the 1988 Saguenay earthquake.

It is noted that the applicability of the simplified method has not been explicitly demonstrated for very silty sands (more than 35% fines), sandy silts and silts, or for tailings composed primarily of nonplastic fines. It is also noted that the fines content has a significant and complex effect on the liquefaction resistance of soil, particularly above a critical percentage, and that correlations of the penetration resistance of sands may not be applicable to these soils.

Use of the Simplified Method below a depth of about 20 m is not recommended (Youd et al., 2001) because empirical observations of liquefaction at the ground surface have generally been limited to liquefaction that occurred within 15 m of the ground surface. However, the Simplified Method has been commonly used to predict liquefaction at depths of 50 m or more (Byrne et al., 2004).

2.3.1.2 Earthquake Loading

The loading of an earthquake on an element of soil is represented by the cyclic stress ratio, CSR, the ratio of the average cyclic shear loading to the initial effective vertical stress on the element (Seed & Idriss, 1982):

$$\mathrm{CSR} = \frac{\tau_{av}}{\sigma'_v} = 0.65 \cdot \frac{a_{max}}{g} \frac{\sigma_v}{\sigma'_v} \cdot r_d \qquad (2\text{-}5)$$

where:

τ_{av} is the average shear stress;

σ'_v is the initial vertical effective stress;

a_{max} is the peak horizontal ground acceleration;

g is the acceleration due to gravity (9.81 m/s^2);

σ_v is the initial total vertical stress; and

r_d is the stress reduction coefficient (described below).

The factor of 0.65 is the result of empirical observation that the average shear stress generated by an earthquake is approximately 65% of the maximum shear stress generated during the occurrence of the peak horizontal ground acceleration (Seed & Idriss, 1970). The peak horizontal ground acceleration, a_{max} (or PGA) can be estimated in three ways:

1) By applying existing attenuation relationships to a specific fault for a given earthquake magnitude that are compatible with the type of faulting expected, regional geology, and local site conditions. In general these relationships are valid for relatively shallow, stiff soil sites and bedrock (Kramer, 1996);

2) Through site response analysis using computer programs such as SHAKE (Schnabel et al., 1972), EERA (Bardet et al. 2000), NERA (Bardet & Tobita 2001), or FLAC (Itasca, 2005). These types of analyses require an actual or artificial acceleration ground motion record in numerical format scaled to the peak horizontal acceleration on rock expected at the site, which can be obtained from existing attenuation relationships. The selected ground motion should have a duration and frequency content consistent with the expected ground motion. The programs simulate the dynamic response of the soil profile assuming no generation of excess porewater pressure. SHAKE and EERA use equivalent linear analysis to simulate the dynamic response of the soil profile, while NERA and FLAC use nonlinear analysis. SHAKE, EERA, and NERA assume a one-dimensional soil profile. FLAC can be used for one, two or three-dimensional profiles and can be programmed to include the effects of porewater pressure generation.

3) The PGA on rock can be obtained from published sources (e.g. Adams & Halchuk, 2003), and generic amplification factors based on a generalization of the soil profile can be applied to estimate the PGA on the ground surface (Finn & Wightman, 2003). This method is the least accurate; Youd et al. (2001) recommend "caution and considerable engineering judgment" in its use.

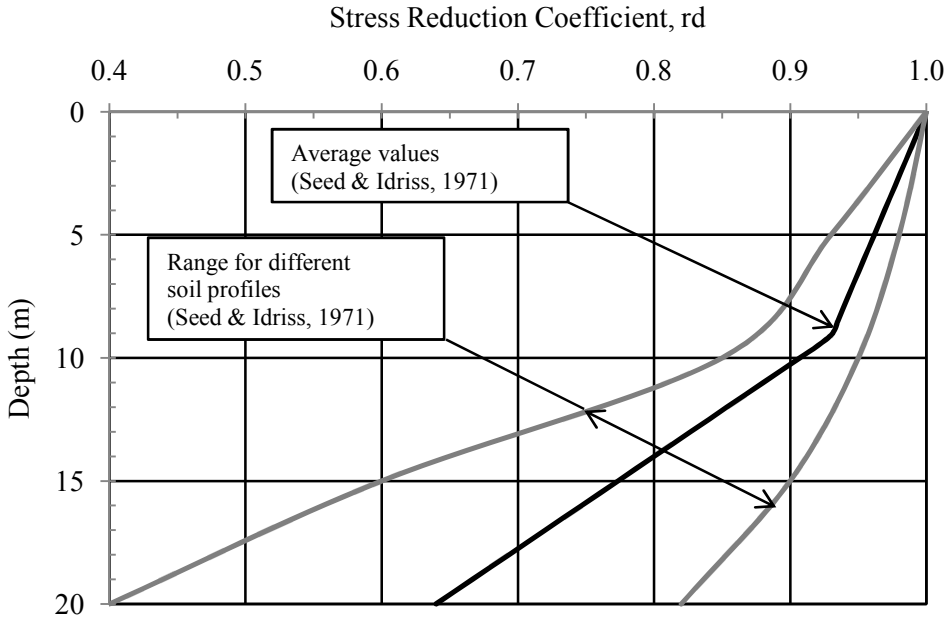

Figure 2-17 – Stress reduction coefficient for use in the Simplified method. (from Seed & Idriss, 1982; Youd et al., 2001).

The stress reduction coefficient, r_d, accounts for the deformability of the soil column and is highly dependent on the properties of the soil. It is essentially the inverse of the

amplification and can be derived from site response analysis or generic charts and equations such as Figure 2-17 or Equation 2-6.

The earthquake magnitude is implicitly considered in the calculation of the cyclic stress ratio.

$$r_d = 1.0 - 0.00765z, \text{ for } z \leq 9.15 \text{ m} \quad (2\text{-}6a)$$

$$r_d = 1.174 - 0.0267z, \text{ for } 9.15 \text{ m} < z \leq 23 \text{ m} \quad (2\text{-}6b)$$

where:

z is the depth below the ground surface in meters.

2.3.1.3 Liquefaction Resistance

The ability of a soil element to resist liquefaction is represented by the cyclic resistance ratio, CRR. The cyclic resistance ratio is the ratio of the average shear resistance for a given number of cycles of loading to the initial vertical effective stress. It is typically estimated from empirical correlations between the occurrence and non-occurrence of visible signs of liquefaction on level ground sites subject to earthquakes and in situ measurements of the soil at these sites. Standard penetration testing (SPT) and cone penetration testing (CPT) are the most commonly used in situ testing techniques used to evaluate the potential for liquefaction.

Figures 2-18 and 2-19 are examples of these correlations using the corrected standard penetration test blow count, $(N_1)_{60}$, and the corrected cone penetration test tip resistance, q_{c1N}, respectively. Figures 2-18 and 2-19 are "clean sand" curves and apply to sands with 5% or less of nonplastic fines. Youd et al. (2001) recommend correcting the $(N_1)_{60}$ and q_{c1N} values with respect to the fines content and using the "clean sand" curves to estimate the CRR. The in situ testing values must also be corrected to account for differences in

the equipment and techniques used in testing and for overburden stress. The corrections to in situ testing values are described in detail in Youd et al. (2001) and discussed below.

Correction of the Standard Penetration Test Blow Count, N

Following the methodology of Youd et al. (2001), the measured standard penetration test blow count, N, can be corrected using the following formula:

$$(N_1)_{60} = N \cdot C_N C_E C_B C_R C_S \tag{2-7}$$

where C_N, C_E, C_B, C_R, and C_S are correction factors for the effective overburden stress, hammer energy (efficiency), diameter of the borehole, length of rods (depth of the borehole), and sampling method, respectively. The factor C_N normalizes the blow count to an effective overburden stress of 100 kPa. Recommended values and formulas for the correction factors are presented in Youd et al. (2001).

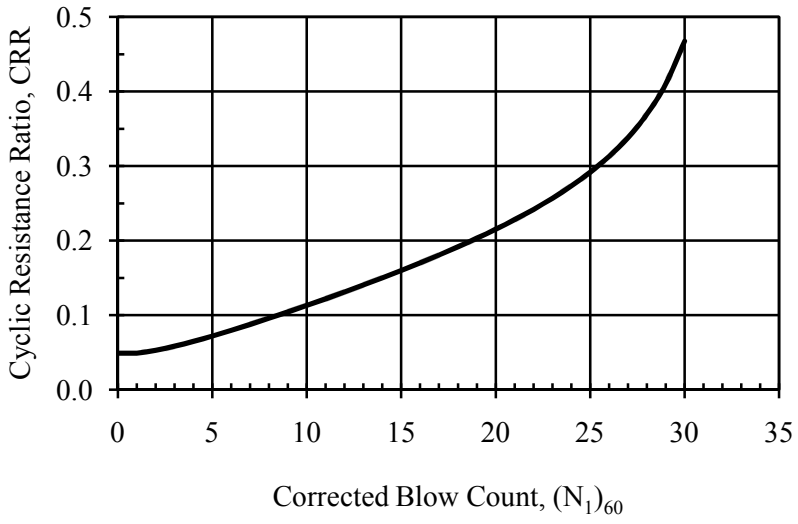

Figure 2-18 – SPT clean-sand base curve for magnitude 7.5 earthquakes based on liquefaction case histories (adapted from Youd et al., 2001).

Youd et al. (2001) also recommend that the penetration resistance be adjusted for the influence of the fines content as shown below.

$$(N_1)_{60-CS} = \alpha + \beta(N_1)_{60} \quad (2\text{-}8)$$

Where $(N_1)_{60\text{-}CS}$ is the corrected, clean-sand standard penetration resistance and the factors α and β vary as shown on Figure 2-20.

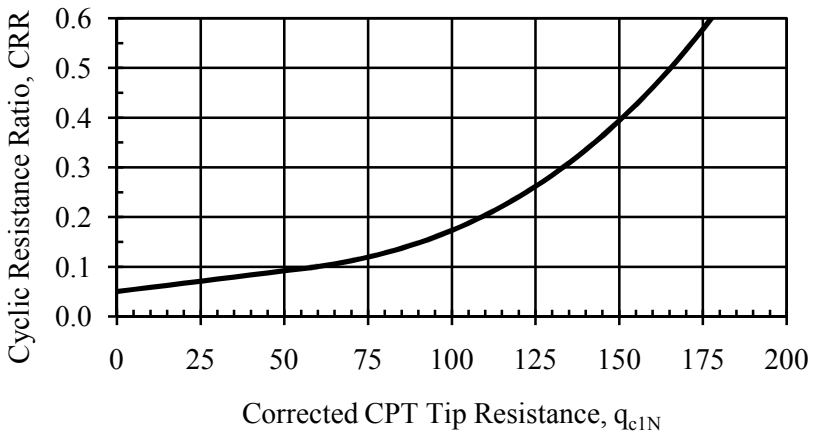

Figure 2-19 – CPT clean-sand base curve for magnitude 7.5 earthquakes based on liquefaction case histories (adapted from Youd et al., 2001).

The standard penetration test blow count is unchanged for soils containing 5% or less of nonplastic fines, is factored by 1.2 and increased by 5 for soils containing 35% or more of nonplastic fines, and intermediate adjustments are made used for soils containing more than 5% and less than 35% nonplastic fines. Increasing the blow count with the fines content assumes that the presence of silt increases the liquefaction resistance (or decreases the penetration resistance) to particular level at 35% fines after which the liquefaction resistance (or penetration resistance) is constant. However, as described

earlier, based on the research of Polito & Martin (2001), the interaction of silt with sand is known to be significantly more complex. Thus, the fines correction of Youd et al. (2001) may not be applicable to all types of soils, particularly those with large proportions of fines or entirely composed of fines (very silty sands, sandy silts, silts, and hard rock tailings).

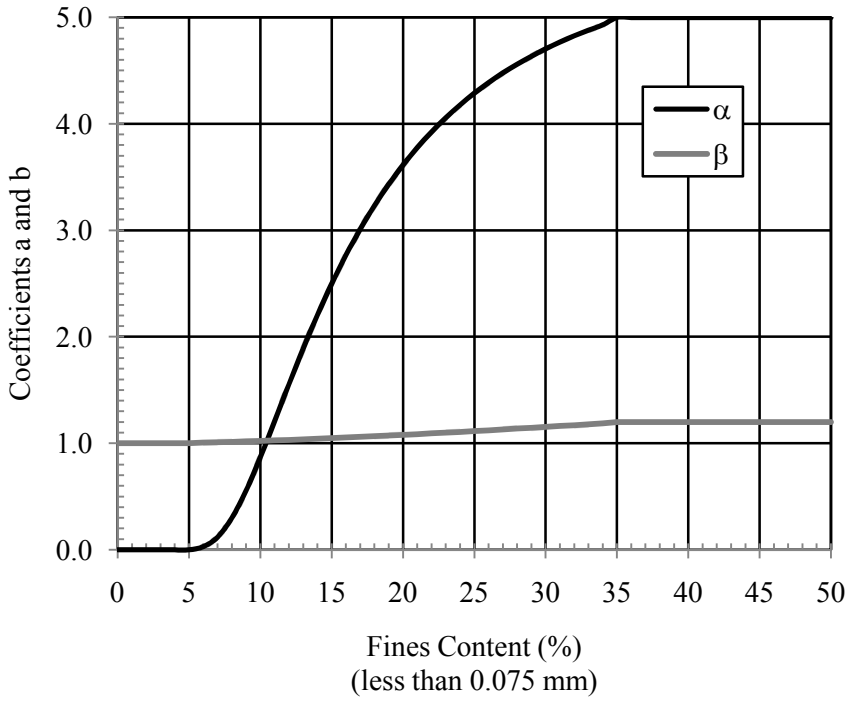

Figure 2-20 – Coefficients α and β for correction of fines content of standard penetration testing (adapted from Youd et al., 2001).

2.3.1.4 Correction of the Cone Penetration Test Tip Resistance, q_c

Youd et al. (2001) recommend correcting the cone tip resistance for overburden stress, fines content, soil type, and the thickness of the soil layer. The fines content and soil type are determined through empirical correlations with the tip resistance, sleeve friction, and overburden stress. Details of the correction procedures are presented in Robertson and Wride (1998) and Youd et al. (2001).

2.3.1.5 Magnitude Scaling Factor

A moment magnitude of 7.5 is implicit in the calculation of the CRR. For comparative purposes, either the CSR must be scaled to a magnitude of 7.5 or the CRR must be scaled to the magnitude of the CSR. Seed & Idriss (1970) developed the magnitude scaling factor, MSF, for this purpose:

$$\mathrm{CRR_M} = \mathrm{MSF} \cdot \mathrm{CRR_{7.5}} \tag{2-9}$$

$$\mathrm{CRR_{7.5}} = \frac{\mathrm{CSR_M}}{\mathrm{MSF}} \tag{2-10}$$

Where the subscripts 7.5 and M denote a moment magnitude 7.5 and an arbitrary magnitude, respectively.

There has been a significant amount of research regarding magnitude scaling factors and values have been presented by various researchers (Ambraseys, 1988; Arango, 1994 & 1996; Andrus & Stokoe, 1997 & 1999; Youd and Noble, 1997a & 1997b). Magnitude scaling factors are generally estimated in either of two ways: by observation of the number of significant cycles produced by earthquakes of known magnitudes (e.g. Seed & Idriss 1970), or by calculation of the energy content of the ground motions produced by earthquakes of known magnitudes (e.g. Arango, 1994 & 1996). Due to the random nature of earthquake ground motion, there is considerable variation in the magnitude scaling factors produced by the various researchers.

Arango (1994) conducted extensive research of the 1988 Saguenay (Quebec) earthquake and other eastern North America earthquakes and developed magnitude scaling factors for earthquakes east of the Rocky Mountains based on the energy content of the recorded ground motions. These magnitude scaling factors differ slightly from those recommended by Youd et al. (2001) for engineering practice.

The magnitude scaling factors recommended by Youd et al. (2001) for engineering practice and those recommended by Arango (1994) for earthquakes east of the Rocky Mountains are presented on Table 2-2. Also shown on the table are the number of significant cycles of loading, N, given by Seed & Idriss (1982) and Arango (1994). MSF values for intermediate magnitudes may be interpolated from the data given.

Table 2-2 – Recommended magnitude scaling factors, MSF, and number of equivalent cycles, N_{EQ}.

Moment Magnitude	Youd et al. (2001) MSF		Seed & Idriss (1982)		Arango (1994)	
	Lower Bound	Upper Bound	MSF	N	MSF	N
5.5	2.20	2.8	1.43	3-4	3.00	1.5
6.0	1.76	2.1	1.32	5-6	2.00	4
6.5	1.44	1.6	1.19	8	-	6
7.0	1.19	1.25	1.08	12	1.25	10
7.5	1.00		1.00	15	1.00	15
8.0	0.84		0.94	22	0.75	27
8.5	0.72		0.89	26	-	45

2.3.1.6 Correction Factors for Overburden Stress and Static Shear Stress

As previously mentioned, the liquefaction resistance of soil increases with the effective overburden (confining) stress. This increase is independent of adjustments made to in situ testing values for effective confining stress. A number of researchers have studied the effect of overburden stress on liquefaction resistance (Seed & Idriss, 1982; Seed, 1983; Seed and Harder, 1990; Thevanayagam, 1998; Hynes and Olson, 1999; Steedman et al., 2000; Vaid et al., 2001; Moss et al., 2006). Youd et al. (2001) recommend the method of Hynes and Olsen (1999) to correct the liquefaction resistance of sand, silty sands and gravels for overburden stress:

$$K_\sigma = (\sigma'_{vo}/P_a)^{(f-1)} \quad (2\text{-}11)$$

where:

K_σ is the overburden stress correction factor;

σ'_{vo} is the effective overburden stress;

P_a is atmospheric pressure (100 kPa);

f is 0.7 to 0.8 for relative densities of 40 to 60%, and 0.6 to 0.7 for relative densities of 60 to 80%.

The resulting correction factors are considered conservative (Youd et al., 2001).

The presence of static deviatoric shearing stresses, such as those below embankments and foundations, effects the liquefaction resistance. Generally, the liquefaction resistance of dilative soils is increased while that of contractive soils is decreased (Seed, 1983; Ishibashi et al., 1985; Youd et al., 2001; Vaid et al., 2001). Despite the research that has been done on this topic, refer to Harder & Boulanger (1997) for a summary. There is currently no consensus as to how this correction should be applied in practice. Youd et al.

(2001) recommend that the existing relationships not be used in routine engineering practice. More recent work by Vaid et al. (2001) on Fraser River sand (D_{50} of 0.30 mm, C_u=1.8 and D_r ranging from 25 to 85%) indicates that the effects of state deviatoric shear stress, effective overburden stress, and relative density should be considered together due to the interactive nature of their influence on the cyclic resistance.

2.3.1.7 Factor of Safety

The factor of safety (FS) with respect to a soil element subjected to a given earthquake loading may be calculated as shown below (Youd et al., 2001).

$$FS = \frac{CRR_{7.5}}{CSR} \cdot MSF \cdot K_\sigma K_\alpha \qquad (2\text{-}12)$$

Factors of safety, FS, greater than 1.0 infer that liquefaction is not likely to occur, with the likelihood decreasing with increasing values of FS. However, high excess porewater pressures may be developed for factors of safety near 1.0. Factors of safety less than 1.0 infer that liquefaction is likely to occur with the likelihood increasing with decreasing values of FS. Marginal factors of safety, around 1.0, infer that liquefaction may or may not occur, but high excess porewater pressures will be developed in either event.

2.3.2 Comments on In Situ Testing

The in situ testing methods most commonly used for liquefaction evaluation are standard penetration testing (SPT) and cone penetration testing (CPT). Others less commonly used methods include shear wave velocity measurements in all types of soil and the Becker penetration test (BPT) in gravelly soil.

SPT is well known and it's assumed that the reader is familiar with it. Basic familiarity with CPT is also assumed. Cone penetration testing has undergone developments in recent years that have expanded its capabilities. Cones are now typically equipped with sensors for measurement of the porewater pressure response of the soil to penetration and

the dissipation of the porewater response. This type of cone penetration testing is referred to as “CPTu” or “piezo-cone”. Another type of cone now available is the “seismic” cone, “SCPT” or “CPT-V_s”. This type of cone is equipped with geophones which are used in combination with a surface source (a hammer striking a steel beam or plate) to develop a shear wave velocity profile in addition to the other measurements made by the cone (Robertson et al., 1992). A CPTu type device was used in the field exploration for this research project.

Conversion factors have been developed for the conversion of cone penetration tip resistance values into standard penetration blow counts and are widely used (Robertson and Wride, 1998). These conversion factors are based on empirical correlations from naturally occurring soils, where it was found the tip resistance, and thus the conversion factor, varies with the gradation of the soil. Ulrich and Hughes (1994) used SPT and CPT data from within 16 tailings impoundments in the western United States in a study of the SPT/CPT correlations and found that:

- The existing correlations based on gradation over-predicted the SPT blow count from CPT tip resistance;
- The conversion of CPT tip resistance to SPT blow count was independent of gradation; and
- Converting the CPT tip resistance to SPT blow count using a conversion factor associated with coarse sand (about 5.5) resulted in converted SPT values equivalent to the measured values.

2.3.3 Other Methods

There are several other methods of evaluating the potential for liquefaction of a soil deposit, e.g. cyclic strain methods, energy dissipation methods, and effective stress-based

response methods. However, none of these methods are widely used for engineering application and very few have been verified (Kramer, 1996).

Several probabilistic methods for the evaluation of the liquefaction potential of soil have also been developed over the last few decades. They tend to fall into one of two categories: those based on probabilistic characterization of the parameters known to influence the generation of excess porewater pressure during cyclic loading, and those based on in situ-based characterization of liquefaction resistance.

The accuracy of these methods depends on the accuracy of the approach used to quantify the liquefaction resistance of the soil. Numerous authors, including Heymsfield (1999), Juang et al. (2002), and Toprak & Holzer (2003), have developed probabilistic methods for the evaluation of the liquefaction potential. These methods are based on the Simplified method as described above. The Summary Report from the 1996 NCEER and 1998 NCEER/NSF Workshops on Evaluation of Liquefaction Resistance of Soils (Youd et al., 2001) states that "probabilistic procedures are still under development and not sufficiently formulated for routine engineering practice."

2.3.4 Laboratory Testing

Laboratory testing is extensively used in liquefaction research to quantify the liquefaction resistance of specific types of soil, to isolate and investigate specific properties and conditions so that their influence on the dynamic behavior and liquefaction resistance can be studied, to analyze specific behaviors associated with liquefaction, to evaluate the effects of liquefaction, and to determine the influence of measures for reducing the potential for liquefaction or mitigating it effects. There are four basic types of laboratory testing used for liquefaction research: conventional dynamic, advanced dynamic, shaking table, and centrifuge testing. Conventional dynamic testing includes cyclic simple shear tests and cyclic triaxial tests and these are the most commonly used laboratory test

methods used in liquefaction research and in engineering practice. Advanced dynamic testing is used mainly for research and rarely in engineering practice. It includes torsional shear and resonant column testing.

Cyclic simple shear, cyclic triaxial, shaking table, and centrifuge testing form the basis of much of our understanding of liquefaction and its effects. These tests are described in the following sections. For additional information on torsional shear testing and resonant column testing refer to Bhatia et al. (1985), Woods (1994) and Ishihara (1996).

2.3.4.1 Cyclic Simple Shear and Cyclic Triaxial Testing

Conventional dynamic testing of soil is accomplished using either cyclic simple shear or cyclic triaxial devices. Figures 2-21 and 2-22 are schematics of typical cyclic simple shear and cyclic triaxial compression testing devices, respectively.

The cyclic simple shear device was developed by Seed and Lee (1966) and subsequently modified by others (Finn, 1985; Budhu, 1988). A commonly used cyclic simple shear device is the NGI-type developed at the Norwegian Geotechnical Institute (Woods, 1994). The NGI-type device is described below.

Samples used in cyclic simple shear testing are placed or formed within a cylindrical mold containing a rubber membrane. When the mold is removed and the sample is consolidated under vertical stress, circumventing horizontal metal wires within the membrane restrict deformation of the sample on horizontal planes leading to an assumed at-rest (K_o) condition. Loading is conducted by stress-controlled or strain-controlled horizontal action of the upper platen while both the lower and upper platen are restrained from vertical movement to create constant-volume conditions. The stress states imposed by cyclic simple shear testing are very similar to those imposed by earthquake ground motions, including rotation of the principle stresses (Finn, 1985). Cyclic simple shear testing is typically accomplished under constant volume conditions without verification

of the saturation or direct measurement of the porewater pressures. The development of excess porewater pressures is inferred from decreases in the effective vertical stress. Testing may also be conducted on dry samples. Finn (1985) indicates that the test results for saturated and dry samples are consistent. This is because the presence of water does not affect the behavior of the soil with respect to contraction under cyclic loading and the associated decrease in effective stress at constant volume (Finn, 1985).

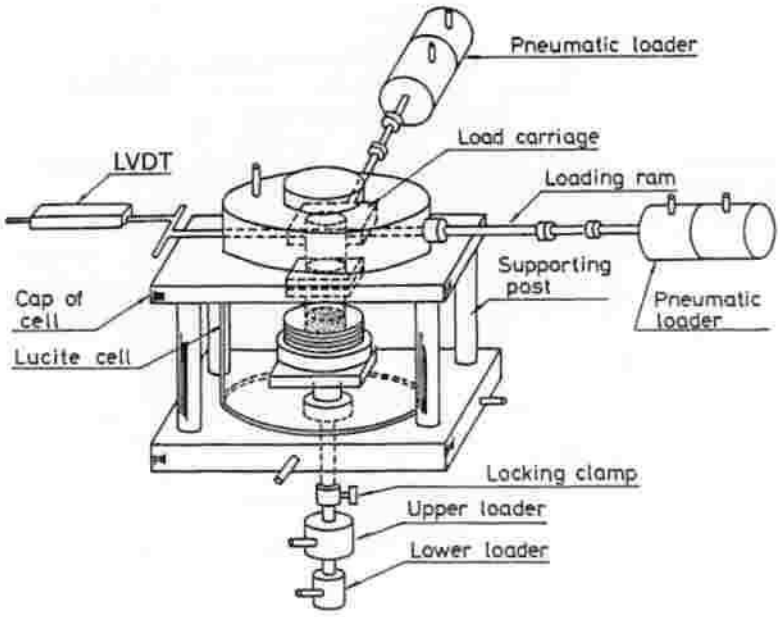

Figure 2-21 – Typical cyclic simple shear test device (from Ishihara, 1996).

Finn (1985) notes that the boundary conditions in some types of simple shear devices, including the NGI-type, create reasonably uniform stress conditions at shear stain levels less than about 0.5%.

Based on numerical analysis, the NGI-type cyclic simple shear device creates non-uniform stresses within samples that are dependent on the sample size and the magnitude of the shear strain applied or produced. However, the effect of the non-uniform stresses is significantly reduced in soil characterized by strain-softening, nonlinear behavior (Shen et al., 1978). As a result, the shear modulus measured using and NGI-type device is believed to be 5 to 15% lower than the actual shear modulus of the material (Shen et al. 1978).

Seed & Peacock (1970) indicate that the cyclic stress ratio causing liquefaction in cyclic simple shear testing in one dimensional loading, CSR_{CSS}, is related to the cyclic resistance ratio under multi-directional ground motion in the field (actual earthquake loading), CRR, by:

$$CRR \cong 0.9 \cdot CSR_{CSS} \tag{2-13}$$

With cyclic triaxial testing (Figure 2-22), a membrane-enclosed, cylindrical sample is consolidated isotropically or anisotropically to a given state of stress. A cyclic deviatoric vertical load (load-controlled test) or cyclic vertical displacement (strain-controlled test) is then applied to the top of the sample. This loading produces a maximum cyclic shear stress within the sample on an angle of $45^{o}+\phi/2$ from the horizontal; where ϕ in the friction angle of the sample.

The loading in cyclic triaxial devices is substantially different from loads applied by earthquakes that consist of upwardly propagating shear waves that induce angular distortion and rotation of the principle stress axis.

The application of back pressure is a common technique to enhance the degree of saturation of samples used in triaxial testing. As mentioned previously, the liquefaction

resistance of soil increases significantly with minimal decreases in the saturation below 100%. Xia & Hu (1991) found that the application of back pressure in cyclic triaxial testing significantly changed the inter-particle forces such that liquefaction resistances of the samples were substantially increased.

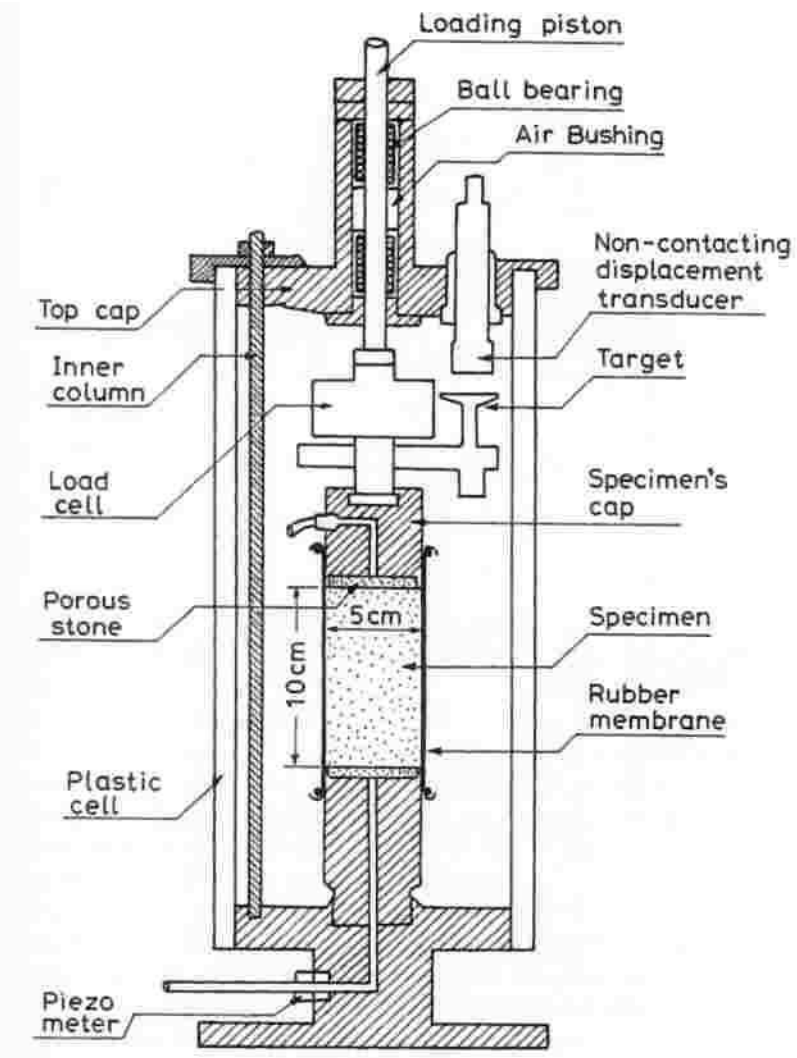

Figure 2-22 – Typical cyclic triaxial compression test device (from Ishihara, 1996).

Despite the cyclic triaxial test being non-representative of field conditions, Kramer (1996) indicates that the cyclic stress ratio causing liquefaction in cyclic triaxial testing, CSR_{TRX}, can be related to the cyclic resistance ratio due to multi-directional ground motion in the field, CRR, by:

$$CRR \cong C_r CSR_{TRX} = C_r \left(\frac{\sigma_{DEV}}{2 \cdot \sigma'_{vc}}\right) \quad (2\text{-}14)$$

where: C_r is a correction factor equal to 0.55 to 0.72 for K_o=0.4 and 1.0 to 1.15 for K_o=1.0 (isotropic consolidation);

σ_{DEV} is the cyclic deviatoric stress;

σ'_{vc} is the effective vertical consolidation stress.

The cyclic simple shear and cyclic triaxial compression test devices have their limitations. Both use a rather small sample size, generally less than 20 cm in maximum dimension. Small sample sizes limit testing of samples with significant layering or gravel content. The use of small samples also increases the influence of boundary conditions on the response of the sample. Another notable limitation of cyclic simple shear and triaxial testing are the means by which the sample is loaded. Samples in cyclic simple shear devices can be consolidated vertically, but lateral stresses cannot be controlled. At-rest stresses are assumed. The horizontal shearing motion of the cyclic simple shear device is more representative of earthquake loading than the cyclic triaxial device. Conventional dynamic laboratory tests are well-suited for investigating particular aspects of liquefaction, such as the relative liquefaction resistance of a soil, or the effects of confining pressure or fines content. However, due to their inherent limitations (Ishihara,

1996), they generally cannot be used alone to develop a good understanding of some of the more complex aspects of liquefaction and the post-liquefaction behavior of soil.

Laboratory testing of cohesionless soils is rarely conducted using undisturbed samples such as those obtained by freezing. The vast majority of laboratory testing of liquefiable soils is done using reconstituted samples and the method of reconstitution (sample preparation) has a dramatic effect on the liquefaction resistance of the samples because it largely determines the soil structure and thus the response of the sample (Miura and Toki, 1982; Vaid & Sivathayalan, 1999; Robertson et al., 2000a & 2002b). The sample preparation methods that produce soil structures most similar to the hydraulic placement of tailings are fluviation (placement through water) and slurry deposition (Kuerbis & Vaid, 1988).

Conventional dynamic testing is almost exclusively done using one-dimensional loading (one horizontal direction). However there are a few examples of two-dimensional loading (e.g. Boulanger & Seed, 1995).

2.3.4.2 Shaking Table Testing

Shaking table testing has been used extensively in liquefaction research. Testing consists of placing a sample within a container, installing sensors in the sample, and then subjecting the container to horizontal cyclic motion of known amplitude and frequency. Tests are generally conducted with one-dimensional loading, although some two-dimensional loading testing has been reported (Pyke et al., 1974; Ishihara & Nagase, 1985). Shaking table test containers can vary from less than one meter to several meters in size. A height to width ratio on the order of 10:1 is assumed to be necessary to duplicate free field conditions in the central portion of the sample during shaking table testing (DeAlba et al., 1975). DeAlba et al. (1975) used a series of large-scale shaking table tests to research the variation of excess porewater pressure and shear strains during

shaking with relative density. The container used was 230 cm by 105 cm at its base tapering to 190 by 75 cm at its top with a height of 120 cm. The liquefaction resistances and shear strains compared well with the result of cyclic simple shear and cyclic triaxial testing and with empirical data from liquefaction case histories.

Shaking table testing has also been used to research the effect of various methods for controlling the occurrence or effects of liquefaction and to verify numerical models of liquefaction behavior (e.g. Cudmani et al., 2003; Byrne et al., 2004).

Larger-scale tests can be much more representative of field conditions and can be used to evaluate the effects of layering, heterogeneity, stone columns, and other conditions not readily evaluated using conventional testing (e.g. Sasaki and Taniguchi, 1982; Adalier et al., 2003).

Shaking table tests are typically done using a rigid box to contain the sample. The resulting interaction between the walls of the sample box and the sample can have a significant impact on the test results, particularly where the natural period of the sample box is close to that of the dynamic load being applied to the model (DeAlba et al., 1975; Scott, 1994). To reduce this effect, laminar shear boxes with sides that deform with the soil sample were developed (e.g. Scott, 1994; VanLaak et al., 1994).

Shaking table testing is being conducted at the Polytechnique in Montreal, Quebec as a part of on-going research into the liquefaction of hard rock tailings (James et al. 2003). Figures 2-23 and 2-24 are photographs of the sample box in use at the Polytechnique. Details and results of the testing will be published in a Master's thesis by Nicolas Pepin (2009).

Figure 2-23 – The sample box used for shaking table testing at Ecole Polytechnique - Montreal (Photo by Darcy Joliette).

Figure 2-24 – Preparation of a sample for shaking table testing by air pluviation with tamping (Photo by Darcy Joliette).

2.3.4.3 Centrifuge Testing

Centrifuge testing allows the results of small-scale testing to be extrapolated to a larger-scale based on the effects of a higher gravity environment using scaling laws. It can also be used to investigate the effects of time-dependent phenomena (e.g. consolidation) in a relatively brief period, using the effects of scale (Scott, 1994). Centrifuge testing devices can be modified to allow dynamic testing by mounting a conventional shaking table to the arm of the centrifuge. An issue with the use of dynamic centrifuge testing are differences in the scaling laws that apply to various phenomena involved (Scott, 1994). For example the scaling factor for the time with respect to dynamic effects such as porewater pressure generation is n while the scaling factor for time with respect to porewater pressure dissipation is n^2, where n is the ratio of the prototype to the modeled length (Scott 1994).

The VELACS project is an ongoing U. S. National Science Foundation funded study intended to verify the predicted response of numerical solutions of liquefaction behavior using centrifuge testing. The verification is based on predicted versus observed porewater pressure generation, acceleration and displacement time histories (Princeton, 2003).

Examples of the use of centrifuge testing to verify numerical models are provided in Puebla et al. (1997), Byrne et al. (2003), Byrne et al. (2004), Adalier & Aydingun (2003), Aydingun & Adalier (2003), Sriskandakumar (2004), and Wijewickreme (2005b).

2.4 THE LIQUEFACTION OF HARD ROCK TAILINGS

The primary uncertainties regarding the liquefaction of hard rock tailings include:

- To what extent is the liquefaction potential of tailings similar to that of natural soils;

- How to evaluate their susceptibility to liquefaction with respect to a given seismic loading; and
- Determining the in situ state of the tailings in an active impoundment and predicting the in situ state of the tailings at closure.

The hydraulic conductivity of cohesionless, naturally occurring soils most susceptible to liquefaction ranges between 10^{-5} and 10^{-3} cm/s (Terzaghi et al., 1996). Natural soils with lower hydraulic conductivities are generally cohesive and those with higher conductivities are generally sufficiently drained to preclude the development of excessive porewater pressures (unless bounded by less permeable soils). However, tailings from hard rock mining typically contain significant nonplastic fine fractions or consist mostly of nonplastic fines and thus have a lower hydraulic conductivity while possessing none of the cohesion typical of natural soils of similar gradation. Terzaghi et al. (1996) indicates that some types of tailings are susceptible to liquefaction and that the range of gradation of liquefiable tailings is finer than the gradation limit normally associated with naturally occurring soil with a low resistance to liquefaction.

The two factors that appear to be the most critical in the liquefaction of tailings, as opposed to naturally occurring soils, are the lower hydraulic conductivity of the tailings and the possible differences in the inter-particle forces of tailings as compared to natural soils of similar gradation.

As noted in Section 2.2.4 and Appendix A, the inter-particle forces of a soil are determined by the grain size distribution, fine particle content, shape and strength of the individual grains, and soil structure. Inter-particle forces have a strong influence on the behavior of soil with respect to their state and with respect to their deformation and strength during cyclic loading and liquefaction.

2.4.1 Field Observations of Tailings Liquefaction

There have been ample observations of the liquefaction of hard rock tailings as a result of seismic activity (Davies & Lighthall, 2001; WISE, 2009). Some field observations of tailings liquefaction are summarized below.

USA 1994 - On January 17, 1994 the Tapo Canoyon Tailings Dam in southern California failed resulting in the release of impounded tailings which traveled several hundred meters downstream. The failure was attributed to liquefaction of the impounded tailings and possibly portions of the dam which was constructed of tailings and waste rock. The impounded tailings consisted of stratified layers varying from plastic silty clays to nonplastic silts and sands. The liquefaction was induced by the Northridge earthquake. The estimated peak horizontal ground acceleration at the site was 0.3 g (Harder & Stewart, 1996; Davies & Lighthall, 2001).

Japan 1978 - On January 15, 1978 the liquefaction of impounded tailings and foundation materials caused breaches in two tailings dikes at the Mochikoshi gold mine tailings in Japan that resulted in significant environmental contamination of downstream areas (Ishihara, 1984; Davies & Lighthall; 2001). Both of the tailings dikes were constructed of local volcanic soils and were active at the time of their failure.

Dike No. 1 consisted of a roughly 16 m high starter dam and was raised by the upstream method to a height of 20 m. It failed during the magnitude 7.0 Izu-Ohshima-Kinkai earthquake that induced a PGA of about 0.25g at the site. Ishihara (1984) evaluated the stability of the dike using pseudo-static methods while considering the generation of excess porewater pressure in the retained tailings and determined that a seismic coefficient of 0.17 resulted in a factor of safety of unity.

Dike No. 2 was constructed using a 12 m high starter dike and raised to a height of 22 m by the upstream method. It failed the day after the earthquake. Using conventional

seepage analysis and slope stability methods, Ishihara (1984) demonstrated that the seepage pressures caused by the dissipation of the excess porewater pressures were sufficient to destabilize the dike the day after the earthquake.

Chile 1965 - Multiple failures of tailings dams were reported as a result of an earthquake on March 28, 1965, most of the failures were attributed to some extent to liquefaction of the impounded tailings. The failure of the El Cobre Tailings Dam resulted in the release of over 2 million tons of tailings and approximately 200 deaths (Davies & Lighthall, 2001; WISE 2009). Evaluations of the failures of these tailings dams are presented in Dobry and & (1967).

2.4.2 Research on the Liquefaction Potential of Tailings

There is a great deal of uncertainty regarding the liquefaction potential of tailings, specifically whether existing methods of evaluation are applicable and how the dynamic behavior of tailings may differ from those of naturally occurring soils, which have been the primary focus of liquefaction research to-date. Some of the main research on the liquefaction of tailings is summarized below.

Ishihara et al. (1980) - Ishihara et al. (1980) conducted extensive laboratory testing on tailings sand and slimes from gold, copper and lead-zinc mines in Japan and Chile and on fine and coarse-ground quartz, silt and sand-sized, respectively. The grain size distributions of all of the materials lie within the bounds shown on Figure 2.1 for typical hard rock tailings. The plasticity indices of the slimes varied from nonplastic to 28. The samples were prepared by air pluviation with and without tapping or vibratory compaction and by slurry consolidation. Cyclic triaxial compression testing with back pressure saturation and consolidation stresses of 50 or 100 kPa were used to measure the liquefaction resistance of the samples. Liquefaction was defined as the development of a

porewater pressure ratio, r_u, of 1.0, 5% double amplitude strain, or 10% double amplitude strain during cyclic testing.

The research revealed that the liquefaction resistance of all the samples was influenced by the sample preparation method and that the liquefaction resistance of the tailings sands was slightly lower than that of the coarse-grained quartz. The resistance of both materials increased with decreasing void ratio. The liquefaction resistance of the nonplastic tailings slimes (void ratios from 0.55 to 0.9) was significantly lower than that of the tailings sands (void ratios from 0.6 to 0.9) at low void ratios and converged towards that of the tailings sands at higher void ratios. The liquefaction resistance of the more plastic tailings slimes (plasticity index of 15 to 20, void ratios of 1.15 to 1.55) was significantly higher than that of the coarse-grained quartz (void ratios of 0.7 to 0.9). At the higher void ratios, the liquefaction resistance of the tailings sands and nonplastic tailings slimes converged. Overall, the liquefaction resistances of the sand tailings and quartz sand were similar.

Ishihara et al. (1981) - This study evaluated the results of cyclic triaxial compression testing (with back pressure saturation) of undisturbed and reconstituted samples from 15 tailings impoundments in Japan. The study focused on two sites in particular, the Takara copper mine that produced nonplastic, fine-grained tailings with a maximum grain size of 0.07 mm and a D_{50} value of 0.005 mm and the Kamioka lead/zinc mine that produced coarse-grained tailings with a maximum grain size of 0.8 mm and a D_{50} value of 0.15 mm. The undisturbed samples were consolidated to effective stresses 20% greater than the estimated in situ values. The evaluation of the test results indicated that:

- The cyclic resistance of reconstituted samples was significantly less than that of undisturbed samples;

- A cyclic stress ratio of 0.25 caused liquefaction (as defined by 5% double amplitude strain) at 20 cycles in the undisturbed samples and was relatively independent of void ratio (which varied from 0.65 to 1.25) and gradation; and
- The cyclic resistance of fine-grained tailings increased slightly with the plasticity index.

Garga and McKay (1984) - This research consisted of undrained, isotropic and anisotropic, cyclic triaxial testing of 20 samples of hard rock tailings and 12 samples of naturally occurring soil (silt and sand). Testing was conducted on both reconstituted samples and samples from thin-walled drive samplers. Analysis of the testing indicated that:

- The method of sampling and the method of sample preparation had a significant effect on the liquefaction resistance;
- The naturally occurring soils were generally more resistance to liquefaction than the tailings. However, they also tended to be coarser than the tailings; and
- The liquefaction resistance of the natural soils and tailings increased with increasing principal stress ratio, K_0.

Troncoso & Verdugo (1985) and Troncoso (1986) - The influence of the nonplastic fines (<0.075 mm) content on the behavior of tailings from a copper mine in Chile under monotonic and dynamic loadings was studied by Troncoso & Verdugo (1985). In this study, the fines content varied from 0 to 30% by weight and all tests were done at a void ratio of approximately 0.9. The effective angle of internal friction of the tailings was found to vary from 44º to 39º with increasing silt content. The steady state line was found

to move lower with increasing silt content for effective confining stresses between 10 and 588 kPa.

The fines content was found to have a significant influence on the behavior of the tailings in cyclic triaxial testing. The shear modulus and the liquefaction resistance of the tailings decreased with increasing silt content.

In reviewing the results of this research, it should be noted that all of the tests were done at the same void ratio and that as mentioned previously, characterization of the behavior of silty sands based on void ratio may not be sufficient; the sand skeleton void ratio or relative density should be considered where appropriate.

Troncoso (1986) confirmed the results of Troncoso & Verdugo (1985).

Woeller et al. (1996) - Woeller et al. (1996) investigated the use of seismic cone penetration testing to evaluate the liquefaction potential of tailings sand and found that use of the shear wave velocity and tip resistance to quantify the state of the tailings as contractive or dilative gave contradictory results. Empirical correlations with the shear wave velocity indicated the tailings were dilative and not subject to flow liquefaction, while empirical correlations with the tip resistance indicated that the tailings were contractive and could undergo flow liquefaction in the event of an earthquake. The discrepancy in the results was attributed to the fact that existing CPT correlations were developed for naturally occurring soils and may not be applicable to tailings.

Robertson et al. (2000a) and Robertson et la. (2000b) - The Canadian Liquefaction Experiment (CanLex) was a comprehensive study of the liquefaction of soil and tailings using laboratory testing on intact and disturbed samples and large-scale in situ testing. The tailings used in the CanLex study were from oil sands deposits and do not fit within the definition of hard rock mine tailings used herein due to their coarseness (Robertson et al., 2000a; Robertson, 2000b).

Wijewickreme et al. (2005a) - Wijewickreme et al. (2005a) investigated the liquefaction resistance of fine-grained tailings using cyclic direct simple shear testing. The materials tested included undisturbed samples of laterite tailings and copper-gold mine tailings, and both undisturbed and reconstituted samples of copper-gold-zinc tailings. The laterite tailings included samples of low plasticity (PI=12) and of no plasticity. The copper-gold and copper-gold-zinc tailings were of no to very low plasticity (PI of 2). All of the tailings samples were dominated by fine-grained material with only 4 of 36 samples having more than 10% sand (greater than 0.075 mm in size) by weight.

Cyclic testing was conducted using a constant-volume, NGI-type cycle simple shear device. Liquefaction was defined as the occurrence of 3.75% single-amplitude shear strain. The stress-strain and effective stress response of the tailings was similar to that observed in similar tests on silts. That is to say that the sample exhibited considerable shear stain at the onset of loading that continued to failure. Also the decrease in effective stress began at the onset of loading and continued until failure. This indicates that the shear stress required to initiate excess porewater pressure generation in the material was relatively low. The liquefaction resistance of the nonplastic laterite tailings was slightly greater than that of the low plasticity laterite tailings. However, the nonplastic tailings were tested at a confining stress of 200 kPa while the low plasticity tailings were tested at a confining stress of 100 kPa. The copper-gold tailings were tested at a confining stress of 100 kPa and their liquefaction resistance was slightly greater than that of the low plasticity laterite tailings. The copper-gold-zinc tailings were tested at confining stresses ranging from 115 to 460 kPa and their liquefaction resistance was less than that of the other types of tailings, while the results appeared to be independent of confining stress.

Summary - Given the degree of uncertainty involved in the analysis of the liquefaction potential of tailings due to the limited amount of field and laboratory data available and

the constraints of conventional dynamic testing of tailings, there is a need for additional cyclic testing of tailings to determine:

- The extent to which the dynamic response of tailings may differ from that of natural soils;
- Whether the inclusion of zones of finer or coarser material (layering) significantly effects the liquefaction potential; and
- If conventional in situ testing techniques can be used to adequately assess the liquefaction potential of tailings.

There is a specific characteristic of tailings in active tailings deposits that has a very significant effect on the potential for liquefaction that has not been studied, under-consolidation. Due to their low permeability, tailings deposits take years to consolidate and during this process their density can be lower than that associated with the overburden stress and the porewater pressures may be greater than hydrostatic. Moreover, the interpretation of existing in situ testing results are correlated to normally consolidated and over-consolidated soils and may not be applicable to under-consolidated deposits.

2.5 METHODS OF CONTROLLING LIQUEFACTION AND ITS EFFECTS

2.5.1 An Overview

Methods that have been used to reduce the potential for liquefaction of a soil deposit or to limit the effects of liquefaction can be divided into six categories (Hausmann, 1990):

a) Lowering of the groundwater level to reduce the degree of saturation;

b) Compression or densification of the soil deposit;

c) Providing drainage to allow for the partial or complete dissipation of excess porewater pressures as they are developed during seismic loading;

d) Reinforcement of the soil mass to reduce the shear strains and thus the excess porewater pressure generated by seismic loading or to reduce the potential for flow failure in the event of liquefaction;

e) The injection of cement grout or other stabilizing agent to increase the density, stiffness or cohesion of the soil; and

f) Thermal stabilization using heat to fuse the soil particles together creating a soil mass with high shear strength and stiffness.

2.5.2 Stone Columns

Stone columns are the most commonly used method for controlling the occurrence of liquefaction and their effectiveness has been demonstrated on numerous occasions (Hausmann, 1990). For example, gravel drains (stone columns) installed at the Port of Kushiro (Japan) successfully prevented liquefaction of loose sand below wharfs while other areas of the port suffered significant damage due to liquefaction during an earthquake in 1993. As of 1992, over 20,000 stone columns had been installed throughout Japan to reduce the potential for liquefaction (Sonu et al., 1993).

The presence of stone columns has three significant effects on the behavior of a soil mass during an earthquake: a) stone columns can be much more permeable than the surrounding soil, this may allow for the dissipation of excess porewater pressures from the soil surrounding each column as they are generated; b) stone columns are generally much stiffer than the surrounding soil and act to reinforce the soil mass with respect to deformation; and c) due to their stiffness relative to the surrounding soil, stone columns alter the site response and may amplify or dampen the ground motion (Adalier et al., 2003).

Figure 2-25 is an illustration of the use of stone columns to reduce the potential for liquefaction. To be effective, stone columns must have sufficient hydraulic conductivity

to inhibit the development of excess porewater pressures due to seismic loading and have access to sufficient drainage for the discharge of excess porewater. Thus, when an earthquake induces porewater pressures in the surrounding soil, a hydraulic head differential is created between the soil and the stone columns. As a result, water from the soil flows into the columns and excess porewater pressures may not develop sufficiently to induce liquefaction.

Barksdale (1987) provides a design method for the use of stone columns to control the generation of excess porewater pressures. The method is largely based on the work of Seed and Booker (1976) and makes the following assumptions:

- The drainage columns are "infinitely" permeable;
- Darcy's law applies;
- The flow within the surrounding soil during earthquake shaking is entirely horizontal;
- The radial permeability of the soil is constant;
- The coefficient of volumetric compressibility of the soil is constant;
- The earthquake motion is equivalent to a given number of uniform cycles; and

The excess porewater pressure ratio, r_u, is a function of the cyclic loading ratio and can be approximated by the approach of DeAlba et al. (1975).

It should be noted that this approach is based on the assumption of uniform cycles of loading, whereas actual earthquakes produce random cycles of varying amplitude.

The assumption of infinite drainage is assumed to be valid when the hydraulic conductivity of the drain is at least 200 times greater than that of the soil. However, some

limited reduction in the induced porewater pressure can be expected when the hydraulic conductivity of the drains is at least 50 to 100 times that of the soil (Barksdale, 1987).

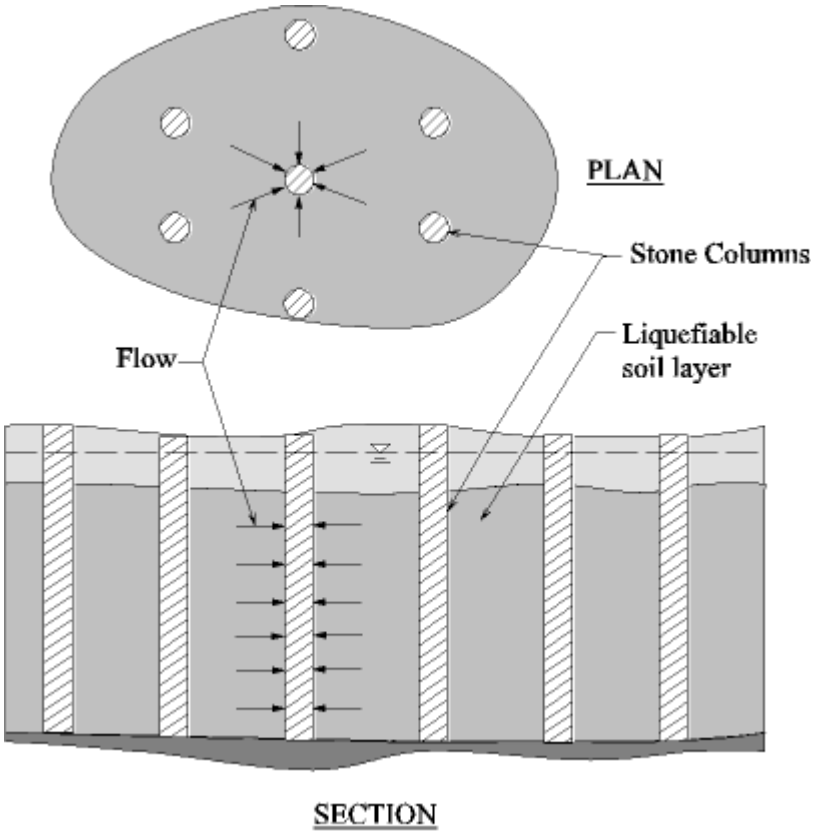

Figure 2-25 - Illustration of the use of stone columns to control liquefaction (adapted from Hausman, 1990).

Barksdale (1987) provides curves relating the induced porewater pressure ratio to the ratio of the diameter of drain to the tributary area of the drain. The appropriate curve is selected based on a dimensionless time coefficient, T_{ad}, defined as:

$$T_{ad} = \frac{4 \cdot k_r \cdot t_d}{\gamma_w \cdot m_{v3} \cdot D^2} \quad (2\text{-}15)$$

where:

k_r is the horizontal hydraulic conductivity of the soil;

t_d is the earthquake duration;

γ_w is the unit weight of water;

m_{v3} is the compressibility of the soil; and

D is the diameter of the stone columns.

Figure 2-26 shows the relationship between the average induced porewater pressure and the drain system parameters (D/D_e and T_{ad}) where the average induced porewater pressure ratio would be approximately 1.0 in the absence of the drains; D_e is the tributary area of the drains and is equal to 1.05 or 1.13 times the spacing of the drains in a triangular or square configuration, respectively. Barksdale (1987) indicates that the typical volume of stone columns required to control liquefaction of a sand deposit is 20 to 30 percent of the total volume of the deposit.

Post-construction evaluation of stone columns indicates that fine-grained material from the surrounding soils may penetrate stone columns as a result of installation methods or fines migration. For purposes of drainage analysis, this phenomenon could be considered to create either a reduced column diameter or a reduced hydraulic conductivity within the column (Barksdale, 1987). Due to the added expense, granular or synthetic filters are not used with stone columns and the material used is not self-filtering.

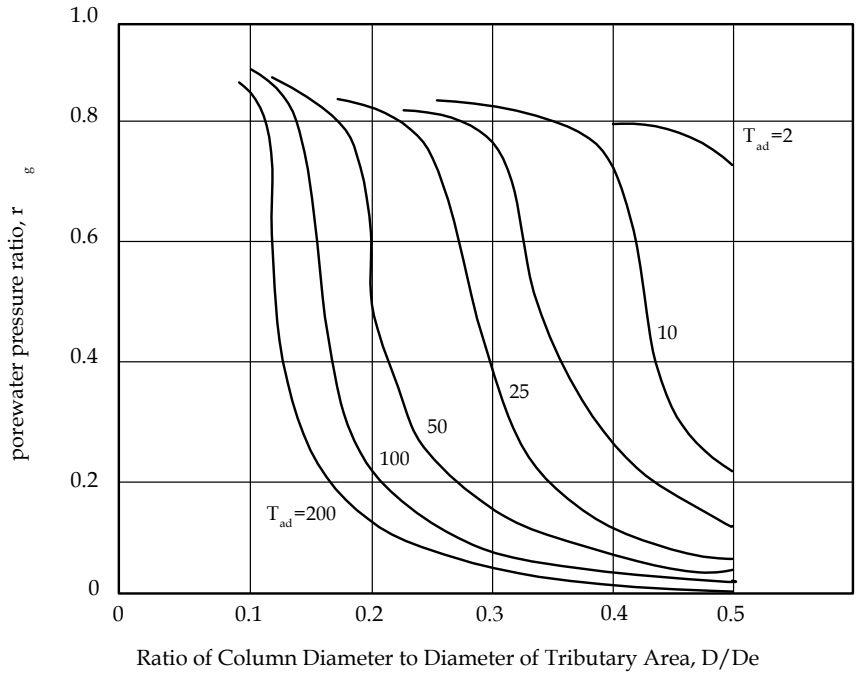

Figure 2-26 – Average induced porewater pressure in the media due to presence of stone columns (from Barksdale, 1987).

2.5.3 Research on the Use of Stone Columns to Control Liquefaction

Relevant research and a case history on the use of stone columns to control the effects of seismically-induced liquefaction are summarized below.

Sasaki & Taniguchi (1982) - Sasaki & Taniguchi (1982) conducted large-scale shaking table tests to evaluate the effectiveness of gravel drains (stone columns) at controlling dynamically-induced liquefaction. These tests were supplemented with conventional cyclic triaxial laboratory testing and numerical modeling. Large-scale testing consisted of the construction of six models in steel boxes which were 12 m long, 3.5 m high and 2 m wide. The models were constructed of uniformly graded fine sand with a D_{50} of 0.28 mm. One model was constructed of only sand and three with sand and gravel drains. The

gravel drains were 40 cm in diameter with a 20 cm diameter inner core of coarse gravel (D_{50} of 22 mm) and a 10 cm thick outer shell of medium gravel (D_{50} of 3.3 mm). The two other models were constructed with a half buried road, one with gravel drains and one without.

The samples were saturated by slow infiltration from the bottom. However, the degree of saturation was not measured. Each sample was shaken horizontally using an acceleration of 0.2 g at a frequency of 5 Hz for 60 seconds.

Shaking led to the development of excess porewater pressures in all of the samples. However, the presence of the gravel drains substantially reduced the generation of excess porewater pressures in the surrounding sand for a distance of approximately 50 cm (1.25 column diameters) and allowed the excess porewater pressures throughout the samples to dissipate much more rapidly than those without gravel drains. Nonetheless, the gravel drains did not perform as well as expected; the zone of influence of the gravel drains was expected to be greater. Sasaki & Taniguchi (1982) attributed the under-performance of the drains to the frequency of the loading which is much higher than that generated by earthquakes in the region. As the rate of increase in porewater pressure is roughly proportional to the rate of loading, in testing where drainage (or partial drainage) is a factor, the rate of loading (frequency) used in testing should reflect the anticipated rate of loading in the field.

Sasaki and Taniguchi (1982) also conducted two-dimensional numerical analysis of the six models. The numerical analyses simulated the generation of excess porewater pressures in the large-scale physical models reasonably well, although the rate of generation of excess porewater pressure in the numerical analysis was much more rapid than in the physical modeling.

Adalier et al. (2003) - Adalier et al. (2003) researched the use of stone columns in nonplastic silty soils through the use of dynamic centrifuge testing using a flexible-wall laminar shear box with interior model dimensions of 0.254 m high, 0.458 m long, and 0.254 m wide. Testing was conducted at gravitational values of 50 g and 63 g, requiring all values and properties to be factored to prototype scale (50 for the 50 g testing and 63 for the 63 g testing). All values and properties in this summary are at prototype scale unless otherwise noted.

The material used in the testing consisted of nonplastic silt with an effective internal friction angle, ϕ', of 25º at a relative density of 60% and "Nevada No. 10" sand which is uniformly graded, subrounded, clean, and has a D_{50} of 0.15 mm, and an effective internal friction angle of 37º at a relative density of 65%. The saturated hydraulic conductivity of the sand was estimated to be 2.6×10^{-3} m/s and 3.3×10^{-3} m/s at 50 g and 63 g, respectively. The hydraulic conductivity of the silt was not provided, but was said to be about 600 times lower than that of the sand.

Overall, the effects of the stone columns were a stiffer response (generally resulting in amplification of the ground motion) the development of excess porewater pressures occurred at a lower rate, porewater pressure ratios were reduced at depth, and settlements were reduced by a factor of 2.

Martin et al. (2004) - Martin et al. (2004) evaluated the performance of high-modulus jet-grout columns at a site in Turkey that was effected by the August 17, 1999 Kocaeli earthquake (moment magnitude 7.4). At the time of the earthquake, the site improvements were under construction. This allowed an evaluation of the differences in behavior between the improved and unimproved areas of the site. Generalized subsurface conditions consisted of, in descending order, 3 m of moderately compacted clayey gravel soil fill, 3.5 m soft to medium stiff silty clay of moderate plasticity, 2.5 m of loose to medium dense silty sand, 1 m of soft to medium stiff silty clay, and 25 m of medium stiff

to stiff silty clay of high plasticity, with a groundwater level within 2 m of the ground surface.

Portions of the site had been improved by the installation of wick drains and the placement of surcharge fills about 3.3 in height (approximately 55 kPa). The surcharge fills had been removed by the time of the earthquake.

Jet grouting was being used to install 60-cm diameter cement soil-cement columns at varying intervals across the site and was about two-thirds completed at the time of the earthquake. Peak horizontal ground accelerations of 0.24 g were estimated at the site.

Foundations consisting of shallow footings, mats and structural slabs had been constructed in some areas of the site at the time to the earthquake. However, none of the structures had yet been completed.

It was found by Martin et al. (2004) that the presence of the soil-cement columns significantly reduced the damage to the site as compared to the unimproved areas of the site. No significant damage was reported in areas of the site containing soil-cement columns. The earthquake caused settlements of from 1 to 5 cm in areas of the site that had been improved by the installation of wick drains and the placement of surcharge fills. These settlements were associated with water found ponded on the surface after the earthquake and were attributed to liquefaction of the silty sand layer, that was reported to have a factor of safety of about 0.6 with respect to liquefaction. No sand boils were observed at the site. Reconnaissance of structures in the surrounding area believed to be on sites with similar subsurface conditions indicated settlements of 5 to 10 cm as a result of the earthquake.

The authors concluded that:

- The placement of surcharge fills on the site led to a small increase in the factor of safety with respect to liquefaction, from 0.6 to 0.7;
- The presence of the wick drains did not relieve excess porewater pressures during shaking, but may have facilitated the dissipation of the excess porewater pressures and allowed more uniform settlement of the ground surface;
- The stiffness of the soil-cement columns changed the response of the site to the ground motion such that shear strains and the resulting excess porewater pressures were lower;
- The reinforcing effect of the soil-cement columns would have reduced settlement had excess porewater pressures been greater.

2.6 THE USE OF WASTE ROCK INCLUSIONS IN TAILINGS IMPOUNDMENTS

2.6.1 An Overview

The use of waste rock inclusions to control the effects of liquefaction in tailings deposits was proposed by Aubertin et al. (2002). It is analogous to the use of stone columns to control liquefaction and its effects in natural soils. Both concepts are of a saturated, finer grained material (sand or tailings) with a relatively low hydraulic conductivity that is penetrated by zones of a more permeable and stiffer material (gravel or waste rock) which provides much shorter drainage paths, and thus more rapid relief of excess porewater pressures generated during earthquakes. The inclusions (or columns) also provide reinforcement against deformation of the finer grained material, this characteristic is more important with silty soils (and tailings) where drainage may be ineffective during the rapid loading of earthquakes. Prefabricated vertical drains (wick drains) have been successfully used to accelerate the consolidation of fine tailings

(bauxite) with good results (Henderson et al., 2002). However, wick drains provide no reinforcement effect.

The design methods which have been established for stone columns assume that the columns are vertical, thus radial horizontal drainage from the surrounding soil is assumed. They also assume that the columns are installed into an existing soil layer with an established and relatively constant phreatic surface. These assumptions affect the analysis and design method for stone columns and will have to be carefully reviewed with respect to the use of waste rock inclusions in tailings which could be constructed prior to, during, or after tailings deposition.

As described earlier, Adalier et al. (2003) used large-scale, dynamic centrifuge testing to investigate the use of stone columns as a liquefaction countermeasure in nonplastic silt. It was found that stone columns were not effective at reducing the development of excess porewater pressures in silt during cyclic loading. However, the dynamic response of the silt was altered by the presence of the stone columns, resulting in reduced deformation and reduced excess porewater pressure development. Given that the hydraulic conductivity of tailings from hard rock mining are fairly similar to those of silts, the findings of this research are an indication of what could be expected from the use of waste rock inclusions in tailings.

Another very important effect of the use of waste rock inclusions would be the accelerated consolidation of the tailings and the strength gains and densification that are associated with consolidation.

Tailings deposits are known to be highly stratified (Aubertin et al., 2002) which may result in the creation of potentially destabilizing water inter-layers within soils under seismic loading. The presence of waste rock inclusions would provide an alternative and preferred place for the accumulation of excess porewater generated during earthquake

activity. The greater horizontal hydraulic conductivity of stratified deposits could enhance this effect.

Environmentally, the placement of potentially acid-generating waste work into tailings impoundments would eliminate generation of acid where the waste rock is submerged and contain any acid or metals generated within the impoundment, as well as eliminating the need for a separate disposal facility for acid generating waste rock.

2.6.2 Potential Placement Methods

The method proposed for the placement of waste rock within mine tailings impoundments is that the waste rock would be spread on the bottom and sides of the impoundment prior to the placement of tailings, particularly against the slopes of the dams or dikes forming the impoundment. This would create drained boundaries within the impoundment and reduce the development of excess porewater pressures against retaining structure(s) in the event of seismic activity. Then additional waste rock would be dumped along pre-designated routes within the impoundment to create inclusions of waste rock as shown on Figure 1-1. The tailings could then be deposited in the impoundment by slurry and the inclusions raised as necessary to keep them above the level of the tailings. When the tailings impoundment is full, it would consist of a deposit of tailings with inclusions of waste rock of a much higher shear strength, shear modulus and hydraulic conductivity.

The layout of the waste rock inclusions could be used to create cells within the impoundment that would limit the amount of material released in the event of a catastrophic failure of the impoundment.

In existing tailings impoundments where liquefaction and stability are of concern, the construction of waste rock columns in the tailings impoundment in proximity to the dams using the techniques conventionally used to install stone columns could be a practical and

cost-effective remediation alternative to strengthening of the impoundment. The most common technique consists of drilling a cased hole and filling the hole with gravel while withdrawing the casing. Waste rock columns could be installed in the impoundment and through dikes constructed of tailings to provide direct reinforcement.

2.6.3 Anticipated Effects

The potential effects of the use of waste rock inclusions in tailings deposits are summarized below:

- Accelerated consolidation resulting in accelerated strength gain and increased impoundment capacity;
- A decrease in the period during which the tailings would be under-consolidated and more vulnerable to liquefaction;
- Reduced excess porewater pressure development during earthquake loading and a reduced tendency for the development of water inter-lenses within the impoundment;
- Decreased deformation due to earthquake loading resulting in lower dynamic loading on the retaining structures;
- The creation of cells would limit the quantity of tailings (and wastewater) released in the event of catastrophic failure of the impoundment;
- The need for a separate facility for the disposal of waste rock could be reduced or eliminated; and
- The waste rock would be contained and could be covered to inhibit acid generation and metal leaching.

Potential drawbacks to the use of waste rock inclusions include:

- More planning would be required in layout of the tailings impoundment;
- Design criteria for the placement of the waste rock inclusions would have to be developed;
- The haul distances for the waste rock may be longer, depending on the location of the impoundment with respect to the shaft or pit and the location of a waste rock pile (if the waste rock were to be disposed of in the conventional manner); and
- In existing tailings impoundments, the installation of waste rock columns would require processing of the waste rock to a gradation suitable for the diameter of the columns and the construction method.

2.7 MODELING LIQUEFACTION AND ITS EFFECTS

2.7.1 Numerical Models of Liquefaction

2.7.1.1 General

In the past two decades or so, a number of constitutive equations (models) capable of simulating the dynamic response of cohesionless soils, including hysteretic deformation, excess porewater pressure generation, liquefaction, and post-liquefaction behavior have been developed. Many of these models have been verified to some extent by conventional dynamic laboratory testing (i.e. cyclic triaxial or cyclic simple shear) or advanced dynamic laboratory testing (i.e. large-scale shaking table or dynamic centrifuge testing).

Implementation and verification of the models in a software program is often done for a specific research project and can be very time consuming and difficult. For proprietary reasons, the specific requirements for integration of the models may not be released to the public. For example, although several papers have been written describing the Wang model (Wang et al., 1990, 2001, 2006; Wang & Makdisi, 1998), insufficient information

has been made available for its numerical implementation into the FLAC finite difference software program (to be described later). Notably, the specific requirements for implementation of the Finn (Martin et al. 1975), Byrne (Byrne, 1991) and UBC Sand (Puebla et al., 1997) models have been made available; the Finn and Byrne models have been incorporated into FLAC (Itasca, 2005).

Although the UBC Sand model has not yet been incorporated into FLAC, a user-defined subroutine of the model has been made available by Itasca Inc. and Professor Peter Byrne of the University of British Columbia. The UBC Sand model (Byrne et al., 1995, 2003, 2004; Puebla et al., 1997; Beatty & Byrne, 1998; Puebla, 1999; Park & Byrne, 2003) was selected for use on this research project and is described in detail in the following section. Examples of the operation of the model are presented in the references listed above.

Table 2-3 presents a list of some published models of soil liquefaction. The models have been evaluated through the use of laboratory testing or using information from case histories. The models range from relatively straightforward correlations between standard penetration testing and the development of porewater pressure under dynamic loading (e.g. the Finn and Byrne models) to relatively complex formulations based on theoretic models of soil behavior (e.g. the UBC Sand and Wang models). All of the models simulate the development of excess porewater pressure during dynamic loading. However, some of them stop there while others can simulate liquefaction and post-liquefaction behavior. The models must be integrated into finite element or finite difference programs to be implemented.

Implementation of the models is usually done for a specific project and can be extremely time consuming and difficult. For this reason, the specific requirements for integration of the models may not be released to the public. For example, although several papers have been written describing the Wang model, insufficient information has been made available for its integration into the FLAC finite difference software program (to be

described later). Notably, the specific requirements for implementation of the Finn, Byrne and UBC Sand models have been made available; the Finn and Byrne models are have been incorporated into FLAC (Itasca, 2005). Although the UBC Sand model has not yet been incorporated into FLAC, a user-defined subroutine of the model has been made available by Itasca Inc. and Professor Peter Byrne of the University of British Columbia.

Table 2-3 – Numerical models developed for liquefaction analysis.

Designation	**Reference(s)**	**Verification Methods**
Adrianopoulos	Adrianopoulos et al. (2006)	Dynamic centrifuge testing.
Arduino and Macari	Arduino & Macari (2001a, 2001b)	Dynamic centrifuge testing.
Byrne	Byrne (1991)	Empirical liquefaction observations.
Egan and Sangrey	Egan & Sangrey (1978)	Unspecified laboratory tests.
Finn	Martin et al. (1975)	Empirical observations.
Imam	Imam et al. (2005)	Cyclic triaxial compression and extension testing.
Papadimitriou	Papadimiitriou et al. (2001)	Cyclic shear testing.
Pastor-Zienkiewicz III	Adalier & Aydigun (2004); Aydigun and Adalier (2003)	Dynamic centrifuge testing.
UBC Sand	Byrne et al. (1995, 2003, 2004); Puebla et al. (1997); Beatty & Byrne (1998); Puebla (1999); Park & Byrne (2003)	Dynamic centrifuge testing, cyclic simple shear testing, and case histories.
Wang	Wang et al. (1990, 2006); Wang & Makdisi (1998); Wang et al. (2001)	Cyclic triaxial testing.
Yang and Ling	Yang & Ling (2005)	Dynamic centrifuge testing.

The UBC Sand model was selected for use on this research project and is described in detail in the following section.

2.7.2 The UBC Sand Model

The UBC Sand model (Byrne et al., 1995, 2003, 2004; Puebla et al., 1997; Beatty & Byrne, 1998; Puebla, 1999; Park & Byrne, 2003) was developed by Dr. Peter Byrne of the University of British Columbia and his collaborators. It is a fully coupled, elastic-plastic, effective stress model for simulating the static and dynamic behavior of sandy soils. Under dynamic loading the model has been shown to simulate the dynamic behavior (porewater pressure and strain development), liquefaction and post-liquefaction behavior of sand (Byrne et al., 2003). The UBC Sand model has been used to simulate and compliment centrifuge modeling and has been verified through conventional and large-scale dynamic laboratory testing and case histories (Puebla et al., 1997; Byrne & Seid-Karbasi, 2003; Byrne et al., 2003; Byrne et al., 2004; Wijewickreme et al., 2005a; Castillo et al., 2006).

The primary reasons for the selection of the UBC model for use on this project included:

- Its ability to simulate the important aspects of the dynamic behavior of cohesionless soils;
- The required soil parameters can be readily determined from in situ or laboratory testing;
- Some of the verification was done using the same cyclic simple shear devices used for the laboratory testing of this research; and
- Implementation of the model using existing software (FLAC) is fairly straight forward.

The equations and assumptions of the model and a discussion of its implementation into FLAC are presented in the following sub-sections.

2.7.2.1 Equations and Assumptions

UBC Sand is a fully coupled, two-dimensional constitutive model for soil behavior. The term "fully coupled" refers to the fact that the mechanical reaction of the soil skeleton, specifically the volumetric strain tendencies, interacts with the porewater pressure response on the basis of the time-step used in the simulation (Byrne et al., 2004). The model is an elasto-plastic effective stress formulation that assumes a hyperbolic relationship between the developed stress ratio (the shear stress divided by the mean effective stress) and the plastic volumetric shear strain.

The primary features of the UBC Sand model include (Beaty & Byrne, 1998):

Yield Surfaces – For each soil element, there is a yield surface defined by the sine of the mobilized friction angle (the ratio of the maximum shear stress to the mean effective stress) which cannot exceed the sine of the peak friction angle. The yield surface is a straight line emanating from the origin and rotates counter-clockwise about the origin as the mobilized friction angle increases. The mobilized friction angle is a function of the loading history, and the rate at which the yield surface rotates is a function of the hyperbolic hardening relationship.

The model assumes a second yield surface consisting of a vertical line at "relatively high confining stresses." However, this surface is not encountered under "typical" undrained stress paths.

Hardening of the Yield Surface – An assumed hyperbolic (power function) relationship between the stress ratio (the sine of the peak friction angle) and the plastic shear strain is used as the yield surface hardener. When an increment of positive plastic shear strain develops, the corresponding value of the plastic shear modulus is obtained from the hyperbolic curve, the existing stress ratio and the peak friction angle. The associated increase in the stress ratio is then computed and the yield surface rotates accordingly.

Combined Elasto-plastic Behavior – Both elastic and plastic behavior are contained in the hardening of the yield surface. The elastic portion is from small-strain linear elastic theory and the plastic portion is based on the hyperbolic relationship, with the plastic strain increment occurring in the direction of the principal shear stress. Overall, the plastic response dominates straining because the elastic response is much stiffer.

Flow Rule – The generation of excess porewater pressure is controlled by the plastic volumetric strain which is determined by a flow rule based on the hyperbolic relationship of the stress ratio with the plastic shear strain. The flow rule is based on these observations:

a) A constant volume friction angle, ϕ_{cv}, defines a stress ratio at which plastic shear strains do not cause plastic volumetric strains (this is analogous to the steady state condition);
b) Stress states below the stress ratio defined by the constant volume friction angle are contractive and those above are dilative; and
c) The maximum contraction or dilation is a function of the current stress ratio and the stress ratio defined by the constant volume friction angle.

The resulting equation is non-associative:

$$\Delta\varepsilon_v^p = (\sin\emptyset_{cv} - \sin\emptyset_d)\Delta\gamma^p = (\sin\psi)\Delta\gamma^p \quad (2\text{-}16)$$

where:

$\Delta\varepsilon_v^p$ is the plastic volumetric strain increment (contraction positive);

ϕ_{cv} is the constant volume friction angle;

ϕ_d is the developed friction angle;

$\Delta\gamma^p$ is the plastic shear strain increment; and

ψ is the dilation angle.

The elastic shear modulus, G^e, and the elastic bulk modulus, B^e, are assumed to be dependent on the mean effective stress, p', and equal to:

$$G^e = k_G^e P_A \left(\frac{p'}{P_A}\right)^{ne} \quad (2\text{-}17)$$

$$B^e = k_B^e P_A \left(\frac{p'}{P_A}\right)^{me} \quad (2\text{-}18)$$

where:

k_G^e is the elastic shear modulus number;

k_B^e is the elastic bulk modulus number;

P_A is atmospheric pressure in compatible units;

ne is the elastic shear modulus number; and

me is the elastic bulk modulus number.

Applicability to Drained, Undrained and Partially Drained Loading – The UBC Sand model operates on the level of the soil matrix and is thus well-suited for the simulation of drained conditions. Undrained and partially drained conditions can be simulated by including the volumetric stiffness (bulk modulus) of the porewater and using a combined mechanical-fluid flow analysis. Full interaction between plastic volumetric strains, porewater pressure and effective stresses is provided.

Dynamic Loading and Damping Considerations – Stress history is incorporated into the model along with recognition of loading, unloading and reloading phases associated with dynamic loading. A linear elastic behavior is assumed between loading and unloading

cycles; thus hysteric damping is not explicitly included. Damping is simulated by the inclusion of a "small viscous component" into the model.

Soil Anisotropy – Anisotropy may be included in the model by making the plastic shear modulus a function of the principal stress direction. However, rotation of the principal stress direction during dynamic simulations may cause rotation of the assumed direction of the anisotropy.

The primary equations of the UBC Sand model are presented below:

Elastic Response - The elastic response is assumed to be incremental linear and isotropic, and is specified by Hooke's law. The incremental elastic strains are related to the stress increments for plane strain by (Puebla et al., 1997):

$$\Delta\varepsilon_x^e = \left(\frac{1-v^2}{E}\right)\Delta\sigma'_x - \left(\frac{v(1+v)}{E}\right)\Delta\sigma'_y \tag{2-19}$$

$$\Delta\varepsilon_y^e = -\left(\frac{v(1+v)}{E}\right)\Delta\sigma'_x - \left(\frac{1-v^2}{E}\right)\Delta\sigma'_y \tag{2-20}$$

$$\Delta\varepsilon_{xy}^e = \frac{\Delta\gamma_{xy}}{2} = \frac{\Delta\tau_{xy}}{2G^e} \tag{2-21}$$

where:

E is Young's modulus;

v is Poisson's ratio;

G^e is the elastic shear modulus;

$\Delta\sigma$' is the effective stress increment;

$\Delta\varepsilon^e$ is the elastic strain increment; and

x and y are the subscripts in the Cartesian coordinate system.

Plastic Shear Response

Plastic shear strains are assumed to be caused by an increase in the stress ratio, Δn.

The developed stress ratio is:

$$n_d = \left(\frac{q}{p'}\right) = \sin\emptyset_d \tag{2-22}$$

where:

n_d is the developed stress ratio;

q is the maximum shear stress;

p' is the effective mean stress or effective confining stress; and

ϕ_d is the developed friction angle.

The incremental plastic shear strain, $\Delta\gamma^p$ is then expressed as:

$$\Delta\gamma^p = \left(\frac{1}{G^*}\right)\Delta n_d \tag{2-23}$$

where:

G* is the normalized plastic shear modulus (see below); and

Δn_d is the developed stress ratio increment.

The developed stress ratio increment is calculated as:

$$\Delta n_d = \left[\left(\frac{\Delta q}{p'}\right) - \left(\frac{q}{(p')^2}\right)\Delta p'\right] \tag{2-24}$$

where:

Δq is the shear stress increment; and

$\Delta p'$ is the mean effective stress increment.

The incremental plastic shear strain can thus be written as:

$$\Delta\gamma^p = \left(\frac{1}{G^*}\right)\left[\frac{\Delta q}{p'} - \left(\frac{n_d}{p'}\right)\Delta p'\right] \quad (2\text{-}25)$$

In the theoretical formulation, the normalized plastic shear modulus, G*, is calculated from:

$$G^* = k_G^p \left(\frac{p'}{P_A}\right)^{np-1}\left[1 - \left(\frac{n_d}{n_f}\right)R_F\right]^2 \quad (2\text{-}26)$$

where:

k_G^p is the plastic shear modulus number;

P_A is atmospheric pressure in the same units as G*;

n_p is the plastic shear modulus exponent;

n_f is the stress ratio at failure, $(q/p')_f = \sin\phi_f$, where ϕ_f is the peak friction angle; and

R_F is the failure ratio, n_f/n_{ult}, generally ranging from 0.5 to 1.0, where n_{ult} is the ultimate strength from the best fit hyperbola.

Plastic Shear-volume Coupling - The plastic volumetric strain increment, $\Delta\varepsilon_v^p$, is calculated using Equation 2-15.

The dilation angle, ψ, is a function of the constant volume friction angle and the developed friction angle:

$$\sin\psi = (\sin\emptyset_{cv} - \sin\emptyset_d) \quad (2\text{-}27)$$

Yield and Plastic Potential Functions - The plastic strain increments are obtained using:

$$\Delta\varepsilon_{ij}^{p} = \lambda\left(\frac{\partial g}{\partial\sigma'_{ij}}\right) \tag{2-28}$$

where λ is a constant of proportionality and is determined from plasticity theory.

The yield function, f, is defined as:

$$f = \sigma'_1 - \sigma'_3 N_{\emptyset} = 0 \tag{2-29}$$

where: $N_{\phi}=(1+\sin\phi_d)/(1-\sin\phi_d)=(1+n_d)/(1-n_d)$.

The plastic potential function, g, used in the flow rule is:

$$g = \sigma'_1 - \sigma'_3 N_{\varphi} = 0 \tag{2-30}$$

where: $N\varphi=(1+\sin\varphi)/(1-\sin\varphi)$.

Combined Response - The combined response of the elastic and plastic components is obtained using:

$$\{\Delta\sigma'\} = [D']\{\Delta\varepsilon\} \tag{2-31}$$

where:

$\{\Delta\sigma'\}$ is the vector of effective stress increments;

[D'] is the constitutive model matrix; and

$\{\Delta\varepsilon\}$ is the vector of total strain increments, $\{\Delta\varepsilon^e\} + \{\Delta\varepsilon^p\}$.

Coupled Response - The response of porewater in the soil matrix is included in the model through the fluid bulk modulus, B_f, which is approximately $2.2\text{x}10^9$ Pa at 20° C. The incremental porewater pressure, Δu, is calculated using:

$$\Delta u = \left(\frac{B_f}{n}\right) \Delta \varepsilon_v^f \tag{2-32}$$

where:

n is the porosity of the soil matrix; and

$\Delta\varepsilon_v^{\ f}$ is the equivalent fluid volumetric strain.

The term B_f/n is the stiffness of the equivalent fluid occupying total volume of the matrix rather than just the volume of voids. For volumetric compatibility, the volumetric strain of the equivalent fluid must be equal to the volumetric strain of the soil matrix (plus or minus any fluid flow from the soil matrix). In matrix form, the incremental porewater pressure is calculated using:

$$\{\Delta u\} = \left[D_f\right]\{\Delta \varepsilon\} \tag{2-33}$$

where:

$\left[D_f\right]$ is the equivalent fluid stiffness matrix; and

$\{\Delta\varepsilon\}$ is the vector of total strain increments.

The coupled stress-strain relationship is:

$$\{\Delta\sigma\} = \left[\ [D'] + \left[D_f\right]\right]\{\Delta\varepsilon\} \tag{2-34}$$

The model operates in total stress. However, as the incremental porewater pressure is calculated for each time-step, the model is a fully coupled effective stress system.

The model does not account for degrees of saturation, the material is assumed to be fully saturated or unsaturated in which case the stiffness of the porewater is neglected.

2.7.2.2 Implementation in FLAC

The UBC Sand model can be implemented in FLAC as a user-defined model (subprogram) in the FISH programming language included with FLAC or as a C++ subroutine compiled as a DLL file (dynamic linked library). In either case the model is loaded into FLAC as needed and executed in the same manner as the built-in models. FISH and DLL versions of the UBC Sand model for implementation in FLAC were provided by the Itasca Consulting Group (Itasca). These versions were developed from FISH models provided to Itasca by Dr. Byrne. The primary differences between the FISH and DLL versions of the model are that the FISH version may be readily customized by editing the text file while the DLL version cannot be customized. However, execution of FLAC with the DLL version is typically faster than with the FISH version. The numerical analysis completed for this research used the DLL version of the model.

The material properties required by the DLL version of model include:

a) The corrected standard penetration blow count, $(N_1)_{60}$, in blows per 0.3 m;
b) The constant volume friction angle, ψ, in degrees;
c) The anisotropic factor, f_{ani};
d) The total density, ρ_{TOTAL}, in Mg/m^3; and
e) The porosity, n.

The parameters $(N_1)_{60}$, ψ, and f_{ani} are specific to the UBC Sand model, while γ_{TOTAL}, k, and n are general FLAC material parameters used in the model. FLAC does not differentiate between saturated and unsaturated hydraulic conductivities, saturated values are provided and are used in all flow calculations. The initial location of the phreatic surface and the distributions of the effective and porewater pressures are obtained by execution of FLAC in “mechanical” and “groundwater” modes which model static and steady state seepage equilibrium conditions.

The elastic shear modulus number, k_G^e, and elastic bulk modulus number, k_B^e, are obtained from measured (or estimated) values of $(N_1)_{60}$ and calculated using the following formulas (Byrne, 2006):

$$k_G^e = 434 \cdot (N_1)_{60}^{0.333} \tag{2-35}$$

$$k_B^e = 0.7 \cdot k_G^e \tag{2-36}$$

The elastic shear modulus exponent, ne, and the elastic bulk modulus exponent, me, are both assumed to equal 0.5 (Byrne, 2006). Refer to Equations 2-16 and 2-17 for the elastic shear modulus and elastic bulk modulus, respectively.

The failure angle (peak friction angle), ϕ_f, in degrees is estimated from the constant volume friction angle, ϕ_{cv}, using:

$$\phi_f = \phi_{cv} + \frac{(N_1)_{60}}{10.0} \tag{2-37}$$

The constant volume friction angle may be obtained from laboratory testing and has been observed to vary from 30 to 33° for sandy soils (Puebla et al., 1997).

The plastic shear modulus number, k_G^P, is assumed to be a function of the elastic shear modulus number, k_G^e, and $(N_1)_{60}$:

$$k_G^P = 0.003 \cdot k_G^e \cdot (N_1)_{60}^2 + 100 \tag{2-38}$$

The plastic shear modulus is calculated through Equation 2-25.

The failure ratio, R_F, is a function of the penetration resistance:

$$R_F = 1.0 - (N_1)_{60}/100 \tag{2-39}$$

R_F is limited to a minimum value of 0.5 and a maximum value 0.99.

The anisotropy factor, F_{ani}, is estimated from $(N_1)_{60}$:

$$F_{ani} = 0.0166 \cdot (N_1)_{60} \quad (2\text{-}40)$$

The allowable values of the anisotropy factor vary from 0.333 for "loose pluviated" material to 1.0 for isotropic material.

As noted earlier, when the developed stress ratio, n_d, equals the stress ratio at failure, n_f, the soil is assumed to be in the steady state condition. The shear strength of the soil in the steady state condition, q_{ss}, is a function of the stress ratio at failure and the mean effective stress, p':

$$q_{ss} = n_f \cdot p' = \sin\emptyset_f \cdot p' \quad (2\text{-}41)$$

Due to the hyperbolic relationship between the stress ratio and the plastic shear strain, the rate of plastic strain development increases exponentially as the steady state condition is approached (refer to Equations 2-23 through 2-26).

2.7.3 Dynamic Numerical Modeling

A number of finite difference and finite element software packages developed (or updated) over the last few years are capable of simulating the dynamic response of earth structures, including liquefaction to some extent. These include:

- FLAC 4.0 (Itasca Consulting Group - Minneapolis, Minnesota, USA);
- Quake/W 2004 (Geo-Slope International – Calgary, Alberta, Canada);
- Plaxis V8 (Plaxis BV – Delft, The Netherlands); and
- DIANA-SWANDYNE II (University of Birmingham – Birmingham, UK).

FLAC (Fast Lagrangian Analysis of Continua) was selected for use in this research project due to its ability to implement the UBC Sand model discussed in the previous section. Furthermore, through user defined models and a relatively open architecture that

allows customization of many of the features, FLAC has the flexibility to be adapted to suit particular needs that may arise during the project.

FLAC was specifically developed for geotechnical engineering applications. In addition to containing intrinsic constitutive models, the operation of the program can readily be modified using a built-in programming language (FISH) and constitutive models can be added to FLAC as dynamic linked libraries (DLLs) from the developer's website database of constitutive models or created by the user. Other technical features of FLAC of interest with respect to this research project include (Itasca 2005):

- FLAC has two and three-dimensional capabilities;
- The ability to specify the statistical distribution or gradient of a property within the model (e.g. the density of a layer of tailings can be varied randomly (within defined limits) or as a factor of other properties, e.g. mean effective stress, to increase the realism of the model);
- The capability of modeling groundwater flow and porewater pressure distribution with interaction between the soil skeleton and the porewater;
- Earthquake loading can be specified using actual ground motion records;
- Hysteric damping can be used to realistically simulate the amplification and damping of ground motions traveling through the model.
- Absorbing or free-field boundary conditions may be specified to simulate the effect of an infinite or semi-infinite elastic medium around the model; and
- It can simulate the large strains associated with liquefaction prior to flow.

2.7.4 Examples of Dynamic Numerical Modeling Studies

There are many examples of the use of numerical models to evaluate the stability of embankment dams under seismic loading where liquefaction (or the generation of excess porewater pressure) is a factor. Most of the examples presented here are of conventional water retention dams, but some tailings dams are included as well:

- Mansouri et al. (1981) – "Dynamic Response and Liquefaction of Earth Dams";
- Mejia & Seed (1983) – "Comparison of 2-D and 3-D Dynamic Analyses of Earth Dams";
- Moriwaki et al. (1998) – "Seismic Deformation Analysis of the Upper San Fernando Dam Under the 1971 San Fernando Earthquake";
- Wieland & Malla (2002) – "Seismic Evaluation of a 117 m High Embankment Dam Resting on a Thick Soil Layer";
- Aydingun & Adalier (2003) – "Numerical analysis of seismically induced liquefaction in earth embankment foundations. Part I. Benchmark model" and
- Adalier & Aydigun (2003) – "Numerical analysis of seismically induced liquefaction in earth embankment foundations. Part II. Application of remedial measures";
- Byrne & Seid-Karbasi (2003) and Seid-Karbasi & Byrne (2004) – "Seismic Stability of Impoundments" and "Embankment Dams and Earthquakes;"
- Adalier & Sharp (2004) – "Embankment Dam on Liquefiable Foundation – Dynamic Behavior and Densification Remediation";
- Escuder et al. (2006) – "FLAC numerical models applied to safety assessment of dams";
- Feng et al. (2006) – "Dynamic response of the Li-yu-tan earth dam subjected to the 1999 Chi-Chi earthquake in Taiwan";

- Ma et al. (2006) – "Liquefaction analysis of a hydraulic fill earth dam";
- Piao et al. (2006) – "Earth Dam Liquefaction and Deformation Analyses Using Numerical Modeling";
- Castillo et al. (2006) – "Non-linear Dynamic Analysis of Heap Leach Pad Under High Phreatic Levels"; and
- Seid-Karbasi and Byrne (2007) – "Seismic Liquefaction, Lateral Spreading, and Flow Slides: A Numerical Investigation into Void Ratio Redistribution."

The studies by Mansouri et al. (1993), Moriwaki et al. (1998), Byrne & Seid-Karbasi (2003), Seid-Karbasi & Byrne (2004), Piao et al. (2006), and Castillo et al. (2006) are briefly summarized in Section 2.8.1.3.

2.8 EVALUATION OF THE STABILITY OF TAILINGS IMPOUNDMENTS

In evaluating the stability of tailings dams, the influence of the tailings behavior should be considered for three primary reasons: a) the tailings constitute a load on the dam and on the foundation materials; b) Many tailings dams are constructed partly or entirely from tailings (generally the coarser fraction), so there is no clear interface between the dam and the tailings; and c) deformation or failure of the dam could initiate a statically-induced liquefaction of the retained tailings resulting in increased load or overtopping of the dam. Therefore, this research project will consider the stability of tailings impoundments – i.e. the retention structure and the tailings.

Under static conditions, the stability of tailings impoundments can be evaluated using conventional geotechnical methods with respect to slope stability, foundation bearing capacity, internal erosion, settlement, surface erosion, etc.

The evaluation of the stability of tailings impoundments under seismic loading has closely followed developments in the evaluation of the stability of conventional water

retention embankment dams. However, the effects of the retained tailings have often been neglected in the evaluation of tailings impoundments.

2.8.1 The Pseudo-static Method

The primary method used in the evaluation of the seismic stability of embankment dams is the pseudo-static method, also known as the seismic coefficient method (Seed and Martin, 1966; Finn, 1993 & 1998; Kramer, 1996). This method consists of using conventional slope stability methods with the earthquake loading represented by a horizontal force applied to an assumed sliding mass and acting in the direction of the assumed failure. The horizontal force is a factor, k, of the weight of the sliding mass. Values of k, the seismic coefficient, typically range from 0.05 to 0.15 and are often based on government regulations, professional guidelines or regional practice. Some of recommendations for use of the pseudo-static method are summarized below:

- Seed (1979) recommend seismic coefficients varying from 0.10 to 0.15 with the magnitude of the expected earthquake and a minimum factor of safety of 1.15 with a maximum 15% reduction in material strengths;
- Hynes-Griffin & Franklin (1984) recommend a seismic coefficient equal to 0.5 of the estimated peak horizontal acceleration on bedrock with a factor of safety of at least 1.0 and a 20% reduction in material strengths; and
- Pyke (1991) suggested seismic coefficients varying from 0.05 for an earthquake magnitude of 6.5 to 0.30 for an earthquake magnitude of 8.25 and a minimum factor of safety of 1.0 with no reduction in material strengths.

The pseudo-static method is known to be a simplistic simulation of the very complex loading and response of embankment dams to earthquakes (Kramer, 1996). A review of dam failures by Seed (1979) found several cases where the dam has an acceptable factor

of safety with respect to pseudo-static analysis and nonetheless failed due to earthquake ground motion. These cases included a tailings dam in Japan.

The pseudo-static method provides an assumed factor of safety against failure. However, it does not describe the expected performance of the dam during earthquake ground motion. As described in Section 2.4.1, Ishihara (1984) successfully used the pseudo-static method in conjunction with assumed excess porewater pressures to analyze the stability of two tailings dams that failed as a result of liquefaction of the retained tailings. In the analyses, Ishihara (1984) back-calculated the pseudo-static coefficients. Using the methodologies described by Seed (1979), Hynes-Griffin & Franklin (1984) and Pyke (1991) above, the evaluation would have indicated adequate factors of safety.

The pseudo-static method was developed for screening level evaluation and its use is not recommended for materials subject to significant strength loss (i.e. liquefaction) during earthquake loading. As a screening level tool, the method is meant to provide an indication if further evaluation using more rigorous methods is required. However, in engineering practice, the results of the method are often considered to be definitive.

2.8.2 Deformation Analysis

Newmark (1965) and Makdisi & Seed (1977, 1978, 1979) developed methods of estimating the deformation of embankment dams based on an analogy between the sliding of a block on an inclined plane and the movement of the mass on an assumed failure surface in an embankment dam during earthquake ground motion. The basic approach of the Newmark method is to calculate a yield acceleration at which movement on the assumed failure surface is initiated. The deformation of the sliding mass is then estimated from relationships developed by Newmark (1965) or later researchers (Kramer, 1996). Beikae (1997) developed a computer program based on a 3-dimensional extension of the Newmark method and applied it to a tailings dam with reasonable results. The

tailings retained by the dam were assumed to be liquefied and represented by mass without shear strength (a fluid). The Makdisi & Seed method also requires calculation of a yield acceleration. However, the movement of the mass on the failure surface is calculated based on correlations developed from numerical analysis of dams using real and synthetic ground motion records.

There are several simplifying assumptions necessary in the use of these approaches. Nevertehless, they are based on the dynamic response of dams and have been found to reasonably predict the deformation of embankment dams in many cases (Kramer 1996). It is noted that these methods are not considered to be applicable to dams subjected to significant strength loss or porewater pressure development during seismic loading (Makdisi & Seed, 1977, 1978, 1979; Kramer, 1996).

2.8.3 Dynamic Numerical Analysis

The use of coupled dynamic numerical analysis to evaluate the dynamic behavior and stability of embankment dams and tailings dams has increased in the last few decades, but remains relatively uncommon compared to pseudo-static analysis. These types of analyses typically require the use of fairly complex finite difference or finite element programs capable of simulating the amplification and damping of earthquake ground motions, the coupled stress-strain response of the soil matrix and porewater and the deformation of the embankment with time.

There are several published examples of the use of numerical analysis to evaluate the dynamic behavior and stability of dams; a few are summarized below.

- Mansouri et al. (1983) used the Finn model in a finite element analysis of the Upper San Fernando Dam that failed due to the February 9, 1971 San Fernando (California) earthquake as a result of liquefaction within the dam.

The results of the analysis were in reasonable agreement with the actual behavior of the dam.

- Moriwaki et al. (1998) evaluated the dynamic response of the Upper San Fernando Dam as a result of the February 9, 1971 San Fernando (California) earthquake using FLAC 3.30 with a custom subroutine to model the development of excess porewater pressures and the degradation of the shear modulus during earthquake shaking. The results of the analysis were reasonable but somewhat larger than the deformations that occurred during the actual earthquake.

- Byrne & Seid-Karbasi (2003) and Seid-Karbasi & Byrne (2004) evaluated the failure of the Mochikoshi tailings dam (an upstream raised structure) in Japan due to the 1978 Izu-Ohshim-Kinkai earthquake using version 4.0 of FLAC. The UBC Sand model was used to simulate the behavior of the tailings. Possible remediation measures were also evaluated. The authors were able to model the dynamic performance of the dam, including site response, cyclic stress ratio generation, excess porewater pressure generation, deformation, and failure. The remedial measures studied include the placement of a buttress fill and the construction of a stabilizing column within the impoundment.

- Piao et al. (2006) used FLAC 4.0 to evaluate the seismic stability, including liquefaction and post-liquefaction responses, of a series of earth dams in the Pacific northwest of the US. It was found that the results of the FLAC analysis were in reasonable agreement with results from the Newmark (1965) method, the Makdisi & Seed (1977, 1978, 1979) method, and the SHAKE (Schnabel et al. 1972) site response computer program.

- Castillo et al. (2006) used FLAC 4.0 and the UBC Sand model to evaluate the stability of a heap leach pad with an elevated phreatic surface due to reduced hydraulic conductivity caused by ore degradation. The parameters of the UBC Sand model were obtained from cyclic direct simple shear testing of the material. Recorded ground motions from the region were modified to the intensities and frequency content expected at the site for the 50, 100 and 500-year earthquakes. The simulations of these events produced excess porewater pressure development and deformation, which were then used to determine whether a flow slide would occur. A few weeks after the analysis was completed, on June 13, 2005 the region was struck by the Tarapaca earthquake (moment magnitude 7.9). The results of the numerical analysis were evaluated with respect to the actual response of the heap leach pad to the Trapaca earthquake and found to be in good agreement.

2.9 REMARKS

Tailings from hard rock mining are a unique type of cohesionless granular with strength characteristics similar to those of sandy soils and deformation behavior similar to that of silt. The deposition of the tailings, typically by slurry, results in a relatively high void ratio wherein the voids are filled with water. All of these factors lend themselves to the creation of a deposit of a material that is particularly vulnerable to liquefaction as a result of seismic activity.

The historic record strongly indicates that tailings are highly vulnerable to liquefaction and that when they liquefy they can flow hundreds to thousands of meters downstream and cause considerable environmental and physical damage. It is important that effective and practical means of determining the liquefaction potential of existing and future tailings impoundments be evaluated and put into practice and that cost-effective means of controlling the liquefaction of impounded tailings be developed.

CHAPTER 3. GEOTECHNICAL STUDY OF A TAILINGS IMPOUNDMENT

3.1 INTRODUCTION

3.1.1 Purposes and Scope

The purpose of this geotechnical study was to evaluate the geotechnical conditions and stability of a representative hard rock tailings impoundment under static and seismic conditions using analytical methods. The results of this study are then compared to numerical analyses of liquefaction (Chapter 4) and of the seismic behavior of the tailings impoundment (Chapter 5).

This phase of the doctoral research included:

- Review of documents pertaining to the site;
- Field exploration (site reconnaissance, test pits and cone penetration testing);
- Conventional and dynamic laboratory testing;
- An evaluation of site and subsurface conditions;
- Level-ground liquefaction evaluation of the tailings based on the results of in situ testing and of laboratory testing; and
- Geotechnical evaluation of the static and dynamic stability of the impoundment using analytical methods.

The example used in this study is the tailings impoundment formed by Dike No. 1 at the Laronde Mine in Pressiac, Quebec. Where noted, some elements and parameters in this study were changed to be more typical of hard rock tailings impoundments and less site-specific. Therefore, the results and conclusions of this study may not be directly applicable to the impoundment at Laronde Mine and may differ from more site-specific studies.

3.1.2 The Laronde Mine

The Laronde Mine is located on Regional Highway 395 in the municipality of Pressiac, Quebec, approximately two kilometers north of Highway 117. It is approximately midway between the cities of Rouyn-Noranda and Val d'Or which lie to the west and east, respectively. The location the Laronde Mine (site) is shown on Figure 3-1.

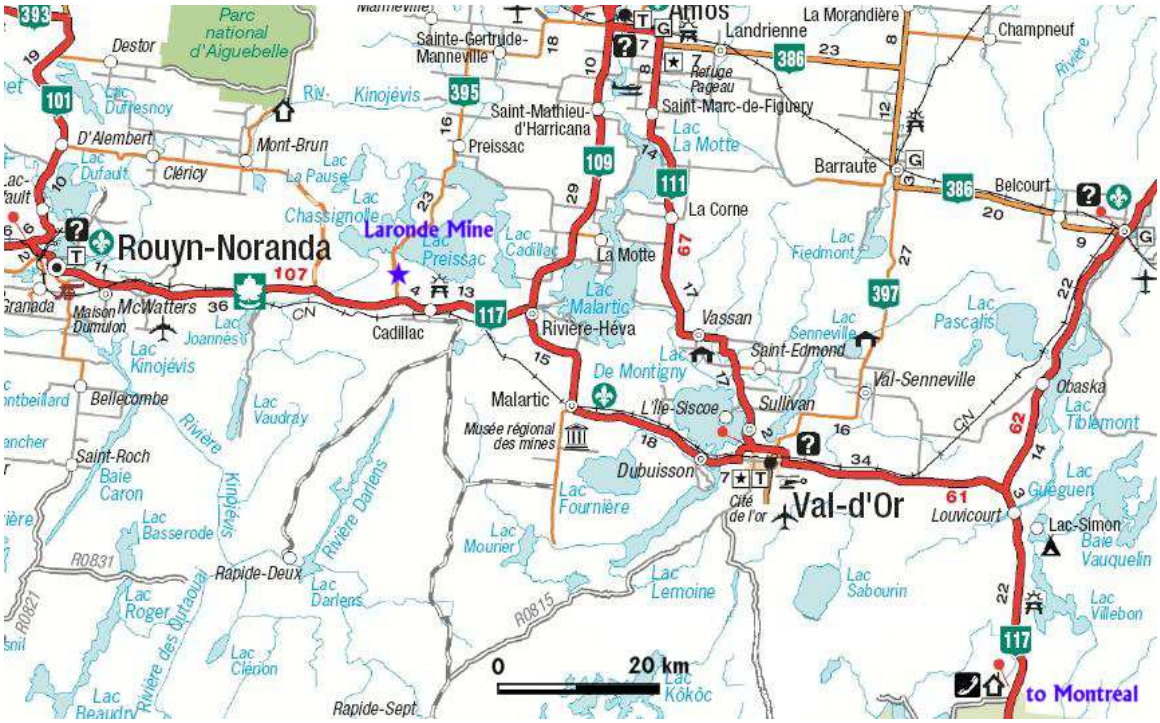

Figure 3-1 – Location of the Laronde Mine.

Production at Laronde Mine began in October 1988. By 2003 the mine had produced over 2 million ounces (56.8 tonnes) of gold, more than 9 million ounces (256 tonnes) of silver, 41,800 tonnes of copper, and 135,000 tonnes of zinc from 12,060,000 tonnes of ore mined (Gosselin, 2003). In total, approximately 177,000 tonnes of metal were processed from the ore resulting in a ratio of all metals to ore of roughly 0.015 and a ratio

of gold to ore of $5.0x10^{-6}$. In 2008, the mine is expected to produce 215,891 ounces (6.12 tonnes) of gold from the extraction of an estimated 2,635,000 tonnes of ore (Agnico-Eagle, 2008).

Mining activities at the site produce both waste rock and tailings from the processing of the mineral bearing rock to extract economically viable minerals. The processing methods used at Laronde produce tailings slurry where the solid particles are colloid to sand-sized particles of the parent rock. The tailings slurry from hard rock mines typically contains about 30% solids by weight (Vick, 1990; Aubertin et al., 2002). The fluid in the slurry is water containing various chemical agents used in the processing or leached from the parent rock. All of the waste rock and tailings produced from the mine to-date have been disposed of on-site. The waste rock is either stockpiled or used for the construction of roads and containment dikes. The tailings are used to make paste backfill for underground openings or placed in an impoundment, with the majority being impounded. Other impoundments at the site are used for the storage or processing of wastewater. The principal facilities at the Laronde Mine are shown on Figure 3-2.

The estimated in-place volume of tailings produced by the mine as of 2003 was $4.25x10^6$ m^3 and assuming 25% of the mineral deposits at the site were exploited and the mineral to ore ratio is relatively constant, the mine will produce an additional $12.75x10^6$ m^3 of tailings during its remaining lifespan. The in-place volume of the tailings was estimated assuming that the void ratios of the intact ore and in-place tailings are 0 and 0.6, respectively.

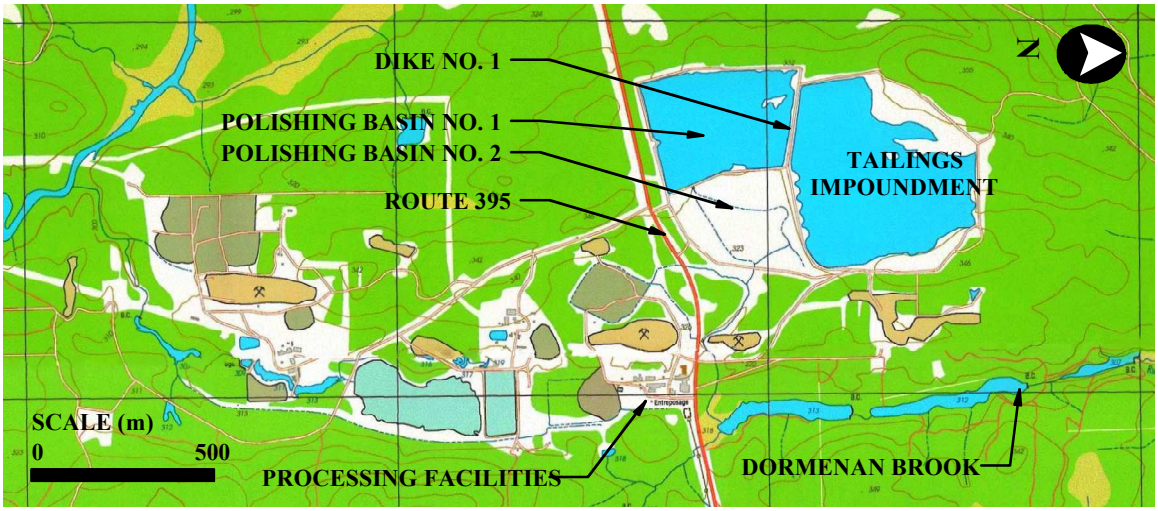

Figure 3-2 – Plan view of the Laronde Mine facility -
from maps 32D08-200-0101 and 32D08-200-0201 (MRN, 2000)

3.1.3 Previous Studies

In 2002, Golder Associés Ltée. conducted a geotechnical study at the site for the raising of Dike No. 1. A report on the study (Golder, 2002) was provided to the Industrial NSERC Polytechnique-UQAT Chair on Environment and Mine Wastes Management for use on this project, with the consent of Agnico Eagle Ltd. Applicable information from this study has been included in this study.

3.2 Document Review

As a part of the geotechnical study, documents containing relevant information on surface and subsurface conditions, the construction of the impoundment, the topography of the project area before and after construction of the impoundment, and local and regional geology and seismicity were reviewed. These documents included:

- Plans for raising of the dike;
- Daily reports (including photographs) from the first and second raisings of the dike;

- Topographic maps of the site and surrounding area;
- Aerial photographs; and
- Geologic maps and reports.

Information from these documents has been incorporated into this geotechnical study.

3.3 GEOLOGIC CONDITIONS

3.3.1 Local Geology

Geologic conditions in the vicinity of the Laronde Mine consist of three east-west trending lithographic units that dip steeply to the south so as to be nearly vertical. From north to south the units are: the Kewagama group, the Blake River group and the Cadillac group. The Kewagama group is a 400-meter-thick formation of interbedded wacke. The Blake River group is a 1,600-meter-thick formation of volcanic rocks which contains all of the known economically viable deposits at the mine. The Cadillac group is a 600-meter-thick formation of wacke interbedded with pelitic schist and a minor iron formation (Gosselin, 2003).

3.3.2 Regional Seismicity

Historically, the Abitibi-Temiscamingue region has experienced one significant earthquake, the moment magnitude 6.2 Temiscamingue earthquake of 1935 (NRC, 2008). Earthquakes in the region typically occur on the fault zones that divide it into blocks (MRN, 1994). The closest known fault zone to the site is the Cadillac-Larder fault zone, approximately 22 km to the south-southwest (SIGEOM, 2000). However, it is not known if the this fault is considered active.

3.3.3 Site Seismicity

The site lies in the Western Quebec Seismic zone. This zone has experienced three significant earthquakes in the historic record (NRC, 2008):

- The 1732 Montreal earthquake (M_w=5.8);

- The 1935 Temiscamingue earthquake (M_w=6.2); and
- The 1944 Cornwall-Massena earthquake (M_w=5.6).

Seismic hazard calculations for the site were obtained from NRC (2008). The calculations provided the peak horizontal ground acceleration (PGA) on class "C" soil which is defined as soil with a shear wave velocity between 360 and 760 m/s (NRCC, 2005). Adams & Halchuk (2003) recommend dividing the PGA values by a reference ground condition (rgc) factor of 1.39 to estimate the PGA values on "hard rock" which is defined as rock with a shear wave velocity greater than 1,500 m/s (NRCC, 2005).

In the "Robust" or "R" model of the seismicity of Canada (Adams & Halchuk, 2003), the site lies in the Cochran (COC) source zone and within 50 km of the Iapetan Rift Background (IRB) source zone. Using the method of Weichert (Weichert, 1980; ACRES, 1990; Kramer, 1996), the parameters given for these source zones were used to estimate the moment magnitudes of the earthquakes associated with various recurrence intervals. The calculations are shown in Appendix E. Recurrence intervals of up to 10,000 years were selected to match the intervals recommended by the Canadian Dam Association (2007).

The earthquake loadings (PGA and moment magnitude) associated with various recurrence intervals at the site are presented on Table 3-1.

The PGA values on hard rock for the site are relatively low, varying from 0.014g to 0.151g with magnitudes varying from 5 to 6.75. As noted in Section 2.2.3, PGA values of less than 0.10g are unlikely to produce liquefaction except in highly susceptible materials subjected to large magnitude earthquakes.

Table 3-1 – Estimated earthquake loadings for various recurrence intervals.

Recurrence Interval (Years)	Annual Probability (%)	PGA on Class "C" Soil (g)	PGA on "Hard Rock" (g)	Moment Magnitude, M_w
100	1.00	0.020	0.014	5
475	0.21	0.047	0.034	5.75
1,000	0.10	0.067	0.048	6.25
2,475	0.0404	0.101	0.073	6.5
5,000	0.02	0.146	0.105	6.75
10,000	0.01	0.210	0.151	6.75

3.4 FIELD EXPLORATION

The field exploration consisted of reconnaissance of the site, the excavation of test pits in the tailings deposit, and cone penetration testing of the tailings deposit.

3.4.1 Site Reconnaissance

Reconnaissance of the site was conducted by the author on June 8 through 10, 2004 and November 16 through 20, 2004. The purpose of the reconnaissance was to observe and note surface features which could have an impact on the condition and behavior of the tailings deposit or which might be indicative of the characteristics of the tailings. Observations made during site reconnaissance have been incorporated into Section 3.6.1 of this report.

3.4.2 Test Pits

Test pits were manually excavated to depths of 0.6 to 1.0 meters at four locations along the tailings beach of the impoundment on June 9 and 10, 2004. The locations of the test pits are shown on Drawing No. 2 (Appendix I). The purpose of the test pits was to obtain bulk samples of the tailings for laboratory testing and visually determine the degree of layering and segregation within the tailings. As encountered in the test pits, the tailings

appeared to be relatively homogeneous and classified in the field as silty sand (SM-ML), loose to medium-dense, moist, slightly mottled grey-brown and yellow-brown, non-plastic, with occasional small clayey pockets. The clayey pockets were less than 20 cm in size and a total of three were encountered in two of the four test pits.

At each test pit, the tailings were shoveled into a 150-liter HDPE barrel that had been filled halfway with water. When the barrels were nearly full, the tailings and water were mixed using a shovel. Within 30 minutes or so of mixing, the tailings would settle and the water would be clear. The water was then carefully removed from the barrels by bailing and siphoning. Additional water was added to the barrels and the mixing process was repeated twice more for each barrel. The barrels were then sealed, labeled and transported to École Polytechnique in Montreal.

No visible layering or segregation was observed in the test pit excavations.

It should be noted that the tests pits were all located on the tailings beach downstream (east) of the berm. Placement further into the impoundment was not possible due to the softness of the surface.

3.4.3 Cone Penetration Testing

Cone penetration testing was conducted within the impoundment on November 20, 2004. Testing was completed by the IRNS (*Institut National de la Recherche Scientifique)* under contract to École Polytechnique. Eleven (11) cone penetration tests (CPTs) were conducted to depths varying from 2.42 to 8.95 meters below the surface of the tailings. The objective of the testing was to obtain geotechnical information for the characterization of subsurface conditions, including the depth of the impoundment, layering and the characteristics of the tailings.

The CPTs were designated S1 through S11 and were located on both sides of the berm located on the tailings impoundment. CPTs S1 through S8 were located between Dike No. 1 and the berm. CPTs S9, S10 and S11 were located within the area of the

impoundment enclosed by the berm as far into the impoundment as the rig could safely venture due to the softness of the tailings. At these locations, the rig was supported on wooden pallets to prevent it from sinking into the tailings. The locations of the CPTs are shown on Drawing No. 2 (Appendix I). The approximate locations, surface elevations and depths of the cone testing completed for this study and for a previous study at the site by Golder Associes (2002) are given in Table 3-2.

Testing was accomplished using a cone system mounted on a Geotech 605D tracked rig. The cone had a tip diameter of 3.6 cm (an ASTM standard area of 10 cm^2), a sleeve length of 15 cm, and was attached to a digital data acquisition system. Sensors in the cone measured the tip resistance, sleeve friction, and porewater pressure during penetration. The cone was advanced using 1-meter-long, 3.6-cm-diameter aluminum rods through which the data acquisition system cables were threaded. The operation of the CPT rig is shown on Figures 3-3 and 3-4 and the cone is shown on Figure 3-5

All of the CPTs were advanced to refusal (when the load on the cone was sufficient to lift the front of the rig off of the surface of the tailings). A screw anchor mounted on the front of the CPT-rig to increase the load capacity on the cone was ineffective in the loose tailings.

The advance of the cone tip was controlled manually by the operator and varied between 1.5 and 3.0 cm/s. The ASTM standard is 2.0 cm/s. The advance of the cone was paused for 30 to 90 seconds at 1-meter intervals to allow additional segments of rod to be added. The data acquisition system took readings of the tip resistance, sleeve friction, and porewater pressures at regular intervals in time that correspond to 0.02 to 0.03-meter intervals of depth. Logs of cone penetration testing completed for this study and for a previous study by Golder Associes are presented in Appendix B.

Six dissipation tests were conducted during the cone penetration testing in 2004. However, due to an equipment malfunction the test results are unusable.

Figure 3-3 - Operation of the CPT rig on the impoundment.

Figure 3-4 - Operation of the CPT rig.

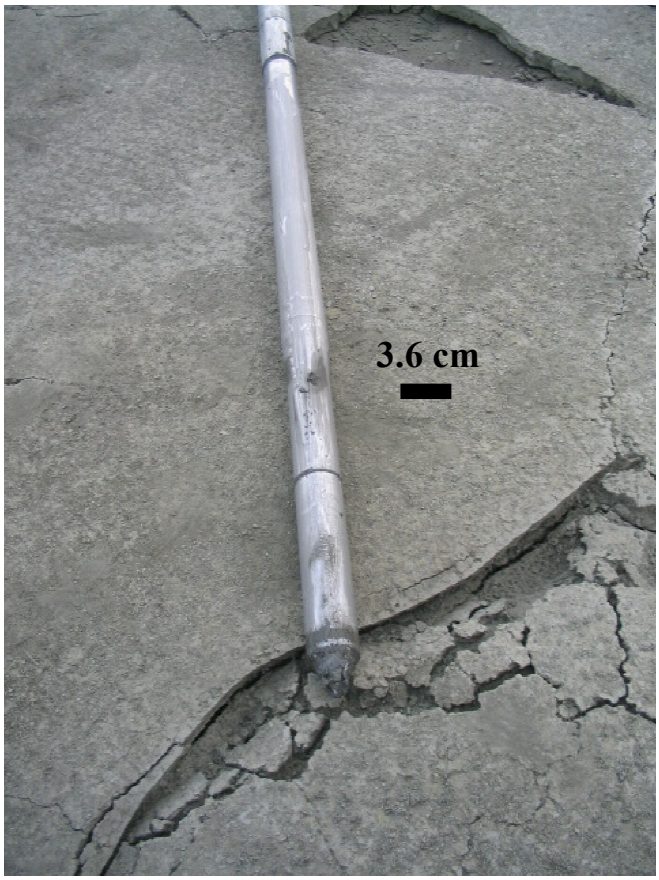

Figure 3-5 - Close up of the cone on the tailings.

3.4.4 Logs of Boreholes

Appendix C contains log of boreholes completed at the site by Golder Associes for a previous study at the site. The locations of these boreholes are shown on Drawing No. 2 in Appendix I.

Table 3-2 – Cone penetration test locations.

CPT Designation	Approximate Location	Surface Elevation (m)	Depth (m)
Polytechnique/INRS (2004)			
S1	Sta. 1+900, 22 m north of center-line of Dike No. 1.	342.2	8.95
S2	Sta. 1+700, 55 m northeast of center-line of Dike No. 1.	342.4	7.51
S3	Sta. 1+500, 25 m east of center-line of Dike No. 1.	342.2	7.55
S4	Sta. 1+300, 26 m east of center-line of Dike No. 1.	342.3	6.47
S5	Sta. 1+100, 25 m east of center-line of Dike No. 1.	342.4	7.21
S6	Sta. 0+900, 25 m east of center-line of Dike No. 1.	342.2	7.81
S7	Sta. 0+700, 22 m southeast of center-line of Dike No. 1.	342.4	4.63
S8	Sta. 0+550, 12 m south of center-line of Dike No. 1.	342.6	2.42
S9	Sta. 1+200, 65 m east of center-line of Dike No. 1.	342.6	5.22
S10	Sta. 1+400, 71 m east of center-line of Dike No. 1.	342.0	5.14
S11	Sta. 1+300, 71 m east of center-line of Dike No. 1.	342.1	7.71
Golder Associes (2002)			
02-02	Sta. 0+900, 70 m east of center-line of Dike No. 1.	338.5	13.65
02-03	Sta. 1+300, 60 m east of center-line of Dike No. 1.	338.6	11.63
02-04	Sta. 1+800, 40 m northeast of center-line of Dike No. 1.	339.1	10.55

3.5 LABORATORY TESTING

Laboratory testing was conducted on samples of the tailings retrieved during the field exploration. Testing consisted of specific gravity measurements, grain size analyses, one-dimensional consolidation measurements, direct shear testing, and cyclic direct simple shear testing. Results of petrographic analysis of the tailings were provided by another researcher. The following sections present descriptions of the laboratory testing and summaries of test results. Details of the laboratory testing are contained in Appendix D. Derivation of the properties of the tailings based on the laboratory results are presented in Section 3.7.1.

Specific gravity (relative density in Canadian Geotechnical Society nomenclature) and grain size analyses were conducted in the mining laboratory at Ecole Polytechnique, Montreal. Consolidation, direct shear and cyclic simple shear testing were conducted at the University of British Columbia's mining and civil engineering laboratories. All laboratory testing was conducted by the author, except where noted otherwise.

3.5.1 Petrographic Analysis

Petrographic analysis of a sample of tailings the Laronde Mine was provided by Mr. Bassam El Husseini, Ph.D. of McGill University. Testing was conducted on a bulk sample retrieved from the ore processing facilities at Laronde Mine in April 2005.

The analysis indicates that the sample was composed of 60% pyrite, 35% quartz, and 5% muscovite/sericite, by volume, with trace amounts of several other minerals. The pyrite consisted of 15μm to 0.3mm size broken, angular fragments. The quartz also consisted of broken, angular fragments varying from 15μm to 0.3mm in size. Muscovite was encountered as aggregates and as single grains varying from 20μm to 0.3mm in size. Sericite existed in the tailings as aggregates.

The composition of the tailings in the impoundment may vary somewhat from that of the sample analyzed due to natural variation in the composition of the parent rock.

The detailed petrographic analysis is presented in Appendix D.

3.5.2 Specific Gravity

The specific gravity of the tailings was measured using ASTM Standard Test Method No. C128-04a "*Standard Test Method for Density, Relative Density (Specific Gravity), and Absorption of Fine Aggregate."* Testing was completed by Hubert Guimont, a graduate student at Ecole Polytechnique.

Specific gravity measurements of the tailings samples results are shown in Table 3-3. The average and standard deviation of the test series are 3.881 and 0.275, respectively.

Table 3-3 – Specific gravity measurements.

Sample No.	1st Measurement	2nd Measurement	3rd Measurement	Average
1	3.881	3.925	3.882	3.896
2	4.251	4.257	4.262	4.257
3	3.733	3.765	3.762	3.753
4	3.607	3.621	3.628	3.619

3.5.3 Grain Size Distribution

The grain size distributions of four bulk samples of the tailings taken from the test pits were evaluated by Hubert Guimont of Ecole Polytechnique following the procedures of ASTM Standard Test Method No. D422-63(2002) "*Standard Test Method for Particle-Size Analysis of Soils*." The results are shown on Figure 3-6 and summarized on Table 3-4.

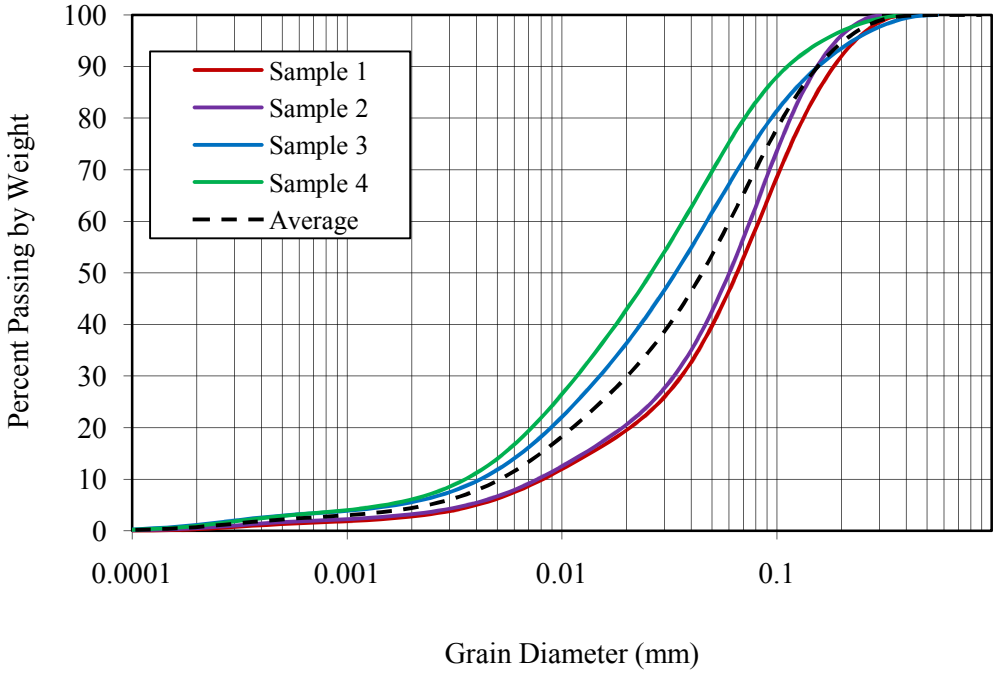

Figure 3-6 - Gradation of the tailings samples.

Table 3-4 – Gradation parameters of the tailings samples.

Sample No.	D_{10} (mm)	D_{30} (mm)	D_{50} (mm)	D_{60} (mm)	D_{95} (mm)
1	0.0082	0.0360	0.065	0.0826	0.24
2	0.0077	0.0332	0.060	0.0751	0.19
3	0.0042	0.0150	0.035	0.0473	0.22
4	0.0036	0.0117	0.025	0.0366	0.16
Averages	0.0059	0.0240	0.046	0.0604	0.20

3.5.4 Consolidation

A consolidation test was conducted on a composite sample of the tailings from the four test pits. Testing conformed to ASTM Standard No. D2435-04 "*Standard Test Methods for One-Dimensional Consolidation Properties of Soils Using Incremental Loading*"

except for sample preparation. The sample was prepared by combining oven-dried tailings with water to form a slurry with at a water content (ratio of the weight of water to the weight of solids) of approximately 27.5% (a void ratio of 1.07). It was found that tailings slurries prepared at this water content could be readily poured into a sample mold without visible segregation of the particles that occurred at higher water contents.

The consolidation testing device was inadvertently disturbed (bumped) during the second load increment, when the sample was being consolidated under a vertical stress of 48 kPa. The disturbance affected the degree of consolidation and time rate of consolidation during the second load increment and the time rate of consolidation during the third load increment. Otherwise the test results appear to have been unaffected by the disturbance.

The results of consolidation testing are shown on Figure 3-7. Based on these results, the compression index, C_c, is estimated to be 0.08 and the recompression index, C_r, is estimated to be approximately 0, indicating no significant rebound due to unloading. The average coefficient of consolidation, c_v, was 1.81×10^{-4} cm^2/s. This value is in the lower part of the ranges given for silt and clay of low plasticity by Holtz & Kovacs (1981).

In the reduction of laboratory test results, the specific gravity of the tailings was assumed to be 3.88, the average measured value.

Detailed consolidation test results can be found in Appendix D.

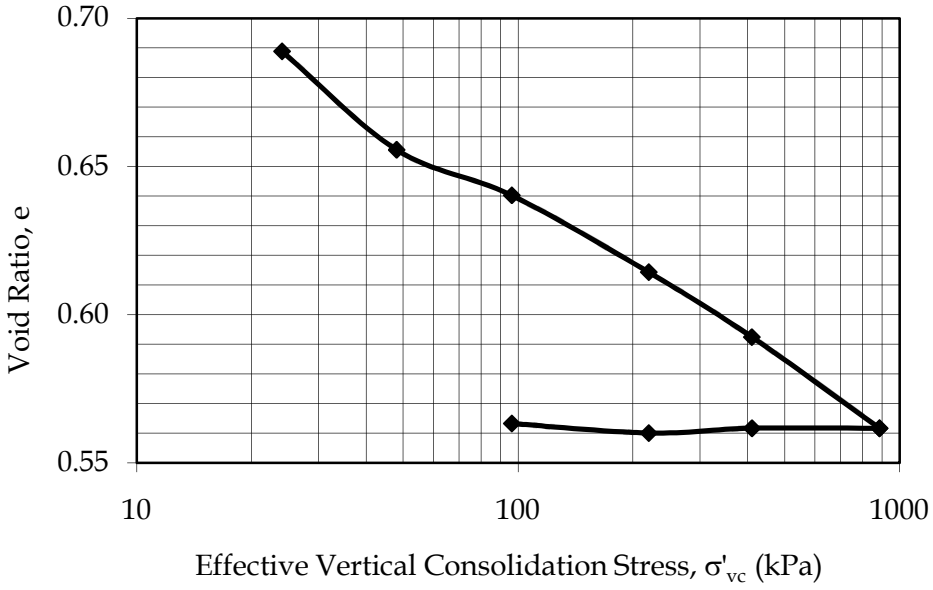

Figure 3-7 - Results of consolidation testing.

3.5.5 Direct Shear Testing

A total of five direct shear tests were conducted on composite samples of the tailings from the test pits. Testing was completed in accordance with ASTM Standard No. D 3080-98 "*Standard Test Method for Direct Shear Test of Soils Under Consolidated Drained Conditions*." The samples were prepared as slurries with water contents of approximately 27.5% and then consolidated under vertical confining stresses varying from 50 to 300 kPa. These stress levels are similar to those expected within the impoundment. A strain rate of 2.54 mm/minute was used due to the low permeability of the tailings as indicated by their grain size characteristics.

Direct shear test results are summarized on Table 3-5 and detailed test results are presented in Appendix D. The test results shown in Table 3-5 are all with respect to 5 mm of shear displacement. As shown on Figure 3-8, all of the samples reached a maximum level of shear stress at a shear displacement of 5 mm or less.

Table 3-5 – Summary of direct shear test results.

Test No.	Effective Vertical Consolidation Stress, $\sigma'_{v,c}$ (kPa)	Void Ratio at end of consolidation, e_c	Maximum Shear Stress τ_{max} (kPa)	Effective Angle of Internal Friction, ϕ'
DS01	103.19	0.701	74.03	35.7º
DS02	199.56	0.581	153.02	37.5º
DS03	299.28	0.641	204.44	34.3º
DS04	54.97	0.723	43.37	38.3º
DS05	103.19	0.683	78.37	37.2º

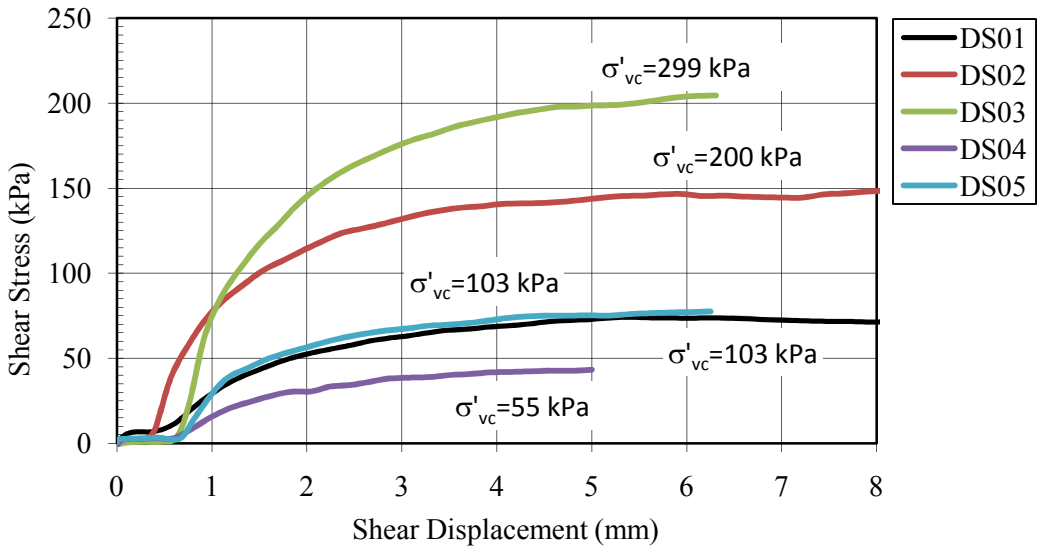

Figure 3-8 – Shear displacement vs. shear stress curves from direct shear testing (effective vertical consolidation stresses, σ'_{vc}, as shown).

The average effective angle of internal friction, ϕ'. from direct shear testing is 36.6º for the five tests. This is shown graphically on Figure 3-9. From the figure it appears that the effective angle of internal friction may decrease slightly with effective consolidation stress.

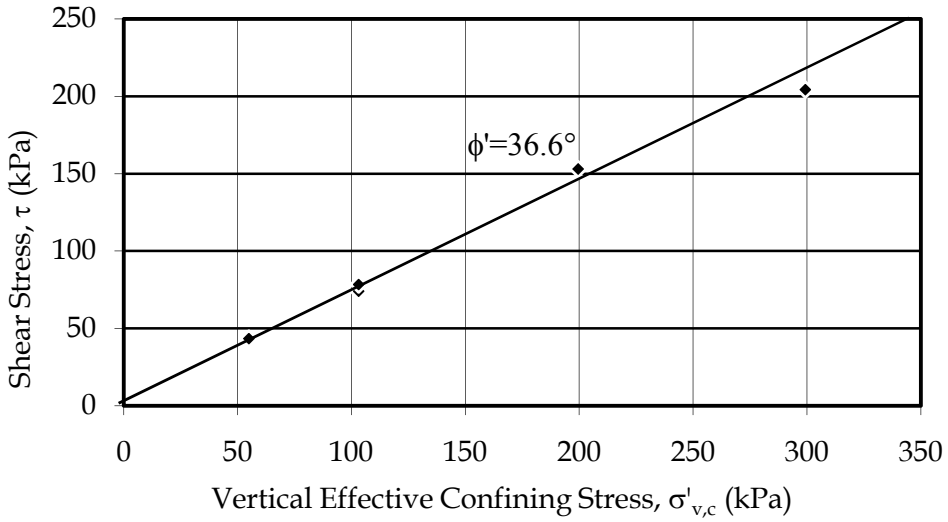

Figure 3-9 – Interpretation of effective angle of internal friction from direct shear test results.

3.5.6 Cyclic Direct Simple Shear Testing

Cyclic direct simple shear testing (CDSS) of reconstituted tailings samples from the test pits was conducted at the University of British Columbia (UBC). Testing was conducted by Lalinda Weerasekara (a Master's student at UBC) and the author under the supervision of Professor Dharma Wijewickreme of UBC.

Testing was conducted using an automated NGI-type cyclic direct simple shear device with a specimen size of about 70 mm in diameter and 20 to 25 mm in height.

Tailings samples were prepared from oven-tried tailings mixed with water to form slurries with water contents of about 27.5% (a void ratio of approximately 1.07), poured into the sample mold and consolidated to effective vertical stresses varying from 100 kPa to 400 kPa prior to cyclic testing. Based on the average dry unit weight estimated within the impoundment (23.2 kN/m^3), this range of effective vertical stresses corresponds to depths of 5.7 to 22.9 m in a normally consolidated tailings deposit with the phreatic level at the surface of the tailings.

During cyclic loading, near-constant volume conditions were maintained by locking the top and bottom platens against vertical displacement and a steel wire-reinforced latex membrane that prevented radial strain. The sample was allowed access to water through porous stones on the top and bottom platens during the consolidation and cyclic loading phases. Finn et al. (1978) and Dyvik et al. (1987) demonstrated that the change in vertical effective stress during cyclic loading in near-constant volume (drained) cyclic direct simple shear is equivalent to the porewater pressure development in undrained cyclic testing. Instrumentation attached to the device measured the effective vertical stress and shear strain continuously during testing. The porewater pressure was not measured, it was inferred from the change in the effective vertical stress during data processing which was done using a proprietary software program.

Cyclic loading of the samples consisted of unidirectional, symmetrical, sinusoidal shear waves with a frequency of 0.1 Hz and amplitudes equivalent to constant cyclic stress ratios, CSR ($CSR = \tau_{CYC} / \sigma'_{VC}$, where τ_{CYC} is the applied cyclic shear stress and σ'_{vc} is the effective vertical consolidation stress) varying between 0.075 and 0.15.

For the cyclic direct simple shear testing, liquefaction was defined as the reduction in the vertical effective stress to zero or the development of 3.75% shear strain, γ, in the sample. Post-cyclic testing was conducted on five samples and consisted of undrained, monotonic shear testing at a shear strain rate of 10% per hour to a maximum shear strain of 25%.

A shear strain of 3.75% was assumed to be the initiation of liquefaction as per NRC (1985), which recommends 2.5% shear strain in cyclic triaxial testing as the point for "triggering of liquefaction." In cyclic direct simple shear testing, 3.75% shear strain is considered to be equivalent to 2.5% shear strain in cyclic triaxial testing (Wijewickreme et al., 2005a). The point for "triggering of liquefaction" is analogous to the steady state condition as discussed by Castro (1975) and Kramer (1996) as described in Section 2.3.3.

The test results are shown on Figure 3-10 and summarized in Tables 3.6 and 3.7 for the cyclic and post-cyclic test results, respectively. Detailed test results are contained in Appendix D.

All of the samples developed 3.75% shear strain prior to the development of porewater pressure ratios of 1.0. However, testing was continued until the porewater pressure ratios reached 1.0. The development of excess porewater pressures in the samples during cyclic loading was relatively uniform. Liquefaction as defined by the development of shear strains in excess of 3.75% occurred within 2 to 85 load cycles with the number of load cycles required for reach this shear strain level increased with decreasing cyclic stress ratio.

The CDSS test results are presented on Figure 3-11 along the with CDSS results on "Fraser River" sand by Sriskandakumar (2004) and Sivathayalan (1994) using the same testing equipment. As tested, the Fraser River sand had a D_{50} of 0.30 mm, a maximum grain size of 0.6 mm, less than 1% non-plastic fines by weight, and a specific gravity of 2.72 (Sivathayalan, 1994). The data from Sivathayalan (1994) is from samples that were water pluviated, tapped with a rubber mallet and consolidated at an effective vertical stress of 100 kPa resulting in an average void ratio of 0.812 (a relative density, or density index, of 40%). The samples used by Sriskandakumar (2004) were prepared by air pluviation (and tapped with a rubber mallet) and consolidated at an effective confining stress of 100 kPa resulting in the same average void ratio as the water pluviated samples. At the consolidation stress levels used in the testing of the tailings, the cyclic resistance

of the tailings was higher than that of the air pluviated Fraser River sand and lower than that of the water pluviated Fraser River sand. As shown on Figure 3-11, the tailings tested for this research and the soils tested by Sriskandakumar (2004) and Sivathayalan (1994) exhibited similar tendencies with respect to the increase in number of cycles to liquefaction with decreasing cyclic stress ratio.

Cyclic testing of the Fraser River sand conducted at effective confining stresses varying from 50 to 400 kPa indicated that the effective consolidation stress had a significant impact on the cyclic resistance. At corresponding void ratios, the cyclic resistance of the sand decreased significantly with increasing effective consolidation stress Sivathayalan (1994).

An important conclusion that can be drawn from the test results is that for a given cyclic stress ratio, the liquefaction resistance of the tailings was not significantly affected by the effective consolidation stress. This is attributed to the predominance of silt-sized material within the tailings and the resulting particle interaction within the tailings as described by Polito & Martin (2001) and discussed in Section 2.2.4.

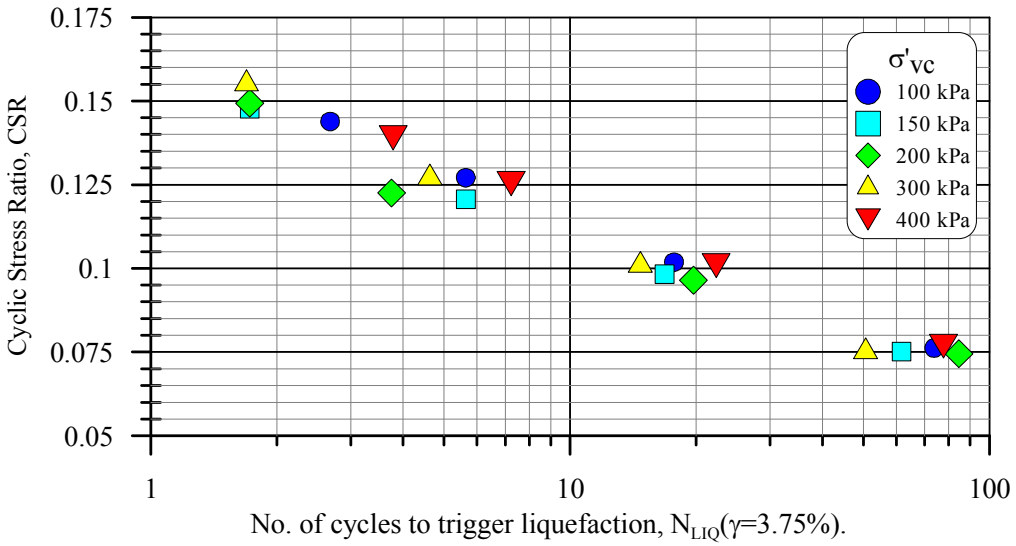

Figure 3-10 - Summary of cyclic direct dimple shear test results - liquefaction defined by a shear strain of 3.75%.

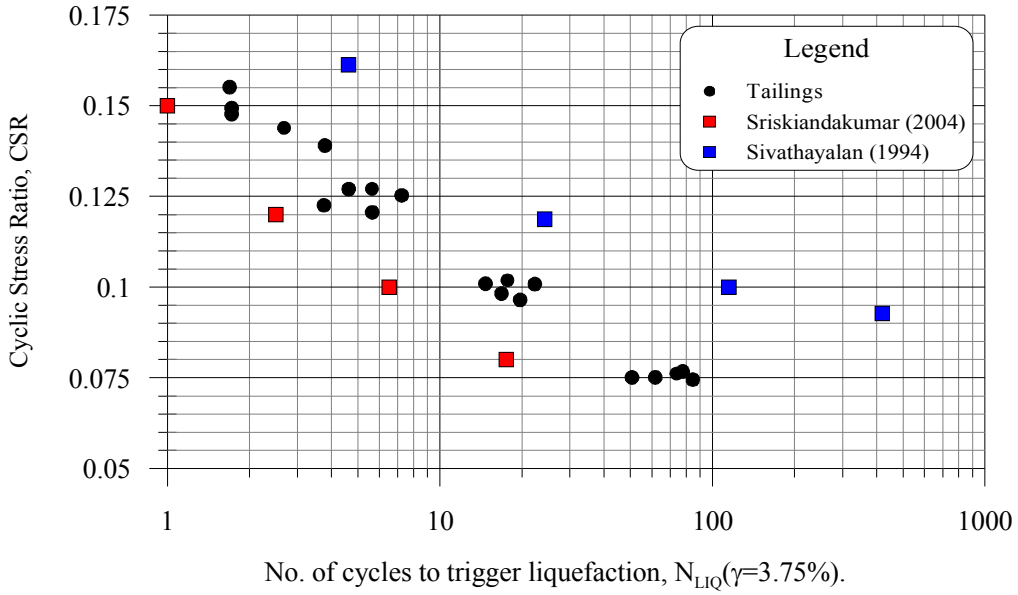

Figure 3-11 - Summary of cyclic direct dimple shear test results on tailings (this research) and on Fraser River Sand by Sivathayalan (1994) and Sriskandakumar (2004).

Details of typical results from the CDSS testing of the tailings are shown on Figure 3-12. These results are from Test No. TL-01, which was consolidated to 102.2 kPa and subjected to a cyclic shear load with an amplitude of 10.2 kPa (CSR=0.10). The dot on the charts represents the occurrence of liquefaction as defined by 3.75% shear strain. Charts a through e of Figure 3-12 are discussed below:

(a) This plot shows the CSR applied to the sample during cyclic testing. The amplitudes of the loading are relatively uniform;

(b) The magnitude of the peak shear strains, γ, increased at a very low rate, until the porewater pressure ratio, r_u, approached 0.75, then the peak shear strains increased dramatically;

(c) The development of the excess porewater pressure, as indicated by the porewater pressure ratio, r_u, was nearly linear during the cyclic loading;

(d) The plot of effective normal stress, σ', vs. shear stress, τ, shows a typical behavior for sand during cyclic loading, including the slight tendency for strain-hardening behavior after the on-set of liquefaction; note that the effective normal stress increases during the loading portion of the cycles after liquefaction;

(e) The shear strain, γ, vs. shear stress, τ, plot is indicative of overall strain-softening with each cycle of load.

(f) The results of the CDSS testing are summarized on Table 3-6. The number of cycles to liquefaction as defined by the shear strain or excess porewater ratio, decreased with increasing cyclic stress ratio and shear strains of 3.75% occurred before the development of excess porewater ratios approaching 1.0.

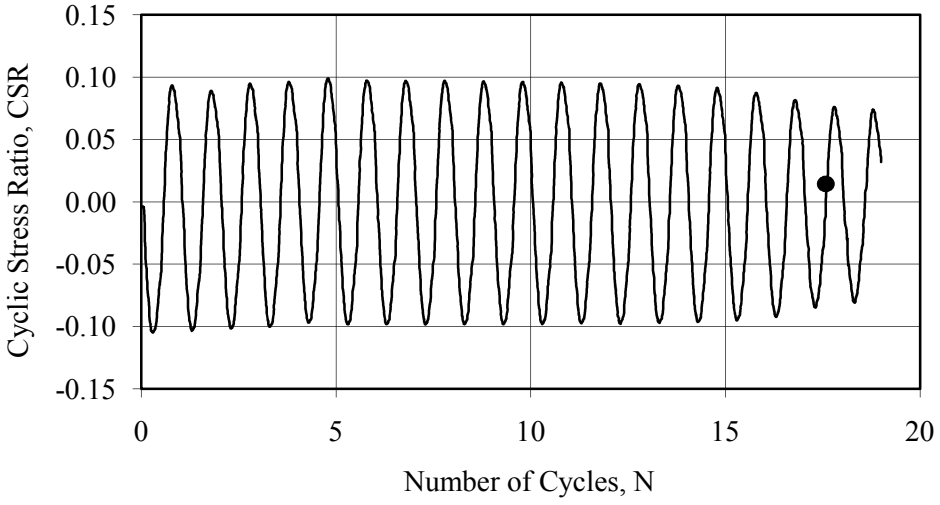

(a) Number of cycles vs. CSR.

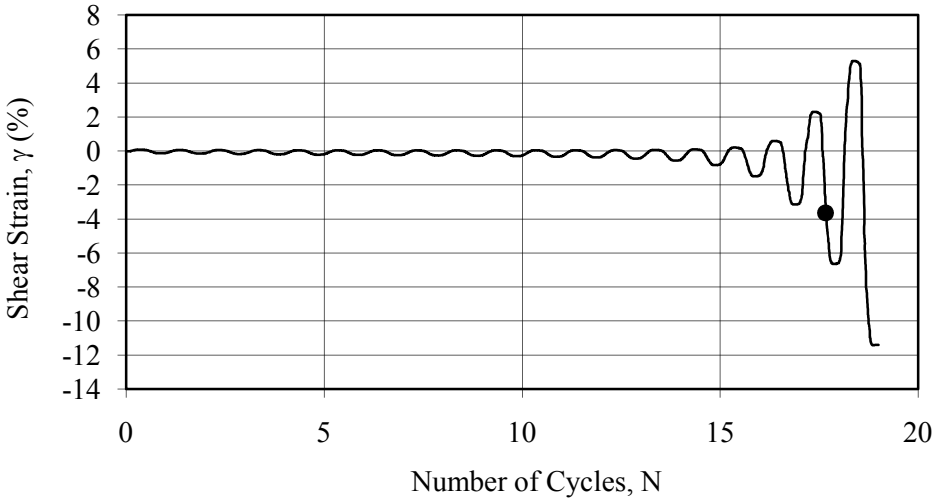

(b) Number of cycles vs. shear strain.

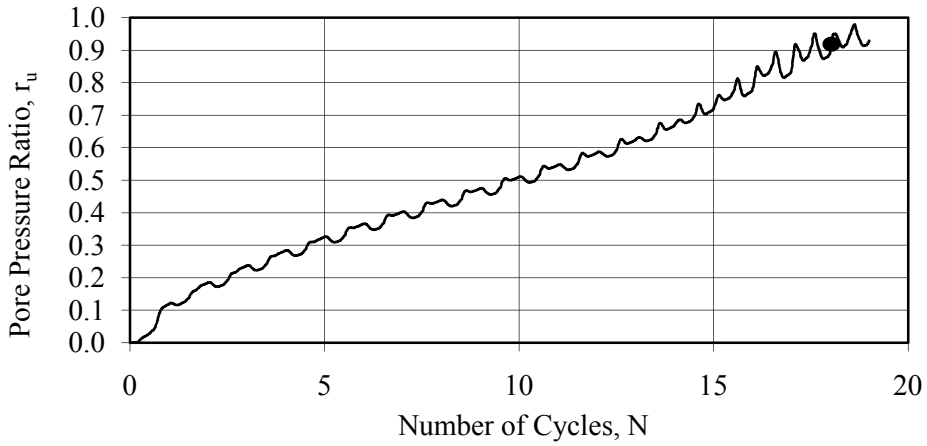

(c) Number of cycles vs. porewater pressure ratio.

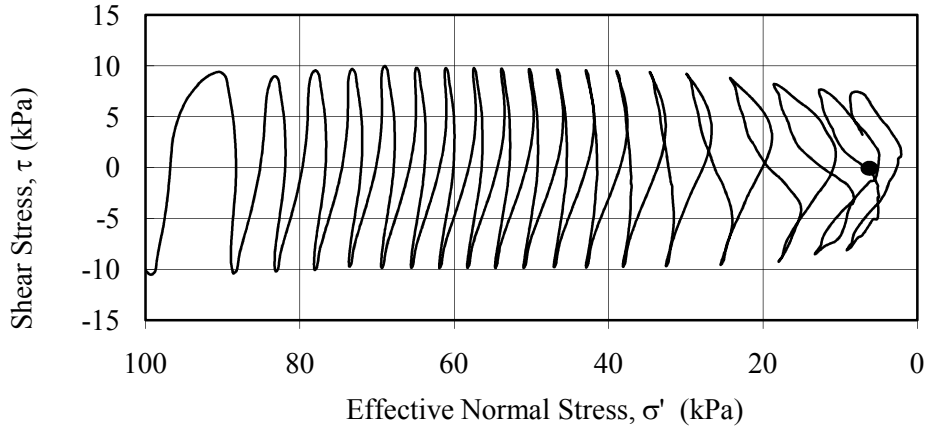

(d) Effective normal stress vs. shear stress.

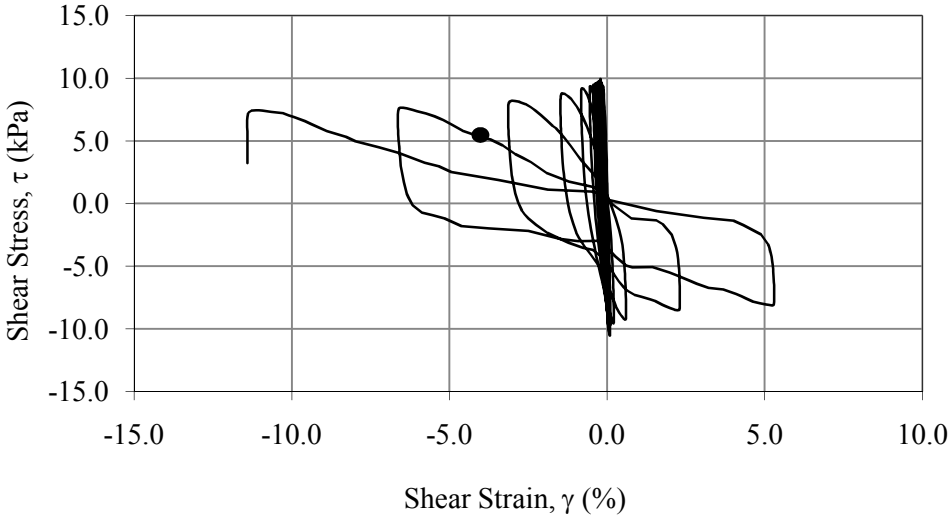

(e) Shear strain vs. shear stress.

Figure 3-12 - Typical CDSS Test Results ($\sigma'_{v,c}$=102.2 kPa, CSR=0.10) (the dots indicate 3.75% shear strain).

Table 3-6 – Summary of cyclic direct simple shear (CDSS) testing.

Test Series	Test No.	$\sigma'_{v,c}$ (kPa)	e_c	$\tau_{cyc}/\sigma'_{v,c}$	N_{LIQ} γ=3.75%	$\Delta u/\sigma'_{v,c}$ γ=3.75%	N_{LIQ} r_u=1.0
100 kPa	TL-03	99.5	0.677	0.076	73.8	0.97	80.5
	TL-01	102.2	0.622	0.102	17.7	0.91	18.6
	TL-04	96.3	0.632	0.127	5.6	0.93	7.0
	TL-02	98.0	0.618	0.144	2.7	0.74	3.6
150 kPa	TL-12	149.7	0.680	0.075	61.7	0.92	64.6
	TL-09	150.3	0.686	0.098	16.8	0.80	19.6
	TL-10	149.7	0.633	0.121	5.6	0.93	7.5
	TL-11	152.6	0.677	0.148	1.7	0.70	2.6
200 kPa	TL-08	200.4	0.655	0.074	84.7	0.92	90.5
	TL-05	200.6	0.610	0.960	19.7	0.89	23.0
	TL-07a	201.0	0.650	0.123	3.8	0.73	5.6
	TL-06	198.8	0.604	0.149	1.7	0.70	3.0
300 kPa	TL-15	300.7	0.638	0.075	50.7	0.88	53.5
	TL-13	299.6	0.639	0.101	14.7	0.82	18.6
	TL-14a	300.0	0.619	0.127	4.6	0.86	6.0
	TL-16	300.9	0.635	0.155	1.7	0.69	2.7
400 kPa	TL-19	400.5	0.582	0.077	77.7	0.83	81.6
	TL-17	400.6	0.611	0.101	22.3	0.82	25.0
	TL-18	400.4	0.590	0.125	7.2	0.79	8.7
	TL-20	400.7	0.618	0.139	3.8	0.68	4.8

$\sigma'_{v,c}$ Effective vertical, consolidation stress;
e_c Void ratio at the end of consolidation;
$\tau_{cyc}/\sigma'_{v,c}$ Cyclic stress ratio (CSR);
r_u Excess porewater pressure ratio, $r_u=\Delta u/\sigma'_{v,c}$;
Δu Change in porewater pressure;
$N_{LIQ}(\gamma=3.75\%)$ Number of cycles to liquefaction defined by a shear strain of 3.75%;
$N_{LIQ}(r_u=1.0)$ Number of cycles to liquefaction as defined by a porewater pressure ratio of 1.0.

The results of post-cyclic strength testing are presented on Table 3-7. The liquefied strength ratios (the ratios of the peak post-cyclic shear strength to the effective consolidation stress) varied from 0.08 to 0.12 and the average value was about 0.10.

Table 3-7 – Summary of Post-cyclic Testing.

Test No.	$\sigma'_{v,c}$ (kPa)	$\tau_{max\text{-}pc}$ (kPa)	γ_{pc} (%)	$\tau_{max\text{-}pc}/\sigma'_{v,c}$
TL-01	102.2	11.5	15.4	0.11
TL-19	400.5	37.0	22.2	0.09
TL-17	400.6	32.7	21.8	0.08
TL-18	400.4	35.8	22.2	0.09
TL-20	400.7	47.9	18.8	0.12

$\tau_{max\text{-}pc}$ Maximum post-cyclic shear stress (peak post-cyclic shear strength);
γ_{pc} Peak post-cyclic shear strain; and
$\tau_{max\text{-}pc}/\sigma'_{v,c}$ Liquefied strength ratio.

3.6 SITE CONDITIONS

3.6.1 Surface Conditions

The Laronde Mine occupies an area of approximately 550 hectares in Pressiac, Quebec, on the on both sides of Route 395, approximately two kilometers north of the intersection with Route 117. From a review of aerial photographs, prior to the development of the site in the 1980s, the area consisted of dense woodlands.

The topography in the vicinity of the site is shown on Drawing No. 1 (Appendix I). The topography of the vicinity is characterized by low rolling hills with no general trend in orientation (MRN, 2000a; 2000b).

Facilities at the site include mine shafts, ore processing plants, an administrative building, mechanical, construction and treatment plants, storage buildings, wastewater treatment

basins, waste rock piles, parking areas, paved and unpaved roadways, and a tailings impoundment. The structures and mine shafts are located in the southern area of the site. The single tailings impoundment is situated in the north-central area of the site. Major existing facilities of the Laronde Mine are shown on Drawing No. 1 (Appendix I).

The tailings impoundment consists of a main section with an area of approximately 3 km^2 (overall plan dimensions of about 2,000 m by 2,000 m) and an eastern extension with an area of 2 km^2 (overall plan dimensions of roughly1,500 m by 1,400 m). Tailings have been placed in both parts of the impoundment, but primarily in the main area. The main section of the impoundment is the subject of this project and will be referred to as the 'impoundment' herein. Figure 3-13 is a panoramic view of the impoundment.

Figure 3-13 - Panoramic view of the impoundment from the southwest.

The impoundment was formed by the construction of Dike No. 1 to the west and Dike No. 2 to the east, which partially separates it from the eastern extension. Polishing Basins Nos. 1 and 2 lie to the west of Dike No. 1. To the north and south, the boundaries of the impoundment are formed by extensions of Dike No. 1 and naturally higher terrain.

Dike No. 1 was constructed in the late 1980s and the placement of tailings began soon thereafter. It was initially constructed to a nominal elevation of 337 m. All elevations in this report are references to CGVD28 (mean sea level). Dike No. 1 is a zoned-earthfill structure composed of local materials with an upstream impervious blanket of compacted clayey till. Dike No. 1 was raised twice by the centerline method to elevations of 340 and 343 meters, with the last raise constructed in 2002. Both additions to the dam include

impervious cores of compacted clayey till. The core of the first addition is keyed into the upstream blanket of the initial dike.

In 2004, the capacity of the impoundment was increased by the construction of a berm within the impoundment, as much as 67 meters upstream of Dike No. 1. The crest elevation of the berm is 344 m and the crest width is 9.0 m. The berm is constructed of waste rock with a low permeability wedge of compacted tailings beneath the upstream slope. The berm allows tailings to be placed within the impoundment (upstream of the berm) without affecting the freeboard of Dike No. 1. A typical cross-section of Dike No. 1 is presented on Figure 3-14.

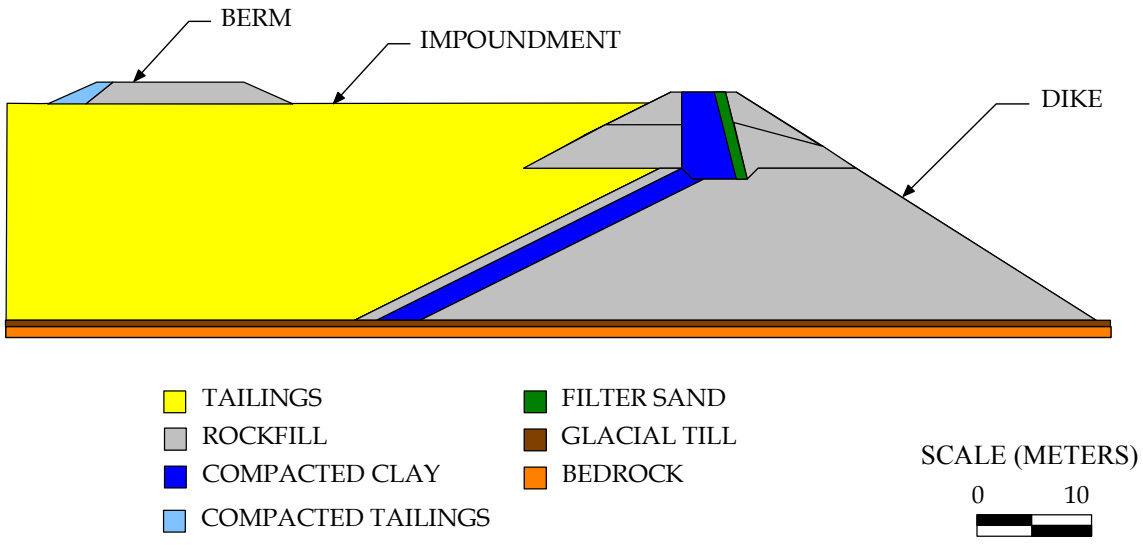

Figure 3-14 – Typical cross-section of Dike No. 1

During the site reconnaissance in November 2004, tailings and wastewater were being placed in the impoundment, upstream of the berm, from outlet pipes which are relocated periodically to distribute the tailings around the western perimeter of the impoundment.

In November 2004, the surface of the tailings within the impoundment varied between elevations 342.0 m and 342.6 m, and the central and eastern portions of the impoundment were submerged. On the western side of the impoundment, the tailings were generally soft though there were significant areas of surface freezing each afternoon through the next morning.

The surface of the tailings was relatively flat by observation, but actually sloped very slightly down and away from the berm. Several erosion channels were observed on the surface of the tailings. These were caused by the flow of wastewater and slurry from inlet pipes and are typically 1 to 2 meter wide and 1 m deep.

There is no vegetation or animal life in the immediate vicinity of the impoundment. The undeveloped areas to the north and west of the impoundment are heavily vegetated with trees and shrubs.

The *Ruisseau Dormenan* (Dormenan Brook) flows from west to east just south of site and is the receptor of final effluent from the mine. *Ruisseau Dormenan* is tributary of the *Rivière Noire* (Black River).

3.6.2 Subsurface Conditions

The following description of subsurface conditions beneath the impoundment is based on a review of borehole and test pit logs produced by Golder (2002) for the last raising of Dike No. 1 as well as logs of boreholes by other organizations from previous investigations that are included in the Golder report. The logs of boreholes are provided in Appendix C.

The impoundment is underlain by of approximately 40 cm of topsoil. The topsoil is in turn underlain by native soils consisting of silty clay and dense glacial till to seven meters in thickness and ultimately bedrock composed of schist and andesite.

Topsoil - The topsoil consists of either hard silty clay or loose sandy silt, both of which are black, laden with organic matter and contains some timber debris, probably from stripping of the site. The thickness of the topsoil varies from 0.4 to 0.6 meters.

Silty Clay - Medium stiff to hard, grey or brown silty clay as much as 5.8 meters thick was encountered beneath topsoil in Boreholes TF-02-02 and TF-02-04.

Glacial Till - Dense glacial till underlies the silty clay at the locations of Boreholes TF-02-02 and TF-02-04. The till consists of silt sand and gravel and is approximately 1-meter-thick.

Bedrock - Bedrock was encountered below topsoil in Boreholes TF-02-01 and TF-03 and below the glacial till in Boreholes TF-02-02 and TF-02-04. At the locations of Boreholes TF-02-01 and TF-02-03 bedrock is composed of schist of medium quality with near vertical joints. Rock Quality Designations (RQD) values of 65% and 70% were measured. Andesite underlies the glacial till at the locations of Boreholes TF-02-02 and TF-02-04. The RQD values of the andesite varied from 0 to 65%, indicating that the rock is of very poor to medium quality.

Groundwater Conditions - During the field exploration, the water level within the impoundment was generally at or above the level of the tailings. However, at the location of tailings beaches, where the water level appeared to be as much as one meter below the top of the tailings due to the slope of the tailings beach.

It is assumed that the piezometeric level in the underlying soils is determined by the long-water level within the impoundment.

3.7 CHARACTERIZATION OF THE TAILINGS

The depth of the tailings varies within the impoundment and is assumed to be as great as 15 meters based on the height of the dike, the topography of the area and cone penetration testing.

The laboratory and in situ testing provided information for evaluation of the characteristics and properties of the tailings. The laboratory testing program used fully consolidated, homogenized samples of the tailings and thus the results are applicable when the tailings are fully consolidated. As discussed in Section 2.1.1.2, tailings typically gain strength through ageing after the completion of consolidation. Thus, the properties derived from the laboratory testing would be conservative when applied to the tailings after they have aged. The cone penetration testing measured properties within the active tailings impoundment and the results can be applied to the tailings in their current state, under-consolidated with respect to existing loads. However, existing procedures for the derivation of material properties from CPT results are based on fully consolidated and over-consolidated materials and the extent of their applicability to under-consolidated materials is not known.

3.7.1 Geotechnical Characteristics and Properties Derived from Conventional Laboratory Testing of the Tailings

This section provides properties of the tailings as derived from the results of laboratory testing (see section 3.5). These values are compared to typical values for hard rock tailings given in Section 2.1.1.2.

3.7.1.1 Specific Gravity

Laboratory test results indicated an average specific gravity (or relative density CGS terms) of 3.88 for the tailings with low and high values of 3.62 and 4.26, respectively. These values are significantly higher than the specific gravities of most naturally occurring soils and rocks and may be explained by the composition of the tailings. From petrographic analysis, the tailings are approximately 60% pyrite, 35% quartz and 5% muscovite. Pyrite, quartz and muscovite have specific gravities of approximately 5.1, 2.65 and 2.8, respectively. The estimated specific gravity of the tailings based on these values is 4.13. Thus, the specific gravity as measured by laboratory testing is appears to be realistic.

The laboratory test samples were from test pits excavated in the tailings beach east of the berm. The sample used for petrographic analysis was obtained directly from the processing plant. The good agreement between the specific gravities of the test pit and processing plant samples is evidence that they are of similar mineral composition.

3.7.1.2 Grain Size Distribution

The grain size distribution of the tailings is presented in Section 3.5.3. It indicates that the tailings consist of colloid to sand-sized particles with respective average D_{10}, D_{50} and D_{95} values of 0.0059 mm, 0.0240 mm and 0.20 mm. The tailings contain 15 to 50 percent sand, where sand is defined as particles larger than 0.075 mm. The grain size distributions in Figure 3-6 are remarkably similar to those presented in Vick (1990) for gold-silver tailings and by Bussière (2007) for hard rock tailings.

3.7.1.3 Plasticity Index

The tailings were determined to be non-plastic based on the author's observations in the field and laboratory. However, very small, isolated pockets of clayey material were encountered in the test pits. Vick (1990) notes that gold-silver ores generally contain little to no clay and are generally of low plasticity or nonplastic. The gold tailings tested by Qui & Sego (2001) were also non-plastic. Bussière (2007) indicates that hard rock tailings typically have no or very little plasticity.

For the purposes of this project, the tailings will be assumed to be non-plastic.

3.7.1.4 Classification

According to the Unified Soil Classification System (Holtz & Kovacs, 1981), the tailings are sandy silt (ML) to silty sand (SM-ML) based on their gradation and lack of plasticity.

3.7.1.5 Drained Shear Strength

As with cohesionless soils, the drained shear strength of the tailings is derived from internal friction with no appreciable contribution from cohesion. From direct shear testing

an average effective angle of internal friction, ϕ', of 36.6° and an effective cohesion, c', of 0 were estimated.

The effective angles of internal friction derived from direct shear testing are comparable to those given in the literature (Vick, 1990; Bussière, 2007).

3.7.1.6 In-place Dry Unit Weight

The in-place dry unit weight of the tailings when normally consolidated was estimated from the results of consolidation testing. Data from one dimensional consolidation testing can be used to estimate the in situ density of normally consolidated soil when there is no lateral component of consolidation, as with deposits of large extent and a level ground surface.

The relationship between the void ratio, e, and the effective vertical consolidation stress, $\sigma'_{v,c}$, is shown on Figure 3-15 and can be represented by:

$$e = -0.035 \cdot ln(\sigma'_{vc}) + 0.800 \qquad (3\text{-}1)$$

The coefficient of determination, R^2, of this relationship is 0.999.

Assuming an average specific gravity of 3.88, the variation in the dry unit weight, γ_d, with depth, z, and effective vertical consolidation stress, σ'_{vc}, is shown on Figure 3-16.

The average dry unit weight, γ_d, and void ratio, e, in the center of the 15-m-thick tailings deposit would be 23.2 kN/m^3 and 0.64, respectively, when normally consolidated.

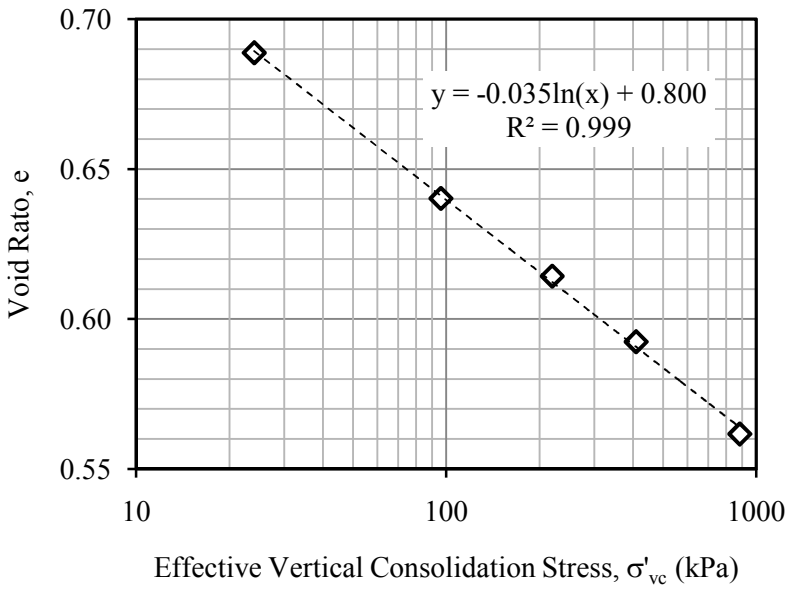

Figure 3-15 – Relationship of the void ratio, e, to the effective vertical consolidation stress, σ'_{vc}, from consolidation testing.

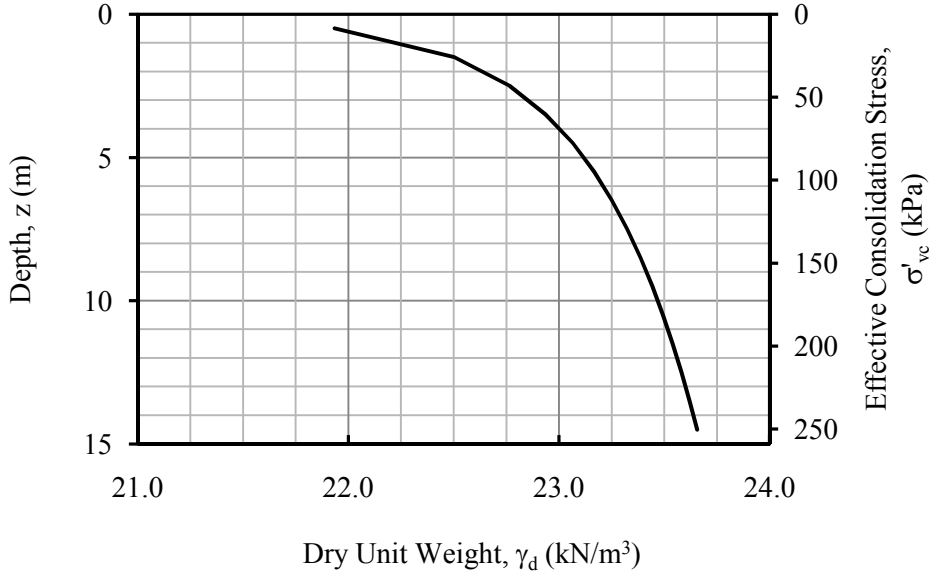

Figure 3-16 - Variation of dry unit weight, γ_d, with depth, z, and effective vertical consolidation stress, σ'_{vc}, based on the results of consolidation testing.

The unit weight of the tailings is significantly greater than that given for gold 'slimes' by Vick (1990), hard rock tailings by Aubertin et al. (1996), Qiu & Sego (2001) and Bussière (2007). However, the specific gravity of the Laronde tailings are significantly higher than those referenced in these sources.

3.7.1.7 Consolidation

The compression index, C_c, and recompression index, C_r, of the tailings were determined through laboratory testing to be 0.08 and 0, respectively. These values are in good agreement with those given my Aubertin et al. (1996), Qiu & Sego (2001), and Bussière (2007).

The coefficient of consolidation, c_v, of the tailings was estimated to vary from 9.35×10^{-3} cm^2/s at a vertical confining stress of 24 kPa to 8.38×10^{-3} cm^2/s at a vertical confining stress of 886 kPa with an average value of 8.80×10^{-3} cm^2/s. These values are one order of magnitude lower than those measured by Aubertin et al. (1996) for hard rock tailings and in very good agreement with those measured by Qiu & Sego (2001) for gold tailings and those reported by Bussière (2007) for hard rock tailings.

3.7.1.8 State

Hydraulically-deposited tailings consolidated under their own weight are typically contractive (Vick, 1990). The tailings displayed contractive behavior during direct shear testing when normally consolidated to effective vertical stresses varying from 50 to 300 kPa. All of the samples reached peak shear stresses at approximately 5 mm of lateral displacement. The contractive behavior continued throughout shearing to a maximum of lateral displacement of 9.5 mm and during subsequent load cycles. The void ratios of the samples are presented on Table 3-5.

During cyclic direct simple shear testing all of the samples experienced a reduction in effective stress to near zero and excessive shear strain, as is expected with contractive samples. None of the limited shear strain characteristic of dilative samples (cyclic mobility) was observed.

The tailings deposit will be contractive when it is fully consolidated. The state of the tailings in their current condition (unconsolidated) is discussed in Section 3.7.3.7.

3.7.1.9 Saturated Hydraulic Conductivity

The saturated hydraulic conductivity of the tailings was estimated from consolidation testing. The values are shown on Table 3-8. The average of these values is 1.19×10^{-5} cm/s. The estimated saturated hydraulic conductivities of the tailings are slightly lower than those given by Aubertin et al. (1996) for various hard rock tailings at similar void ratios and by Qiu & Sego (2001) for gold tailings at similar void ratios. The estimated values are within the range given in Bussière (2007) for hard rock tailings from several sources. However, estimating the hydraulic conductivity from consolidation test results is known to be relatively inaccurate.

Table 3-8 – Estimated saturated hydraulic conductivities from consolidation testing.

Effective vertical, consolidation Stress, $\sigma'_{v,c}$ (kPa)	Void Ratio e_c	Saturated Hydraulic Conductivity, k (cm/s)
24	0.689	2.7×10^{-5}
220	0.614	1.1×10^{-5}
410	0.592	6.0×10^{-6}
886	0.562	3.3×10^{-6}

Given that the tailings are nonplastic, the granular formulation of Mbonimpa et al. (2002) can be used to estimate the saturated hydraulic conductivity of the tailings:

$$k_{SAT}[cm/s] = G_C \frac{\gamma_W}{\mu_W} \frac{e^{3+x}}{1+e} C_u^{1/3} D_{10}^2 \qquad (3\text{-}2)$$

where: G_C is a constant equal to 0.1;

γ_W is the unit weight of water (9.81 kN/m^3);

μ_W is the dynamic viscosity of water (1x10^{-3} Pa);

e is the void ratio;

x is a parameter equal to 2.0 for granular and low plasticity soils;

C_u is the coefficient of curvature of the soil; and

D_{10} is the sieve size (cm) corresponding to 10% of the soil passing by weight.

Using the average gradation properties of the tailings from Table 3-4:

$$k_{SAT}[cm/s] = 0.1\frac{9.81}{0.001}\cdot\frac{0.63^5}{1+0.63}10.24^{0.333}0.00059^2 = 4.5x10^{-5}cm/s$$

This value is mid-range for silt based on the observations of Freeze & Cherry (1979).

The k_{SAT} values from 1-dimensional consolidation testing varied from 3.3x10^{-6} cm/s to 2.7x10^{-5} cm/s with an average value of 1.2x10^{-5} cm/s. There was reasonable agreement between these values and those calculated using the formulation of Mbonimpa et al. (2002).

Based on these findings, the hydraulic conductivity of the homogenized tailings is estimated to be 4.5x10^{-5} cm/s. As noted in Section 2.1.1, the hydraulic conductivity of hydraulically deposited tailings tends to be 2 to 10 times, or more, greater in the horizontal direction than the vertical direction.

Assuming the hydraulic conductivity of the homogenized tailings is equivalent to the hydraulic conductivity of the tailings deposit at an orientation of 45º from the horizontal, and that horizontal value in the field is on average 5 times that the of vertical value, the hydraulic conductivities of the tailings deposit can be estimated using the following formulas:

$$k_{sat-h} = 5 \cdot k_{sat-v} \quad (3\text{-}3)$$

where: k_{sat-h} is the saturated horizontal conductivity; and

k_{sat-v} is the saturated vertical conductivity.

$$\frac{1}{k_{sat-\theta}} = \frac{cos^2\theta}{k_{sat-h}} + \frac{sin^2\theta}{k_{sat-v}} \quad (3\text{-}4)$$

where: $k_{sat-\theta}$ is the saturated horizontal conductivity at an angle θ above the horizontal (Freeze & Cherry, 1979).

The estimated saturated horizontal and vertical conductivities of the tailings are thus 2.25×10^{-4} cm/s and 4.5×10^{-5} cm/s, respectively.

3.7.2 Dynamic Properties of the Tailings from CDSS Testing

The dynamic properties of reconstituted, consolidated samples of the tailings were investigated using the cyclic direct simple shear (CDSS) test results. This type of testing is described in Section 2.3.3.1 and the methods used and test results are presented in Section 3.5.6.

3.7.2.1 Liquefaction Resistance

All of the samples subjected to CDSS testing underwent liquefaction in a manner consistent with contractive soils under cyclic loading.

As noted in Section 2.3.3.1, the CSR causing liquefaction in CDSS testing is approximately 90% of the CSR that would cause liquefaction under actual earthquake loading, where the CSR is calculated as per the simplified method (refer to Section 2.3.1). Thus, by factoring the results of the laboratory testing, by 0.9, to account for field conditions a graph of the estimated liquefaction resistance of the tailings was created and is presented on Figure 3-17. Also shown on the figure are a curve and an equation

describing the trend of the data. The coefficient of determination of the equation is 0.975 indicating a very good fit to the data. The cyclic resistance of the tailings may be estimated by:

$$CRR = 0.153\mathrm{N}^{-0.188} \tag{3-5}$$

where N is the number of loading cycles.

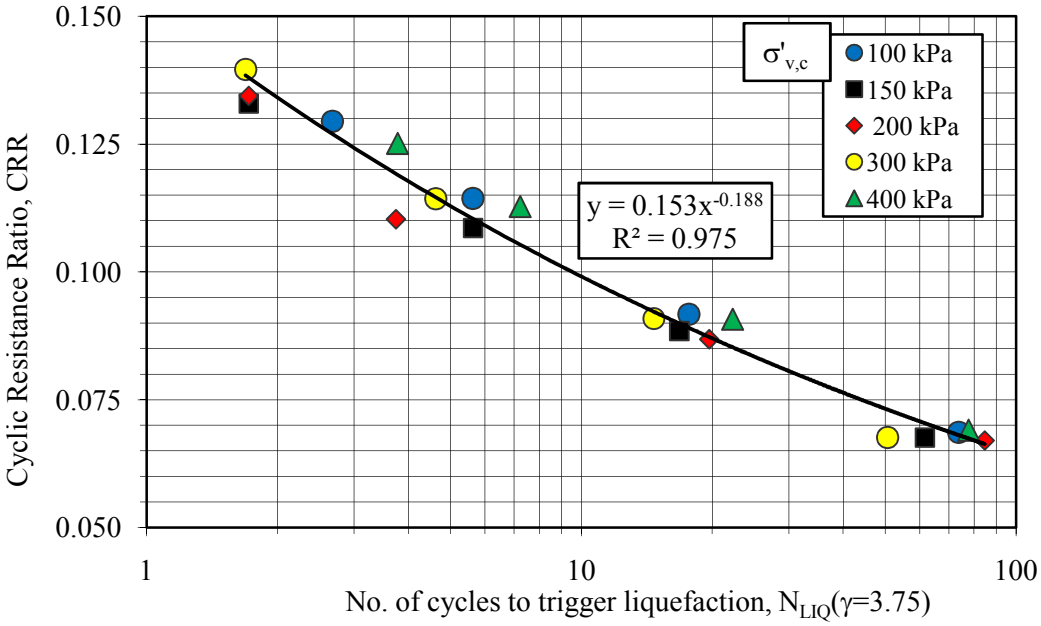

Figure 3-17 – Cyclic resistance of tailings from CDSS testing factored by 0.9 for field conditions.

The magnitude scaling factors (MSF) used in the simplified method are related to the energy content of the earthquake or the number of significant cycles of loading (Seed & Idriss, 1982; Arango, 1994; Youd et al., 2001). The numbers of significant cycles for earthquakes of various magnitudes as determined by Arango (1994) for events east of the

Rocky Mountains are shown in Table 2-2. Figure 3-18 presents the CRR curve for the tailings (from Equation 3-3) with the number of cycles associated with various earthquake magnitudes indicated on the graph. This graph can be used to evaluate the liquefaction potential of the tailings by calculating the CSR induced by a given earthquake and comparing it to the CRR scaled from the chart for the appropriate earthquake magnitude. For example, a magnitude 6 earthquake inducing a CSR of 0.10 at some depth in the tailings deposit would not cause liquefaction at that depth because the CRR of the tailings (read from the graph) would be about 0.117 and the factor of safety with respect to liquefaction would be 0.117/0.10=1.17. As the testing was conducted on consolidated samples, the chart is applicable to consolidated tailings and would be unconservative with respect to under-consolidated deposits and conservative with respect to consolidated, aged deposits.

The MSF values of Arango (1994) were used rather than those of Youd et al. (2001) because the values from Arango (1994) were based on extensive research using real and artificial ground motions for eastern North America, particularly from the 1988 Saguenay (Quebec) earthquake.

Figure 3-18 is analogous to the CRR graph for the Simplified method as presented in Youd et al. (2001), (refer to Figures 2-18 and 2-19). The graphs by Youd et al. (2001) represent corrected penetration resistance vs. CRR of clean sand for an earthquake magnitude of 7.5. Figure 3-18 is of earthquake magnitude v. CRR for a known condition of the soil (hydraulically deposited, saturated and normally consolidated).

The results of CDSS testing can be compared to the Simplified method in two ways:

- The first method consists of factoring the CRR values of the tailings for various earthquake magnitudes from Figure 3-18 by the appropriate MSF (Table 2-2) to obtain the $CRR_{7.5}$ values and estimating the corrected penetration resistances, $(N_1)_{60\text{-}cs}$ and $q_{1N\text{-}CS}$, for each value of $CRR_{7.5}$ (Figures

2-18 and 2-19). The corrected penetration resistances of the $CRR_{7.5}$ values should be roughly equivalent.

- The second method consists of calculating MSF factors based on the results of CDSS testing and then determining the equivalent corrected penetration resistance values for the magnitude 7.5 event (Figures 2-18 and 2-19). As noted in Section. 2.3.1, the CSR (CRR) charts of the Simplified method assume a magnitude 7.5 event.

- The results of the first method, using the Arango (1994) and Seed & Idriss (1982) MSF values, are shown on Table 3-9.

- For the Arango (1994) MSF values, the $CRR_{7.5}$ values vary from 0.047 for the magnitude 5.5 test results to 0.109 for the magnitude 8 rest results. As noted above, these values were expected to be approximately equivalent. The significant differences between the values indicates that the Arango (1994) MSF values may not be applicable with respect to the CDSS testing of the tailings. This is confirmed by the variation in the corrected penetration resistances presented in Table 3-9 (e.g. the $(N_1)_{60\text{-}cs}$ values vary from 0.75 blows/300 mm for the magnitude 5.5 test results to 9.5 blows/300 mm for the magnitude 8.5 results).

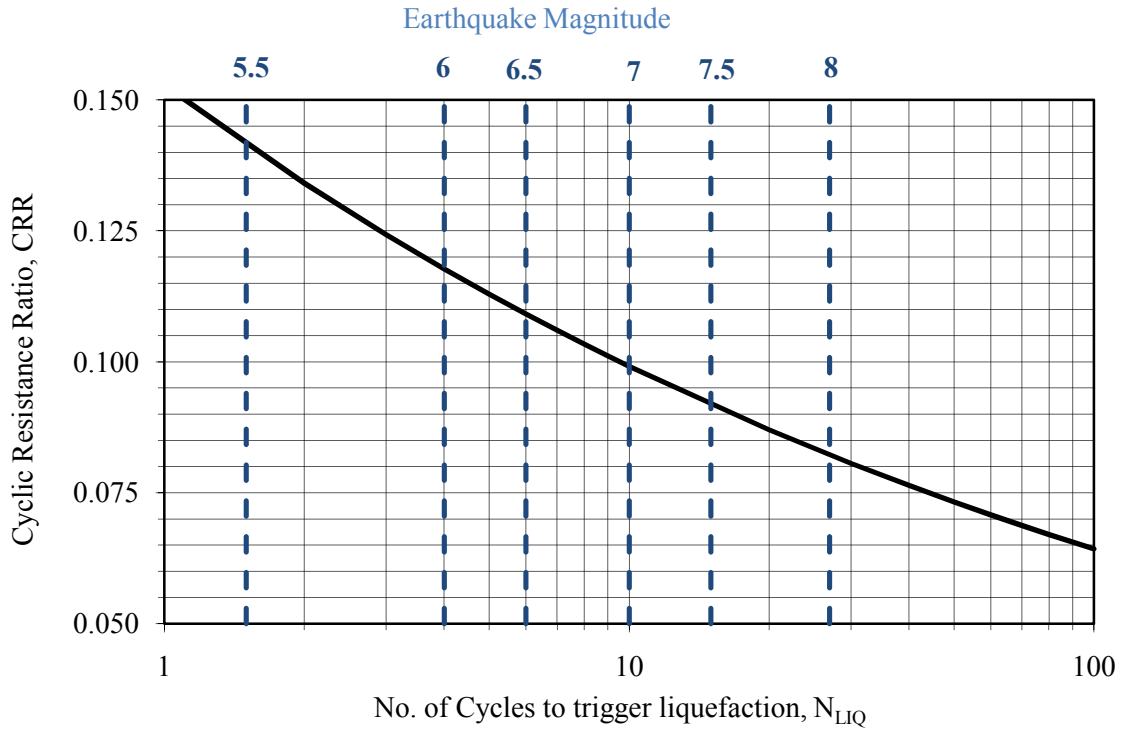

Figure 3-18 – CRR of the tailings from CDSS testing factored by 0.9 for field conditions with earthquake magnitudes shown based on Arango (1994).

For the Seed & Idriss (1982) MSF values, the results were much more consistent. The $CRR_{7.5}$ values varied between 0.083 and 0.092 and the corresponding values of $(N_1)_{60\text{-}cs}$ and $q_{c1N\text{-}cs}$ were also relatively consistent with average values of 7 (blows/300 mm) and 50. The results of CDSS testing are in reasonable agreement with the magnitude scaling factors given by Seed & Idriss (1982).

Table 3-9 – Estimation of equivalent corrected penetration resistances from CDSS testing using Arango (1994) and Seed & Idriss (1982) magnitude scaling factors (MSF).

Analysis using Arango (1994) MSF Values					
Earthquake Magnitude, M_w	CRR from CDSS Testing	MSF	$CRR_{7.5}$	$(N_1)_{60\text{-}cs}$ (blows/ 300 mm)	$q_{c1N\text{-}CS}$
5.5	0.142	3.00	0.047	0.75	0.5
6	0.118	2.00	0.059	3.25	11
6.5	0.109	1.60	0.068	4.5	22
7	0.099	1.25	0.079	5.75	35
7.5	0.092	1.00	0.092	7.5	50
8	0.082	0.75	0.109	9.5	68
Analysis using Seed & Idriss (1982) MSF Values					
Earthquake Magnitude, M_w	CRR from CDSS Testing	MSF	$CRR_{7.5}$	$(N_1)_{60\text{-}cs}$ (blows/ 300 mm)	$q_{c1N\text{-}CS}$
5.5	0.121	1.43	0.085	6.75	45
6	0.110	1.32	0.083	6.5	40
6.5	0.104	1.19	0.087	7	45
7	0.096	1.08	0.089	7.25	50
7.5	0.092	1.0	0.092	7.5	55
8	0.086	0.94	0.092	7.5	55

The second method, estimating magnitude scaling factors from the CDSS test results, using the magnitude 7.5 results as a datum, used the number of equivalent cycles for various magnitude earthquakes estimated by Arango (1994) and by Seed & Idriss (1982) (see Table 2-2). The results of this method are summarized on Table 3-10. Based on the Arango (1994) values, the magnitude scaling factors calculated from the CDSS test results vary from 1.54 for the magnitude 5.5 test results to 0.89 for the magnitude 8 test results. These MSF values differ from those given by Arango (1994) by factors of 0.5 to 1.2. Based on the Seed & Idriss (1982) N values, the calculated MSF values vary from 1.32 for the magnitude 5.5 test results to 0.093 for the magnitude 8 test results. These

MSF values differ from those given by Seed & Idriss (1982) by factors of 0.92 to 1.01 and indicate reasonable agreement between the MSF values of Seed & Idriss (1982) and those calculated from the CDSS test results.

Table 3-10 – Estimated magnitude scaling factors from CDSS testing based on number of equivalent cycles from (Arango, 1994) and Seed & Idriss (1982)

Earthquake Magnitude, M_w	Based on Arango (1994)		Based on Seed & Idriss (1982)	
	CRR from CDSS Testing	Estimated MSF	CRR from CDSS Testing	Estimated MSF
5.5	0.142	1.54	0.121	1.32
6	0.118	1.28	0.110	1.20
6.5	0.109	1.18	0.104	1.13
7	0.099	1.08	0.096	1.04
7.5	0.092	1.00	0.092	1.00
8	0.082	0.89	-	-

A possible reason for the differences in the magnitude scaling factors estimated using the two methods was the rate of cyclic loading used in the CDSS testing. Cyclic loading was applied at a frequency of 0.1 Hz. This rate is significantly less than that of earthquake loadings and less than the than that typically used for cyclic triaxial testing which is 1 Hz. Sriskandakumar (2004) states that the undrained behavior of sand in cyclic loading is essentially independent of the frequency of the loading. However, the energy content of the loading decreases with increasing frequency (the energy content is proportional to the area enclosed by the load diagram) and Ishihara (1996) states that the dynamic shear modulus of soil increases with increasing frequency. Thus, the frequency of loading has some effect on the cyclic resistance and may have affected the results of CDSS testing. Arango (1994) found that the number of cycles required to cause liquefaction in stress controlled, cyclic triaxial testing increased slightly with increasing frequency. However,

for practical purposes, the liquefaction resistance of was found to be independent of frequency.

The corrected penetration resistance for the magnitude 7.5 test results were an $(N_1)_{60\text{-}cs}$ value of 7.25 blows/300 mm and a $q_{1N\text{-}cs}$ value of 50. Given the relatively slow rate of loading and the significance of shear strain (shear modulus) in the development of excess porewater pressures as well as the large number of cycles (15) associated with the magnitude, these penetration resistances should be considered upperbound values with respect to the tailings as tested (normally consolidated).

3.7.2.2 Shear Modulus and Dynamic Damping

The CDSS device used for this research measured the shear strain in increments of 0.01%, thus reliable estimates of the shear modulus at shear strains less than 0.01% was not possible. However, the shear modulus was calculated at the shear strains corresponding to the first 1/4 of the first load cycle and at the lowest reliable value of shear strain for the tests completed at a cyclic shear strain of 0.075. These values are presented in Table 3-11, and plotted on Figure 3-19. The figure shows a clear trend of decreasing shear modulus with increasing shear strain and of generally increasing shear modulus with increasing consolidation stress, both of which are expected.

The curves on the figure were taken from Seed et al. (1984) and show the degradation of the shear modulus with increasing shear strains (shear strain v. G/G_{MAX}) for sand under mean principle effective stresses of 25 kPa (A), 50 kPa (B), 100 kPa (C), and 200 kPa (D).

The theoretical at-rest pressure coefficient in cohesionless media can be approximated by $K_0 = 1 - sin\emptyset'$ (Holtz & Kovacs, 1981). Thus for the tailings:

$$K_0 = 1 - sin\emptyset' = 1 - \sin(36.6°) = 0.40$$

Assuming at-rest conditions in the cyclic direct simple shear testing prior to the development of significant excess porewater pressures, the mean effective principal

stresses within the sample, $(\sigma'_x+\sigma'_y+\sigma'_z)/3$, were approximately 0.6 of the effective vertical consolidation stresses. Thus, CDSS test results at 150 and 200 kPa are roughly comparable to the Seed et al. (1984) curve for a mean principal effective stress of 100 kPa and the results at 300 and 400 kPa are comparable to the curve for a stress of 200 kPa. From Figure 3-19, it can be inferred that the maximum (or low strain) shear modulus of the tailings varies from 45 to 55 GPa with increasing consolidation stress. The modulus reduction behavior of the tailings appears to be very similar to that of sands.

Seed et al. (1984) provides the following relationship for the shear modulus of sand:

$$G = 48 \cdot K_2 \left(\frac{\sigma'_m}{21}\right)^{0.5} \quad (3\text{-}6)$$

where: G is the shear modulus in kPa;

K_2 is the soil modulus coefficient and varies with the strength, effective vertical stress condition and density of the soil; and

σ'_m is the mean principle effective stress in kPa.

Using the shear modulus values of 45 to 50 GPa, the K_2 value of the tailings varies from 15 to 30. This is slightly lower than the value of 34 given by Seed et al. (1984) for loose, moist sand. However, no values for loose, saturated sand were provided.

Bowles (1996) provides a representative range of the shear modulus of clean, dense, quartz sand that varies from 12 to 20 MPa.

Bowles (1996) also provides an equation for estimating the shear modulus of "angular-grained" materials with void ratios greater than 0.6:

$$G = \frac{3230(2.97-e)^2}{1+e}\sqrt{\sigma'_m} \quad (3\text{-}7)$$

where: G is the maximum shear modulus in kPa;

e is the void ratio;

σ'_m is the mean principle effective stress in kPa.

Using Equation 3-7 and assuming an average void ratio of 0.63 and mean effective stresses of 100 and 200 kPa gives shear moduli of 108 and 152 MPa, respectively.

There is a significant discrepancy between the values of the shear modulus estimated from different empirical correlations for sands. The values from laboratory test are within the range of the empirical correlations and deemed to be more appropriate based on the observations of Shen et al. (1978) which indicate that the shear moduli estimated from cyclic simple shear testing using NGI-type devices may be 5 to 15% lower than the actual values.

Based on the CDSS testing, the shear modulus of tailings is estimated to be 50 MPa at the effective overburden stresses expected in the impoundment. The use of a constant shear modulus independent of the effective overburden stress is supported by the laboratory test results which were not significantly affected by the magnitude of the effective consolidation stresses at the same shear stress ratio.

Table 3-11 – Estimated shear moduli (from CDSS testing).

Test Series	Test No.	$\sigma'_{v,c}$ (kPa)	e_c	CSR	$\gamma_{(N=0.25)}$ (%)	G (kPa)
$\sigma'_{v,c}$= 100 kPa	TL-03	99.5	0.677	0.076	0.07	10,743
	TL-03	99.5	0.677	0.076	0.03	16,267
	TL-01	102.2	0.622	0.102	0.08	12,963
	TL-04	96.3	0.632	0.127	0.08	14,850
	TL-02	98.0	0.618	0.144	0.21	6,752
$\sigma'_{v,c}$= 150 kPa	TL-12	149.7	0.680	0.075	0.04	25,800
	TL-12	149.7	0.680	0.075	0.04	25,050
	TL-09	150.3	0.686	0.098	0.04	34,875
	TL-10	149.7	0.633	0.121	0.08	14,850
	TL-11	152.6	0.677	0.148	0.20	10,980
$\sigma'_{v,c}$= 200 kPa	TL-08	200.4	0.655	0.074	0.09	16,522
	TL-08	200.4	0.655	0.074	0.03	22,450
	TL-05	200.6	0.610	0.960	0.11	17,463
	TL-07a	201.0	0.650	0.123	0.17	13,847
	TL-06	198.8	0.604	0.149	0.31	9,668
$\sigma'_{v,c}$= 300 kPa	TL-15	300.7	0.638	0.075	0.12	18,767
	TL-15	300.7	0.638	0.075	0.04	31,488
	TL-13	299.6	0.639	0.101	0.21	13,943
	TL-14a	300.0	0.619	0.127	0.28	13,429
	TL-16	300.9	0.635	0.155	0.49	9,200
$\sigma'_{v,c}$= 400 kPa	TL-19	400.5	0.582	0.077	0.17	17,794
	TL-19	400.5	0.582	0.077	0.02	37,550
	TL-17	400.6	0.611	0.101	0.23	16,813
	TL-18	400.4	0.590	0.125	0.33	14,776
	TL-20	400.7	0.618	0.139	0.42	13,010

where: $\gamma_{(N=0.25)}$ is the shear strain measured at the at first 1/4 of a cycle of load;
G is the shear modulus.

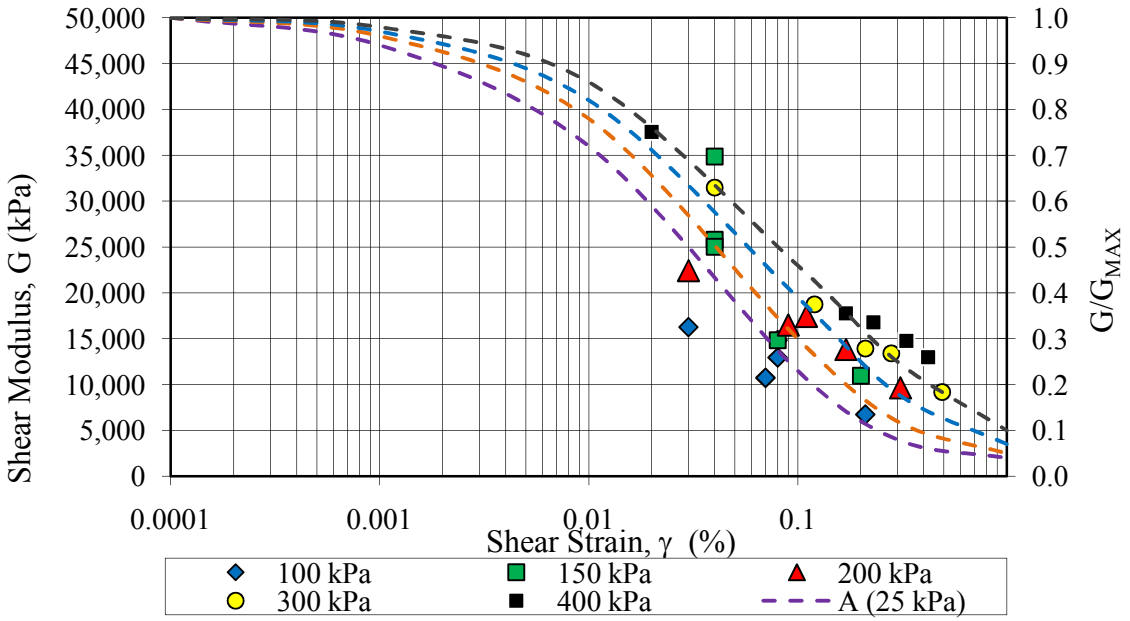

Figure 3-19 – Shear moduli from CDSS testing
(data grouped by consolidation stress) and G/G_{MAX} curves from Seed et al. (1984) for mean effective stresses of 25, 50, 100, and 200 kPa.

3.7.2.3 Post-cyclic Shear Strength

Post-liquefaction shear strength tests were conducted on five of the CDSS tested samples (refer to Table 3-7). The post-liquefaction shear strengths, $S_{u\text{-}PC}$, varied from 11.5 to 47.9 kPa and the average liquefied strength ratio, $S_{u\text{-}PC}/\sigma'_{v,c}$, was 0.10.

Wijewickreme et al. (2005a) conducted a series of CDSS tests with post-cyclic strength testing on normally consolidated, undisturbed and reconstituted samples of copper-gold-zinc tailings from a single source and measured $S_{u\text{-}PC}/\sigma'_{v,c}$ values varying from 0.130 to 1.070, with an average value of 0.343, for 20 undisturbed samples with void ratios varying from 0.54 to 1.43 and from 0.272 to 0.320 for three reconstituted samples with void ratios of 0.84, 0.86 and 087.

Seed et al. (1988) provides residual (post-liquefaction) shear strengths for loose to medium dense, clean sands that vary from near zero to 50 kPa. This range is in good agreement with the results of laboratory testing in Table 3-7.

3.7.3 Geotechnical Characteristics and Properties Derived from Cone Penetration Testing of the Tailings

Some of the characteristics and properties of the tailings can be estimated using the results of cone penetration testing. It is expected that some of these properties and characteristics will evolve as the tailings continue to consolidate. The methods currently available for interpreting CPT data were based on studies of naturally occurring, normally and over-consolidated soils and may be of limited applicability to under-consolidated tailings.

Graphs of the cone tip resistance, q_c, sleeve friction, f_s, and porewater pressure, u, measured during the cone penetration testing are presented in Appendix B, which also contains graphs of the soil behavior type index, I_c. The cone tip resistance is the most significant parameter developed from CPT testing and is directly related to the strength and compressibility of the soil (Robertson & Campanella, 1986). The soil behavior type index can be used to classify the soil following the method of Robertson & Wride (1998) as recommended in Youd et al. (2001). The method used in the calculation of the soil behavior type index is presented in Appendix B.

Example CPT testing results are presented on Figure 3-20. The other results are presented in Appendix F.

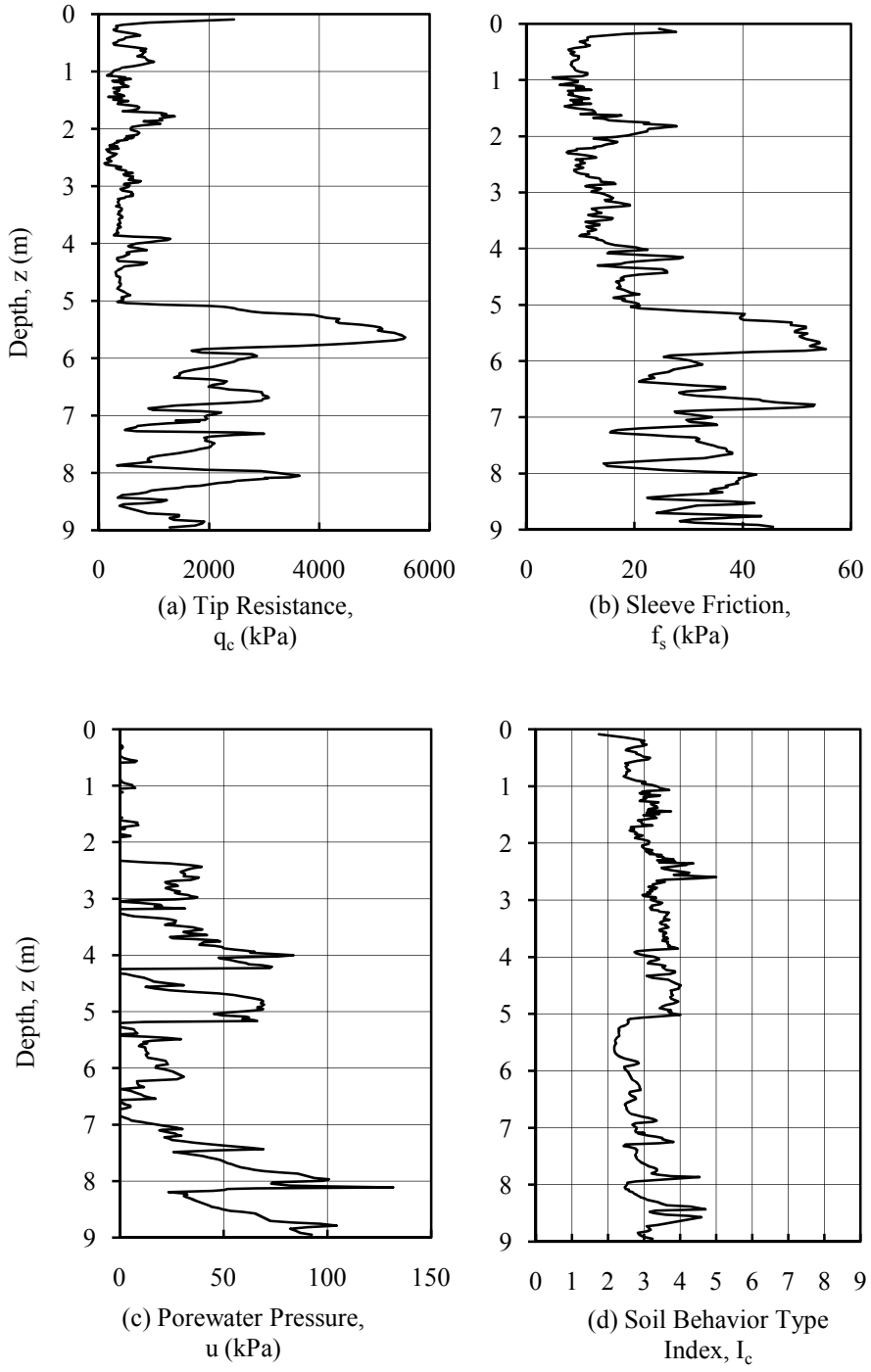

Figure 3-20 – Values of CPT S2: (a) tip resistance, q_c; (b) sleeve friction, f_s; (c) porewater pressure, u; and (d) Soil Behavior Type Index, I_c.

3.7.3.1 Normalization of CPT Results

Youd et al. (2001) recommend normalization of cone test results. The normalization consists of factoring the tip resistance to an effective, vertical overburden pressure of 100 kPa based on the soil type as determined from the ratio of the tip resistance to the sleeve friction. The resulting normalized cone tip resistance, q_{c1N}, is dimensionless. The method and equations for normalization are presented below. Profiles of the normalized tip resistances are presented in Appendix B.

The tip resistance was normalized using the following equations:

$$q_{c1N} = C_Q(q_c/P_a) \quad (3\text{-}8)$$

$$C_Q = \text{maximum}[(P_a/\sigma'_{vo})^n, 1.7] \quad (3\text{-}9)$$

where: C_Q is the normalizing factor with a maximum value of 1.7;

P_a is equal to 1 atmosphere of pressure in the same units as q_c;

σ'_{vo} is the effective vertical overburden stress in the same units as q_c;

n is an exponent equal to 0.5 for clean sands, 1.0 for clays, and "intermediate values" for silts, sandy silts, and silty sands.

An exponent, n, of 0.5 was used to normalization of the tip resistance in the tailings based on the assumption that their behavior is more like sand than silty soil, particularly considering the results of the direct shear testing and the findings of Ulrich and Hughes (1994) that the measured tip resistances of tailings were similar to those of coarse sand and unlike those of silt and silty sand.

3.7.3.2 Layering within the Tailings Deposit

Two typical profiles of the cone tip resistance, q_c, from the cone penetration testing are presented on Figure 3-21. As shown on the figure, the tip resistance varies significantly with depth. This variation is common in active tailings deposits (Ulrich and Hughes, 1994; Woeller et al., 1995) and is due to the method of placement that results in relatively thin lenses of tailings being placed in the impoundment at various locations at intermittent intervals such that the degree of consolidation of the lenses varies greatly. The zones of lower penetration resistance represent significantly under-consolidated lenses (Ulrich and Hughes, 1994), which are weaker and more compressible. With time, these lenses should consolidate and develop strength comparable to the consolidated lenses. The strength of some of stronger lenses in the deposit may be the result of desiccation or consolidation by capillary pressure after placement as the water level within the impoundment is sometimes below the surface of the tailings or due to chemical precipitation resulting in thin "hard pan" zones.

Based on the variations observed in the CPT logs, the tailings deposit consists of layers of variable consolidation that vary from 5 to 20 cm in thickness.

3.7.3.3 Classification

CPT data can also be used to classify the soil based on empirical correlations involving the tip resistance, sleeve friction, and assumed in situ stresses. Evaluation of the CPT data using the method proposed by Robertson (1990) infers that the tailings consist of normally to slightly over-consolidated lenses of silty clay, clayey silt, silt, and silty sand. However, this method is based on correlations with naturally occurring soils and does not appear to be applicable to the tailings given the results of laboratory testing and the petrographic analysis of tailings, which indicate that the tailings consist of non-plastic colloid to sand-sized particles. For reference, the classification parameters and the applicable chart from Robertson (1990) are contained in Appendix B.

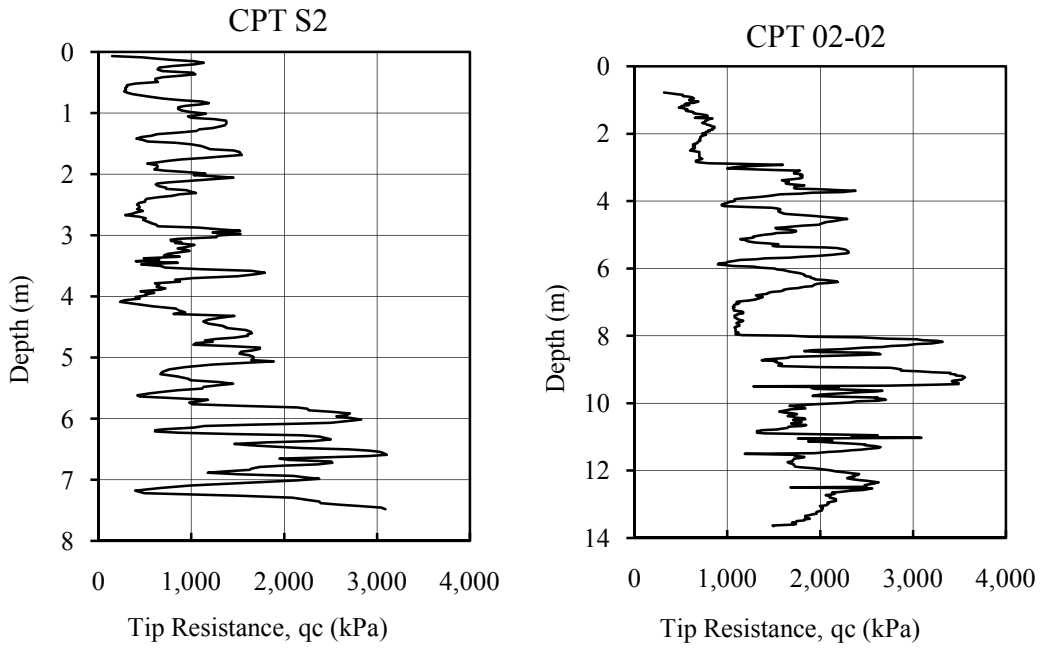

Figure 3-21 – Typical tip resistance profiles from cone penetration testing.

3.7.3.4 Relative Density

Robertson & Campanella (1986) provide a chart relating the penetration resistance of uncemented, normally consolidated quartz sands to the relative density, D_r, over a range of effective, vertical consolidation stresses (Figure 3-22). The range of the measured tip resistance and vertical effective stresses within the tailings are shown on Figure 3-22. Assuming that this chart is applicable to the tailings, it is inferred that the relative density of the tailings varies significantly throughout the depth of the deposit.

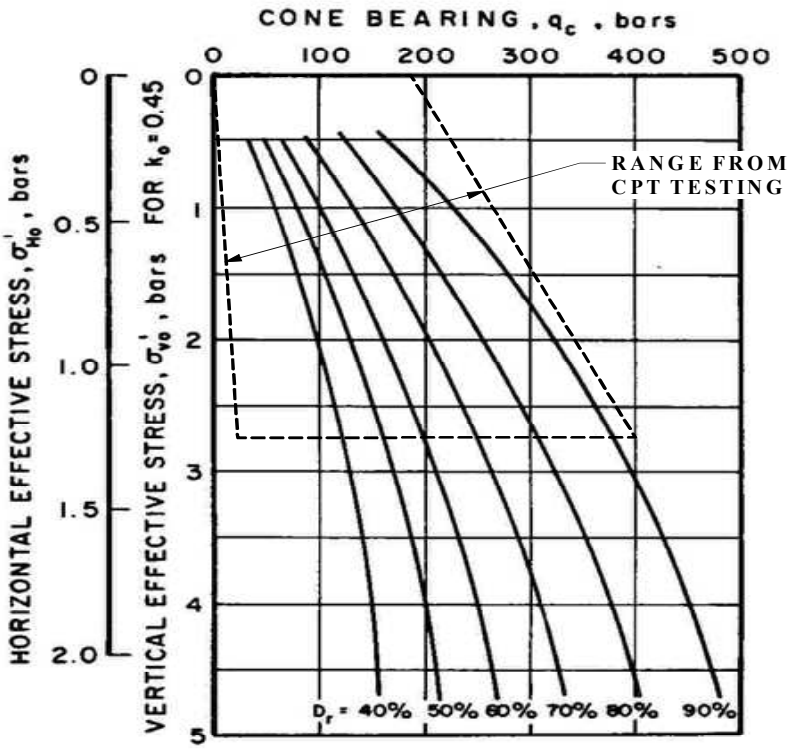

Figure 3-22 – Relative density/CPT tip resistance relationship (Robertson, 1990) with range of CPT data.

3.7.3.5 Effective Angle of Internal Friction

There are methods for the estimating the effective angle of internal friction of soil based on CPT data, including a method by Robertson & Campanella (1983) modified by Chen & Juang (1996) for highly compressible sands and another by Chen & Juang (1996) based on cavity-expansion theory. However, these methods assume the soil is fully consolidated under existing loads.

The modified Robertson and Campanella method (Chen & Juang, 1996) for highly compressible sands is in the form of:

$$\tan\phi' = \frac{1}{6.079}\ln\left\{\frac{q_c/\sigma_v'}{0.340}\right\} \quad (3\text{-}10)$$

where: ϕ' is the drained angle of internal friction;

σ'_v is the effective, vertical overburden stress.

Applying Equation 3-10 to the cone penetration testing results in estimated effective angles of internal friction generally varying between 25 and 45º with lower and higher values in less and more consolidated zones, respectively. Profiles of the effective angle of internal friction for CPT S2 and CPT 02-02 are presented on Figure 3-23. The higher internal friction angles near the surface of CPT S2 are attributed to desiccation or freezing near the ground surface at the time of testing which increased the penetration resistance.

An average value of 36.6º for the effective internal friction angle was determined from direct shear testing. This value is in relatively good agreement with the profiles of Figure 3-23 considering that the tailings are generally under-consolidated with some minor zones of overconsolidation.

3.7.3.6 Equivalent Standard Penetration Resistance

CPT tip resistance values are often converted into standard penetration test values because the majority of empirical correlations for soil properties are based on standard penetration test data and to allow direct comparisons between CPT and SPT test results.

Robertson & Campanella (1986) contains a widely used chart used to determine the equivalent SPT resistance, N, from CPT tip resistance, q_c, (see Figure 3-24). This chart is derived from research on naturally occurring silty sands and sands. Note that the characteristic grain size (D_{50} value) of the material has a strong influence on the ratio of the CPT tip resistance to the SPT blow count.

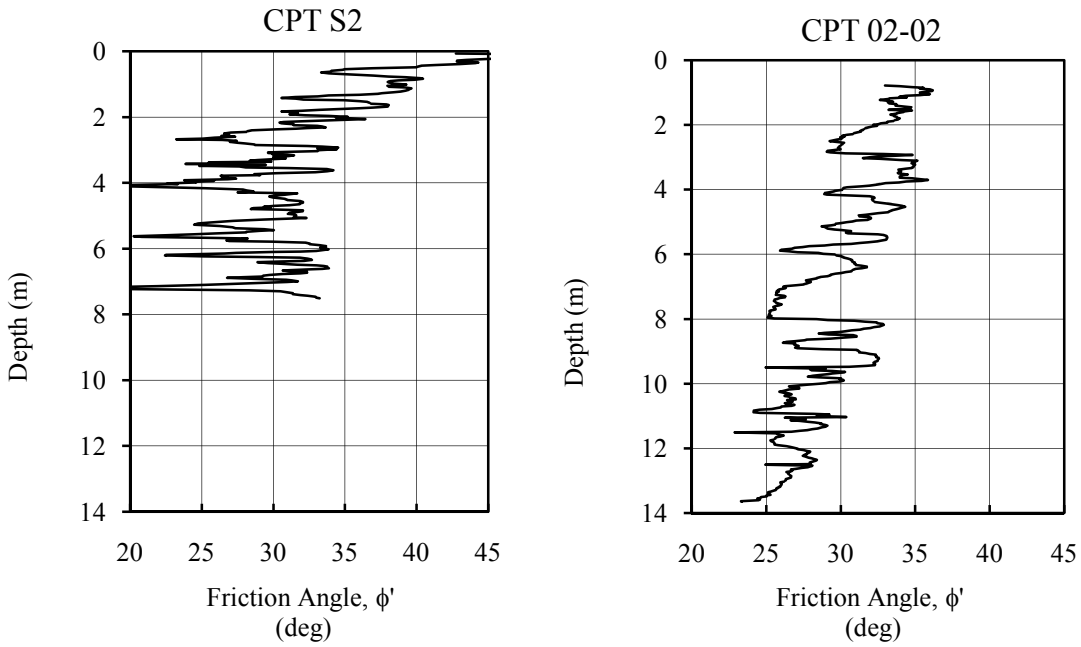

Figure 3-23 – Estimated effective angle of internal friction for CPT S2 and CPT 02-02 based on the method of Robertson & Campanella (1983) by Chen & Juang (1996).

A study by Ulrich & Hughes (1994) on the relationship between the tip resistance and the blow count for mine tailings indicates that the correlation between the tip resistance and the blow count for mine tailings was not affected by the grain size distribution, but may be a function of the ore-type (composition of the tailings). For the sites studied by Ulrich & Hughes (1994), it was found that the ratio of q_c to N for tailings was equivalent to that for coarse sand, q_c/N equals about 5 to 6, where q_c is measured in bars.

The penetration resistance conversions described above are associated with the uncorrected resistances, N and q_c. As presented in Section 2.3.1, the cyclic resistance of soil is correlated to the corrected penetration resistances with the correction for the effective overburden stress being the most important factor. Due to the different methods used to correct the SPT resistance, N, and the CPT tip resistance, q_c, for the effective overburden stress (refer to Section 2.3.1), the applicability of the conversions described

in evaluating the liquefaction resistance of soil is questionable. However, the curves relating the CRR ratio to the corrected penetration resistance values, $(N_1)_{60}$ and q_{c1N} (Figures 2-18 and 2-19) can be used to develop conversion factors for the corrected penetration resistance values as shown below.

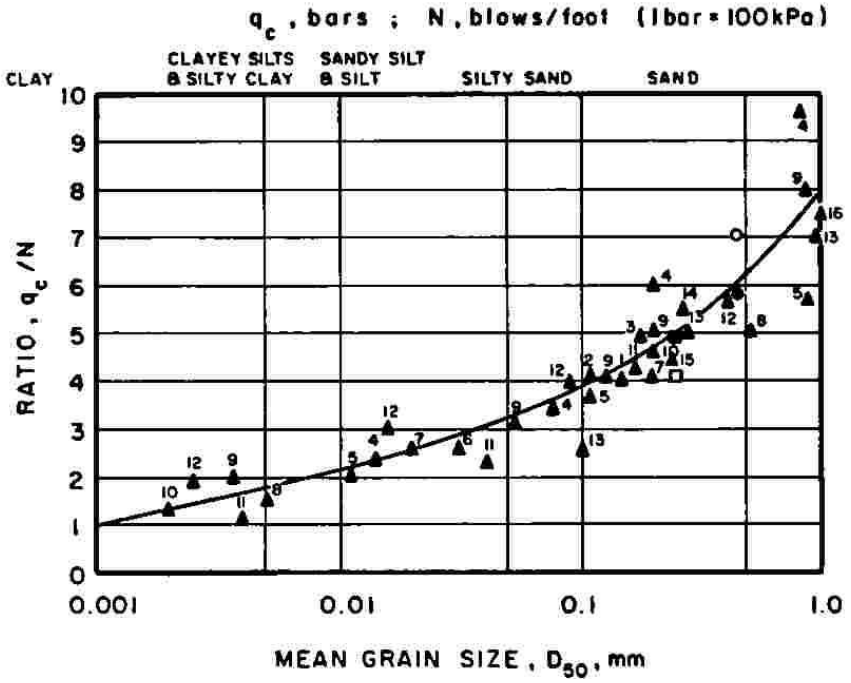

Figure 3-24 – Correlation of the CPT tip resistance with the SPT blow count for naturally occurring soils (from Robertson & Campanella, 1986).

Table 3-12 contains the corrected penetration resistances, q_{c1N} and $(N_1)_{60}$ for a range of CRR values from the clean-sand base curves of the simplified method of liquefaction evaluation (Figures 2-18 and 2-19) and the ratios of the corrected tip resistance to the corrected standard penetration blow count. From the table it is noted that the ratio of the q_{c1N} to $(N_1)_{60}$ varies from 7.06 at a CRR value of 0.10 to 5.41 at a CRR value of 0.50 with the average ratio being 5.70. The average value is in the range recommended by Ulrich

and Hughes (1994) for the conversion of uncorrected penetration resistance values (5 to 6). Given this and the fact that loose, saturated tailings deposits are particularly susceptible to liquefaction and are thus more likely to liquefy under the lower levels of cyclic loading that typically precede the peak loading in earthquake ground motions, an $(N_1)_{60}/q_{c1N}$ ratio of 6 is considered appropriate for the tailings at Laronde Mine.

Table 3-12 – Estimated conversion factors for corrected penetration resistance values based on the CRR charts of the simplified method of Seed & Idriss (1982).

CRR	q_{c1N}	$(N_1)_{60}$ (blows/300 mm)	$q_{c1N}/(N_1)_{60}$
0.10	60	8.5	7.06
0.15	90	14	6.43
0.20	110	18.75	5.87
0.25	120	22.5	5.33
0.30	135	25.5	5.29
0.35	145	27.5	5.27
0.40	150	28.75	5.22
0.45	160	29.75	5.38
0.50	165	30.5	5.41
		Average:	5.70

Conversion of the corrected tip resistances of the cone penetration testing to corrected standard penetration test blow counts results in values varying between 2 and 20 blows per 300 mm in the upper 6 m of the tailings with a majority of the values being less than 4 blows per 300 mm. Below a depth of 6 m the results blow counts are typically less than 4 blows per 300 mm.

3.7.3.7 Porewater Pressure Response

The porewater pressure response within the tailings was measured during cone penetration testing. The measured porewater pressure response of a soil is significantly

affected by the size and location of the piezometeric sensor with respect to the cone, the rate of penetration and the type and state of the soil. Piezometeric sensors are typically located on the face of the cone or behind the cone. Porewater pressures measured behind the cone appear to be dominated by the shear behavior of the soil in a zone of normal stress relief, while those measured on the face of the cone are dominated by increases in normal stresses in a zone of maximum compression and increased normal stress (Robertson & Campanella, 1986). The device used in this study used a piezometer located behind the cone.

Typically, the porewater response of the tailings to cone penetration was to generate excess porewater pressures in areas of lower tip resistance and reduced porewater pressures (less than hydrostatic) in areas of higher tip resistance. This trend is evident in Figure 3-25 where profiles of the penetration resistance and porewater development of CPT S6 are presented.

There is no direct correlation between the porewater pressures measured during cone penetration testing and hydrostatic porewater pressures, except in instances where testing is paused to allow measurement of a stabilized porewater pressure level (Robertson & Campanella, 1986). When the porewater pressure sensor is located behind the cone, saturated medium dense silts generally produce zones of porewater pressure less than the hydrostatic pressure, while loose silts typically produce zones of porewater pressures as much as 1.5 greater than the hydrostatic pressure (Robertson & Campanella, 1986). These responses are comparable to those of the cone penetration testing of the tailings in this study.

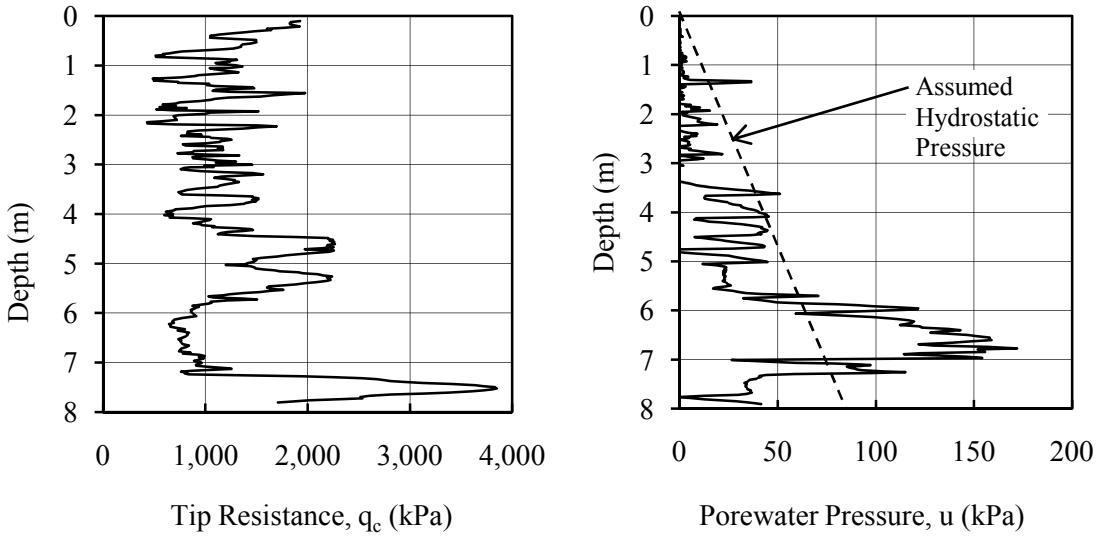

Figure 3-25 – Profiles of the tip resistance and porewater pressure response of CPT No. S6.

3.7.3.8 Shear Modulus

Robertson and Campanella (1986) provide correlations between the tip resistance, q_c, and low strain shear modulus (maximum shear modulus), G_{MAX}, for normally consolidated, uncemented quartz sands (refer to Figure 3-25). At tip resistances lower than 5,000 kPa, such as encountered in the tailings, the relationship between the tip resistance, q_c, and the small strain shear modulus, G_{MAX}, is approximately linear for values of qc less than 50 bars (500 kPa) and may be estimated using:

$$G_{MAX} = 12.5 \cdot q_c \qquad (3\text{-}11)$$

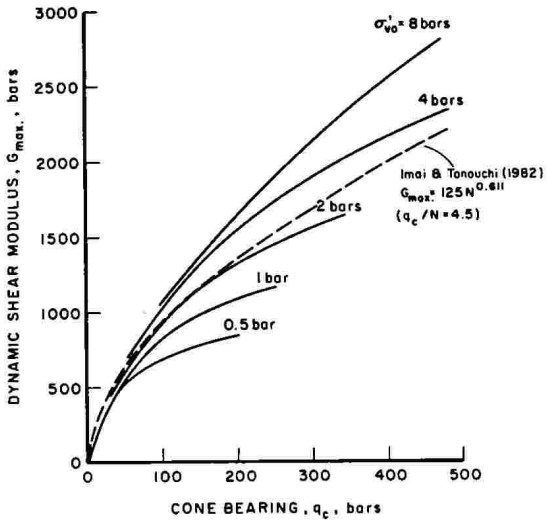

Figure 3-26 – Correlation of the modulus with cone penetration testing for normally consolidated, uncemented quartz sands (from Robertson & Campanella, 1986).

3.7.4 Summary of Geotechnical Properties of the Tailings

The geotechnical properties of the tailings as derived from conventional and dynamic laboratory testing and cone penetration testing are summarized Table 3-13.

Table 3-13 – Average geotechnical properties of the tailings.

Property	Laboratory Testing	CPT
G_S	3.88	-
D_{10}	0.006 mm	-
D_{30}	0.024 mm	-
D_{50}	0.046 mm	
D_{60}	0.060 mm	-
Percent Fines (<0.075 mm)	60%	-
Atterberg Limits	Non-plastic	-

(continued…)

Table 3-13 (continued).

Property	Laboratory Testing	CPT
Classification	ML/SM	CL/ML/SM
ϕ'	36.6º	25 to 40º
c'	0	0
γ_d	23.2	-
e	0.64	-
C_c	0.08	-
C_r	0	-
c_v	$8.8x10^{-3}$ cm^3/s	-
State	Contractive	Contractive
k_{SAT-H}	$2.25x10^{-4}$ cm/s	-
k_{SAT-V}	$4.5x10^{-5}$ cm/s	-
G_{MAX}	50 MPa	$12.5 \cdot q_c$

3.8 STABILITY EVALUATION CRITERIA AND ASSUMED EARTHQUAKE LOADS

3.8.1 Stability Evaluation Criteria

In the province of Quebec, the criteria used for the evaluation of the stability of tailings impoundments are generally based on the 2007 Dam Safety Guidelines of the Canadian Dam Association (CDA, 2007) and the Guidelines for Preparing a Mining Site Rehabilitation Plan and General Mining Site Rehabilitation Requirements of the *Minstère des Ressources naturelles (et faune)* of the province of Quebec (MRN, 1997). The provincial regulations specifically refer to closed mines. However, they are generally applied to operating mines as well.

For purposes of this study, the evaluation criteria of the CDA (2007) guidelines will be applied with respect to the stability of the impoundment under static and seismic conditions.

For static conditions, the minimum factor of safety of the impoundment is 1.5. Due to the presence of the tailings on the upstream side of the dike, the dike is not subject to the

seepage forces associated with rapid drawdown, thus stability under a rapid drawdown condition is not a concern. For seismic conditions using the pseudo-static method, the minimum factor of safety is 1.1 with the pseudo-static coefficient assumed to be equal to 3/4 of the PGA on rock (Seed & Martin, 1966; Hynes-Griffin & Franklin, 1984; Pyke, 1991).

3.8.2 Assumed Earthquake Loads

The estimated site-specific earthquake loads on the tailings impoundment at Laronde Mine are presented in Table 3-1. As noted in Section 3.3.3, these loads are relatively low. They are probably not sufficient to cause liquefaction of the impounded tailings or failure of the dike because it is constructed of compacted earthfill. To evaluate the seismic behavior of the tailings and performance of the impoundment under a range of earthquake loads, rather than the relatively low level site-specific earthquake loads, the earthquake loads used in this study will consist of seismic events with moment magnitudes of 6.5, 6.75, 7, 7.25, and 7.5 with assumed horizontal distances from the fault rupture to the site of 30 km. These loadings were selected because they range from the zone of "satisfactory performance" to the zone of "potential problems" identified by Lo & Klohn (1995) as shown on Figure 2-4.

The parameters associated with the selected earthquake ground motions are given on Table 3-14 and the calculations of these values are presented in Appendix E. As discussed in Section 2.2.3, the Arias intensity is a measure of the intensity of ground motion and represents the total energy per unit weight absorbed by an idealized set of oscillators (Kayen & Mitchell, 1997).

Table 3-14 – Estimated Parameters of earthquakes selected for evaluation of the example impoundment.

No.	Moment Magnitude, M_w	Peak Ground Acceleration (on hard rock), PGA (g)	Arias Intensity, I_h (m/s)
E1	6.5	0.159	0.515
E2	6.75	0.195	0.916
E3	7	0.238	1.629
E4	7.25	0.292	2.897
E5	7.5	0.357	5.151

3.8.3 Modeling of Earthquake Loads

The transverse ground motion record from Site S16 of the 1988 Saguenay (Quebec) earthquake (record S16T) (NRC, 2003) was used as a basis for modeling the ground motions of the earthquakes used in the liquefaction evaluation. This record is shown on Figure 3-27. The rationale and calculations for the selection and modification of this ground motion record are presented in Appendix E. In brief, the acceleration and time-scale of the record were factored such that the Arias Intensities, I_x, in two-dimension analysis (one dimension of horizontal shaking) were equivalent to the three-dimensional (real world) shaking intensities, I_h, (two dimensions of horiziontal shaking) given in Table 3-14.

The estimated PGA values of the simulated ground motions in Table 3-15 are significantly higher than the PGA values of the evaluation earthquakes given in Table 3-14. However, as noted in Section 2.3.1.1, PGA values represent relatively random, isolated peak values and are not a very accurate method of representing earthquake loads

(Seed & Idriss, 1982; Kramer 1996). The timesteps of the modified ground motions varied from 0.005 s to 0.008 s.

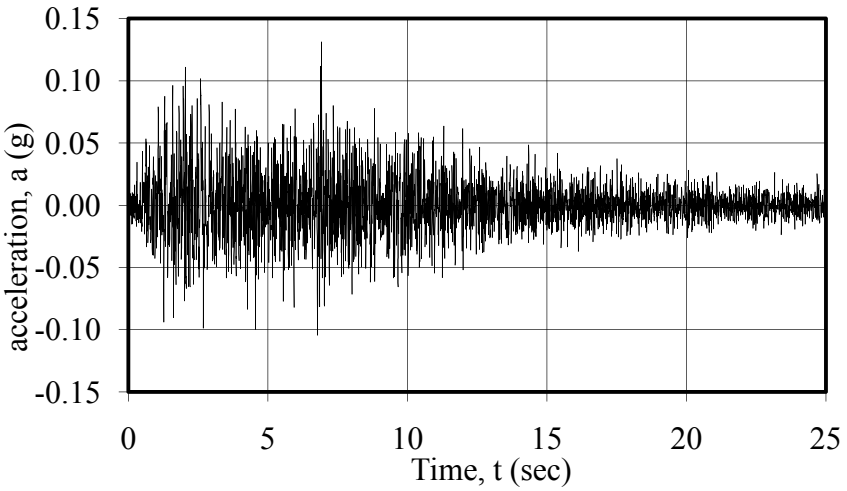

Figure 3-27 – Ground motion of the 1988 Saguenay earthquake - Site S16T (NRC, 2003).

Simulated ground motion records of Earthquakes E1, E2 and E3 are presented on Figure 3-28 and those for Earthquakes E4 and E5 are presented on Figure 3-29. Details on the development of the simulated groundmotion records and spectral acceleration diagrams are presented in Appendix E.

Table 3-15 – Parameters of simulated earthquake ground motions.

No.	Moment Magnitude, M_w	PGA (on hard rock), (g)	Arias Intensity (one dimensional shaking), I_x (m/s)	Duration of Shaking (seconds)
E1	6.5	0.229	0.309	25.0
E2	6.75	0.408	0.550	25.0
E3	7	0.659	0.977	27.5
E4	7.25	0.859	1.738	37.5
E5	7.5	1.432	3.091	40.0

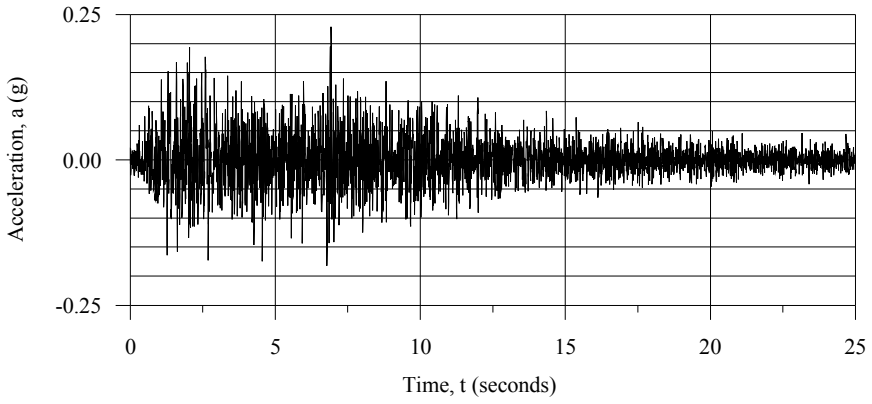

(a) Earthquake E1, M_w=6.5, PGA=0.229 g

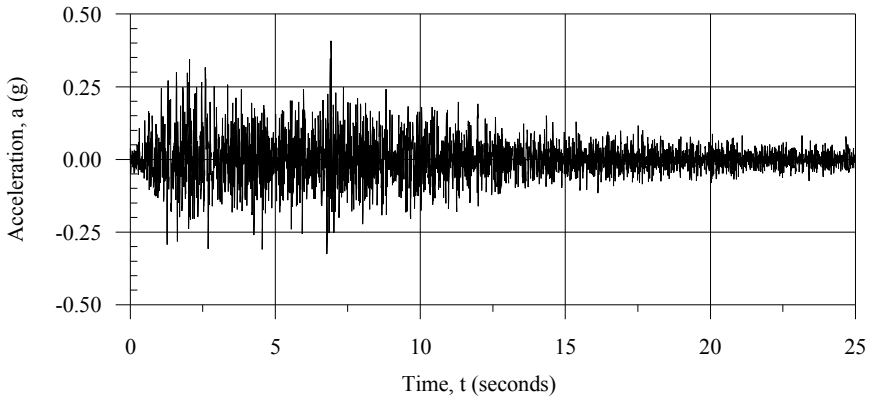

(b) Earthquake E2, M_w=6.75, PGA=0.408 g

Figure 3-28 – Ground motion records of Earthquakes E1 and E2 (see Table 3-15).

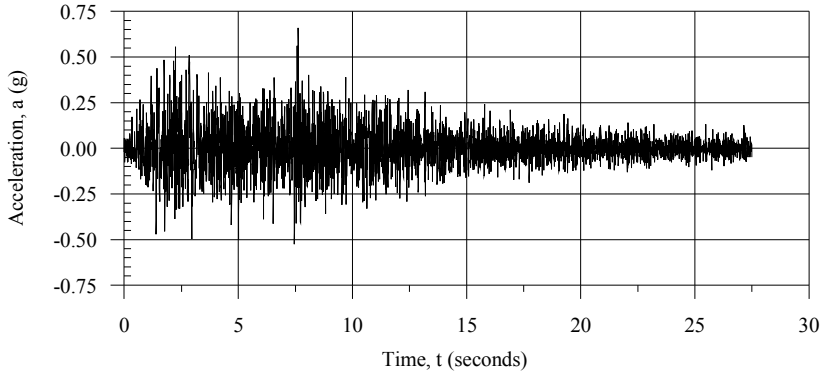

(a) Earthquake E3, M_w=7, PGA=0.659g

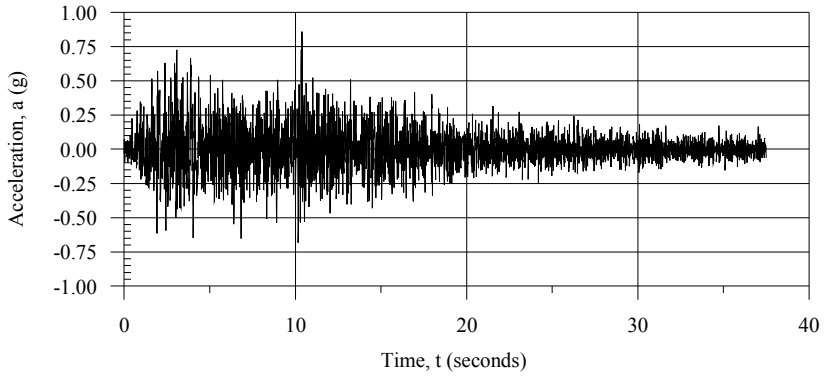

(b) Earthquake E4, M_w=7.25, PGA=0.859g

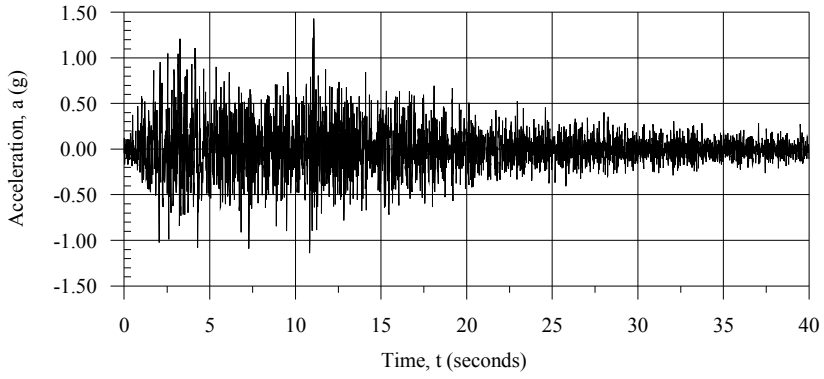

(c) Earthquake E5, M_w=7.5, PGA=1.432 g

Figure 3-29 – Simulated ground motion records of Earthquakes E3, E4 and E5 (see Table 3-15 for details).

3.9 LIQUEFACTION EVALUATION

Evaluations of the potential for liquefaction of the tailings due to various earthquake loadings were conducted using data obtained from the cone penetration testing and laboratory testing programs. There will be essentially three phases in the lifespan of the tailings deposit with respect to the potential for liquefaction:

a) A consolidation phase that exists while the impoundment is active and extends for some years after closure until the deposit is normally consolidated. The behavior of the tailings during this phase can be evaluated using cone penetration testing. However, the results are only applicable to the deposit at the time of testing and may be not be applicable with time due to ongoing consolidation of the deposit;

b) A normally consolidated phase during which the properties of the tailings are relatively stable and can be evaluated from cone penetration testing or laboratory testing of undisturbed or reconstituted samples; and

c) An ageing phase characterized by an increase in liquefaction resistance with time. The liquefaction resistance of the deposit at this time can be evaluated using in situ testing or by the laboratory testing of undisturbed samples. The use of reconstituted samples would probably provide overly-conservative results as they would not include the effects of ageing.

The phase of a tailings deposit must be considered in the analyses of the potential for liquefaction because it determines the applicability and degree of conservatism of the testing and evaluation methods. The phase of a tailings deposit may also be a factor in selecting the earthquake recurrence interval, as the probability of a particular event occurring during a phase depends on the duration of that phase; e.g. if the consolidation phase will last for 5 years, the probability of the 5,000-year earthquake occurring during that phase is about 0.1%.

The liquefaction evaluation assumed “level ground” conditions as defined by the Simplified method of Seed & Idriss (1982) and are applicable to the interior of the impoundment, away from the dynamic influence of the dike.

The liquefaction evaluations of the tailings considered the magnitude 6.5, 7 and 7.5 earthquake loadings (Earthquakes E1, E3 and E5, respectively).

3.9.1 Liquefaction Evaluation using Cone Penetration Test Results

Cone penetration testing of the tailings deposit at the Laronde Mine site was conducted in November 2004. The results are applicable to that period as the properties of the tailings, particularly the degree of consolidation may have changed since then. In areas where no additional tailings have been placed, the degree of consolidation has increased and the tailings liquefaction resistance of the tailings may be greater. In areas where additional tailings have been placed, the degree of consolidation may have decreased and the resistance of the tailings may have decreased.

Evaluation of the liquefaction potential of the tailings involved the following:

a) Modeling of assumed conditions, including soil properties and groundwater level;

b) Site response analyses of the anticipated earthquake loadings;

c) Calculation of the cyclic stress ratios induced by the earthquake (CSR), the cyclic resistance ratios of the tailings (CRR) and the resulting factors of safety with respect to liquefaction;

d) Evaluation of the potential for liquefaction based on the factors of safety.

3.9.1.1 Assumed Conditions

In addition to the assumption of level ground conditions, the following assumptions were made for the liquefaction analysis based on the CPT data:

a) The properties of the tailings as derived from cone penetration testing (Section 3.7.2) and conventional laboratory testing (Section 3.7.1) are applicable;
b) The liquefaction resistance of the tailings can be estimated using the Simplified method of Seed & Idriss (1981) for cone penetration testing and assuming the resistance of the tailings is similar to that of "clean" sand. This assumption is based on the findings that the conversion factor for the penetration resistances (q_c and N) was found to be similar to that for sand rather than silty sand (Section 3.7.3.6) and the dynamic behavior and liquefaction resistance of the tailings in CDSS testing was similar to that of sand (Section 3.5.6);
c) The phreatic surface coincides with the surface of the tailings and porewater pressures within the tailings are hydrostatic;
d) The tailings deposit is 15-m-thick; and
e) The tailings are underlain by a 2-m-thick layer of glacial till over hard bedrock.

3.9.1.2 Analyses and Results

The site response analyses and calculation of the CSR and CRR values and the corresponding factors of safety with respect to liquefaction are presented in Part 3 of Appendix E. The results of the analyses are presented below.

Liquefaction calculation spreadsheets for all of the CPT logs with the three earthquake loadings considered in the analysis are presented in Appendix F. The estimated profiles of the CSR, CRR and factor of safety with respect to liquefaction for Earthquakes E1, E3 and E5 (Mw=6.5, 7 and 7.5 respectfully) are also presented in Appendix F.

Site response analyses were completed using NERA (Bardet & Tobita, 2001). The results of the site response analyses are summarized on Table 3-16. The amplification factors, F_a were calculated using the following formula:

$$F_a = \frac{PGA_x}{PGA_{BR}} \quad (3\text{-}12)$$

where: PGA_x is the peak (horizontal) ground acceleration at some reference point (e.g. the ground surface); and

PGA_{BR} is the peak (horizontal) ground acceleration on the top of bedrock.

The amplification factors vary from 0.109 and 0.424 and decrease with the intensity of the applied earthquake load. Application of the ground motions (horizontal accelerations) resulted in severe damping of the accelerations as the ground motion traveled from the bedrock to the surface. The reason for the severe damping of the accelerations was the relatively low shear modulus of the tailings and the drastic reduction of the shear modulus with shear strain.

Table 3-16 – Summary of site response analyses based on CPT 02-02 data with respect to Earthquakes E1, E3 and E5.

Earthquake	Moment Magnitude, M_w	PGA on Rock (g)	PGA on Surface of Tailings (g)	Amplification Factor, F_a
E1	6.5	0.229	0.097	0.424
E3	7	0.659	0.127	0.193
E5	7.5	1.432	0.156	0.109

Profiles from the analysis of CPT 02-02 for Earthquakes E1, E3 and E5 are presented in Figures 3-30, 3-31 and 3-32, in sequence. The profiles from CPT 02-02 are typical of the profiles from the liquefaction evaluation of the cone penetration testing data.

As shown on Figure 3-30, the CSR induced in the tailings modeled on the results of CPT 02-02 vary from about 0.05 near the surface to about 0.14 at a depth of 13.5 m and the CRR (based on the tip resistance) is relatively uniform with depth and varies between

0.065 and 0.075. The corresponding factors of safety with respect to liquefaction vary from about 1.25 near the ground surface to about 0.5 at a depth of 13.5 m.

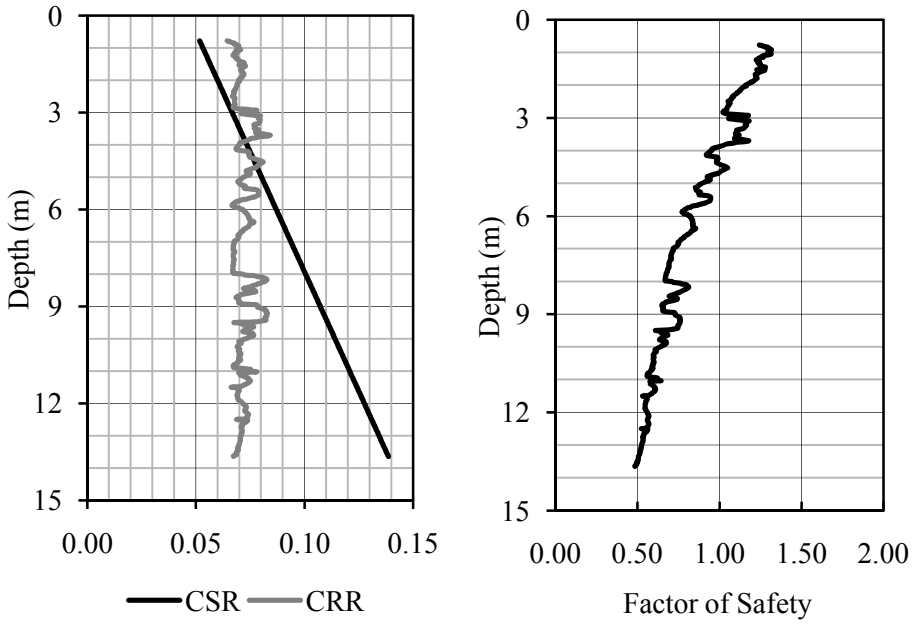

Figure 3-30 – Profiles of the CSR and CRR and of the factor of safety with respect to liquefaction based on the log of CPT 02-02 for Earthquake E1 (M_w=6.5).

Liquefaction analysis of the data from CPT 02-02 for Earthquake E3 is presented on Figure 3-31. The CSR increases from about 0.08 near the surface of the tailings to about 0.3 at a depth of 13.5 m while the CRR varies roughly between 0.06 and 0.075. The resulting factor of safety profile varies from about 0.75 near the surface of the tailings, and decreases to less than 0.25 at a depth of 13.5 m.

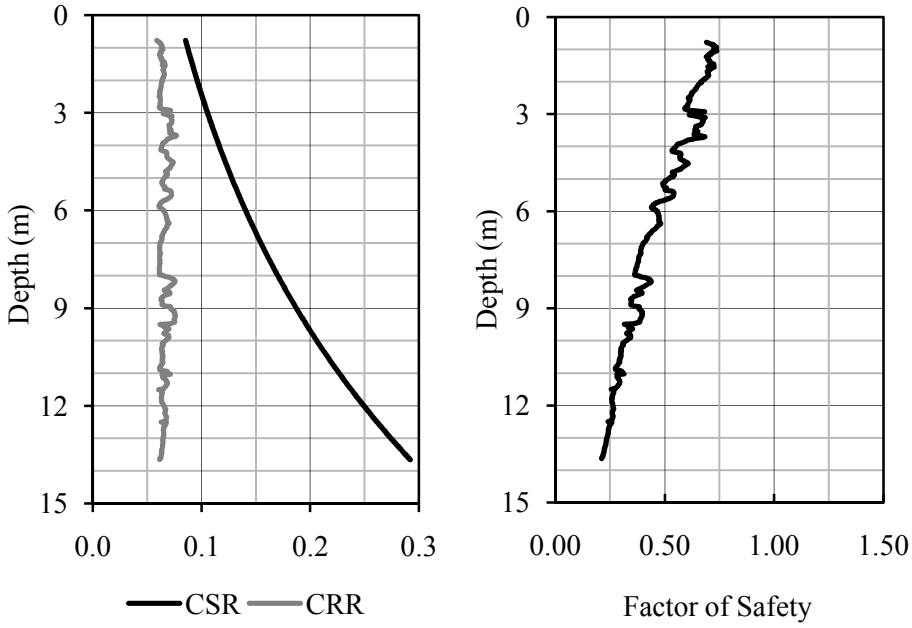

Figure 3-31 – Profiles of the CSR and CRR and of the factor of safety with respect to liquefaction based on the log of CPT 02-02 for Earthquake E3 (M_w=7.0).

Analysis of the potential for liquefaction of the tailings due to Earthquake E5 using the CPT 02-02 data is presented on Figure 3-32. The CSR is approximately 0.1 near the ground surface and increases to 0.5 at a depth of 13.5 m. The CRR varies between 0.055 and 0.07. The factor of safety with respect to liquefaction varies from about 0.6 near the surface of the tailings to approximately 0.12 at a depth of 13.5 m.

In the three cases presented, the CSR, the dynamic loading on the tailings, increased with increasing earthquake loading, while the CRR, the dynamic resistance of the tailings, decreased with increasing earthquake loading. The increase in the CSR is primarily due to the influence of the peak horizontal ground acceleration (a_{max} in Equation 2-5) and the decrease in the CRR is primarily due to the magnitude scaling factor, MSF.

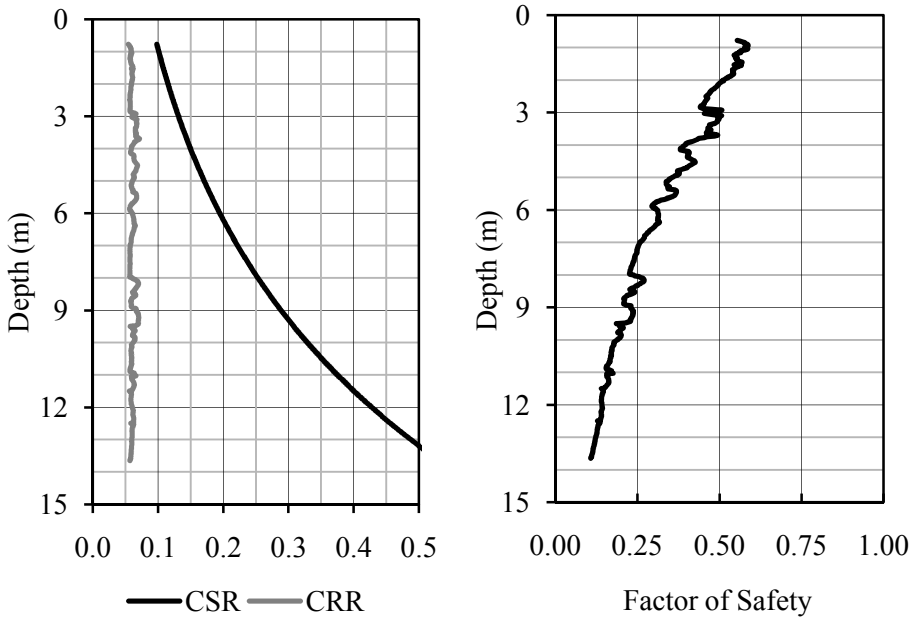

Figure 3-32 – Profiles of the CSR and CRR and of the factor of safety with respect to liquefaction based on the log of CPT 02-02 for Earthquake E5 (M_w=7.5).

In general, liquefaction analysis of all of the CPT data provided similar results. However, there were some isolated zones of increased cone tip resistance, q_c, on some of the CPT logs that gave higher liquefaction resistance (see Appendix F). As noted previously, these zones are believed to be the result of over-consolidation and hard pan in zones of the tailings due to exposure and desiccation during placement.

3.9.1.3 The Potential for Liquefaction

The potential for liquefaction of the tailings was evaluated based on the calculated factors of safety with respect to liquefaction as defined in Section 2.3.1.5.

Factors of safety below 1.0 indicate that liquefaction is very likely to occur in the event of the selected earthquakes, with the likelihood of liquefaction increasing as the factor of safety decreases. Factors of safety above 1.0 indicate that liquefaction is unlikely to

occur, with the likelihood of liquefaction decreasing with increasing with the factor of safety. Marginal values in the area of 1.0 indicate that liquefaction is likely.

Low factors of safety, below 0.7 for instance, indicate that liquefaction may occur well before the end of shaking.

Based on laboratory testing with uniform cycles of dynamic loading, DeAlba et al. (1975) indicate that the porewater pressure development due to cyclic loading is approximately linear. This finding can be extrapolated to an assumption that the porewater pressure ratio developed in soil due to earthquake loading that does not induce liquefaction, can be approximated by the inverse of the factor of safety. For example, an earthquake loading that produces a factor of safety of 2, induces half of the cyclic loading required to induce liquefaction (where liquefaction is defined as r_u=1.0) and this loading produces an r_u value of 0.5.

Based on the liquefaction analysis of the CPT data, the occurrence of any of the evaluation earthquakes (E1 through E5) would result in widespread liquefaction of the tailings. Although the liquefaction analyses for Earthquake E1 indicated that the factors of safety with respect to liquefaction in the upper 4 to 5 m of the tailings would be slightly above 1.0, they would generally be less than 1.2 and there would still be a significant probability of liquefaction as defined by the occurrence of the steady state condition rather than an excess porewater ratio, r_u, of 1.0 (refer to Section 2.2.2.2).

As noted previously, the CPT data represents the existing condition of the impoundment where the tailings are under-consolidated. However, assuming that the tip resistance accounts for the under-consolidated state of the tailings, the estimated factors of safety are representative of the liquefaction potential of the tailings at the time of testing.

3.9.2 Liquefaction Analyses Using CDSS Test Results

The cyclic direct simple shear testing conducted on consolidated tailings samples was used to estimate the cyclic resistance of the tailing within the deposit under normally

consolidated conditions. This does not represent the current condition of the tailings. It represents the conditions of the tailings at some time in the future when the deposit will be normally consolidated.

The potential for liquefaction of the tailings deposit was evaluated in four steps:

a) Modeling of assumed conditions, including topography, soil properties and groundwater levels;

b) Site response analyses of the anticipated earthquake loads (E1, E3 and E5);

c) Calculation of the cyclic stress ratios (CSR) induced by the earthquake, the cyclic resistance ratios (CRR) of the tailings and the corresponding factors of safety with respect to liquefaction; and

d) Evaluation of the potential for liquefaction based on the factors of safety.

3.9.2.1 Assumed Conditions

The liquefaction evaluation assumed the following:

a) Level ground conditions;

b) The properties of the tailings can be derived from the conventional and CDSS laboratory testing;

c) The liquefaction resistance of the tailings can be determined from the CDSS test results;

d) The phreatic surface is located at the surface of the tailings and porewater pressures are hydrostatic;

e) The tailings deposit is 15-m-thick; and

f) The tailings are underlain by a 2-m-thick layer of glacial till over hard bedrock.

3.9.2.2 Analyses and Results

The site response analyses and calculation of the CSR and CRR values and the corresponding factor of safety with respect to liquefaction are presented in Part 4 of Appendix E. The results of the analyses are presented below.

The site response analyses produced the amplification factors, F_a, of 0.694, 0.420 and 0.233 for Earthquakes E1, E3 and E5, respectively (refer to). All of the ground motions were damped as they transited the tailings with the degree of damping increasing with the intensity of the loading. The amplification factors produced in the site response analyses using CDSS test results were roughly double those produced in the analysis using CPT results (see Table 3-16), indicating significantly less damping in the normally consolidated tailings compared to the under-consolidated tailings.

Table 3-17 – Results of site response analyses based on CDSS test results.

Earthquake	Moment Magnitude, M_w	PGA on Rock (g)	PGA on Surface of Tailings (g)	Amplification Factor, F_a
E1	6.5	0.229	0.159	0.694
E3	7	0.659	0.277	0.420
E5	7.5	1.432	0.334	0.233

The CSR, CRR profiles and the resulting factor of safety profiles for Earthquakes E1, E3 and E5 are shown respectively on Figures 3-33, 3-34 and 3-35.

For Earthquake E1, the CSR induced in the tailings varies from about 0.11 near the ground surface to 0.20 at a depth of 15 m while the CRR of the tailings is about 0.11 and constant with depth (refer to Figure 3-33). The variation in the CSR is due to the influence of the stress reduction factor, r_d, and the uniformity of the CRR is due to the lack of influence of the effective consolidation stress on the cyclic resistance of the

tailings in CDSS testing. The factor of safety with respect to liquefaction varies from about 1 near the ground surface to about 0.5 at a depth of 15 m.

Figure 3-34 shows the results of the liquefaction analysis for Earthquake E3 (M_w=7.0) based on CDSS test results. The CRR is uniformly about 0.1 with depth while the CSR varies from 0.19 near the ground surface to 0.44 at a depth of 0.44 m. The factor of safety varies from 0.6 near the surface to about 0.2 at the bottom of the tailings (z = 15 m).

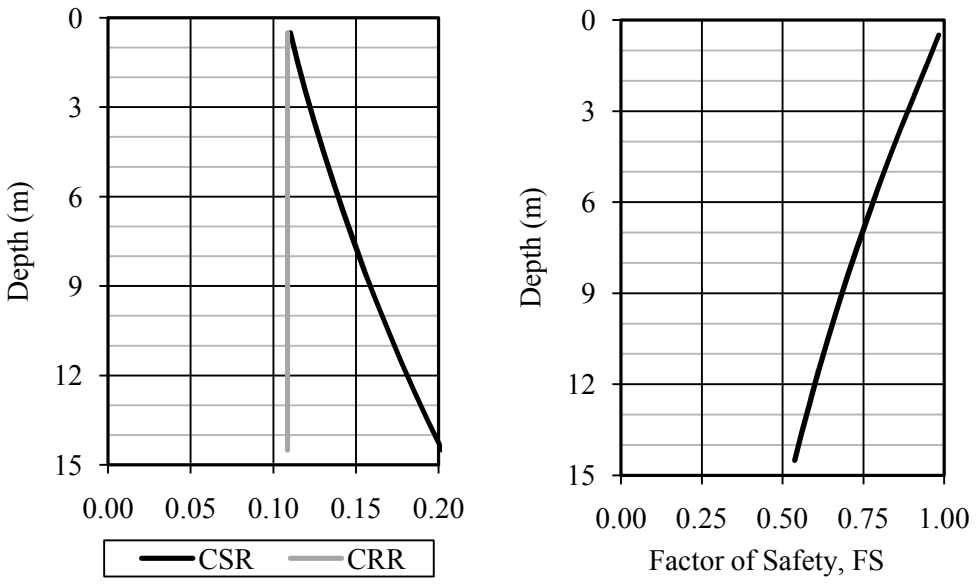

Figure 3-33 – Profiles of the CSR and CRR and of the factor of safety with respect to liquefaction based on CDSS test results for Earthquake E1 (M_w=6.5).

The profiles of CSR, CRR and FS for the analysis of the CDSS data with respect to Earthquake E5 are shown on Figure 3-35. The CSR is constant with depth at a value of about 0.08 while the CRR is just under 0.25 at the surface and increases to about 0.85 at a depth of 15 m. The resulting factor of safety is about 0.4 near the surface and 0.1 near the bottom of the tailings.

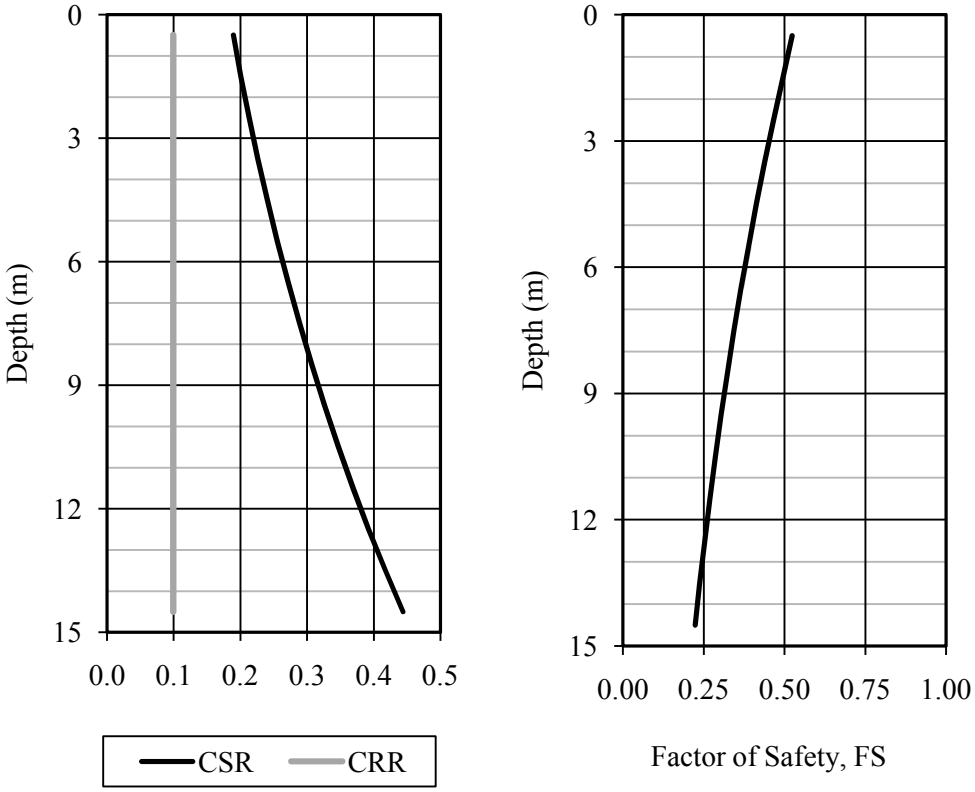

Figure 3-34 – Profiles of the CSR and CRR and of the factor of safety with respect to liquefaction based on CDSS test results for Earthquake E3 (M_w=7.0).

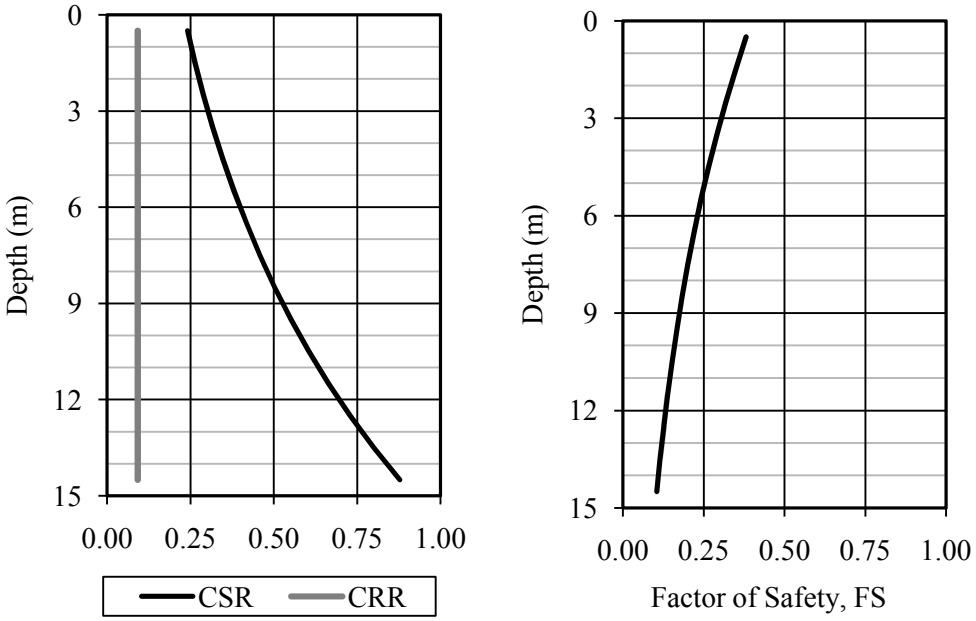

Figure 3-35 – Profiles of the CSR and CRR and of the factor of safety with respect to liquefaction based on CDSS test results for Earthquake E5 (M_w=7.5).

3.9.2.3 The Potential for Liquefaction

Based on the analyses, the tailings would be subject to widespread liquefaction in the event of any of the earthquakes considered. The factors of safety due to Earthquake E1 (M_w=6.5) vary from 0.5 to 1, indicating liquefaction throughout the depth and extent of the tailings. The factors of safety due to Earthquakes E3 and E5 are even lower, ranging from 0.2 to 0.6 for Earthquake E3 and from 0.15 to 0.4 for Earthquake E5. These very low values indicate that liquefaction would occur well before the end of significant shaking.

3.9.3 Remarks on the Liquefaction Analyses

The results, amplification factors and factors of safety, of the liquefaction analyses using CPT and CDSS test data are summarized on Table 3-18.

Table 3-18 – Summary of the liquefaction analyses based on CPT and CDSS test data.

		Earthquake E1 (M_w=6.5)	Earthquake E3 (M_w=7.0)	Earthquake E5 (M_w=7.5)
CPT	F_a	0.424	0.193	0.109
	F.S.	1.25 – 0.5	0.75 – 0.25	0.65 – 0.1
CDSS	F_a	0.694	0.420	0.233
	F.S.	1.0 – 0.5	0.55 – 0.2	0.4 – 0.1

F_a – amplification factor; F.S. – factor of safety with respect to liquefaction.

Comparing the results of the liquefaction analyses based on the cone penetration testing of under-consolidated tailings and the CDSS testing of normally consolidated tailings, the following general observations are noted:

- The amplification factors from the CDSS test data (consolidated tailings) were significantly larger than from the CPT data (unconsolidated tailings). The difference is attributed to the consolidated tailings being stiffer based on the shear modulus.

- Cyclic loading (CSR) in the consolidated tailings is 30 to 50% greater than in the unconsolidated tailings. This is attributed to the greater stiffness of the consolidated tailings which resulted in less damping.

- The cyclic strength (CRR) of the consolidated tailings is about 30 to 40% greater than that of the unconsolidated tailings. This increase in strength is be attributed to the consolidation of the tailings.

- Generally, the factors of safety with respect to liquefaction of the consolidated tailings were slightly less than those of the under-consolidated tailings. This can be attributed in part to the stiffness of the consolidated tailings, which led to greater amplification of the ground motion and great cyclic stress ratios,

and the fact that this was not counteracted entirely by gain in cyclic resistance with consolidation.

Recall that the software used for site response analyses (NERA) is not capable of considering the effect of excess porewater pressure generation during shaking. This is true for other site response analyses programs, including the most commonly used, Shake (Schnabel, 1972). The effect of excess porewater generation during shaking is to reduce the effective stress and thus the shear modulus of the soil, in addition to any reduction due to shear strain. However, the influence of excess porewater pressure generation can be incorporated in dynamic numerical analysis as is shown in Chapter 4 of this thesis.

3.10 PRELIMINARY STABILITY EVALUATION OF THE REPRESENTATIVE TAILINGS IMPOUNDMENT

A preliminary evaluation of the stability of the example impoundment under static and seismic conditions was undertaken using conventional limit equilibrium methods and the Geo-Slope© 2004 computer software package (version 6.21 by Geo-Slope International Ltd. (2004). This program is very widely used in engineering practice and academic research in the analysis of slopes, embankments, dams, and dikes. The purpose of the preliminary stability evaluation was to establish benchmark values on the stability of the impoundment under static and dynamic conditions prior to the FLAC analysis presented in Chapter 5 of this thesis.

The assumed cross-section of the dike used in the evaluation is shown on Figure 3-36. This cross-section is based on Drawing No. 3 in Appendix I. The model duplicates the geometry of the dike as shown in the typical cross-section. However, the berm was not included in the model as it is not a typical feature of tailings impoundments.

The material properties used in the analysis are also shown in Table 3-19. The materials were assumed to be homogeneous and isotropic. The properties of the tailings were derived from the laboratory testing and the tailings were assumed to be normally consolidated. The properties of the rockfill were estimated from Leps (1970) and Sherard

et al. (1963). The properties of the compacted clayey till and sand filter were estimated from Bowles (1996). Milligan (1976) was used to estimate the properties of the glacial till. The typical properties of similar rock were used to estimate the properties of the bedrock (Goodman, 1989). Hydraulic conductivities for all of the materials except the tailings were estimated from typical values provided in Freeze and Cherry (1979).

The liquefaction evaluations of the tailings indicated widespread liquefaction of the tailings in the event of any of the assumed earthquakes. Due to the low factors of safety with respect to liquefaction estimated in the liquefaction evaluation, it is assumed that the tailings will be either be fully liquefied or develop very high excess porewater pressures prior to the end of significant shaking. Thus, a liquefied strength ratio of 0.1 was applied to the tailings in the seismic analysis (refer to Section 3.7.2.3). This strength can be modeled in Slope/W by reducing the effective friction angle such that the tangent of the effective friction angle is equal to 0.1. The reduced effective frictional angle is therefore equal to 5.7°.

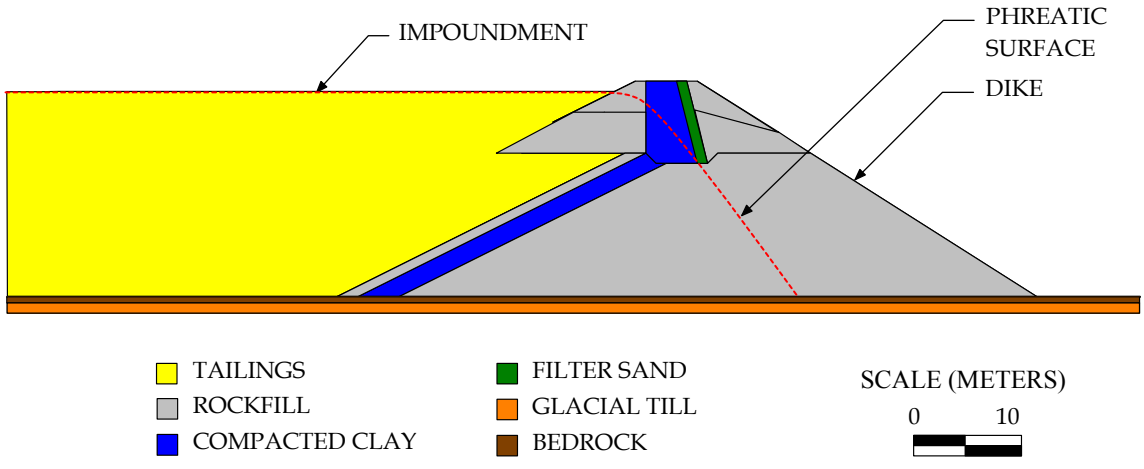

Figure 3-36 – Assumed cross-section of the dike at the example impoundment.

The level of the phreatic surface was estimated through finite element seepage analysis using the Seep/W© computer program, part of the Geo-Slope software package.

Stability analyses were conducted using the Slope/W© computer program that is also part of the Geo-Slope software package. Stability analyses used the Morgenstern-Price half-sine function to estimate inter-slice forces and the slip surfaces were found using the built-in iterative auto-locate function with a minimum slip surface thickness of 5 m, except where otherwise noted. A minimum slip surface thickness was used to disregard shallow slip surfaces that are common in cohesionless materials but are generally not a threat to stability of the structure.

The model created in Geo-Slope is shown on Figure No. 1 (Appendix G).

Table 3-19 – Material properties used in seepage and slope stability analysis.

Material Description	Dry Unit Weight, γ_d (kN/m^3)	Void Ratio, e	Effective Friction Angle, ϕ'	Cohesion, c (kPa)	Hydraulic Conductivity, k_{sat} (m/s)
Tailings (static case)	23.2	0.64	36.6	0	$2.25x10^{-6}$ H $4.50x10^{-7}$ V
Tailings (seismic case)	23.2	0.64	5.7	0	$2.25x10^{-6}$ H $4.50x10^{-7}$ V
Rockfill (0-150 mm)	22.2	0.15	46.0	0	0.1
Rockfill (0-300 mm)	22.2	0.15	46.0	0	0.1
Compacted clayey till	19.6	0.18	32.0	200	$1.0x10^{-7}$
Sand (filter)	19.6	0.30	34.0	0	$1.0x10^{-4}$
Glacial till	19.6	0.18	36.0	250	$1.0x10^{-7}$
Bedrock	26.0	0.02	25.0	50,000	$1.0x10^{-8}$

3.10.1 Seepage Analysis

The purpose of the seepage analysis was to determine the level of the phreatic surface within the impoundment as well as the distributions of hydrostatic and seepage pressures. Boundary conditions consisted of hydrostatic pressure heads along the sides of the impoundment corresponding to the surface elevation, elevation 340 m on the upstream side of the model and elevation 320 m on the downstream side of the model. The bottom of the model was assumed to be an impermeable boundary.

The results of the seepage analysis are shown on Figure No. 2 (Appendix G). Within the impoundment, the phreatic surface is at the surface of the tailings. Within the dike, the phreatic surface is roughly parallel to the compacted clayey till core. Downstream of the core, the phreatic is near the surface of the bedrock.

The results of the seepage analysis were directly incorporated into stability analyses, so the hydrostatic and seepage pressures generated in the seepage analysis were considered in the stability analyses.

3.10.2 Static Stability

Using Slope/W, the factor of safety of the dike under static conditions was calculated to be 3.07 with the critical slip surface extending from just upstream of the crest to the downstream toe of the dike (refer to Figure No. 3 of Appendix G).

This factor of safety is well above the minimum of 1.5 recommended by the CDA (2007) for tailings dikes under static conditions. The dike is considered to be stable with respect to the static loading evaluated.

3.10.3 Seismic Stability

The seismic stability of the impoundment under the five earthquake loads described in Section 2.8.2 was analyzed using the pseudo-static method as described in Section 2.8.1.1. Based on the various recommendations for the selection of a pseudo-static coefficient, k, described in Section 2.8.1.1 and the CDA (2007), the pseudo-static

coefficient was assumed to equal 3/4 of the PGA (on rock) with reduction in material strengths.

The results of the pseudo-static analysis are summarized on Table 3-20.

The factors of safety range from 2.27 for Earthquake E1 (M_w=6.5) to 0.88 for Earthquake E5 (M_w=7.5). The factors of safety for Earthquake E4 (M_w=7.25) and E5 are below the minimum value of 1.1 recommended by the CDA (2007). However, due to the known inaccuracy of the pseudo-static method (refer to Section 2.8.1.1), the low factors of safety associated with Earthquakes E4 and E5 are not necessarily indicative of failure. They indicate the need for additional analyses using dynamic numerical methods as recommended by the Dam Safety Guidelines of the CDA (2007).

Table 3-20 – Summary of pseudo-static analysis of Dike 1.

Earthquake	M_w	PGA (on rock) (g)	Pseudo-static Coefficient, k	Factor of Safety	Figure No. (Appendix G)
E1	6.5	0.159	0.119	2.27	4
E2	6.75	0.195	0.146	1.65	5
E3	7	0.238	0.179	1.24	6
E4	7.25	0.292	0.219	1.03	7
E5	7.5	0.357	0.268	0.88	8

The modes of potential failure indicated by the slip surfaces are interesting. The slip surface associated with Earthquake E1 is similar to that of the static analysis and characterized by a moderately deep failure within the dike that does not directly involve the impounded tailings, as shown on Figure No. 4 (Appendix G). The slip surface associate with Earthquake E2 extends from 70 m in to the impoundment and encompasses the two raises of the dike and the downstream slope. The geometry of this failure surface indicates that the low strength and relatively high mass of the

liquefied tailings within the impoundment have a significant and detrimental effect on the seismic stability of the dike. This effect is due to the horizontal loading of the tailings on the dike simulated by the pseudo-static coefficient and the high unit weight and reduced shear resistance of the tailings. For Earthquakes E3, E4 and E5, the slip surfaces extend far into the impoundment and though the dike at the approximate boundary between the initial dike and the first raise. The geometries of these surfaces are also ascribed to the effect of the liquefied tailings on the seismic stability of the dike.

For comparative purposes, a pseudo-static analysis of the impoundment subject to Earthquake E5 was also conducted assuming a conventional circular slip surface. This resulting factor of safety is 1.50 and the slip surface is characterized by a moderately deep arc in the downstream slope of the dike (refer to Figure No. 9 of Appendix G). The mode of failure developed by the assumption of a circular slip surface is remarkably unconservative given the findings using a randomly generated slip surface through the "auto-locate" function in Slope/W. In this instance, the mode of failure developed with a circular slip surface is non-critical and could be misleading with respect to the seismic stability of the impoundment.

The non-circular slip surfaces generated by the "auto-locate" function are kinematically admissable considering that:

a) The use of the pseudo-static coefficient actually imparts a lateral component of gravity to the model that may change the shape and orientation of the failure surface;

b) The liquefied tailings have very low strength and a greater unit weight than the rockfill, thus with increasing pseudo-static coefficient, the tendency for a horizontal failure surface through extending through the tailings increases;

c) The intersection of the lower portion of the dike with the first raise represents a weakness (a thinner section) through the rockfill dike that was exploited as the pseudo-static coefficient increased; and

d) Similar potential failure surfaces were developed in dynamic numerical analyses of the dike using ground motions from the 1988 Saguenay and 1994 Northridge earthquakes (James et al., 2006).

Non-circular failure surfaces are generally associated with geometric features within or underlying slopes (Duncan & Wright, 2005; Chen & Lau, 2008)

3.11 REMARKS ON THE GEOTECHNICAL STUDY

In brief, the following findings and conclusions were developed in the geotechnical study:

a) The properties and characteristics of the tailings from the example site are similar to those given for hard rock tailings in published sources;

b) The shear strength of the tailings is significantly greater than that of naturally occurring soils of similar gradation (silts and silty sands);

c) Cone penetration testing indicates that the degree of consolidation of the tailings varies significantly with depth. However, the tailings are generally under-consolidated although there some lenses of over-consolidated material;

d) The dynamic behavior and liquefaction resistance of the tailings, as measured by CDSS testing, is very similar to that of loose, fine-grained sand;

e) During CDSS testing, the liquefaction resistance of the tailings was not affected by the effective vertical consolidation stress for a given magnitude of cyclic shear ratio;

f) A 15 cycles of loading, equivalent to a moment magnitude 7.5 earthquake, the cyclic resistance of the tailings was equivalent to a clean sand with a corrected

standard penetration blow count, $(N_1)_{60}$ of 7.5 blows per 300 mm or a corrected tip resistance, q_{c1N}, of 50. However, a value of 6 was found to be an appropriate conversion factor for converting q_{c1N} values to $(N_1)_{60}$ values;

g) The liquefied shear strength ratio of the tailings is estimated to be 0.10;

h) Based on similarities between the liquefaction potential as estimated from the cone penetration testing and the CDSS testing, the Simplified method, as described by Youd et al. (2001) appears to be suitable for the evaluation of the liquefaction resistance of tailings. However, the correction of the penetration resistances and the magnitude scaling factors should be evaluated for each specific case;

i) The maximum shear modulus, G_{max}, of the tailings was found to relatively low and essentially independent of effective consolidation stress;

j) Shaking resulted in relatively large shear strains in the tailings that led to large decreases in the shear modulus and high damping;

k) The shear modulus reduction curves of the tailings may be approximated by the curves for sand presented in Seed et al. (1984);

l) Evaluation of the liquefaction potential of the tailings deposit at the representative site indicated a very high potential for liquefaction under all the earthquake loadings considered; and

m) Pseudo-static evaluation of the example impoundment found that loss of strength within the tailings due to liquefaction has a deleterious effect on the seismic stability of the impoundment.

CHAPTER 4. PRELIMINARY NUMERICAL ANALYSIS OF THE DYNAMIC BEHAVIOR OF THE TAILINGS

4.1 INTRODUCTION

The use of waste rock inclusions to control the effects of liquefaction in tailings impoundments was evaluated using dynamic numeral modeling. Evaluations of the representative tailings impoundment and of a conceptual upstream-raised tailings impoundment, both with and without waste rock inclusions, are presented in Chapters 5 and 6, respectively. However, as a preliminary step it was necessary to calibrate and validate the selected system of analysis, which consists of FLAC (Section 2.7.3) and the UBC Sand model (Section 2.7.2), with respect to its ability to simulate the dynamic behavior of the tailings, including excess porewater pressure development, shear strain, and liquefaction. The CDSS testing results were used as a benchmark for calibration of the UBC Sand model and to determine the ability of the system to simulate the dynamic behavior of the tailings.

The liquefaction potential of the representative tailings deposit was evaluated, using FLAC and the UBC Sand model, with respect to earthquakes of various intensities and assuming level ground conditions. The liquefaction evaluations were completed assuming the tailings were either in an under-consolidated condition or normally consolidated. The degree of under-consolidation of the tailings was assumed to be the same as that in the representative impoundment based on cone penetration testing and the properties of the consolidated tailings were derived from the CDSS testing. The results of the liquefaction evaluations were compared with the analytical liquefaction evaluations based on the cone penetration test results and CDSS test results presented in Chapter 3.

This chapter contains descriptions and the results of the calibration and validation of the system of analysis, estimated parameters for applying the UBC Sand model to the tailings, the dynamic numerical evaluations of the liquefaction potential of the representative tailings deposit under level ground conditions, and comparisons of the results of analytical and numerical liquefaction evaluations.

4.2 SYSTEM OF ANALYSIS

The system used in the analysis consisted of the FLAC software program and the UBC Sand numerical model. Additional information on FLAC and the UBC Sand model are provided in Sections 2.7.3 and 2.7.2, respectively.

Version 5.00.346 (single precision) of the FLAC computer program by Itasca Consulting Group Inc. was used in the numerical analyses completed for this research. The program uses the explicit finite difference method to simulate material and fluid behavior and was specifically designed for geotechnical applications in two dimensions. Itasca (2005) recommends using the double precision version of FLAC when the accumulated value of a property is 6 orders of magnitude greater than the incremental values associated with the time steps. As that condition was not encountered, the single precision version of FLAC was found to be sufficient for this research.

The UBC Sand model can be implemented in FLAC as a user-defined model (subprogram) with the FISH programming language included with FLAC or as a C++ subroutine compiled as a DLL file (dynamic linked library). The numerical analysis completed for this research used the DLL version of the model.

Initial verification of the operation of the model was completed using the verification example created by Dr. Peter Byrne of the University of British Columbia and provided by The Itasca Consulting Group Inc. of Minneapolis, Minnesota and indicated proper functioning of the FISH and DLL versions of the model.

4.3 NUMERICAL MODELING OF THE CDSS TESTING

The UBC Sand model was developed to simulate the dynamic behavior of sand. Therefore, its applicability to the tailings was verified through FLAC modeling of the cyclic direct simple shear testing conducted for this research project (refer to Section 3.5.6) with the UBC Sand model used to simulate the behavior of the tailings. The modeling was also used to determine the appropriate UBC Sand model parameters for the

tailings, specifically the standard penetration test blow count, $(N_1)_{60}$, and the constant volume friction angle, ψ_{cv}.

4.3.1 Model Geometry

The CDSS testing device was modeled two-dimensionally in plane stress using two elements. An upper element represented the steel upper platen of the testing device, while a lower element represented the sample (tailings). It was not necessary to model the lower platen due to it's being stationary during testing. As noted in the Section 3.5.6, the actual samples were disc-shaped with diameters of 70 mm and heights varying between 20 and 25 mm giving a height to width ratio through the center of 0.286 to 0.357. However, during the numerical analysis it was found that using height to width ratios similar to those of the actual samples resulted in significant deviation in the behavior of the model relative to the CDSS testing, particularly at lower cyclic stress ratios (e.g. samples modeled with CSR values of 0.075 liquefied much sooner than expected based on the test results). Through an iterative process it was determined that using a height to width ratio of 0.714 significantly reduced this deviation. The height to width ratio of the actual samples varied between 0.286 and 0.357 when measured through the center of the samples. The height to width ratios of the samples actually varied from 0.286 through the center to greater than 1.0 near the sides. Thus, the height to width ratio used in the modeling was more representative of the average height to width ratio of each sample.

The samples were modeled using a height of 50 mm and a width of 70 mm. The upper platen was assumed to be 5 mm thick. The actually upper platen is much larger. However, for modeling purposes, that size of the platen is not significant. It need only be very rigid with relative to the sample. The geometry of the model is shown on Figure 4-1.

The steel-wire reinforced rubber membrane used to contain the sample during CDSS testing was not simulated in this FLAC model.

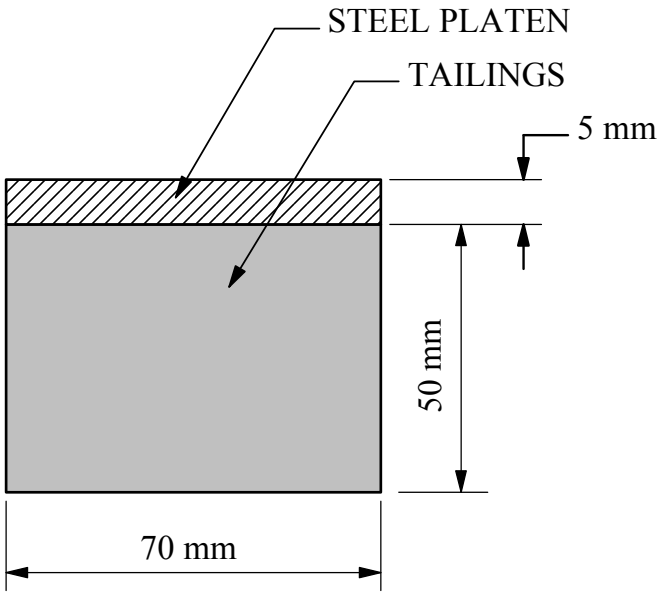

Figure 4-1 – Schematic of FLAC model of CDSS test apparatus.

4.3.2 Material Properties

The upper platen was assumed to consist of steel that was simulated using the "Elastic" material model in FLAC with the material properties shown in Table 4-1. The hydraulic conductivity was assigned to represent the characteristics of the drain stone within the platen during consolidation. During the dynamic loading, no flow was permitted through the upper platen.

Table 4-1 - Material properties of steel platen used in modeling of the CDSS testing.

Property	Value
Density, γ	77.0 kN/m^3
Shear modulus, G	7.5x10^7 kPa
Bulk modulus, K	1.62x10^8 kPa
Hydraulic conductivity, k	1.0 m/s

As noted, the tailings were simulated using the UBC Sand model. The properties of the tailings were based on the average values of the dry density, void ratio and hydraulic conductivity as determined from laboratory testing (refer to Section 3.7). In trial runs, varying the dry density and porosity of tailings based on the effective vertical consolidation stress has no significant effect on the results. The constant volume friction angle, ψ_{cv}, was determined using Equation 2-37, assuming that the corrected standard penetration test blow count, $(N_1)_{60}$, would be approximately 10 blows/300 mm based on typical $(N_1)_{60}$ values for loose sand (Terzaghi et al., 1996). The material properties used for the tailings are given in Table 4-2. The value of the UBC Sand model parameter associated with the corrected standard penetration blow count was a variable that was determined during the FLAC analysis. A value of 2.2×10^6 kPa was used for the bulk modulus of water (Itasca, 2005).

Table 4-2 - Material properties of tailings used in FLAC modeling of CDSS testing.

Property	Value
Dry density, γ_d	23.2 kN/m^3
Void ratio, e	0.64
Hydraulic conductivity, k	4.5×10^{-7} m/s
Constant volume friction angle, ψ_{cv}	35.6°

4.3.3 Assumptions

The following assumptions were made regarding the numerical simulation of the CDSS testing:

- Plane stress modeling with a sample size of 70 mm wide by 50 mm high was assumed to be equivalent to CDSS testing with a sample diameter of 70 mm and a height of 20 to 25 mm;
- The tailings were assumed to be fully saturated;
- The effects of the membrane on CDSS test behavior and results were assumed to be included in the modified geometry;
- The properties of and stresses within the sample were assumed to uniform. This condition was enforced by the use of a single element to model the sample; and
- Liquefaction was defined by the occurrence of a shear strain, γ, of 3.75% (for consistency with the CDSS testing) or the development of an excess porewater pressure ratio, r_u, of at least 0.97.

The use of an excess porewater pressure ratio, r_u, of at least 0.97 was included in the definition of liquefaction in the modeling due to the fact that in some cases the maximum post-liquefaction shear strain, γ, of the sample was less than 3.75% despite the development of r_u values near 1.0 over a number of cycles. The limitation of the shear strain may have been due to the dimensions of the model and the assumption of plane stress conditions.

4.3.4 Methodology and Procedure

The modeling followed the methodology used in the laboratory testing and used the same load frequency (0.1 Hz). The effective consolidation stresses and cyclic stress ratios used in the modeling were approximately equal to those used in the testing. The value of $(N_1)_{60}$ used in the modeling was incrementing the initial value of 10 (blows per 300 mm) by ±0.25 until a value that produced a reasonable overall approximation of each of the 20 the CDSS test results was obtained with the primary criterion being the number of cycles required to produce liquefaction as defined in Section 4.3.3. The corresponding value of $(N_1)_{60}$ was found to be 11 blows/300 mm.

4.3.5 Results of Modeling and Comparison With CDSS Test Results

The results of the FLAC modeling and the CDSS laboratory testing are summarized in Table 4-3 and presented on Figure 4-2. Generally, the number of cycles of loading required to produce liquefaction, N_{LIQ}, in the numerical modeling were reasonably similar to those required to produce liquefaction in the CDSS testing (refer to Figure 4-2). However, for the five tests conducted at a CSR of 0.15, the number of cycles to produce liquefaction in the numerical modeling varied from 4 to 5 with an average value of 4.3 while the number required in the CDSS testing varied from 1.7 to 3.8 with an average value of 2.3. At CSR levels of 0.075 and 0.10 the number of cycles to liquefaction in the modeling and testing were in very good agreement. At a CSR level of 0.125 the agreement between the modeling and testing was good, although the average number of cycles to liquefaction of the modeling, 7.7, was somewhat higher than that of the testing, 5.4.

As with the CDSS testing, the level of the effective, vertical consolidation stress used in the modeling had no significant effect on the liquefaction resistance of the tailings.

Given that earthquakes of moment magnitude 6.5 to 7.5 typically produce 5 to 15 cycles of significant loading, respectively (see Table 2-6), the discrepancies between the modeling and test results at higher CSR values (0.15) are not deemed to be critical with respect to the evaluation of the liquefaction potential for the earthquake loads considered because less than 5 cycles of significant loading are required to cause liquefaction under CSR values of this magnitude.

There were some differences between the behavior observed in the laboratory testing and the numerical modeling, particularly with increasing shear strain. These differences were apparent in Test No. TL-05 which was the keystone test in the numerical modeling. Testing parameters consisted of an effective, vertical consolidation stress of 200 kPa and a cyclic stress ratio of 0.10. Liquefaction as defined by a shear strain of 3.75% occurred at 19.7 and 17 cycles, respectively, in the laboratory testing and numerical modeling.

Table 4-3 – Summary of results of CDSS testing and FLAC modeling.

Test No.		CDSS Testing			FLAC Modeling		
		$\sigma'_{v,c}$ (kPa)	CSR	N_{LIQ} (γ=3.75%)	$\sigma'_{v,c}$ (kPa)	CSR	N_{LIQ} (γ=3.75% or $r_u \geq 0.97$)
$\sigma'_{v,c}$=100 kPa	TL-03	99.5	0.076	73.8	100	0.075	89
	TL-01	102.2	0.102	17.7	100	0.10	19
	TL-04	96.3	0.127	5.6	100	0.125	8
	TL-02	98.0	0.144	2.7	100	0.15	5
$\sigma'_{v,c}$=150 kPa	TL-12	149.7	0.075	61.7	150	0.075	58
	TL-09	150.3	0.098	16.8	150	0.10	17
	TL-10	149.7	0.121	5.6	150	0.125	7.5
	TL-11	152.6	0.148	1.7	150	0.15	4
$\sigma'_{v,c}$=200 kPa	TL-08	200.4	0.074	84.7	200	0.075	50
	TL-05	200.6	0.096	19.7	200	0.10	17
	TL-7a	201.0	0.123	3.8	200	0.125	8
	TL-06	198.8	0.149	1.7	200	0.15	4.5
$\sigma'_{v,c}$=300 kPa	TL-15	300.7	0.075	50.7	300	0.075	60
	TL-13	299.6	0.101	14.7	300	0.10	20
	TL-14a	300.0	0.127	4.6	300	0.125	8
	TL-16	300.9	0.155	1.7	300	0.15	4
$\sigma'_{v,c}$=400 kPa	TL-19	400.5	0.077	77.7	400	0.075	59
	TL-17	400.6	0.101	22.3	400	0.10	17
	TL-18	400.4	0.125	7.2	400	0.125	7
	TL-20	400.7	0.139	3.8	400	0.15	4

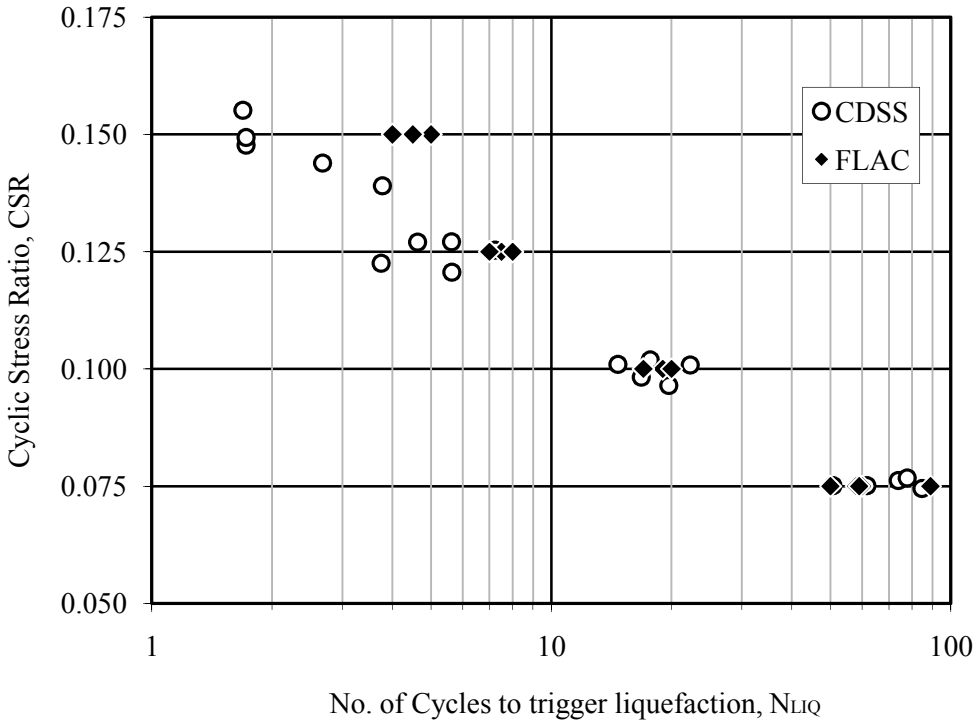

Figure 4-2 – CSR vs. Number of cycles to liquefaction
from CDSS testing and FLAC modeling.

Figure 4-3 is a plot of shear strain, γ, vs. number of cycles, N, for TL-05 as tested and as modeled. As shown on the figure, the modeled response was stiffer than the tested response through the 15th cycle. After this point the shear strain in the model increased rapidly and reached 3.75% (liquefaction) within two cycles while the shear strain of the test also increased, but at a less rapid rate and did not reach 3.75% until about the 20th cycle.

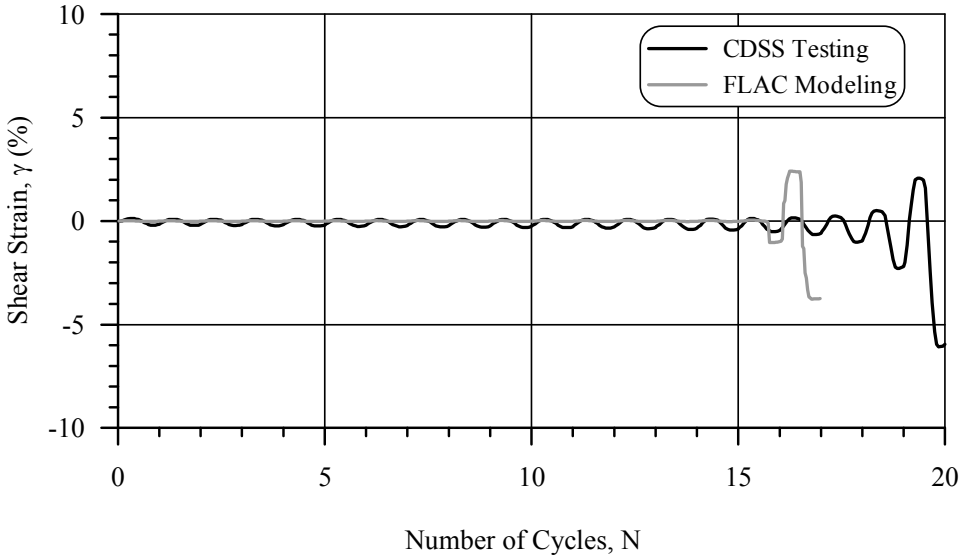

Figure 4-3 - Number of cycles vs. shear strain for CDSS Test No. 05 (from laboratory testing and FLAC Modeling).

The tested and modeled shear strain, γ, vs. shear stress, τ, response for Test No. TL-05 is presented on Figure 4-4. The stiffness of the model relative to the test is apparent. However, as shear strains increased the behavior of the model was very similar to that of the test.

The excess porewater pressure ratios, r_u, developed in the model and test of Test No. TL-05 are plotted on Figure 4-5. The excess porewater pressure ratios developed similarly until the 15th cycle. From the 16th cycle onwards the excess porewater pressure ratio of the test continued to develop at a relatively constant rate with moderate peaks and valleys until the 18th cycle when the magnitude of the peaks and valleys increased. Even after an excess porewater ratio of 1.0 was reached in test, the pattern of peaks and valleys continued. In the case of the FLAC simulation, during the 16th cycle, the value of r_u suddenly increased by about 0.1 and then underwent relatively large oscillations between 0.82 and 1.0.

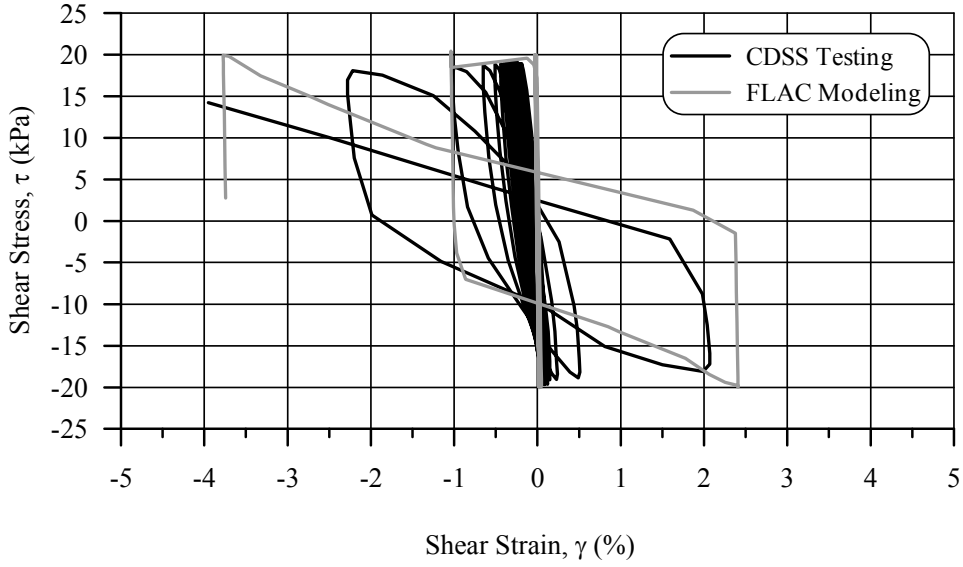

Figure 4-4 – Shear strain v. shear stress for CDSS Test No. 05
(from laboratory testing and FLAC Modeling).

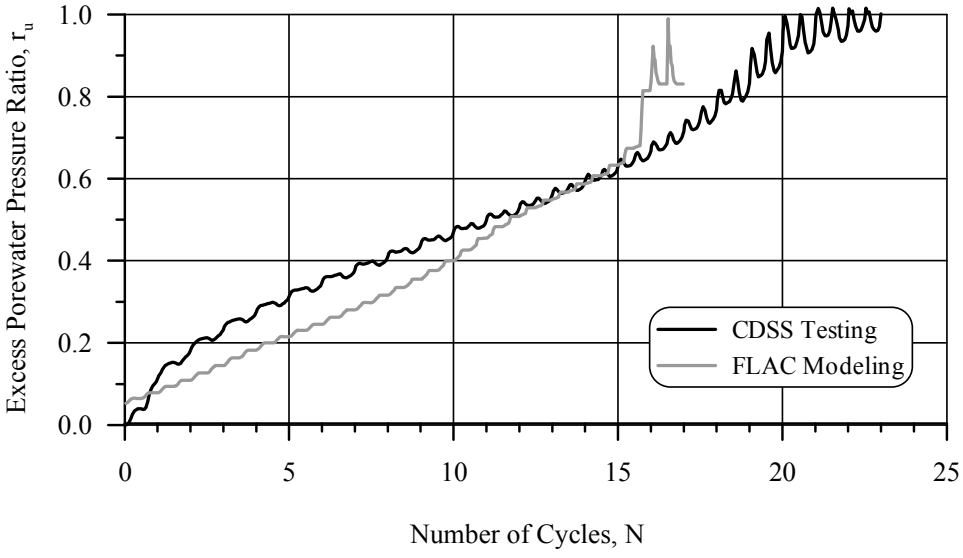

Figure 4-5 – Number of cycles v. excess porewater pressure ratio for CDSS Test No. 05
(from laboratory testing and FLAC Modeling).

On Figure 4-6 the vertical effective stress, σ'_v, vs. shear stress, τ, for the testing and modeling are plotted. The testing results show a typical reduction in the normal stress from 200 kPa towards 0 with cyclic loading and post-liquefaction hysteresis. The results of the modeling are relatively similar to the testing until an effective, vertical stress of 60 kPa was reached. Then there was a sudden decrease in the modeled effective, vertical stress to about 40 kPa and a hysteresis loop significantly wider than that of the testing response developed.

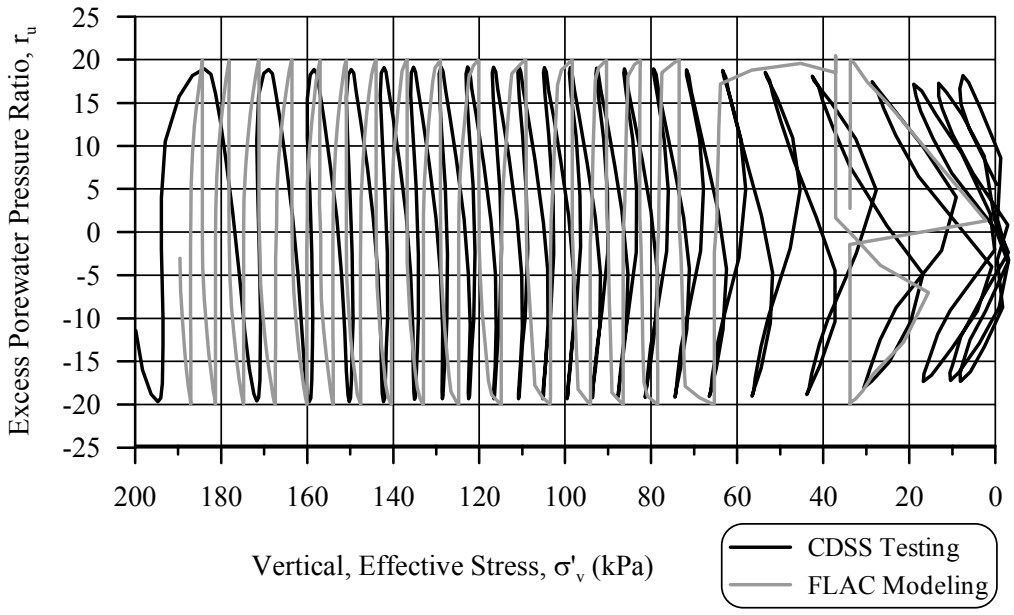

Figure 4-6 – Normal stress v. shear stress for CDSS Test No. 05
(from laboratory testing and FLAC Modeling).

There were a number of important differences between the laboratory testing and modeling that account for the differences in the observed behavior. The most obvious

difference was that the laboratory testing was three dimensional while the modeling was two dimensional and assumed plane stress conditions. Other differences included:

- The laboratory samples were prepared from slurries to increase the degree of homogeneity, but they may not have been homogeneous or isotropic; while the modeled samples were assumed to be homogeneous and isotropic;
- Mechanical damping in the numerical simulation was limited to that incorporated into the UBC Sand model and the amount, if any, of mechanical damping the laboratory testing equipment is not known; and
- The steel-reinforced metal membrane used in the testing was not modeled in the numerical simulation. The effects, if any, of the membrane on the test results are not known. However, they are believed to be significant because in testing the samples did not undergo excess strain when the applied shear stress exceeded the shear strength of the soil prior to liquefaction.

Additionally, the analysis of the raw data from laboratory testing at the University of British Columbia was done using proprietary software that was not provided for evaluation; thus, it is not known what types or degree of corrections or adjustments are made to the raw testing data to produce the output provided.

4.3.6 Remarks on the Numerical Modeling of the CDSS Testing

Overall, the results of numerical modeling were in reasonably good agreement with the results of the laboratory testing. The modeling indicates that the UBC Sand model can be used to simulate the dynamic behavior of the tailings and that a corrected standard penetration test blow count, $(N_1)_{60}$, of 11 (blows per 300 mm) and a constant volume friction angle, ψ_{cv} of 35.6° may be used to represent the tailings, when normally consolidated.

These values were used to simulate consolidated tailings using the UBC Sand model in the numerical analyses presented in Chapters 4, 6 and 7.

4.4 NUMERICAL EVALUATION OF THE LIQUEFACTION POTENTIAL OF THE TAILINGS

The potential for liquefaction of the tailings deposit at the representative tailings impoundment was evaluated using dynamic numerical methods that assumed level ground conditions and the results of these evaluations were compared to the analytical liquefaction evaluations presented in Chapter 3. The liquefaction resistances of the tailings used in the numerical analyses were based on the results of cone penetration testing for unconsolidated tailings and on the CDSS laboratory testing for normally consolidated tailings.

4.4.1 Model Geometry and Material Properties

The tailings deposit was assumed to be 15-m-high and to be underlain by 2 m of dense glacial till and then hard bedrock, the same conditions assumed in the analytical evaluations. The model used in the evaluation was a relatively simple, two-dimensional grid with respective horizontal and vertical dimensions of 150 m and 18 m and composed of 2,700 1-m-square elements. The size of the elements was 1-m-square. The geometry of the model is presented on Figure 4-7.

Square elements were used in the model for accuracy as recommended by Itasca (2005). The selected element size was a compromise between: a) accuracy, which improves with decreasing element size; b) solution time, which increases with increasing element size; and c) the requirement that the model provide for a gradual change in properties (e.g. stress, strain, density) within the depth of the impoundment. It was found that using 1-m-square elements was sufficient to meet the objectives of the modeling.

The impounded tailings were assumed to be 130-m-wide and 15-m-high, resulted in a width to height ratio of 8.67. Through an iterative process it was found that a ratio of at

least 5 was required to avoid the influence of the ends of the model in the center of the tailings.

The solution time for dynamic analysis in FLAC is based on the time steps required for dynamic or fluid flow, with the smaller time step controlling. The time steps are determined by the element size, the material and fluid properties, and dynamic damping parameters. Solution time for a 40 second earthquake using this model was about 1.5 hours on a desktop computer equipped with an Intel® Pentium® Dual E2200 central processing unit (CPU) with a rated speed of 2.2 GHz.

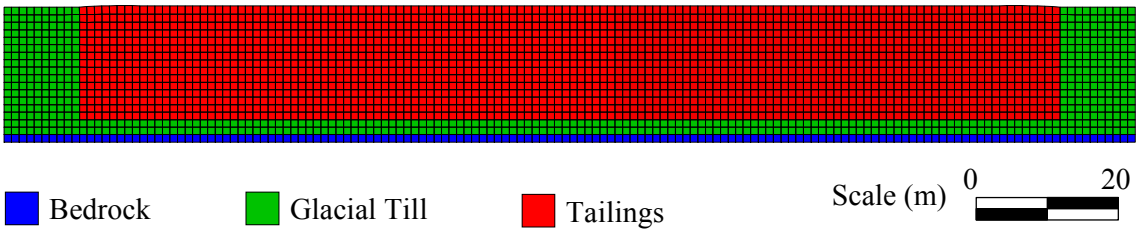

Figure 4-7 - Geometry of the FLAC model used to evaluate the liquefaction resistance of the tailings.

The intent of the modeling was to evaluate the liquefaction response of the tailings deposit with respect to the "level ground" of infinite extent conditions assumed by the analytical methods. Thus, only the response at the center of the model was considered. The presence of the glacial till on the sides of the model was necessary for stability reasons.

The properties used in the modeling are summarized on Table 4-4. The properties of the tailings were derived from the laboratory testing, cone penetration and the numerical modeling of the CDSS testing (Section 4.3). The properties of the glacial till and bedrock

were derived from published sources. The properties of the tailings, glacial till and bedrock are the same as those used in the analytical evaluations described in Chapter 3.

Table 4-4 – Material properties assumed in the dynamic numerical liquefaction analyses.

Material Property	Tailings	Glacial Till	Bedrock
Corrected standard penetration resistance, $(N_1)_{60}$ (blows/300 mm)	3.5 (unconsolidated) 11 (consolidated)	-	-
Constant volume friction angle, ψ_{cv}	35.6º	-	-
Dry density, γ (kg/m^3)	2,375 (average)	2,000	2,200
Internal friction angle, ϕ	-	36º	25º
Cohesion, c (kPa)	0	250	50,000
Dilation angle, ϕ_d	-	10º	15º
Porosity, n	0.39 (average)	0.15	0.02
Shear modulus, G (MPa)	87.2 (average)	360	7,690
Bulk modulus, K (MPa)	61.0 (average)	780	16,700
Hydraulic conductivity, k (m/s)	2.25×10^{-5} (H) 4.5×10^{-6} (V)	1.0×10^{-7}	1.0×10^{-8}

4.4.1.1 Tailings

The material properties for the tailings were derived from the cone penetration and laboratory testing conducted for this research (Chapter 3). As noted, the tailings are under-consolidated with respect to existing loads and the typical corrected standard penetration test blow count, $(N_1)_{60}$, from conversion of the CPT results was less than 4 (see Section 3.7.3.6).

The principal parameters of the UBC Sand model are the $(N_1)_{60}$ value and ψ_{cv} (the constant volume friction angle). Based on the evaluation of the CPT results an average $(N_1)_{60}$ value of 3.5 was used to for the tailings. This value was randomized using the "rdev" function in FLAC to produce standard deviations of 0.5 to simulate the heterogeneity of tailings the deposit, to some extent. The resulting values had an average of 3.5 and a standard deviation of 0.5. Using Equation 2-27, the ψ_{cv} of the tailings was determined to be 36.25° based on the effective friction angle from direct shear testing (ϕ=36.6°) and the typical $(N_1)_{60}$ value from the CPT results.

The dry unit weight and porosity of the tailings were based on the consolidation testing (Equation 3-1). At mid-depth (7.5) m in the impoundment, these properties were 2,375 kg/m^3 and 0.39, respectively. The resulting values were for normally consolidated material. However, as the excess porewater pressure response of the UBC Sand model is based primarily on the $(N_1)_{60}$ values, the slightly greater unit weights and porosity of the tailings relative to their under-consolidated values, was not significant with respect to the dynamic behavior of the tailings. Estimation of the horizontal and vertical saturated hydraulic conductivities of the tailings is presented in Section 3.7.1.9 and was based on consolidation testing, empirical correlations with the grain size distribution and published values (k_h=2.25x10^{-4} cm/s and k_v=4.5x10^{-5} cm/s). These values were assumed to be averages and the "rdev" function was used to assign standard deviations of one half an order of magnitude. The use of hydraulic conductivity values for consolidated tailings rather than unconsolidated tailings did not have an appreciable effect on the modeling due to the rapid rate of loading relative to the hydraulic conductivities.

From direct shear testing, the tailings were determined to have no appreciable cohesion; accordingly, they were assigned no cohesion.

Other properties of the tailings (e.g. shear and bulk moduli) were automatically calculated by the UBC Sand model based on the parameters provided (see Section 2.7.2.1).

4.4.1.2 Glacial Till

As noted in Section 3.6.2, the impoundment is underlain by dense glacial till. The properties of the glacial till used in the modeling were based on reported values for dense and well-compacted glacial till provided in Milligan (1976) and Bowles (1996).

4.4.1.3 Bedrock

The bedrock at the site consists of schist of medium quality and andesite of poor to medium quality (Section 3.6.2). Properties for similar rock were obtained from Goodman (1989) and Itasca (2005).

4.4.2 Static Conditions

As a first step in the FLAC analysis, the static conditions were established by solving for mechanical and hydraulic stability of the model. These conditions differed very slightly for the models where the tailings were assumed to be unconsolidated versus consolidated, due to differences in the elastic moduli of tailings. Accordingly, only the results of the static analysis of the consolidated tailings model are presented herein.

Boundary conditions for the static analyses consisted of fixing the bottom of the model against vertical movement, fixing the sides against lateral movement and applying fixed hydrostatic porewater pressures to the bottom and sides of the model.

Under static conditions (prior to dynamic loading), the magnitude of the effective vertical stresses within the tailings varied from 0 to about 250 kPa with depth as shown on Figure 4-8. In FLAC, compression stresses are negative and tensile stresses are positive. The slight non-uniformity of the stresses in the central portion of the model is due to the method used by FLAC to estimate the contours from average stresses in the centers of the elements and the heterogeneity assigned to the tailings properties. The stress discontinuities on the sides of the model are due to differences in the elastic properties of the glacial till and tailings.

Analytically, the vertical effective stress at the bottom of the tailings was estimated as follows:

$$\sigma_v' = 15\ m \cdot (23.5\ kN/m^3\ - 0.6 \cdot 9.81\ kN/m^3) = 264\ kPa.$$

The vertical effective stresses calculated in the numerical modeling was in agreement with the analytical estimate and was deemed to be reasonable.

The porewater pressure, u, contours within the model under static conditions are presented on Figure 4-9. The porewater pressures varied from about 0 near the surface to just over 175 kPa at the bottom of the model and are indicative of a steady-state, hydrostatic condition as determined below:

$$u = 18\ m\ \cdot 9.81\ kN/m^3 = 176.58\ kPa$$

The porewater pressure distribution in the model was deemed to be reasonable.

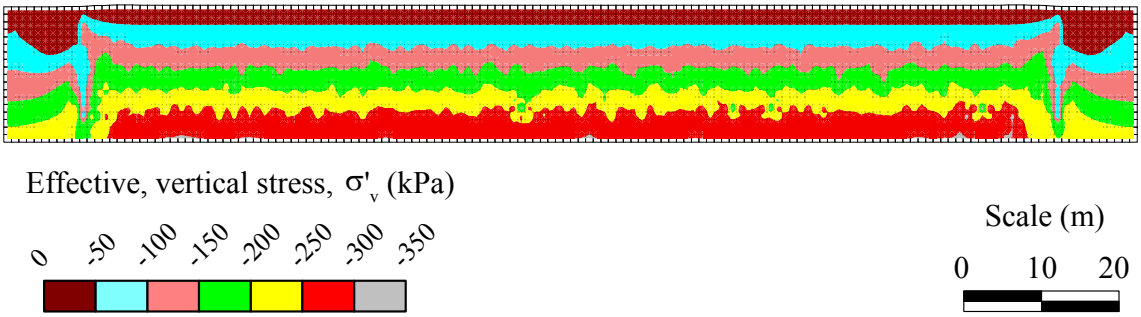

Figure 4-8 - Contours of the effective vertical stress within the consolidated tailings deposit under static conditions.

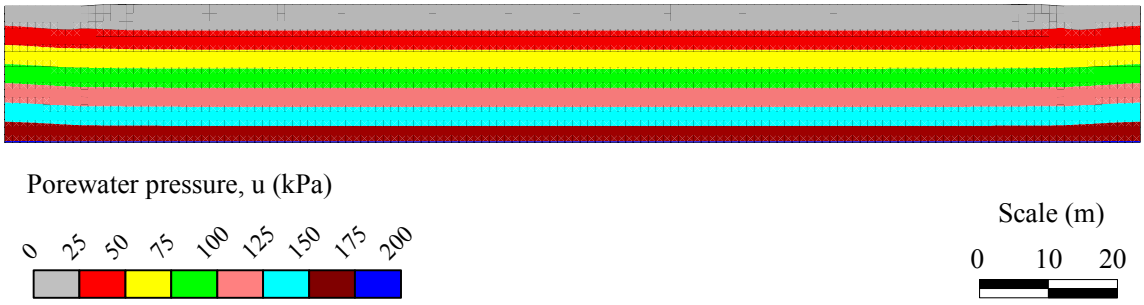

Figure 4-9 – Contours of the porewater pressure within the consolidated tailings deposit under static conditions.

4.4.3 Earthquake Loadings

The earthquake loadings used in the dynamic numerical analyses of liquefaction were the same as those used in the analytical analyses of liquefaction, evaluation earthquakes E1, E3 and E5, which are associated with moment magnitudes of 6.5, 7 and 7.5, respectively. Modeling of the earthquake loadings is described in Section 3.8.3.

4.4.4 Execution Parameters for Dynamic Loading

Boundary conditions for the dynamic analyses consisted of: a) removing the fixity on the bottom and sides of the model; b) applying a vertical velocity of 0 to the bottom of the model, and applying "free field" boundary conditions to the sides of the model. Free field boundaries of single columns of elements placed on the sides of the model that simulate the dynamic response of and extended medium, including the absorption and rebound of shear waves (Itasca, 2005).

Groundwater flow between the elements was permitted during the dynamic analyses. A bulk modulus of 2.2×10^5 kPa was used for the porewater; although this value is an order of magnitude lower than the actual value of 2.2×10^6 kPa, in trial runs it had no significant effect on the results. Using a reduced modulus significantly increased the run time of the simulations and is recommended by Itasca (2005) and Castillo (2006).

A Rayleigh stiffness dynamic damping factor of 0.005 at a frequency of 20 Hz was applied to the entire model to prevent excessive amplification of the ground motion at low levels of shear strain. This amount of damping resulted in no appreciable amplification or dampening of the ground motion within the 1-m-thick layer of bedrock at the bottom of the model. This procedure is recommended by Itasca (2005).

During the dynamic portions of the simulations, several properties were monitored and recorded at intervals of depth along a vertical line through the middle of the tailings. These properties included the horizontal acceleration, cyclic stress ratio, the vertical effective stress, and the excess porewater pressure ratio.

Six cases were analyzed. The cases consisted of the unconsolidated and the normally consolidated tailings deposit under the three earthquake loads considered and are listed in Table 4-5

Table 4-5 – Cases used in liquefaction analysis.

Case	Earthquake	State of Tailings
1	E1 (M_w=6.5)	Normally consolidated
2	E3 (M_w=7.0)	Normally consolidated
3	E5 (M_w=7.5)	Normally consolidated
4	E1 (M_w=6.5)	Under-consolidated
5	E3 (M_w=7.0)	Under-consolidated
6	E5 (M_w=7.5)	Under-consolidated

4.4.5 Results of the Liquefaction Modeling

In the six cases analyzed, the applied earthquake loading resulted in liquefaction of the tailings, where liquefaction is defined as the occurrence of porewater pressure ratios, r_u, near unity to consistency with the analytical methods of liquefaction presented in Chapter

3. The depth of liquefaction varied with the assumed condition of the tailings and the earthquake loading. Conditions within the central area of the model during and after shaking were relatively uniform. This indicates that the presence of the glacial till on either side of the model for stability did not have a significant effect on the dynamic behavior of the tailings within this area. Specific behaviors and findings of the liquefaction analyses follow.

The following sections focus on the results of the consolidated tailings to Earthquake E1 and the unconsolidated tailings to Earthquake E5. These results bracket the results of all 6 analyses conducted. Detailed results for all of the analyses are presented in Appendix H.

4.4.5.1 Site Response

As noted in Chapter 3, the response of a site to earthquake loading is generally evaluated base on the amplification factors, F_a (see Equation 3-12). Recall that the amplification factor is the ratio of the peak (horizontal) ground acceleration, PGA, at a given location to the PGA on the top of bedrock.

Calculated PGA values at the top of bedrock, at the bottom of the tailings (top of the glacial till) and surface of the tailings at the center of the model and the resulting amplification factors between the top of bedrock and the tailings for the cases considered are presented on Table 4-6. As can be observed from the table, within the 2 m of dense glacial lying between bedrock and the tailings, the PGA values increased considerably indicating amplification of the ground motion. The corresponding amplification factors vary from 1.347 to 2.146 with an average value of 1.8.

With respect to consolidated tailings the PGA values on the surface of the tailings were significantly amplified for Earthquake E1 (M_w=6.5), slightly amplified for Earthquake E3 (M_w=7.0) and highly damped for Earthquakes E5 (M_w=7.5). The amplification factors were 2.064, 1.138 and 0.320 for Earthquake E1, E3 and E5, respectively. This indicates that the site response is a function of the characteristics of the earthquake loading as well

as the subsurface conditions with more intense loadings resulting in less amplification (more damping) of the ground motion due to the increased shear strain. In the analyses with under consolidated tailings, the PGA values indicated slight amplification of Earthquake E1 and significant damping of Earthquakes E3 and E5 which resulted in amplification factors of 1.117, 0.383 and 0.229, respectively. As expected, the presence of unconsolidated tailings resulted in significantly more dampening of the ground motion due to the lower shear modulus. It is noted that PGA values represent isolated maximum values of the ground motion and may not be indicative of the amplification (or damping) of the entire ground motion.

Table 4-6 – PGA values on bedrock and surface and amplification factors from dynamic numerical liquefaction analysis.

Earthquake	Earthquake Magnitude, M_w	PGA (g) Top of Bedrock	PGA (g) Bottom of Tailings	PGA (g) Top of Tailings	Amplification Factor, Fa (Surface/ Bedrock)
Consolidated Tailings					
E1	6.5	0.251	0.338	0.518	2.064
E3	7	0.768	1.443	0.874	1.138
E5	7.5	1.510	2.430	0.483	0.320
Under Consolidated Tailings					
E1	6.5	0.249	0.441	0.278	1.117
E3	7	0.759	1.629	0.291	0.383
E5	7.5	1.513	2.241	0.347	0.229

4.4.5.2 Site Response of Consolidated Tailings to Earthquake E1

Figure 4-10 presents the ground motion (horizontal accelerations) recorded at (a) the top of bedrock, and (b) the bottom, (c) mid-height, and (d) the surface of the tailings for the analysis with consolidated tailings subjected to Earthquake E1 (M_w=6.5). The figures in this Section presenting ground motions recorded during the numerical analysis show

every 250th data point for convenience (1,000 out of 250,000 points for Earthquake E1). Thus, some resolution is lost in the figures. Figures showing every data point are presented in Appendix H. The applied ground motion is shown on Figure 3-28. There were no significant differences between the ground motion applied to the bottom of the model and the ground motion recorded on the top of bedrock (Figure 4-10a).

Comparing Figure 4-10a with Figure 4-10b indicates that there was moderately high amplification of the ground motion within the 2-m-thick layer of glacial till between bedrock and the bottom of the tailings, particular in the first 15 seconds of shaking. Amplification of the ground motion continued within the tailings, resulting in increasingly larger peak acceleration values towards the surface.

4.4.5.3 Site Response of Unconsolidated Tailings to Earthquake E5

The recorded ground motions from the numerical analysis of unconsolidated tailing subject to the Earthquake E5 (M_w=7.5) are shown on Figure 4-11, where (a) is the top of bedrock, and (b) is the bottom, (c) is mid-height, and (d) is the surface of the tailings. The ground motion applied to the bottom of the model (the bottom of bedrock) is shown on Figure 3-29. There was no significant difference between the applied ground motion and that on the surface of the bedrock (Figure 4-11a).

As the ground motion passed through the glacial till is was considerately amplified for the duration of shaking (see Figure 4-11b). However, within the unconsolidated tailings, the ground motion was highly to severely damped. The damping within the tailings is attributed to the low shear modulus of the unconsolidated tailings as well as the high shear strains and the generation of excess porewater pressures that would have been induced by the very strong applied ground motion.

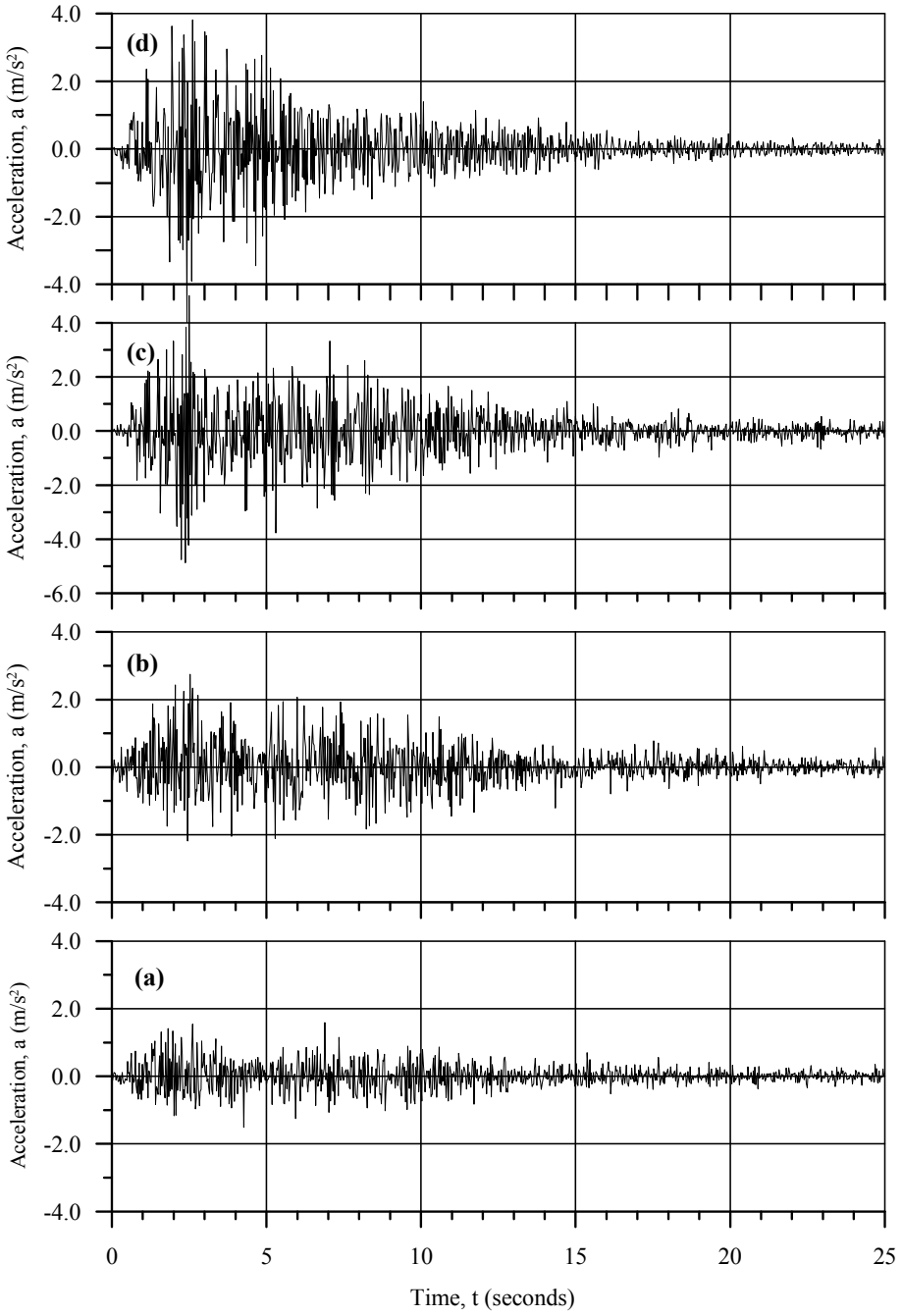

Figure 4-10 – Acceleration at (a) top of bedrock and at the (b) bottom, (c) mid-height and (d) the top of the consolidated tailings subject to Earthquake E1 (M_w=6.5).

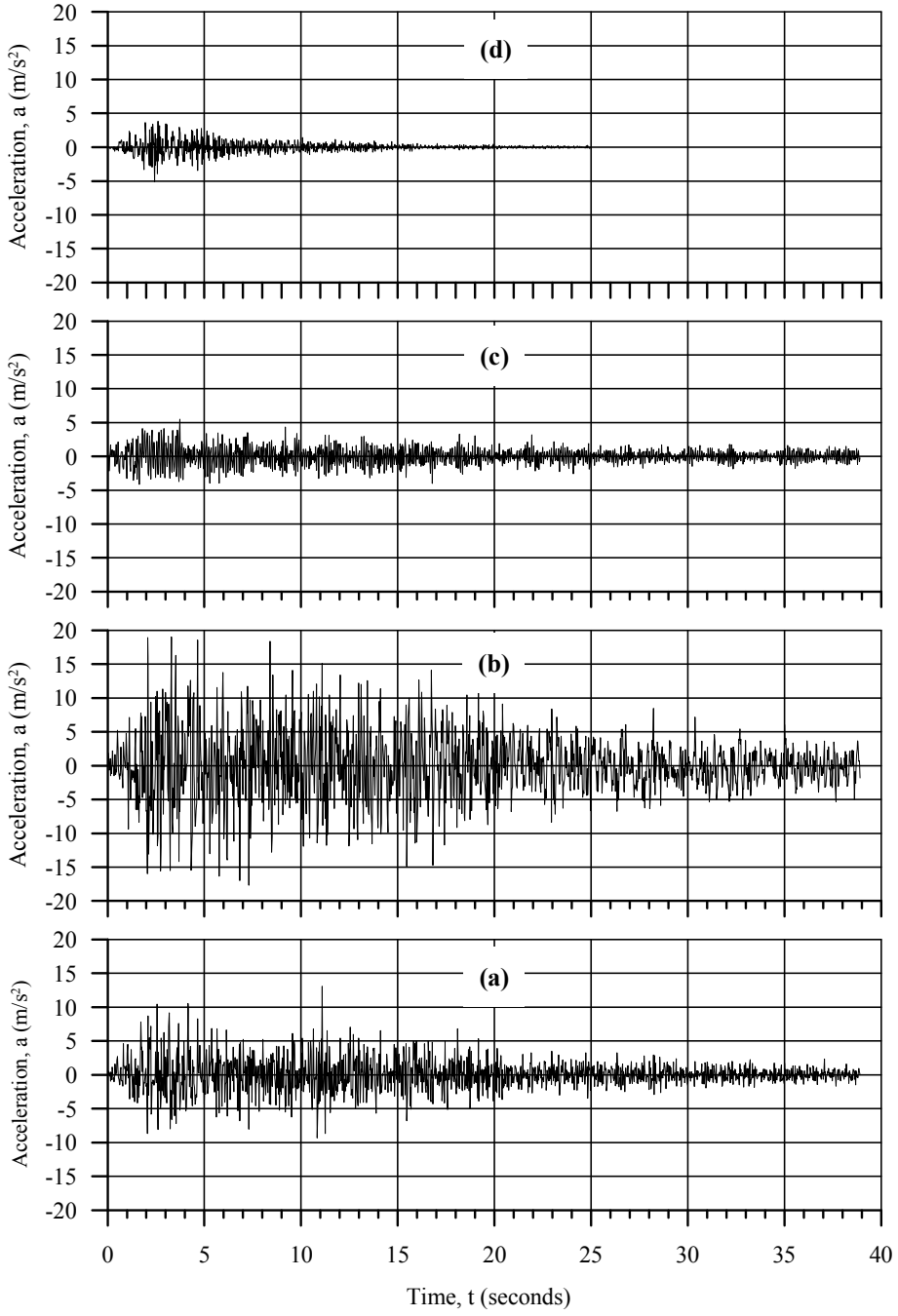

Figure 4-11 – Acceleration at (a) top of bedrock and at the (b) bottom, (c) mid-height and (d) the top of the unconsolidated tailings subject to Earthquake E5 (M_w=7.5).

4.4.5.4 Summary of the Site Responses

In summary, the site responses of the six cases evaluated were characterized by:

- For the consolidated tailings, Earthquake E1 produced moderately high amplification, E3 produced slight amplification and E5 produced very high damping;
- For the unconsolidated tailings, Earthquake E1 produced slight amplification while E3 and E5 produced very high damping;
- The occurrence and amount of amplification (or damping) appeared to be a function of the subsurface conditions (consolidated vs. unconsolidated tailings) as well as the intensity of the earthquake loading;
- The ground motion was moderately to highly amplified within the 2-m-thick layer of glacial till underlying bedrock in all cases.

It is interesting to note here that Taiebat et al. (2009) recently used dynamic numerical analyses to study the propagation of shear waves through liquefied soils. It was found that the development of high excess porewater pressures at the bottom of a 10-m-thick soil layer resulted in severe damping of the horizontal accelerations and the associated shear strains in the overlying material. The findings of Taiebat et al. (2009) are in agreement with the findings of this research.

4.4.5.5 CSR Development in Consolidated Tailings for Earthquake E1

As described in Section 2.3.1.1, the cyclic stress ratio, CSR, is the means by which the dynamic shear loadings that result in the generation of excess porewater pressure and liquefaction are measured. The CSR at various depths in the center of the tailings was calculated using the following equation:

$$CSR = \frac{\tau}{\sigma'_{v,o}} \qquad (4\text{-}1)$$

where: τ is the calculated shear stress on an element; and

$\sigma'_{v,o}$ is the initial vertical effective stress on the element.

Equation 4-1 differs from Equation 2-5 of the Simplified method in that Equation 4-1 considers all of the sources of shear stress on an element, where Equation 2-5 only considers the shear stress due directly to the horizontal accelerations applied by earthquake loading.

The cyclic stress ratios recorded at 0.25H (a), 0.5H (b) and 0.75H (c) in the consolidated tailings subjected to Earthquake E1 are shown on Figure 4-12, where H is the height of the tailings deposit measured from the bottom to the surface (H = 15 m).

At 0.25H the peak values of the CSR during the first 4 seconds of shaking were about 0.15. After the 4th second the peak values of the CSR declined gradually until they were less than 0.05 by the 12th second and remained at this level for the remainder of shaking. The patterns of CSR development at 0.5H and 0.75H were very similar to that at 0.25H, except that the peak values for the first 4 seconds of shaking were roughly 0.18 at 0.5H and 0.25 at 0.75 H.

The cyclic stress ratios were all approximately 0 at the start of shaking and were reasonably symmetrical about the horizontal axis, indicating no significant initial static shear and no bias in the shear during shaking, both of which are consistent with the assumption of level ground conditions.

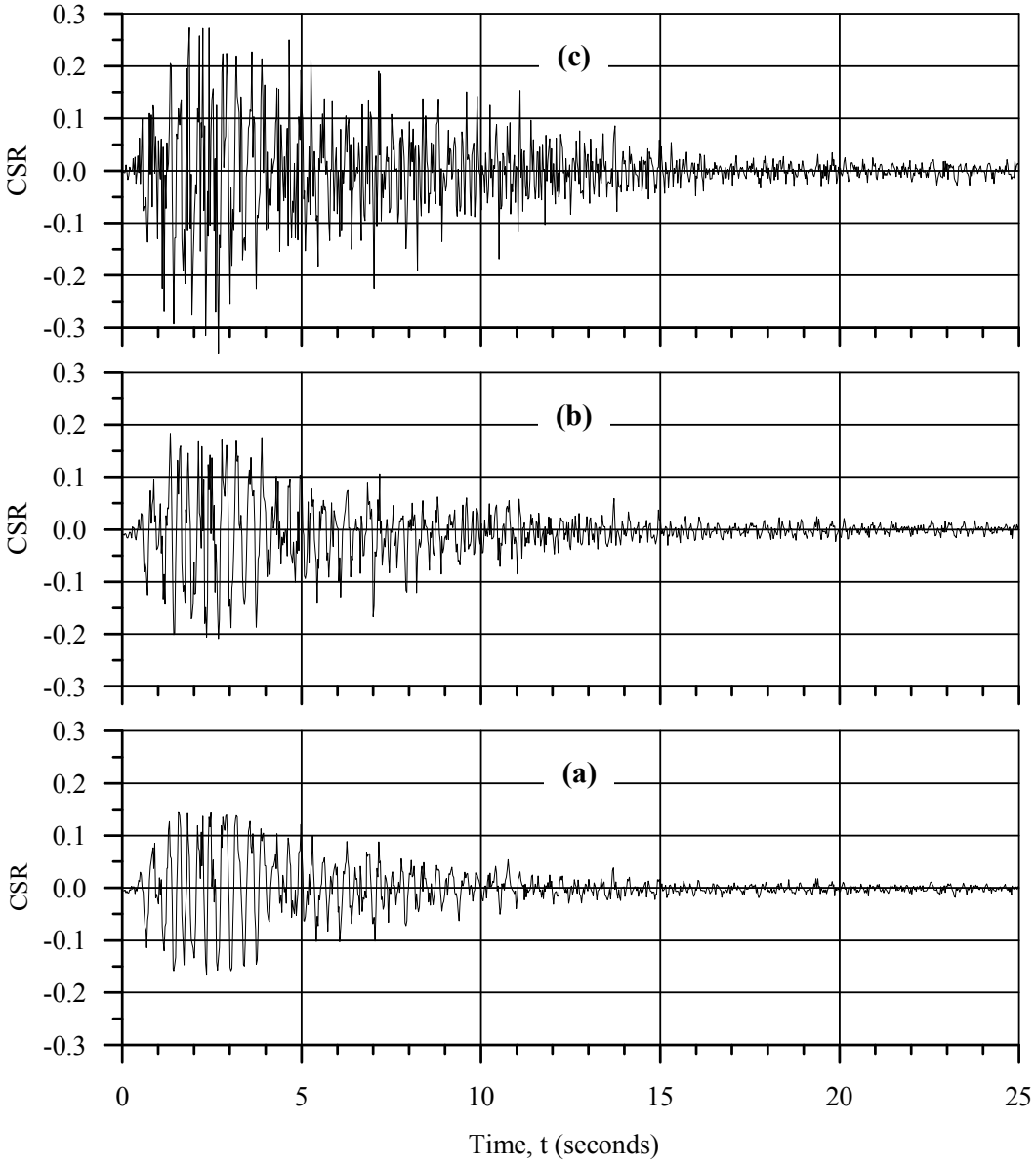

Figure 4-12 – Cyclic stress ratios developed at (a) 0.25H, (b) 0.5H and (c) 0.75H in the consolidated tailings due subject to Earthquake E1 (M_w=6.5).

4.4.5.6 CSR Development in Unconsolidated Tailings for Earthquake E5

The cyclic stress ratios recorded in the unconsolidated tailings during the liquefaction analysis for Earthquake E5 are presented on Figure 4-13 for 0.25H (a), 0.5H (b) and 0.75H (c).

At 0.25H the CSR development was characterized by intense loading cycle with a maximum value of about 0.18 in the 1st second of shaking, followed by a rapid and significant reduction in the peak CSR values to negligible values by the 4th second. After the 4th second there was no significant shear load in the tailings at this level in the tailings. At 0.5H the CSR development followed a very similar pattern with slightly greater peak values. The CSR development at 0.75H consisted of roughly 4 cycles with peak values of 0.15 to 0.18 in the first 3 seconds, followed by a rapid decline to peak CSR values of less than 0.03 by the 4th second. The remainder of shaking was characterized by negligible shear loading at 0.75H.

The symmetry of the CSR plots about the horizontal axial and the near zero initial CSR within the unconsolidated tailings are indicative of level ground conditions.

The minimal loading within the tailings after the 4th second of shaking is attributed to high shear strain and the development of high excess porewater pressures, either of which would have caused considerable damping within the tailings. These issues are discussed in the following sections.

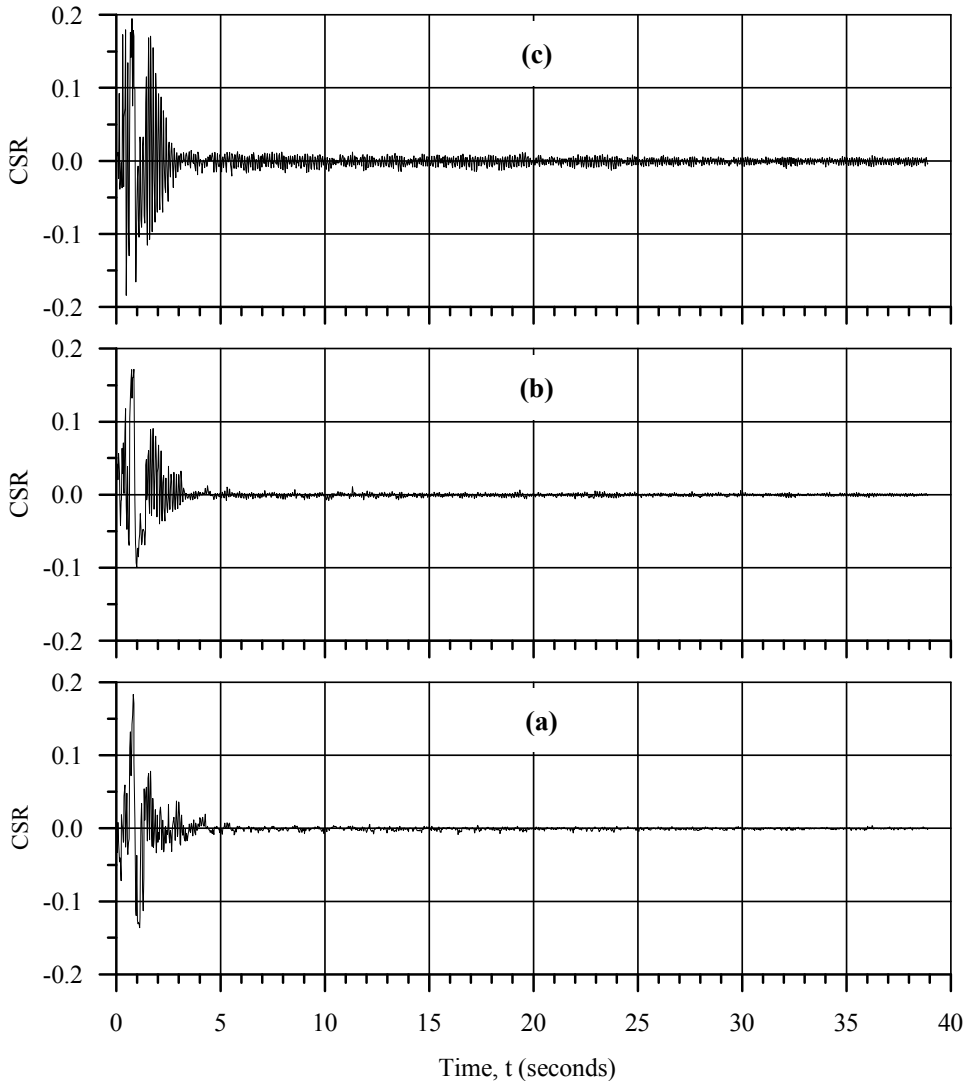

Figure 4-13 – Cyclic stress ratios developed at (a) 0.25H, (b) 0.5H and (c) 0.75H in the unconsolidated tailings due subject to Earthquake E5 (M_w=7.5).

4.4.5.7 Maximum Shear Strains

The average of the maximum shear strains developed through the depth of tailings in the center of the model during shaking are shown on Table 4-7. The average maximum shear strains in the consolidated tailings were slightly to significantly less than in the

unconsolidated tailings and the amount of shear strain increased by an order of magnitude with increased earthquake loading.

Referring to the Seed et al. (1984) shear modulus reduction curves for sand that are shown on Figure 3-19 and considered applicable to the tailings, the average shear modulus of the tailings would have been reduced by roughly 60% and 80% for Earthquakes E1 and E3 and by greater than 90% for Earthquake E5. Thus, these levels of shear strain would have been associated with significant damping.

Table 4-7 – Maximum shear strains in tailings from numerical liquefaction analyses.

Earthquake Loading	Maximum Shear Strains (%)	
	Consolidated Tailings	Unconsolidated Tailings
E1 (M_w=6.5)	0.063	0.058
E3 (M_w=7.0)	0.17	0.18
E5 (M_w=7.5)	0.65	2.1

4.4.5.8 Excess Porewater Pressure in Consolidated Tailings for Earthquake E1

The development of excess porewater pressures during shaking in the center of the model at various depths in the tailings were monitored through calculation and recording of the excess porewater ratio, r_u. The formula used to calculate r_u was:

$$r_u = \frac{\sigma'_{vo} - \sigma'_v}{\sigma'_{vo}} \quad (4\text{-}2)$$

where:

σ'_{vo} is the initial vertical effective stress;

σ'_v is the vertical effective stress at the time under consideration.

This formula was used in lieu of the conventional formula ($r_u=\Delta u/\sigma'_{vo}$), because it considers changes in the effective stress that might occur due to dynamic loading that are not caused by excess porewater pressure generation, as could occur if the degree of saturation of the soil was less than 1.0.

Graphs of the excess porewater ratio recorded in the consolidated tailings for the numerical analysis of Earthquake E1 are presented on Figure 4-14. In the upper 4.5 m of the tailings (0.7H) the earthquake loading resulted in an initial decrease in the porewater pressure resulting in negative values of r_u for the first 2 to 5 seconds of shaking. The decrease in the porewater pressure may be attributed the relatively low initial effective consolidation stresses in this depth (less than 40 kPa). As shown on the figure, the excess porewater pressures within this depth increased relatively rapidly after the 2nd second. Below a depth of 4.5 m (0.7H), the excess porewater ratios within the tailings increased rapidly and reached maximum values during the 5th second of shaking. In the upper 4.5 m (0.7H), the r_u values varied from 0.8 to 0.95 at the end of shaking. Below a depth of 4.5 m the r_u values varied from 0.5 to 0.7 at the end of shaking.

The stabilization of the excess porewater pressures below a depth of 4.5 after 5 seconds of shaking indicates that the applied cyclic stresses were not sufficient to generate additional excess porewater pressures.

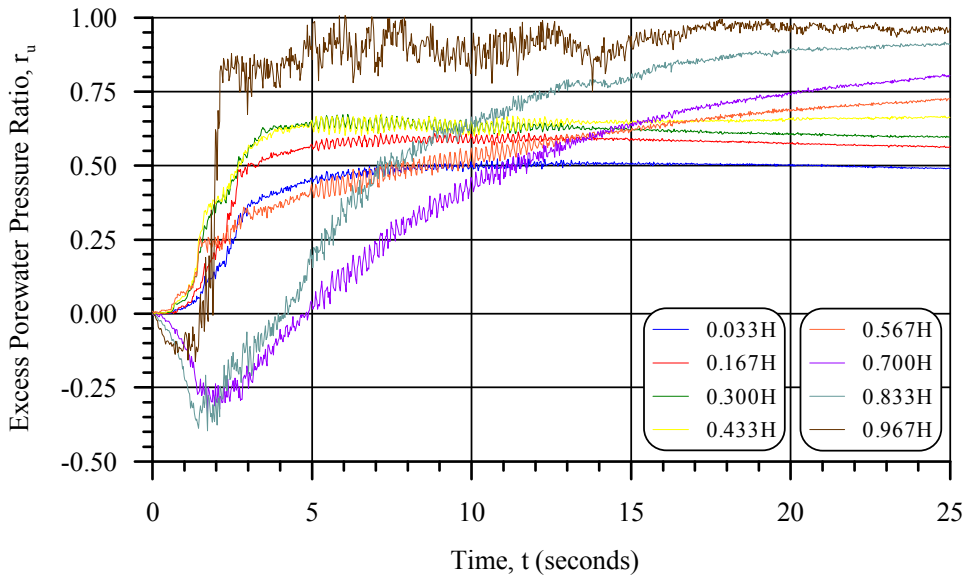

Figure 4-14 – Development of the excess porewater pressure ratio, r_u, in the consolidated tailings during Earthquake E1 (M_w=6.5).

4.4.5.9 Excess Porewater Pressure in Consolidated Tailings for Earthquake E3

The excess porewater pressure generation in the consolidated tailings with respect to Earthquake E3 is presented on Figure 4-15. At the start of shaking the upper 4.5 m of tailings (0.7H) experienced a brief, less than 2 seconds, decrease in porewater pressure followed by a relatively rapid increase to values between 0.85 and 0.95 by the end of shaking. Below 0.7H, the excess porewater pressure generation was very rapid from the start of shaking and maximum r_u values of 0.95 were attained within 6 seconds of start of shaking.

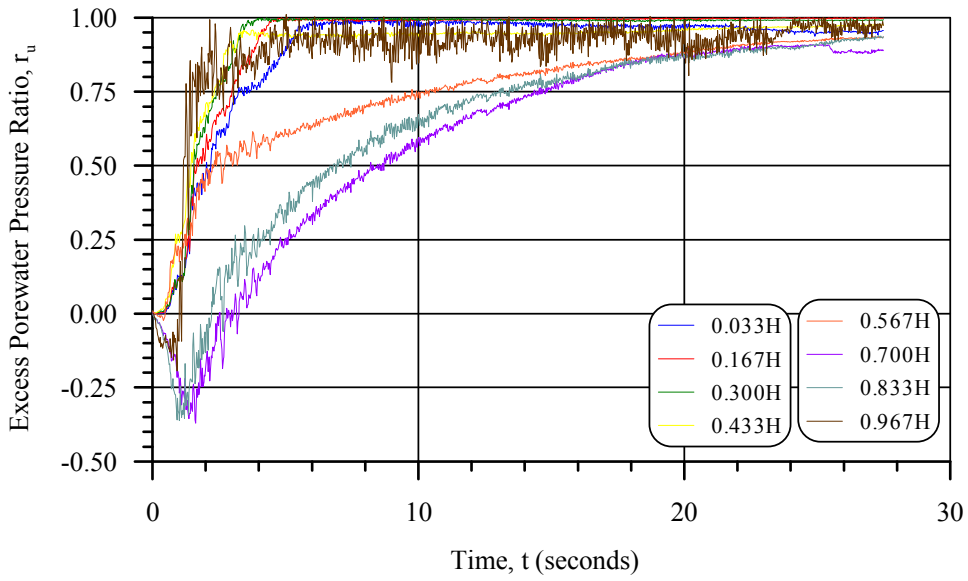

Figure 4-15 – Development of the excess porewater pressure ratio, r_u, in the consolidated tailings during Earthquake E3 (M_w=7.0).

4.4.5.10 Excess Porewater Pressure in Consolidated Tailings for Earthquake E5

As shown on Figure 4-16, Earthquake E5 resulted in the rapid generation of excess porewater pressure ratios close to 1.0 thorough the depth of the consolidated tailings. As with Earthquakes E1 and E3, there was a decrease in the porewater pressure in the upper 4.5 m of the tailings (0.7H) in the first 2 seconds of shaking which was followed by a fairly rapid increase. Below a depth of 4.5 m r_u values close to 1.0 occurred within 4 seconds. Above a depth a 4.5 m, r_u values approaching 1.0 occurred within 4 to 18 seconds.

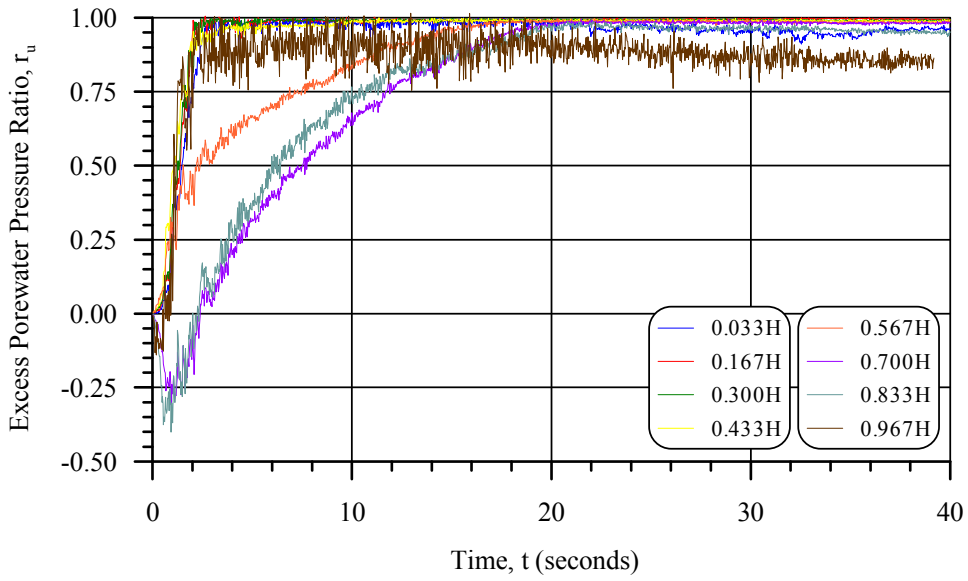

Figure 4-16 – Development of the excess porewater pressure ratio, r_u, in the consolidated tailings during Earthquake E5 (M_w=7.5).

4.4.5.11 Excess Porewater Pressure in Unconsolidated Tailings for Earthquake E1

The excess porewater pressure development in the unconsolidated tailings due to Earthquake E1 is presented on Figure 4-17. In the upper 4.5 m of the tailings (0.7H) there was a decrease in the porewater pressure during the first 2 seconds of shaking that resulted in negative values of r_u. As noted earlier the decrease in the porewater pressure may be due to the relatively low effective confining stresses in this zone, which were less than 70 kPa. By the 4th second the upper 2.5 m of tailings (0.83H) has begun to generate excess porewater pressures that resulted in values near 1.0 by the 20th second. However, drainage at the surface of the tailings and the severe damping of the ground motion resulted in a decrease in the value of r_u in the upper 2.5 m of tailings such that the values of r_u at the end of shaking decreased to between near 0 and 0.65. Below a depth of 4.5 m (0.7H) , the excess porewater pressures developed moderately rapidly at the start of shaking and then by the 10th second the rate of development was fairly low. At the end of shaking the r_u values in the lower 10.5 m of tailings varied from 0.65 at the bottom of the

tailings to about 1.0 at a depth of 8.5 m. Between depths of 4.5 to 8.5 m (0.7H to 0.43H) the value of r_u at the end of shaking was about 1.0.

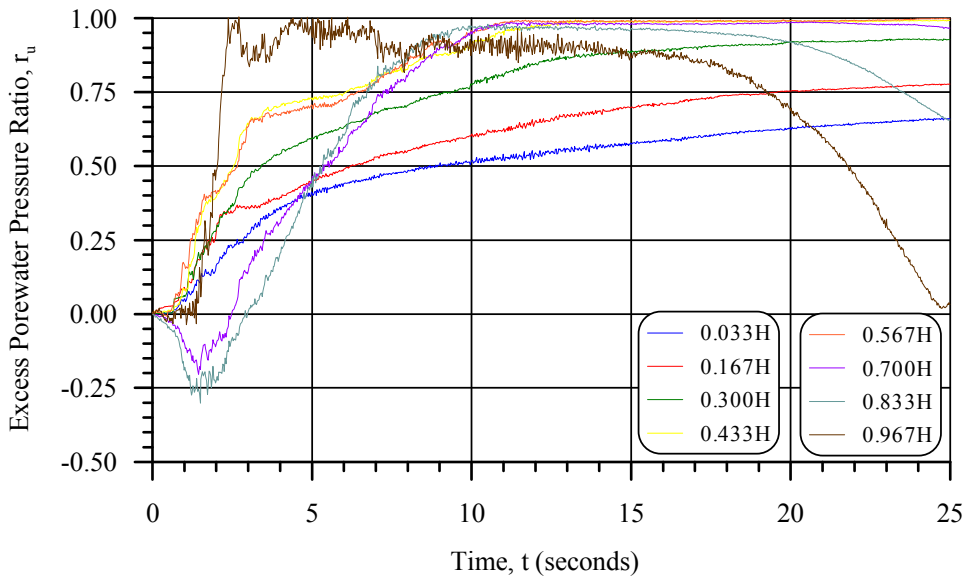

Figure 4-17 – Development of the excess porewater pressure ratio, r_u, in the unconsolidated tailings during Earthquake E1 (M_w=6.5).

4.4.5.12 Excess Porewater Pressure in Unconsolidated Tailings for Earthquake E3

Earthquake E3 resulted in the rapid development of excess porewater pressure ratios between 0.85 and 1.0 in the unconsolidated tailings below a depth of 4.5 m (see Figure 4-18). Within 4.5 m of the surface there was a sudden decrease in the porewater pressure that lasted for less than 2 seconds and was followed by a relatively rapid development in excess porewater pressures to values of about 0.85 by the end of shaking.

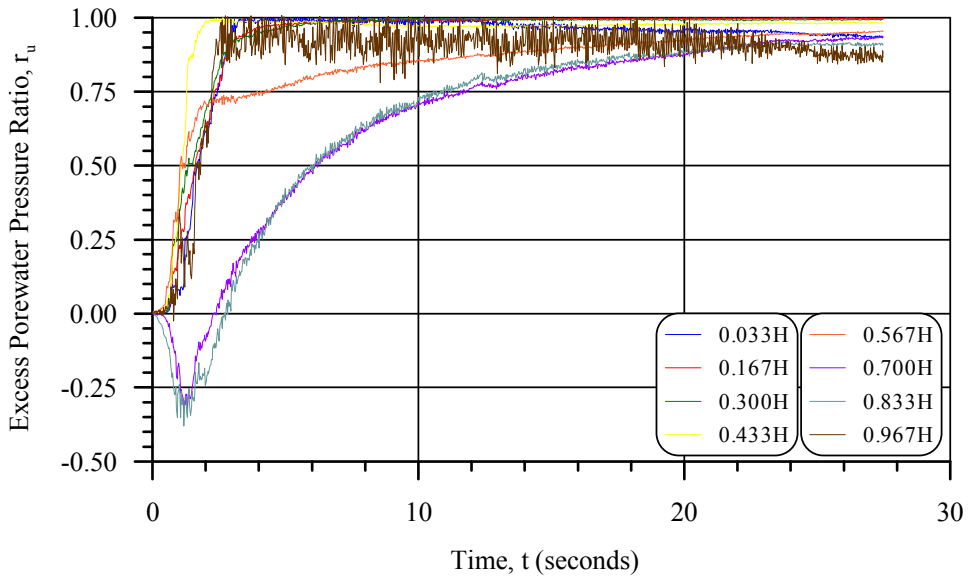

Figure 4-18 – Development of the excess porewater pressure ratio, r_u, in the unconsolidated tailings during Earthquake E3 (M_w=7.0).

4.4.5.13 Excess Porewater Pressure in Unconsolidated Tailings for Earthquake E5

The excess porewater pressure development in the unconsolidated tailings subject to Earthquake E5 is show on Figure 4-19. In the upper 4.5 m of the tailings (0.7H) there was an initial decrease in the porewater pressure resulting in r_u values as low as -0.4 in the first 2 seconds of shaking. From the start of shaking below a depth of 4.5 m and after the 2nd second above a depth of 4.5 m, the excess porewater pressures developed very rapidly and values near 1.0 were attained by the 4th second and maintained for the duration of shaking. Significant variation of the r_u value occurred at the just below the surface of tailings. This variation is attributed to random deformation of the unconfined surface of the tailings under the very intense loading of Earthquake E5.

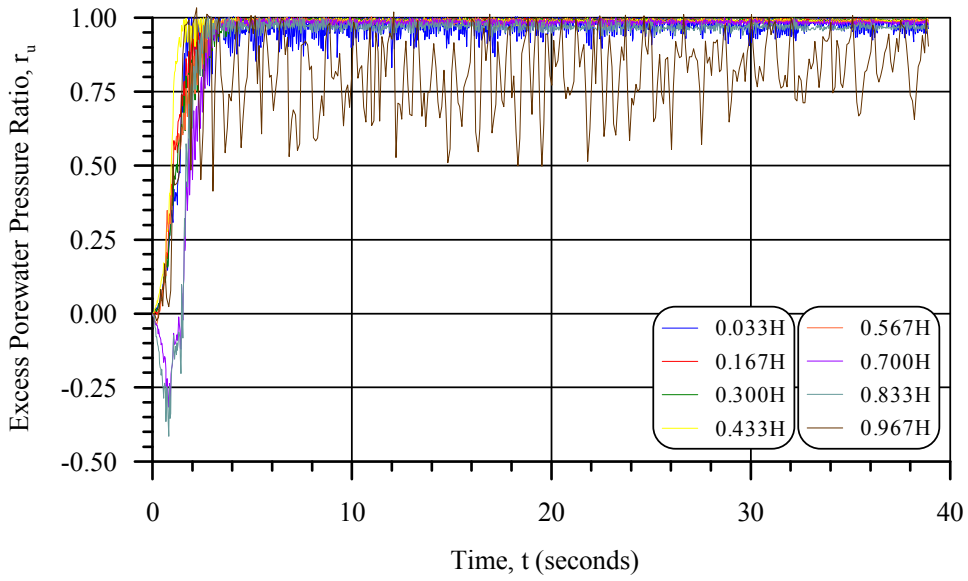

Figure 4-19 – Development of the excess porewater pressure ratio, r_u, in the unconsolidated tailings during Earthquake E5 (M_w=7.5).

4.4.5.14 Factors of Safety and the Potential for Liquefaction

In the Simplified method of liquefaction analysis (Section 2.3.1), liquefaction is defined as the occurrence of excess porewater pressure ratios of 1.0 and the factor of safety (with respect to liquefaction), FS, is the ratio of the cyclic resistance ratio of the soil, CRR, to the cyclic stress ratio, CSR (see Equation 2-12). Furthermore, the Simplified method assumes the cyclic loading and development of excess porewater pressures during shaking are relatively uniform (Seed and Idriss, 1982). Given this, the following was assumed:

a) If the r_u value approaches 1.0 towards the end of dynamic loading, the FS is about 1.0;
b) If the r_u value approaches 1.0 before the end of dynamic loading, the FS is less than 1.0 and decreases with more rapidly r_u approaches 1.0 from the start of the loading; and

c) If r_u value does not approach 1.0 during shaking, the FS is greater than 1.0 and may be approximated by the inverse of the r_u value.

Using these assumptions, the factors of safety with respect to liquefaction for the six cases analyzed were approximated and are presented on Table 4-8. The ranges of factors of safety shown in Table 4-8 represent the variations of the factors of safety within the depth of the tailings.

Table 4-8 – Approximate factors of safety with respect to liquefaction from the dynamic numerical evaluations.

Earthquake Loading	Approximate Factor of Safety
Normally Consolidated Tailings	
E1 (M_w=6.5)	0.25 – 2.0
E3 (M_w=7.0)	0.25 – 0.75
E5 (M_w=7.5)	0.25 – 0.5
Under-consolidated Tailings	
E1 (M_w=6.5)	0.25 – 1.5
E3 (M_w=7.0)	0.25 – 0.75
E5 (M_w=7.5)	0.25

Based on the estimated factors of safety, the liquefaction potential of the normally consolidated tailings was very high under the earthquake loads considered and increased with increasing earthquake intensity. For the under-consolidated tailings, the liquefaction potential was moderate to high with respect to Earthquake E1 and high with respect to Earthquakes E3 and E5.

4.4.6 Remarks on the Liquefaction Evaluation

The differences in the responses of the consolidated and unconsolidated tailings to the earthquake loads considered can be summarized as follows:

a) The greater stiffness of the consolidated tailings relative to the unconsolidated tailings resulted in more amplification (or less damping) of the ground motion as it traveled through the tailings;
b) The greater amplification (less damping) within the consolidated tailings was evident in the CSR development during shaking;
c) Although the consolidated tailings experienced greater cyclic loading, due to greater amplification, the generation of excess porewater pressure in the consolidated and unconsolidated tailings was fairly similar due to the greater cyclic resistance of the consolidated tailings; and
d) The average maximum shear strains in the consolidated and unconsolidated tailings were roughly equivalent for the magnitude 6.5 and 7 earthquake loadings. However, for the magnitude 7.5 earthquake loading, the average maximum shear strains in the consolidated tailings were about 3 times lower than those of the unconsolidated tailings.

4.4.7 Comparisons of Analytical and Numerical Liquefaction Evaluations

In Section 3.9.1 the evaluation of the potential for liquefaction of the (under-consolidated) tailings based on the cone penetration is presented. That analysis was based on the Simplified method as presented by Youd et al. (2001). An analytical evaluation of the potential for liquefaction of the tailings when normally consolidated was completed using the CDSS testing data (refer to Section 3.9.2). The findings of the analytical liquefaction evaluations and the FLAC evaluation are summarized on Table 4-9. As shown on the table, there is a considerable difference in the results of the liquefaction evaluations.

The site response analyses completed for the analytical evaluations did not consider the effects of porewater pressure generation which were considered in the dynamic numerical evaluations.

Considering results for the unconsolidated tailings, it is noted that the amplification factors from the numerical methods are significantly greater than those of the analytical method. The very low values obtained from the CPT data (varying from 0.11 to 0.42) are attributed to the presence of zones of very low tip resistance and thus low shear modulus within the tailings which were assumed to be of infinite extent in the analysis. If these zones are actually of limited extend, then their influence on the site response would be somewhat reduced. The corresponding F_a values from the numerical analyses were 0.23 to 1.12.

The factors of safety with respect to liquefaction from the CPT and FLAC analyses were in general agreement at the three earthquake loads considered.

The differences in the results of the analytical and numerical liquefaction evaluation of the unconsolidated tailings can be primarily attributed to the following:

- The analytical evaluation did not consider the effect of excess porewater pressure development, which was considered in the numerical evaluation; and
- The corrected standard penetration test resistance values, $(N_1)_{60}$, used in the numerical evaluation to characterized the strength, cyclic resistance and elastic properties of the tailings was an average value based on conversion of the CPT tip resistance and did not accurately reflect the considerable heterogeneity encountered in the field.

In the evaluations of the consolidated tailings the amplification factors from the numerical method were 0.4 to 3 times greater than those from the analytical method using CDSS testing data. However, it was expected that the opposite would be the case since the numerical method includes the damping effect of excess porewater pressure

generation. However, a review of the ground motions from the numerical evaluation (see Appendix H), indicates that the peak accelerations on the surface occurred very early in the shaking and may not have been influenced by the generation of excess porewater pressures.

For the normally consolidated tailings, the factors of safety estimated by analysis of the CDSS test results and using FLAC were in general agreement.

Table 4-9 – Comparison of analytical and numerical liquefaction evaluations.

Factors	CPT	FLAC	CDSS Testing	FLAC
State of Tailings	Under-consolidated		Normally Consolidated	
Earthquake E1 (M_w=6.5)				
Amplification Factor	0.42	1.12	0.69	2.06
FS	0.25 – 1.25	0.25 - 1.5	0.5 - 1	0.25 – 2
Earthquake E3 (M_w=7.0)				
Amplification Factor	0.19	0.38	0.42	1.14
FS	0.25 – 0.75	0.25 – 0.75	0.55 – 0.2	0.25 – 0.75
Earthquake E5 (M_w=7.5)				
Amplification Factor	0.11	0.23	0.23	0.32
FS	0.1 – 0.65	0.25	0.1 – 0.4	0.25 – 0.5

4.5 REMARKS ON THE PRELIMINARY NUMERICAL MODELING

This chapter included an evaluation of the system of analysis used in the numerical modeling based on the results of cyclic simple shear testing, and numerical liquefaction analyses of both consolidated and unconsolidated tailings deposits under various earthquake loadings that were compared to the results of analytical modeling.

The following conclusions are drawn from the preliminary numerical modeling:

1. The system of analysis (FLAC and the UBC Sand model) is capable of simulating the dynamic behavior of the tailings over a wide range of earthquake loadings.

2. The 2-dimensional model of the CDSS testing provided reasonable results, particularly over the range of cyclic loadings that would normally produce liquefaction in hydraulically deposited, cohesionless granular material.

3. UBC Sand model parameters, $(N_1)_{60}$ and ψ_{cv} of 11 blows/300 mm and 35.6º, respectively, can be used to model the dynamic behavior of consolidated tailings.

4. The factors of safety with respect to liquefaction of the analytic and numerical liquefaction evaluations of the tailings when under-consolidated and normally consolidated were in reasonable agreement, despite significant differences in the site responses as measured by the amplification factors.

CHAPTER 5. NUMERICAL ANALYSIS OF THE REPRESENTATIVE TAILINGS IMPOUNDMENT

5.1 INTRODUCTION

This chapter presents an evaluation of the representative tailings impoundment based on dynamic numerical analyses. The objectives of the evaluation were to:

- Present dynamic numerical analyses of the representative impoundment, with and without waste rock inclusions;
- Evaluate and compare the dynamic behavior of the representative tailings impoundment, with and without waste rock inclusions; and
- Evaluate the dynamic behavior of the representative impoundment for comparison with: a) the level ground liquefaction analyses presented in Chapters 3 and 4; and b) the analytical pseudo-static stability evaluation presented in Chapter 3.

5.2 METHOD OF ANALYSIS

The dynamic behavior of the impoundment was analyzed using numerical analysis and evaluated based on the site response, cyclic stress ratio and excess porewater pressure development, and the pattern and magnitude of deformations.

The analyses were conducted using the FLAC finite difference software program with the UBC Sand model used to simulate the tailings. The analyses consisted of two phases: a static phase and a dynamic phase. In the static phase, the states of stress, strain and porewater pressure within the models under conditions of steady state mechanical and fluid equilibrium were developed. In the dynamic phase, horizontal accelerations were applied to the bottom of the model to simulate the occurrence of an earthquake of known intensity.

In the dynamic phase of the modeling, FLAC was set to solve for mechanical, fluid and dynamic equilibrium simultaneously. This required the generation of two time steps, one

for fluid flow and another for dynamic behavior, that were calculated automatically by the software based on the material properties, geometry and damping parameters of the model. The actually time step used by FLAC was the smaller of the two and controlled the progress of the simulation.

The time step used by FLAC in the dynamic phase of the modeling was the dynamic time step which averaged $4x10^{-5}$ seconds. Solution time for the dynamic phase was about 5.5 hours for the simulated earthquake, which had a duration of 40 seconds, using a computer with an Intel® Pentium® Dual E2200 central processing unit (CPU) with a rated speed of 2.2 GHz.

The values of several parameters at locations of interest in the model were recorded at intervals of 1,000 time steps during the dynamic phase for evaluation and use in this report. Some of the parameters were calculated automatically by FLAC (e.g. horizontal acceleration, porewater pressure, and displacement) and others were calculated using subroutines included in the FLAC execution files (e.g. the cyclic stress ratio and the excess porewater pressure ratio).

A critical element in numerical modeling is the generation of the mesh, particularly the size and shape of the individual elements. Itasca (2005) recommends using square elements wherever possible for greater accuracy, smaller elements where more detail is required and larger elements where less detail is required. The number of elements used in a model has a direct correlation with the time required for simulation.

The models were created on a 250 (horizontal) by 35 (vertical) element grid (8,750 elements) with a typical element size of 1 m by 1 m. It was found that this mesh achieved the following.

a) The computational time for the dynamic phase was about 4.5 hours for a 40 second ground motion, which was considered reasonable;

b) A relatively gradual distribution of calculated results and parameters (void ratios, stresses, accelerations, strains, etc.) through the depth of the impoundment; and
c) The geometry of the representative impoundment was accurately duplicated.

The element size selected (1 m by 1 m) was a compromise between limiting computational time (larger elements) and accuracy considerations (smaller elements) and provided a degree of accuracy sufficient for the needs of this research, which was to make comparative evaluations of the responses of tailings impoundment with and without waste rock inclusions. The convergence criteria was to have relatively smooth transitions of material properties, stresses, pressures, and accelerations within the depth of the tailings with the dynamic analyses taking less than 12 hours to complete for the selected ground motions.

5.3 MODEL GEOMETRY, MATERIAL PROPERTIES AND BOUNDARY CONDITIONS

A typical section through the dike at the representative impoundment is presented on Figure 3-14, which is duplicated on Figure 5-1. Recall that the dike is a zoned rockfill structure and is not typical of tailings dam construction, particularly the presence of the berm on the surface of the tailings. To make the analyses more general in nature, the berm was not considered in the analyses.

5.3.1 Model Geometry

The finite difference grid (or mesh) created in FLAC to model the impoundment is presented on Figure 5-2. Also shown on the figure are the points (red dots) where parameters calculated during the analyses were recorded. Note that most of the points coincide with either of two vertical lines in the impoundment that are labeled “P1” and “P2.” These lines are profiles where the recorded parameters could be presented with respect to depth. P1 and P2 were located 46 m and 56 m upstream of the crest of the dike, respectively. In the conventional impoundment, P1 and P2 were located in the impounded tailings. In the reinforced impoundment, P1 was located in the impounded tailings between waste rock inclusions and P2 was located in the center of a waste rock inclusion.

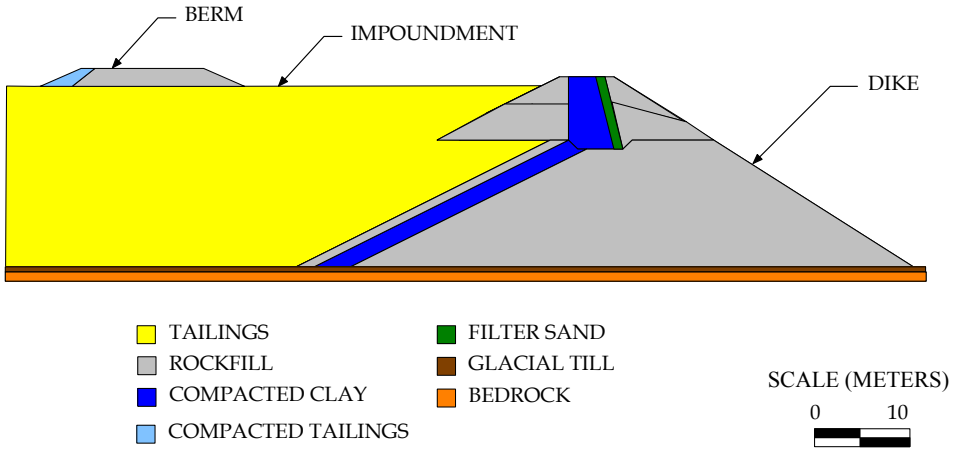

Figure 5-1 – Typical section of the dike at the representative impoundment.

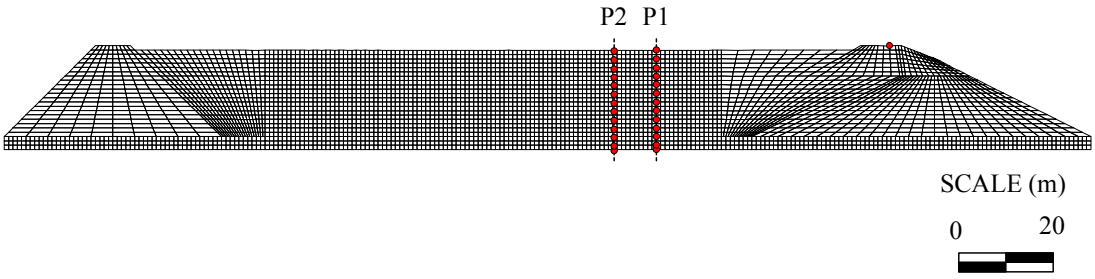

Figure 5-2 – Finite difference grid (mesh) used to model the representative impoundment.

The models of the representative impoundment, with and without waste rock inclusions, with the material designations shown are presented on Figures 5-3 and 5-4, respectively. Comparing these figures to the typical cross-section of the dike of the representative impoundment (Figure 5-1) demonstrates the models are comparable to the actual impoundment, except for the absence of the berm on the surface of the tailings. The model of the impoundment with inclusions (Figure 5-4) includes three waste rock inclusions. The waste rock inclusions are 8-m-wide and spaced 20 m apart, measured center-to-center, with the first inclusion being 32 m upstream of the crest of the dike.

Layers of waste rock, 1-m-thick were assumed on the bottom and sides of the impoundment.

A buttress was placed on the upstream end of the model for stability reasons. During numerical modeling, it was found that simulating tailings at the upstream end of the model resulted in excessive deformation sufficient to terminate program execution under relatively low dynamic loads and that placing a very stiff material at the upstream end resulted in excessive dynamic loads on the dike that resulted in excessive deformation. Eventually, it was discovered that the upstream side of the model could consist of either a moderately stiff vertical zone with a dynamic free field boundary (see Section 4.4.4) or of a dam-like structure that was stronger than the dam or dike being analyzed. It was also discovered that the width of the impounded tailings was very important in that an insufficient width resulted in excessive deformation due to dynamic interaction between the two sides of the model. Height to width ratios of the impounded tailings of 1:5 or greater were found to the sufficient to prevent this dynamic interaction and create "level ground" conditions within the impoundment. The area of the impounded tailings in the models was 122 m wide (measured from the downstream toe of the buttress to the upstream toe of the dike) and 20 m deep, resulting in a height to width ratio of 6.1 that was considered to be sufficient to prevent significant dynamic interaction between the ends of the model.

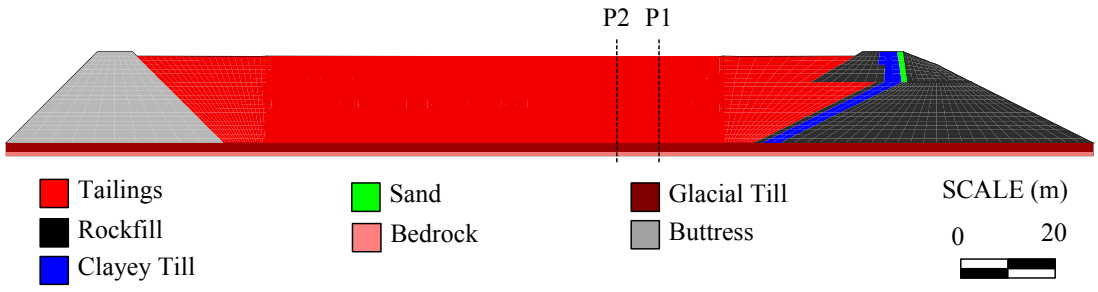

Figure 5-3 – Model of the representative impoundment (without inclusions).

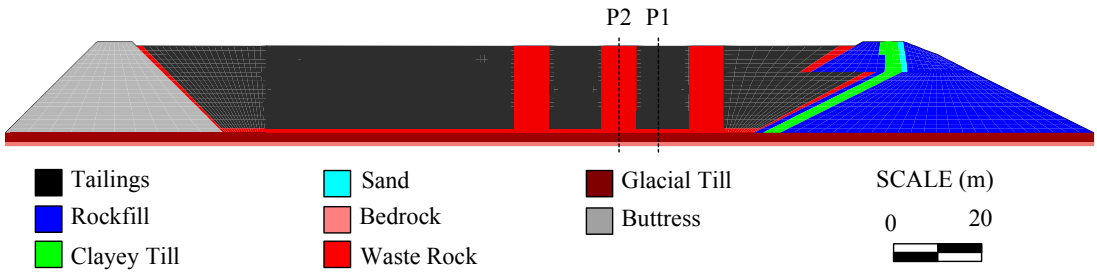

Figure 5-4 – Model of the representative tailings impoundment (with inclusions).

5.3.2 Material Properties

The tailings were simulated using the UBC Sand model (refer to Section 2.7.2). All other materials were simulated using FLAC's built-in Mohr-Coulomb model. The properties of the materials, excluding the tailings, are summarized on Table 5-1.

5.3.2.1 Tailings

The material properties for the tailings were derived from the cone penetration and laboratory testing conducted for this research (Chapter 3). As noted, the tailings are under-consolidated with respect to existing loads and the typical corrected standard penetration test blow count, $(N_1)_{60}$, from conversion of the CPT results was less than 4 (see Section 3.7.3.6).

The principal parameters of the UBC Sand model are the $(N_1)_{60}$ value and ψ_{cv} (the constant volume friction angle). Based on the evaluation of the CPT results an average $(N_1)_{60}$ value of 3.5 was used to for the tailings. This value was randomized using the "rdev" function in FLAC to produce standard deviations of 0.5 to simulate the heterogeneity of tailings the deposit. The resulting values had an average of 3.5 and a standard deviation of 0.5. Using Equation 2-27, the ψ_{cv} of the tailings was determined to be 36.25° based on the effective friction angle from direct shear testing (ϕ=36.6°) and the typical $(N_1)_{60}$ value from the CPT results.

The dry unit weight and porosity of the tailings were based on the consolidation testing (Equation 3-1). At mid-depth (7.5) m in the impoundment, these properties were 2,375 kg/m^3 and 0.39, respectively. The resulting values were for normally consolidated material. However, as the excess porewater pressure response of the UBC Sand model is based primarily on the $(N_1)_{60}$ values, the slightly greater unit weights and porosity of the tailings relative to their under-consolidated values, was not significant with respect to the dynamic behavior of the tailings. Estimation of the horizontal and vertical saturated hydraulic conductivities of the tailings is presented in Section 3.7.1.9 and was based on consolidation testing, empirical correlations with the grain size distribution and published values (k_h=2.25x10^{-4} cm/s and k_v=4.5x10^{-5} cm/s). These values were assumed to be averages and the "rdev" function was used to assign standard deviations of one half an order of magnitude. The use of hydraulic conductivity values for consolidated tailings rather than unconsolidated tailings did not have an appreciable effect on the modeling due to the rapid rate of loading relative to the hydraulic conductivities.

From direct shear testing, the tailings were determined to have no appreciable cohesion; accordingly, they were assigned no cohesion.

Other properties of the tailings (e.g. shear and bulk moduli) were automatically calculated by the UBC Sand model based on the parameters provided (see Section 2.7.2.1).

5.3.2.2 Rockfill

The total density of the rockfill (2,200 kg/m^3) was based on typical values provided in Sherard et al. (1963). The friction angle of the rockfill was estimated using Leps (1970) and assuming that the rockfill was well-graded and at an average vertical effective stress of 100 kPa. The dilation angle of the rock fill (10°) was taken from Itasca (2005). The shear and bulk moduli were derived from the following relationships between the effective normal stress and the moduli based on Seed et al. (1984) and Rollins et al. (1998) and assuming a Poisson's ratio, μ, of 0.3 and a coefficient of earth pressure at-rest, K_0, of 0.4:

$$G = 2650 \cdot \left(0.6 \cdot \sigma'_{v,o}\right) \quad (5\text{-}1)$$

$$K = 2.3833 \cdot G \quad (5\text{-}2)$$

where: G is the shear modulus;

K is the bulk modulus; and

$\sigma'_{v,o}$ is the initial vertical effective stress.

The shear and bulk moduli of each element were calculated iteratively within FLAC using a "FISH" subroutine. The hydraulic conductivity of the rockfill was estimated from published values for gravel (Freeze and Cherry, 1979). The porosity was estimated to be 0.25 based on the unit weight.

The rockfill was assigned a cohesion of 10 kPa to represent interlocking of the grains. The cohesion served to prevent excessive deformation in areas of low effective stress due to seepage or dynamic loads (Castillo et al., 2006; James et al., 2006).

The material properties assumed for the compacted clay/till core were based on published values for medium stiff clay from Holtz & Kovacs (1981), Bowles (1996) and Itasca (2005).

For the sand (filter), the material properties were derived from values provided in Holtz & Kovacs (1981), Bowles (1996) and Itasca (2005) for medium dense sand.

As noted in Section 3.6.2, the impoundment is underlain by dense glacial till. The properties of the glacial till used in the modeling were based on reported values for dense and well-compacted glacial till provided in Milligan (1976) and Bowles (1996).

The bedrock at the site consists of schist of medium quality and andesite of poor to medium quality (Section 3.6.2). Properties for similar rock were obtained from Goodman (1989) and Itasca (2005).

Table 5-1 – Material properties used in FLAC Modeling of the representative impoundment.

Material Property	Bedrock	Glacial Till	Rockfill	Clay/Till Core	Sand Filter
Model	Mohr	Mohr	Mohr	Mohr	Mohr
Dry unit weight, γ_d (kg/m^3)	2,200	2,000	2,000	1,800	1,850
Friction angle, ϕ	25º	36º	45º	30º	37º
Cohesion, c (kPa)	50,000	250	10	100	10
Dilation angle, φ_d	15º	10º	10º	10º	10º
Porosity, n	0.10	0.15	0.25	0.25	0.30
Shear modulus, G (MPa)	$7.69x10^3$	360	Varied[1]	76.9	17.3
Bulk modulus, K (MPa)	$1.67x10^4$	780	Varied[1]	166.7	37.5
Hydraulic conductivity, k (m/s)	$1.0x10^{-8}$	$1.0x10^{-7}$	$1.0x10^{-3}$	$1.0x10^{-8}$	$1.0x10^{-2}$

[1] The moduli of the rockfill varied with the vertical effective stress as per Equations 5-1 and 5-2.

The waste rock was assigned the same material properties as the rockfill.

The buttress used for stability on the upstream side of the model was assigned the same material properties as the glacial till, except that the hydraulic conductivity was $1x10^{-3}$ m/s.

5.3.2.3 Homogeneity and Isotropy

All of the materials were assumed to be homogeneous and isotropic except for the tailings and rockfill. Recall that the $(N_1)_{60}$ values of the tailings were randomized about an average value, as were the vertical and horizontal hydraulic conductivities of the tailings. The density and porosity of the tailings were varied with the depth. The shear and bulk moduli of the rockfill varied with the vertical effective stress.

5.3.2.4 Dynamic Damping

During the dynamic analyses, hysteretic damping corresponding to the upper range for sand in Seed and Idriss (1970) was applied to all of the materials except for the tailings and Bedrock. The UBC Sand model includes a "small viscous component" that simulates hysteretic damping (Beaty and Byrne, 1998). Hysteric damping was not applied to the bedrock, because bedrock was considered to be the "source" of the earthquake loading and the application of hysteretic damping may have fundamentally altered the ground motion as it passed through the 1-m-thick layer of bedrock assumed on the bottom of the model.

A Rayleigh dynamic stiffness damping factor of 0.01 at a frequency of 20.0 Hz was applied to the entire model. This is recommended by Itasca (2005) and Cundall (2006) to prevent excessive amplification of the ground motion at very low levels of shear strain when hysteretic damping is not effective. These particular values were selected because they resulted in no significant change (amplification or damping) of the ground motion within the 1-m-thick layer of bedrock simulated on the bottom of the model.

5.3.3 Boundary Conditions

The boundary conditions on the models during the static analyses are shown on Figure 5-5. The effect of the boundary conditions was to simulate a pond on the surface of the impoundment with seepage through the dike and upstream buttress. No flow was permitted to or from the bottom of the model.

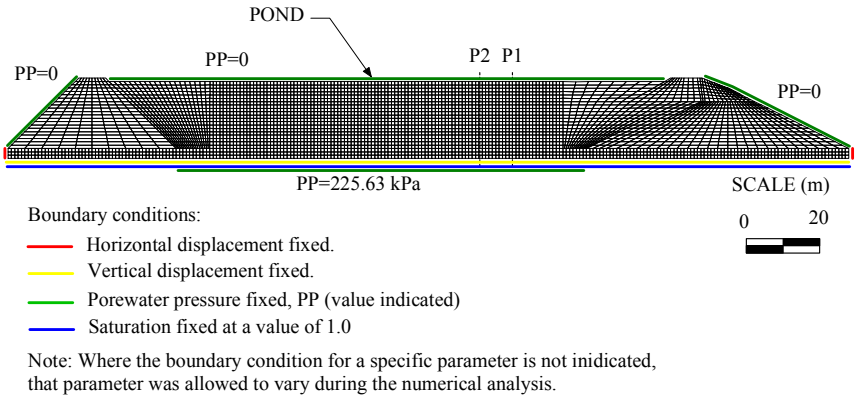

Figure 5-5 – Boundary conditions applied to the model of the representative impoundment during static analyses.

5.4 STATIC CONDITIONS

The results of the static analyses that were conducted to establish the states of stress, strain and porewater pressure in the impoundment prior to dynamic analyses are summarized in the following sections.

5.4.1 The Representative Impoundment (without inclusions)

The static vertical effective stresses in the impoundment are shown on Figure 5-6. They vary from 0 at the surface of the tailings to about 350 kPa at the bottom of the tailings. Analytically, the vertical effective stress at the bottom of the tailings was estimated as follows:

$$\sigma_v' = 20\ m \cdot (23.5\ kN/m^3\ - 0.6 \cdot 9.81\ kN/m^3) = 352\ kPa.$$

The vertical effective stresses calculated in the numerical modeling were in agreement with the analytical estimate and is deemed to be reasonable.

The lack of uniformity in the stress distribution on Figure 5-6 and other stress contours extracted from FLAC and presented in this thesis are the result of: a) the manner in which FLAC creates stress contours from the average stresses calculated within in each element; and b) the heterogeneity applied to the values of $(N_1)_{60}$ used for the tailings. Recall that

the elastic moduli of the tailings were estimated from the $(N_1)_{60}$ values. The linear divisions (separations) evident on the stress contours are the result of the manner in which the grid was created (by attaching elements from different sections of the mesh), and have no significance with respect to the results.

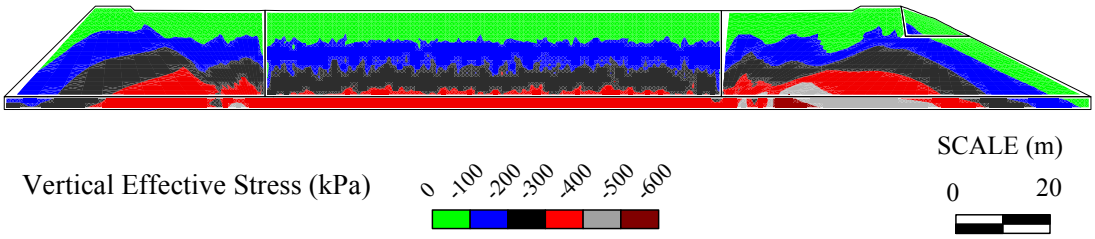

Figure 5-6 – Static vertical effective stresses in the representative impoundment (without inclusions).

The static horizontal effective stresses within the impoundment are presented on Figure 5-7. Within the tailings, these stresses varied from 0 near the surface to about 150 kPa at the bottom. The ratio of the horizontal stresses to the vertical stresses (150 kPa/350 kPa) corresponds to an at-rest pressure coefficient of approximately 0.43. For the tailings:

$$K_0 = 1 - sin\emptyset = 1 - \sin(36.6°) = 0.40$$

Given this, the static horizontal effective stresses within the impoundment are deemed to be reasonable.

The higher horizontal effective stresses in the lower areas of the dike are due to stress transfer resulting from the geometry of the impoundment and to the rockfill of the dike being stiffer than the tailings.

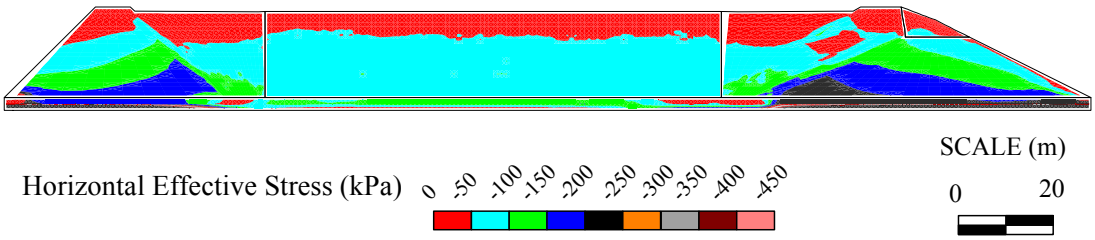

Figure 5-7 – Static horizontal effective stresses in the representative impoundment (without inclusions).

The porewater pressure distribution within the conventional impoundment is shown on Figure 5-8. In the central part of the impoundment, static porewater pressures varied from about 0 near the surface to 196 kPa at the bottom of the tailings and 225 kPa at the bottom of the model. These values are in agreement with the assumption of hydrostatic conditions which results in calculated porewater pressure, u, values of 196 kPa at the bottom of the tailings and 226 kPa at the bottom of the model ($u=\gamma_w \cdot z$, where γ_w is the unit weight of water and z is depth).

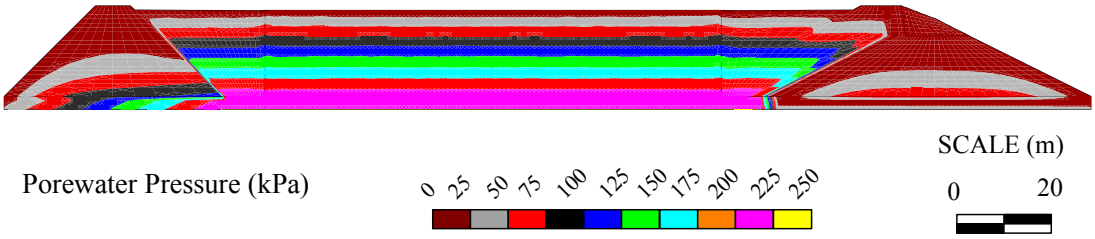

Figure 5-8 – Hydrostatic porewater pressures in the representative impoundment (without inclusions)

The factor of safety of the impoundment (without inclusions) under static conditions was calculated using FLAC. This required that the model used to simulate the tailings be changed from the UBC Sand model to the Mohr-Coulomb model and the assignment of

equivalent elastic and strength properties. FLAC calculates the factor of safety using the strength reduction method with a bracketing approach (Itasca, 2005). The resulting factor of safety against slope failure of the dike was 2.33.

5.4.2 The Representative Impoundment (with inclusions)

The vertical effective stresses in the representative impoundment with waste rock inclusions are shown on Figure 5-9. The stress distribution is very similar to that for the impoundment without waste rock inclusions (Figure 5-6), except in the area of the waste rock inclusions where stress transfer from the adjacent tailings to the waste rock inclusions is evident. This is due to the relative stiffness of the two materials, with the waste rock being much stiffer than the tailings. Vertical effective stresses in the tailings adjacent to the inclusions are 50 to 100 kPa lower than those in the tailings away from the inclusions.

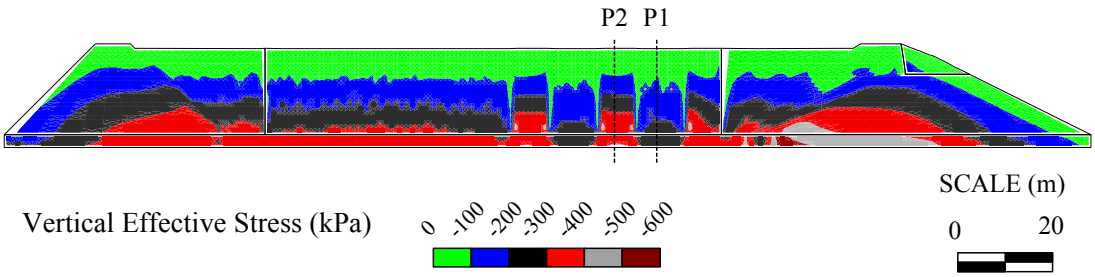

Figure 5-9 – Static vertical effective stresses in the representative impoundment (with inclusions).

Figure 5-10 shows the horizontal effective stresses in the impoundment with inclusions. Generally, these stresses are similar to those for the impoundment without inclusions (Figure 5-7), except for slightly higher stresses in the bottom of the inclusions. These higher stress zones are attributed to the greater friction angle of the waste rock compared to the tailings (45° versus 36.6°), which would have resulted in greater at-rest pressures,

and the greater vertical effective stresses in the bottom of the inclusions due to the stress transfer described above.

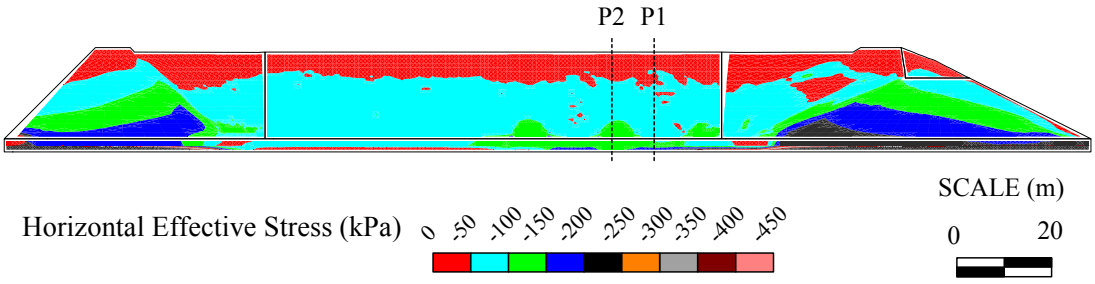

Figure 5-10 – Static horizontal effective stresses in the representative impoundment (with inclusions).

The porewater pressure distribution in the impoundment with inclusions is plotted on Figure 5-11 and is the same as that in the impoundment without inclusions (Figure 5-8).

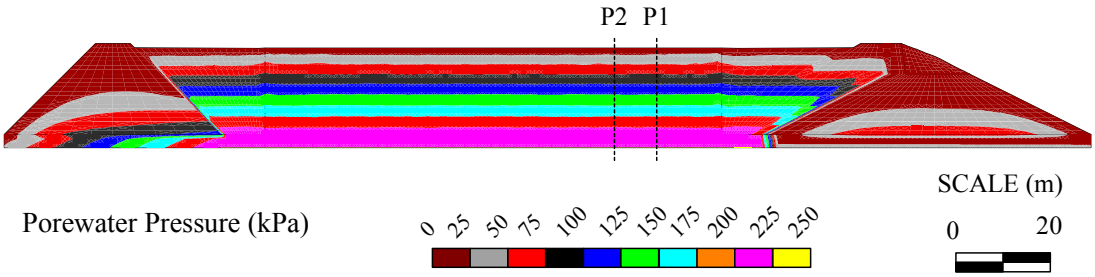

Figure 5-11 – Hydrostatic porewater pressures in the representative impoundment (with inclusions)

The factor of safety of the representative impoundment with inclusions under static conditions was calculated using FLAC and determined to be 2.33, the same as the impoundment without inclusions.

5.5 DYNAMIC ANALYSES

Dynamic analyses of the impoundments was conducted by removing the boundary conditions against lateral movement of the sides and vertical movement of the bottom of the model and applying a vertical velocity of 0 and a ground motion (horizontal accelerations) to the bottom of the model. The fluid boundary conditions used in the static analyses were retained.

5.5.1 Earthquake Loading

The ground motion applied to the bottom of the models in the dynamic analyses was that developed for Earthquake E5. This ground motion simulates the occurrence of a moment magnitude 7.5 earthquake with a fault-rupture to site distance of 30 km and the associated parameters are a PGA of 1.432 g, an Arias Intensity, I_x, of 3.091 m/s, and a duration of 40 s. Additional information on the Earthquake E5 ground motion is presented in Section 3.8.3 and Appendix E.

5.5.2 Dynamic Analysis of the Representative Impoundment (without inclusions)

The dynamic analysis of the representative tailings impoundment without waste rock inclusions is presented in the following sections that describe the behavior of the impoundment during shaking and the conditions within the impoundment at the end of shaking. Based on the behavior of the dike during shaking and the fact that the dike is a zoned rockfill structure, post-shaking analysis was not considered necessary and was not conducted.

5.5.2.1 Site Response

The peak horizontal ground accelerations, PGA, at locations of interest in the impoundment were extracted from FLAC and the corresponding amplification factors, F_a, were calculated using Equation 3-12. The values are listed on Table 5-2. Based on the amplification factors, the ground motion (horizontal accelerations) was slightly amplified as it passed through the 2-m-thick layer of dense glacial till overlying bedrock and

severely damped within the tailings. The F_a value of 0.68 calculated for the crest of the dike is indicative of moderate damping. However, as previously noted, PGA values represent isolated points on accelerograms that tend to be quite complex and may not accurately represent the damping or amplification of the entire ground motion. A more accurate depiction of the site response can be obtained by reviewing the acceleration time histories at specific locations.

Table 5-2 – Calculated amplification factors – representative impoundment (without inclusions).

Location	Peak Horizontal Ground Acceleration, PGA (g)	Amplification Factor (F_a)
Top of bedrock	1.53	-
Top of glacial till	1.61	1.05
Surface of Impoundment at P1	0.08	0.05
Surface of Impoundment at P2	0.09	0.06
Crest of dike	1.04	0.68

The horizontal accelerations input to the bottom of bedrock (a) and calculated on the top of bedrock (b), on the top of glacial till (c), and at 0.275H in the tailings (d) at location P1 (see Figure 5-2) are shown on Figure 5-12. The input ground motion was that for Earthquake E5 (M_w=7.5) and is also shown on Figure 3-29. From Figure 5-12 it is noted that the horizontal accelerations at the top of bedrock are virtually identical to those input to the bottom of bedrock, there was moderately low amplification of the horizontal accelerations within the 2-m-thick layer of dense glacial till overlying bedrock, and at 0.275H in the tailings the horizontal accelerations were damped by a factor of about 3. "H" refers to the height of tailings in the impoundment (20 m), measured from the bottom to the top; thus, 0.275H is 5.5 m above the bottom of the tailings.

The amplification within the dense glacial till was attributed to the shear modulus of the till being significantly lower than that of the bedrock, but being sufficiently stiff so as not to undergo high shear strains that would have resulted in significant damping.

The horizontal accelerations calculated at 0.275H, 0.475H, 0.675H, and 0.875H in the tailings at location P1 (see Figure 5-2) are presented on Figure 5-13. Within the tailings, the damping of the ground motion increased as it rose towards the surface. The horizontal accelerations at 0.875H are almost an order of magnitude lower than those at the bottom of the tailings. Note that the horizontal accelerations at 0.275H are shown on Figure 5-12 as well for comparison with underlying ground motions.

The horizontal accelerations were severely damped within the tailings. The damping is attributed to shear strains in the tailings due to their relatively low shear modulus and the generation of excess porewater pressures during shaking that would have reduced the effective stresses in the tailings and further reduced the shear modulus. These issues will be discussed further in the following sections.

The horizontal accelerations on the crest of the dike (refer to Figure 5-2 for the exact location) are presented on Figure 5-14. Comparison of the these accelerations with those on the top of bedrock (Figure 5-12b) indicates that the horizontal acceleration on the crest was slightly damped for the first 15 seconds of shaking and then moderately amplified for the remainder of shaking. The response at the crest of a dam or dike is significantly influenced by the material properties and geometry of the structure and the intensity and frequency content of the ground motion. However, in the case of tailings impoundments, the presence of the retained tailings has some effect as well. Generally, with conventional water retention dams and earth embankments, the PGA values on the crest are amplified by a factor of 1.5 to 2.5 (Makdisi & Seed, 1977, 1978, 1979; Kramer, 1996; Cascone & Rampello, 2003; Rampello et al., 2008).

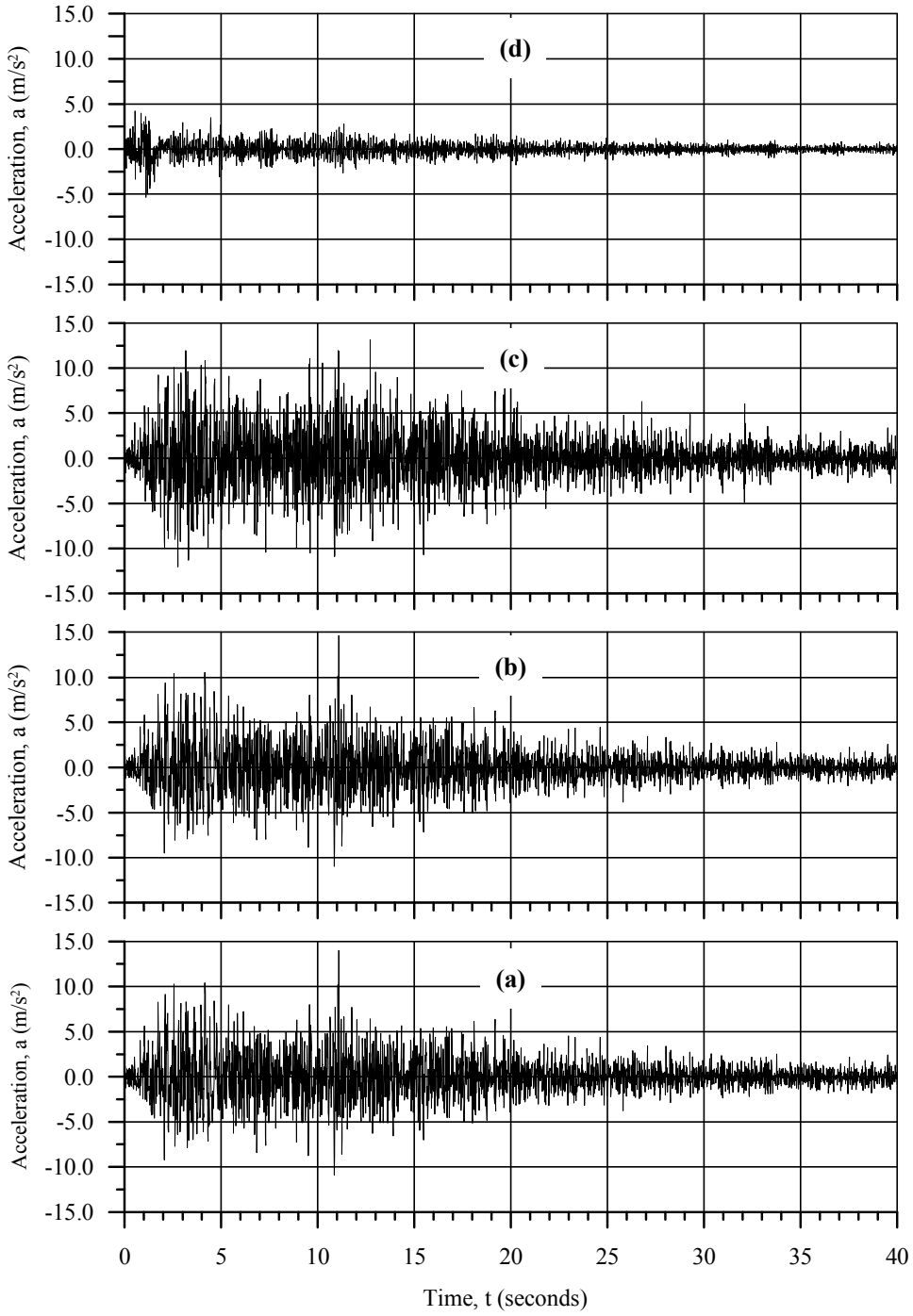

Figure 5-12 – Horizontal accelerations at P1: input to the bottom of bedrock (a) and calculated on the top of bedrock (b), on the top of glacial till (c), and at 0.275H in the tailings (d) – Representative impoundment (without inclusions).

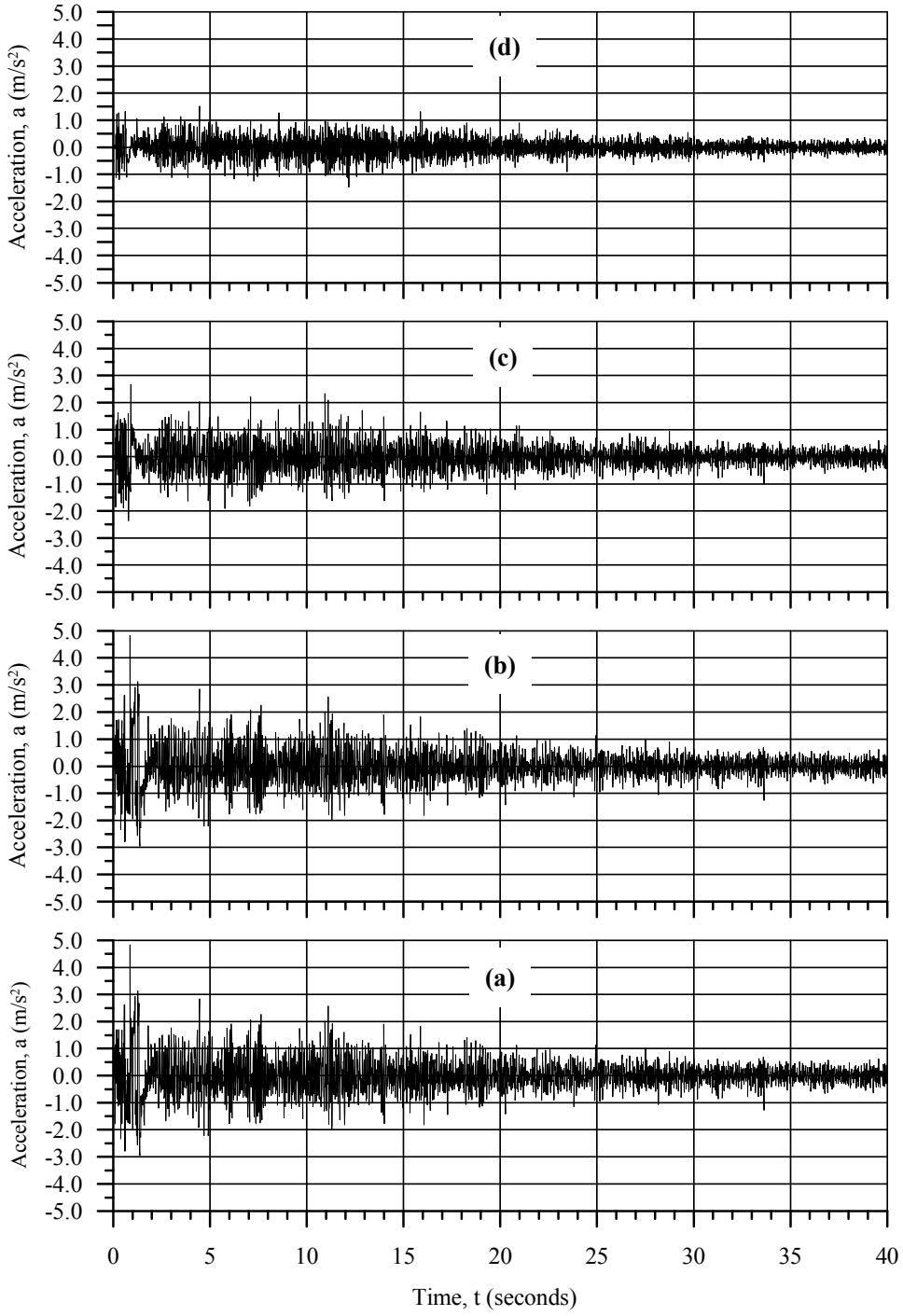

Figure 5-13 – Horizontal accelerations at P1: calculated at 0.275H (a), 0.475H (b), 0.675H (c), and 0.875H (d) – Representative impoundment (without inclusions).

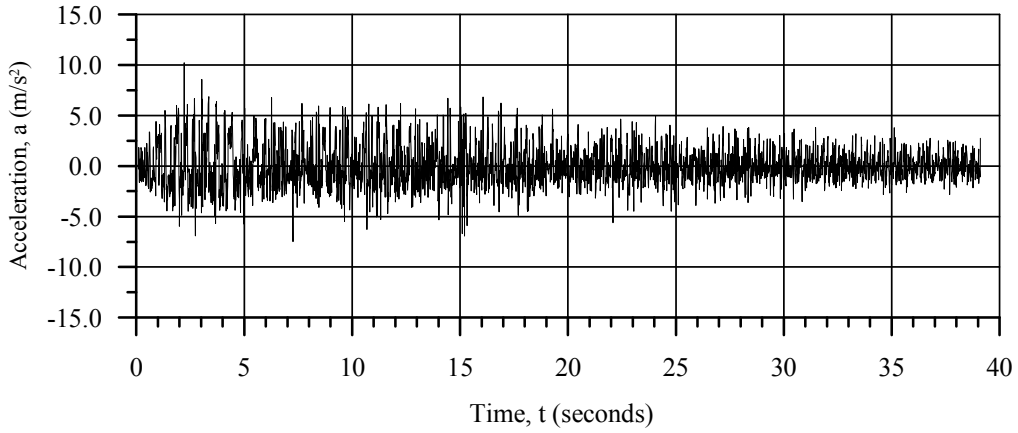

Figure 5-14 – Horizontal accelerations calculated on the crest of the dike - representative impoundment (without inclusions).

5.5.2.2 Cyclic Stress Ratio Development

During the dynamic analysis, the cyclic stress ratio, CSR, within the tailings was calculated using Equation 4-1, which is the ratio of the calculated shear stress to the initial vertical effective stress. This definition of the CSR includes all of the shear stresses incident on the tailings at a particular location and height, not just the shear stresses directly due to the earthquake loading as per the Simplified method of liquefaction evaluation (Equation 2-5).

Figure 5-15 presents the CSR development in the tailings at 0.275H, 0.475H, 0.6754H, and 0.875H at location P1 (Figure 5-3) during shaking. Generally, the CSR development was characterized by relatively large amplitudes during the first 2 seconds of shaking, with maximum values varying from 0.24 at 0.275H to 0.1 at 0.875H, followed by a sudden decline to maximum amplitudes of 0.025 or less for the next 10 to 15 seconds, and then no significant CSR development for the remainder of shaking.

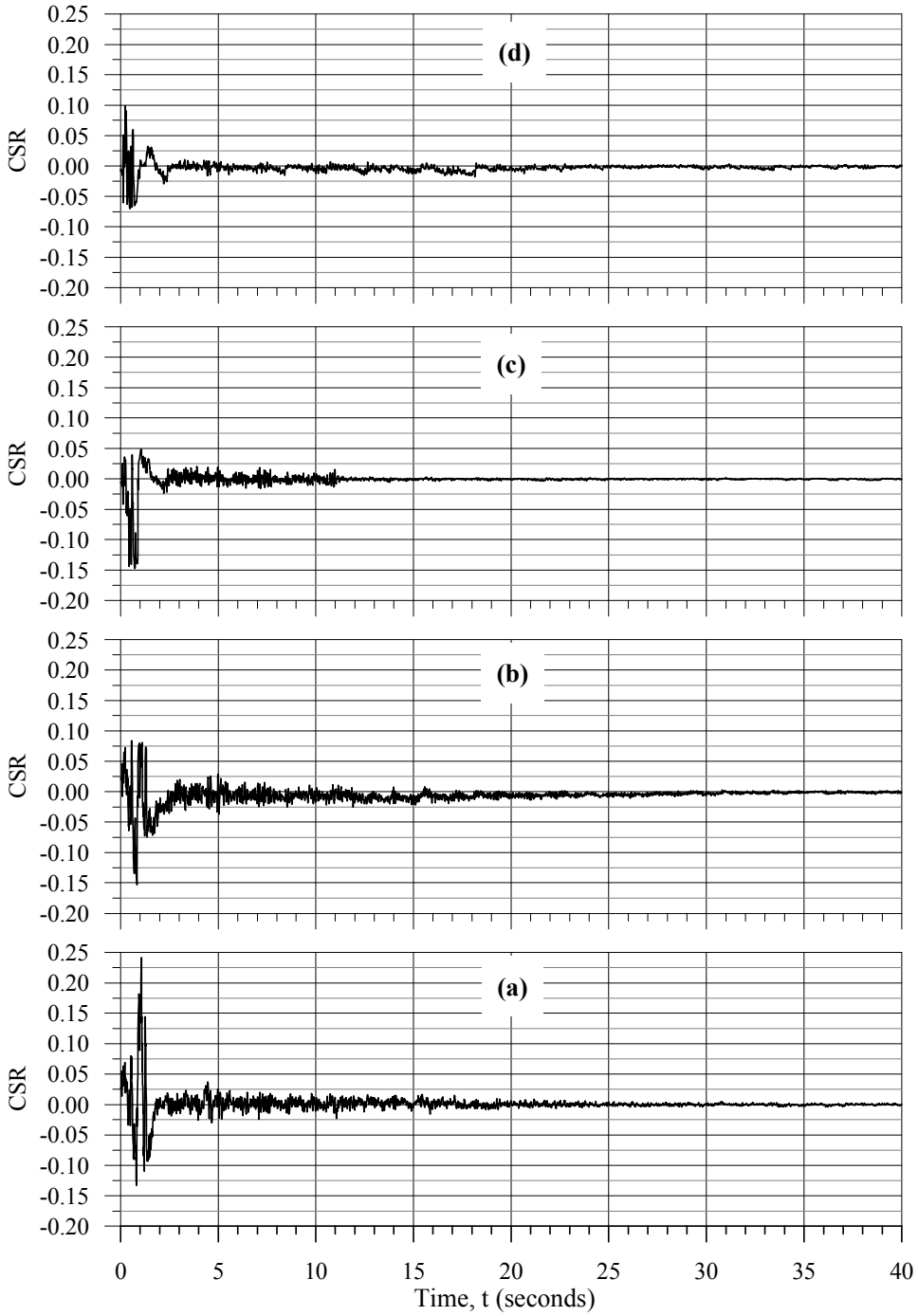

Figure 5-15 – CSR development at P1: calculated at 0.275H (a), 0.475H (b), 0.675H (c), and 0.875H (d) – Representative impoundment (without inclusions).

The CSR values at the start of shaking (t = 0 s) were approximately zero indicating that there were no significant shear stresses on horizontal planes in the tailings at the start of shaking and corresponds "level ground" conditions with respect to liquefaction analysis.

The rapid decline in the CSR, and thus the shear loading in the tailings, is attributed to the development of high excess porewater pressures in the tailings that are described in the following section.

The CSR development in the tailings at location P2 was very similar to that at P1 and was not included for brevity. The CSR development at P2 is presented in Appendix H.

5.5.2.3 Excess Porewater Pressure Development

The excess porewater pressure ratio, r_u, was used to represent the excess porewater pressure development in the tailings. Figure 5-16 provides plots of the r_u values developed at various heights in the tailings at location P1 (Figure 5-3). The r_u values were calculated using Equation 4-2 and include any changes in the vertical effective stresses due to excess porewater pressure generation or other causes. As noted previously, this equation was used because dynamic loading can cause changes in the effective stress not related to excess porewater generation, particularly in soils where the degree of saturation is less than 1.0.

As shown on Figure 5-16, the development of excess porewater pressure in the tailings was very rapid at all levels in the tailings at P1. By the 2nd second of shaking the r_u values varied between 0.65 and 1.0, by the 20th second were greater than 0.9 and remained greater than 0.9 for the remainder of shaking.

The high r_u values coincided with very low, less than 0.025, CSR values (Figure 5-15). Values of r_u approaching 1.0 indicate an almost complete nullification of the effective stress and thus the shear strength of cohesionless materials, as a result, these materials are no longer able to resist or transmit any appreciable shear stress.

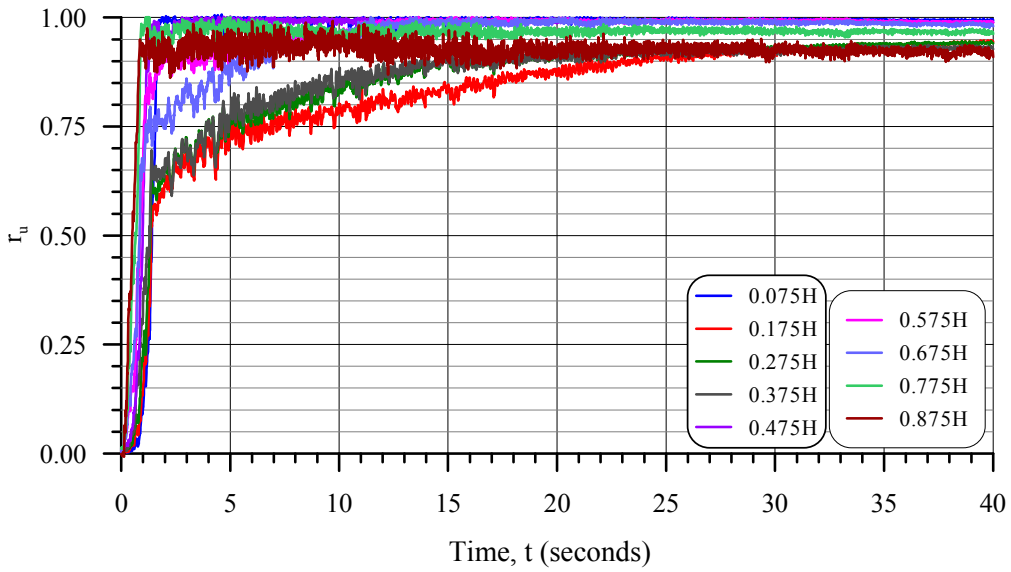

Figure 5-16 – Excess porewater pressure ratio, r_u, development in the tailings at location P1 during shaking in the representative impoundment (without inclusions).

5.5.2.4 Displacement of the Crest of the Dike

The displacement of the crest of the dike (Figure 5-2) during shaking is presented on Figure 5-17. Horizontally, the crest moved downstream at a rate of about 35 mm/s during the first 20 seconds of shaking, after which the rate of displacement decreased to near zero. The horizontal displacements were 0.83 m at t = 20 s and 0.95 m at t = 40 s. Vertically, the rate of displacement was lower and the crest moved downwards by 0.3 m by the end of shaking.

Referring back to the horizontal accelerations calculated on the crest of the dike (Figure 5-14), the amplification observed on the crest after the first 15 seconds of shaking was not associated with increased displacement of the crest. The majority of the displacement occurred during the first 20 seconds of shaking and the rate of displacement of the crest declined during the period of amplification.

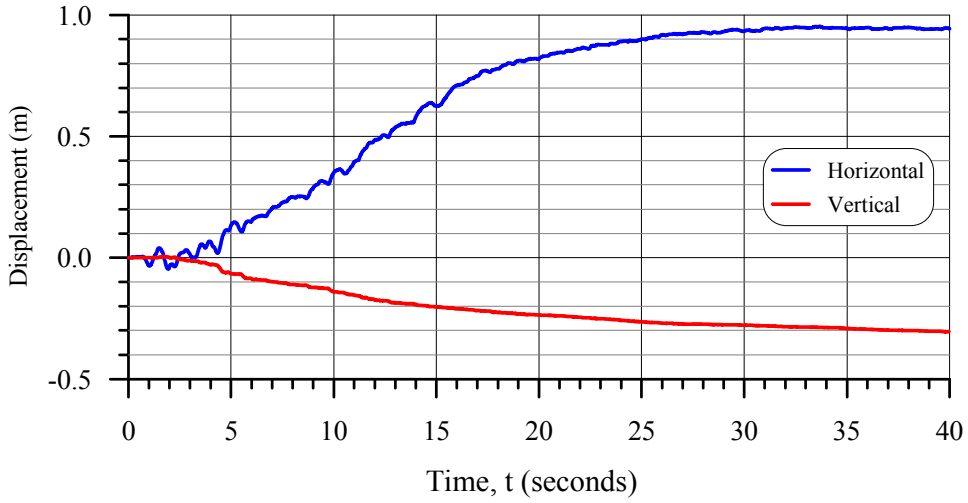

Figure 5-17 – Displacement of the crest of the dike during shaking in the representative impoundment (without inclusions).

5.5.2.5 Conditions at the End of Shaking

The vertical effectives stresses in the impoundment at the end of shaking (t = 40 s) are shown on Figure 5-18. Within the tailings, the vertical effective stresses were less than 100 kPa, compared to the 0 to 350 kPa prior to shaking (Figure 5-6). Moderate stress decreases occurred in the rockfill of the dike, typically about 50 kPa.

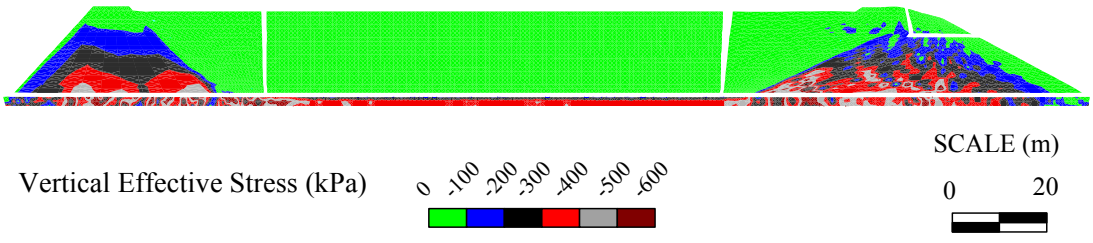

Figure 5-18 – Vertical effective stresses in the representative impoundment at the end of shaking (without inclusions).

Figure 5-20 shows the horizontal effective stresses at the end of shaking. Within the tailings, the horizontal effective stresses were less than 50 kPa, indicating a significant reduction from static levels (Figure 5-7) and moderate reductions in the horizontal effective stress occurred in the dike.

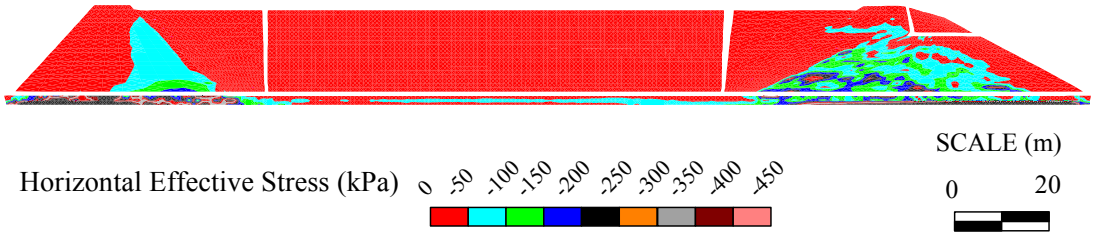

Figure 5-19 – Horizontal effective stresses in the representative impoundment at the end of shaking (without inclusions).

The porewater pressure distribution in the impoundment at the end of shaking is shown on Figure 5-20. The porewater pressure, u, varied from 0 at the surface of the tailings to just over 500 kPa at the bottom of the tailings and was indicative of significant excess porewater pressure development compared to the static pressures (0 to 226 kPa).

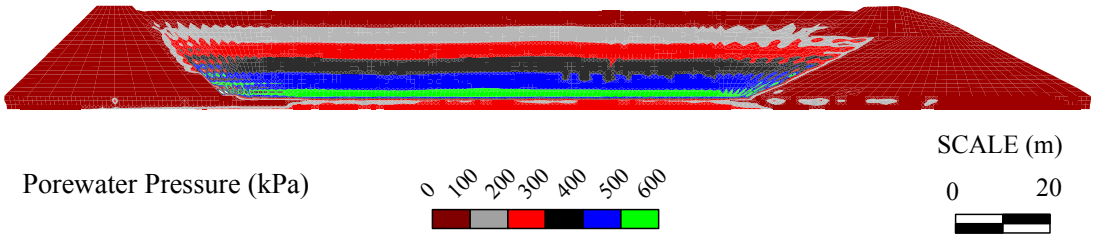

Figure 5-20 – Porewater pressures in the representative impoundment at the end of shaking (without inclusions).

Figure 5-21 shows areas in the impoundment where the vertical effective stress was less than 10 kPa at t = 40 s. Generally, vertical effective stresses in the tailings were less than 10 kPa, except for several zones in the lower portion of the tailings.

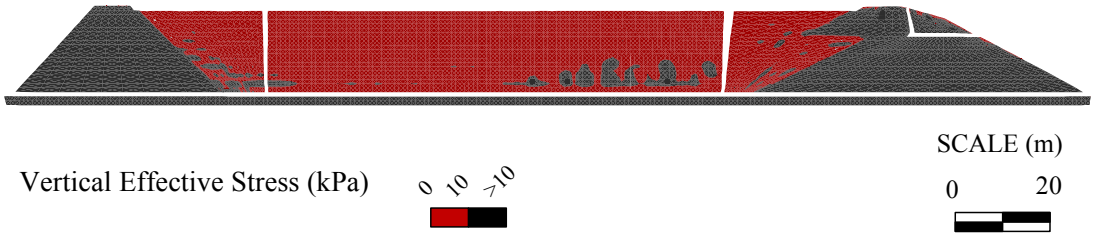

Figure 5-21 – Vertical effective stresses of 10 kPa or less in the representative impoundment at the end of shaking (without inclusions).

The horizontal deformation of the impoundment at the end of shaking is plotted on Figure 5-22. Maximum deformations of about 1.5 m downstream occurred on the downstream slope of the dike, particularly in the upper portion of this slope, and extended at decreasing magnitude to about 70 m into the impoundment.

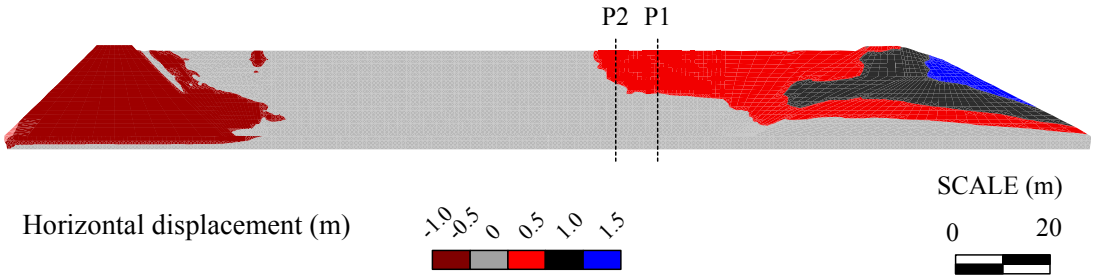

Figure 5-22 – Horizontal deformation of the representative impoundment at the end of shaking (without inclusions).

5.5.3 Analysis of the Representative Impoundment with Inclusions

The dynamic analysis of the representative tailings impoundment with waste rock inclusions is presented in the following sections that present the behavior of the impoundment during shaking and the conditions within the impoundment at the end of shaking. Based on the behavior of the dike during shaking and the fact that the dike is a zoned rockfill structure, post-shaking analysis was deemed to be unnecessary.

5.5.3.1 Site Response

The site response of the impoundment was evaluated using amplification factors and ground motion records extracted from the FLAC analysis.

Based on the amplification factors, F_a, calculated using Equation 3-12 with PGA values extracted from the FLAC analysis (Table 5-3), the ground motion was slightly amplified within the 2-m-thick layer of dense glacial till between bedrock and the tailings (F_a = 1.19). The F_a values of 0.31 and 0.35 indicate that the horizontal accelerations were highly damped on the surface of the tailings at P1 (Figure 5-2) and on the top of the waste rock inclusion at P2 (Figure 5-2). On the crest of the dike, the F_a value of 1.0 indicates that there was no appreciable damping of amplification of the ground motion at this location during shaking.

The horizontal accelerations input to the bottom of bedrock and calculated at the top of bedrock, top of the glacial till, and at 0.275H in the tailings (all at P1) are graphed on Figure 5-23. Amplification of the ground motion was very slight on the top of bedrock and moderately low on the top of the glacial till, corresponding to that observed for the impoundment without inclusions (Figure 5-12). At 0.275H in the tailings, the horizontal accelerations were highly damped, but to a lesser degree than in the impoundment without waste rock inclusions.

Table 5-3 – Calculated amplification factors – representative impoundment (with inclusions).

Location	Peak Horizontal Ground Acceleration, PGA (g)	Amplification Factor (F_a)
Top of bedrock	1.55	-
Top of glacial till	1.84	1.19
Surface of Impoundment at P1	0.48	0.31
Surface of Impoundment at P2	0.55	0.35
Crest of dike	1.55	1.00

Figure 5-24 presents the horizontal accelerations calculated at 0.275H, 0.475H, 0.675H, and 0.875H at location P1 (in the tailings). The ground motion was highly damped at these four levels and the degree of damping was comparable at these levels, except at 0.875H where there were isolated amplitudes as great as 0.7 g at t = 5 s.

Figure 5-25 presents the horizontal accelerations calculated at 0.275H, 0.475H, 0.675H, and 0.875H at location P2 (in the center of a waste rock inclusion, Figure 5-4). The degree of damping of the ground motion varied from slight at 0.275H to high at 0.875H.

The amplitudes of the horizontal acceleration at P1 (in the tailings) were, generally, less than 0.2 g for the first 20 seconds of shaking and less than 0.1 for the remainder of shaking. At P2 (in the inclusion), the amplitudes were generally two to three times greater than at the same heights in P1.

The horizontal accelerations calculated on the crest of the dike during shaking are shown on Figure 5-26. Compared to the horizontal accelerations measured on the top of bedrock (Figure 5-23), the ground motion was slightly damped during the first half of shaking (t = 0 to 20 s) and slightly amplified during the second half of shaking (t = 20 to 40 s).

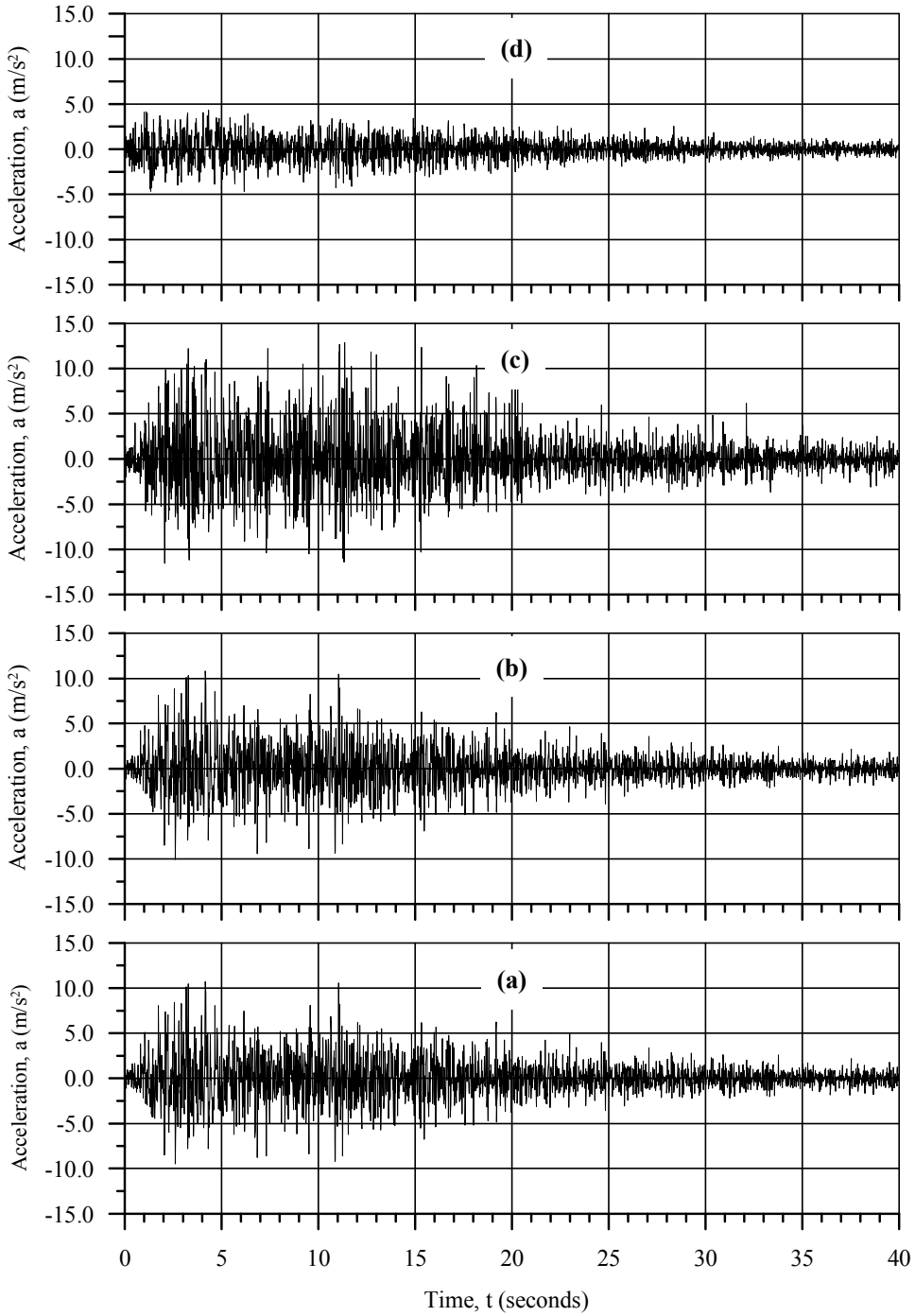

Figure 5-23 – Horizontal accelerations at P1: input to the bottom of bedrock (a), calculated on the top of bedrock (b), on the top of glacial till (c), at 0.275H in the tailings (d) – Representative impoundment (with inclusions).

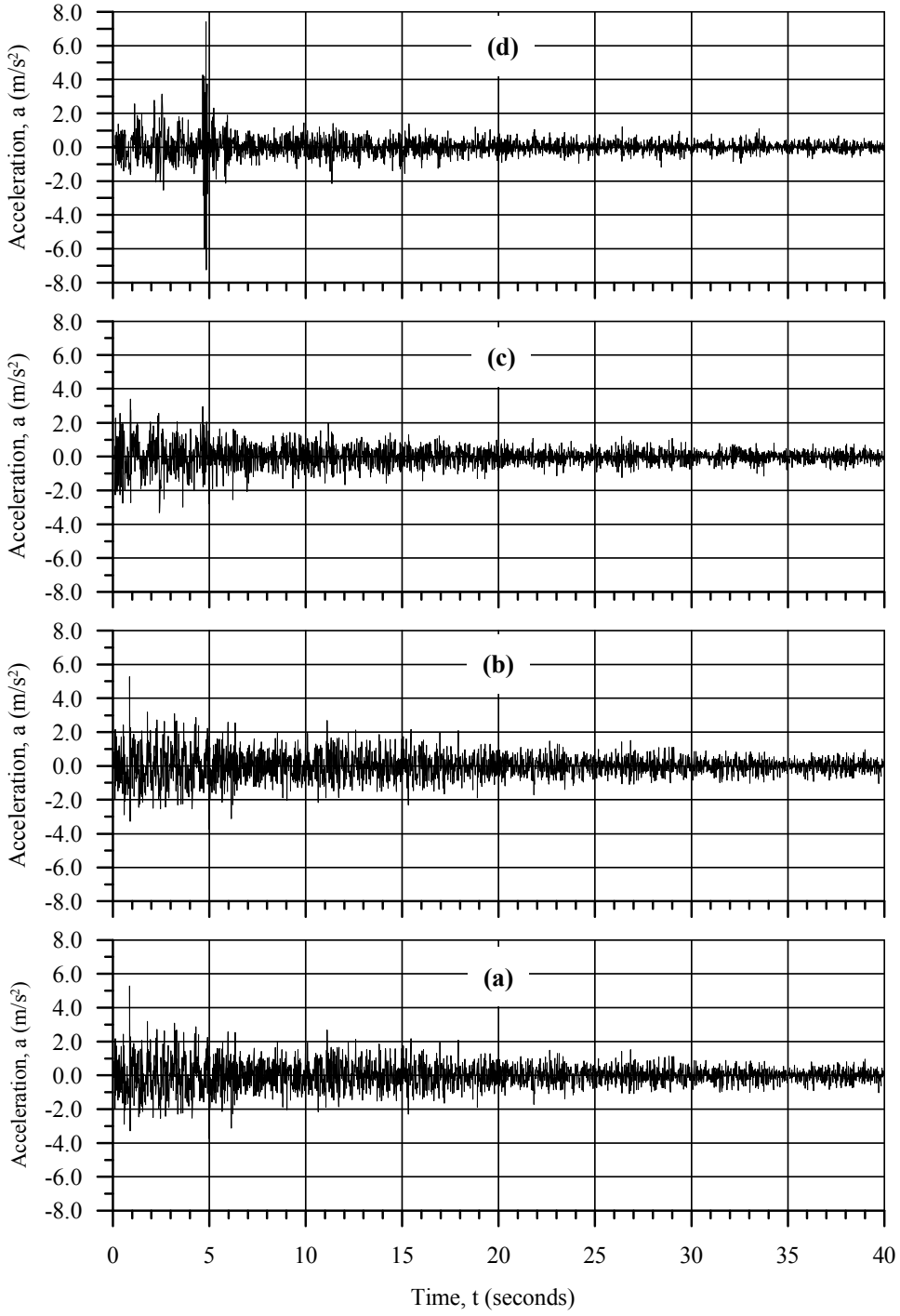

Figure 5-24 – Horizontal accelerations at P1: calculated at 0.275H (a), 0.475H (b), 0.675H (c), and 0.875H (d) – Representative impoundment (with inclusions).

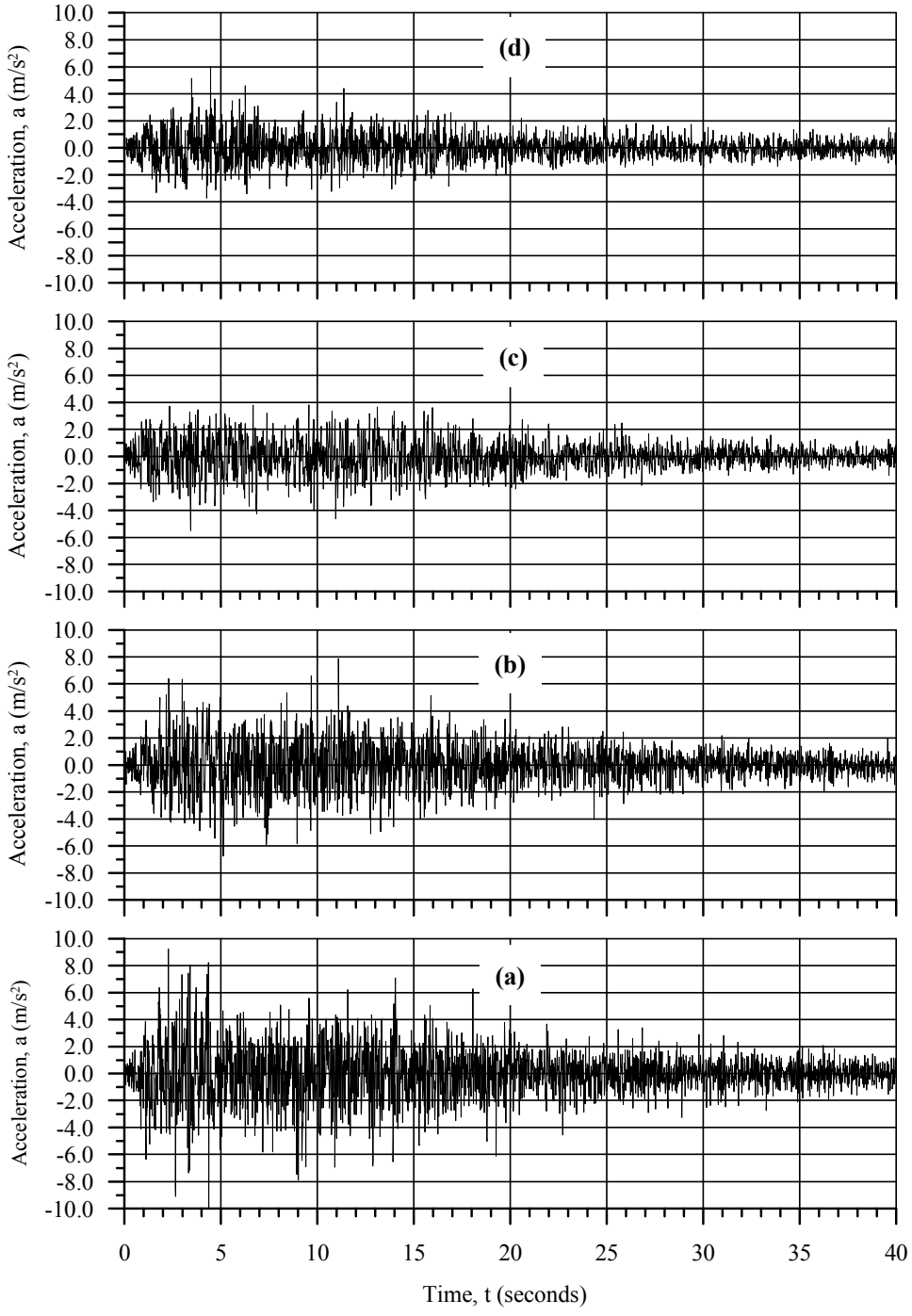

Figure 5-25 – Horizontal accelerations at P2: calculated at 0.275H (a), 0.475H (b), 0.675H (c), and 0.875H (d) – Representative impoundment (with inclusions).

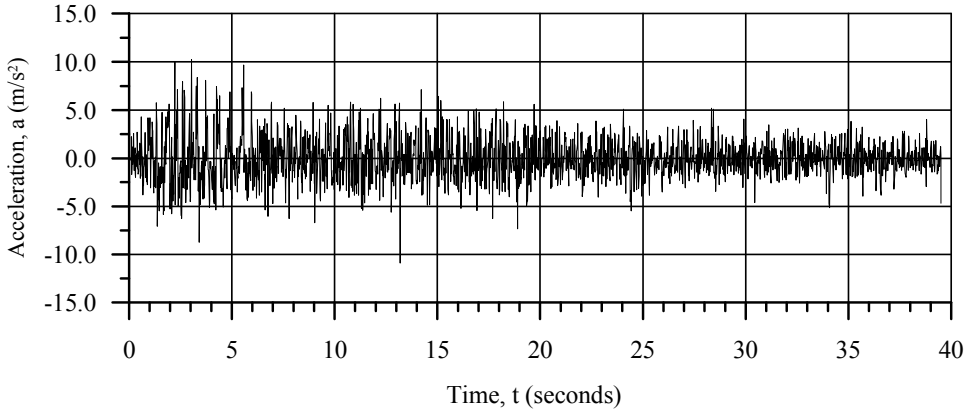

Figure 5-26 – Horizontal accelerations calculated at the crest of the dike - representative impoundment (with inclusions).

5.5.3.2 Cyclic Stress Ratio Development

The cyclic stress ratio in the impoundment was calculated using Equation 4-1, which as previously noted, considers the shear stress from all sources, not just that directly from the applied horizontal accelerations.

Figure 5-27 presents the cyclic stress ratio development in the tailings at P1 (Figure 5-2) during shaking. The initial values of the cyclic stress ratio were approximately 0, indicating that there were no significant shear stresses in the tailings at this location prior to shaking. Significant amplitudes of cyclic stress ratio were developed in the first 2 to 4 seconds. The cyclic stress ratio amplitudes varied from 0.2 at 0.275H to 0.05 at 0.875H. At 0.275H, 0.475H and 0.675H, the cyclic stress ratio values in the tailings after the 5th second of shaking were negligible. At 0.875H, the cyclic stress ratio values varied roughly between -0.025 and 0.025 after the 5th second of shaking.

Figure 5-28 presents the cyclic stress ratio development in the waste rock inclusion at location P2 (Figure 5-4). At the four levels reported (0.275H, 0.475H, 0.675H, and 0.875H), the cyclic stress ratio development was characterized by 5 to 10 second trends

of generally increasing or decreasing cyclic stress ratio with high frequency oscillations from the general trends. The high frequency oscillations varied from 0.1 to 0.25 in magnitude and were generally greater with increasing height, H, and smaller with time, t. The trends in the cyclic stress ratio development were more pronounced in the upper portion of the inclusion (0.875H) than the lower portion (0.275H).

The pattern of cyclic stress ratio development indicates that in addition to the dynamic loading that caused the high frequency oscillations, there were significant shear stresses acting on the inclusion during shaking. These shear stresses are attributed to loading of the impounded tailings on the inclusions due to the strength loss associated with the generation of high excess porewater pressures.

The cyclic stress ratio development at 0.675H was typical and is described further. At the start of shaking, the cyclic stress ratio was approximately 0, indicating that no static shear stresses were present. From the t = 0 s to t = 7 s, the cyclic stress ratio increased to 0.35 while undergoing oscillations as great as ±0.3 about the trend. From t = 7 s to t=14 s, the cyclic stress ratio decreased to -0.15 with oscillations of about ±0.25 from the general trend. From the t = 14 s the cyclic stress ratio value increased to 0.25 at t = 19 s, leveled off to 0.35 at t = 27 s, declined to 0.1 at t = 30 s where it remained until the end of shaking. From t = 14 s to the end of shaking, the amplitude of the oscillations was about 0.1.

The cyclic stress ratios developed in the waste rock inclusion (location P2) were significantly greater that those developed in the adjacent tailings (location P1). In fact, after the first few seconds of shaking, the tailings made no contribution to resisting the shear loading induced directly by the earthquake shaking or by the impounded tailings.

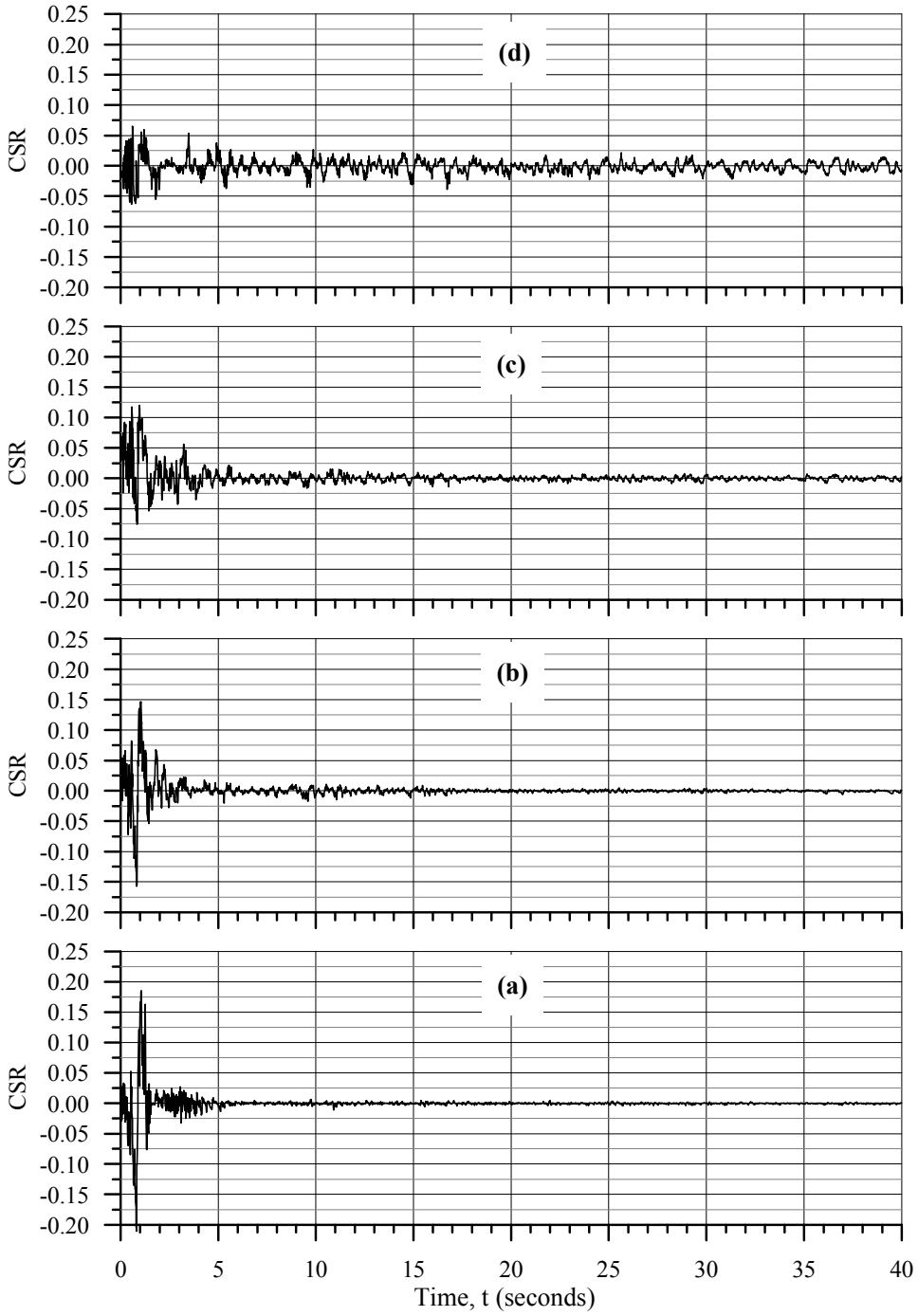

Figure 5-27 – CSR development at P1: calculated at 0.275H (a), 0.475H (b), 0.675H (c), and 0.875H (d) – Representative impoundment (with inclusions).

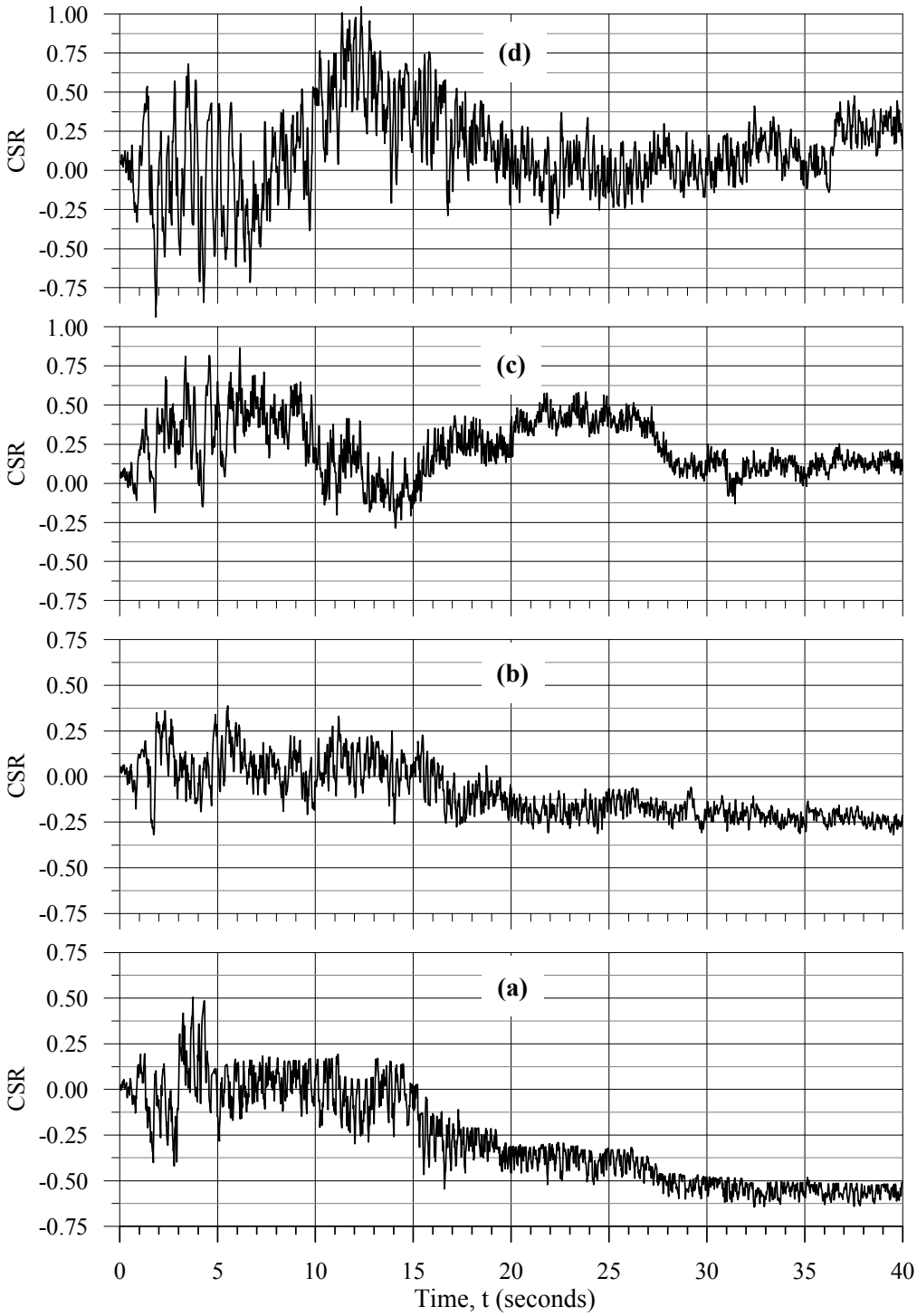

Figure 5-28 – CSR development at P2: calculated at 0.275H (a), 0.475H (b), 0.675H (c), and 0.875H (d) – Representative impoundment (with inclusions).

5.5.3.3 Excess Porewater Pressure Development

Figure 5-29 provides graphs of the r_u values developed at various heights in the tailings at location P1 (Figure 5-2). The r_u values were calculated using Equation 4-2 and include any changes in the vertical effective stresses due to excess porewater pressure generation or other causes. As noted previously, this equation was used because dynamic loading can cause changes in the effective stress not related to excess porewater generation, particularly in soils where the degree of saturation is less than 1.0.

The development of excess porewater pressure in the tailings was very rapid at all levels in the tailings at P1. By the 2nd second of shaking the r_u values varied between 0.8 and 1.0. By the 8th second the r_u values were generally greater than 0.9 and remained at this level until the end of shaking.

The high r_u values coincided with CSR values of less than 0.025 at location P1 (Figure 5-27).

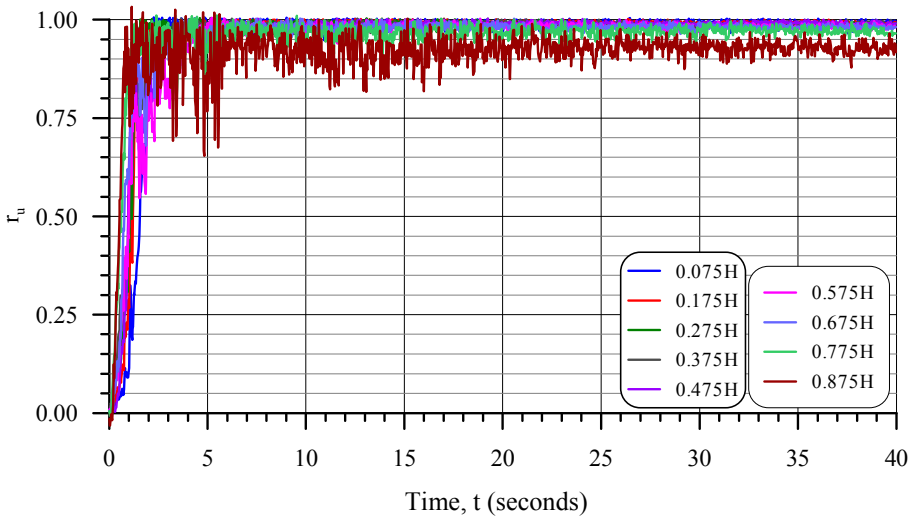

Figure 5-29 – Excess porewater pressure ratio, r_u, development in the tailings at location P1 during shaking in the representative impoundment (with inclusions).

The porewater pressures calculated within FLAC at location P1 (in the tailings) during shaking are plotted on Figure 5-30. The porewater pressure increase was rapid and the maximum levels were reached within a few seconds of the start of shaking. From then until the end of shaking, the porewater pressures were relatively constant, except for very small magnitude variations attributed to volumetric strains during the ongoing dynamic loading.

The porewater pressure development confirms the excess porewater pressure development shown on Figure 5-29.

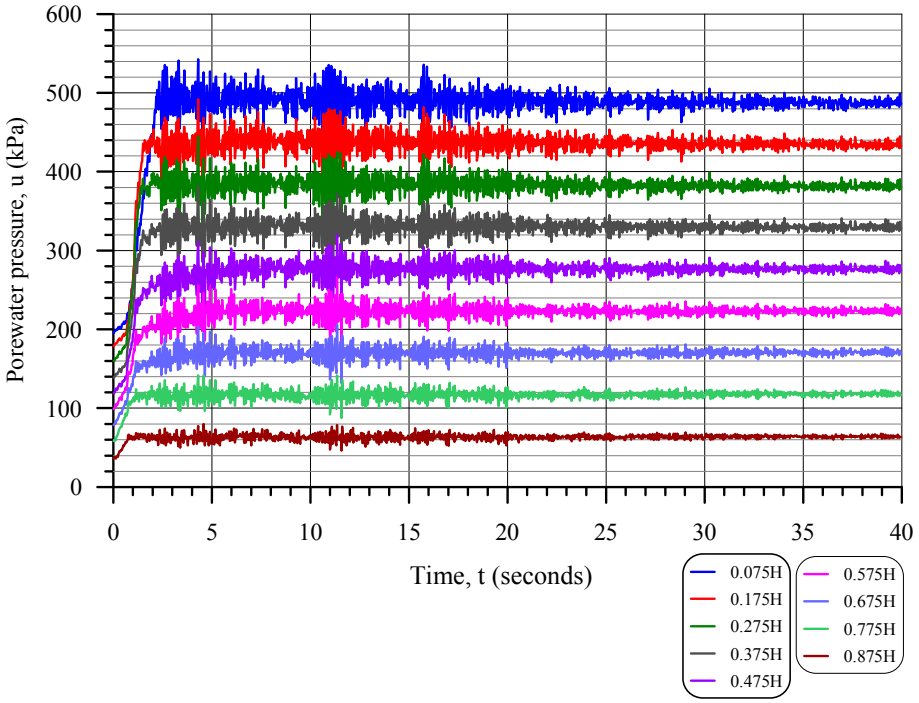

Figure 5-30 – Porewater pressure, u, development in the tailings at location P1 during shaking in the representative impoundment (with inclusions).

Figure 5-31 shows the development of the r_u values at various depths at location P2 (in a waste rock inclusion). The figure indicates that there was a general increase in the r_u values in the first 1 to 2 seconds of shaking which was followed by a general decrease for the rest of shaking. By the end of shaking, the r_u values in the waste rock inclusion varied from -1.9 to 0.25 with negative r_u values for 8 of the 9 heights presented.

The porewater pressures calculated in the waste rock inclusion at P2 during the dynamic analysis are shown on Figure 5-32. They show some initial small increases in the porewater pressure at the onset of shaking that are followed by generally decreasing porewater pressure for the remainder of shaking. The maximum porewater pressure at the height evaluated was reduced from over 180 kPa at the start of shaking to less 50 kPa at the end of shaking.

The decreases in the porewater pressure in the waste rock inclusion are consistent with monotonic shear loading of dilative materials. As discussed in Appendix A, dilative soils tend to generate porewater pressure decreases in response to monotonic shear loads. This further supports the finding that the waste rock inclusion was under shear loading from the impoundment and not solely from shear stresses imparted by the earthquake ground motion as it rose through the impoundment.

From equation 4-1, it is observed that negative r_u values can occur if the vertical effective stress increases or the porewater pressure decreases as a result of the loading under consideration. However, given the effective unit weight of the waste rock and the unit weight of water, 11.28 kN/m^3 and 9.81 kN/m^3, respectively, a decline in the porewater pressure alone could result in a minimum r_u value of about -0.9 and does not explain the values near -2.0 that were obtained. That leads to the conclusion that the effective vertical stress within some zones the waste rock inclusion increased during shaking, irrespective of the changes in the porewater pressure.

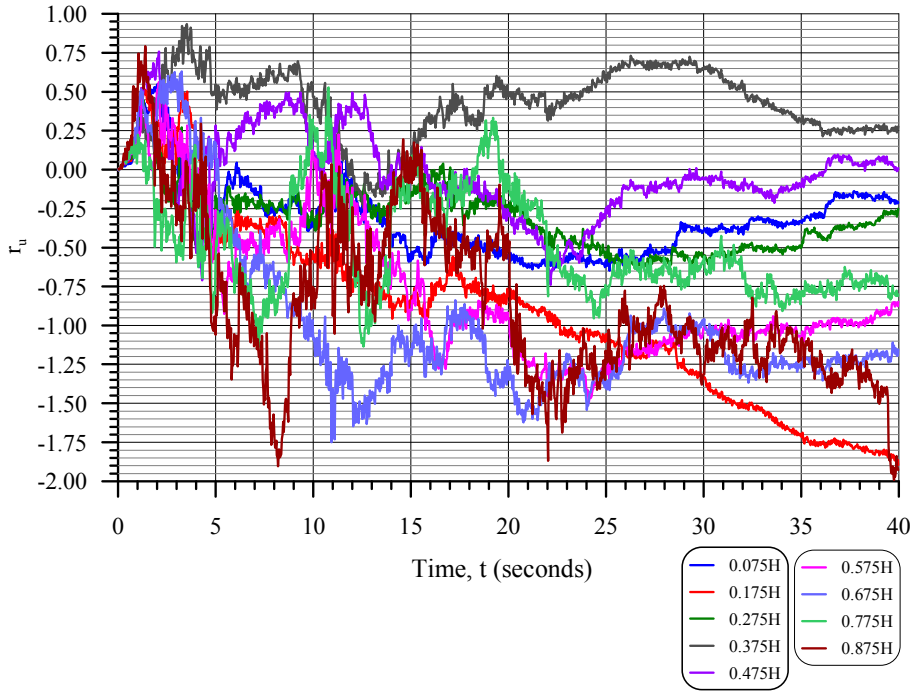

Figure 5-31 – Excess porewater pressure ratio, r_u, development in the inclusion at location P2 during shaking in the representative impoundment (with inclusions).

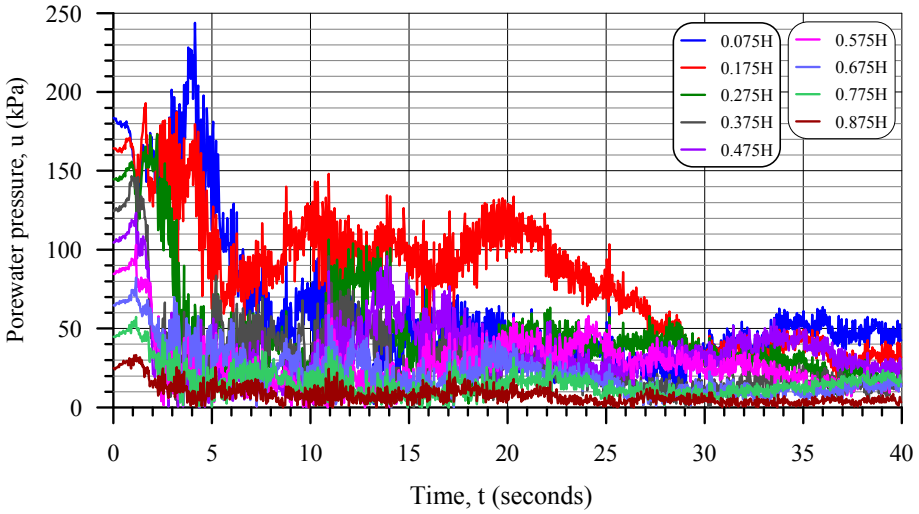

Figure 5-32 – Porewater pressure, u, development in the inclusion at location P2 during shaking in the representative impoundment (with inclusions).

5.5.3.4 Displacement of the Crest of the Dike

The displacement of the crest of the dike (see Figure 5-2 for the specific location) during shaking is shown on Figure 5-33. Horizontally, the crest moved 0.62 m downstream during shaking and displacement during the last 5 seconds of shaking was about 0.1 m upstream. Vertically, the crest moved 0.25 m downwards during shaking.

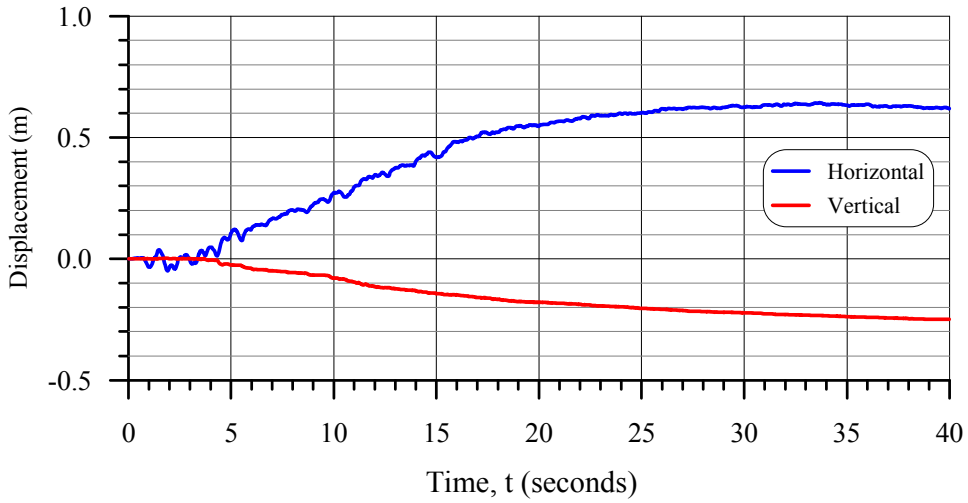

Figure 5-33 – Displacement of the crest of the dike during shaking – representative impoundment (with inclusions).

5.5.3.5 Conditions at the End of Shaking

Contours of the vertical effective stresses within the impoundment are presented on Figure 5-34. Compared to the stressed prior to shaking (Figure 5-6) the following is noted:

a) The vertical effective stresses in the tailings were reduced to less than 100 kPa. They were as much as 350 kPa prior to shaking;
b) The vertical effective stresses in the waste rock inclusions were lower in the upper areas of the inclusions and higher in the lower area of the inclusions.

There were small zones of stresses in the range of 400 to 500 kPa within the lower areas of the inclusions.

c) The stress transfer that was evident prior to shaking was no longer evident after shaking; and

d) There was zone of high stress (as much as 500 kPa) within the dike.

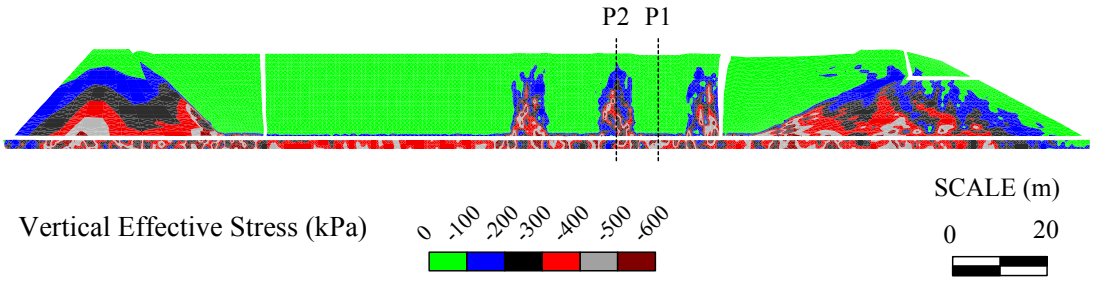

Figure 5-34 – Vertical effective stresses in the representative impoundment at the end of shaking (with inclusions).

The porewater pressure distribution in the impoundment at the end of shaking is shown on Figure 5-35. Within the tailings, the porewater pressure varied from 0 near the surface to about 600 kPa at the bottom of the tailings, a substantial increase from the values prior to shaking (0 to 200 kPa). Within the waste rock inclusions, the porewater pressure was less than 100 kPa, a substantial reduction from the values prior to shaking. The non-uniformity in the porewater pressures at the end of shaking, specifically the vertical features in the tailings between and adjacent to the inclusions, are attributed to the dynamic interaction of the inclusions and tailings.

Figure 5-36 shows areas in the impoundment where the vertical effective stress was less than 10 kPa at the end of shaking. Generally, vertical effective stresses in the tailings were less than 10 kPa, except for some small zones between the inclusions and the dike.

The horizontal deformation of the impoundment at the end of shaking is presented on Figure 5-37. Maximum displacements of about 1 m occurred on the downstream face of the dike and were oriented downstream. The displacements extended out 50 m into the impoundment with decreasing magnitude.

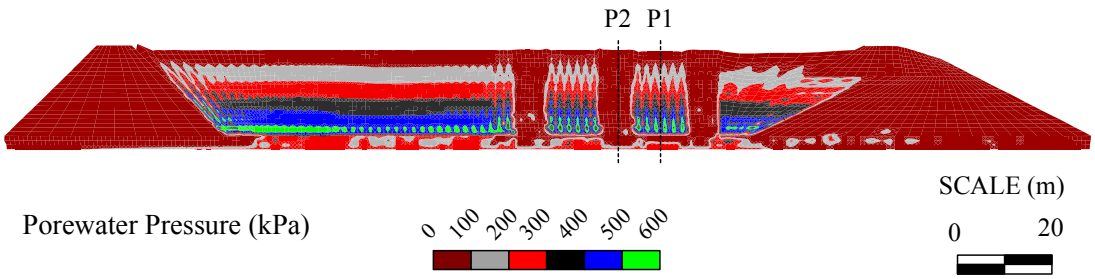

Figure 5-35 – Porewater pressures in the representative impoundment at the end of shaking (with inclusions).

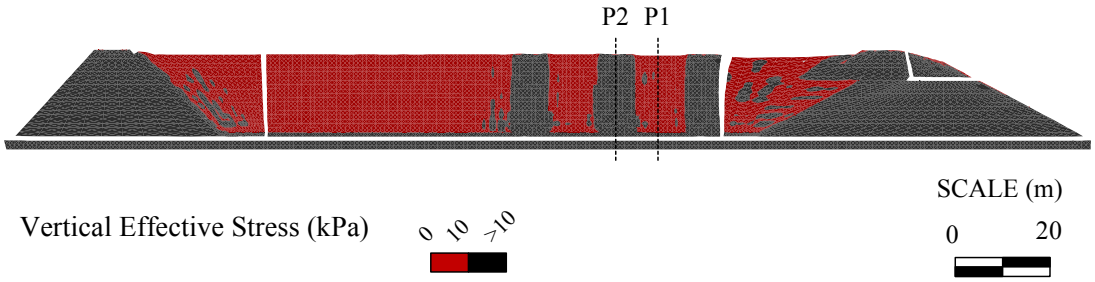

Figure 5-36 – Vertical effective stresses of 10 kPa or less in the representative impoundment (with inclusions) at the end of shaking.

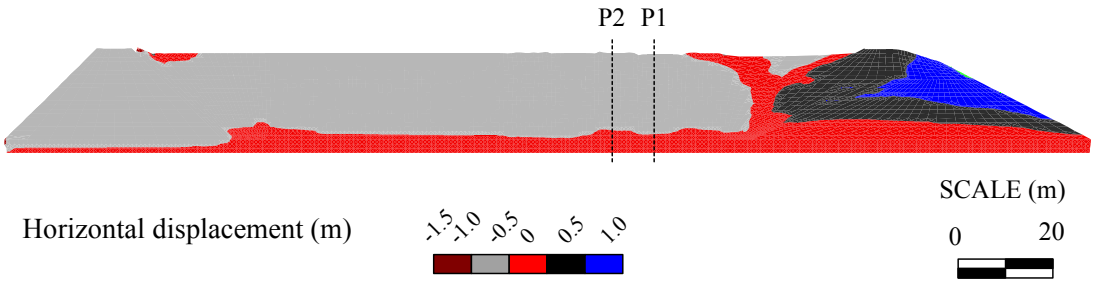

Figure 5-37 – Horizontal deformation of the representative impoundment (with inclusions) at the end of shaking.

5.5.4 Comparison of the Dynamic Responses

Except for the presence of the waste rock inclusions and the 1-m-thick layer of waste rock on the bottom and sides of the impoundment, the geometry, material properties, boundary conditions, and applied loads of the analyses of the impoundment were identical. Therefore, any significant differences in their dynamic behavior may be attribute to the present of the waste rock inclusions (and the waste rock layer on the bottom and sides of the impoundment). The differences in the dynamic responses of the representative impoundment, with and without waste rock inclusions, are summarized as follows.

a) The presence of the waste rock inclusions caused a stiffer response that resulted in less damping within the tailings in the vicinity of the waste rock. Amplification factors on the surface of impoundment at P1 and P2 were 0.05 and 0.06, respectively, without inclusions and 0.31 and 0.35 with inclusions.

b) Based on the cyclic stress ratio development, the tailings in the impoundment without inclusions were unable to resist shear loading resulting from earthquake shaking and lateral deformation of the impoundment was resisted by the dike. However, in the impoundment with inclusions, although the tailings were unable to resist shear loading, the inclusions developed considerable shear stresses, indicating that they and the dike were resisting

lateral deformation of the impoundment. This finding is supported by the fact that the horizontal deformation of the crest of the dike was reduced due to the presence of the inclusions.

c) The excess porewater pressure development in the tailings at P1 was similar for the impoundment with and without waste rock inclusions. However, porewater pressures in the waste rock inclusions were reduced significantly by the dynamic loading.

d) The downstream horizontal displacement of the crest of the dike was reduced from 0.95 m to 0.61 m and the downwards vertical displacement of the crest was reduced from 0.30 to 0.25 m by the presence of the inclusions. The reduction in the horizontal displacement is attributed to the contribution made by the inclusions to retaining the tailings during the earthquake loading.

e) The outwards horizontal deformation of the downstream crest was reduced by about 0.5 m and the extent of the deformation into the impoundment was reduced by about 20 m due to the waste rock inclusions.

5.6 COMPARISON OF THE DYNAMIC RESPONSE OF THE TAILINGS WITH THE LEVEL GROUND ANALYSES

Section 4.4 presents level ground liquefaction evaluation of the tailings based on numerical analyses. The analysis for unconsolidated tailings subjected the Earthquake E5 loading in that section was compared with the analysis presented in this chapter for the representative impoundment without waste rock inclusions, specifically the dynamic response of the tailings at location P1 and P2. The material properties using the level ground liquefaction analyses and the analyses in that chapter were identical.

The following observations were drawn from the comparison:

a) The amplification factor on the surface of the tailings in the level ground analysis was 0.229 (Section 4.4.5.1) which is significantly higher than the factors of 0.05 and 0.06 obtained from the analysis of the representative impoundment (Section 5.5.2.1). This difference was evident in the graphs of

the horizontal accelerations from the analyses (refer to Sections 4.4.5.3 and 5.5.2.1).

b) In the level ground liquefaction analysis, the cyclic stress ratios at 0.275H, 0.475H and 0.775H in the tailings were characterized by maximum amplitudes of about 0.18 and significant cycles for the first 2 seconds of shaking (Section 4.4.5.6). In the analysis of the representative impoundment, the CSR in the tailings was significant during the first 2 seconds of shaking, and the maximum amplitudes varied from 0.25 at 0.275H to 0.1 at 0.875H (Section 5.5.2.1).

c) The excess porewater pressure development in the two analyses were similar (refer to Sections 4.4.5.13 and 5.5.2.3). However, the rate of excess porewater pressure development in the upper portion of the tailings was lower for the analysis of the impoundment versus the level ground analysis.

d) Both analyses indicated excess porewater pressure ratios exceeding 0.9 through the depth of the tailings well before the end of shaking.

The differences between the two analyses are appreciable, but not significant, and are directly related to the site response, which was stiffer for the level ground analysis relative to the analysis of the impoundment. The difference in the site responses are attributed to the presence of the rockfill dike forming the representative analysis, which was the only variable between the analyses.

5.7 COMPARISON OF THE DYNAMIC RESPONSE OF THE REPRESENTATIVE IMPOUNDMENT WITH THE ANALYTICAL STABILITY EVALUATION

In Section 3.10, an analytical evaluation of the seismic stability of the representative impoundment with respect to Earthquake E5 (M_w=7.5) using the pseudo-static method was presented. The analysis assumed that the tailings would be liquefied by the earthquake loading well before the end of shaking. Accordingly, a liquefied strength was assigned to the tailings. The resulting factor of safety was 0.88 and indicated the potential for failure of the impoundment. The potential failure surface was a roughly horizontal

line that passed through the dike just below the raises and extended about 80 m into the impoundment.

The pattern of horizontal deformation at the end of the dynamic analysis of the representative impoundment (Figure 5-22) indicated a potential failure surface that extended from the lower part of downstream slope of the dike to the surface of the impoundment about 80 m upstream.

Itasca (2005) recommends using the velocities of a model to determine the location and extent of potential failure surfaces. Figure 5-38 is a plot of the horizontal velocities in the impoundment at the end of shaking that was extracted from the FLAC analysis. The pattern of the horizontal velocities is suggestive of additional deformation of the upper portion of the dike.

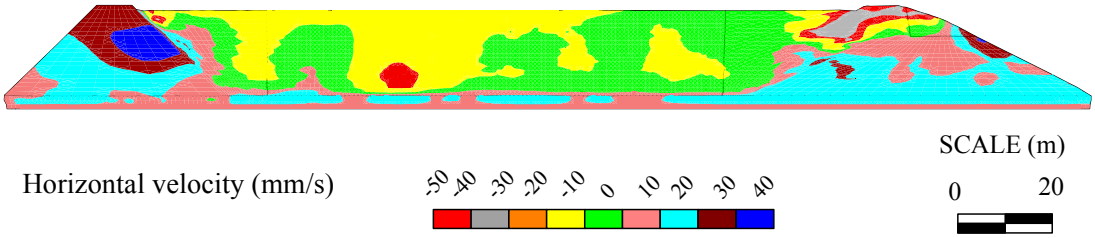

Figure 5-38 – Horizontal velocities in the representative impoundment (without inclusions) at the end of shaking.

5.8 REMARKS ON THE NUMERICAL ANALYSES OF THE REPRESENTATIVE IMPOUNDMENT

The following remarks are offered with respect to the numerical analysis of the representative impoundment:

a) The use of waste rock inclusions in the representative tailings impoundment resulted in an improvement in the seismic behavior as evidenced by a reduction in the deformation of the dike.

b) The waste rock inclusions led to a stiffer dynamic response within the impoundment. However, there was no significant effect on the excess porewater pressure generation during shaking.

c) Comparing the numerical analysis of the representative impoundment with the level ground liquefaction analysis revealed appreciable differences in the site response as well as the associated cyclic shear stress and excess porewater pressure development. These differences were attributed to the presence of the rockfill dike, specifically, the effect of topography with respect to ridges on earthquake ground motions as noted by Kramer (1996) and Sigaran-Loria & Hack (2006).

d) The analytical seismic stability evaluation of the impoundment presented in Chapter 3 indicated possible failure of the impoundment based on a pseudo-static factor of safety of 0.88. None of the results from the numerical analysis presented in Chapter 5 are indicative of failure. However, the potential failure surface identified in the pseudo-static analysis is somewhat similar to the pattern of deformations from the dynamic analysis at the end of shaking that indicated downstream displacement of the upper raises of the dike.

The tailings in the representative impoundment, with and without waste rock inclusions, were assumed to be unconsolidated. However, the presence of waste rock inclusions (and relatively thin layers of waste rock on the bottom and sides of an impoundment) would probably acceleration consolidation resulting in an increased degree of consolidation and, possibly, improved seismic behavior (less deformation and increased stability). Additional consolidation of the tailings due to the waste rock inclusions was not assumed in this research because the focus was on the primary effect of the inclusions during seismic loading and quantification of the degree of consolidation due to the use of waste rock inclusions in an active tailings impoundment was beyond the scope of this research.

CHAPTER 6. EVALUATION OF THE USE OF WASTE ROCK INCLUSIONS

6.1 INTRODUCTION

6.1.1 Objectives and Scope

The primary objectives of this chapter are to:

a) Analyze and evaluate the behavior of a conceptual tailings impoundment, with and without waste rock inclusions, subject to various earthquake loadings; and
b) Determine the effects of waste rock inclusions on the dynamic behavior of impoundments, particularly the ability of the inclusions to control the effects of liquefaction.

The dynamic behaviors of the impoundments were analyzed using numerical analysis and evaluated based on the dynamic site response, excess porewater pressure development, and the pattern and magnitude of deformations.

As noted in Chapter 2, upstream-raised tailings impoundments tend to be more susceptible to seismically-induced failure than centerline or downstream-raised impoundments. Accordingly, an upstream-raised impoundment was used in the analysis.

Parametric analyses and evaluations of the conceptual tailings impoundments with and without waste rock inclusions are presented in Chapter 7.

6.1.2 Method of Analysis

The methods of analysis were similar to those described in Chapter 5 for the evaluation of the example impoundment. In summary, the dynamic behavior of a conceptual impoundment subject to various earthquake loadings was simulated using the FLAC finite difference software program.

The numerical analyses were conducted in three phases: a) a static analysis; b) a dynamic analysis; and, when applicable, c) a post-shaking analysis. Post-shaking analysis was not conducted when failure occurred during the dynamic analysis.

Static analyses were conducted to develop the states of stress and strain and porewater pressures within the models under a condition of steady state mechanical and fluid equilibrium. In the dynamic analyses an earthquake ground motion was applied to the models to simulate occurrence of earthquake loadings of known intensity. In the post-shaking analysis, the model was returned to a condition of steady state mechanical and fluid equilibrium, if possible.

Post-shaking analyses were used to simulate the mode of failure observed by Ishihara (1984) for Dike No. 2 at the Mochikoshi gold mine in Japan, where seismically-induced failure occurred hours after the end of shaking and was attributed to the slow dissipation of excess porewater pressures generated during an earthquake (refer to Section 2.4.1.2). Post-shaking analysis of dams is recommended in the Dam Safety Guidelines of the Canadian Dam Association (2007).

In the dynamic and post-shaking phases of the modeling, FLAC was set to solve for mechanical, fluid and dynamic equilibrium simultaneously. This requires the generation of two time steps, one for fluid flow and another for dynamic behavior. Both of these time steps were calculated automatically by the software based on the material properties and damping parameters of the model. The actually time step used by FLAC was the smaller of the two and controlled the progress of the simulation.

In the dynamic phases of the modeling, the time step used by FLAC was the dynamic time step which averaged 4×10^{-5} seconds. Solution time for the dynamic phases varied from 3.5 to 5.5 hours for simulated earthquakes with durations of 25 to 40 seconds on a computer with an Intel® Pentium® Dual E2200 central processing unit (CPU) with a rated speed of 2.2 GHz.

It was determined from preliminary modeling that at least 4 hours of simulated time would be required for substantial dissipation of the excess porewater pressures generated during the dynamic phase and that the associated computational time for the post-shaking phases would have been about 2,000 hours (83 days). The value of the bulk modulus of

water used in FLAC modeling has a significant effect on the calculated time steps. Itasca (2005), Byrne et al. (2003) and Castillo et al. (2006) recommend reducing the value of the bulk modulus of water to decrease the fluid and dynamic time steps and they indicate that this does not have a significant effect on the modeling as long as there is a significant difference between the bulk modulus of water and that of the soil. Therefore a value of $2.2x10^5$ kPa was using for the bulk modulus of water in the post-shaking phases of the analyses to decrease the dynamic time step, that controlled the simulation time step, to about $1x10^{-4}$ seconds. Parametric analysis indicated that the reduction in the bulk modulus of water had no appreciable effect on the results of the modeling. The actual (correct) value of the bulk modulus of water, $2.2x10^6$ kPa (Itasca, 2005), was used in the static and dynamic phases of the analyses.

The reduction in the bulk modulus of water during the post-shaking phase reduced the estimated computational time from 2,000 hours to 800 hours (33 days) per simulation. A further reduction in the computational time of the post-shaking phase was accomplished by increasing the hydraulic conductivities of all of the materials in the model by two orders of magnitude. By this means, the simulated time for substantial dissipation of the excess porewater pressures generated during the dynamic phase was reduced from 4 hours to about 3 minutes, and combining this with the reduction in the bulk modulus of water reduced the computational time for the post-shaking phase to about 10 hours. Parametric analysis indicated that increasing the hydraulic conductivity to reduce the time step had no significant effect on the behavior of the models during the post-shaking phase, except to increase the rate of dissipation of excess porewater pressure generating during shaking.

An alternative method that was considered, but rejected, for modeling of the post-shaking phase consisted of re-establishing the boundary conditions used for the corresponding static phase and solving for the static, steady state mechanical and fluid equilibrium of the model with no dynamic computations. This method resulted in slightly less

deformation of the model, probably due to the absence of dynamic effects, and is considered to be somewhat unconservative.

The values of over 100 parameters were recorded during the dynamic and post-shaking phases of the numerical analyses. The recorded parameters included horizontal accelerations, vertical effective stresses, porewater pressures, cyclic stress ratios, excess porewater pressure ratios, and horizontal and vertical displacements. Most of the recorded parameters were automatically generated by FLAC (i.e. horizontal accelerations, vertical effective stresses, and displacements), while others were user-defined variables calculated using FLAC's FISH language subroutines (i.e. cyclic stress ratios, excess porewater pressure ratios). The parameters were recorded at critical locations on the model and profiles of specific parameters through the depth of the tailings were recorded along vertical lines at three locations: 10 m, 84 m and 110 m upstream of the crest of the dike. These locations were annotated as P1, P2 and P3, respectively. The recorded parameters were stored in text files to produce graphs to illustrate the behavior of the models. These graphs are presented later in the Chapter.

The models were saved (stored as data files) after each of the three phases of analyses so that "snapshots" of the distribution of a particular parameter, the vertical effective stress for example, could be extracted and used as figures in this report.

6.1.3 Notes on the Numerical Modeling

6.1.3.1 The Modeling Process

As noted by Barbour & Krahn (2004), geotechnical numerical modeling is the mathematical simulation of very complex, interactive mechanical, fluid and dynamic processes. Applying Barbour & Krahn (2004) to this research, the following four steps were undertaken:

- Step 1 - The definition of the purpose of the model and the development of a conceptual model that fulfils that purpose;

- Step 2 - Selecting appropriate theoretical models of the important processes (mechanical, fluid, and dynamic in this case);
- Step 3 - Development and verification of the numerical model; and
- Step 4 - Calibration, interpretation and validation of the numerical model using analytical results as well as empirical data.

The purpose of the conceptual model was to determine the effectiveness of waste rock inclusions at controlling the effects of liquefaction on the stability of tailings impoundments. Therefore, the conceptual model that was developed was susceptible to excessive deformation and potential failure as a result of liquefaction of the retained tailings.

The theoretical models applied, specifically UBC Sand (static and dynamic behavior of cohesionless media), Mohr-Coulomb (elasto-plastic behavior of soil and rock), Darcy's law (fluid flow), Biot's theory (fluid mechanical interaction), and hysteric damping (shear modulus reduction and dynamic damping), simulated all of the important processes required to simulate the performance of the conceptual model under static, dynamic and post-shaking conditions.

The development, calibration, interpretation, and validation of the model are described in Chapters 3, 4 and 5.

6.1.3.2 Limitations of the Modeling

There were a number of limitations inherent to the numerical modeling that should be noted, including:

a) Although FLAC was run with the "large strain" option, excessive deformation of individual elements occasionally resulted in fatal errors that terminated execution. In these cases the performance of the impoundment was evaluated using the magnitude and pattern of deformation and the velocity of movement at the end of execution;

b) FLAC was not capable of modeling the separation of elements, such as would occur during the development of a catastrophic failure of an impoundment; and

c) The development of tension cracks, fissures, water inter-lenses (thin seams of water between soil layers of different hydraulic conductivity) and sand boils could not be modeled. The occurrence of these features would probably have increased the deformation of the models.

6.1.3.3 Generation of the Mesh

A critical element in numerical modeling is the generation of the mesh, particularly the size and shape of the individual elements. Itasca (2005) recommends using square elements wherever possible for greater accuracy, smaller elements where more detail is required and larger elements where less detail is required. The number of elements used in a model has a direct correlation with the time required for simulation. In dynamic analysis, the size and stiffness of the elements determines the dynamic time step and thus the time required for simulation.

Through a process of trial and error, it was found that by creating the models on a 255 by 35 element grid (8,925 elements) with typical dimensions of 1 m by 1 m, the following was achieved:

d) The computational time per simulation varied from 4 hours for a 25-second dynamic analysis to 10 hours for a 160-second post-shaking analysis, and was considered to be reasonable;

e) A relatively gradual distribution of calculated results and parameters (void ratios, stresses, accelerations, strains, etc.) in the depth of the impoundment; and

f) The geometry of the conceptual impoundment was duplicated quite accurately.

Using a typical element size of 0.75 m by 0.75 m or 0.5 m by 0.5 m would have approximately doubled and quadrupled the computational time per simulation, respectively, while increasing the accuracy somewhat. Using a typical elements size greater than 1 m by 1 would have reduced computational time, but would have decreased the resolution (accuracy) of the modeling.

The element size selected (1 m by 1 m) was a compromise between computational time and accuracy considerations and provided a degree of accuracy sufficient for the needs of this research, which was to make comparative assessments of the responses of tailings impoundments with various configurations of waste rock inclusions and loading conditions.

6.2 EARTHQUAKE LOADINGS

The earthquakes loadings used in the dynamic phase of the analyses are described in Section 3.8.3 and Appendix E. Briefly, one-dimensional earthquake ground motions with the equivalent Arias intensities of earthquakes of moment magnitudes 6.5, 6.75, 7.0, 7.25, and 7.5 with fault-rupture to site distances of 30 km were developed from the ground motion recorded at site S16T during the 1988 Saguenay (Quebec) earthquake and factored to account for the effects of two-dimensional shaking. The parameters of the simulated ground motions are presented in Table 3-15 and reproduced in Table 6-1 for convenience. In this thesis, the simulated ground motions are referred to as Earthquakes E1 through E5.

Table 6-1 – Parameters of simulated earthquake ground motions.

Ground Motion	Moment Magnitude, M_w	PGA (on hard rock), (g)	Arias Intensity (one dimensional shaking), I_x (m/s)	Duration of Shaking (seconds)
E1	6.5	0.229	0.309	25.0
E2	6.75	0.408	0.550	25.0
E3	7	0.659	0.977	27.5
E4	7.25	0.859	1.738	37.5
E5	7.5	1.432	3.091	40.0

6.3 CONCEPTUAL TAILINGS IMPOUNDMENT

A conceptual upstream-raised tailings impoundment was used in the analysis and evaluation. The relevant dimensions of the impoundment were based on typical ranges of dimensions reported in Mittal and Morgenstern (1977), US EPA (1994), ICOLD (2001), and Aubertin et al. (2002a). The material properties applied to the model were from the in situ and laboratory testing conducted for this research as well as published sources; these were in the general ranges reported for similar materials. Due to the wide range of variability in these characteristics among tailings impoundments, the behavior of the conceptual impoundment cannot be considered representative of any specific tailings impoundment.

The impoundment was assumed to be active or recently closed, thus the impounded tailings were assumed to be under-consolidated with respect to existing conditions. The degree of consolidation was assumed to be the same as that estimated for the representative impoundment (Laronde Mine) based on the results of cone penetration testing (refer to Section 3.7.3).

6.3.1 Geometry of the Conceptual Impoundment

The conceptual tailings impoundment was assumed to be an upstream-raised structure consisting of a 4-m-high starter dam, three 4-m-high raises and one 5-m-high raise, resulting in a total height of 21 m. The starter dam was assumed to be constructed of compacted glacial till and the raises were assumed to be constructed of cycloned tailings. A crest width of 8 m was assumed for the starter dike and first 3 raises and a crest width of 6 m was assumed for the final raise. Downstream and upstream slopes of 2:1 (H:V) were assumed for the starter dike and raises. It was assumed that tailings were placed in the impoundment up to one meter below the level of the crest (1 m of freeboard) and the surface of the tailings was assumed to be level. The geometry of the conceptual impoundment is presented on Figure 6-1.

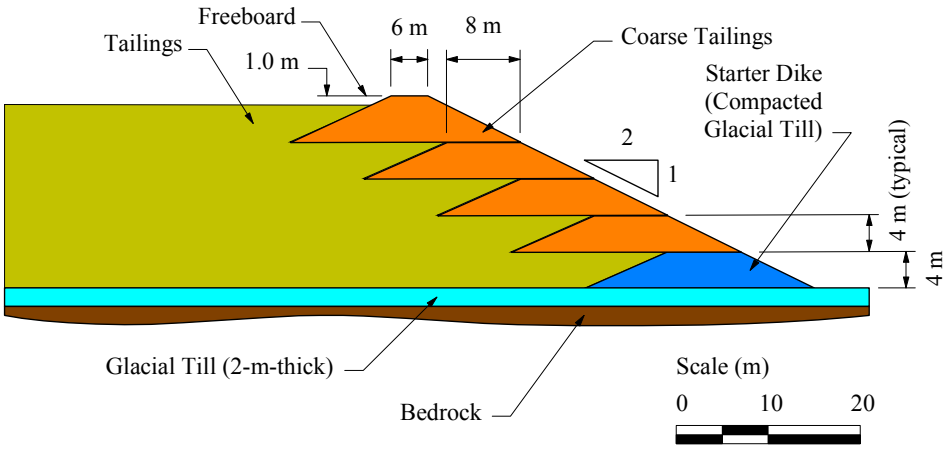

Figure 6-1 – Assumed configuration of the conceptual impoundment.

6.3.2 Subsurface Conditions

Subsurface conditions (below the impoundment) were assumed to consist of a 2-m-thick layer of dense glacial till underlain by hard, moderately fractured bedrock.

6.3.3 Groundwater Conditions

The pond level within the impoundment was assumed to be at the surface of the tailings and the beach width, the distance from the pond to the upstream side of the dike, was assumed to be 100 m. The hydrostatic pressures and seepage conditions resulting from the presence of the pond were calculated by FLAC during the static analyses during which the mechanical and fluid equilibrium of the system was established.

6.3.4 Material Properties

The assumptions and derivations of the properties for all of the materials, excluding the coarse tailings forming the dikes, are described in detail in Section 5.3.1. In summary:

- The impounded tailings were assumed to be under-consolidated with respect to existing loads and their properties were derived from the in situ and laboratory testing conduced for this research project;
- Bedrock was assumed to consist of hard, moderately fractured andesite and its properties were based on published values for similar rock;
- The glacial till overburden was assumed to be very dense and typical values from published sources were assumed;
- The glacial till used to construct the starter dam was assumed to be a well-compacted and typical values from published sources were used; and
- The properties used to characterize the waste rock (inclusions) were based on published sources for rockfill.

The material properties of the bedrock, glacial till, compacted glacial till, and waste rock (inclusions) are summarized in Table 6-2. These materials were all modeled using the elasto-plastic Mohr-Coulomb model as implemented in FLAC. The failure envelope of this model is a shear yield function with a tension cutoff. The tension cutoff is assumed to equal the cohesion divided by the tangent of the internal friction angle. The shear flow rule is non-associated and the flow rule is associated (Itasca, 2005).

Table 6-2 – Assumed material properties of bedrock, glacial till, rockfill, and waste rock inclusions.

Material Property	Bedrock	Glacial Till	Compacted Glacial Till	Waste Rock Inclusions
Constitutive Model (Yield Criteria)	Mohr-Coulomb	Mohr-Coulomb	Mohr-Coulomb	Mohr-Coulomb
Dry Density, ρ_{DRY} (kg/m^3)	2,200	2,000	2,000	2,000
Friction angle, ϕ'	25º	36º	32º	46º
Cohesion, c (kPa)	50,000	250	200	0
Dilation angle, ϕ_d	15º	10º	10º	10º
Porosity, n	0.02	0.15	0.15	0.20
Shear modulus, G (MPa)	$7.69x10^3$	360.0	192.3	Varied[1]
Bulk modulus, K (MPa)	$1.67x10^4$	780.0	416.7	Varied[1]
Hydraulic conductivity, k (m/s)	$1.0x10^{-8}$	$1.0x10^{-7}$	$1.0x10^{-7}$	$1.0x10^{-6}$

[1] The shear and bulk moduli of the waste rock were varied with the mean effective stress per Seed et al. (1984).

The assumed material properties of the impounded tailings and coarse tailings are summarized in Table 6-3.

The impounded tailings and the coarser tailings used to construct the dike raises were modeled using the UBC Sand model (refer to Section 2.7.2). However, due to software stability issues, the outer elements of the dike raises were modeled using the Mohr-Coulomb model instead of the UBC Sand model. This stability issue is discussed later in this section.

The properties of the impounded tailings were estimated from the in situ and laboratory testing conducted on the tailings of the representative impoundment (Laronde Mine). The degree of consolidation of the tailings in the conceptual impoundment was assumed to be similar to that of the representative impoundment, which is an active tailings impoundment in which the tailings are under-consolidated with respect to existing loads.

The standard penetration blow count, $(N_1)_{60,}$ a key parameter in the UBC Sand model, were used to simulate the degree of consolidation of the tailings. As noted in Section 2.7.2, this parameter is associated with the stiffness and cyclic resistance of the material being modeled, that are the characteristics most affected by the degree of consolidation. An alternative procedure would have been to calculate the excess porewater pressures within the tailings due to the consolidation process. However, this would have required more elaborate modeling of the placement of the tailings since the initiation of deposition, including the random exposure of the surface to produce zones of over-consolidation, and was considered beyond the scope of this research.

The coarse tailings composing the dike raises were assumed to consist of cycloned tailings that would thus be somewhat coarser than the impounded tailings, but would be essentially the same material. As a base case, it was assumed that these coarser tailings would not be compacted but would be normally consolidated. Accordingly, the coarse tailings were assumed to be somewhat denser and more permeable than the impounded tailings. The increased density of the coarser tailings was reflected in the average corrected standard penetration blow count, $(N_1)_{60}$, and dry density, ρ_{dry}, 11 blows/300 mm and 2,400 kg/m^3, respectively. To account for the increased coarseness, the hydraulic conductivities used for the coarse tailings were twice those used for the impounded tailings. The effect of compaction of the coarse tailings was investigated in the parametric evaluations described later in this chapter.

Table 6-3 – Assumed material properties of tailings.

Material Property	Tailings	Coarse Tailings	Coarse Tailings on Edges
Constitutive Model (Yield Criteria)	UBC Sand	UBC Sand	Mohr-Coulomb
Dry density, ρ (kg/m^3)	Varied[1]	Varied[1]	2,400
Constant volume friction angle, ϕ'_{cv}	36.25º	35.5º	-
Corrected SPT blow count, $(N_1)_{60}$ (blows per 300 mm)	3.5[2]	11[2]	-
Friction angle, ϕ'	36.6º	36.6º	36.6º
Cohesion, c (kPa)	0	0	25.0
Dilation angle, ψ	Varied[3]	Varied[3]	0º
Porosity, n	Varied[1]	Varied[1]	0.40
Shear modulus, G (MPa)	Varied[4]	Varied[4]	30.52
Bulk modulus, K (MPa)	Varied[4]	Varied[4]	21.36
Hydraulic conductivity[5]			
Horizontal, k_h (m/s)	2.25×10^{-6}	4.5×10^{-6}	4.5×10^{-6}
Vertical, k_v (m/s)	4.5×10^{-7}	9.0×10^{-7}	9.0×10^{-7}

[1]The dry density and porosity were functions of the vertical effective stress based on Equation 3-1.

[2] The values shown are the averages; the standard deviation of these values was 0.5 blows/300mm.

[3]In the UBC Sand model, the dilation angle is a function of the constant volume friction angle, ϕ'_{cv} and the developed friction angle, ϕ_d (see Equation 2-27).

[4] In the UBC Sand model, the shear and bulk moduli are calculated from the corrected SPT blow count and the mean effective stress (refer to Equations 2-17, 2-18, 2-35, and 2-36).

[5] The hydraulic conductivities shown are the average values. The actual values were randomized in FLAC to simulate a standard deviation of one half of an order of magnitude.

Seepage in existing slopes composed of cohesionless silty or sandy soils typically induces shallow failures that are not associated a general with instability of the slope. To prevent fatal errors in the execution of FLAC due to the excessive distortion of individual elements during the static, dynamic and post-shaking analyses caused by seepage forces on the downstream slopes of the impoundments, the outer elements on the downstream slope and on the crest of the dike were simulated using the Mohr-Coulomb model with strength and deformation properties comparable to the UBC Sand model properties and a minimal cohesion of 25 kPa. Cohesion cannot be given to a material simulated with the UBC Sand model that was used to model the impounded tailings and most of the coarse tailings. The use of a minimal cohesion to prevent excessive deformation in elements on the exterior of slopes subjected to seepage is discussed in Castillo et al. (2006). The cohesion can be considered to represent the effect of particle interlocking and vegetation on the slope.

6.3.5 Dynamic Damping

The damping parameters used in the modeling were the same as those used in the modeling of the representative impoundment (refer to Section 5.3.1). Hysteric damping was used to model both dynamic damping and shear modulus reduction with shear strain in the glacial till, compacted glacial till, coarse tailings on the slope, and waste rock. Damping within the tailings and coarse tailings was explicitly included through the use of the UBC Sand model (refer to Section 2.7.2). As recommended by Itasca (2005) and confirmed by parametric evaluation during the modeling, Rayleigh stiffness damping of 0.005 at a frequency of 20 Hz was applied to the entire model to simulate damping at low levels of acceleration. The application of the Rayleigh stiffness damping resulted in no significant amplification or damping of the ground motion as it transited from the bottom of the bedrock, where it was applied, to the top of the bedrock. The purpose of the Rayleigh damping was to provide damping under very low levels of shear strain where

hysteretic damping is ineffective due to its inability to simulate the damping that occurs at zero to very low shear strains.

6.3.6 The Waste Rock Inclusions

As a base case, the waste rock inclusions were assumed to consist of five rows of waste rock placed parallel to the dike. The inclusions were assumed to be 8 m wide on average and to be spaced at 16 to 20 m apart (measured center to center) starting 12 m upstream of the starter dam. The assumed configuration of the impoundment with waste rock inclusions is shown on Figure 6-2. It was also assumed that 1-m-thick layers of waste rock would be placed on the bottom and sides of the impoundment (not shown on Figure 6-2).

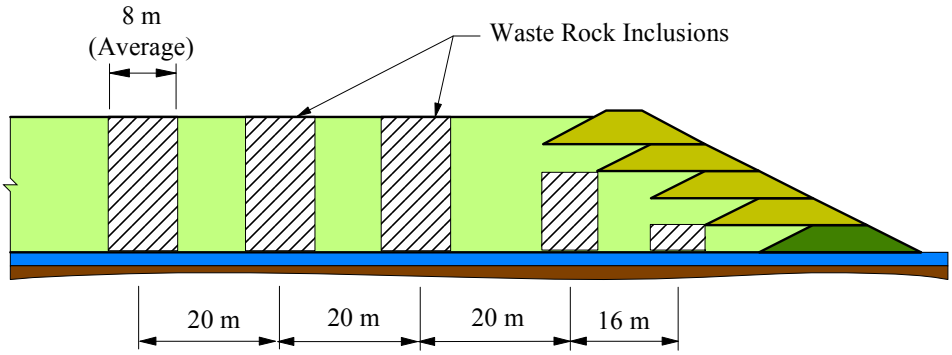

Figure 6-2 – Assumed location and dimensions of waste rock inclusions in cross-sectional view of the conceptual impoundment.

6.4 Analysis and Evaluation of the Conceptual Impoundment

The conceptual impoundment, with and without waste rock inclusions, was analyzed and evaluated using the five earthquake loadings described in Table 6-1. The responses of the impoundments to Earthquake E3 (M_w=7.0) are described in detail. The responses of the impoundments to Earthquakes E1 (M_w=6.5), E2 (M_w=6.75), E4 (M_w=7.25), and E5

(M_w=7.5) are provided in the summary of this section; detailed results of these responses are presented in Appendix H.

For convenience, the conceptual impoundment without waste rock inclusions may be referred to as the "conventional impoundment" and the conceptual impoundment with waste rock inclusions may be referred to as the "reinforced impoundment."

6.4.1 The Geometry of the Models

The geometry of the model of the conventional impoundment is shown on Figure 6-3. The overall length and height of the model were 255 m and 24 m, respectively. A buttress assumed to be composed of glacial till was placed on the upstream end of the model for stability reasons. The resulting width of the area of impounded tailings was 148 m, as measured from the upstream end of the crest of the dike to the toe of the buttress, and the depth of the impoundment, H, was 20 m.

The glacial till buttress was used on the upstream side of the model for stability during dynamic modeling for the following reasons:

a) Extending the tailings to the upstream size of the model resulted in excessive local deformation that resulted in fatal program errors. This deformation was due to the relatively low elastic moduli of the tailings;
b) Placing stiffer elements on the upstream side of the model that were subject to earthquake loads from the side caused very high lateral loads in the tailings that resulted in failure of the impoundment; and
c) During preliminary modeling, it was found that placing a glacial till buttress on the upstream side of the model avoided both of the phenomena described above and that failure surfaces in the tailings, as evidenced by deformation patterns, tended to extend from the dike into the impoundment and exit at the surface of the impoundment downstream of the buttress. This indicated that the presence of the buttress had no significant effect on the stability of the

impoundment/dike and that the distance from the dike to the buttress was sufficient.

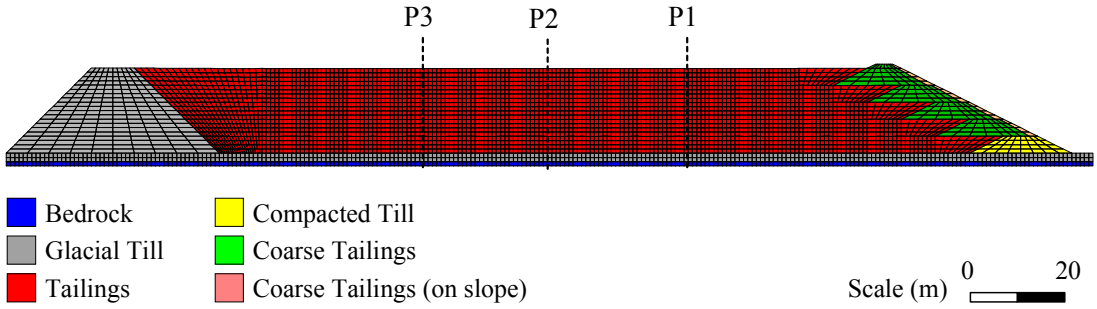

Figure 6-3 – Mesh of the typical impoundment modeled without waste rock inclusions (conventional impoundment).

The geometry of the model used for the impoundment with waste rock inclusions (the reinforced impoundment) is presented on Figure 6-4.

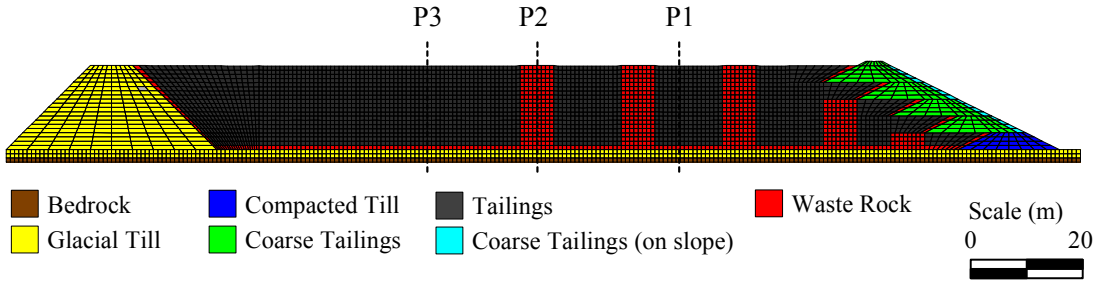

Figure 6-4 – Mesh of the typical impoundment modeled with waste rock inclusions (reinforced impoundment).

6.4.2 Boundary Conditions Applied to the Models

The mechanical and fluid boundary conditions applied to the models of the conventional and reinforced impoundments during the static phase of the analysis are shown on Figure 6-5. The conditions applied to the boundaries consisted of fixed horizontal and vertical displacements and fixed values of porewater pressure and saturation. Where a specific boundary condition was not applied, the associated parameter was allowed to vary freely during the static analysis. The operation of FLAC with respect to the fluid boundary conditions is described in Section 5.3.1.

The boundary conditions applied during the dynamic phase of the analysis consisted of the application of the "free field" boundary in place of the fixed horizontal displacement boundaries used in the static analysis and the application of the appropriate ground motion (Earthquake E1, E2, E2, E4, or E5) to the bottom of the model in the form of applied horizontal accelerations. Free field boundaries are single columns of elements placed on the sides of the grid. These elements simulate the behavior of an extended medium, including the absorption and rebound of shear waves (Itasca, 2005).

For the post-shaking phase of the analysis, the applied ground motion was removed and replaced with an applied velocity of 0. All other boundary conditions remained unchanged.

The fluid boundary conditions of the static phase of the analysis were retained during the dynamic and post-shaking phases of the analysis.

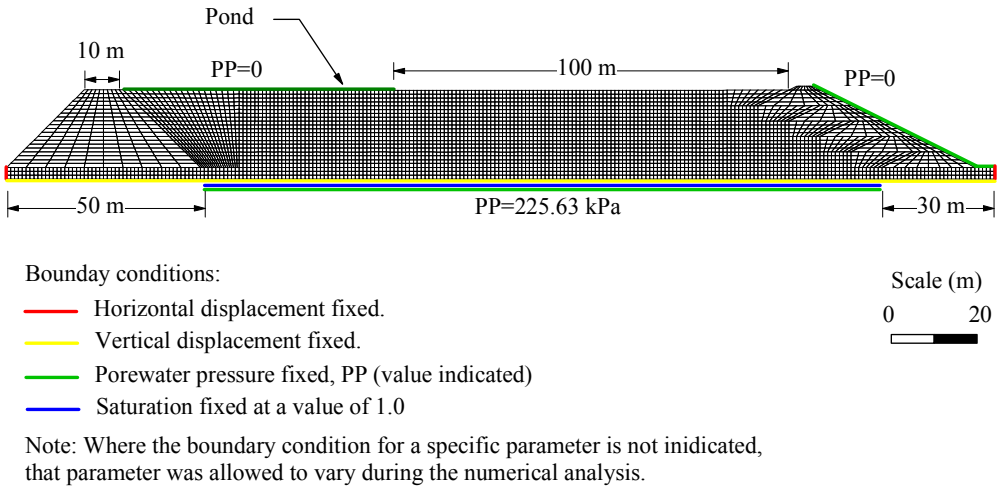

Figure 6-5 – Mechanical and fluid boundary conditions applied to the model during the static phase of the analysis.

6.4.3 Parameters Recorded During Analyses of the Models

As noted earlier, critical parameters calculated within FLAC were recorded at regular intervals of time during the dynamic and post-shaking phases of the analyses. The parameters were recorded at intervals of 1,000 time steps that were equivalent to increments of approximately 0.04 seconds and 0.1 seconds for the dynamic and post-shaking phases, respectively.

The recorded parameters included:

- Horizontal accelerations input to the model as well as those developed at the top of bedrock and at the top of the glacial till (all at P1), on the crest of the dike, and at 2 m increments of depth in the tailings at P1, P2 and P3;
- The porewater pressure, cyclic stress ratio, CSR, and excess porewater pressure ratio, r_u, at P1, P2 and P3 at 2 m increments of depths in the tailings and at 5 locations in the tailings below the slope of the dike; and

- The horizontal (x) and vertical (y) displacements of the center of the crest of the dike.

The cyclic stress ratio, CSR, was calculated using Equation 4-1 and the excess porewater pressure ratio, r_u, was calculated using Equation 4-2.

The locations where the critical parameters were recorded are shown as red dots on Figure 6-6. The response of the model at the interface between the tailings and a waste rock inclusion was also evaluated. However, the results were difficult to interpret due to numerical instability observed at that location.

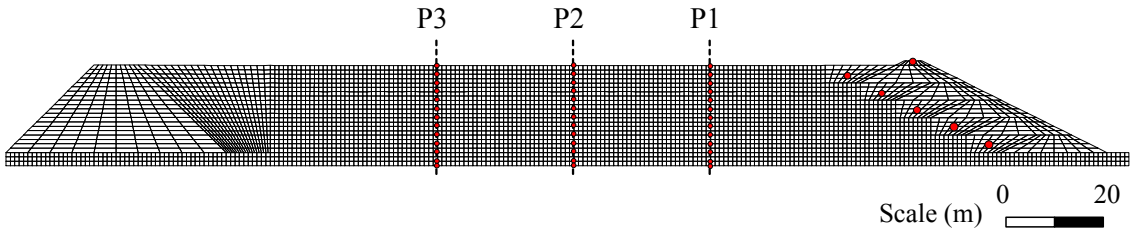

Figure 6-6 – The locations (red dots) on the models where critical parameters were recorded during the dynamic and post-shaking phases of the analyses.

6.4.4 Static Analyses

Static analyses were conducted to establish the state of the conventional and reinforced impoundments prior to dynamic analyses. The results of static analyses are summarized in the following sections.

The modeling was done assuming instantaneous construction of the impoundment followed by the application of gravity. In the impoundment with waste rock inclusions, this resulted in the development of stress transfer to the waste rock inclusions from the adjacent tailings. However, given that in an actual impoundment the tailings would undergo a period of consolidation upon placement and with the deposition of additional

tailings, stress transfer from the relatively softer tailings to the waste rock inclusions would be expected. Accordingly, the stress transfer in the model is deemed to be reasonable.

6.4.4.1 Conventional Impoundment

The static vertical effective stresses within the conventional impoundment are shown on Figure 6-7. Within the tailings, they varied from 0 near the surface of the impoundment to 350 kPa at the bottom of the impoundment. The vertical effective stress at the bottom of the impoundment calculated analytically using the unit weight and porosity assigned to the tailings is:

$$\sigma_v' = 20\ m \cdot (23.5\ kN/m^3\ - 0.6 \cdot 9.81\ kN/m^3) = 352\ kPa$$

The results shown on Figure 6-7 agree with the vertical effective stresses calculated analytically and are thus deemed reasonable. The irregularities observed in the distribution of the vertical effective stresses (and other stresses to be presented) are a result of two factors: 1) heterogeneity that was provided to the tailings by statistically varying the $(N_1)_{60}$ value, and thus the elastic moduli, in FLAC using a function that provides randomized values given an average and a standard deviation (see Section 4.4.1.1); and 2) the manner in which FLAC calculates the stresses and the distribution of stresses. In FLAC, stresses are estimated based on forces calculated at the nodes of each element and as a result the distribution of stresses contains some irregularity.

The linear separations (discontinuities) seen in the plot of the vertical stress distribution (as well as other stress distributions to be presented) are the result of the grid generation method and occurs where elements have been attached to create a particular geometry. The presence of these attachments has no effect on the simulation, but it does create separation in the graphic presentation of some of the properties.

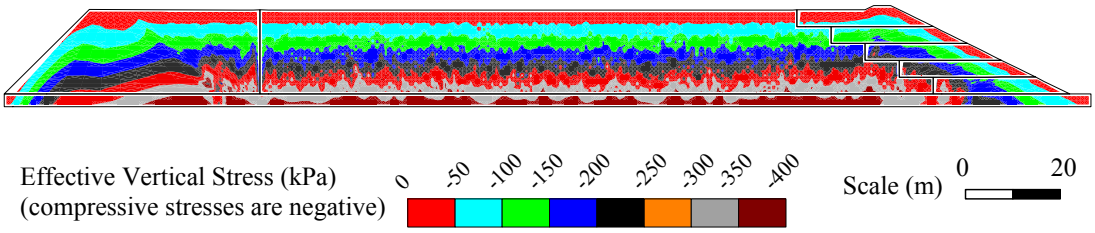

Figure 6-7 – Static vertical effective stresses in the conventional impoundment.

The static horizontal effective stresses within the conventional impoundment are presented on Figure 6-8. Within the tailings, these stresses varied from 0 near the surface of the impoundment to 150 kPa at the bottom of the impoundment. The ratio of the horizontal stresses to the vertical stresses (150 kPa/350 kPa) correspond to an at-rest pressure coefficient of approximately 0.43. As noted previously, the theoretical at-rest pressure coefficient of the tailings is 0.40. Given this, the static horizontal effective stresses within the impoundment are deemed to be reasonable.

The relatively high horizontal effective stresses within the starter dike, bedrock and the glacial till buttress reflect the influence of their stiffness (shear and bulk moduli) compared to the tailings and each other as well as the geometry and mechanical boundary conditions of the model.

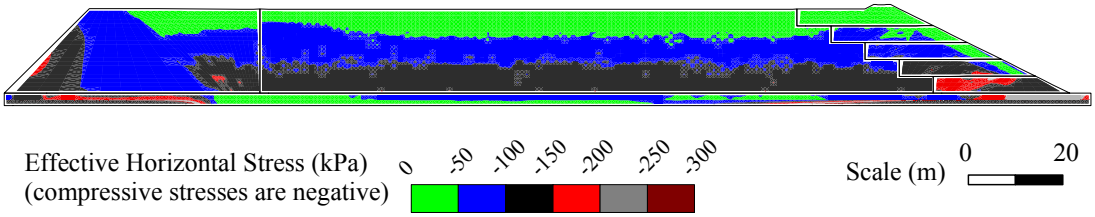

Figure 6-8 – Static horizontal effective stresses in the conventional impoundment.

The porewater pressure distribution within the conventional impoundment is shown on Figure 6-9. In the central part of the impoundment, static porewater pressures vary from about 0 near the surface to 196 kPa at the bottom of the tailings and 225 kPa at the bottom of the model. These values are in agreement with the assumption of hydrostatic conditions which results in calculated porewater pressure, u, values of 196 kPa at the bottom of the tailings and 226 kPa at the bottom of the model ($u=\gamma_w \cdot z$, where γ_w is the unit weight of water and z is depth).

Within the impoundment, the static water level was at the surface of the tailings and the degree of saturation of all of the retained tailings and most of the tailings used to construct the dike was 100%. Thin zones (less than one meter in depth) with degrees of saturation less than 1.0 occurred at the crest and in the upper 1/3 of the downstream slope of the dike. The saturation in these zones was between 98 and 100%.

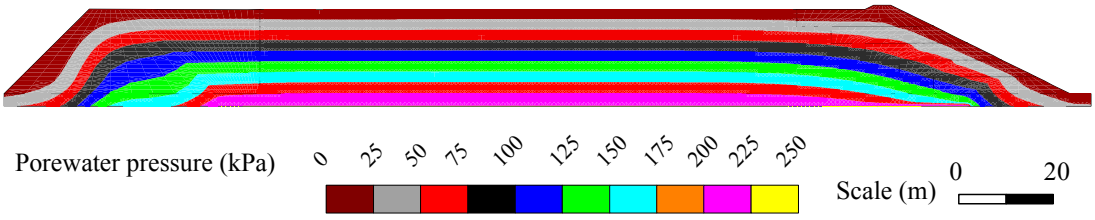

Figure 6-9 – Porewater pressures in the conventional impoundment under static conditions.

The horizontal and vertical effective stresses and the porewater pressures within the conventional impoundment for the condition of static equilibrium were thus in agreement with analytical estimates.

6.4.4.2 Reinforced Impoundment

The static vertical effective stresses within the impoundment with waste rock inclusions are shown on Figure 6-10. Within the tailings away from the inclusions, the static vertical

effective stresses vary from 0 at the surface to 350 kPa at the bottom of the tailings and correspond to the analytically calculated values of 0 at the surface and 353 kPa at the bottom of the tailings. In the vicinity of the inclusions, the vertical effective stresses in the tailings vary from 0 at the surface of the impoundment to 275 kPa. Within the waste rock inclusions, the vertical effective stresses varied from 0 near the surface of the impoundment to between 375 and 475 kPa at the bottom of the impoundment. The corresponding values from analytical calculations using the assumed material properties are 0 at the surface and 235 kPa at the bottom of the impoundment. The presence of the inclusions has changed the distribution of the effective stresses in their vicinity. Stress transfer from the tailings to the inclusions has resulted in vertical effective stresses that were lower in the tailings and higher in the waste rock inclusions. This was expected given the assumed instantaneous construction of the impoundment and because the inclusions are much stiffer than the tailings. Some degree of stress transfer would occur in a stage construction sequence due to the consolidation of the tailings.

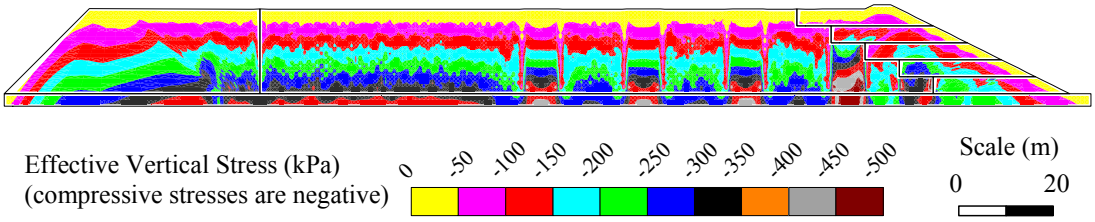

Figure 6-10 – Static vertical effective stresses within the reinforced impoundment.

The static horizontal effective stresses within the reinforced impoundment are presented on Figure 6-11. Within the tailings away from the inclusions, these stresses varied from 0 near the surface of the impoundment to 150 kPa at the bottom of the impoundment. Away from the inclusions, the ratio of the horizontal stresses to the vertical stressed correspond to an at-rest pressure coefficient of about 0.43. The theoretical at-rest pressure coefficient

of the tailings is 0.40. Given this, the static horizontal effective stresses within the impoundment (away from the inclusions) are deemed reasonable.

In the vicinity of the inclusions, the horizontal effective stresses at the bottom of the impoundment were 100 kPa in both the tailings and waste rock. Using Equation 6-1, the coefficient of at-rest pressure for the waste rock is 0.28. The values approximated from the FLAC analysis are 100 kPa/275 kPa=0.36 for the tailings and 100 kPa/400 kPa=0.25 for the waste rock. Based on these results, the static horizontal effective stresses within the impoundment (in the area of the inclusions) are deemed to be reasonable.

The horizontal effective stresses within the starter dike, bedrock and the glacial till buttress reflect the influence of their stiffness (shear and bulk moduli) relative to the tailings and each other as well as the geometry and mechanical boundary conditions of the model.

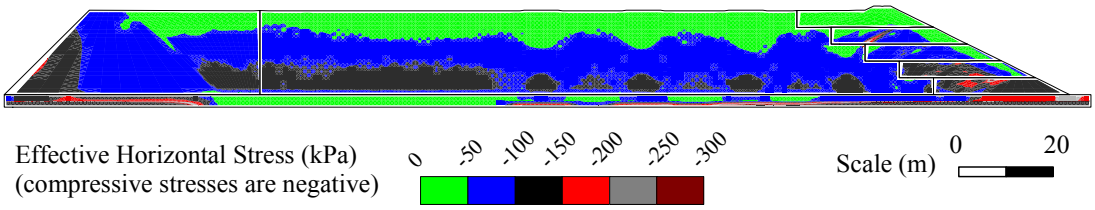

Figure 6-11 – Static horizontal effective stresses within the reinforced impoundment.

The hydrostatic porewater pressures in the reinforced impoundment are shown on Figure 6-12 and are the same as those for of the conventional impoundment.

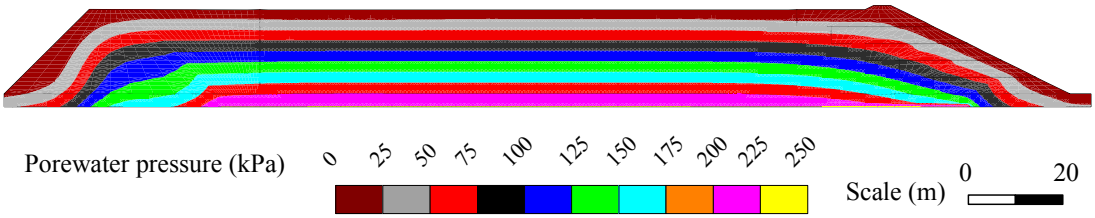

Figure 6-12 – Porewater pressure distribution in the reinforced impoundment under static conditions.

Within the impoundment, the static water level was at the surface of the tailings and the degree of saturation of all of the retained tailings and most of the tailings used to construct the dike was 100%. Thin zones (less than one meter in depth) with degrees of saturation less than 100% occurred on the surface of the impoundment in the area of the waste rock inclusions and at the crest and in the upper 1/3 of the downstream slope of the dike. The degree of saturation in these zones was between 98 and 100%.

The effective stresses and porewater pressures within the reinforced impoundment are in good agreement with what would be expected based on the assumed material properties and geometry.

6.4.5 Dynamic Analysis of the Conventional Impoundment – Earthquake E3 (M_w=7.0)

The model of the conventional impoundment was subject to dynamic loading that simulated the occurrence of Earthquake E3. The static conditions in the impoundment at the onset of the dynamic analysis are presented in Section 6.4.4.

The ground motion that was applied to the bottom of the model to simulate the occurrence of Earthquake E3 is presented on Figure 3-28(c). The record represents a moment magnitude 7 earthquake with an assumed horizontal fault rupture to site distance of 30 km. The event is characterized by a PGA of 0.659g and a duration of 27.5 seconds.

Details on the creation of the ground motion records used to simulate the earthquakes in the dynamic analyses are presented in Section 3.8.3 and Appendix E.

6.4.5.1 Site Response

The response of a site to an earthquake is usually evaluated based on the values of the peak horizontal ground accelerations (PGA) within the soil profile and at the surface. However, as noted in Section 2.2.3.1, the PGA values represent isolated maximum values of acceleration and may not be representative of the intensity of the ground motion or of the amplification (or damping) of the ground motion as it rises through the soil profile. Therefore, the response of the impoundment will be evaluated here using PGA values and horizontal acceleration records (ground motions) extracted from FLAC during the dynamic analyses.

The PGA values extracted from FLAC during the dynamic analysis are shown on Table 6-4 along with the associated amplification factors, F_a. Recall that the amplification factor, F_a, is a ratio of the PGA value at a given location to that at a reference location, generally, the top of bedrock (refer to Equation 3-12). The ground motion applied at the bottom of the model was slightly amplified as it passed through the 1-m-thick layer of bedrock assumed on the bottom of the model. Thus, the PGA value on the top of bedrock was 0.764g, 15.9% higher than the PGA of the applied ground motion (0.659g).

Based on the amplification factors of Table 6-4, the response of the site to the earthquake loading was moderately high amplification of the ground motion within the 2-m of glacial till overlying bedrock (based on an F_a value of 1.902), severe damping within the impounded tailings (F_a values of 0.169 and 0.124 at P1 and P2, respectively) and moderately low amplification on the crest of the dike (the F_a was 1.237). However, as noted above, PGA values represent isolated peaks and may not be representative of the ground motion at any particular point in the subsurface or on the surface.

Table 6-4 – Calculated amplification factors
– conventional impoundment, Earthquake E3 (M_w=7.0).

Location	Peak Horizontal Ground Acceleration, PGA (g)	Amplification Factor (F_a)
Top of bedrock	0.764	-
Top of glacial till	1.453	1.902
Surface of Impoundment at P1	0.129	0.169
Surface of Impoundment at P2	0.095	0.124
Crest of dike	0.945	1.237

Figure 6-13 presents ground motions extracted from FLAC at location P1 (see Figure 6-6). They consist of the horizontal accelerations applied to the bottom of the model (Earthquake E3) and those calculated at the top of bedrock and at the top of the glacial till (the bottom of the tailings). Comparing Figure 6-13(a) to Figure 6-13(b), the horizontal acceleration was slightly amplified within the bedrock. Within the 2-m of glacial till assumed to lie between the top of bedrock and the bottom of the tailings, the acceleration was moderately amplified for the duration of shaking (see Figure 6-13). The amplification of the acceleration within the glacial till was due to two factors: 1) The shear modulus of the glacial till was significantly lower than that of the bedrock and shear waves (which transmit accelerations) are generally amplified when passing through a medium of lower shear modulus than the medium from which they originated (Kramer, 1996); and 2) the shear modulus of the glacial till was sufficient to transfer the acceleration through shear waves without developing excessive strains that would have produced significant damping. The maximum shear strains in the glacial till during the dynamic analysis were generally less than 0.001.

The horizontal accelerations extracted from FLAC contain every 10^{th} data point (60,000 data points out of 600,000 for Earthquake E3 which has a duration of 27.5 seconds).

Thus, some isolated peaks were excluded and the PGA values of the accelerations on the figures may be slightly less than the actual PGA values of the accelerations However, the overall shape and intensity of the ground motion was unchanged. This is applicable to all of the ground motion records extracted from FLAC that are presented in this report.

Figure 6-14 presents the ground motions (horizontal accelerations) within the tailings at location P1 (refer to Figure 6-6) for 0.275H, 0.475H, 0.675H, and 0.975H, where H is the height of the tailings within the impoundment measured from the bottom to the surface (H=20 m). The horizontal accelerations within the tailings were damped significantly during the first 3 seconds earthquake shaking with the degree of damping increasing towards the surface. PGA values varied from 0.612g at 0.275H (Figure 6-14a) to 0.153g at 0.975H (Figure 6-14d). After the 3rd second of shaking, the accelerations within the tailings were severely damped and peak values were less than 0.05g for the duration of shaking. The damping in the tailings is attributed to the development of excess porewater pressures (to be described later) and the development of high shear strains. For the conventional impoundment, maximum shear strains in the impounded tailings typically varied between 0.01 and 0.05 during the dynamic analysis. In the area of the dike, the maximum shear strains were typically between 0.05 and 0.2.

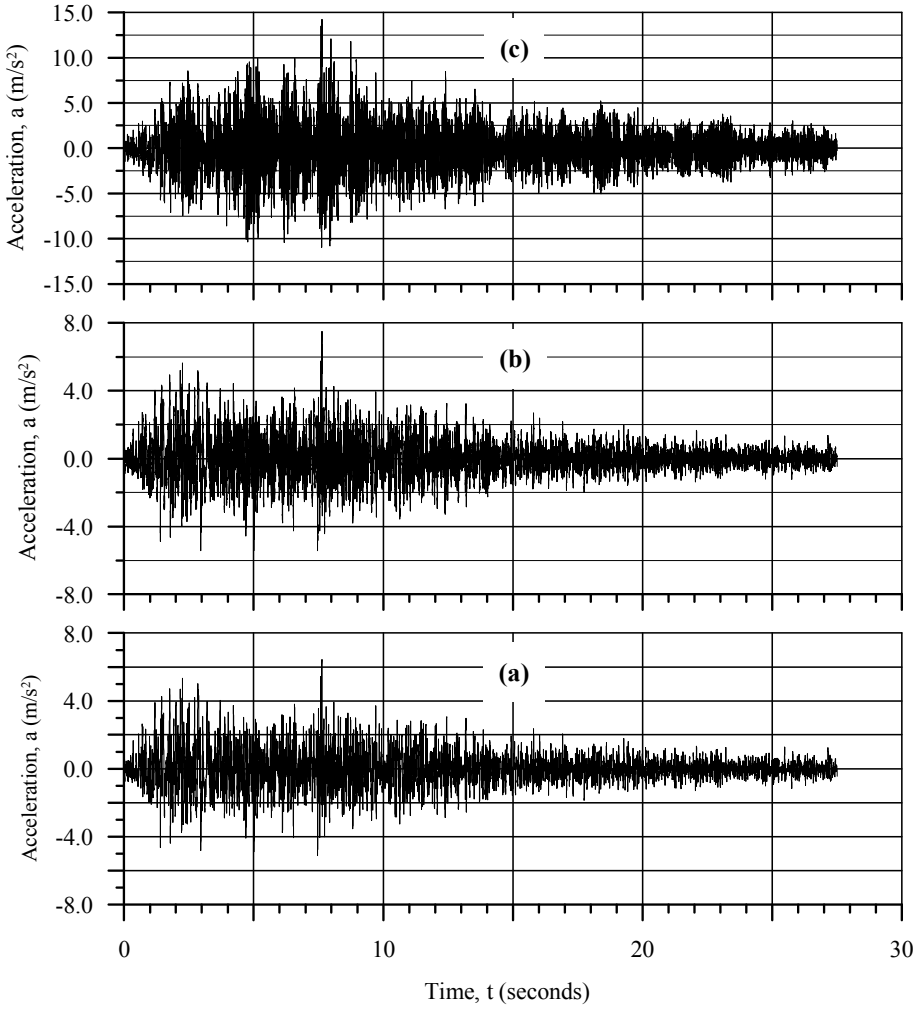

Figure 6-13 – Horizontal acceleration applied to the bottom of the model (a), and recorded on the top of bedrock (b), and on the top of glacial till (c) at location P1 – conventional impoundment, Earthquake E3 (M_w=7.0).

The horizontal accelerations measured on the crest of the dike are presented on Figure 6-16. The horizontal acceleration on the crest was slightly damped through the 10th second of shaking and then was slightly to moderately amplified for the remainder of shaking. The response of the crest is attributed to the development of shear strains and excess porewater pressures in the underlying material, which produced damping, and to the geometry, which would have produced amplification (e.g. Kramer, 1996).

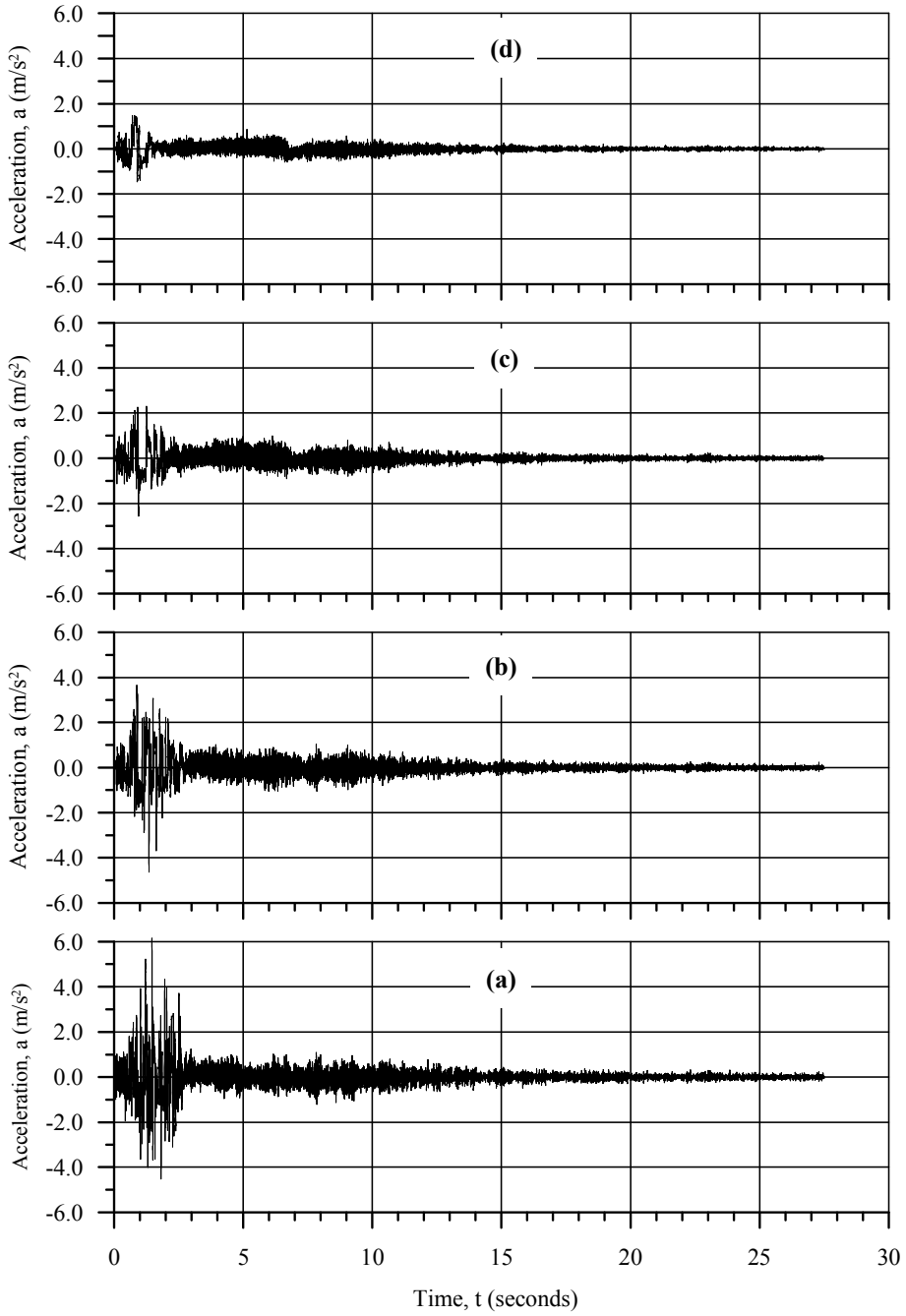

Figure 6-14 – Horizontal acceleration at 0.275H (a), 0.475H (b), 0.675H (c), and 0.875H (d) in the tailings at P1 – conventional impoundment, Earthquake E3 (M_w=7.0).

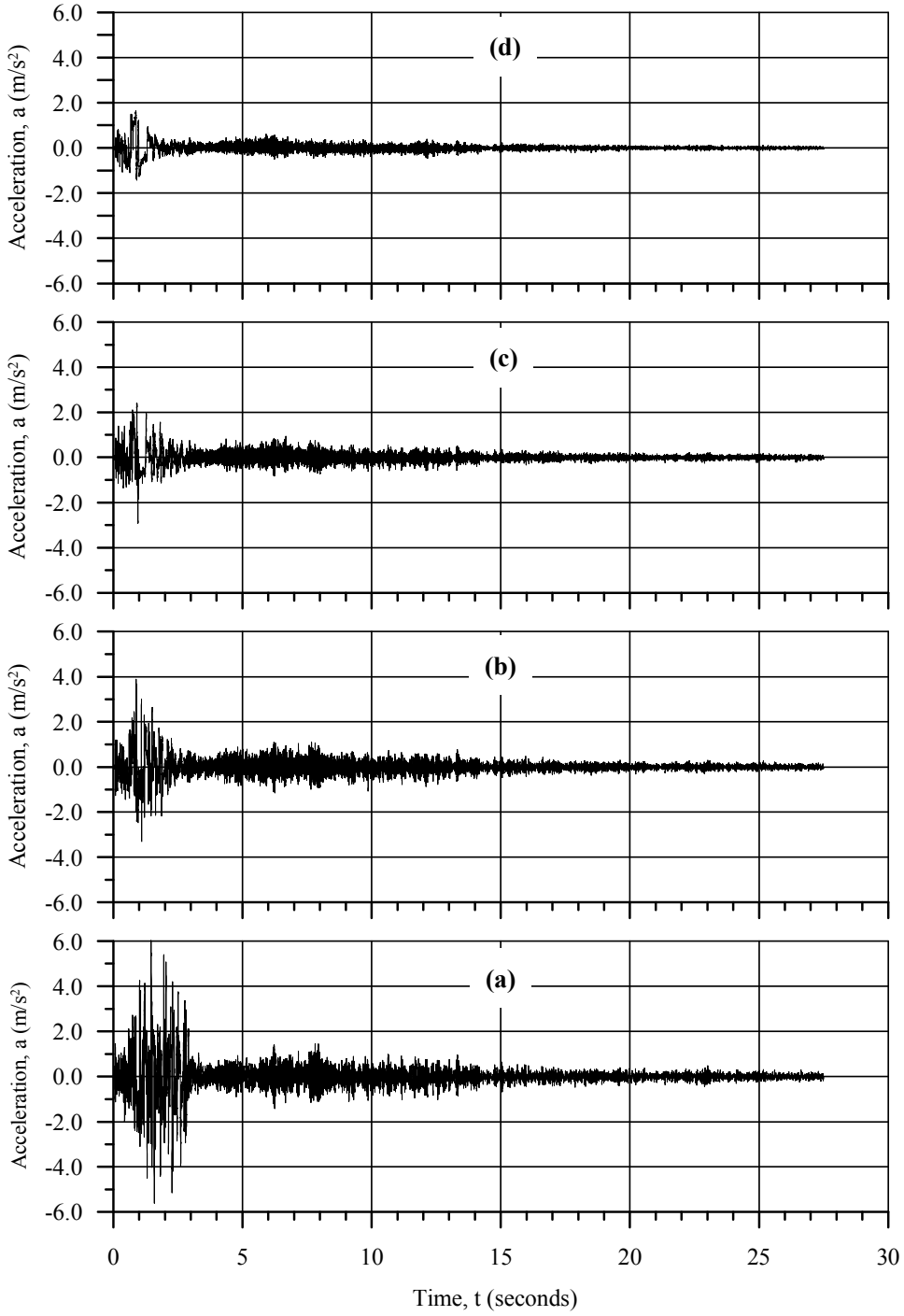

Figure 6-15 – Horizontal acceleration at 0.275H (a), 0.475H (b), 0.675H (c), and 0.875H (d) in the tailings at P2 – conventional impoundment, Earthquake E3 (M_w=7.0).

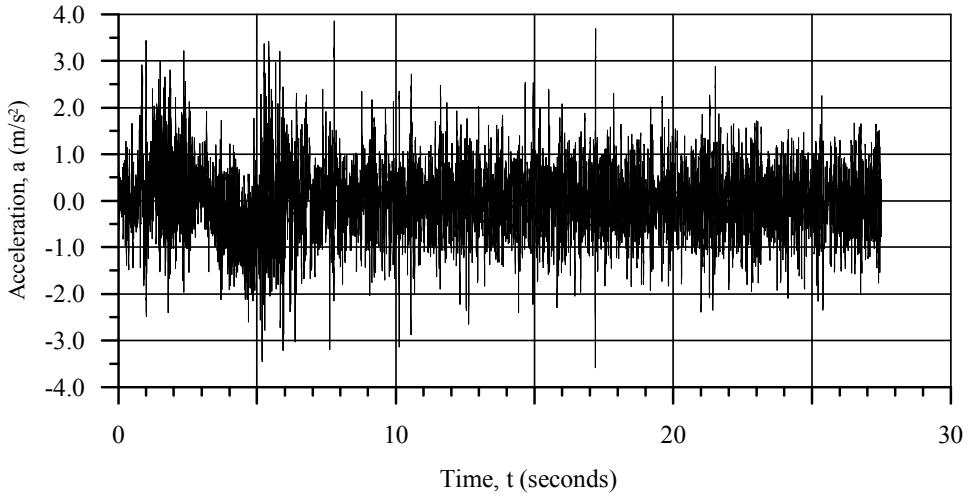

Figure 6-16 – Horizontal acceleration on the crest of the dike – conventional impoundment, Earthquake E3 (M_w=7.0).

Section 3.9.1 presents the result of level ground liquefaction analysis of unconsolidated tailings based on the results of cone penetration testing. Amplification factors from that analysis are presented on Table 3-16. For Earthquake E3, the F_a value at the surface of the tailings was 0.193 which is comparable to the results from locations P1 and P2 from the dynamic analysis of the convention impoundment (Table 6-4). NRCC (1995) recommends and amplification factors of 1.5 for "very loose and loose coarse-grained soils with depth greater than 15 m" and 2.0 for "very soft and soft fine-grained soils with depth greater than 15 m." Either of these descriptions could be applied to the retained tailings. NRCC (2005) does not recommend amplification factors for liquefiable soils (e.g. under-consolidated or normally consolidated tailings); instead it recommends dynamic site response analysis such as that in Section 3.9.1 or in this section of the thesis.

6.4.5.2 Cyclic Stress Ratios

The cyclic stress ratios, CSR, developed at location P1 (see Figure 6-6) at elevations 0.275H, 0.475H and 0.675H within the tailings are shown on Figure 6-17. As mentioned

previously, the CSR is the ratio of the applied shear stress to the initial vertical effective stress. CSR values within the tailings were calculated in FLAC during the dynamic analysis using Equation 4-1. Recall that the shear stress used to calculate the CSR consists of the shear stress induced directly by the earthquake loading as per Equation 2-5 and the shear stresses induced by static loadings and other dynamic loadings, such as those generated to resist movement along a potential failure surface during earthquake loading. However, the CSR value is limited by the shear strength of the soil. Thus, the maximum value of the CSR decreases as excess porewater pressures are generated and the shear strength of the soil decreases.

The CSR development in at P1 is summarized as follows.

a) At the start of shaking (t=0 seconds), the values of the CSR at the elevations shown on Figure 6-17 were approximately 0 (a maximum value of 0.03 was recorded at 0.675H). This indicates that the static shear stresses within the tailings impoundment at location P1 (see Figure 6-3) were relatively small, a condition associated with the assumption of level ground conditions.

b) At 0.275H, the amplitudes of the CSR reached a maximum magnitude of 0.15 in the first second of shaking and then decreased rapidly to 0.03 by the end of the 3rd second (Figure 6-17a). From then on, there were no significant CSR values recorded at this location. Thus, there was no significant shear loading in the impoundment at this location and elevation for the remainder of shaking.

c) The patterns of CSR development during shaking at 0.475H, 0.675H, and 0.875H in the tailings were very similar to that at 0.275H, except as noted below.

d) At 0.475H, the CSR reached a maximum magnitude of 0.18 by the 1st second of loading and then declined to about zero by the 4th second of loading. From then until the end of shaking, there was no appreciable cyclic change in the CSR. However, from the 5th second to the 14th second the value of the CSR

decreased to about -0.025 as if the tailings at this level were subjected to a relatively low, monotonic shear loading (refer to Figure 6-17b).

e) At 0.675H (Figure 6-17c), the value of the CSR varied from -0.11 to 0.13 for the first two seconds of shaking and then abruptly decreased to near 0 by 3rd second. For the remainder of shaking, the value of the CSR was close to 0, except for the period from 5 to 7 seconds when it decreased to about -0.25. This decrease is attributed to a shear loading associated with a potential failure surface within the impoundment.

f) Near at the surface of the impoundment (0.875H), the first 2 seconds of shaking were characterized by the development of CSR amplitudes as great as 0.15. During the next 6 seconds, the value of CSR varied between -0.03 and 0.03. From the 8th second to the 15th second, the value of the CSR declined roughly from about 0 to -0.05 and it remained at this level for the rest of shaking. The relatively constant value of the CSR in the last 12.5 seconds of shaking indicates a shear loading within the impoundment at this location and elevation associated with a potential failure surface.

g) The development of the cyclic stress ratios within the tailings did not directly correlate with the development of the accelerations within the tailings, despite the direct correlation between the applied shear and the acceleration implicit in the Simplified method of liquefaction evaluation (see Section 2.3.1 and Equation 2-5). The reasons for the lack of direct correlation appears to be the development of excess porewater pressures within the tailings that reduced the capacity of the tailings to sustain and transmit shear stresses as well as the occurrence of shear stresses not directly related to the horizontal accelerations.

h) Referring to Section 2.3.1.2, the threshold level of CSR considered necessary for the development of excess porewater pressures in loose sand is about 0.04. This level of CSR was only exceeded within the tailings at P1 and P2 for a few cycles at the start of shaking. However, the severe decrease in the amplitude of the cyclic stress ratios is indicative of the development of high

excess porewater pressures in the tailings and/or the development of relatively high shear strains in the tailings, either of which would have caused a significant reduction in the horizontal accelerations and thus the CSR values in the overlying tailings.

The CSR values developed in the tailings below the slope of the dike at the five locations shown on Figure 6-6 are plotted on Figure 6-18 and summarized as follows:

a) In the lower elevations (0.1H, 0.3H and 0.5H), static shear stress in the tailings caused initial CSR values ranging from -0.15 to -0.35, increasing in magnitude with depth. In the upper elevations (0.7H and 0.9H), the static shear resulted in initial CSR values of about 0.05. At 0.1H, 0.3H and 0.5H, the values of the CSR varied between -0.92 and 0 during the first 10 seconds of shaking, and then remained relatively constant, except for a decrease in the CSR value at 0.3H during the last 10 seconds of shaking.

b) The variation in the values of the CSR at 0.7H and 0.9H was much less than in the lower zone of the tailings. At these levels the CSR varied between -0.15 and 0.15 for the first 5 seconds of shaking and were then relatively stable, generally not varying by more than 0.05 for the remainder of shaking.

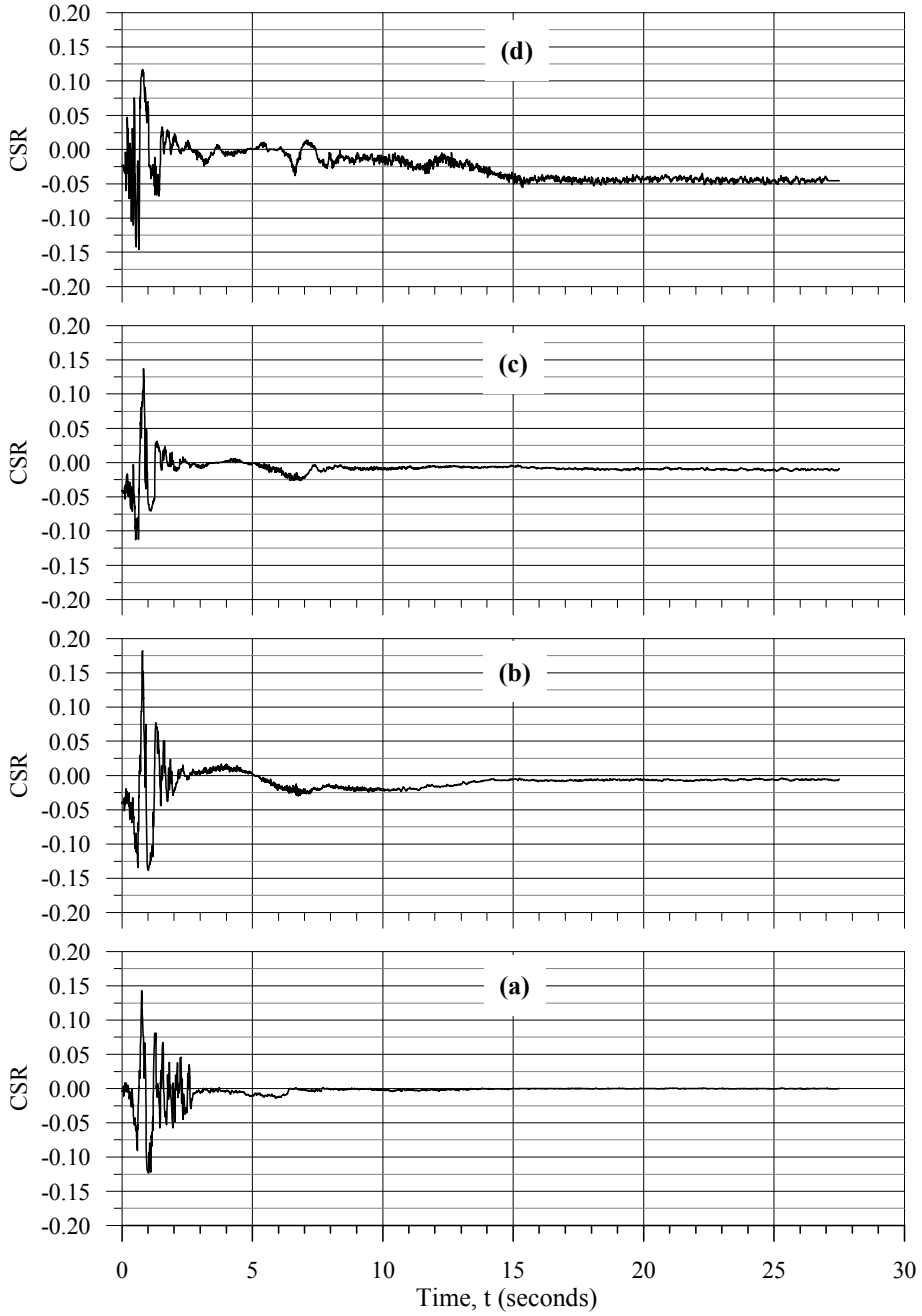

Figure 6-17 – Cyclic stress ratio at 0.275H (a), 0.475H (b), 0.675H (c), and 0.875H (d) in the tailings at P1 – conventional impoundment, Earthquake E3 (M_w=7.0).

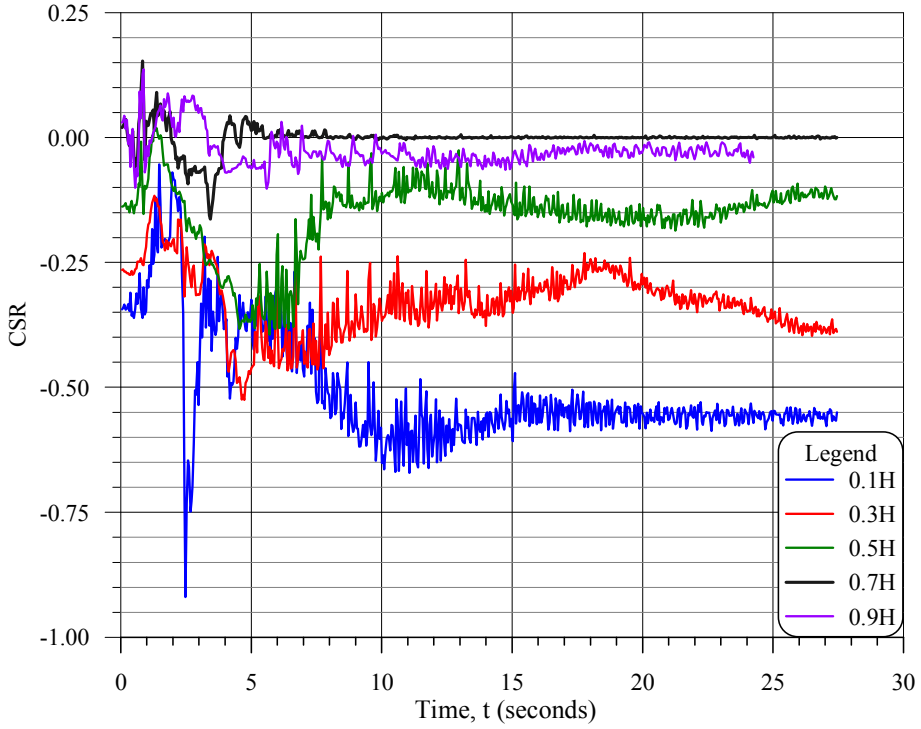

Figure 6-18 – Cyclic stress ratios developed in the tailings below the dike – conventional impoundment, Earthquake E3 (M_w=7.0).

6.4.5.3 Excess Porewater Pressure Development

The development of excess porewater pressures and liquefaction in the tailings was evaluated using the excess porewater pressure ratio, r_u. During the dynamic and post-shaking phases of the numerical analysis, the value of r_u at various locations on the model was calculated at each time step using Equation 4-2. The calculated values and the associated times were extracted and saved to a text data file.

Recall that Equation 4-2 defines r_u as the ratio of the difference in the vertical effective stress to the initial vertical effective stress $[(\sigma'_{vo}-\sigma')/\sigma'_{vo}]$, rather than the conventional definition as the ratio of the change in porewater pressure to the initial vertical effective stress $(\Delta u/\sigma'_{vo})$. The reason for the use of the change in the vertical effective stress is to capture vertical effective stress changes due to stress redistribution, stress transfer and

dynamic loading as well as excess porewater pressure development. As a result the value of r_u may be negative if and when vertical effectives stresses at some location within the impoundment increase to levels greater than their initial values during or after dynamic loading.

The excess porewater pressure ratios, r_u, developed at various levels in the tailings at location P1 (refer to Figure 6-6) at shown on Figure 6-19. From 0.175H to 0.875H, the excess porewater pressure ratios increased dramatically at the onset of shaking and were greater than 0.9 by the third second of shaking. At 0.975H, the r_u value increased to above 0.95 by the 2nd second of shaking and then decreased to 0.88 by the 3rd second. The rapid development of the r_u values coincided with the relatively large amplitude horizontal accelerations and cyclic stress ratios at this location. At all levels, except for 0.875H and 0.975H, the r_u values were relatively constant and remained above 0.9 for the remainder of earthquake. At 0.975H, and to a lesser extent at 0.875H, there was significant variation in the r_u values between the 3rd and 12th second and then a gradual decline to values of 0.87 at 0.875H and 0.7 at 0.975H at the end of shaking (t=27.5 seconds).

The variations in the r_u values at 0.875H and 0.975H from the 3rd to 12th second are attributed to the lack of confinement at the surface of the impoundment that would have allowed volumetric strain and associated porewater pressure changes. The declines in the excess porewater pressure ratios 0.875H and 0.975H during the latter half of shaking are attributed to drainage at the surface of the impoundment.

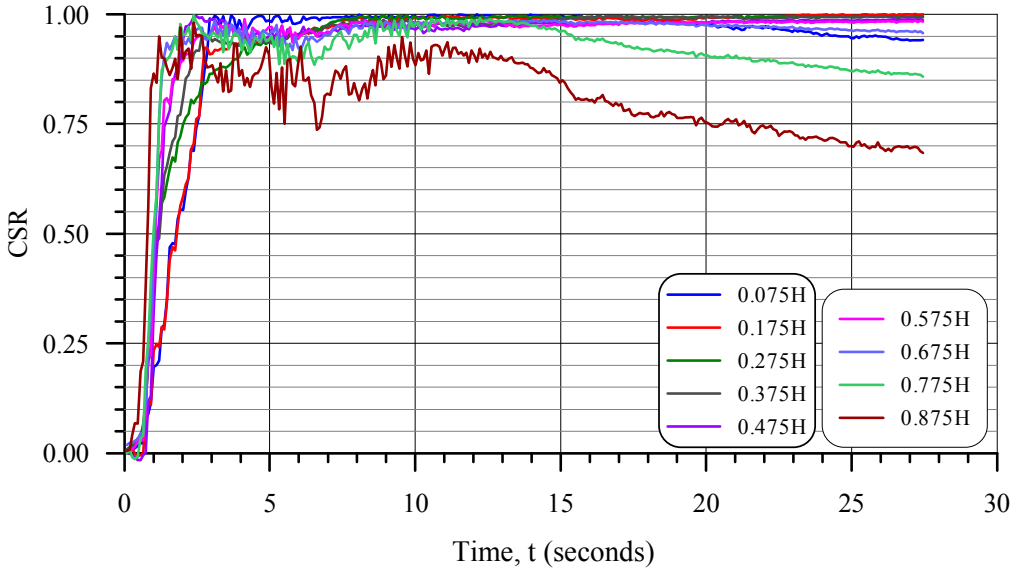

Figure 6-19 – Excess porewater pressure ratio development at various depths in the tailings at location P1 – conventional impoundment, Earthquake E3 (M_w=7.0).

The excess porewater pressure ratios developed in the tailings below the dike (see Figure 6-6 for the locations) are shown on Figure 6-20. During the first 2 seconds of shaking the r_u values increased to between 0.5 and 0.99, from the 2nd to the 5th second they fluctuated dramatically, particularly the value at 0.1H which varied between -0.35 and 0.85 during this period. This period of fluctuation occurred during similar fluctuations in the cyclic stress ratio (see Figure 6-18). Between the 5th and 10th seconds of shaking, the r_u values became relatively stable for the duration of shaking with the values at the end of shaking varying from -0.05 at 0.1H to 0.99 at 0.9H. Negative values of r_u are associated with an increase in the vertical effective stress. Given the contractive nature of the tailings and the dynamic nature of the loading, the vertical effective stress was expected to decrease due to increased porewater pressure (refer to Section 2.2.2.1). However, the increased vertical effective could have been caused by deformation of the impoundment that resulted in localized areas of volumetric expansion or by shear loading associated with strain along a potential failure surface.

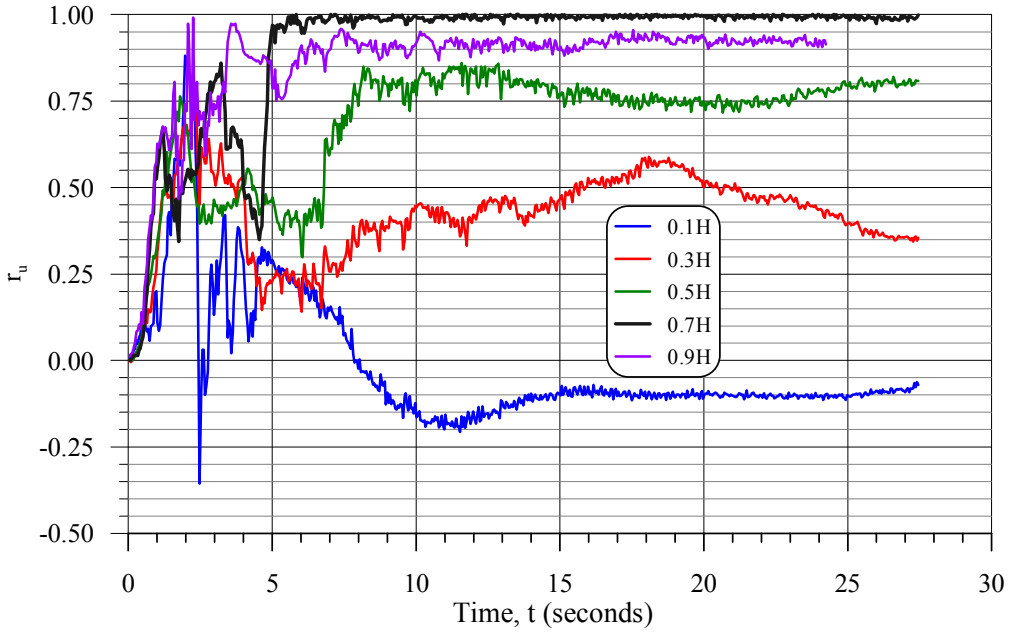

Figure 6-20 – Excess porewater pressure ratios, r_u developed in the tailings below the dike – conventional impoundment, Earthquake E3 (M_w=7.0).

6.4.5.4 Displacement of the Crest of the Dike

The horizontal and vertical displacements of the center of the crest of the dike (refer to Figure 6-6) during shaking are presented on Figure 6-21. The seismic loading resulted about 2.77 m of downstream displacement and 0.66 m of downwards displacement of the crest with almost all of the displacement occurring within the first 5 seconds of shaking.

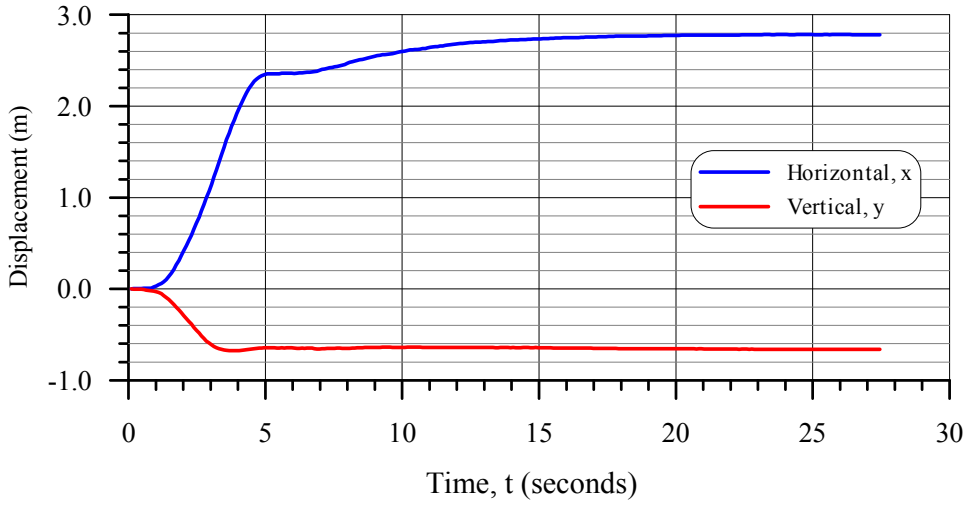

Figure 6-21 – Displacement of the crest of the dike during shaking – conventional impoundment, Earthquake E3 (M_w=7.0).

6.4.5.5 Conditions at the End of Shaking

The vertical effective stresses within the impoundment at the end of shaking are shown on Figure 6-22. The stresses at the end of shaking were considerably lower than those before shaking (Figure 6-7) as a result of the development of excess porewater pressures, particularly within the retained tailings. Note that below the lower portion of the dike, vertical effective stresses were not significantly lower than they were prior to shaking. Based on laboratory testing, Vaid et al. (2001) theorized that the presence of static shear stresses in contractive soil would facilitate shear stress reversals and thus excess porewater pressure generation (refer to Section 2.2.4). However, this was not apparent in the tailings below the lower portion of the embankment. From Figure 6-21 it is observed that there were significant downstream movement of the crest at the onset of shaking. This movement is indicative of volumetric expansion of the embankment which could have significantly reduced the development of excess porewater pressures in the underlying tailings.

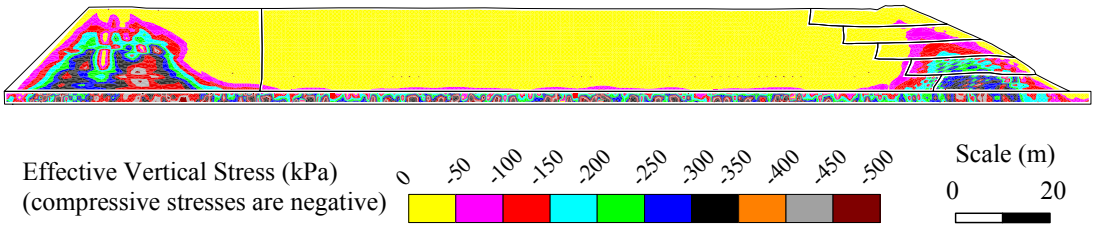

Figure 6-22 – Vertical effective stresses at the end of shaking – conventional impoundment, Earthquake E3 (M_w=7.0).

The porewater pressure within the impoundment at the end of shaking is presented on Figure 6-23. Compared to Figure 6-9 (the static porewater pressures), the porewater pressures within the tailings varied nearly linearly with depth, from 0 at the surface to 500 kPa at the bottom. The static porewater pressure at the bottom of the tailing was 196 kPa. As discussed above, the porewater pressures below the lower portion of the dike were not significantly higher than before shaking.

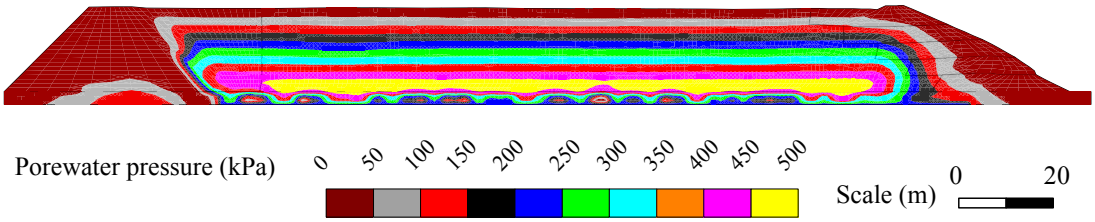

Figure 6-23 – Porewater pressures at the end of shaking – conventional impoundment, Earthquake E3 (M_w=7.0).

The horizontal displacement of the impoundment at the end of shaking is plotted on Figure 6-24. A maximum displacement of about 3 to 3.5 m developed at mid-height on the downstream slope. The extent of the displacement shows the importance of the width of the model as the material 100 m or more upstream appears to have some effect on the

stability of the impoundment. This is expected given the equivalent friction angle of the liquefied tailings is anticipated to be in the range of 2° to 4° (refer to Section 2.2.5.3). The displacement in the area of the dike appears to confirm the volumetric expansion below the dike discussed in Section 6.4.5.3 regarding the excess porewater pressure development below the embankment.

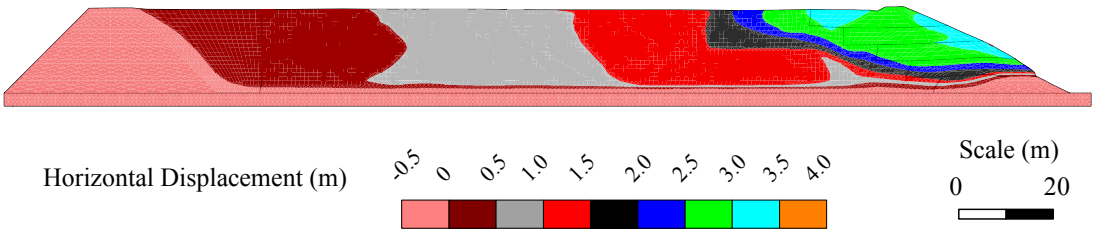

Figure 6-24 – Horizontal displacement at the end of shaking – conventional impoundment, Earthquake E3 (M_w=7.0).

The vertical displacement of the impoundment at the end of shaking is shown on Figure 6-25. The downward displacement of the lower crest of the dike and adjacent tailings coupled with the upwards displacement of the lower portion of the embankment confirms the rotational-type movement noted above. Within the retained tailings, vertical displacements were generally less than 0.25 m.

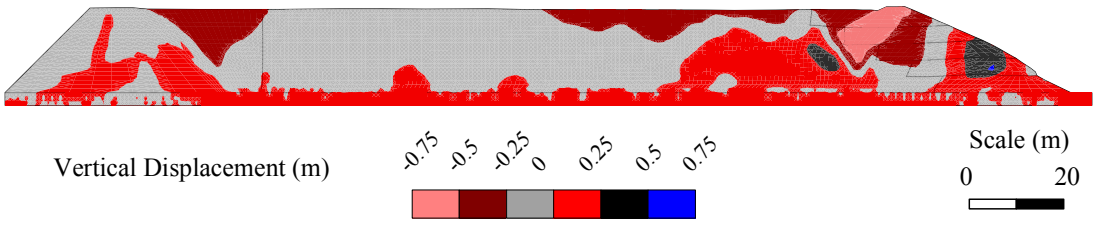

Figure 6-25 – Vertical displacement at the end of shaking – conventional impoundment, Earthquake E3 (M_w=7.0).

6.4.5.6 Summary of the Dynamic Analysis

The dynamic analysis of the conventional tailings impoundment with respect to Earthquake E3 (M_w=7.0) is summarized as follows:

a) The applied ground motion (horizontal accelerations) resulted in high amplification within the glacial till underlying the bedrock (F_a=1.902), severe damping within the retained tailings (F_a=0.169 and 0.124) and moderate amplification on the crest of the dike (F_a=1.237);
b) The severe damping of the horizontal accelerations in the tailings was the result of the generation of excess porewater pressures and high shear strains in the tailings, both of which would have resulted in significant damping;
c) Within 3 seconds of the start of shaking, there were high excess porewater pressures in the retained tailings, except for the tailings located below the dike where high excess porewater pressures were limited to the upper portion of the tailings;
d) The crest of the dike underwent horizontal and vertical displacements of 2.77 m downstream and 0.66 m downwards with most of the displacement occurring within the first 5 seconds of shaking;
e) From the 18th second to the end of shaking (t=27.5 seconds) there was no appreciable movement of the crest of the dike; and
f) The displacement pattern within the impoundment extended from just above the starter dike to the surface of the impoundment, 40 m upstream of the crest of the dike.

6.4.6 Post-shaking Analysis of the Conventional Impoundment – Earthquake E3 (M_w=7.0)

As noted in Section 6.1.2.1, the analysis of the post-shaking behavior was conducted by continuing the dynamic analysis by removing the applied ground motion from the bottom

of the model and applying a a horizontal velocity of 0. The hydraulic conductivity of all of the materials was increased by two orders of magnitude and the bulk modulus of water was reduced by one order of magnitude to decrease the processing time of each post-shaking simulation from 2,000 hours to 10 hours. The effect of increasing the hydraulic conductivities was to increase the flow rate for the dissipation of the excess porewater pressures and the effect of reducing the bulk modulus of water was to increase the processing speed. Through parametric analysis it was found that there was no significant effect on the deformation characteristics of the impoundment due the increase in the hydraulic conductivities or the reduction in the bulk modulus of water. Summaries of the parametric analyses of the effects of increasing the hydraulic conductivities and decreasing the bulk modulus of water are presented in Appendix H.

6.4.6.1 Excess Porewater Pressure Dissipation

The development of the excess porewater pressure ratio at various depths at location P1 (see Figure 6-6) in the impoundment (during and after Earthquake E3) is graphed on Figure 6-26. After the end of shaking (t=27.5 seconds) the excess porewater pressures that had developed within the impoundment during shaking dissipated through flow towards the surface and through the dike. Note that the rate of dissipation was effected by the increase in the hydraulic conductivities to acceleration the analysis. This applies to all of the post-shaking analyses and is not reflected in the time-scales used on the figures. The disturbances in the otherwise relatively smooth decreases in the excess porewater pressure were attributed to the random distribution of the hydraulic conductivities and $(N_1)_{60}$ values within the tailings and coarse tailings and to non-uniform excess porewater pressure development. As observed on the figure, the porewater pressures at location P1, as measured by the r_u values, reached a state reasonably close to a steady state condition by the 200^{th} second (172.5 seconds after the end of shaking).

The porewater pressures at many of the levels shown on Figure 6-26 did not return to their original values as the steady state condition was approached. The r_u values at 200 seconds varied between -0.3 to 0.25. As discussed previously, the difference between the

r_u values prior to shaking (that were typically near 0) and after the dissipation of excess porewater pressures was due to changes in the vertical effective stress as a result of stress redistribution and transfer, and non-uniform changes in the elastic properties of the tailings caused by shear strains.

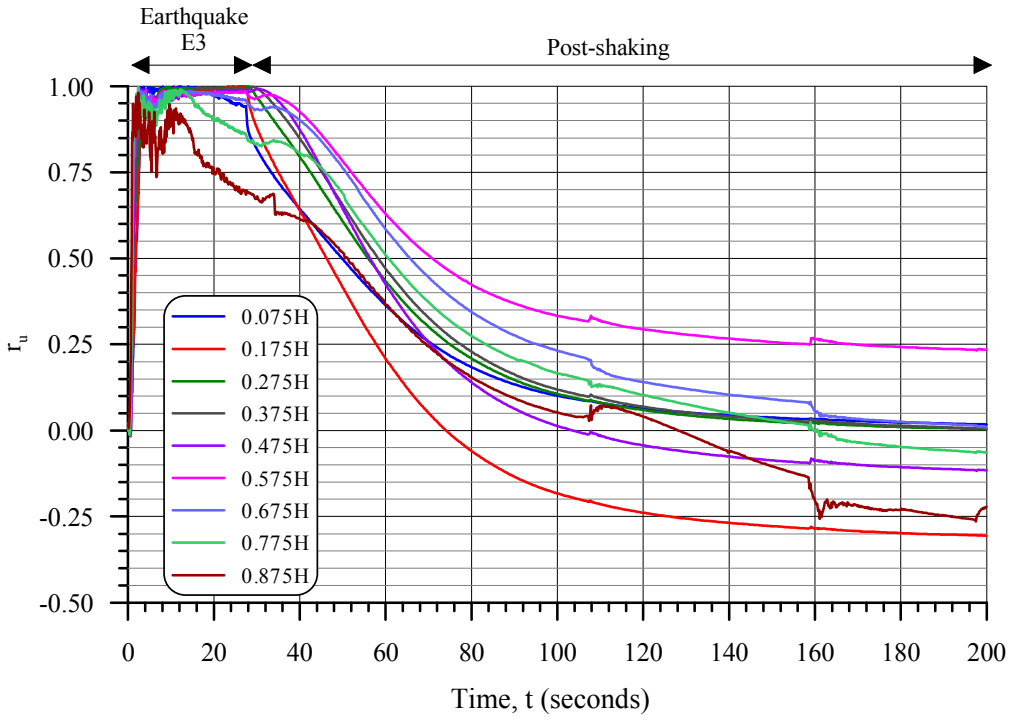

Figure 6-26 – Post-shaking dissipation of porewater pressure ratio at various depths at location P1 - conventional impoundment, Earthquake E3 (M_w=7.0).

6.4.6.2 Post-shaking Displacement of the Crest of the Dike

Figure 6-27 is a plot of the displacement of the center of the crest of the dike (refer to Figure 6-6) during and after shaking. As can be seen on the figure, the crest of the dike underwent no significant displacement during the post-shaking analysis.

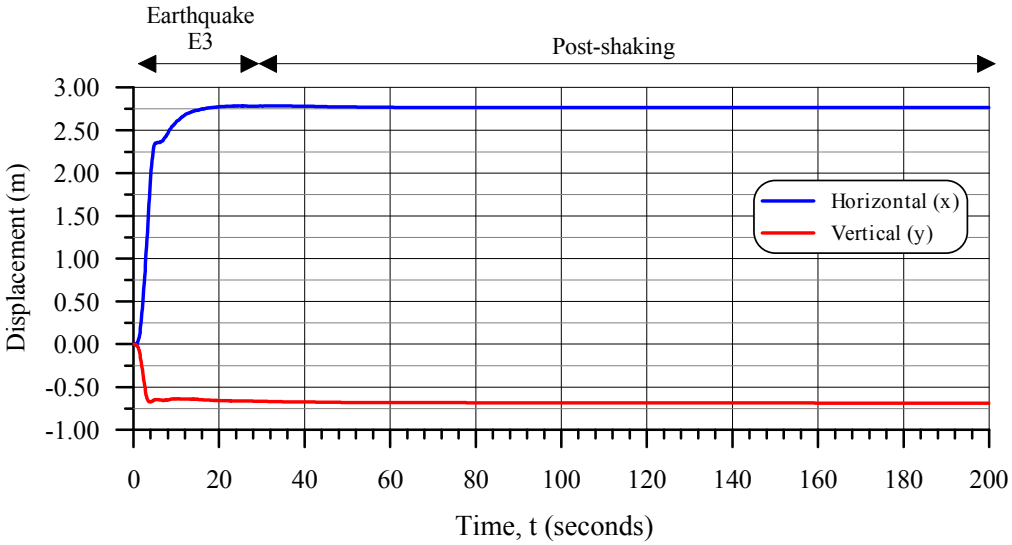

Figure 6-27 – Post-shaking displacements of the crest of the dike – conventional impoundment, Earthquake E3 (M_w=7.0).

6.4.6.3 Conditions at the End of the Post-shaking Analysis

Figure 6-28 presents the horizontal displacement of the impoundment at the end of the post-shaking analysis (t=200 s). By comparing this figure to the horizontal displacements at the end of shaking that are presented on Figure 6-24 (t=27.5 s), it can be observed that there was no appreciable horizontal movement of the impoundment during the post-shaking analysis, except for about 0.5 m of outwards horizontal displacement of the downstream slope. This displacement was associated with seepage forces acting on the slope.

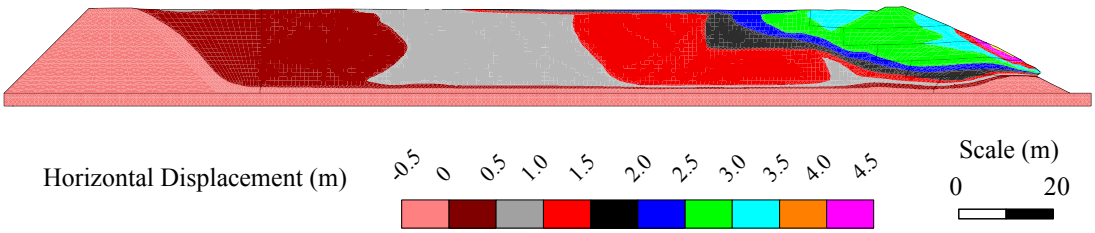

Figure 6-28 – Post-shaking horizontal displacement – conventional impoundment, Earthquake E3 (M_w=7.0).

The vertical effective stresses in the impoundment at the end of the post-shaking analysis (t=200 s) are plotted on Figure 6-29. Except for some minor stress concentrations in the lower portion of the impoundment, below the dike, the vertical effective stresses are very similar to those estimated during the static analysis of the impoundment as shown on Figure 6-7. As noted previously, the non-uniformity evident in the stress distribution is attributed to the heterogeneity in the material properties, stress redistribution, and the manner in which FLAC calculates the stress contours.

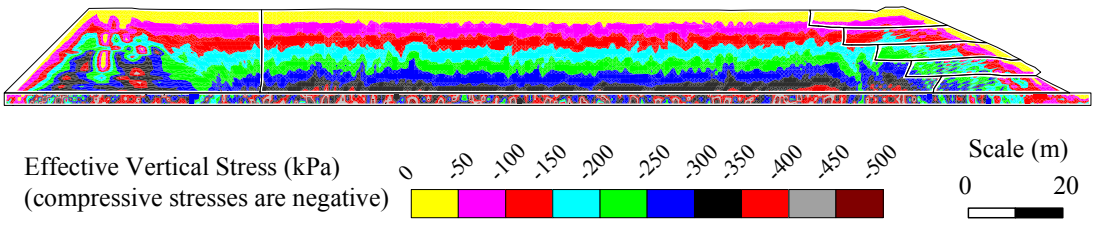

Figure 6-29 – vertical effective stresses at the end of the post-shaking analysis – conventional impoundment, Earthquake E3 (M_w=7.0).

The porewater pressures within the impoundment at the end of the post-shaking analysis are presented on Figure 6-30. Through comparison with the porewater pressures from the

static analysis (Figure 6-9), it can be seen that the porewater pressures in the impoundment have returned to a hydrostatic condition characterized by values varying linearly from 0 at the surface of the tailings to 196 kPa at the bottom of the tailings.

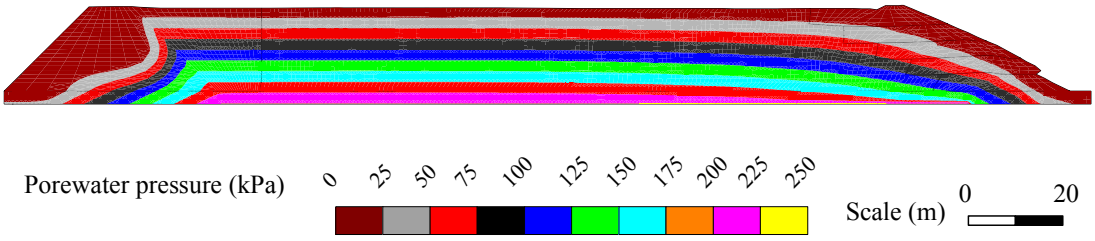

Figure 6-30 – Porewater Pressures at the end of the post-shaking analysis – conventional impoundment, Earthquake E3 (M_w=7.0).

6.4.6.4 Summary of the Post-shaking Analysis

During the post-shaking analysis, the excess porewater pressures developed during earthquake shaking dissipated and porewater pressures within the impoundment returned to hydrostatic conditions without significant additional deformation to the impoundment, except for 0.5 m of bulging of the downstream slope above the starter dike that was associated with seepage pressures.

6.4.7 Dynamic Analysis of the Reinforced Impoundment – Earthquake E3 (M_w=7.0)

The model of the reinforced impoundment was also subject to the dynamic loading used to simulate the occurrence of Earthquake E3. The effective stresses and porewater pressures in the reinforced impoundment at the onset of dynamic loading are presented in Section 6.4.4.2.

6.4.7.1 Site Response

PGA values at selected locations in the model were extracted from FLAC and are presented on Table 6-5 along with the associated amplification factors, F_a.

The PGA value from the top of bedrock (0.745 g) is somewhat greater than that of the input ground motion (0.659 g), indicating that there was a low level of amplification within the 1-m-thick layer of bedrock at the bottom of the model. The amplification factor on the top of the 2-m-thick layer of dense glacial till overlying bedrock was 1.681, indicating moderately high amplification of the horizontal accelerations within the glacial till. As noted previously, the amplification of the acceleration within the glacial till was due to the lower shear modulus of the glacial till relative to the bedrock and stiffness (shear modulus) of the glacial till being sufficient for the horizontal accelerations to pass through without inducing high shear strains that would lead to significant damping. The maximum shear strains measured in the glacial till during shaking were less than 0.001.

On the surface of the impoundment at location P1 (see Figure 6-6), which was situated in the tailings between waste rock inclusions, the amplification factor was 0.196. This value is indicative of very high damping of the horizontal acceleration (ground motion) within the tailings and is comparable to the values obtained from the surface of the conventional impoundment which were 0.169 and 0.124 at locations P1 and P2, respectively. The damping within the tailings is attributed to the relatively low stiffness of the tailings and the generation of excess porewater pressures in the tailings during shaking. The relatively low stiffness of the tailings and the generation of excess porewater pressures would, respectively, have reduced the shear modulus of the tailings and their ability to transmit shear stresses. At location P2, on the top of a waste rock inclusion, the amplification factor was 1.048. This value indicates that there was no significant amplification or damping of the horizontal accelerations at P2 relative to the top of bedrock. The value of F_a on the crest of the dike was 0.552 and indicates significant damping. This is significantly lower than the F_a recorded for the conventional impoundment which was 1.237 and indicated moderate amplification.

Within the impoundment, the maximum shear strains in the tailings and waste rock inclusions during shaking generally varied between 0.001 and 0.005. In the area of the dike, the maximum shear strains generally varied between 0.01 and 0.02.

Table 6-5 – Calculated amplification factors – reinforced impoundment, Earthquake E3 (M_w=7.0).

Location	Peak Horizontal Ground Acceleration, PGA (g)	Amplification Factor (F_a)
Top of bedrock	0.745	-
Top of glacial till	1.252	1.681
Surface of impoundment at P1	0.146	0.196
Surface of impoundment at P2	0.781	1.048
Crest of dike	0.441	0.552

The horizontal accelerations applied to the base of the model and recorded on the top of the bedrock and top of the of the glacial till (all at location P1) during the dynamic simulation are shown on Figure 6-31. There was no significant difference between the horizontal accelerations applied to the bottom of the model and those recorded on the top of the bedrock. Within the glacial till, there was significant amplification of the horizontal accelerations during the simulation.

The horizontal accelerations within the tailings at location P1 (see Figure 6-6) are presented on Figure 6-32. At 0.275H in the tailings, the amplitudes of the accelerations were 0.3 g for the first 12 seconds of shaking, 0.2 g from the 12th to the 23rd second of shaking and less than 0.15 g for the remainder of shaking. Compared to the horizontal accelerations on the bottom of the tailings (top of the glacial till) shown on Figure 6-31, horizontal accelerations at 0.275H were moderately dampened during the first 10 seconds

of shaking and slightly amplified during the remainder of shaking. The difference is attributed to the 1-m-thick layer of waste rock on the bottom of the impoundment. At 0.475H the ground motion was characterized by 4 seconds of horizontal acceleration amplitudes as great as 0.3 g followed by moderately high damping until the end of shaking that resulted in acceleration amplitudes of 0.1 g or less. A similar pattern occurred at 0.675H. However, at 0.675H the damping was more severe and after the 4th second the acceleration amplitudes were typically less than 0.1 g. At 0.875H the ground motion was characterized by 4 seconds of acceleration amplitudes of 0.1 g and severe damping for the rest of shaking that resulted in maximum acceleration amplitudes of less than 0.05 g.

The horizontal accelerations recorded at location P2 (see Figure 6-6) are shown on Figure 6-33. This location corresponds to the center of a waste rock inclusion. At 0.275H the horizontal accelerations where generally characterized by low to moderate damping throughout shaking with punctual occurrences of high amplification as great as 0.9 g occurring at the 1st and 3rd second of shaking. A similar pattern occurred at 0.475H, except that overall the ground motion was moderate to highly damped, with maximum accelerations at 1st and 3rd seconds as great as 0.7 g. At 0.675H, this pattern continued with high damping throughout shaking and maximum acceleration values of as much as 0.4 g for the first 3 seconds. Near the surface, at 0.875H, the ground motion was severely damped. For the first 4 seconds of shaking, the maximum amplitudes of the horizontal acceleration were 0.35 g; afterwards, they gradually declined to become less than 0.05 g by the end of shaking.

Comparing the horizontal accelerations at locations P1 and P2, it can be seen that the site responses at these locations are relatively similar, except for the isolated high amplitudes of acceleration at the 1st and 3rd second of shaking at location P2 and the response at P1 indicated somewhat more damping.

The horizontal accelerations recorded on the crest of the dike (refer to Figure 6-6 for the exact location) are plotted on Figure 6-34. The amplitudes of the acceleration were

relatively constant during shaking, generally varying between -0.2g and 0.25g, with frequent isolated peaks of as much as 0.4g in magnitude.

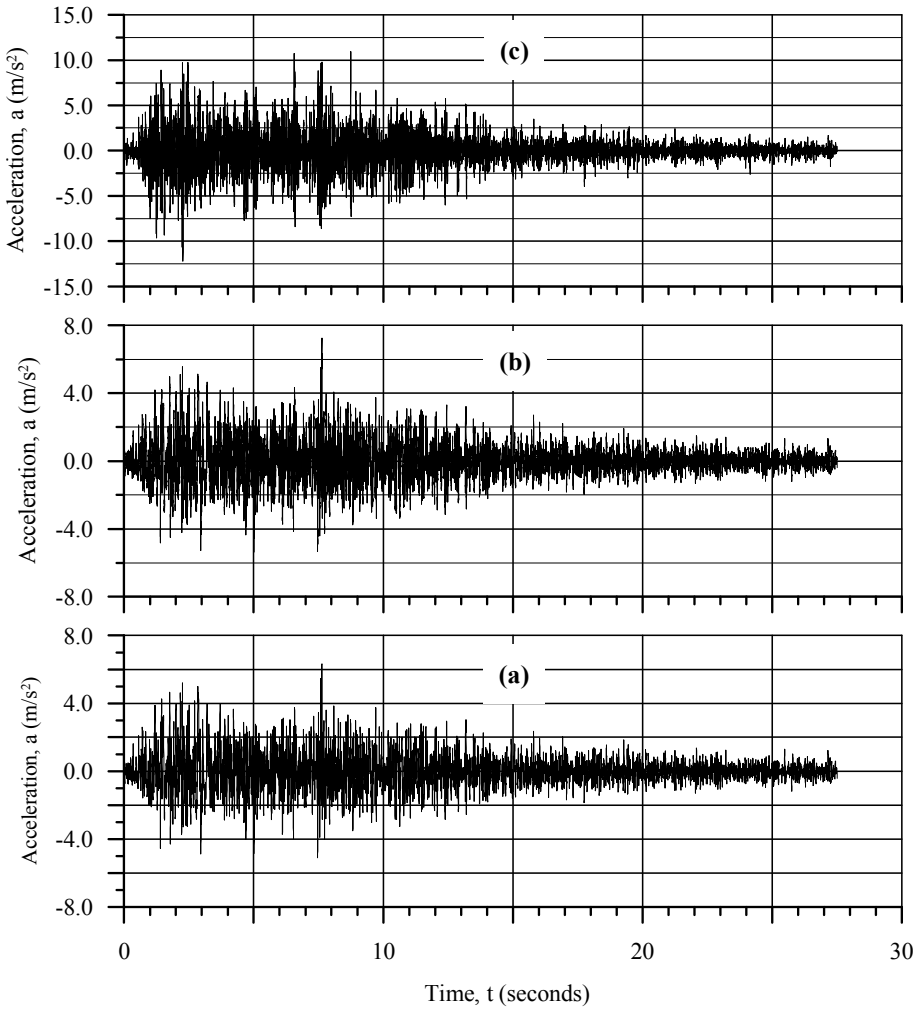

Figure 6-31 – Horizontal acceleration applied to the bottom of the model (a), and recorded on the top of bedrock (b) and on the top of glacial till (c) at location P1 – reinforced impoundment, Earthquake E3 (M_w=7.0).

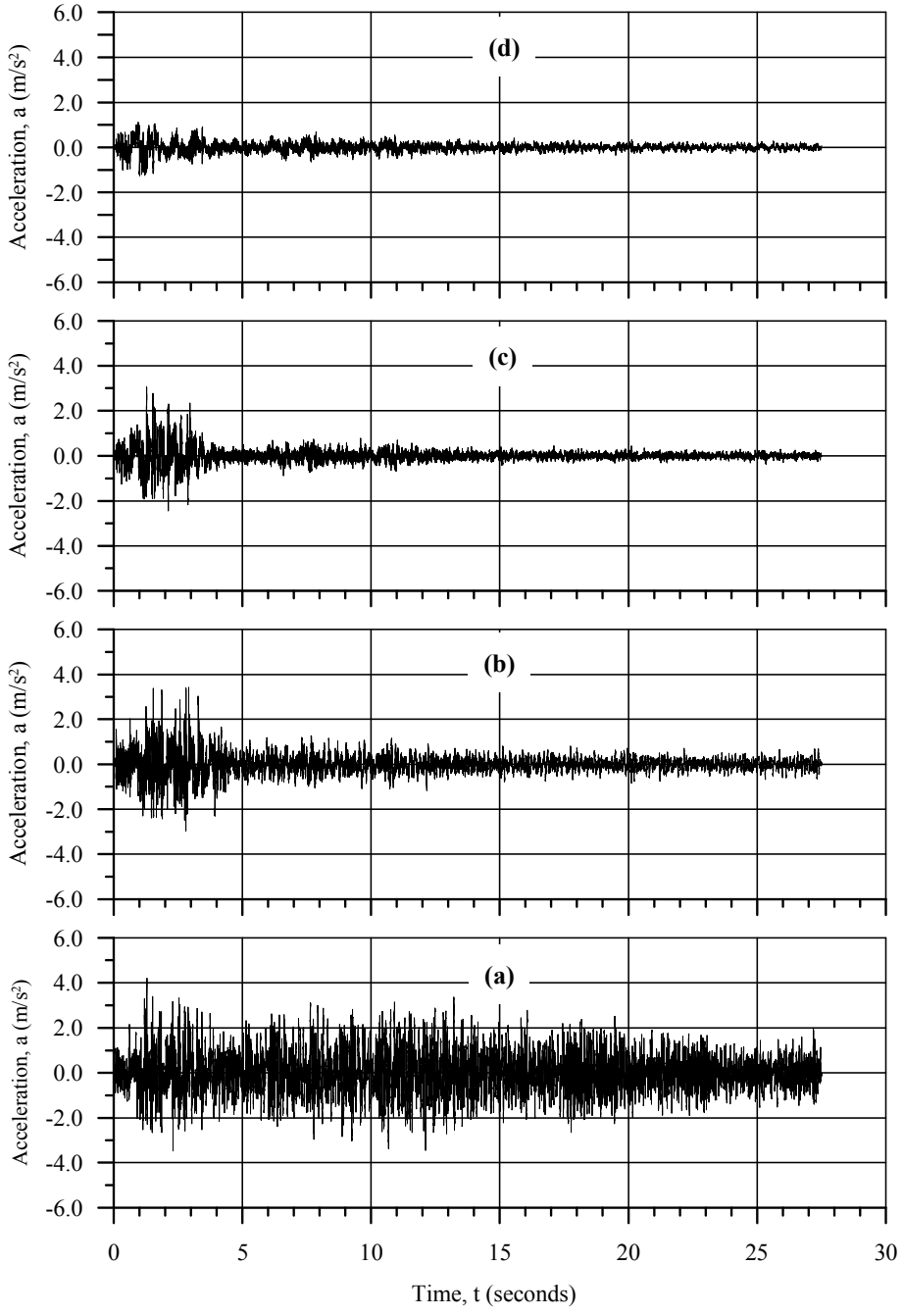

Figure 6-32 – Horizontal acceleration at 0.275H (a), 0.475H (b), 0.675H (c), and 0.875H (d) in the tailings at P1 – reinforced impoundment, Earthquake E3 (M_w=7.0).

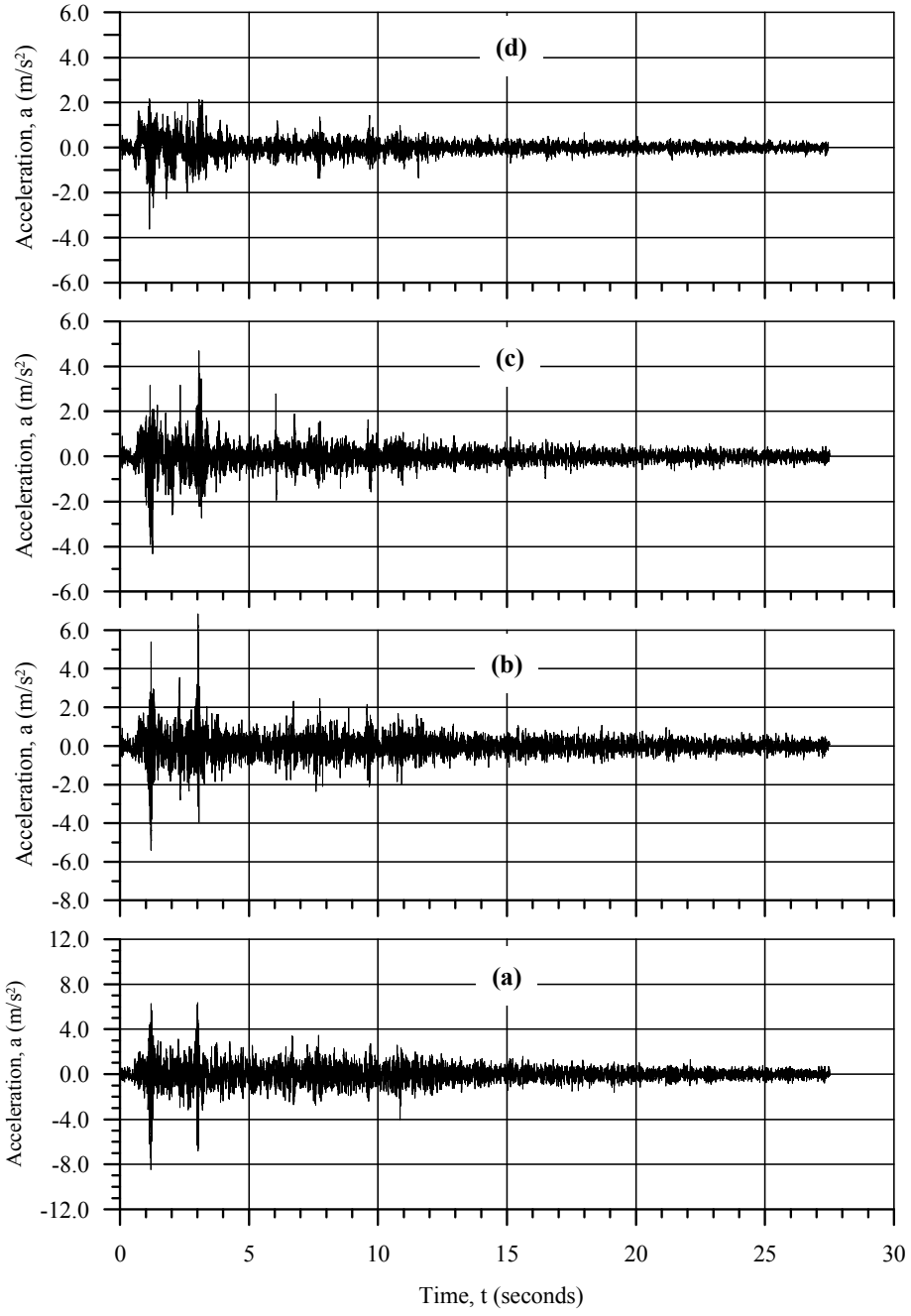

Figure 6-33 – Horizontal acceleration at 0.275H (a), 0.475H (b), 0.675H (c), and 0.875H (d) in the tailings at P2 – reinforced impoundment, Earthquake E3 (M_w=7.0).

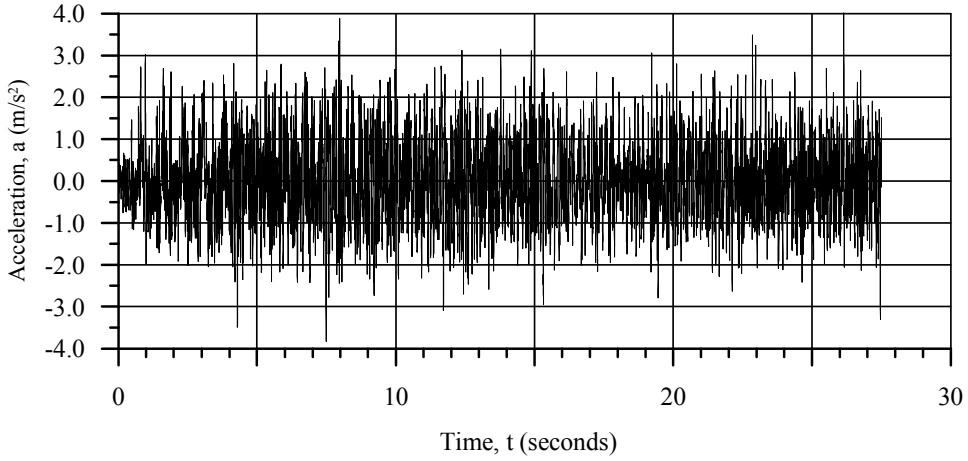

Figure 6-34 – Horizontal acceleration on the crest of the dike – reinforced impoundment, Earthquake E3 (M_w=7.0).

6.4.7.2 Cyclic Stress Ratios

The cyclic stress ratios developed in the tailings at location P1 are plotted on Figure 6-35. At the onset of shaking (t=0), the CSR values were 0.05 or less, indicating that there was no significant static shear stress within the tailings at this location. At 0.275H, 0.475H and 0.675H significant shear stresses were developed in the tailings during the first 4 seconds of shaking resulting in peak CSR values of 0.2, 0.17 and 0.075, respectively. After the 4th second of shaking, the CSR values declined and there were no significant shear stresses developed in the tailings. At 0.975H in the tailings, the CSR values varied between 0.15 and 0.075 for the first 1.5 seconds of shaking and then were characterized by amplitudes varying between -0.025 and 0.05 until the end of shaking.

The following observations are noted with respect to the development of the CSR in the reinforced impoundment:

a) The cyclic stress ratios developed in the tailings at P1 were significantly higher than the threshold level associated with the development of excess

porewater pressures and liquefaction, which is 0.04 as discussed in Section 2.3.1.1.

b) Figure 6-36 presents the cyclic stress ratios recorded at location P2 (in the center of a waste rock inclusion) during the dynamic analysis. The initial CSR values at the start of shaking varied between 0 and 0.1. These initial values indicate that the inclusion was under a low shear loading prior to shaking. Throughout shaking, there was significant variation in the CSR at the four levels shown on Figure 6-36. These variations included cyclic changes as well as overall increases and decreases in the value of the CSR with time. For example, at 0.275H, the CSR value was characterized by a general increase from 0.03 to 0.3 for the first 3 seconds of shaking, followed by variation between 0.2 and 0.3 until the 13th second, and then by a sudden decrease to 0.1. From there, the CSR value varied between 0.05 and 0.15 until the end of shaking (t=27.5 seconds).

c) The nature of the CSR development at location P2 indicates that the inclusions were subjected to significant shear stresses during the earthquake loading in addition to the direct dynamic loading of the earthquake that produced the 0.05 to 0.1 amplitude cyclic variations shown on Figure 6-36. It is inferred that the shear stresses within the inclusions were acting to resist the displacement of the tailings in the impoundment.

d) Comparing the CSR development at P1 (Figure 6-35) to that at P2 (Figure 6-36), indicates that there were no significant shear stresses developed in the tailings at P1 after the 3rd second of shaking, while significant shear stresses were developed in the waste rock inclusion at P2. The waste rock inclusions thus appears to be acting to retain the impoundment with respect to the shear loads imposed by the earthquake.

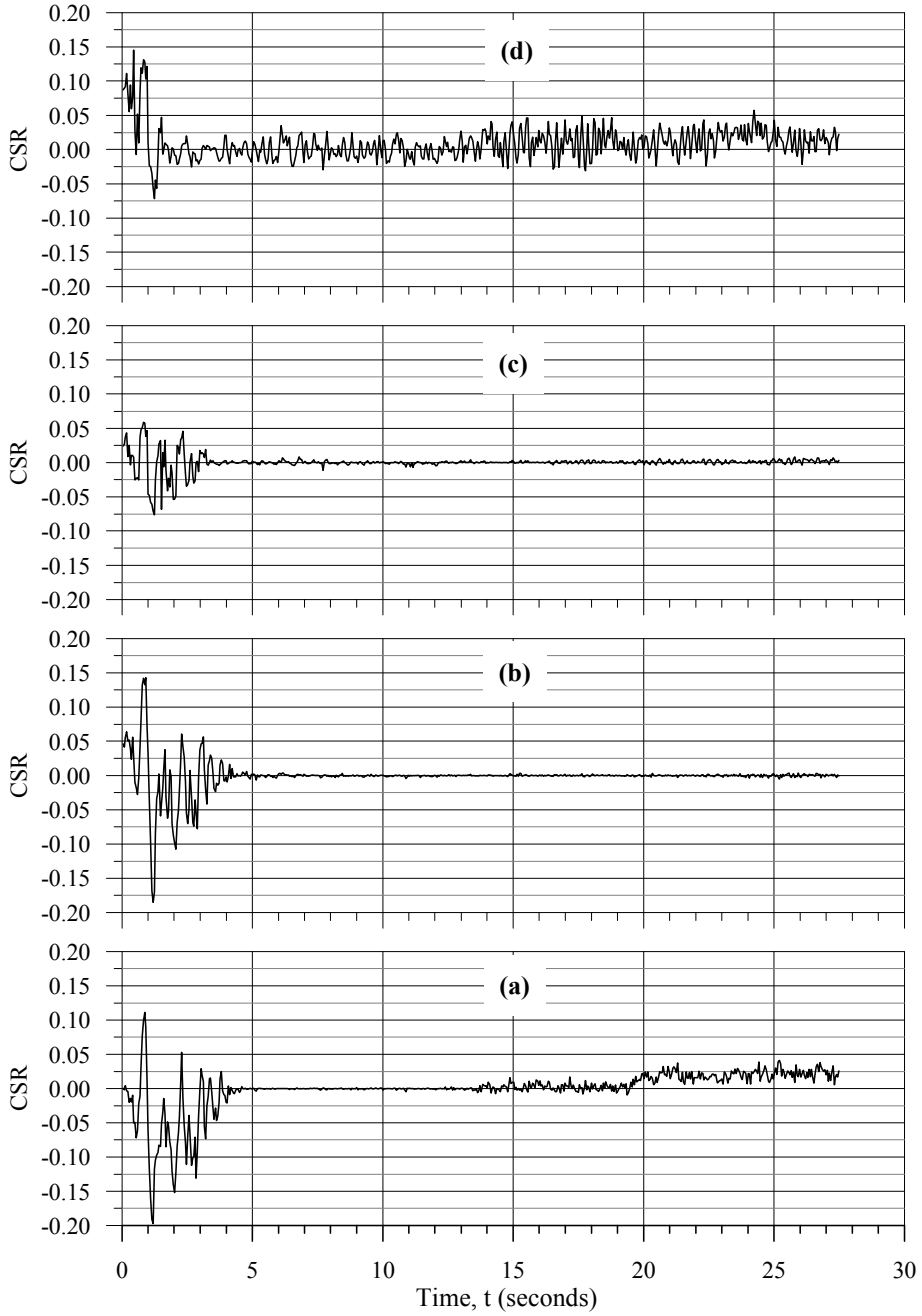

Figure 6-35 – Cyclic stress ratio at 0.275H (a), 0.475H (b), 0.675H (c), and 0.875H (d) in the tailings at P1 – reinforced impoundment, Earthquake E3 (M_w=7.0).

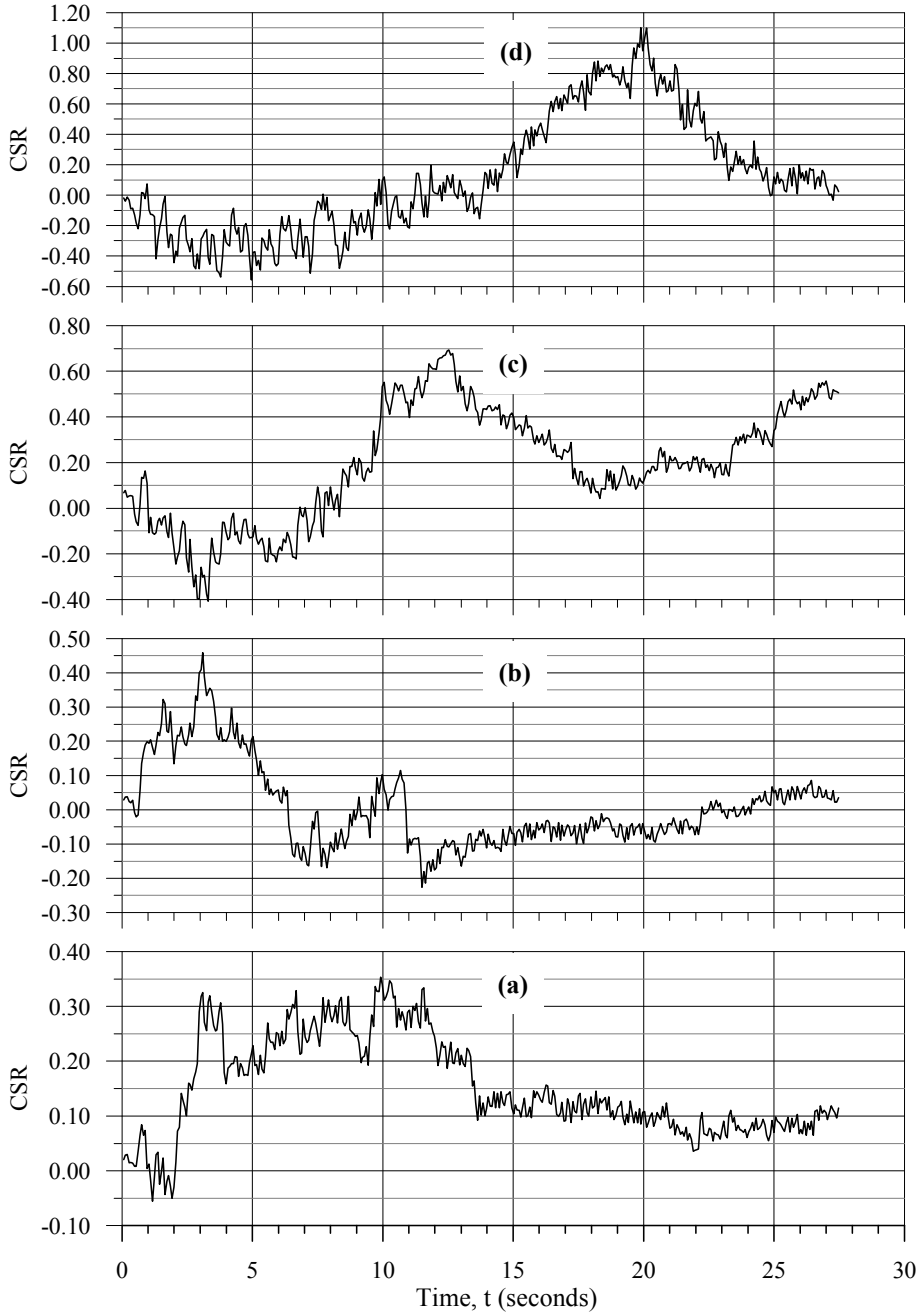

Figure 6-36 – Cyclic stress ratio at 0.275H (a), 0.475H (b), 0.675H (c), and 0.875H (d) in the impoundment at P2 – reinforced impoundment, Earthquake E3 (M_w=7.0).

6.4.7.3 Excess Porewater Pressure Development

The development of excess porewater pressures at location P1 in the impoundment was monitored using the excess porewater pressure ratio, r_u, calculated using Equation 4-2. The r_u values recorded at various depths in the tailings at P1 are shown on Figure 6-37. Within the first 3 seconds of shaking the porewater pressures within the tailings developed rapidly and reached values exceeding 0.85 at all levels, except at 0.075H. At this level, the value of r_u attained a maximum of 0.52 during the 3rd second and then declined rapidly to 0.06 by the 4th second; afterwards, it varied between -0.03 and 0.12 before becoming relatively stable between 0.1 and 0.15 for the remainder of shaking. At 0.175H, after reaching a peak value of 0.87 during the 6th second, the value of r_u declined gradually to 0.57 by end of shaking. At the other levels (0.275H though 0.875H), the excess porewater pressure ratio remained relatively constant or declined slightly after the 4th second, resulting in values varying between 0.85 to 0.97 at the end of shaking.

The decrease in the excess porewater pressures in the lower portion of the tailings (0.075H and 0.175H) is attributed to drainage caused by the presence of the 1-m-thick layer of waste rock on the bottom of the impoundment. The slight decreases in the r_u values at 0.275H and 0.875H are attributed to drainage through the surface of the impoundment.

The development of the excess porewater pressure ratio, r_u, at location P2 is illustrated on Figure 6-38. This location P2 coincides with the center of a waste rock inclusion.

Within 3 seconds of the start of shaking, there was a rapid increase in the r_u values at all levels, except near the surface of the impoundment (0.875H). At 0.875H there was a decline in the r_u value to -0.6 during the 2nd second of shaking. After the 3rd second, the variation in the excess porewater pressures at P2 was extremely random with time and depth. By the end of shaking, the r_u values varied from 0.1 at 0.175H to 0.9 at 0.775H. In general, the r_u values at the end of shaking were lower with depth.

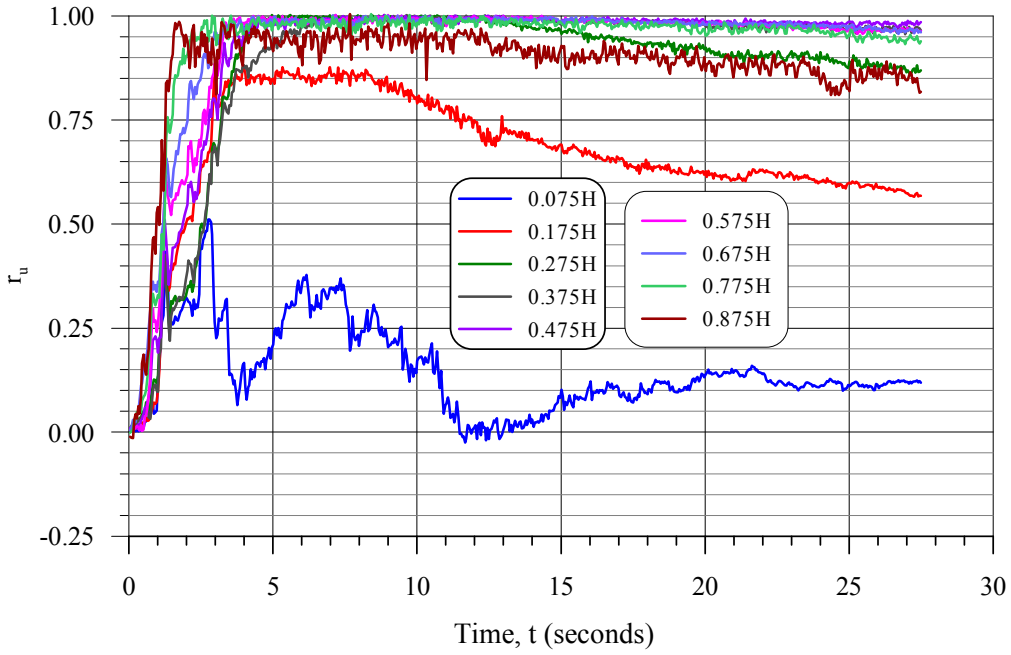

Figure 6-37 – Excess porewater pressure ratio development at various depths in the tailings at location P1 – reinforced impoundment, Earthquake E3 (M_w=7.0).

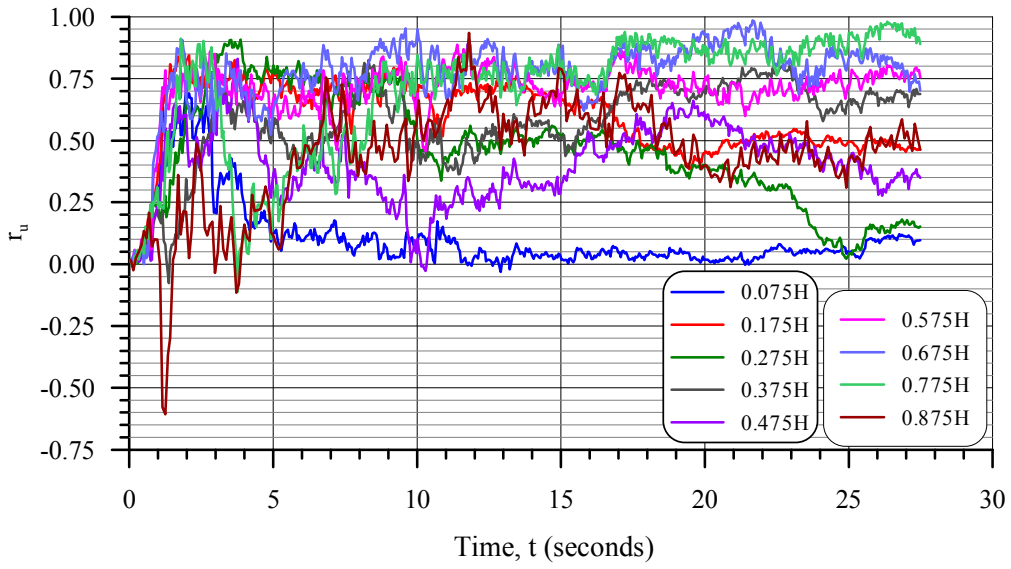

Figure 6-38 – Excess porewater pressure ratio development at various depths in the tailings at location P2 – reinforced impoundment, Earthquake E3 (M_w=7.0).

6.4.7.4 Displacement of the Crest of the Dike

The horizontal and vertical displacement of the crest of the dike during shaking is presented on Figure 6-39. Horizontally, the crest of the dike moved downstream 0.15 m within the first 3 seconds of shaking, and a maximum downstream displacement of 0.17 m occurred during the 11th second. By the end of shaking, the downstream displacement decreased to 0.12 m. Vertically, the crest moved downwards and reached a maximum displacement of 0.12 m during the 22nd second of shaking which remained constant to the end of shaking.

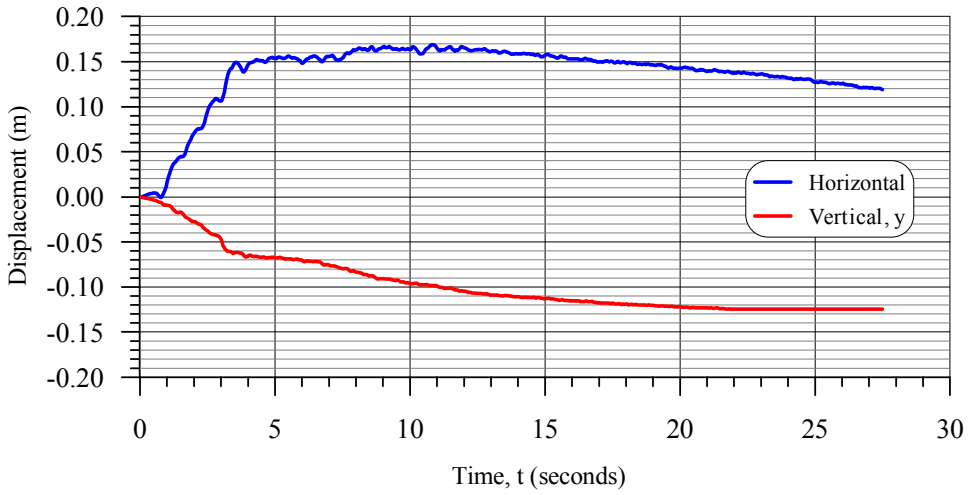

Figure 6-39 – Displacement of the crest of the dike during shaking - reinforced impoundment, Earthquake E3 (M_w=7.0).

6.4.7.5 Conditions at the end of Shaking

The vertical effective stresses within the impoundment at the end of shaking (t=27.5 s) are shown on Figure 6-40. The vertical effective stresses within the retained tailings and the uppermost portions of the waste rock inclusions varied from 0 to 50 kPa and were

significantly lower than those prior to shaking (see Figure 6-10) due to the development of excess porewater pressures. However, below the dike, the vertical effective stresses in the tailings are not significantly lower than prior to shaking. Generally, the vertical effective stresses within the tailings were greater near the 1-m-thick layer of waste rock on the bottom of the impoundment and near the waste rock inclusions, indicating that the presence of the waste rock inclusions reduced the development of excess porewater pressures in the tailings compared to the tailings in the conventional impoundment (Figure 6-23).

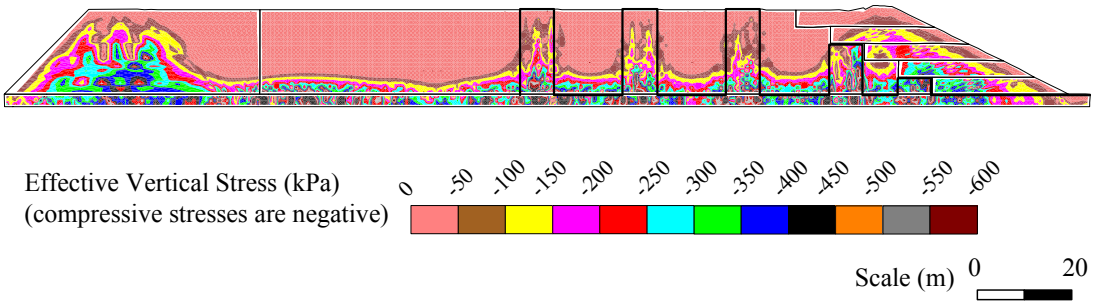

Figure 6-40 – Vertical effective stresses at the end of shaking – reinforced impoundment, Earthquake E3 (M_w=7.0).

The porewater pressure distribution in the impoundment at the end of shaking is presented on Figure 6-41. The loading of Earthquake E3 resulted in the development of porewater pressures of 450 kPa at 1/3 H in the tailings. The presence of the waste rock inclusions and waste rock on sides and bottom of the impoundment limited the development of excess porewater pressures in the immediate vicinity of the waste rock. In the three waste rock inclusions in the interior of the impoundment, porewater pressures in the lower zones decreased by 50 to 150 kPa during shaking. The decrease in the porewater pressure in the inclusions is similar to that experienced by dilative granular materials under monotonic loading (refer to Section 2.2.2.1 and Figure 2-7). The shear

loading in the inclusions from the impounded tailings during shaking as indicated by the CSR development at P2 (see Figure 6-36). Referring back to the dynamic analysis of the conventional impoundment, Figure 6-24 presents the horizontal displacement of the impoundment due to Earthquake E3, showing that there was a general movement of the impounded tailings towards the downstream. The earthquake loading would have initiated that same type of movement in the reinforced impoundment, except for the shear resistance of the inclusions. The shear loading on the inclusions produced a decrease in the porewater pressure within the waste rock inclusions.

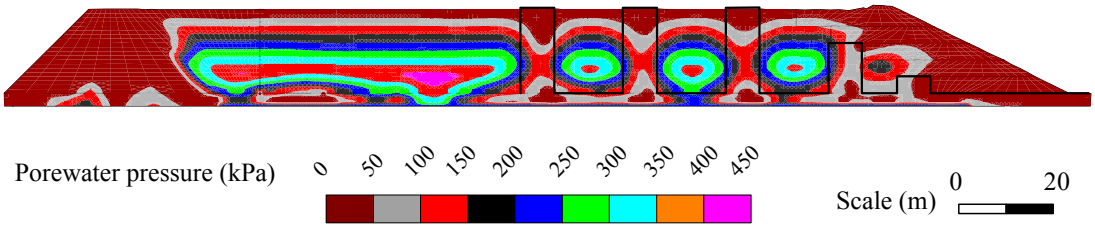

Figure 6-41 – Porewater Pressures at the end of shaking – reinforced impoundment, Earthquake E3 (M_w=7.0).

The horizontal displacements of the impoundment at the end of shaking are presented on Figure 6-42. Although the horizontal displacement inside of the impoundment was minimal, horizontal displacements in the zone below the downstream slope was significant and varied from 0 to 0.25 m and on the face of the slope were as great as 0.75 m. However, the horizontal displacement of the crest of the dike was limited to 0.12 m (see Figure 6-39). The greatest horizontal displacements occurred on the surface of the tailings immediately upstream of the dike. In this area, the tailings formed a small bulge on the upstream slope of the dike for a distance of less than 1.75 m.

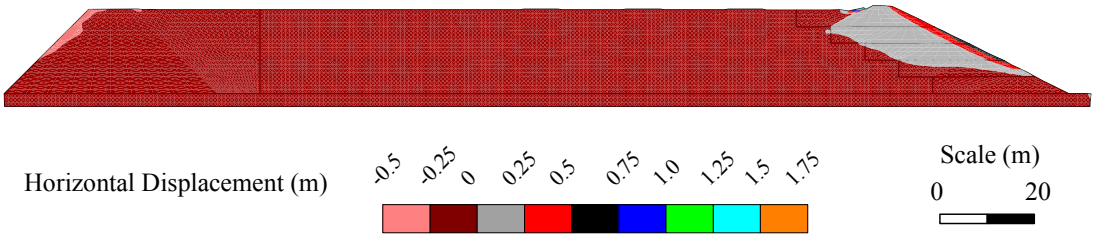

Figure 6-42 – Horizontal displacements at the end of shaking – reinforced impoundment, Earthquake E3 (M_w=7.0).

6.4.7.6 Summary of the Dynamic Analysis

The dynamic analysis of the reinforced impoundment under the loading of Earthquake E3 (M_w=7.0) is summarized as follows:

a) The site response to the dynamic loading was characterized by high amplification in the 2-m-thick layer of glacial till overlying bedrock (the value of F_a on the top of glacial till was 1.681), moderately high to severe damping in the tailings at location P1 with the degree of damping increasing towards the surface of the impoundment (F_a was equal to 0.196 at the surface),and moderate to high damping at location P2 which coincided with the center of a waste rock inclusion. An F_a value of 1.048 was calculated for the surface at P2. However, this was an isolated peak and was not representative of the entire ground motion (refer to Figure 6-33d).

b) The damping of the horizontal accelerations at locations P1 was the result of high shear strains and excess porewater pressure development in the tailings.

c) The CSR development at locations P1 and P2 indicates that there was some shear loading of the tailings at P1 for the first 4 seconds of shaking, but that after this period, the shear loads within the impoundment (in the area of the inclusions) were almost entirely resisted by the inclusions (refer to Figures 6-35 and 6-36).

d) At location P2 (the center of a waste rock inclusion), the pattern of r_u development indicated significant reduction in vertical effective stresses during shaking (Figure 6-38). The cause for this will be discussed in Section 6.4.8.1.

e) The vertical effective stresses at the end of shaking (Figure 6-40) suggest that liquefaction developed in the impounded tailings between and upstream of the waste rock inclusions but did not develop in the lower 3 m of the tailings due to drainage provided by the waste rock lining the bottom of the impoundment.

f) Porewater pressures within the lower sections of the waste rock inclusions decreased by a significant amount during shaking (Figure 6-41). This was attributed to the shear stress of the waste rock under the loading of the impounded tailings.

g) The crest of the dike displaced 0.12 m downstream and 0.12 m downwards as a result of the dynamic loading with most of the downstream movement occurring within the first 4 seconds of shaking and the downwards movement being more gradual. The horizontal displacement of the crest peaked at 0.17 m in the downstream direction during the 10^{th} second of shaking and then decreased to 0.12 m by the end of shaking (Figure 6-39).

6.4.8 Post-shaking Analysis of the Reinforced Impoundment – Earthquake E3 (M_w=7.0)

The post-shaking analysis of the reinforced impoundment was completed using the same methods used for the conventional impoundment. Briefly, the hydraulic conductivities of all of the materials were increased by two orders of magnitude to increase the rate of dissipation of the excess porewater pressures and the bulk modulus of water was decreased to 2.2×10^{-5} kPa to increase the controlling time-step. The combined effect was to reduce the time required to complete the post-shaking analysis from 2,000 to 10 hours.

6.4.8.1 Excess Porewater Pressure Dissipation

Changes in the effective vertical stress and porewater pressure during the post-shaking analysis at various depths at locations P1 and P2 are presented on Figures 6-43 and 6-44 using the excess porewater pressure ratio, r_u, that was calculated in FLAC using Equation 4-2. Recall that the rate of dissipation of the excess porewater pressures was accelerated by the increase in the hydraulic conductivities of the model during the post-shaking analysis.

Immediately after the end of shaking (the start of the post-shaking analysis), t=27.5 s, the excess porewater pressures developed at P1 and P2 during shaking began to dissipate rapidly. Generally, the rate of dissipation was more rapid at P1 (within the tailings) than at P2 (within a waste rock inclusion). The reasons for the more rapid dissipation in the tailing were: 1) the horizontal conductivity of the tailings (2.25×10^{-4} m/s) was greater than that of the waste rock inclusions (1×10^{-4} m/s); and 2) higher excess porewater pressures were recorded at P1 than P2 resulting in a greater hydraulic head.

By the 100^{th} second (72.5 seconds after the end of shaking), the porewater pressures at P1 and P2 reached states reasonably close to the condition of steady state flow, except near the surface (0.775H and 0.875H) at both P1 and P2, where the r_u values continued to decrease with time until 140 seconds and 200 seconds, respectively.

As previously noted, Equation 4-2 which was used to calculate r_u considers changes in the effective stress as well as the porewater pressure. At t=200 s, the values of r_u varied from -0.25 to 0.12 at P1 and from -0.8 (0.875H) to 0.53 (0.175H) at P2. These values indicate that there was a considerable redistribution of stresses within the impoundment during the dynamic and post-shaking phases of the analysis, particularly in the vicinity of the waste rock inclusions. Recall that the static vertical effective stresses within the reinforced impoundment were non-uniform and reflected stress transfer from the tailings to the stiffer waste rock inclusion as shown on Figure 6-10. The dynamic loading significantly reduced this stress transfer in addition to causing a redistribution of stresses.

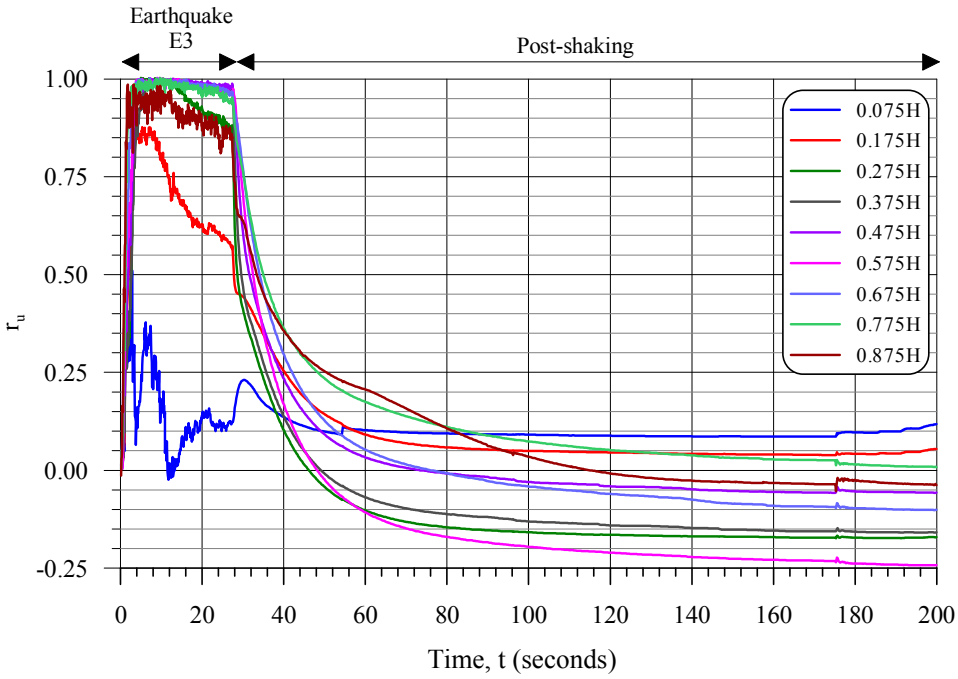

Figure 6-43 – Post-shaking development of the porewater pressure ratio at various depths at location P1 – reinforced impoundment, Earthquake E3 (M_w=7.0).

The development of porewater pressures at various levels at P2 (the center of a waste rock inclusion) in the reinforced impoundment are presented on Figure 6-44. During shaking, from t=0 to t=27.5 s, the porewater pressures declined and approached zero, and then increased somewhat, but not enough to return to hydrostatic pressure levels (t=0 s). Following shaking, the porewater pressures increased rapidly to exceed the hydrostatic pressures. These increases are attributed to the flow of excess porewater from the tailings surrounding the inclusion and were followed by gradual dissipation of the porewater pressure to hydrostatic levels.

Comparison of Figures 6-43 and 6-44 indicates that the changes in the excess porewater pressure ratios values between the start of shaking (t=0 s) and the end of the post-shaking analysis, were due to changes in the vertical effective stress (both decreases and

increases) that cannot be attributed to the changes in the porewater pressure. The changes in the vertical effective stress are attributed to stress redistribution within the impoundment.

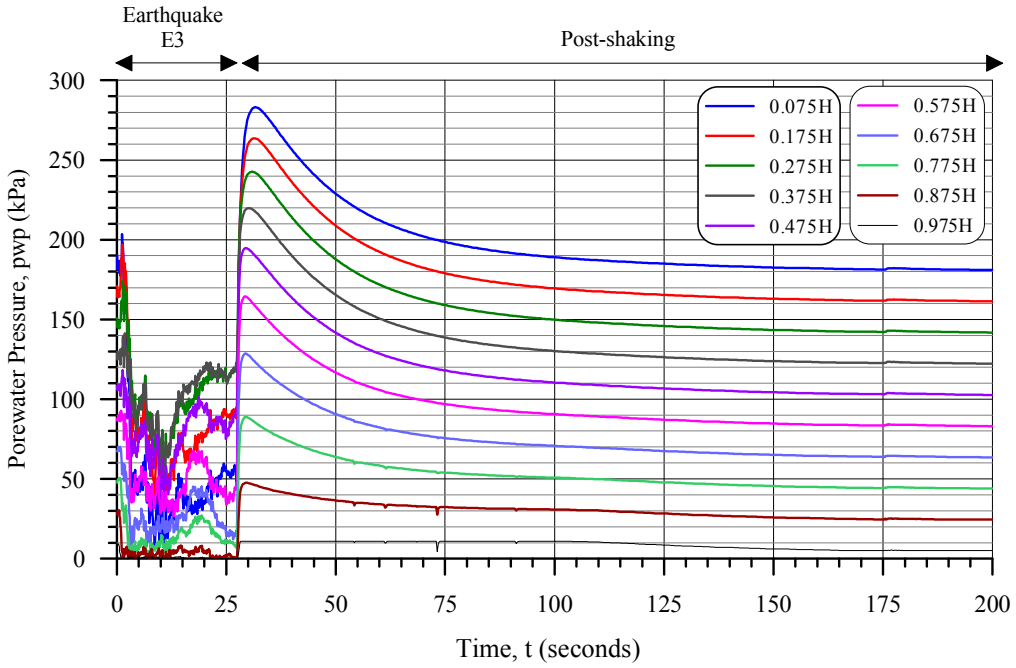

Figure 6-44 – Porewater pressure development at various depths
in the tailings at location P2 – reinforced impoundment, Earthquake E3 (M_w=7.0).

6.4.8.2 Displacement of the Crest of the Dike

The horizontal and vertical displacement of the crest of the dike during the dynamic and post-shaking phases of the analysis are shown on Figure 6-45. The exact point on the crest where the displacements were recorded is shown on Figure 6-6. There was no significant displacement of the crest during the post-shaking analysis.

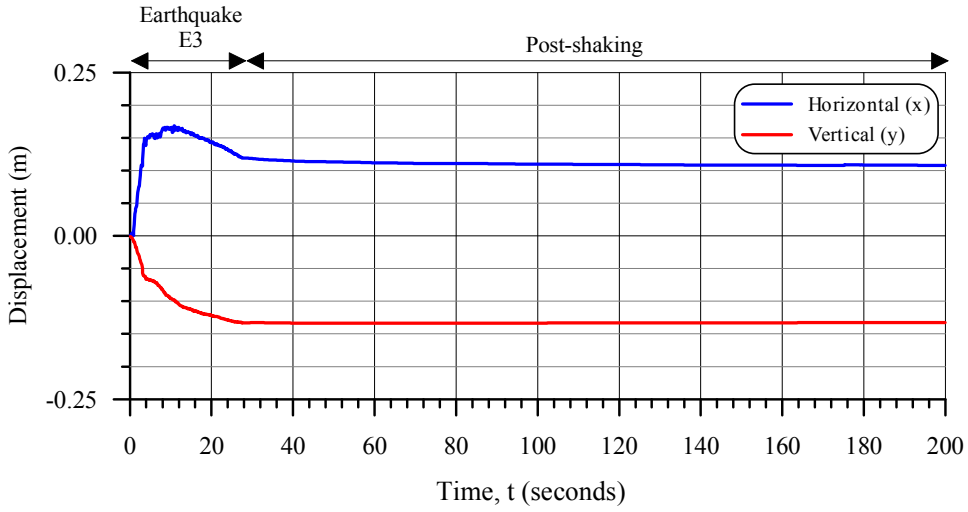

Figure 6-45 – Post-shaking displacements of the crest of the dike – reinforced impoundment, Earthquake E3 (M_w=7.0).

6.4.8.3 Conditions at the End of the Post-shaking Analysis

Contours of the horizontal displacement of the impoundment at the end of the post-shaking analysis are provided on Figure 6-46. By comparing this figure to that of the horizontal displacements of the impoundment after shaking (Figure 6-42) it is observed that horizontal displacements during the post-shaking analysis were limited to 0.25 m of bulging on the downstream slope of the dike and minor movement of the impounded tailings on the upstream slope of the dike.

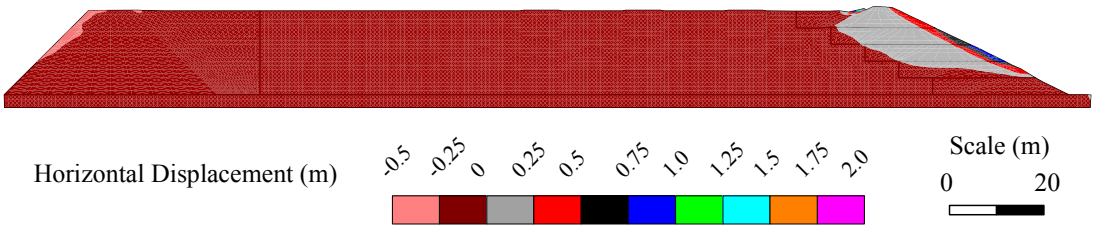

Figure 6-46 – Post-shaking horizontal displacement – reinforced impoundment, Earthquake E3 (M_w=7.0).

The static vertical effective stresses in the impoundment at the end of the post-shaking analysis are contoured on Figure 6-47. Within the impounded tailings, the magnitude of the vertical effective stresses varied from 0 at the surface to between 300 and 350 kPa at the bottom of the tailings. A similar range of stress occurred within the waste rock inclusions. However, there were zones of stress concentration as great as 400 kPa in magnitude in the lower zones of the waste rock inclusions within the impoundment and throughout the waste rock inclusions below the dike.

The pronounced stress difference between the inclusions and tailings that was observed as a result of the static analysis (see Figure 6-10) and attributed to stress transfer, was significantly lower after the post-shaking analysis. The vertical effective stresses in the lower portions of the inclusions were generally 50 to 100 kPa lower after the post-shaking analysis than after the static analysis, while those in the lower portion of the tailings in the vicinity of the inclusions were typically 50 kPa greater.

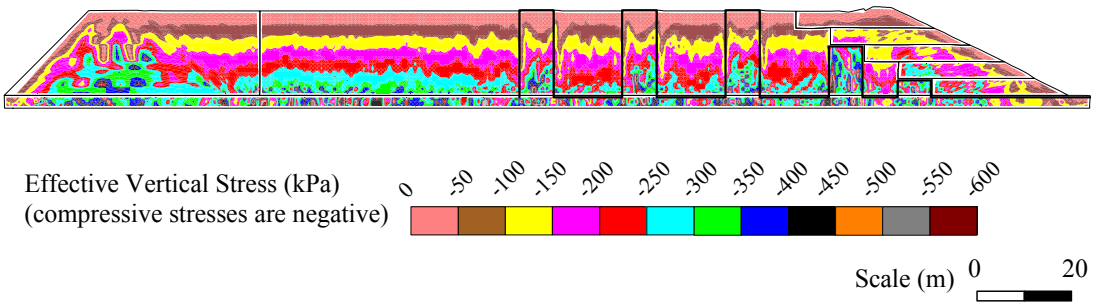

Figure 6-47 – Vertical effective stresses at the end of the post-shaking analysis – reinforced impoundment, Earthquake E3 (M_w=7.0).

Figure 6-48 presents contours of the porewater pressure within the impoundment as a result of the post-shaking analysis. Within the interior of the impoundment, porewater

pressures varied from 0 at the surface to 196 kPa at the bottom of the tailings and 226 kPa at the bottom of the model, indicating hydrostatic conditions and matching the conditions determined by the static analysis (refer to Figure 6-12).

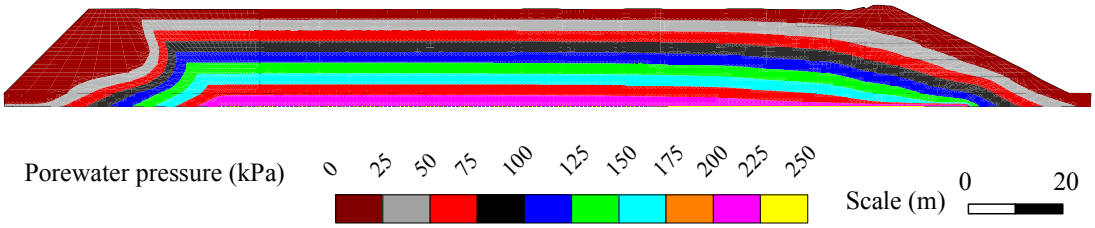

Figure 6-48 – Porewater Pressures at the end of the post-shaking analysis – reinforced impoundment, Earthquake E3 (M_w=7.0).

6.4.8.4 Summary of the Post-shaking Analysis

During the post-shaking analysis, the excess porewater pressures developed in the impoundment during the dynamic analysis, dissipated and returned to hydrostatic conditions without significant deformation of the impoundment. However, there was 0.25 m of additional outwards displacement on the downstream slope of the dike due to seepage pressures.

6.4.9 Comparison of the Responses of the Conventional and Reinforced Impoundments – Earthquake E3

Various aspects of the responses of the conventional and reinforced impoundments subjected to Earthquake E3 are described in the previous two sections. Given that the only difference between the impoundments was the presence of the waste rock inclusions and the 1-m-thick layer of waste rock on the bottom and sides of the impoundment, and that the same earthquake loading was applied to the impoundments, the differences in their responses was attributed to the presence of the waste rock inclusions. The responses

of the conventional and reinforced impoundments are summarized on Table 6-6. More detailed results are provided in Appendix H.

Table 6-6 – Summary of the responses of the conventional and reinforced impoundments (Earthquake E3, M_w=7.0).

Aspect	Conventional Impoundment	Reinforced Impoundment
Site response	High to severe damping on surface at P1 and P2.	High to severe damping on surface at P1 and P2, but less than in conventional impoundment.
CSR development	At P1 – CSR of 0.1 to 0.15 developed in first 3 seconds of shaking, with significant CSR for duration of shaking. Below dike – Significant CSR values developed in lower portion of tailings throughout shaking.	At P1 (tailings) – CSR of 0.05 to 0.2 developed in first 4 seconds of shaking, with significant CSR for duration of shaking. At P2 (inclusion) – Considerable shear loading from impoundment.
Excess porewater pressure development	At P1 – Rapid development of r_u to values near 1.0. Below dike – Significant variation in r_u values during shaking.	At P1(tailings) – Rapid development of r_u to values near 1.0, except in lower portion due to drainage. At P2 (inclusion) – Significant variation during shaking with r_u values at the end of shaking varying between 0.1 and 0.9.
Deformation and shear strains	Crest of dike displaced 2.77 m outwards and 0.66 m downwards during shaking. Shear strains in impoundment an order of magnitude higher than with inclusions.	Crest of dike displaced 0.75 m outwards and 0.12 m downwards during shaking. Shear strains in impoundment an order of magnitude lower than without inclusions.
Post-shaking behavior	No significant deformation of impoundment during dissipation of excess porewater pressures.	Dissipation of excess porewater pressures was more rapid with inclusions and there was no significant deformation during dissipation.

The results indicate that the presence of the waste rock inclusions altered the dynamic behavior of the conceptual impoundment by:

a) Providing a stiffer response to the dynamic loading (maximum shear strains in the impoundment were reduced by an order of magnitude);
b) Resisting the shear loading of the impoundment;
c) Reducing the generation of excess porewater pressures to a limited extent in tailings by providing drainage; and
d) Reducing the deformation of the dike, including the displacement of the crest, by an order of magnitude.

6.4.10 Analyses of the Conceptual Impoundment - Earthquake E1 (M_w=6.5)

The models of the conventional and reinforced conceptual impoundments were analyzed using Earthquake E1 which simulated a moment magnitude 6.5 event with a PGA of 0.229g (on hard rock) and a duration of 25 seconds.. The results are summarized in this section. Additional details are contained in Appendix H. The static conditions are presented in Sections 6.4.4.1 and 6.4.4.2 for the conventional and reinforced models, respectively.

6.4.11 Summary of Numerical Analyses

The models of the conceptual tailings impoundment, with and without waste rock inclusions, were subjected to five earthquake loads of increasing intensity (Earthquakes E1 through E5) and their behavior during and after shaking was evaluated with respect to the site response, cyclic stress ratio development, the generation and dissipation of excess porewater pressures, the effective stresses and displacements at the end of shaking and after the dissipation of excess porewater pressures. This section provides a brief summary of the findings of the numerical analyses.

6.4.11.1 Site Response Analyses

The peak horizontal accelerations, PGA, amplification factors, F_a, of the conceptual impoundments are summarized on Table 6-8. As noted, the amplification factors may be used to evaluate the site response of the impoundments. However, a more accurate evaluation can be developed using the accelerograms (records of horizontal acceleration) provided in Appendix H.

Based on the amplification factors in Table 6-8 the site responses of the impoundments were summarized as follows:

In the conventional and reinforced impoundments, application of the earthquake loads resulted in amplification factors on the top of the 2-m-thick layer of glacial till overlying bedrock that varied from 1.213 to 2.068 and tended to be slighter higher for the reinforced impoundment relative to the conventional impoundment. The amplification was attributed to the glacial till being less stiff (lower shear modulus) than the bedrock but having sufficient stiffness to withstand the dynamic loading without developing excessive shear strains that would have produced substantial damping. The factors for the reinforced impoundment were on average 18% greater than those for the conventional impoundment, this difference is not significant given the variation typical in site responses and the punctual nature of PGA values, and is attributed to the presence of the waste rock inclusions which would have affected the response of the underlying glacial till by that added shear resistance. Finn & Wightman (2003) recommend a Foundation Factor, F (amplification factor) of 1.0 for "dense and very dense coarse-grained soils from 0 to 15 m deep." However, that recommendation is generic and not site-specific. Site-specific response analyses are considered more applicable than generic site amplification factors (Kramer, 1996; Finn & Wightman, 2003).

The amplification factors on the surface of the conventional impoundment varied from 0.088 (E5 at P2) to 0.402 (E1 at P2) and generally decreased with increasing intensity of the earthquake loading. In the conventional impoundment, there was no significant

difference in the amplification factors at P1 and P2. This was expected given that more intense loadings were expected to generate larger shear strains and thus greater damping within the tailings. The damping in the tailings was attributed to shear strains and to the generation of excess porewater pressure during shaking. Finn & Wightman (2003) recommend site-specific response analyses for sites subject to liquefaction, no amplification factors are provided. Significant excess porewater pressures were developed in all of the dynamic analyses conducted and the associated reduction in the vertical effective stresses was generally greater than 70% and often greater than 90%. This would have resulted in very high to severe damping of the horizontal accelerations that are transmitted through shear stress.

In the reinforced impoundment, P1 was located in the tailings between waste rock inclusions and the amplification factors at the surface varied from 0.196 to 0.537, indicating moderate to high damping. The site response at this location was dominated by shear strain and excess porewater development in the tailings, but would have been significantly affected by the presence of the waste rock inclusions as the relatively stiffer inclusions would have reduced the shear strain in the tailings. This is borne out by the fact that the amplification factors at P1 in the reinforced impoundment were on average 64% higher than those at P1 in the conventional impoundment.

At P2 in the reinforced impoundment (the center of a waste rock inclusion), the amplification factors varied from 0.723 to 1.922, indicating moderate damping to high amplification. Generally, the more intense loadings resulted in more amplification. The site response at this location was a result of conflicting mechanisms. There was the relatively stiff and narrow waste rock inclusion that would have produced amplification, but there were softer tailings on both sides of the inclusion that would have produced damping. Ultimately the response was variable. For example an F_a value of 0.723 (moderate damping) was produced by Earthquake E2 and an F_a value of 2.068 (high amplification) was produced by Earthquake E5. For the E2 loading it appears that the

damping in the tailings predominated and for the E5 loading it appears that the amplification in the waste rock inclusion predominated.

The amplification factors on the crest of the dike varied from 1.266 to 2.667 (average 1.698) for the conventional impoundment and from 0.552 to 2.137 (average 1.357) for the reinforced impoundment. Amplification of the horizontal acceleration at the crests of dams and embankments is a well known phenomenon (Makdisi & Seed, 1977, 1978, 1979; Kramer, 1996). However, the research on this aspect of dynamic behavior has focused on water-retention dams constructed of earthfill, rather than tailings impoundments.

The amplification of horizontal accelerations on the crests of ridges can be roughly approximated by $2\pi/\phi$ where ϕ is the vertex (interior) angle of the ridge (Kramer 1996). Applying this approximation to the conceptual impoundments gives an amplification factor of 2.3. In the dynamic numerical analysis of an earth dam situated on medium stiff to still alluvium over "deep" bedrock, Cascone & Rampello (2003) found that the amplification of the PGA on the crest of the dam was about 2 times greater than that of the ground motion on bedrock. Rampello et al. (2008) conducted dynamic numerical analysis of the same dam evaluated by Cascone & Rampello (2003) using 10 ground motions and calculated amplification factors on the crest of the dam that varied from 0.62 to 1.51. It is noted that the approximations and evaluations discussed above were for water-retention, earthfill dams composed of materials not subject to excess porewater pressure generation. Therefore, the resulted may not be strictly applicable to the conceptual impoundment. However, the results of the numerical analysis conducted for this research are in general agreement with the approximation and published values.

Given the material properties and geometry of the conceptual impoundments, the variation of the applied ground motions, and considering the affects of excess porewater pressure generation, the site responses of the impoundments are in general agreement with the expected and published behavior and are thus deemed reasonable.

Table 6-7 – Summary of site responses of the conceptual impoundments to Earthquakes E1 through E5.

Earthquake	PGA Values (g)					Amplification Factors, F_a			
	Top of Bedrock	Top of Glacial Till	Surface at P1	Surface at P2	Crest of Dike	Top of Glacial Till	Surface at P1	Surface at P2	Crest of Dike
Conventional Impoundment									
E1	0.249	0.315	0.095	0.100	0.664	1.265	0.382	0.402	2.667
E2	0.451	0.547	0.093	0.123	0.625	1.213	0.206	0.273	1.386
E3	0.764	1.453	0.129	0.095	0.945	1.902	0.169	0.124	1.237
E4	0.917	1.580	0.124	0.086	1.772	1.723	0.135	0.094	1.932
E5[a]	1.526	2.394	0.299	0.135	0.888	1.569	0.196	0.088	1.266
Reinforced Impoundment									
E1	0.255	0.486	0.116	0.250	0.545	1.906	0.455	0.980	2.137
E2	0.466	0.811	0.113	0.337	0.446	1.740	0.242	0.723	0.957
E3	0.745	1.252	0.146	0.781	0.411	1.681	0.196	1.048	0.552
E4	0.905	1.487	0.312	1.739	1.297	1.643	0.345	1.922	1.433
E5	1.539	3.182	0.826	1.882	2.629	2.068	0.537	1.233	1.708

[a] Analysis of the conventional impoundment under Earthquake E5 was terminated due to excessive deformation of one or more elements of the model.

6.4.11.2 Cyclic Stress Ratio Development

The cyclic stress development due to the Earthquake E3 loading is described in Sections 6.4.5.2 and 6.4.8.2 for the conventional and reinforced impoundments, respectively. The CSR development in the impoundments for the other earthquake loadings considered is presented in Appendix H.

Generally, the development of the CSR coincided with the horizontal accelerations at a given location. In some locations, particularly under the downstream slope of the dike, the CSR was significantly influenced by shear stresses developed within the

impoundment to resist horizontal displacement. However, at some locations the development of excess porewater pressures approaching 1.0 negated the shear strength of the soil and the CSR values approached 0 for remainder of shaking. In the tailings underlying the dike, the development of the CSR was strongly influenced by shear forces developed to resist horizontal displacement of the impounded tailings.

A similar pattern of CSR development under the slope of a dike was observed by Seid-Karbasi & Byrne (2004) in the dynamic numerical evaluation of the Mochikoshi Tailings Dams in Japan.

The CSR development in the impoundments appears to be reasonable.

6.4.11.3 Excess Porewater Pressure Development

Generally, the development of excess porewater pressures was quite rapid for the conventional and reinforced impoundments under the earthquake loadings considered. In the conventional impoundment, excess porewater pressures developed throughout the retained tailings to high levels (r_u values greater than 0.8), except under the dike. In the reinforced impoundment, excess porewater pressures in the upper 16 m of the retained tailings and away from the immediate vicinity of the waste rock inclusions reached this level. In the tailings adjacent to waste rock inclusions and in the lower part of the reinforced impoundment, the development of excess porewater pressures was limited by drainage and possibly by the stiffness of the inclusions which reduced shear strains.

In the conventional and reinforced impoundments, the excess porewater pressures in the tailings below the dike were significantly affected by the shear stresses developed to resist movement of the impoundment and as a result the development of excess porewater pressures was limited or porewater pressures decreased. Liquefaction was unlikely in this zone.

The development of excess porewater pressures in the retained tailings of the conventional and reinforced impoundments was consistent with the expected behavior

and the results of analytical calculations (Section 3.9) and "level ground" liquefaction modeling (Section 4.4.5). In their analysis of excess porewater development based on the numerical modeling of an earth dam, Seid-Karbasi & Byrne (2004) found that the r_u values developed below the downstream slope of the dam ranged from 0.17 to 1.0 whereas values ranging from 0.7 to 1.0 were expected from "level ground" conditions.

Given that the excess porewater pressure development meets the current understanding regarding the generation of excess porewater pressures, is in agreement with the analytical and "level ground" numerical analysis, and is supported by Seid-Karbai & Byrne (2004), the excess porewater pressure generation observed in the models is deemed reasonable.

6.4.11.4 The Dissipation of Excess Porewater Pressures

The dissipation of excess porewater pressures following shaking was quite rapid due to the increase of the hydraulic conductivities by two orders of magnitude (to decrease the simulation time). In all of the post-shaking analyses, the models returned to a condition close to steady state mechanical and fluid equilibrium as determined by r_u values that were relatively constant with time.

The dissipation caused minor additional deformation on the downstream slopes of the impoundments due to seepage pressures. Recall that cohesion was applied to the outer elements on the downstream slopes of the dikes to prevent localized failures (shallow sloughing) due to seepage pressures that would have terminate program execution.

6.4.11.5 Displacements

The displacements of the crest of the conceptual impoundments at the end of the post-shaking analyses are shown on Figure 6-49 and summarized on Table 6-8.

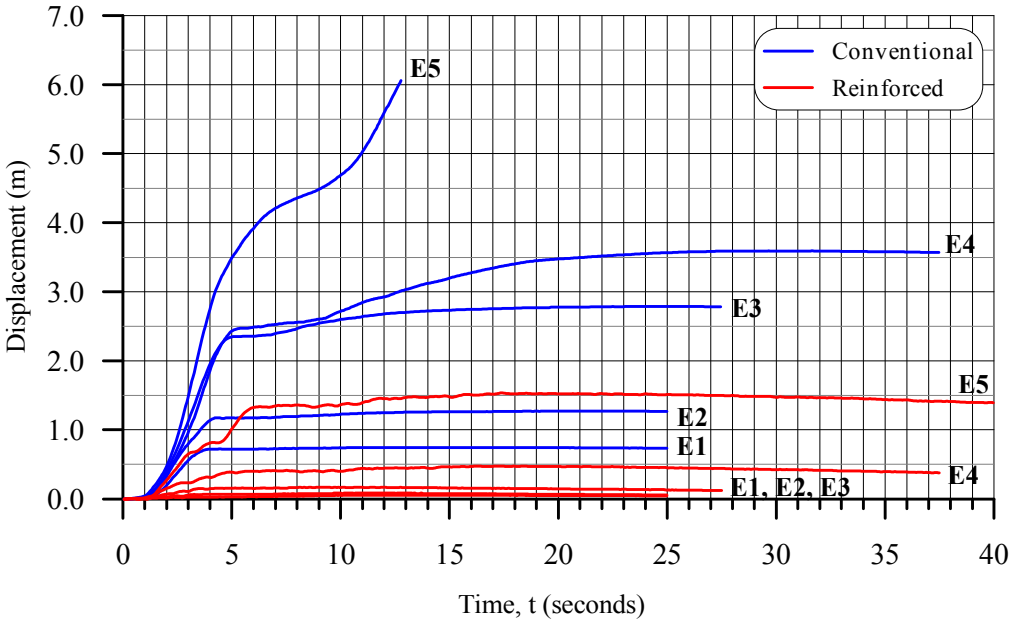

Figure 6-49 – Horizontal displacements of the crests of the conventional and reinforced impoundments for the earthquakes considered.

For the conventional impoundment, the horizontal and vertical displacements of the crest increased with the earthquake loading. All horizontal displacements of the crest were downstream and all vertical displacements were downwards. The horizontal displacement of the crest varied from 0.75 m (E1) to 6.05 m (E5) and vertical displacement varied from 0.45 m (E1) to 0.95 m (E5). The displacements of the crest of the reinforced impoundment were significantly lower under all earthquake loadings. The horizontal displacements varied from 0.04 m (E1) to 1.40 m (E5) and the vertical displacements varied from 0.06 (E1) to 0.85 (E5).

The displacement patterns of the conventional impoundment indicated movements that extended far into the impoundment, indicated that failure of the impoundment would result in the release of most of the retained tailings. Regarding the reinforced impoundment, the displacement patterns indicated movements that were generally limited to the area of the dike and sometimes shallow zones that did not extend beyond the crest

of the dike. This indicates that a limited amount of tailings would be released in the event of a failure of the reinforced impoundment.

Table 6-8 – Summary of analysis in the conceptual impoundments.

Earthquake	Horizontal Displacement of Crest (m)	Vertical Displacement of Crest (m)
Conventional Impoundment		
E1	0.75	-0.45
E2	1.26	-0.55
E3	2.77	-0.66
E4	3.60	-0.60
E5	6.05	-0.95
Reinforced Impoundment		
E1	0.04	-0.06
E2	0.06	-0.07
E3	0.12	-0.12
E4	0.38	-0.28
E5	1.40	-0.85

Note: Horizontal displacements are positive in the downstream direction (negative upstream) and vertical displacements are positive upwards and negative downwards.

6.5 DISCUSSIONS ON LIQUEFACTION AND STABILITY

6.5.1 Liquefaction Evaluation

6.5.1.1 Evaluation Criteria

Liquefaction is defined in Section 2.2.1 as the generation of excess porewater pressure within saturated, contractive, cohesionless soil due to static or dynamic loading, sufficient

to bring the soil the steady state condition or a condition of zero (or very low) effective stress leading to excessive deformation under gravity or external loading.

In applying this definition to the numerical analyses presented, it is noted that the tailings consisted of a saturated, contractive, cohesionless soil and were subjected to a dynamic loading that resulted in very low effective stresses. However, the tailings did not exhibit excessive deformation under gravity or external loading, due to their being retained by the dike and by the waste rock inclusions in the case of the reinforced impoundment. So, the question that remains is whether the tailings reached the steady state condition as a result of the applied loadings. The answer lies with the UBC Sand model (refer to Section 2.7.1).

In the UBC Sand model, the steady state (critical state) condition assumed when the developed stress ratio, n_d, equals the stress ratio at failure, n_f.

Recalling the pertinent equations (Puebla et al., 1997):

$$n_d = \left(\frac{q}{p\prime}\right) = sin\phi_d \tag{2-22}$$

where:`

n_d is the developed stress ratio;

q is the maximum shear stress;

p' is the effective mean stress or effective confining stress; and

ϕ_d is the developed friction angle.

The failure angle (peak friction angle), ϕ_f, (in degrees) is estimated from the constant volume friction angle, ϕ_{cv}, using:

$$\phi_f = \phi_{cv} + \frac{(N_1)_{60}}{10.0} \tag{2-37}$$

Also recall that the stress ratio at failure is equal to the sine of the failure angle, or peak friction angle, $sin(\emptyset_f)$.

The tailings were assigned an average $(N_1)_{60}$ value of 3.5 (blows per 300/mm) with a statistical distribution giving a standard deviation of 0.5 and a ϕ_{cv} value of 36°. The resulting average stress ratio at failure was 0.5927 ± 0.0014 assuming a range of two standard deviations.

The coarse tailings were assigned an average $(N_1)_{60}$ value of 11 with a statistical distribution giving a standard deviation of 0.5 and a ϕ_{cv} value of 36°. The resulting average stress ratio at failure was 0.6032 ± 0.0014, assuming a range of two standard deviations.

For discussion purposes, values of n_d of 0.58 or greater will be associated with the critical state condition in the tailings (impounded) and values of 0.6 or greater will be associated with the critical state condition in the coarse tailings (dike raises).

6.5.1.2 Liquefaction of the Tailings

Figures 6-50 and 6-51 present contours of the developed stress ratio within the conventional impoundment at the end of shaking due to Earthquakes E1 and E5, respectively.

For Earthquake E1, the zones in the tailings where the developed stress ratio was at least 0.59 coincided with the limit shown for 0.6 (Figure 6-50). These zones were limited to an area underlying the dike raises and to small, isolated pockets in the impoundment. Based on the criteria presented above, the coarse tailings were close to, but not in, the critical state condition at the end of shaking. Generally, the n_d values within the impounded tailings were less than 0.5 and the tailings were not at the critical state at the end of shaking. The area of tailings under the dike raises is considered to have been in a state of liquefaction at the end of shaking.

With respect to Earthquake E5 (Figure 6-51), the n_d values in the tailings were at least 0.59 throughout the depth of the impoundment from the dike to 40 m upstream. Further upstream, the n_d values were generally less than 0.3. The zone of high n_d values (0.5 to 0.6) on the upstream side of the model is attributed to the presence of the stability buttress. The impounded tailings from the dike to 40 m upstream are considered to have been in a state of liquefaction at the end of shaking. The coarse tailings of the dike raises were close to, but not in, the critical state condition at the end of shaking.

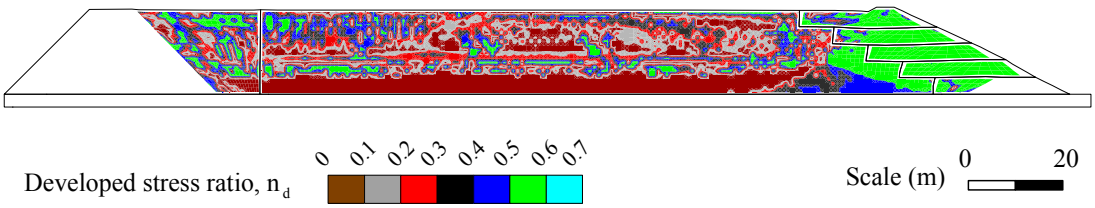

Figure 6-50 – Contours of the mobilized stress ratio in the tailings at the end of shaking – conventional impoundment, Earthquake E1 (Mw=6.5).

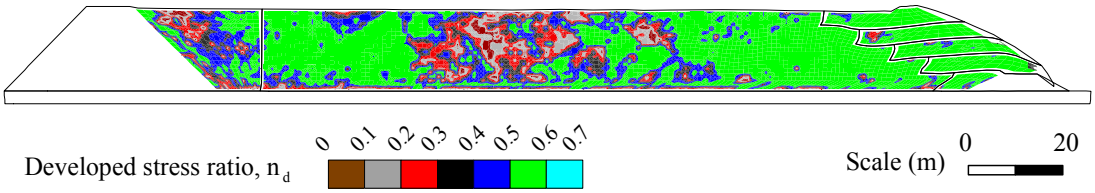

Figure 6-51 – Contours of the mobilized stress ratio in the tailings at the end of shaking – conventional impoundment, Earthquake E5 (Mw=7.5).

The developed stress ratios in the reinforced impoundment at the end of shaking as a result of Earthquakes E1 and E5 are presented on Figures 6-52 and 6-53, respectively.

As a result of E1 (Figure 6-52), the developed stress ratios were generally less than 0.3 and the zones in the critical state condition were small and isolated. In the coarse tailings

of the dike raises, there were considerable zones with n_d values of 0.6 or greater, indicating the critical state condition. At the end of shaking, there were small, isolated zones of liquefaction in the impounded tailings and considerable zones of liquefaction in the coarse tailings of the dike raises.

The n_d values in the reinforced impoundment due to Earthquake E5 are plotted on Figure 6-53. Based on these values, small to moderate zones of liquefaction were evident in the impounded tailings, particularly between the waste rock inclusions and below the dike raises, and considerable areas of the coarse tailings of the dike raises were in a critical state (liquefaction) at the end of shaking.

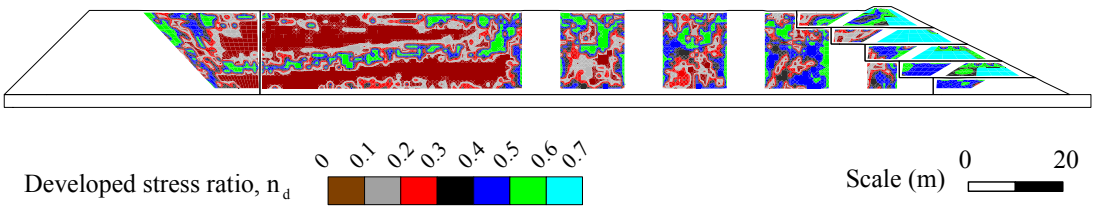

Figure 6-52 – Contours of the mobilized stress ratio in the tailings at the end of shaking – reinforced impoundment, Earthquake E1 (Mw=6.5).

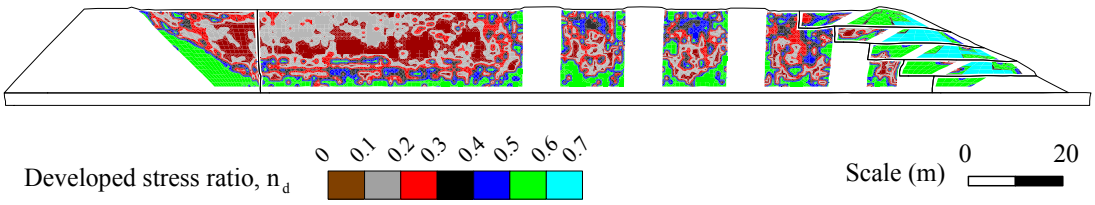

Figure 6-53 – Contours of the mobilized stress ratio in the tailings at the end of shaking – reinforced impoundment, Earthquake E5 (Mw=7.5).

A question that immediate comes to mind is, why didn't the impoundments undergo considerably more deformation, particularly where the coarse tailings of the dike raises

were in a state of liquefaction at the end of shaking. Recall, that in fact, the displacement of the crests of the impoundments stopped well before the end of shaking (except for the conventional impoundment under the Earthquake E5 loading). The answer may lie in a combination of factors:

a) Stress transfer to the relatively strong starter dike or waste rock inclusions, where present;
b) Effective stress changes due to excess porewater pressure generation and dissipation and due to dynamic loading which would have made the state of the tailings evolve with time; and
c) On-going strains and the lack of confinement, that would have allowed for volumetric changes (recall from Appendix A that the critical state condition is a constant volume condition).

Using the definition of liquefaction commonly applied in engineering practice, the development of excess porewater ratios approaching 1.0:

- In the conventional impoundment, liquefaction occurred due to Earthquakes E1 through E5 throughout the depth and extent of the impounded tailings, except below the dike, and did not occur within the coarse tailings of the dike raises.
- In the reinforced impoundment, liquefaction due to Earthquakes E1 through E5 was limited to the upper 2/3 to 3/4 of the impounded tailings between and upstream of the waste rock inclusions.

The dissipation of excess porewater pressures through the surface of the impoundment and downstream slope of the dike after any of the earthquakes considered, would cause the development of sand boils and fissures and the ejection of a considerable amount of water from the impoundment. This is the evidence of liquefaction that was used by Seed and Idriss (1982) in the development of the Simplified method of liquefaction evaluation.

6.5.2 Stability Evaluation

6.5.2.1 Evaluation Criteria

In evaluating the stability of the impoundments with respect to the earthquake loading, failure was defined, rather narrowly, as collapse of the impoundment.

The criteria used to assess the stability of the conceptual impoundments with respect to the various earthquake loads were as follows:

a) If mechanical equilibrium could not be restored to the model during the post-shaking phase and the velocity of the movement at the completion of the analysis indicated continued deformation of the dike in the downstream direction, collapse of the impoundment (failure) was assumed;

b) Excessive deformation of the dike not meeting the above criteria for failure, but sufficient to halt execution of the simulation due to the excessive deformation of one or more elements, where the velocity of movement at the end of execution was indicative of collapse (movement of the dike in the downstream direction) was considered failure of the impoundment; and

c) Deformation of the impoundment not meeting the criteria given above was not considered failure of the impoundment. However, any significant deformation of the slope or crest of the dike would probably required re-grading of the slope or crest and the restoration of erosion control measures and flow control devices, or could cause overtopping of the crest.

The cohesion added to the outer elements of the downstream slopes of the impoundments was included in the analysis to prevent shallow surface failures due to seepage and was not sufficient to prevent excess deformation of the impoundment due to the earthquake loadings.

Although FLAC has the capacity to calculate the factor of safety (and associated potential failure surface), the factor of safety function is not applicable to dynamic analysis and cannot applied when the UBC Sand model is in use.

Shear strain was considered as a criterion for to evaluate the stability of the impoundment, but there was no basis for their use and the shear strain patterns provided no more additional information than the deformation patterns.

6.5.2.2 Stability Evaluation

The horizontal velocities in the conventional impoundment at the post-shaking analysis following the application of Earthquake E1 (M_w=6.5) are plotted on Figure 6-54. The velocities varied from -2.5 mm/s to 2 mm/s and distribution of the velocities indicate that there was no significant downstream movement of the dike suggestive of collapse. The upper portion of the dike and the tailings in the vicinity were actually moving upstream. A small zone of downstream movement on the slope of the dike, just above the starter dike, is attributed to the seepage pressures.

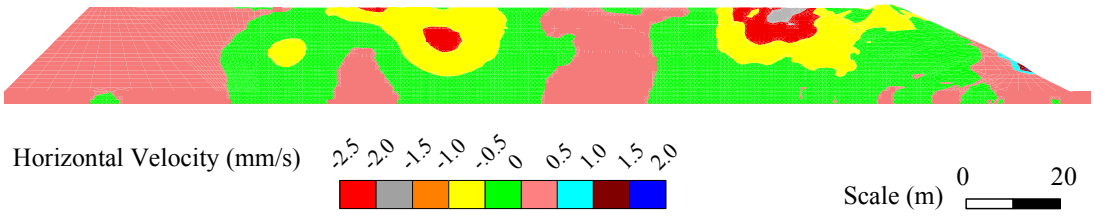

Figure 6-54 – Horizontal velocities at the end of the post-shaking analysis – conventional impoundment, Earthquake E1 (M_w=6.5).

Figure 6-55 presents the horizontal velocities in the conventional impoundment at the termination of the analysis (t=12.8 s) due the excessive deformation of one or more elements under the loading of Earthquake E5 (M_w=7.5). The velocities varied from -500 mm/s to more than 2,500 mm/s with the great velocities occurring on the downstream

slope of the dike, above the starter dike. The pattern of the velocities indicates movement extending to the upstream buttress and that collapse of the dike is imminent, particularly given that dynamic analysis would have continued for another 12.2 seconds had it not been for the excessive deformation that caused program execution to terminate.

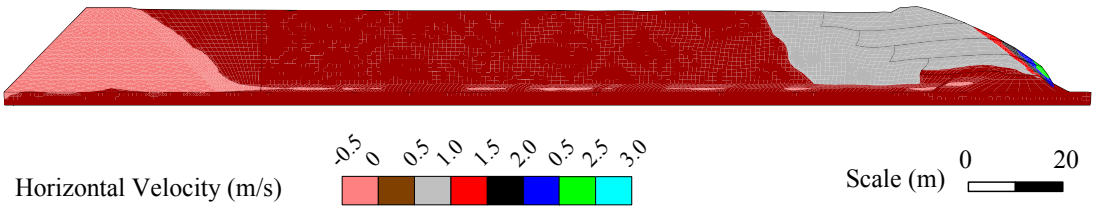

Figure 6-55 – Horizontal velocities at t=12.8 s (termination of program due to excessive deformation) – conventional impoundment, Earthquake E5 (M_w=7.5).

Figure 6-56 shows the horizontal displacements due to Earthquake E5 in the reinforced impoundment after the end of the post-shaking analysis. Except for a small area of downstream velocities as great as 1.5 mm/s on the slope above the starter dike, the velocities varied from -0.25 mm/s to 0.25 mm/s. The concentrated area of velocities above the starter dike are attributed to seepage pressures.

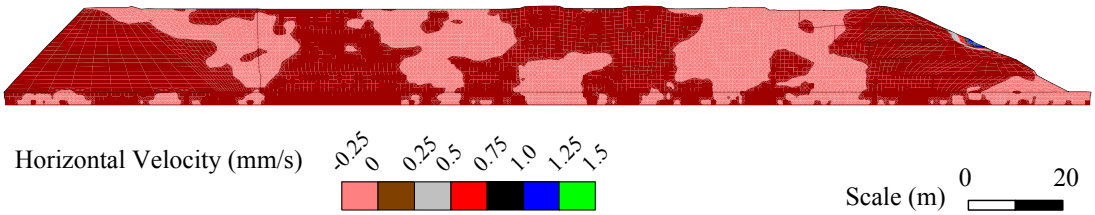

Figure 6-56 – Horizontal velocities at the end of the post-shaking analysis – reinforced impoundment, Earthquake E5 (M_w=7.5).

Horizontal velocity plots for the cases analyzed in this chapter are presented in Appendix H. In general, the horizontal velocities of the conventional impoundment due to Earthquakes E1 through E4 are similar to Figure 6-54 and those for the reinforced impoundment due to Earthquakes E1 through E5 are similar to Figure 6-56.

Based on the criteria presented above, the conventional impoundment is considered to have failed as a result of the Earthquake E5 loading and no other instances of failure were indicated.

6.6 REMARKS ON THE EVALUATION OF WASTE ROCK INCLUSIONS

The use of waste rock inclusions had the following effects on the behavior of the conceptual tailings impoundment:

a) Under static conditions, there was a significant stress transfer from the tailings to the waste rock inclusions that resulted in reduced vertical effective stresses in the tailings adjacent to the inclusions and increased vertical effective stresses in the waste rock inclusions. Stress transfer from the tailings to the waste rock inclusions is expected in actual impoundments due the stiffness of the waste rock relative to the tailings and due to consolidation of the tailings as the impoundment is raised.

b) The presence of the waste rock inclusions caused a stiffer response to the earthquake loads (less damping). The maximum shear strains in the reinforced impoundments were an order of magnitude lower than those in the conventional impoundment.

c) The inclusions reduced the generation of excess porewater pressure in the adjacent tailings and on the bottom of the impoundment. However, some infiltration of the tailings into the waste rock inclusions would be expected and this would probably decrease the drainage capacity of the inclusions. This phenomena is the subject of ongoing research at Ecole Polytechnique.

d) The displacements and deformation of the impoundment with waste rock inclusions were substantially lower than those in the impoundment without waste rock inclusions, in some instances and order of magnitude lower.

e) The extent of deformation into the impoundment was dramatically reduced by the presence of the inclusions, implying that less tailings would be released in the event of a failure of the impoundment.

The use of waste rock inclusions as described thus far, resulted in a significant decrease in the displacements over the range of earthquake loadings considered.

CHAPTER 7. PARAMETRIC EVALUATIONS AND DISCUSSION

The chapter presents parametric evaluations and a general discussion on the research.

Parametric evaluations were completed to determine the relative influence of various properties and characteristics on the dynamic behavior of the conventional and reinforced impoundments. The methodology consisted of changing a specific property or characteristic and conducting the dynamic and post-shaking analyses, if necessary, and evaluating the behavior with respect to a base case taken from the analysis described in Chapter 6. The analyses of the parametric evaluations were conducted using Earthquakes E4 (M_w=7.25) and E5 (M_w=7.5) because these loading produced the most deformation in the conventional and reinforced impoundments and the greatest difference in behavior between the two types of impoundments.

Observations, conclusions and tendencies deduced from the parametric evaluations are limited to the analyses conducted in terms of the impoundment geometry, material properties, waste rock configurations, earthquake loads, and methods and may not be applicable elsewhere.

The discussion section encompasses all of the research presented in this document. Its purpose is to provide a general overview of the research, the findings of the research and how the different elements of the research (e.g. literature review, field investigation, laboratory testing, and numerical analyses) interacted and will contribute to the conclusions and recommendations presented in Chapter 8.

7.1 PARAMETRIC EVALUATION OF THE CONVENTIONAL IMPOUNDMENT

Numerical analyses were conducted to evaluate the influence of the following factors on the dynamic behavior of the conceptual tailings impoundments:

a) The degree of consolidation of the impounded tailings as expressed by the corrected standard penetration test blow count, $(N_1)_{60}$; and

b) The degree of compaction of the coarse tailings used to construct the dike as expressed by the corrected standard penetration test blow count, $(N_1)_{60}$.

The results of the analyses are summarized in the following sections.

7.1.1 Degree of Consolidation of the Impounded Tailings

In the numerical analysis of the conceptual impoundments presented in Chapter 6, the impounded tailings were assumed to be under-consolidated and the degree of consolidation was expressed using the corrected standard penetration blow count, $(N_1)_{60}$, a key parameter of the UBC Sand model. In Section 3.7.3.6 the average $(N_1)_{60}$ value of the under-consolidated tailings in the representative impoundment was estimated to be 3.5 (blows per 300 mm) based on the results of cone penetration testing. From the numerical simulation of CDSS testing presented in Section 4.3, the $(N_1)_{60}$ value of the tailings normally consolidated samples from the representative impoundment was estimated to be 11.

Dynamic analysis, and post-shaking analysis where deemed applicable, were conducted for the conventional impoundment using an $(N_1)_{60}$ value of 2.5 to represent a degree of consolidation less than that evident in the representative impoundment, such as may have occurred if the rate of tailings placement had been more rapid. Analyses were also conducted using $(N_1)_{60}$ values varying from 4.5 to 11, representative of increasing degrees of consolidation of the tailings. To simulate somewhat the heterogeneity typical of active tailings deposits, the $(N_1)_{60}$ values used in the analyses were average values and standard deviations of 0.5 were specified to create statistical distributions. All other material properties and conditions used in the analyses were unchanged from those presented in Chapter 6. Recall that in the numerical analysis of the conceptual impoundments, downstream displacements are positive, upstream displacement are negative, while upwards displacements are positive and downwards displacements are negative.

The results of the analyses are summarized in Table 7-1. The results for under-consolidated tailings, $(N_1)_{60}$=2.5 and $(N_1)_{60}$=4.5, are shown on Figures 7-1 and 7-2, respectively. The results of analysis for normally consolidated tailings, $(N_1)_{60}$=11, are shown on Figure 7-3. Figures for all of the results summarized in Table 7-1 are contained in Appendix H.

Assuming the tailings to be less consolidated than in the representative impoundment by using an average $(N_1)_{60}$ value of 2.5 and applying the Earthquake E4 ground motion (M_w=7.25, t=37.5 s) resulted in large deformations of the dike and impoundment. As shown on Figure 7-1, the excess porewater pressure development in the tailings was quite rapid and r_u values exceeded 0.9 during shaking, though there was evidence of some drainage near the surface (0.875H). Horizontal displacement of the crest was 3.5 m (downstream) by the 6th second of shaking and continued at a decreasing rate until t=32.5 s when execution was terminated due to excessive deformation. Vertical displacement of the crest surpassed 1.0 m (downwards) during the 4th second of shaking and then decreased slightly to 0.8 m (downwards). The horizontal deformations extended the width of the impoundment.

At the end of the analyses, the horizontal velocities of the impoundment for all of the cases considered were indicative of significant continued deformation.

The analysis of the conventional impoundment assuming a slightly higher degree of consolidation than in the representative impoundment, an $(N_1)_{60}$ value of 4.5 rather than 3.5, and subjected to the Earthquake E5 loading (M_w=7.5, t=40 s) is presented on Figure 7-2. In summary:

a) The excess porewater pressure generation was rapid and the r_u values exceeded 0.9 during most of shaking, except near the surface; and
b) The horizontal displacement of the crest was 5.4 m (downstream) and increasing at 19.6 seconds, when program execution was terminated due to excessive deformation. The maximum vertical displacement was 0.8 m

(downwards) at t=4 s. However, subsequent upwards movement of the crest resulted a downwards displacement of 0.5 m at the end of the analysis.

Figure 7-3 presents the results of analysis of the conventional impoundment assuming the retained tailings were normally consolidated and an $(N_1)_{60}$ value of 11 was applicable. The results indicate:

a) The development of excess porewater pressures was rapid and r_u values varied between 0.65 and 0.9 during shaking;
b) Horizontal and vertical displacements of the crest were 4.2 m (downstream) and 1.2 m (downwards) at the end of shaking (t=40 s) and horizontal displacements were on-going at a low rate; and
c) Horizontal deformation of the impoundment at the end of shaking indicated a maximum outwards displacement of the downstream slope of the dike of about 6 m and that horizontal displacements extending the width of the impoundment.

Dynamic analyses using Earthquake E5 (M_w=7.5) and assuming average $(N_1)_{60}$ values of 5.5, 6.5, 7.5, and 9.5 blows per 300 mm in the tailings resulted in crest displacements that varied from 4.0 to 5.9 m (downstream) and 1.0 to 1.2 m (downwards). The r_u development in all of these cases was rapid and values at P1 and P2 varied between 0.75 and 1.0 by the end of the analyses. Results are presented in Appendix H.

The horizontal velocities of the impoundments at the end of all of the analyses conduced were indicative of significant continued deformation.

The analyses of the impoundment considering the degree of consolidation of the tailings, as represented by $(N_1)_{60}$, indicates that the degree of consolidation of the tailings had a discernable, but not significant, impact on the dynamic behavior of the impoundment with the deformations decreasing with increasing consolidation.

Table 7-1 – Summary of Analysis – Effect of degree on consolidation of the tailings in the conventional impoundment.

$(N_1)_{60}$ of Tailings (Blows/300 mm)	Earthquake	Horizontal Displacement of Crest (m)	Vertical Displacement of Crest (m)	Notes
3.5	E5	5.1	-1.0	**Base case** (see Section 6.4.13). Analysis stopped due to excessive deformation at t=12.8 s.
2.5	E4	5.0	-0.8	Analysis stopped due to excessive deformation at t=32.5 s.
4.5	E5	5.4	-0.5	Analysis stopped due to excessive deformation at t=19.6 s.
5.5	E5	5.9	-1.0	Analysis stopped due to excessive deformation at t=15.6 s.
6.5	E5	5.1	-1.0	Analysis stopped during post-shaking analysis due to excessive deformation (t=43.2 s).
7.5	E5	5.0	-1.1	Analysis stopped due to excessive deformation at t=28.2 s.
9.5	E5	4.5	-1.2	
11.0	E5	4.2	-1.2	

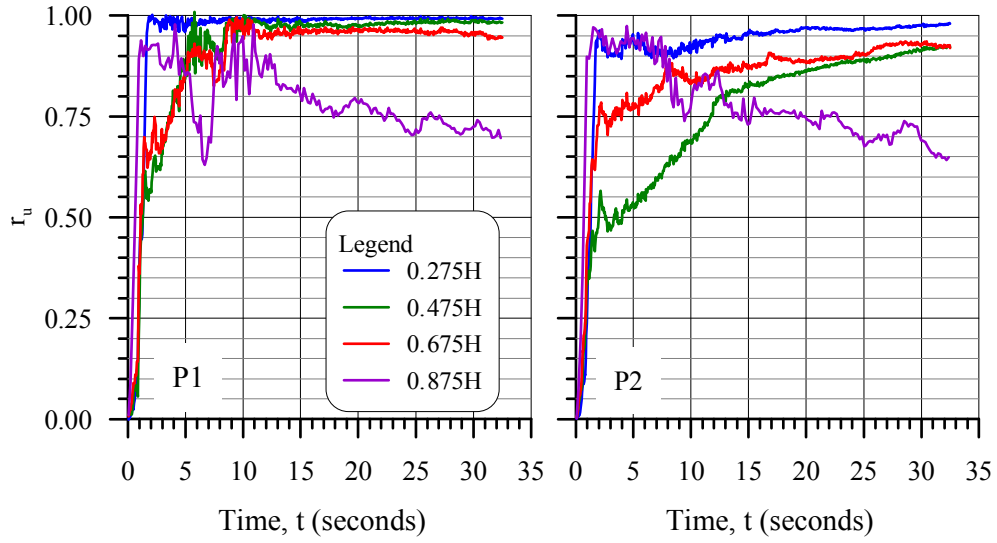

(a) Excess porewater pressure ratio at P1 and P2.

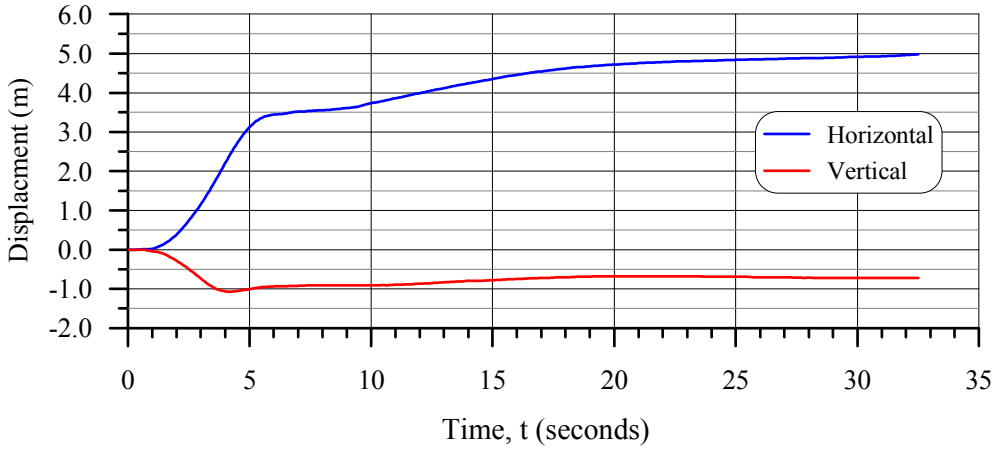

(b) Displacement of the crest of the dike during shaking.

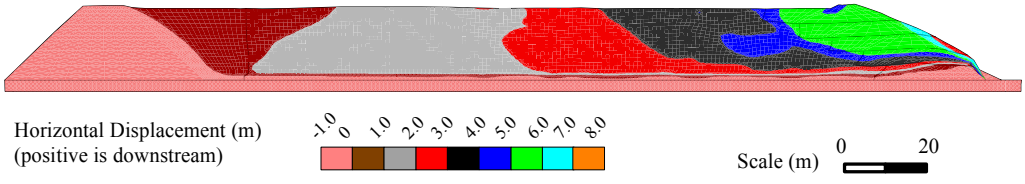

(c) Horizontal displacements at the end of shaking.

Figure 7-1 – Results of dynamic analysis of the conventional impoundment – $(N_1)_{60}$=2.5, Earthquake E4 (M_w=7.25).

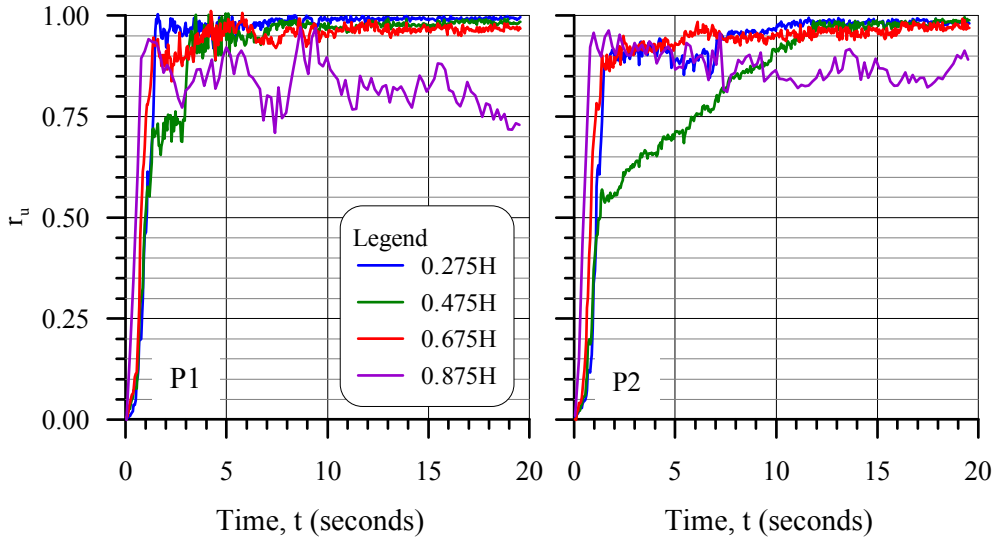

(a) Excess porewater pressure ratio at P1 and P2.

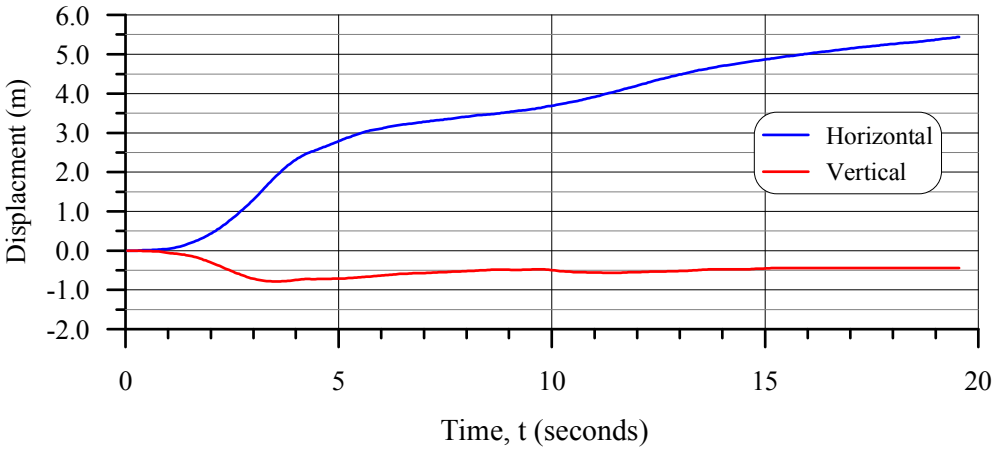

(b) Displacement of the crest of the dike during shaking.

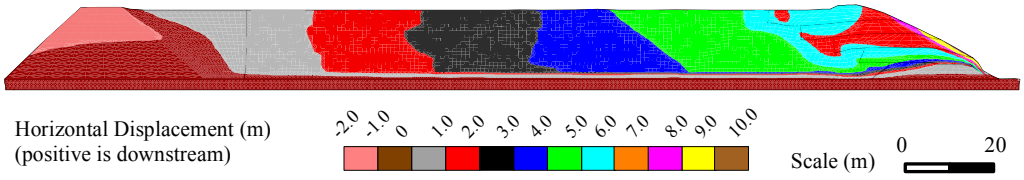

(c) Horizontal displacements at the end of shaking.

Figure 7-2 – Results of dynamic analysis of the conventional impoundment – $(N_1)_{60}$=4.5, Earthquake E5 (M_w=7.5).

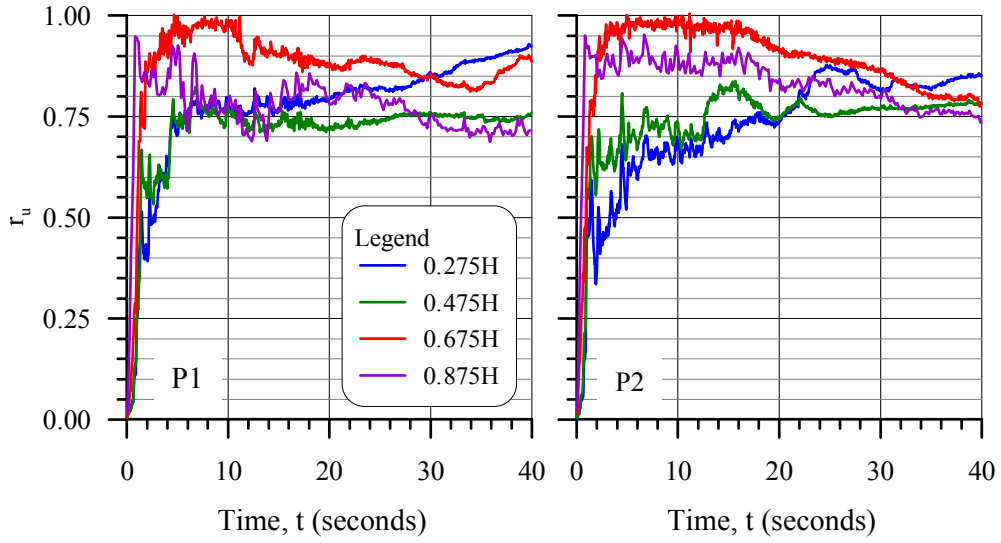

(a) Excess porewater pressure ratio at P1 and P2.

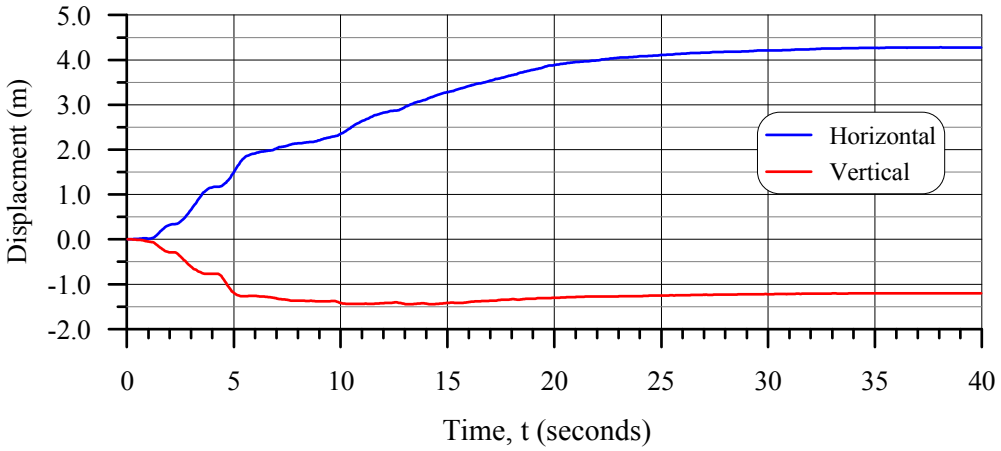

(b) Displacement of the crest of the dike during shaking.

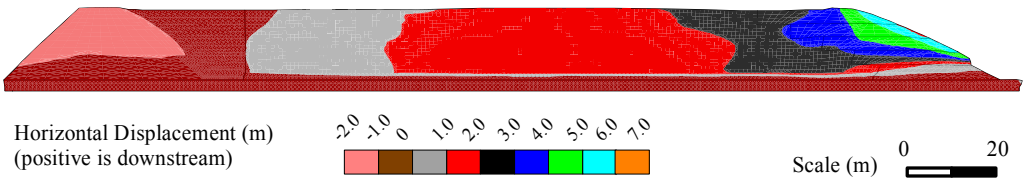

(c) Horizontal displacements at the end of shaking.

Figure 7-3 – Results of dynamic analysis of the conventional impoundment – $(N_1)_{60}$=11, Earthquake E5 (M_w=7.5).

7.1.2 Compaction of Coarse Tailings Forming the Dike

The degree of compaction of the coarse tailings used to construct the dike was represented by the $(N_1)_{60}$ value, with greater values indicating an increasing degree of compaction. In the evaluation of the impoundments presented in Chapter 6 the coarse tailings of the dike were assumed to be constructed of normally consolidated tailings with minimal compaction effort.

The effect of compaction of the coarse tailings on the behavior of the impoundment was evaluated by assigning $(N_1)_{60}$ values of 13, 15 and 22 to the tailings and then conducting static and dynamic analyses using Earthquake E5 (M_w=7.5, t=40 s). The analyses are summarized as follows:

- An $(N_1)_{60}$ value of 13 represents a low compaction effort on the dike raises. As shown on Figure 7-4, this had no appreciable impact on the behavior of the impoundment compared to the base case. The dynamic analysis was terminated a t=8.3 s due to excessive deformation.
- An $(N_1)_{60}$ value of 15 indicated a moderately low compaction effort. During dynamic analysis, the crest of the impoundment moved 6.1 m downstream and 0.3 m downwards before execution was stopped at t=19.5 s due to excessive deformation (Figure 7-5).
- An $(N_1)_{60}$ value of 22 would be attained through a moderately high compaction effort. The crest of the dike was displaced 6.1 m downstream and 2.5 m downwards by t=19.6 s when the analysis was ended due to excessive deformation (Figure 7-6).
- The horizontal velocities of the impoundment at the end of analyses for the three cases considered indicated continued displacement.

The analyses indicated that compaction of the coarse tailings used to construction the dike had no significant impact on the dynamic behavior of the impoundment.

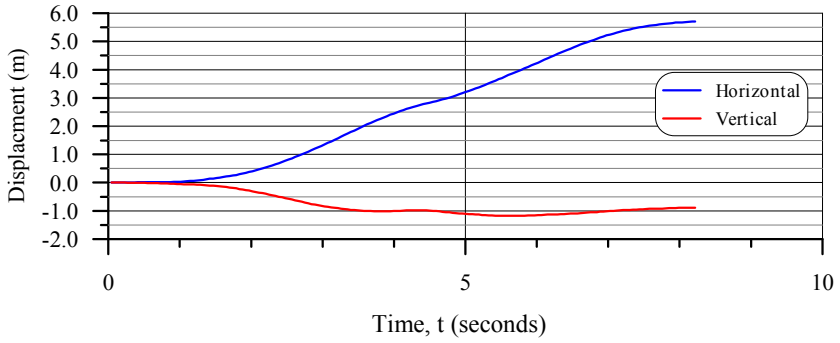

(a) Displacement of the crest of the dike during shaking.

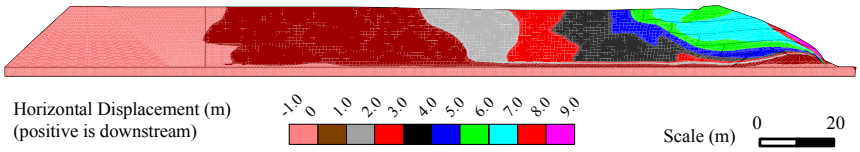

(b) Horizontal displacements at the end of shaking.

Figure 7-4 – Results of dynamic analysis of the conventional impoundment – Coarse tailings, $(N_1)_{60}$=13 – Earthquake E5 (M_w=7.5).

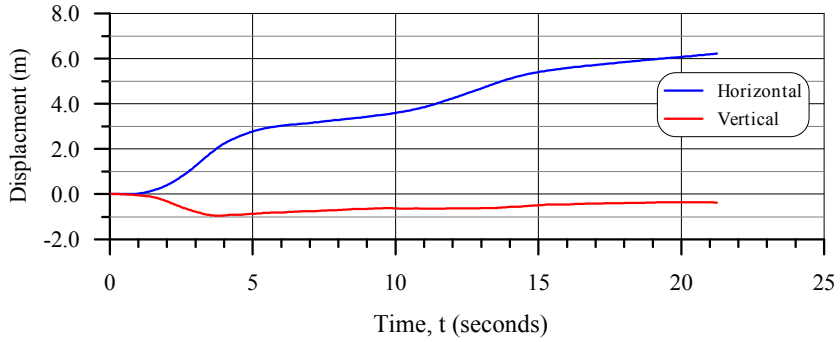

(a) Displacement of the crest of the dike during shaking.

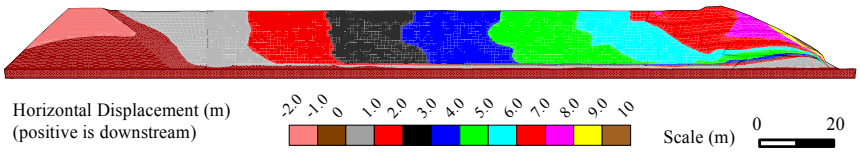

(b) Horizontal displacements at the end of shaking.

Figure 7-5 – Results of dynamic analysis of the conventional impoundment – Coarse tailings, $(N_1)_{60}$=15 – Earthquake E5 (Mw=7.5).

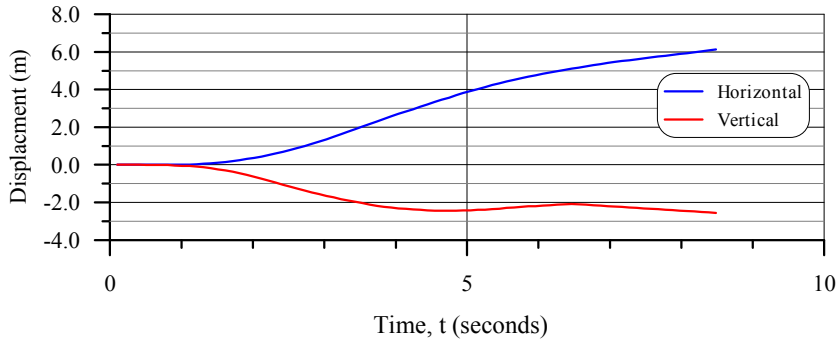

(a) Displacement of the crest of the dike during shaking.

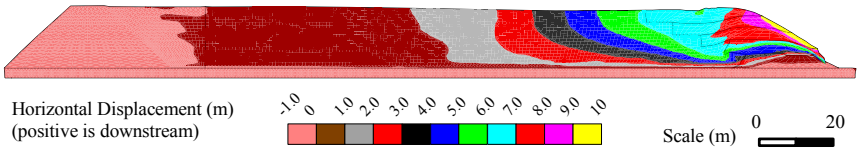

(b) Horizontal displacements at the end of shaking.

Figure 7-6 – Results of dynamic analysis of the conventional impoundment – Coarse tailings, $(N_1)_{60}$=22 – Earthquake E1 (M_w=7.5).

7.2 PARAMETRIC EVALUATIONS OF THE REINFORCED IMPOUNDMENT

The following factors were evaluated in the parametric evaluation of the conceptual impoundment with waste rock inclusions:

a) The hydraulic conductivity of the waste rock inclusions;

b) The configuration of the waste rock inclusions;

c) Placing waste rock on the upstream side of the dike raises; and

d) Waste rock inclusions consisting of closely-spaced columns.

The results are described in the following sections.

7.2.1 Hydraulic Conductivity of the Inclusions

As noted in Chapter 6, the waste rock inclusions in the reinforced impoundment exhibited some capacity to limit excess porewater pressure generation in the adjacent tailings during earthquake shaking, despite the hydraulic conductivity of the waste rock being not much higher than that of the tailings. Recall that the hydraulic conductivity of the waste rock, k_{WR}, was assumed to be $1x10^{-6}$ m/s (isotropic) and that the hydraulic conductivity of the tailings was assumed to be $2.25x10^{-6}$ m/s (horizontal) and $4.5x10^{-7}$ m/s (vertical) with standard deviations of one half an order of magnitude. The effect of a greater hydraulic conductivity of the waste rock was evaluated by changing its hydraulic conductivity to $1x10^{-4}$ m/s and conducting the dynamic analyses using the Earthquake E1, E3 and E5 loadings. The results are summarized on Table 7-2 and shown on Figures 7-7, 7-8 and 7-9, respectively.

Table 7-2 – Summary of results: The hydraulic conductivity of the waste rock inclusions.

Earthquake	$k_{WR}=1.0x10^{-6}$ m/s		$k_{WR}=1.0x10^{-4}$ m/s	
	Horizontal Displacement of Crest (m)	Vertical Displacement of Crest (m)	Horizontal Displacement of Crest (m)	Vertical Displacement of Crest (m)
E1 (M_w=6.5)	0.04	-0.06	0.025	-0.06
E3 (M_w=7.0)	0.12	-0.12	0.10	-0.12
E5 (M_w=7.5)	1.4	-0.85	1.5	-0.6

For Earthquake E1 (M_w=6.5), the r_u development, displacement of the crest during shaking and the deformation of the impoundment at the end of shaking due to the

increased waste rock hydraulic conductivity (Figure 7-7) were essentially unchanged from the analysis with k_{WR} equal to $1x10^{-6}$ m/s (see Appendix H).

For Earthquake E3, there was no discernable difference in the r_u development and displacement of the crest during shaking with the increased hydraulic conductivity (Figure 7-8) than with than with the initial value (refer to Figures 6-37 and 6-39). The horizontal deformation of the downstream slope of the dike at the end of shaking was slightly greater in the analysis with $k_{WR}=10x^{-4}$ m/s (Figure 7-8) than in the analysis with $k_{WR}=1x10^{-6}$ m/s (Figure 6-42). However, this difference is small enough to be due to the inherent variability of dynamic numerical modeling.

The dynamic response of the reinforced impoundment with the increased waste rock hydraulic conductivity (Figure 7-9) to the Earthquake E5 loading was virtually identical to that with the initial waste rock hydraulic conductivity (see Appendix H).

The results of the dynamic analyses of the reinforced impoundments with respect to the increased hydraulic conductivity of the waste rock inclusions and Earthquakes E1, E3 and E5 indicated that the hydraulic conductivity of the waste rock inclusions had no significant effect on the dynamic behavior of the reinforced impoundment.

Post-shaking analyses were note conducted for these cases. Given that in the post-shaking analyses presented in Chapter 6, the hydraulic conductivities of all of the materials were increased by two orders of magnitude to decrease the rate of excess porewater dissipation and that no appreciable deformation occurred during the analyses, post-shaking analyses were not considered necessary for this element of the parameter evaluation.

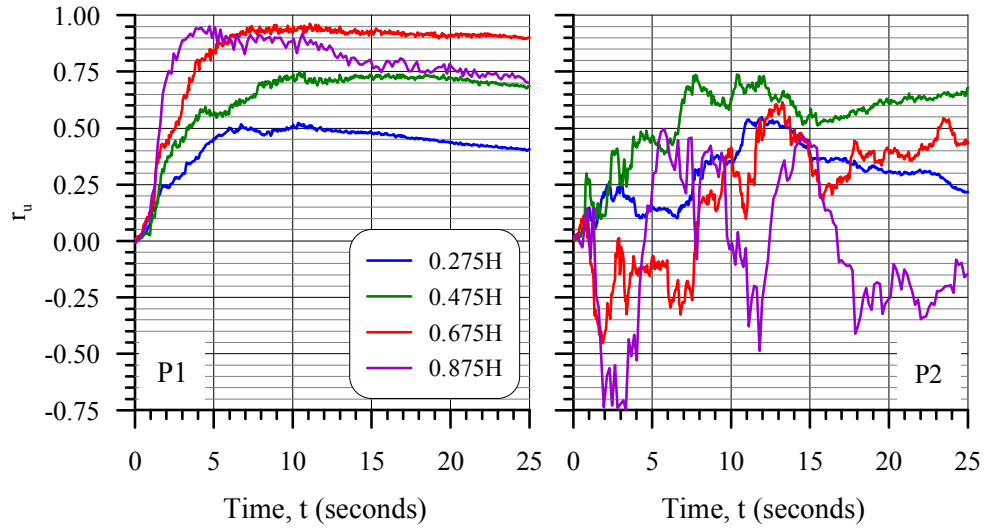

(a) Excess porewater pressure ratio at P1 and P2.

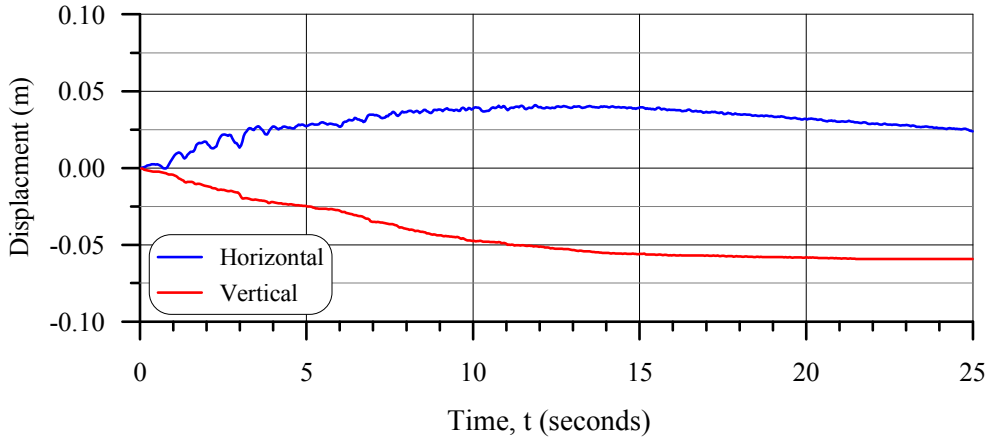

(b) Displacement of the crest of the dike during shaking.

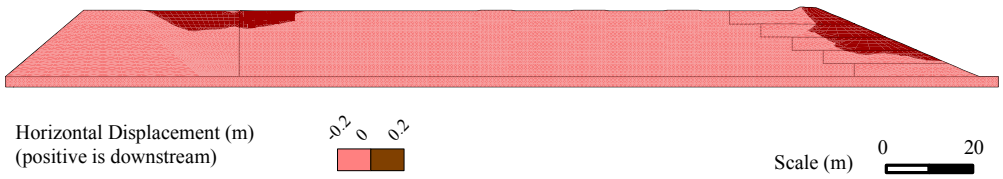

(c) Horizontal displacements at the end of shaking.

Figure 7-7 – Results of dynamic analysis of the reinforced impoundment – k_{WR}=1x10^{-4} m/s – Earthquake E1 (M_w=6.5).

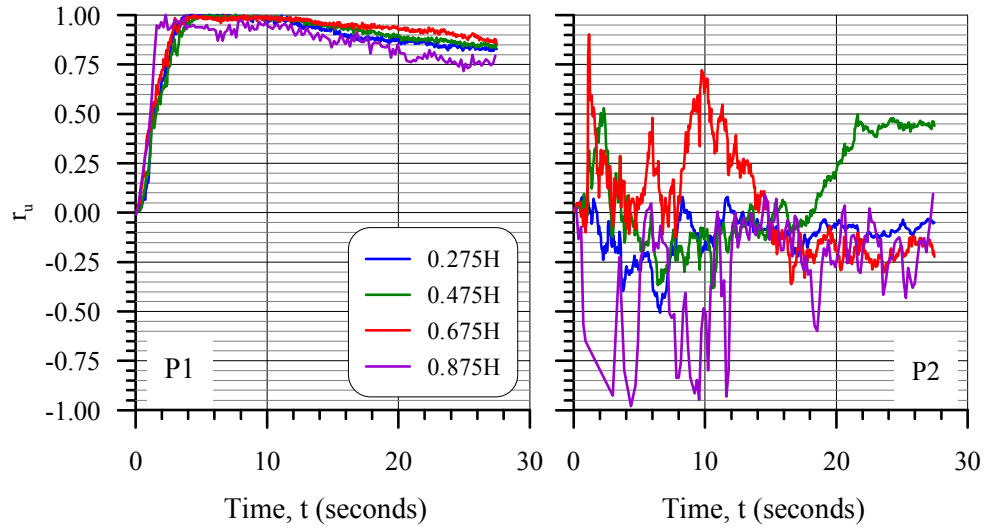

(a) Excess porewater pressure ratio at P1 and P2.

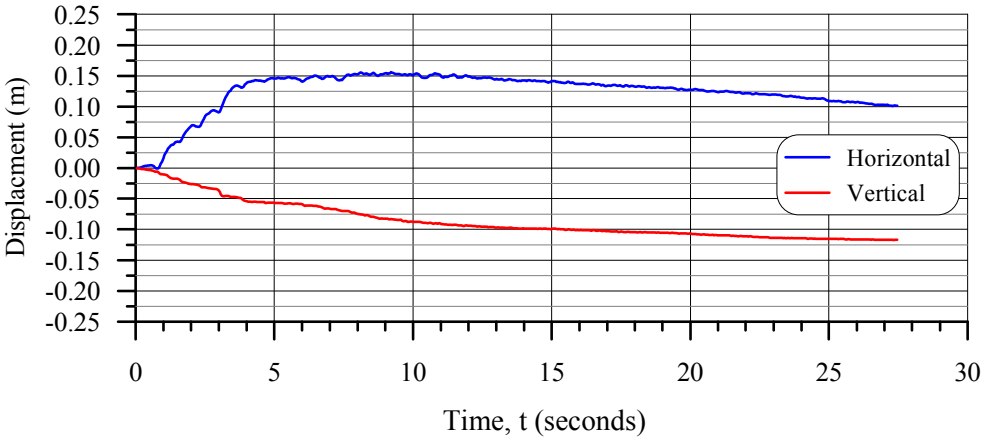

(b) Displacement of the crest of the dike during shaking.

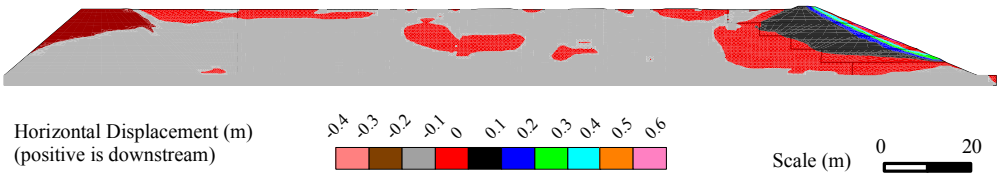

(c) Horizontal displacements at the end of shaking.

Figure 7-8 – Results of dynamic analysis of the reinforced impoundment – k_{WR}=1x10^{-4} m/s – Earthquake E3 (M_w=7.0).

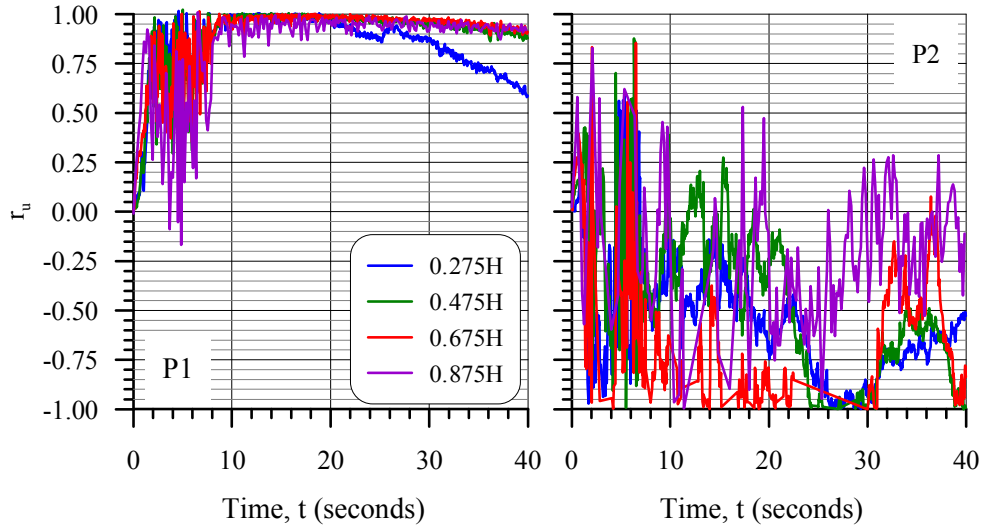

(a) Excess porewater pressure ratio at P1 and P2.

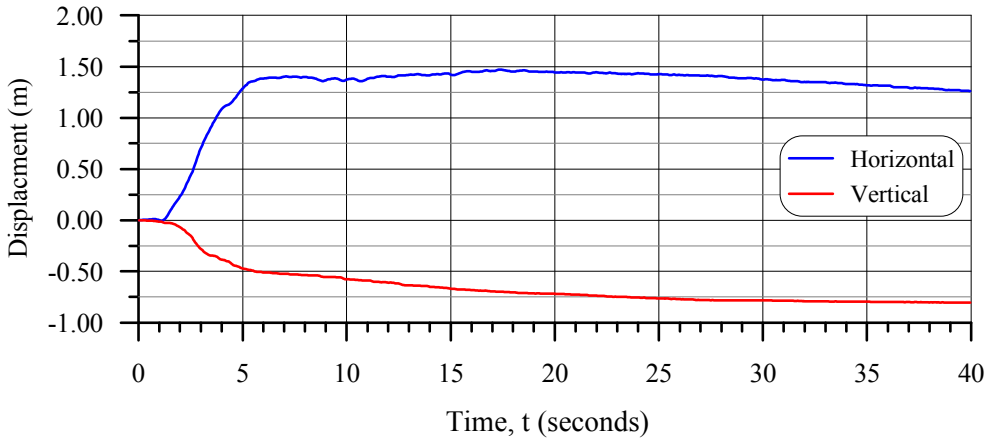

(b) Displacement of the crest of the dike during shaking.

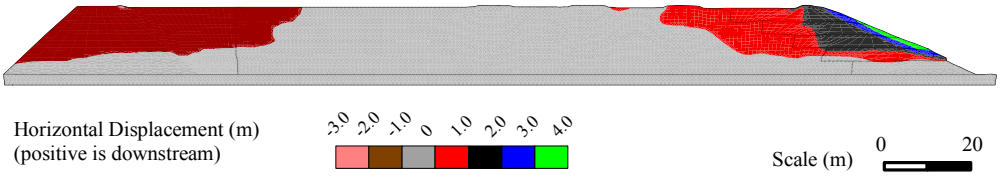

(c) Horizontal displacements at the end of shaking.

Figure 7-9 – Results of dynamic analysis of the reinforced impoundment – k_{WR}=1x10^{-4} m/s – Earthquake E5 (M_w=7.5).

7.2.2 Configuration of the Waste Rock Inclusions

In all of the analyses described thus far, the configuration of the waste rock inclusions in the reinforced impoundment was the same and consisted of five, 8-m-wide inclusions. The first inclusion (from the downstream) was located 12 m upstream of the starter dike, the second was 16 m upstream of the first (measured center-to-center) and next three were at 20 m intervals, measured center-to-center, refer to Figure 6-2. This configuration is the Base Case. This section describes the results of analyses of five alternative configurations of waste rock inclusions (Cases A through E) with respect to Earthquake E5 (M_w=7.5, t=40 s). The results of the analysis are summarized on Table 7-3.

Table 7-3 – Summary of results: Configuration of the waste rock inclusions – Earthquake E5 (M_w=7.5).

Description of Inclusions	Horizontal Displacement of Crest (m)	Vertical Displacement of Crest (m)
Base Case: Five 8-m-wide inclusions at 16 to 20-m center to center.	1.4	-0.85
Case A: Three 8-m-wide inclusions at 16 to 20-m center-to-center	1.1	-0.75
Case B: Five 4-m-wide inclusions at 16 to 20-m center-to-center.	0.9	-0.65
Case C: Two 8-m wide inclusions at 16-m center-to-center.	1.3	-0.75
Case D: Five 6-m-wide inclusions at 16 to 20-m center-to-center.	1.1	-0.70
Case E: Five 8-m-wide inclusions at 24-m center-to-center (see Note 1).	5.0	-1.75

Note 1: The execution of the dynamic analysis for Case E was terminated due to excessive deformation at t=18.5 s.

All of the material properties used in these analyses were the same as those used in Chapter 6. Thus, any differences in the dynamic behavior of the impoundments may be attributed to the configuration of the waste rock inclusions.

The results of the analyses are summarized as follows:

- Case A (Figure 7-10) considered three 8-m-wide waste rock inclusions and is the same the base case without the two upstream inclusions located furthest upstream. The displacements of the crest of the dike for case A at the end of shaking were slightly less than those for the Base Case. However, the horizontal deformation of the downstream slope was about 1 m more for Case A than the Base Case.
- Case B (Figure 7-11) consisted of five 4-m-wide waste rock inclusions at the same spacing as the Base Case. At the end of shaking, the horizontal and vertical displacements of the crest of the dike for this case were 0.9 m (downstream) and 0.65 m (downwards), respectively, and were thus 25 to 35% lower than those of the Base Case. The horizontal deformation of the downstream slope was slightly greater for this case than for the Base Case.
- For Case C (Figure 7-12) there were two 8-m-wide inclusions at 16 m center-to-center (the two downstream inclusions of the Base Case). At the end of shaking, the horizontal displacement of the crest was slightly less than that of the Base Case, the vertical displacement of the crest for this case was the same as the base case, and the horizontal deformations of the impoundment were comparable to those of the Base Case, although they extended 20 m further into the impoundment.
- Figure 7-13 presents the model and results for Case D which was composed of five 6-m-wide inclusions at the same spacing as the Base Case. Compared to the Base Case, this configuration resulted in slightly reduced

displacements of the crest of the dike and a similar pattern and magnitude of horizontal deformation at the end of shaking.

- For Case E (Figure 7-14), there were 8-m-wide inclusions spaced at 24 m center-to-center with the first inclusion located 12 m upstream of the starter dike. The dynamic loading resulted in excessive deformation leading to an end in program execution at t=18.5 s when the crest had displaced 5.0 m downstream and 1.75 m downwards.
- The horizontal velocities within the impoundment at the end of the analyses for Cases A through D were relatively low and not indicative of significant continued deformation. For Case E, the horizontal velocities at t=18.5 s were indicative of significant continued deformation.

Post-shaking analyses were not completed for Cases A through D as it was not considered necessary due to the dynamic performance of the reinforced impoundment being very similar to that of the Base Case, which did not exhibit significant deformation during post-shaking analyses due to Earthquakes E1 through E5.

The parametric evaluation of the configuration of indicates the following:

a) The width of the waste rock inclusions (4, 6 or 8 m) had no significant impact on the dynamic behavior of the impoundment;
b) The number of waste rock inclusions (2, 3, 4 or 5) had no significant impact on the dynamic behavior of the impoundment. The inclusions nearest to the dike appeared to be the critical ones; and
c) Increasing the center-to-center spacing of the inclusions (from 20 m to 24 m) has a detrimental impact on the dynamic behavior of the impoundment and resulted in excessive deformations.

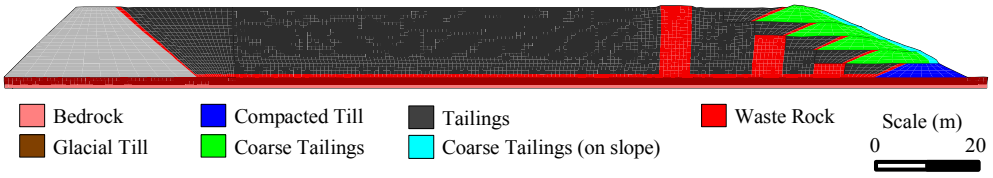

(a) Model of reinforced impoundment with three 8-m-wide inclusions.

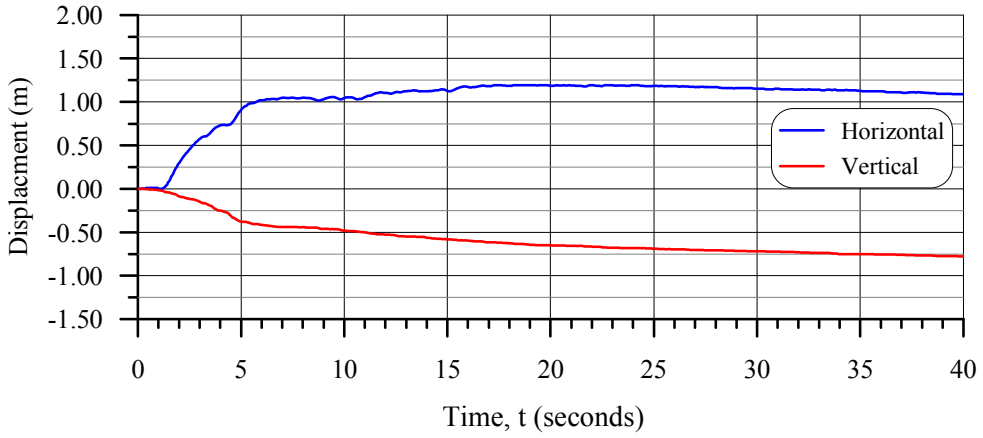

(b) Displacement of the crest of the dike during shaking.

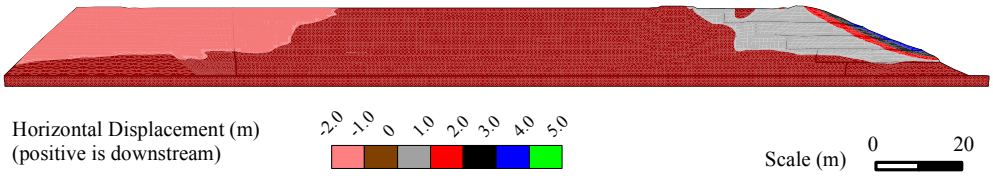

(c) Horizontal displacements at the end of shaking.

Figure 7-10 – Case A: Model and results of analysis of impoundment with three 8-m-wide waste rock inclusions – Earthquake E5 (Mw=7.5).

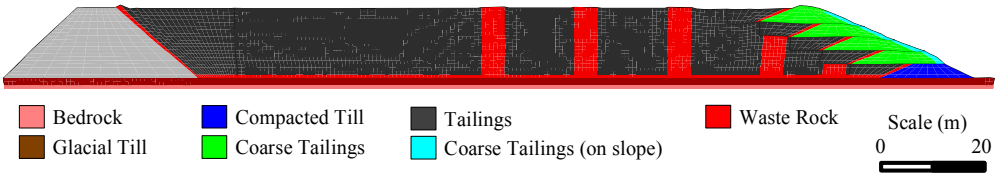

(a) Model of reinforced impoundment with five 4-m-wide inclusions.

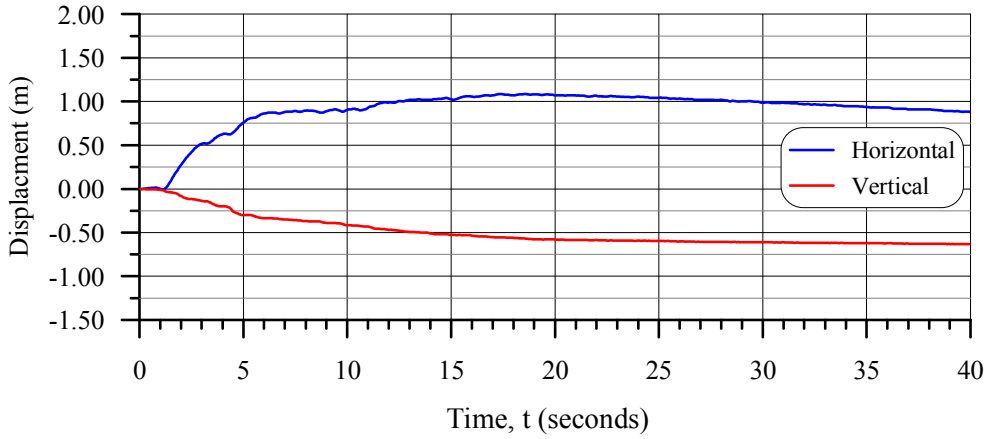

(b) Displacement of the crest of the dike during shaking.

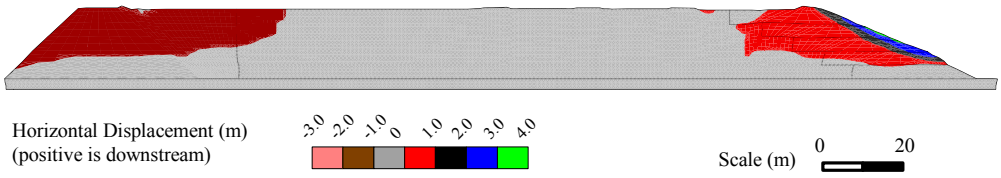

(c) Horizontal displacements at the end of shaking.

Figure 7-11 – Base B: Model and results of analysis of impoundment with five 4-m-wide waste rock inclusions – Earthquake E5 (Mw=7.5).

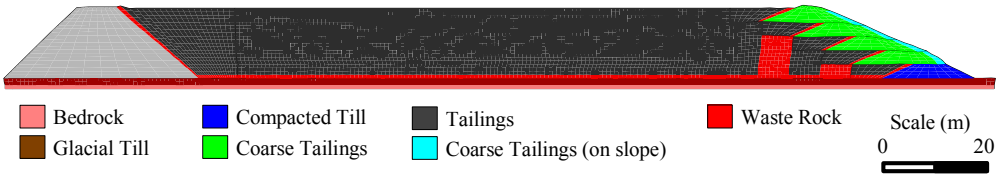

(a) Model of reinforced impoundment with two 8-m-wide inclusions.

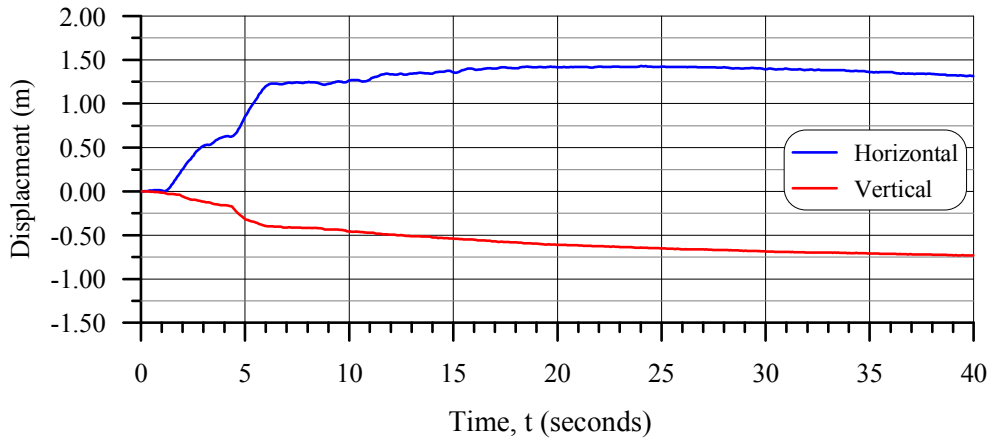

(b) Displacement of the crest of the dike during shaking.

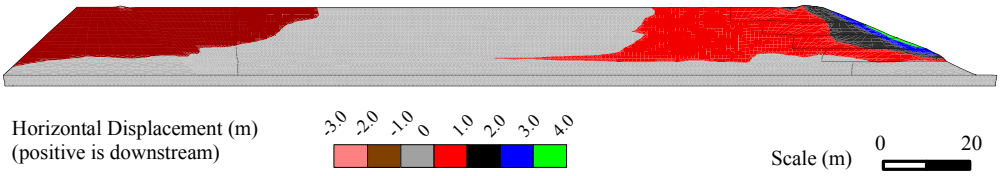

(c) Horizontal displacements at the end of shaking.

Figure 7-12 – Case C: Model and results of analysis of impoundment with two 8-m-wide waste rock inclusions – Earthquake E5 (Mw=7.5).

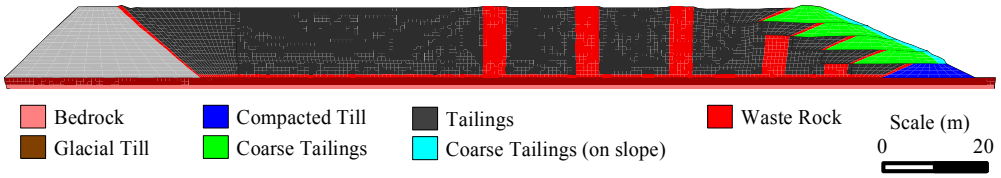

(a) Model of reinforced impoundment with five 6-m-wide inclusions.

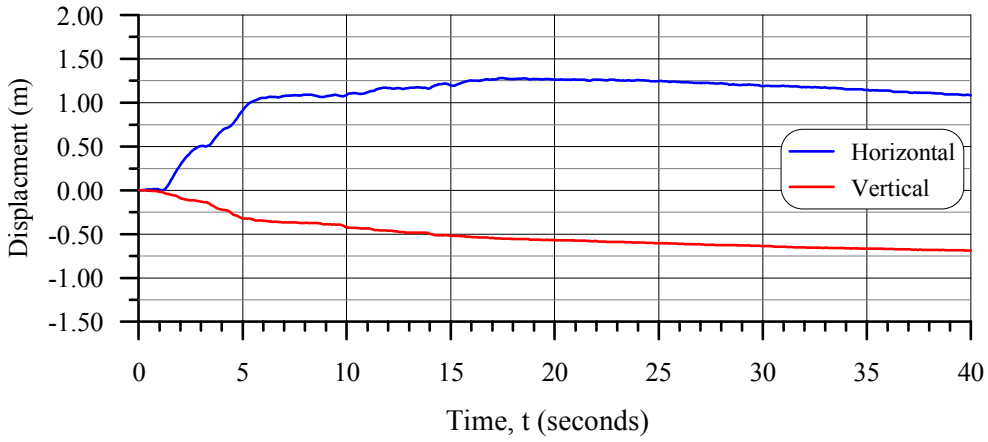

(b) Displacement of the crest of the dike during shaking.

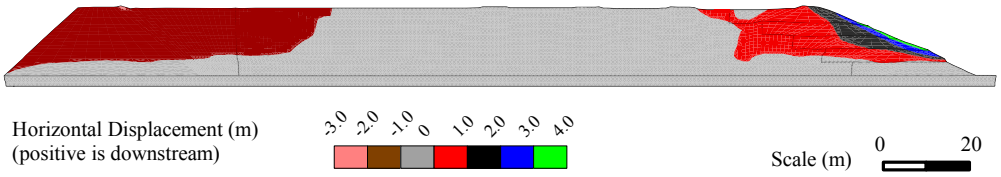

(c) Horizontal displacements at the end of shaking.

Figure 7-13 – Case D: Model and results of analysis of impoundment with five 6-m-wide waste rock inclusions – Earthquake E5 (Mw=7.5).

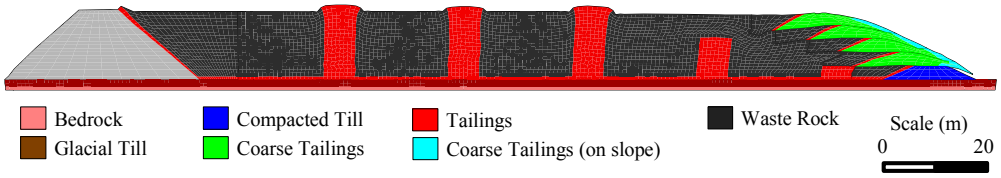

(a) Model of reinforced impoundment with 8-m-wide inclusions at 24-m spacing (center to center).

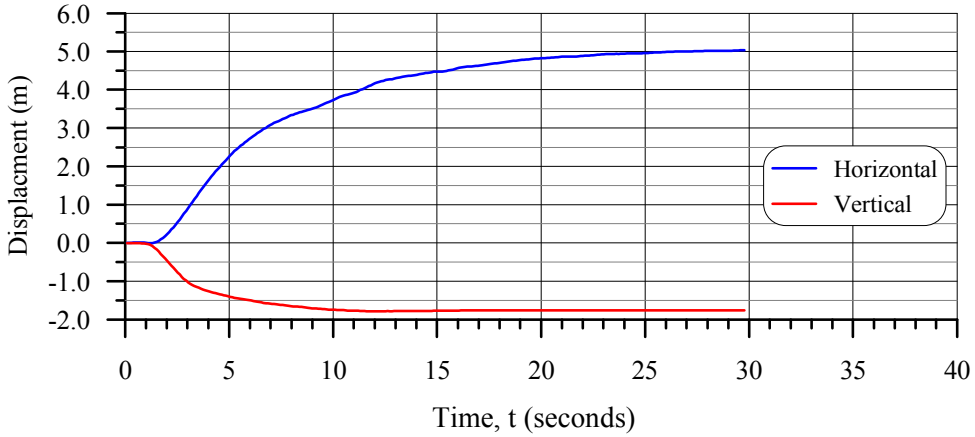

(b) Displacement of the crest of the dike during shaking.

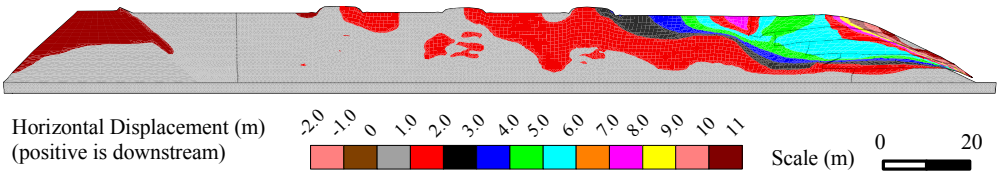

(c) Horizontal displacements at the termination of the simulation (t=29.8 seconds).

Figure 7-14 – Case E: Model and results of analysis of impoundment with five 8-m-wide waste rock inclusions at 24-m on-center – Earthquake E5 (Mw=7.5).

7.2.3 Inclusions Constructed Adjacent to the Dike

An alternative method for the construction of waste rock inclusions in tailings impoundments would consist of placing waste rock adjacent to the starter dike and dike raises before each stage of tailings placement. The result of placement method is illustrated on Figure 7-15a, which shows 16-m-wide zones of waste rock (inclusions) placed on the upstream side of the dike.

This model was subject to the Earthquake E4 (M_w=7.25) ground motion and the results are shown on Figure 7-15. The crest of the dike displaced 1.3 m downstream and 0.3 m upwards during shaking and displacements were essentially complete by the 20th second of shaking. The horizontal deformation of the impoundment varied from 2 m on the downstream slope of the dike to zero 100 m upstream.

The pattern of horizontal deformations suggests that the impounded tailings were being pushed over the starter dike by the dynamic loading. Note that horizontal displacements of the starter dike are at least a 1 m lower than those of the tailings upstream of the starter dike and the dike raises above it. This finding is supported by the rise of the crest of the dike during shaking.

Figure 7-16 presents the results of the dynamic analysis for the impoundment with waste rock placed upstream of the dike as shown on Figure 7-15, but with respect to Earthquake E5 (M_w=7.5). The horizontal displacement of the crest during shaking was 4 m (downstream) with most of the displacement occurring by t=20 s. Vertical displacement of the crest during shaking was 0.1 m upwards. The horizontal deformation of the impoundment was a maximum on the downstream slope of the dike, approaching 7 m, and extended about 100 m into the impoundment. The movement of the impounded tailings over the starter dike was more pronounced here than in the Earthquake E4 analysis presented above.

The horizontal velocities of the impoundment after shaking, for Earthquakes E4 and E5, were relatively low and not indicative of continued deformation.

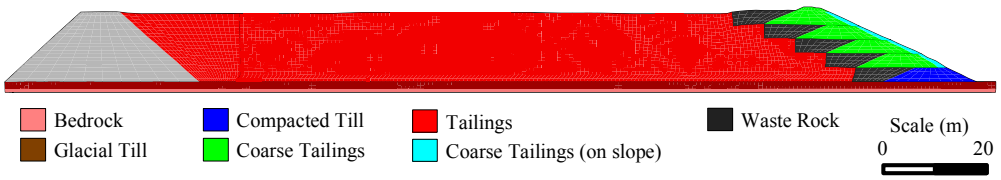

(a) Model of reinforced impoundment 16-m-wide inclusions against dike.

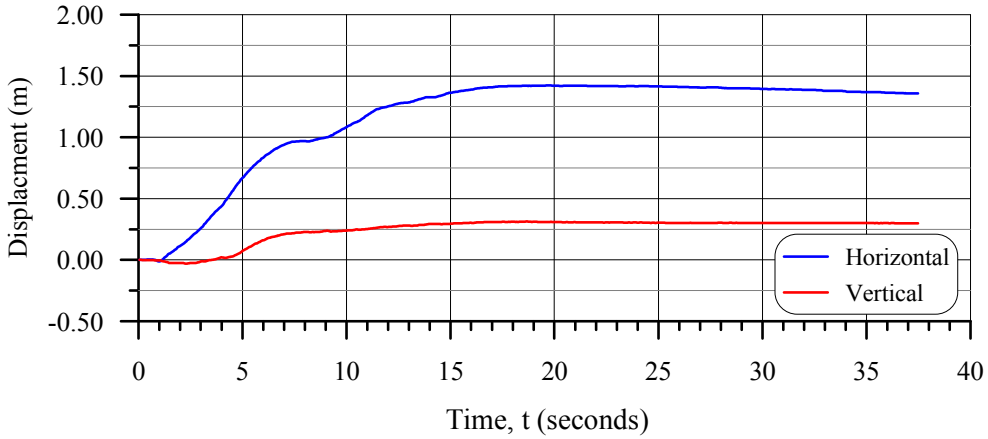

(b) Displacement of the crest of the dike during shaking.

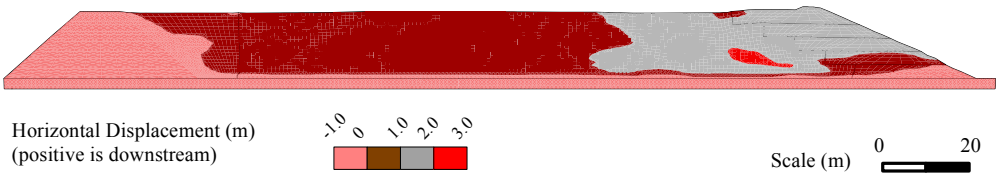

(c) Horizontal displacements at the end of shaking.

Figure 7-15 – Model and results of analysis of impoundment with 16-m-wide waste rock inclusions adjacent to dike – Earthquake E4 (Mw=7.25).

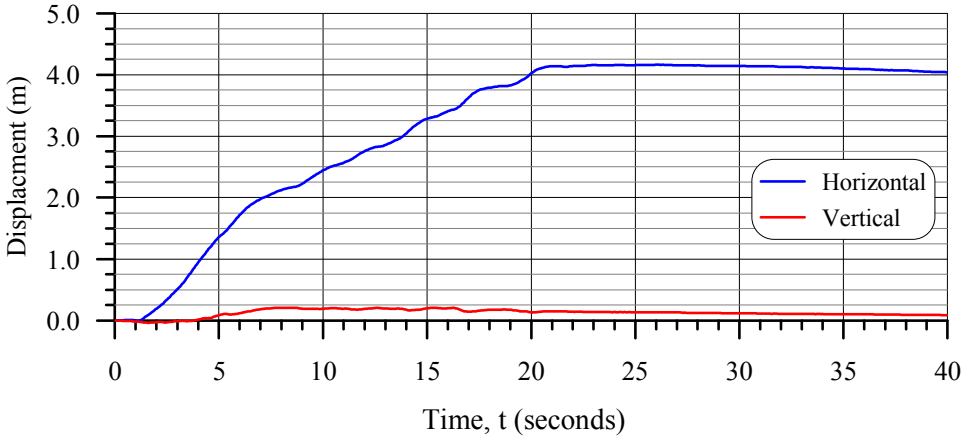

(a) Displacement of the crest of the dike during shaking.

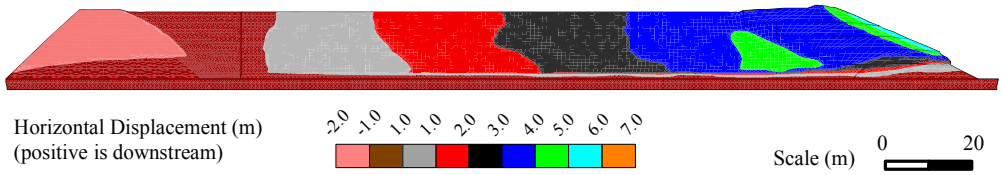

(b) Horizontal displacements at the end of shaking.

Figure 7-16 – Results of analysis of impoundment with 16-m-wide waste rock inclusions adjacent to dike – Earthquake E5 (Mw=7.5).

7.2.4 Inclusions as Closely-spaced Columns

As noted in Section 2.6.2, a possible placement method of waste rock inclusions into existing impoundments would be to construct waste rock columns within the tailings. This would be comparable to the construction of gravel (or stone) columns in soil deposits to control the effects of liquefaction and would require the waste rock to be crushed to the size of gravel (to a maximum grain size of approximately 75 mm diameter) so it could be placed into drilled holes.

The inclusions were assumed to consist of 10 rows, of 1-m-diameter waste rock columns, spaced at 3 m center-to-center and starting 16 m upstream of the crest (refer to

Figure 7-17a). This model was subject to the Earthquake E4 (M_w=7.25) and E5 (M_w=7.5) loadings. The results are described below.

As presented on Figure 7-17, the displacements of the crest during Earthquake E4 were 2.5 m downstream and 2.7 m downwards and a majority of the displacement occurred during the first 15 seconds of shaking. Horizontal deformation of the impoundment was generally confined to the area downstream of the waste rock columns and exceeded 6 m.

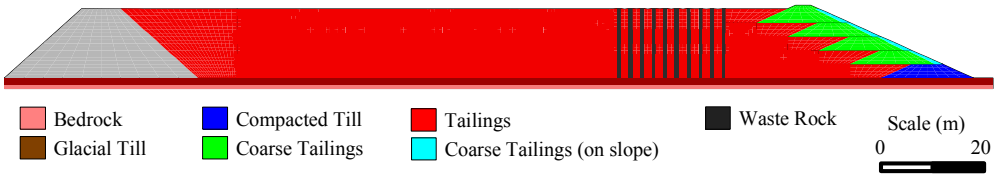

(a) Model of impoundment with 10 rows of 1-m-diameter waste rock columns at 3 m spacing (center-to-center).

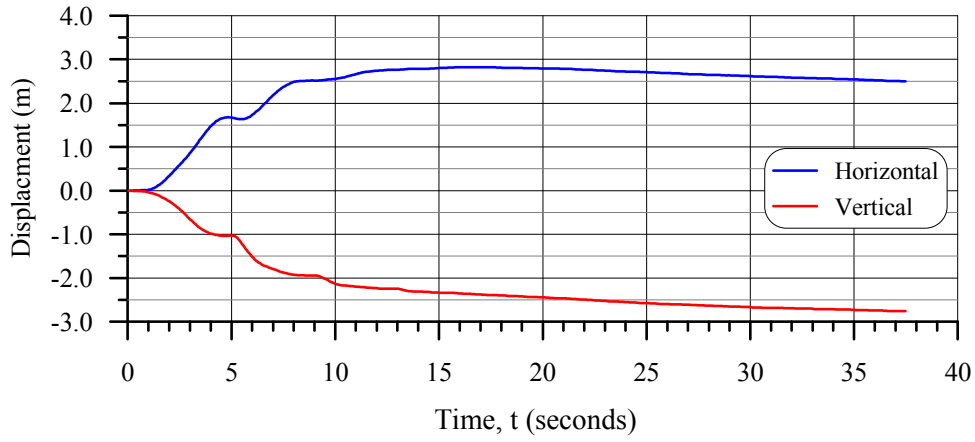

(b) Displacement of the crest of the dike during shaking.

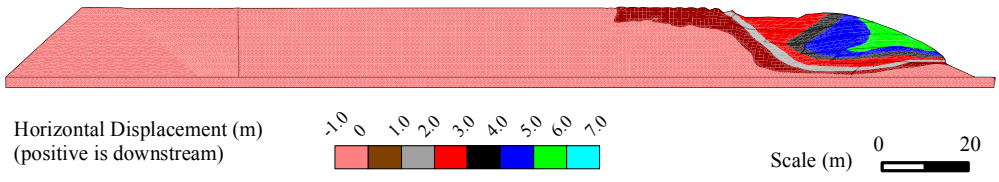

(c) Horizontal displacements at the end of shaking.

Figure 7-17 – Model and results of analysis of impoundment with waste rock columns – Earthquake E4 (M_w=7.25).

The results of the dynamic analysis of the impoundment with respect to Earthquake E5 are provided on Figure 7-18. The analysis was terminated at t=14.1 s into the 40 s ground motion due to excessive deformation. Displacements of the crest of the dike at t=14.1 s were 3.5 m downstream and 2.9 m downwards. The horizontal deformation of the impoundment was generally limited to the area downstream of the waste rock columns and the maximum exceeded 9 m (on the downstream slope). The surface of the impoundment in the area of the waste rock columns moved approximately 1 m downstream by the end of the analysis.

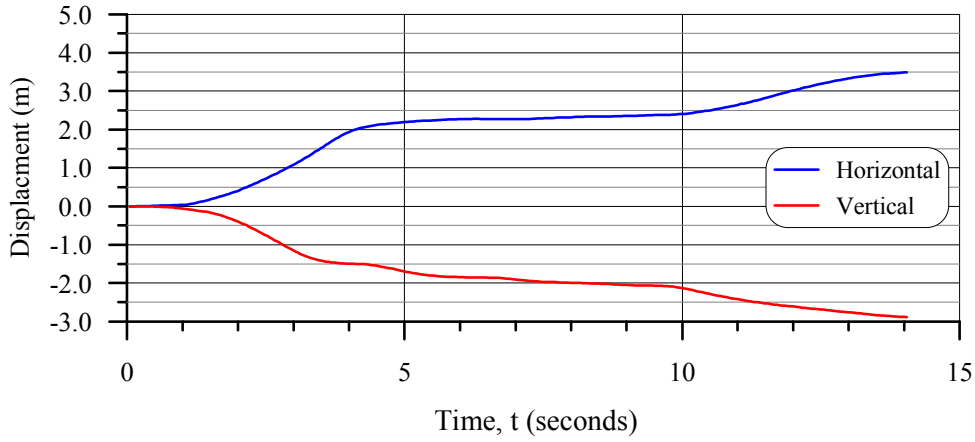

(a) Displacement of the crest of the dike during shaking.

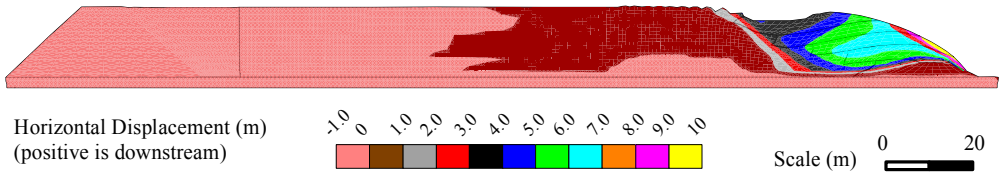

(b) Horizontal displacements at t=14.1 seconds.

Figure 7-18 – Results of analysis of impoundment with waste rock columns – Earthquake E5 (Mw=7.5).

The magnitudes and patterns of horizontal velocity in the impoundment at the end of the Earthquake E4 analysis did not indicate significant continued deformation. However, the horizontal velocities at the end of the Earthquake E5 analysis indicated significant deformation would have occurred had shaking continued.

7.3 REMARKS ON THE PARAMETRIC EVALUATIONS

Observations were developed from the parametric evaluations. The relevancy of these conclusions is limited to the analyses conducted in terms of the impoundment geometry, waste rock configurations considered, material properties, earthquake loads, and methods used in analysis and evaluation. In summary:

- The degree of consolidation of the retained tailings (from highly under-consolidated to normally consolidated) had a minor effect on the dynamic behavior of the conventional impoundment. Generally, deformations decreased slightly with increasing degrees of consolidation.
- Compaction of the coarse tailings used to construct the dike (resulting in $(N_1)_{60}$ values of 11 to 22 blows/300 mm) had no significant effect on the dynamic behavior of the impoundment.
- The saturated hydraulic conductivity of the waste rock inclusions (k_{WR} of $1x10^{-4}$ m/s and $1x10^{-6}$ m/s had no significant effect on the dynamic behavior of the impoundment.
- With respect to the configuration of the waste rock inclusions:
    a) The width of the waste rock inclusions (4, 6 or 8 m) had no significant impact on the dynamic behavior of the impoundment;
    b) The number of waste rock inclusions (2, 3, 4 or 5) had no significant impact on the dynamic behavior of the impoundment. The two inclusions nearest to the dike were critical in improving the seismic performance of the impoundment; and

c) Increasing the center-to-center spacing of the inclusions (from 20 m to 24 m) had a detrimental impact on the dynamic behavior of the impoundment and resulted in excessive deformation.

- Constructing waste rock inclusions against the upstream side of the dike resulted in relatively large deformations, but actually resulted in an increased crest height.
- Constructing columns of waste rock in the impoundment allowed excessive deformation of the tailings and dike downstream of the columns, but limited deformation of the impoundment upstream of the columns.

7.4 DISCUSSION

As described in Chapter 1, the primary elements of this research consisted of:

- A review of the state of knowledge and practice with respect to the various aspects of the research;
- A geotechnical study of a representative tailings impoundment;
- Preliminary numerical modeling;
- Numerical modeling of the representative impoundment;
- Numerical modeling of a conceptual impoundment;
- Parametric evaluation of the conceptual impoundment; and
- The formulation of conclusions and recommendations regarding the research (Chapter 8).

This section presents a general discussion of the and findings of the research presented.

The review of the state of knowledge and practice (Chapter 2) revealed that there are significant areas of uncertainty regarding the evaluation of the liquefaction potential of hard rock tailings, the evaluation of the seismic stability of tailings impoundments and means of improving the seismic stability of tailings impoundments by controlling the effects of liquefaction of the impounded tailings. To be specific:

a) Existing analytical methods for the evaluation of the liquefaction potential of soils, e.g. the Simplified method of Seed & Idriss (1982), may not be directly applicable to tailings due to differences in gradation, strength, and soil fabric.

b) The use of the results of in situ testing of tailings deposits must consider the differences in the behavior and properties of tailings and naturally occurring soils as well as the degree of consolidation of the tailings, particularly when considering correlations developed for normally and over-consolidated naturally occurring soils.

c) Although saturated hard rock tailings are known to be susceptible to liquefaction, there has been a limited amount of research quantifying their liquefaction resistance when under-consolidated or normally consolidated.

d) For decades, gravel inclusions (gravel columns) have been successfully used to control the effects of liquefaction in sands by limiting the development of excess porewater pressures. However, it is not known what the effects of similar inclusions in tailings would be, given that the hydraulic conductivity of tailings is generally much lower than that of sands and tends to be highly anisotropic and might not allow excess porewater pressures dissipation to the inclusions at the same rate as sands (additional work is needed on this aspect).

e) There are a number of numerical models that have been developed to simulate the dynamic behavior of sand. However, their ability to simulate the dynamic behavior of tailings has been demonstrated in only a few cases.

f) Existing analytical methods for the evaluation of the seismic stability of dams, e.g. the pseudo-static method and Makdisi & Seed (1977, 1978, 19793), are widely applied to tailings impoundments in professional practice, even though they were not specifically developed to consider the effects of excess porewater pressure generation and liquefaction of the retained tailings or of the tailings forming the dikes.

g) Dynamic numerical analysis represents the current state of the practice with respect to the evaluation of the seismic stability of tailings impoundments and is specifically required by some agencies, e.g. CDA (2007) and *Directo Superemo No. 248 del Ministerio Mineria*, Chile (2007). However, there are no standards or guidelines regarding how it is to be implemented in terms of the assumptions, methods, and interpretation of the results.

To get to the objective of this research, evaluating the use of waste rock inclusions to control the effects of liquefaction in tailings impoundments, it was necessary to explore all of these areas.

The geotechnical study of the representative tailings impoundment (Chapter 3) was the first step in researching some of the issues raised in Chapter 2. The study consisted of:

- Document review (e.g. geologic and topography maps, aerial photographs, construction drawings);
- Field exploration (test pits and CPT);
- Conventional and dynamic laboratory testing;
- Evaluation of site conditions;
- Characterization of the tailings as under-consolidated and as normally consolidated material;
- Analytical evaluation of the liquefaction potential of the tailings (under-consolidated and normally consolidated) under level ground conditions; and
- Analytical evaluation of the static and seismic stability of the impoundment.

The study found that:

a) The properties and characteristics of the tailings in the representative impoundment were similar to those in published sources for hard rock tailings and thus were deemed to be reasonable;
b) The tailings were found to have greater shear strength than naturally occurring soils of similar gradation (silts and silty sands);

c) The dynamic site response of the tailings deposit differed substantially from published values for loose soil and the variations in the PGA with depth varied substantial from the stress reduction coefficient, r_d, presented in the Simplified method (Youd et al., 2001);

d) The dynamic behavior and liquefaction resistance of the tailings in normally consolidated CDSS testing was similar to that of loose, fine-grained sand and the liquefaction resistance was independent of confining stress ($\sigma'_{v,c}$=100 to 400 kPa). The high silt content of the tailings (35 to 50%), had no apparent effect on the liquefaction resistance, indicating that correcting the penetration resistance of tailings for silt content as recommended in the Simplified method (Youd et al., 2001) might not be necessary.

e) The analytical liquefaction evaluations indicated the tailings had a high potential for liquefaction under the earthquake loads considered; and

f) A pseudo-static evaluation of the impoundment found that liquefaction of the tailings resulted in considerable loading on the dam and had a very negative impact on its stability. The potential failure surface extended far into the impoundment, indicating that the dynamic loading of the liquefied tailings was strongly implicated in the stability.

Numerical analyses of the CDSS testing and level ground liquefaction are presented in Chapter 4. The analyses of the CDSS testing served to calibrate and validate, to some extent, the use of FLAC and the UBC Sand model by reasonably simulating the 20 CDSS tests conducted at various effective vertical consolidation stresses and cyclic stress ratios. Parameters obtained from the modeling were used in the remainder of the numerical modeling for this research. The numerical analyses of level ground liquefaction was compared to the analytical liquefaction evaluations presented in Chapter 3 based on the Simplified method. Generally, it was found that there was reasonable agreement between the results of the analytical and numerical methods for the earthquake loadings used.

Chapter 5 presents the dynamic numerical evaluations of the representative impoundment, that is formed by a raised zoned earthfill dike. The evaluations were conducted on the impoundment in its current condition (as-built) and assuming the presence of waste rock inclusions. The as-built numerical evaluation was compared to the analytical (pseudo-static) evaluation presented in Chapter 3 and to the numerical evaluation with waste rock inclusions. The analytical evaluation indicated a factor of safety of 0.88 under seismic conditions, while the numerical evaluation provided no evidence of unacceptable behavior under an equivalent dynamic loading. The numerical evaluation with waste rock inclusions indicated a significant reduction in deformation due to the presence of the inclusions.

The comparative numerical analyses of the conceptual impoundment, with and without waste rock inclusions, presented in Chapter 6 led to the following observations:

a) At the five earthquake loadings used, the presence of the waste rock inclusions within the impoundment resulted in less damping of the ground motion as it rose through the tailings.
b) The presence of the waste rock inclusions, and the 1-m-thick layer of waste rock in the bottom and sides of the impoundment, reduced the generation of excess porewater pressures in the adjacent tailings.
c) The displacements of the impoundment were reduced by as much as an order of magnitude when the waste rock inclusions were present.
d) The extent of the deformation in the impoundment was significantly reduced by the waste rock inclusions. Typically, significant deformations extended 100 or more into the impoundment without waste rock inclusions, but were limited to the area of the dike in the impoundment with waste rock inclusions.

From the parametric evaluations of the conceptual impoundment presented in Sections 7.1 and 7.2, these observations developed:

a) Neither the degree of consolidation of the retained tailings nor the degree of compaction of the tailings used to form the dike had a significant impact on the dynamic behavior of the tailings impoundment without waste rock inclusions.
b) The hydraulic conductivity of the waste rock inclusions had no significant effect on the dynamic behavior of the impoundment, specifically not on the generation of excess porewater pressures during shaking.
c) Although the size and number of waste rock inclusions had no significant impact on the dynamic behavior of the impoundment, increasing the spacing of the inclusions from 20 m to 24 m (center to center), resulted in much higher deformation of the impoundment in the vicinity of the dike.
d) Constructing waste rock inclusions against the upstream side of the dike raises resulted in relatively large deformations in the vicinity of the dike and the pattern of deformations indicated that the tailings were being pushed over the starter dike.

An issue that has not been addressed thus far is the influence of the starter dam. Recall that the starter dam was assumed to be constructed of compacted glacial till with an effective friction angle of 32° and a cohesion of 200 kPa. These strength parameters represented well-compacted material of good quality and were chosen specifically to avoid excessive deformation of the impoundment due to deformation or failure of the starter dike. In practice, starter dams were typically constructed of whatever material was available at the time, often waste rock, and proper compaction was not a priority. The potential for deformation or failure of the impoundment due to the starter dam was not considered in this research.

The analyses and evaluations presented in this thesis tend to indicate that waste rock inclusions may constitute a viable option to control the effects of liquefaction in tailings impoundments.

CHAPTER 8. CONCLUSIONS AND RECOMMENDATIONS

As stated in Chapter 1, the primary objectives of this research were to: a) evaluate the behavior of a conceptual tailings impoundment subjected to seismic loading and to assess the use of waste rock inclusions to control the effects of liquefaction in tailings impoundments; and b) provide conclusions and recommendations regarding the use of waste rock inclusions. The work that was undertaken to achieve these objectives involved several phases. Observations, conclusions and recommendations were developed from the various phases of the research and are presented in the following sections.

The conclusions and recommendations are based on the research conducted, including the assumed material properties, earthquake loadings, impoundment and waste rock inclusions configurations, and subsurface conditions, and thus may not always be applicable to particular situations.

8.1 CONCLUSIONS

In Chapter 2 (The State of Knowledge and Practice), the need for effective and practical means of determining the liquefaction potential of tailings, evaluating the seismic stability of tailings impoundments and controlling the effects of liquefaction on tailings impoundments was demonstrated. Existing tools and promising approaches were reviewed in relation to the objectives.

From Chapter 3, the geotechnical study of tailings impoundment, the following conclusions were developed:

a) Based on CDSS testing, the dynamic behavior and liquefaction resistance of the tailings evaluated was similar to that of loose, fine-grained sand.

b) The shear strength (effective friction angle) of the tailings was significantly higher than that of sands of similar gradation.

c) The Simplified method of liquefaction evaluation, as described by Youd et al. (2001), may be applicable to tailings. However, the applicability of the

corrections to the penetration resistance, static shear stress and overburden stress correction factors, and magnitude scaling factors may be site-specific based comparisons between the results of CDSS shear testing and analyses using the Simplified method.

d) Based on pseudo-static evaluation of the seismic stability of the representative impoundment, it was found that liquefaction of the tailings resulted in an unacceptable factor of safety on a non-circular potential failure surface that extended relatively far into the impoundment. The result using a circular failure surface was very unconservative. The use of pseudo-static analysis with circular failures surfaces to evaluate the seismic stability of the tailings impoundments may be unconservative because the dynamic loading of the liquefied tailings on the retention structure may be excluded.

Preliminary numerical analyses were presented in Chapter 4 and the following conclusions were derived from the analyses:

a) The FLAC software program and the UBC Sand model could be used to model the dynamic behavior and liquefaction of the tailings.

b) Comparisons of level ground liquefaction analyses conducted using the Simplified (analytical) method and dynamic numerical analyses revealed significant differences in the site responses for all levels of loading and in the expected depth of the liquefied zone for the moment magnitude 6.5 earthquake loading (Earthquake E1).

The following conclusions were developed from Chapter 5, the numerical analyses of the representative impoundment, with and without waste rock inclusions:

a) The potential mode of failure of the impoundment as-built was similar to that of the pseudo-static analysis presented in Chapter 3.

b) The presence of waste rock inclusions in the impoundment resulted in a stiffer response (less damping) within the impoundment and a substantial reduction in the deformation of the impoundment, particularly the dike, due to shaking.

From Chapters 6 and 7, which presented comparative numerical analyses of a conceptual upstream-raised tailings impoundment, with and without waste rock inclusions, under various loadings and parametric considerations, conclusions were developed regarding the use of waste rock inclusions to control the effects of liquefaction in tailings impoundments The presence of waste rock inclusions in the conceptual tailings impoundment led to:

a) Stiffer site responses (less damping of the ground motion) in the area of the inclusions.

b) Decreased excess porewater pressure development in the area of the inclusions.

c) Order of magnitude reductions in the deformations of the impoundment due to seismic loading.

d) The extent of the zones from which tailings would be lost due to failure of the impoundment was reduced to the area in the vicinity of the dike (downstream and above the inclusions), rather than the width of the impoundment.

Regarding the parametric evaluations:

a) Neither the degree of consolidation of the retained tailings nor the degree of compaction of the tailings used to construction the dike had a significant impact on the dynamic behavior of the impoundment without waste rock inclusions.

b) The hydraulic conductivity of the waste rock inclusions had no significant impact on the dynamic behavior of the impoundment with waste rock inclusions.

c) Although the width (4 to 8 m) and number (2 to 5) of inclusions considered did not have a significant impact on the dynamic behavior of the impoundment, increasing the spacing of the inclusions from 20 m to 24 m (center-to-center), resulted in much greater deformation in the area of the dike.

d) Inclusions consisting of 16-m-wide benches of waste rock placed against on the upstream side of the starter dike and subsequent raises allowed relatively large deformation of dike and adjacent portion of the impoundment.

e) The use of columns of waste rock in the conceptual impoundment resulted in large deformations downstream of the columns and relatively small deformations in the areas of the columns and upstream.

In general, the use of waste rock inclusions resulted in a significant improvement in the dynamic performance of the conceptual impoundment under the earthquake loadings considered (M_w=6.5 to 7.5).

8.2 RECOMMENDATIONS

8.2.1 The Use of Waste Rock Inclusions to Control the Effects of Liquefaction in Tailings Impoundments

The following recommendations provide general guidance for the use of waste rock inclusions to control the effects of liquefaction in tailings impoundments.

The use of waste rock inclusions should be considered in proposed tailings impoundments where the risk of excessive deformation or failure due to seismic loading and liquefaction is a concern. In existing tailings impoundments where this concern exists, installing columns of waste rock in the tailings could help control deformation of the impoundment.

Evaluation of the use of waste rock inclusions at a particular site should include the following:

a) In the planning stages of a project, a feasibility study on the placement of the waste rock inclusions during tailings deposition;

b) A geotechnical study of site and subsurface conditions, including the dynamic properties of the tailings; and

c) Comprehensive dynamic numerical analyses of alternative configurations of waste rock inclusions over a range of expected seismic loadings of varying intensity, frequency and duration, with parametric evaluation of material critical properties.

8.2.2 Additional Research

The co-disposal concept of using waste rock inclusions to control the effects of liquefaction in tailings impoundments was initially proposed by Aubertin et al. (2002a), and there are several areas where additional research is recommended for its further development. These areas include:

a) Evaluation of the dynamic behavior and liquefaction potential of unconsolidated and normally consolidated tailings based on in situ testing.

b) The effect of waste rock inclusions on the deposition and consolidation of tailings.

c) The dynamic properties of waste rock.

d) The use of waste rock inclusions in impoundments of various sizes and shapes and in impoundments located on sloped ground.

e) The effects of the shape of the waste rock inclusions due to incremental placement.

f) The effect of earthquake frequency on the performance of impoundments with waste rock inclusions.

g) The effect of the third dimension and two-dimensional shaking in the dynamic behavior of impoundments.

h) The potential and effects of tailings infiltration into the waste rock inclusions.

The research may consist of conventional and dynamic laboratory testing, including shaking table tests on physical models, and dynamic numerical analyses.

Research on the consolidation of tailings due to the presence of waste rock inclusions, including, the effect of infiltration of tailings into the waste rock is currently underway at Ecole Polytechnique.

8.3 CLOSURE

This research was conducted to meet a specific objective, an evaluation of the use of waste rock inclusions to control the effects of liquefaction in tailings impoundments. The information, findings and conclusions presented may not be applicable to any specific site or condition and should not be used for any specific site or condition.

Hopefully, this document provides a sufficient basis for further research and for further study of the liquefaction potential of tailings and the seismic stability of tailings impoundments.

CHAPTER 9. REFERENCES

Acres International Limited (ACRES). (1990). Report: Safety Assessment of Existing Dams for Earthquake Conditions, Volume B, Ground Motion Parameter Maps.

Adalier, K., Elgamal, A., Meneses, J., & Baez J. I. (2003). Stone Columns as Liquefaction Countermeasure in Non-plastic Silty Soils. *Soil Dynamics and Earthquake Engineering,* 571-584.

Adalier, K. & Aydingun, O. (2003). Numerical Analysis of Seismically Induced Liquefaction in Earth Embankment Foundations – Part I: Benchmark Model. *Canadian Geotechnical Journal, 40*, 753-765.

Adalier, K. & Sharp, M. (2004). Embankment Dam on Liquefiable Foundation: Dynamic Behavior and Densification Remediation. *Journal of Geotechnical and Geoenvironmental Engineering, 130*(11)*,* 1214-1224.

Adams, J & Halchuk, S. (2003). Fourth Generation Seismic Hazard Maps of Canada: Values for Over 650 Canadian Localities Intended for the 2005 National Building Code of Canada (Open File Report No. 4459). Ottawa: Geological Survey of Canada.

Adrianopoulos, K. I., Papadimitriou, A. G. & Bouckovalas. (2006). Implementation of a bounding surface model for seismic response of sand*. Proceedings of the 4th International FLAC Symposium on Numerical Modeling in Geomechanics*, *Madrid, Spain.* (pp. 387-393). Minneapolis: Itasca Consulting Group, Inc.

Angnico Eagle (2008). *Laronde Mine.* Agnico Eagle Mines Ltd. Condulted: November 2008. http://www.agnico-eagle.com/English/OperatingMines/LaRondeMine.

Alarcon-Guzman, A., Leonards, G. A. & Chameau, J. L. (1988). Undrained Monotonic and Cyclic Strength of Sands*. Journal of Geotechnical Engineering, ASCE, 114*(10)*,* 1089-1109.

Ambraseys, N. N. (1988). Engineering seismology. *Earthquake Engineering and Structural Dynamics*, 17, 1–105.

American Society of Testing Materials (ASTM). (2000). Standard Classification of Soils for Engineering Purposes (Unified Soil Classification System). ASTM International, D2487-00.

Amini, F & Qi, G. Z. (2000). Liquefaction Testing of Stratified Silty Sands. *Journal of Geotechnical and Geoenvironmental Engineering, 126*(3), 208-217.

Andrus, R. D., and Stokoe, K. H., II. (1997). Liquefaction Resistance Based on Shear Wave Velocity. *Proceeding of the NCEER Workshop on Evaluation of Liquefaction Resistance of Soils*, National Center for Earthquake Engineering Research. State University of New York at Buffalo, (pp. 89–128).

Andrus, R. D. & Stokoe, K. H. II (1999). A Liquefaction Evaluation Procedure Based on Shear Wave Velocity. *Proceedings of the Joint Meeting of the U.S.-Japan Cooperative Program in Natural Resources Panel on Wind and Seismic Effects. Tsukuba, Japan*, (pp. 71-78).

Arango, I. (1994). *Methodology for Liquefaction Potential of Site East of the Rockies.* Technical Report. (Vols. 1 & 2) San Francisco: Bechtel Corporation.

Arango, I. (1996). Magnitude Scaling Factors for Soil Liquefaction Evaluations. *Journal of Geotechnical Engineering, 122*(11), 929-936.

Arduino, P. & Macari, E. J. (2001a). Implementation of Porous Media Formulation for Geomaterials. *Journal of Engineering Mechanics*, *127*(2), 157-166.

Arduino, P. & Macari, E. J. (2001b). Numerical Analysis of Geomaterials within Theory of Porous Media. *Journal of Engineering Mechanics, 127*(2), 167-175.

Aubertin, M., Bussière, B. & Chapuis, R. P. (1996). Hydraulic Conductivity of Homogenized Tailings from Hard Rock Mines. *Canadian Geotechnical Journal, 33*, 470-482.

Aubertin, M., Bussière, B. & Bernier, L. (2002). *Environnement et gestion des rejets miniers* [CD-ROM Manual]. Montréal: Presses Internationales Polytechnique.

Aydingun, O. & Adalier, K. (2003). Numerical Analysis of Seismically Induced Liquefaction in Earth Embankment Foundations – Part II: Application of Remedial Measures. *Canadian Geotechnical Journal, 40*, 766-779.

Barbour, S. L. & Krahn, J. (2004). Numerical Modelling – Prediction or Process? *Geotechnical News*, 44-52.

Bardet, J. P., Ichi, K. & Lin, C. H. (2000). EERA : A Computer Program for Equivalent-linear Earthquake Site Response Analyses of Layered Soil Deposits [computer software]. Los Angeles: University of Southern California – Department of Civil Engineering.

Bardet, J. P. & Tobita, T. (2001). NERA: Nonlinear Earthquake Site Response Analyses of Layered Soil Deposits [computer software]. Los Angeles:University of Southern California - Department of Civil Engineering.

Barksdale, R. D. (1987). *Applications of the State of the Art of Stone Columns – Liquefaction, Local Bearing Failure, and Example Calculations,* Technical Report No. REMR-GT-7, Washington DC: US Army Corps of Engineers.

Basham, P. W., Wiechert, D. H., Anglin, F. M. & Berry, M. J. (1985). New Probabilistic Strong Seismic Ground Motion Maps of Canada, *Bulletin of the Seismological Society of America*, 75, 563-595.

Beaty, M. & Byrne, P. M. (1998). An Effective Stress Model for Predicting Liquefaction Behavior in Sand. *Proceedings of Geotechnical Earthquake Engineering III, Seattle, Washinton*, (Vol. 75, pp. 766-777). Reston VA: ASCE.

Been, K., Crooks, J. H. A., Conlin, B. H. & Horsfield, D. (1988). Liquefaction of Hydraulically Placed Sand Fills. *Hydraulic Fill Structures, SGP 21*, 573-591.

Been, K., Jefferies, M. G. & Hachey, J. (1991). The critical state of sands. *Geotechnique, 41*(3), 365-381.

Beikae, M. (1997). A Seismic Analysis Technique for Tailings Dams. *Proceedings of the International Conference on Tailings and Mine Waste '97, Fort Collins, Colorad* (pp. 181-191). Rotterdam: Balkema.

Bhatia, S., Schwab, J. & Ishibashi, I. (1985). Cyclic Simple Shear, Torsional Shear and Triaxial - A Comparitive Study. In Vijay Khosla (Ed.), *Proceedings of Advances in the Art of Testing of Soils Under Cyclic Conditions*, (Vol., pp. 232-254). New York, NY: ASCE.

Bilham, Roger. (2003) Earthquakes and tectonic plate motions/Historic and future Indian earthquakes. Consulted on December 1, 2006, http://cires.Colorado.edu/~bilham/verbatimaccounts1819.hmml

Bolt, B. A. (2004). Earthquakes (5^{th} edition). New York: W. H. Freeman and Company.

Bolton, M. D. (1986). *The Strength and Dilatancy of Sands. Geotechnique, 36*(1), 65-78.

Bouckovalas, G.D., Andrianopoulos, K. I & Papadimitriou, A.G. (2003). A Critical State Intrepretation of the Cyclic Liquefaction Resistance of Silty Sands. *Soil Dynamics and Earthquake Engineering,* 23, 115-125.

Bouferra, R., Benseddiq, N. & Shahrour, I. (2007). Saturation and Preloading Effects on the Cyclic Behavior of Sand. *International Journal of Geomechanics, 7*(5), 396-401.

Boulanger, R. W. & Seed, R. B. (1995). Liquefaction of Sand Under Bidirectional Monotonic and Cyclic Loading. *Journal of Geotechnical and Geoenvironmental Engineering, 121*(12), 870-878.

Bourdeau, C. (2006). Site Effects Study in the Las Colina Slope (El Salvador, 2001). *Proceedings of FLAC and Numerical Modeling in Geomechanics, Mardrid, Spain* (pp. 205-210). Minneapolis: Itasca Consulting Group, Inc.

Bowles, J. E. (1996). *Foundation Analysis and Design* (5th edition). Toronto, ON : McGraw-Hill College.

Brennan, A. J. & Madabhushi, S. P. G. (2005). Liquefaction and Drainage in Stratified Soil. *Journal of Geotechnical and Geoenvironmental Engineering, 131*(7), 876-885.

Budhu, M. (1988). The Mechanism of Failure Under Cyclic Simple Shear Strain. *Japanese Society of Soil Mechanics and Foundation Engineering, Soils and Foundations, 28*(4), 119-129.

Bussiere, B. (2007). Hydro-Geotechnical Properties of Hard Rock Tailings from Metal Mines and Emerging Geo-environmental Disposal Approaches. *Canadian Geotechnical Journal, 44*(9), 1019-1052.

Byrne, P. (1991). A Cyclic Shear-Volume Coupling and Pore Pressure Model for Sand. *Proceedings of the Second International Conference on Recent Advances in Geotechnical Earthquake Engineering and Soil Dynamics, St. Louis, USA* (pp. 47-55). New York: ASCE.

Byrne, P. M., Debasis, R., Campanella, R. G. & Hughes, J. (1995). Predicting Liquefaction Response of Granular Soils from Pressuremeter Tests. *Proceedings of the ASCE National Conventional, San Diego, USA*, (pp. 122-135).

Byrne, P. M., Park, S. S. & Beaty, M. (2003). Seismic Liquefaction: Centrifuge and Numerical Modeling. *Proceedings of the Third International Symposium on FLAC and FLAC3D Numerical Modelling in Geomechanics, Sudbury, Canada* (pp. 321-331). Lisse, Netherlands: Balkema.

Byrne, P. M. & Seid-Karbasi, M. (2003). Seismic Stability of Impoundments. Proceedings of the 17th Annual Symposium of the Vancouver Geotechnical Society, Vancouver, BC. Retrieved from: http://www.civil.ubc.ca/liquefaction/Publications/VGS12R.pdf.

Byrne, P. M., Park, S.S,, Beaty, M., Sharp, M., Gonzalez, L., & Abdoun, T. (2004). Numeral Modeling of Liquefaction and Comparison with Centrifuge Tests. *Canadian Geotechnical Journal, 41*, 193-211.

Canadian Dam Association (CDA). (2007). Dam Safety Guidelines. Edmonton AB: Canadian Dam Association.

Carter, D. P. & Seed, H. B. (1988). *Liquefaction of Sand Deposits Under Low Levels of Excitation* (Report No. EERC 88/11). Berkeley CA, USA: Earthquake Engineering Research Center.

Castillo, J., Hallman, D., Byrne, P., & Parra, D. (2006). Non-linear dynamic analysis of heap leach pad under high phreatic levels. *Proceedings of FLAC and Numerical Modeling in Geomechanics, Mardrid, Spain* (pp. 187-194). Minneapolis: Itasca Consulting Group, Inc.

Cascone, E. & Rampello, S. (2003). Decoupled Seismic Analysis of an Earth Dam. *Soil Dynamics and Earthquake Engineering.* 23(5). 349-365.

Castro, G. (1969). *Liquefaction of Sands*. Ph.D. unpublished. Harvard University, Boston MA, USA.

Castro, G. (1975). Liquefaction and Cyclic Mobility of Saturated Sands. *Journal of Geotechnical Engineering,* 101(GT6), 551-569.

Chaney, R. (1978). Saturation Effects on the Cyclic Strength of Sand. *Proceedings ASCE Special Conference on Earthquake Engineering and Soil Dynamics*. New York. USA (pp. 342–359). New York: ASCE.

Chen, H. W. & van Zyl, D. J. A. (1988). Shear Strength and Volume-change Behavior of Copper Tailings under Saturated Conditions. *Hydraulic Fill Structures, SGP 21,* 430-451.

Chen, J. W. & Juang, C. H. (1996). Determination of Drained Friction Angle of Sands from CPT. *Journal of Geotechnical Engineering, 122*(5), 374-381.

Chen, Y.M. & Lau, C.K. (2008). *Slope Stability Analysis and Stabilization: New Methods and Insight*. London: Taylor and Francis.

Chien, L.K., Oh, Y.N. & Chang, C.H. (2002). Effect of Fines Content on Liquefaction Strength and Dynamic Settlement of Reclaimed Soil. *Canadian Geotechnical Journal, 39*, 254-265.

Conlin, B. (1987). A Review of the Performance of Mine Tailings Impoundments under Earthquake Loading Conditions. *Proceedings of Earthquake Geotechnique, Vancouver, Canada*.

Cudmani, R. O., Osinov, V. A., Buhler, M. M. & Gudehus, G. (2003). A Model for the Evaluation of Liquefaction Susceptibility in Layered Soils due to Earthquakes. *Proceedings of Soil Rock 2003, Cambridge MA, USA*. Essen: Verlag Gluckauf GMBH.

Cundall, P. A. (2006). A Simple Hysteretic damping function formulation for dynamic continuum simulations. *Proceedings of FLAC and Numerical Modeling in Geomechanics, Mardrid, Spain* (pp. 359-364). Minneapolis: Itasca Consulting Group, Inc..

Davies, M. P. (2002). Tailings Impoundment Failures: Are Geotechnical Engineers Listening? *Geotechnical News,* September. 31-36.

Davies, M. P. & Lighthall, P. C. (2001). Geotechnical Aspects of Several Recent Mine Tailings Impoundment Failures. *Proceedings of the 54th Canadian Geotechnical Conference, Calgary AB, Canada* (pp. 321-326).

DeAlba, P., Chan, C. K. & Seed, H. B. (1975). *Determination of Soil Liquefaction Characteristics by Large-scale Laboratory Tests. (*Report No. EERC 75-14). Berkeley CA: Earthquake Engineering Research Center.

Dobry, R. & Alvarez, L. (1967). Seismic Failures of Chilean Tailings Dams. *Journal of the Soil Mechanics and Foundations Division, 93*(SM6), 237-260.

Duncan, J.M. and Wright, S.G. (2005). *Soil Strength and Slope Stability.* Toronto ON: John Wiley and Sons.

Dyvik, R., Berre, T., LaCasse, S., & Raadim, B. (1987). Comparison of Truly Undrained and Constant Volume Direct Simple Shear Tests. *Géotechnique, 37*(1), 3-10.

Earthquakes Canada. (2006). Seismic Hazard Calculations (www.earthquakescanada.ca). Consulted on February 20, 2006.

Egan, J. A. & Sangrey, D. A. (1978). Critical State Model for Cyclic Load Pore Pressure. *Proceedings from the ASCE Earthquake Engineering and Soil Dynamics Specialty Conference*, Pasadena CA, USA. (pp. 410-424). New York: ASCE.

Erten, D. & Maher, M. H. (1995). Cyclic Undrained Behavior of Silty Sand. *Soil Dynamics and Earthquake Engineering, 4*, 115-123.

Escuder, I., Altarejos, L. & de Membrillera, M. G. (2006). FLAC Numerical Models Applied to Safety Assessment of Dams. *Proceedings of the 4th International Symposium on FLAC and Numerical Modeling in Geomechanics*, Madrid, Spain (pp. 157-160). Minneapolis MN: Itasca Consulting Group, Inc.

Evans, M. D. & Zhou, S. (1995). Liquefaction Behavior of Sand-gravel Composites. *Journal of Geotechncial Engineering, 121*(3), 287-298.

Feng, Z. Y., Chang, Y. H., Tsai, P. H., & Li, J. N. (2006). Dynamic response of Li-yu-tan earthdam subjected to the 1999 Chi-Chi earthquake in Taiwan. *Proceedings of the 4th International FLAC Symposium on Numerical Modeling in Geomechanics*, Madrid, Spain. (pp. 221-227). Minneapolis MN: Itasca Consulting Group Inc.

Fiegel, G. L. & Kutter, B. L. (1994). Liquefaction Mechanism for Layered Soils, *Journal of Geotechnical Engineering*, *120*(4), 737-755.

Finn, W. D. L. (1985). Aspects of Constant Volume Cyclic Simple Shear. *Proceeings of Advances in the Art of Testing of Soils Under Cyclic Conditions, Detroit MI, USA* (pp. 74-98). New York: ASCE.

Finn, W. D. L. (1993). Seismic Safety Evaluation of Embankment Dams. *Proceedings of the International Workshop on Dam Safety Evaluation, Grindelwald, Switzerland* (pp. 91-135). Sutton, UK: Quadrant House.

Finn, W. D. L. (1998). Seismic Safety Evaluation of Embankment Dams - Developments in Research and Practice 1988-1998. *Proceedings of Geotechnical Earthquake Engineering and Soil Dynamics III, Seattle WA, USA* (Vol. 2, pp. 812-853). Reston VA: ASCE.

Finn, W. D. L., Lee, K. W., Maartman, C. H. & Lo, R. (1978). Cyclic Pore Pressures Under Anisotropic Conditions. *Proceedings from the ASCE Earthquake Engineering and Soil Dynamics Specialty Conference*, Pasadena CA, USA. (pp. 457-470). New York: ASCE.

Finn, W. D. L., Ledbetter, R. H. & Wu, G. (1994). Liquefaction in Silty Soils: Design and Analysis. *Proceedings of Ground Failures Under Seismic Conditions, Atlanta GA, USA. GSP(44),* (pp. 51-76). New York: ASCE.

Finn, W. D. L. & Wightman, A. (2003). Ground Motion Amplification Factors for the Proposed 2005 Edition of the National Building Code of Canada. *Canadian Journal of Civil Engineering, 30*, 272-278.

Freeze and Cherry, 1979. Groundwater. Englewood Cliffs NJ: Prentice-Hall.

Gamache-Rochette, A. (2004). *Une Etude de caraterisation en laboratoire et sur le terrain des ecoulements de l'eau dans les roches steriles.* M.Sc. Thesis unpublished. Ecole Polytechnique Montréal PQ, Canada.

Garga, V. & McKay, L. D. (1984). Cyclic Triaxial Strength of Mine Tailings. *Journal of Geotechnical Engineering*, *110*(8), 1091-1105.

Geo-Slope International Limited (Geo-Slope). (2004). *Geo-Studio 2004* (version 6.22). [computer software and user guide]. Calgary AB: Geo-Slope International Ltd. (includes Seep/W and Slope/W).

Goodman, R. E. (1989). *Introduction to Rock Mechanics.* Toronto ON: John Wiley & Sons Inc.

Golder Associes Ltd. (Golder). (2002). *Report: Rapport de conception – Rehaussement des digues du parc a résidus – Division Laronde.*

Gonzalez, L., Abdoun, T., & Sharp, M. K. (2002). Modelling of Seismically Induced Liquefaction under High Confining Stress. *International Journal of Physical Modelling in Geotechnics*, 2(3). 1–15.

Gosselin, G. (2003). *Field Trip Guide: Geological Setting, History, Production and Reserves - A World Class VMS Au-Ag-Cu-Zn Deposit*. Agnico Eagle Mines Ltd, Laronde Mine Division.

Guo, T. & Prakash, S. (1999). Liquefaction of Silts and Silt-Clay Mixtures. *Journal of Geotechnical and Geoenvironmental Engineering, 125*(8), 706-710.

Harder, L. F. Jr. & Stewart, J. P. (1996). Failure of Tapo Canyon Tailings Dam. *Journal of Performance of Constructed Facilities, 10*(5), 109-114.

Harder, L. F., Jr., and Boulanger, R. W. (1997). Application of K_σ and K_α Correction Factors. *Proceedings of the NCEER Workshop on Evaluation of Liquefaction Resistance of Soils, Buffalo NY, USA.* (pp. 167-190). National Center for Earthquake Engineering Research., State University of New York at Buffalo.

Hausmann, M. R. (1990). *Engineering Principles of Ground Modification*, Toronto ON: McGraw-Hill Publishing Company.

Hemysfield, E, (1999). Probabilistic Approach for Determination of Liquefaction Potential. *Journal of Energy Engineering, 125*(1), 18-33.

Henderson, M. E., Purdy, J., & Delaney, T. (2002). Performance of Vertical Wick Drains at the Atlas Moab Uranium Mill Tailings Facility After 1 Year. *Proceedings of Tailings and Mine Waste 2002, Fort Collins CO, USA*. (pp. 387-391). Exton PA: Balkema.

Holtz, R. D. & Kovacs, W. D. (1981). *An Introduction to Geotechnical Engineering*. Englewood NJ: Prentice-Hall, Inc.

Hyde, A., Higuchi, T. & Yasuhara, K. (2006). Liquefaction, Cyclic Mobility, and Failure of Silt. *Journal of Geotechnical and Geoenvironmental Engineering, 132*(6), 716-735.

Hynes-Griffin, M. E. & Franklin, A. G. (1984). *Rationalizing the Seismic Coefficient Method. Paper No. GL-84-13*. Washington DC: US Army Corps of Engineers.

Hynes, M. E. & Olsen, R. S. (1999). Influence of Confining Stress on Liquefaction Resistance. *Proceedings of Physics and Mechanics of Soil Liquefaction, Baltimore MD, USA. P.V. Lade and J. Yamamuro (eds.)* (pp. 145-151). Rotterdam: Balkema.

International Commission on Large Dams (ICOLD). (1989). *Tailings Dams Safety - Guidelines*. Bulletin No. 74. Paris: Commission Internationale des Grands Barrages.

International Commission on Large Dams (ICOLD). (1995). *Tailings Dams and Seismicity – Review and Recommendations.* Bulletin No. 98. Paris: Commission Internationale des Grands Barrages.

International Commission on Large Dams (ICOLD). (2001). *Tailings Dams – Risk of Dangerous Occurrences – Lessons Learnt From Past Experiences*. Bulletin No. 121. Paris: Commission Internationale des Grands Barrages.

Imam, S. M. R., Morgenstern, N. R., Robertson, P. K. & Chan, D. H. (2005). A Critical-state Constitutive Model for Liquefiable Sand. *Canadian Geotechnical Journal, 42*, 830-855.

Ishibashi, Isao; Kawamura, Makoto and Bhatia, Shobha. (1985). Effect of Initial Shear on Cyclic Behaviour of Sand. *Journal of Geotechnical Engineering*, Vol. 111(12). 1395-1410.

Ishihara, K., Sodekawa, M. & Tanaka, Y. (1978). Effects of Overconsolidation on Liquefaction Characteristics of Sands Containing Fines. *Proceedings of Dynamic Geotechnical Testing, Denver CO, USA.* (pp. 246-264). Philadelphia: ASTM.

Ishihara, K. (1984). Post-Earthquake Failure of a Tailings Dam due to Liquefaction of the Pond Deposit. *Proceedings of the International Conference on Case Histories in Geotechnical Engineering, St-Louis USA*, (pp. 1129-1143). New York: ASCE.

Ishihara, K. (1993). Liquefaction and Flow Failure During Earthquakes. *Geotechnique, 43*(3), 351-415.

Ishihara, K. (1996). *Soil Behaviour in Earthquake Geotechnics*. Oxford: Oxford University Press.

Ishihara, K. & Nagase, H. (1985). Multi-directional Irregular Loading Tests on Sand. Proceedings of *Advances in the Art of Testing of Soils Under Cyclic Conditions*, Detroit MI, USA (pp. 99-119). New York: ASCE.

Ishihara, K., Sodekawa, M. & Tanaka, Y. (1981). Cyclic Strength of Undisturbed Mine Tailings. *Proceedings of the International Conference on Recent Advances in Geotechnical Earthquake Engineering and Soil Dynamics, St-Louis USA*. (pp. 53-58. New York: ASCE.

Ishihara, K., Tsuchiya, H., Huang, Y., and Kamada, K. (2001). Recent Studies on Liquefaction Resistance of Sand - Effect of Saturation," (CD-ROM), *Proceedings of Recent Advances in Geotechnical Earthquake Engineering and Soil Dynamics*, San Diego CA, USA (keynote lecture). Reston VA: USA.

Ishihara, K., Troncoso, J., Kawase, Y. & Takahashi, Y. (1980). Cyclic Strength Characteristics of Tailings Materials. *JSSMFE, Soils and Foundations, 20*(4), 127-142.

Itasca Consulting Group, Inc. (Itasca). (2005). FLAC – Fast Lagrangian Analysis of Continua. Version 5.00.377. [computer software and user manual]. Minneapolis MN: Itasca Consulting Group, Inc.

James, M., Aubertin, M. & Wilson, G. W. (2006). Evaluation of the dynamic stability of a tailings dam using FLAC. *Proceedings of the 4th International Symposium on FLAC and Numerical Modeling in Geomechanics*, Madrid, Spain. (pp. 161-169). Minneapolis MN: Itasca Consulting Group, Inc.

James, M., Jolette, D., Aubertin, M. & Bussiere, B. (2003). An Experimental Set-up to Investigate Tailings Liquefaction and Control Measures. *Proceedings of the International Symposium on Major Challenges in Tailings Dams, Montreal PQ, Canada.* (pp. 153-164). Paris: Commission Internationale des Grands Barrages.

James, M., Gomes, P. & Schwenger, R. (2007). The Liquefaction Resistance of Tailings and the Stability of Impoundments. Proceedings of the 60th Canadian Geotechnical Conference, Ottawa ON, Canada. (on CD-ROM). Edmonton AB: Canadian Geotechnical Society.

Jedele, L. P. (2005). Energy-Attenuation Relationships from Vibrations Revisited. *Proceedings of the Geo-Frontiers 2005, Austin, Texas* (pp. 1-14). Reston VA: ASCE.

Jeyapalan, J. K. (1982). A Viscous Model for Flow Slides of Tailings Dams. Proceedings of Numerical Methods in Geomechanics, Edmonton AB, Canada, (pp. 691-697). Rotterdam, Balkema.

Jeyapalan, J. K; Duncan, J. M. & Seed, H. B. (1983). Investigation of Flow Failures of Tailings Dams. *Journal of Geotechnical Engineering, 109*(20), 172-189.

Juang, C. H., Jiang, T. & Andrus, R.D. (2002). Assessing Probabilty-based Methods for Liquefaction Potential Evaluation. *Journal of Geotechnical and Geoenvironmental Engineering, 128*(7), 580-589.

Kayen, R. E. & Mitchell, J. K. (1997). Assessment of Liquefaction Potential During Earthquakes by Arias Intensity. *Journal of Geotechnical and Geoenvironmental Engineering, 123*(2), 1162-1174.

Koester, J. P. (1994). The Influence of Fines Type and Content on Cyclic Strength. *Proceedings of Ground Failures Under Seismic Conditions, Atlatnta GA, USA, GSP 44*. (pp. 17-33). New York: ASCE.

Kokusho, T. & Kojima, T. (2002). Mechanism of Postliquefaction Water Film Generation in Layered Sand. *Journal of Geotechnical and Geoenvironmental Engineering, 128*(2), 129-137.

Kokusho, T., Hara, T. & Hiraoka, R. (2004). Undrained Shear Strength of Granular Soils with Different Particle Gradations. *Journal of Geotechnical and Geoenvironmental Engineering, 130*(6), 621-629.

Kramer, S. L. (1996). *Geotechnical Earthquake Engineering*. Upper Saddle River, NJ: Prentice-Hall Inc.

Kuerbis, R., Negussey, D. & Vaid, Y. P. (1988). Effect of Gradation and Fines Content on the Undrained Response of Sand. Proceedings of *Hydraulic Fill Structures, Fort Collins CO, USA, SGP*(21). (pp. 330-345). New York: ASCE.

LaMontagne, M., Wetmiller R. J. & DuBerger, R. (1990). Some Results from the 25 November, 1988 Saguenay, Quebec Earthquake. *Proceedings of the Canadian Geotechnical Conference, Quebec PQ, Canada,* (pp. 177-182).

Leahy, Denise, Eng., Ph.D. (2008). Personal communication.

Ledbetter, R. H. (1985). *Improvement of Liquefiable Foundation Conditions Beneath Existing Structures* (Technical Report REMR-GT-2). Washington DC: US Army Corps of Engineers.

Leon, E., Gassman, S. L. & Talwani, P. (2006). Accounting for Soil Ageing When Assessing Liquefaction Potential. *Journal of Geotechnical and Geoenvironmental Engineering, 132*(3), 363-377.

Leps, T. M. (1970). Review of Shearing Strength of Rockfill (with discussions). *Journal of the Soil Mechanics and Foundations Division, SM4*, 1159-1170.

Lo, R.C. & Klohn, E. L. (1995). Design Considerations for Tailings Dams. *Proceedings of the 5th International Conference on Tailings and Mine Waste '96, Fort Collins CO, USA,* (pp. 113-121). London: Taylor and Francis.

Lucia, P. C., Duncan, J. M. & Seed, H. B. (1981). Summary of Research on Case Histories of Flow Failures of Mine Tailings Impoundments. *U.S. Bureau of Mines*

Information Circular (pp. 46-53). Washington DC: U.S. Department of the Interior.

Ma, F., Wang, Z. L. & LaVassar, J. (2006). Liquefaction analyses of a hydraulic fill earth dam. *Proceedings of the 4th International FLAC Symposium on Numerical Modeling in Geomechanics, Madrid, Spain* (pp. 395-402). Minneapolis MN: Itasca Consulting Group, Inc.

Makdisi, F. I. & Seed, H. B. (1977). *A Simplified Procedure for Estimating Earthquake-induced Deformations in Dams and Embankments* (Report No. UCB/EERC-77/19). Berkeley CA: Earthquake Engineering Research Center.

Makdisi, Faiz I. & Seed, H. Bolton, 1978, Simplified Procedures for Estimating Dam and Embankment Earthquake-Induced Deformations, *Journal of the Geotechnical Engineering Division*, 104(7), 849-867.

Makdisi, F. I. & Seed, H. B. (1979). Simplified Procedure for Evaluation Embankment Response. *Journal of the Geotechnical Engineering Division, 105*(GT12), 1427-1434.

Mansouri, T. A., Nelson, J.D. & Thompson, E.G. (1983). Dynamic Response and Liquefaction of Earth Dams. *Journal of Geotechnical Engineering, 109*(1), 89-99.

Marcuson, W. F. III, Hynes, M. E., & Franklin, A.G. (1990). Evaluation and Use of Residual Strength in Seismic Safety Analysis of Embankments. *Earthquake Spectra, 6*, 529-572.

Martin, G., Finn, W. D. L. & Seed, H. B. (1975). Fundamentals of Liquefaction Under Cyclic Loading. *Journal of the Geotechnical Engineering Division*, 101(5), 423-438.

Martin, J. R. II, Olgun, C. G., Mitchell, J. K., & Durgunoglu, H. T. (2004). High-modulus Columns for Liquefaction Mitigation. *Journal of Geotechnical and Geoenvironmental Engineering, 130*(6), 561-571.

Mbonimpa, M., Aubertin, M., Chapuis, R. P., & Bussiere, B. (2002). Practical Pedotransfer Functions for Estimating the Saturated Hydraulic Conductivity. *Geotechnical and Geological Engineering, 20*, 235-259.

McNeilman, T. W. & Skaggs, R. L. (1988). In-Place Properties of a Hydraulic Landfill. *Proceedings of Hydraulic Fill Structures, Fort Collins CO, USA, SGP 21*, (pp. 255-273). New York: ASCE.

Mejia, L. & Seed, H. B. (1983). Comparison of 2-D and 3-D Dynamic Analyses of Earth Dams. *Journal of Geotechnical Engineering, 109*(11), 1383-1398.

Milligan, V. (1976). Glacial Till. (Special Publication No. 12.), Legget, R. F. (editor). *Geotechnical Aspects of Glacial Tills* (pp. 269-291). Ottawa: The Royal Society of Canada.

Ministère des Ressources Naturelles, Québec (MRN). 1994. *Géologie du Québec.* Ville de Québec: Gouvernement du Québec.

Ministère des Ressources Naturelles and the Ministère de l'Environnement et de la Faune (MRN). (1997). *Guidelines for Preparing a Mining Site Rehabilitation Plan and General Mining Site Rehabilitation Requirements.* Ville de Québec: Gouvernement du Québec.

Ministère des Ressources Naturelles, Québec (MRN). (2000). 1:20,000 Topographic Maps (Cadillac, 32D01-200-0201 and Lac Pressiac, 32D01-200-0101). Ville de Québec: Gouvernement du Québec.

Mitchell, K. & Soga, K. (2005). *Fundamentals of Soil Behavior.* Toronto ON: John Wiley & Sons, Inc.

Mittal, H. K. & Morgenstren, N. R. (1977). Design and Performance of Tailings Dams. *Proceedings of Geotechnical Practice for Disposal of Solid Waste Materials, Ann Arbor MI, USA* (pp. 475-492). New York: ASCE.

Miura, S. & Toki, S. (1982). A Sample Preparation Method and its Effect on Static and Cyclic Deformation-Strength Properties of Sand. *Soils and Foundations, 22*(1), 61-77.

Moriwaki, Y., Tan, P. & Ji, F. (1998). Seismic Deformation Analysis of the Upper San Fernando Dam Under the 1971 San Fernando Earthquake. *Proceedings of Geotechnical Earthquake Engineering III, Seattle WA, USA* (pp. 854-865). New York: ASCE.

Moss, R. E. S., Seed, R. B. & Olsen, R. S. (2006). Normalizing the CPT for Overburden Stress. *Journal of Geotechnical and Geoenvironmental Engineering, 132*(3), 378-387.

Munro, P. S. & Weichert, D. (1989). *The Saguenay Earthquake of November 25, 1988 - Processed Strong Ground Motion Records* (Open File No. 1996). Ottawa ON: Geological Survey of Canada.

National Research Center (NRC). (1985). Liquefaction of Soils During Earthquakes. Washington DC: National Academy Press.

National Research Center Canada (NRCC). (1995). National Building Code of Canada. Ottawa ON:NRCC.

National Research Center Canada (NRCC). (2005). National Building Code of Canada. Ottawa ON:NRCC.

Natural Resources Canada (NRC). (2003). *Processed Ground Motions Records of the 1988 Saguenay Earthquake*. Website accessed on June 16, 2003. http://www.seismo.nrcan.gc.ca/nwfa/index_e.php

Natural Resources Canada (NRC). (2008). *An Overview of Damage Due to the Eastern Canada Earthquakes of 1925, 1929, 1935, 1944, and 1988.* Lamontagne, M. & Halchuk, S. (editors). Website accessed: November 15, 2008. http://seismescanada.rncan.gc.ca/historic_eq/20th/e_damaging_e.php.

Naeini, S. A. & Bazia, M. H. (2004). Effects of Fines Content on Steady-state Strength of Mixed and Layered Samples of a Sand. *Soil Dynamics and Earthquake Engineering, Elsevier, 24*, 181-187.

Newmark, N. M. (1965). Effects of Earthquakes on Dams and Embankments. *Géotechnique, 15*(2), 139-160.

Oka, F., Sekiguchi, K. & Goto, H. (1981). A Method of Analysis of Earthquake-induced Liquefaction in Horizontally Layered Soil Deposits. *Soils and Foundations, 21*(3), 1-17.

Olson, S. M. & Stark, T. (2002). Liquefied Strength Ratio from Liquefaction Flow Failure Case Histories. *Canadian Geotechnical Journal, 39*, 629-647.

Park, S.-S. & Byrne, P. M. (2003). Practical Constitutive Model for Soil Liquefaction. *Proceedings of the 9th International Symposium on Numerical Modeling in Geomechanics, Sudbury ON, Canada,* October 6-9, (pp. 181-186). London: Taylor and Francis.

Papadimitrious, A., Bouckovalas, G. D & Dafalias, Y. (2001). Plasticity Model for Sand Under Small and Large Cyclic Strains. *Journal of Geotechncal and Geoenvironmental Engineering, 127*(11), 973-983.

Perlea, V. G. (2000). Liquefaction of Cohesive Soils. Proceedings of Geo-Denver 2000, Denver CO, USA, (pp. 58-76). Reston VA: ASCE.

Piao, R. P., Rippe, A. H., Myers, B. & Lane, K. W. (2006). Earth Dam Liquefaction and Deformation Analysis using Numerical Modeling. Proceedings of GeoCongress

2006: Geotechnical Engineering in the Information Age, Atlanta GA, USA (on CD-ROM). Reston VA: ASCE.

Polito, C. P. (1999). The Effect of Nonplastic and Plastic Fines on the Liquefaction of Sandy Soils. Ph.D. thesis (unpublished), Virginia Polytechnic Institute and State University, Blacksburg, VA, USA.

Polito, C. & Martin, J. R. II. (2001) Effects of Nonplastic Fines on the Liquefaction Resistance of Sands. *Journal of Geotechnical and Geoenvironmental Engineering, 127*(5), 408-415.

Poulos, S. J., Gonzalo, C. & France, J. W. (1985). Liquefaction Evaluation Procedure. *Journal of Geotechnical Engineering, 111*(6), 773-792.

Prakash, S. & Sandoval, J. A. (1992). Liquefaction of Low Plasticity Silts. *Soil Dynamics and Earthquake Engineering, 11*, 373-379.

Princeton University. (2003). *General information.* Verification of Liquefaction Analysis by Centrifuge Studies. Consulted on June 5, 2003. http://www.cee.princeton.edu/~radu/soil/velacs/.

Psarropoulos P. N., Tazoh, T., Gazetas, G. & Apostolou, M. (2007). Linear and Nonlinear Valley Amplification Effects on Seismic Ground Motion. *Soils & Foundations*, 47(5). 857-872.

Puebla, H., Byrne, P.M. & Phillips, R. (1997). Analysis of CANLEX Liquefaction Embankments: Prototype and Centrifuge Models. *Canadian Geotechnical Journal, 34*, 641-657.

Puebla, H. (1999). A Constitutive Model for Sand and the Analysis of the CanLex Embankments. Ph.D. Thesis. University of British Columbia, Vancouver BC, Canada.

Pyke, R., Chan, C. K., & Seed, H. B. (1974). *Settlement and Liquefaction of Sands Under Multi-directional Shaking* (Report No. EERC 74-2). Berkeley CA: Earthquake Engineering Research Center.

Pyke, R. (1991). Selection of Seismic *Coefficients for Use in Pseudo-static Slope Stability Analyses*. Consulted on April 17, 2002, http://www.tagasoft.com/tagasoft/discussion/article2_html.

Qiu, Y. & Sego, D. C. (2001). Laboratory Properties of Mine Tailings. *Canadian Geotechnical Journal, 38*(1), 183-190.

Rampello, S., Cascone, E. & Grosso, N. (2008). Evaluation of the Seismic Response of a Homogeneous Earth Dam. *Soil Dynamics and Earthquake Engineering.* 29(5). 782-798.

Riemer, M.F., Gookin, W.B., Bray, J.D. & Arango, I. (1994). Effects of Loading Frequency and Control on the Liquefaction Behavior of Clean Sands (Report No. UCB/GT/94-07). Berkeley CA: University of California.

Robertson, P.K. & Campanella, R.G. (1983). Interpretation of Cone Penetration Tests. *Canadian Geotechnical Journal.* 20 (4). 718-745.

Robertson, P. K. & Campanella, R. G. (1986). *Guidelines for Use and Interpretation of Piezometer Cone Penetration Test.* University of California, Berkeley, Department of Civil Engineering, Soil Mechanics Series. Berkeley CA: University of California.

Robertson, P.K. (1990). Soil Classification Using the CPT. *Canadian Geotechnical Journal.* 27 (1). 151-158.

Robertson, P. K., Woeller, D. J., Kokan, M., Hunter, J. & Luternauer, J. (1992). Seismic Techniques to Evalaute Liquefaction Potential. *Proceedings of the 45th Canadian*

Geotechnical Conference. Toronto ON, Canada, (pp. 5-1 to 5-9). Edmonton AB: Canadian Geotechnical Society.

Robertson, P. K. & Wride, C. E. (1998). Evaluating Cyclic Liquefaction Potential Using the Cone Penetration Test. *Canadian Geotechnical Journal, 35*, 442-459.

Robertson, P. K., Wride, C. E., List, B. R., Atukoral, U., Biggar, K. W., Byrne, P. M. et al (2000a). The Canadian Liquefaction Experiment: An Overview. *Canadian Geotechnical Journal, Volume 37*(3), 499-504.

Robertson, P. K., Wride, C. E., List, B. R., Atukoral, U., Biggar, K. W., Byrne, P. M. et al. (2000b). The CANLEX Project: Summary and Conclusions. *Canadian Geotechnical Journal, 37*(3), 563-591.

Sangrey, D. A., Castro, G., Poulos, S. J. & France, J. W. (1978). Cyclic Loading of Sands, Silts and Clays. *Proceedings of the Earthquake Engineering and Soil Dynamics Specialty Conference*, Pasadena CA, USA (pp. 836-851). New York: ASCE.

Sasaki, Y. & Taniguchi, E. (1982). Shaking Table Tests on Gravel Drains to Prevent Liquefaction of Sand Deposits. *JSSMFE - Soils and Foundations, 22*(3), 1-14.

Schnabel, P. B., Lysmer, J. & Seed, H. B. (1972). *SHAKE: A Computer Program for Earthquake Response Analysis of Horizontally Layered Sites* (EERC Report No. 72-12). Berkeley CA: Earthquake Engineering Research Center.

Schneider, J. A. & Mayne, P. W. (1999). *Soil Liquefaction Response in Mid-America Evaluation by Seismic Piezocone Tests* (Report No. MAE-GT-3A). Urbana, IL: Mid-America Earthquake Center.

Scott, R. F. (1994). Review of Progress in Dynamic Geotechnical Centrifuge Research. *Proceedings of Dynamic Geotechnical Testing II,* San Francisco CA, USA. (pp. 305-329). Philadelphia PA: ASTM.

Seed, H. B. & Lee, K. L. (1966). Liquefaction of Saturated Sands during Cyclic Loading. *Journal of the Soil Mechanics and Foundation Engineering Division.* 92(6). 105-134.

Seed, H. B. (1979). Soil Liquefaction and Cyclic Mobility Evaluation for Level Ground During Earthquakes. *Journal of the Geotechnical Engineering Division, GT2*, 201-255.

Seed, H. B. (1979). Considerations in the Earthquake-resistant Design of Earth and Rockfill Dams. *Geotechnique. 29(3). 215-263.*

Seed, H. B. & Harder, L. F., Jr., 1990, SPT-Based Analysis of Cyclic Pore Pressure Generation & Undrained Residual Strength. *Proceedings of the H. Bolton Seed Memorial Symposium, Berkeley CA, USA.* (Vol. 2, pp. 351-376). Vancouver BC: Bitech Publishers.

Seed, H. B. & Idriss, I. M. (1970). *A Simplified Procedure for Evaluating Soil Liquefaction Potential* (Report No. EERC 70-9). Berkeley CA: Earthquake Engineering Research Center.

Seed, H. B. & Idriss, I. M. (1970). *Soil Moduli and Damping Factors for Dynamic Response Analyses* (Report No. EERC 70-10). Berkeley CA: Earthquake Engineering Research Center.

Seed, H. B. & Idriss, I. M. (1982). *Ground Motions and Soil Liquefaction During Earthquakes*. Berkeley CA: Earthquake Engineering Research Institute.

Seed, H. B. & Martin, G. R. (1966). The Seismic Coefficient in Earth Dam Design. *Journal of the Soil Mechanics and Foundations Division, 92*(SM3), 25-58.

Seed, H. B., Mori, K. & Chan, C. K. (1975). *Influence of Sesimic History on the Liquefaction Characteristics of Sands* (Report No. ERRC 75-25). Berkeley CA: Earthquake Engineering Research Center.

Seed, H. B. & Peacock, W. H. (1970). *Procedures for Measuring Soil Liquefaction Characteristics Under Cyclic Loading*. (Report No. ERRC 70-8). Berkeley CA: Earthquake Engineering Research Center.

Seed, H. B. (1983). Earthquake-Resistant Design of Earth Dams. Proceedings of the Symposium on Seismic Design of Embankments and Caverns, Philadelphia PA, USA (pp. 41-61). New York: ASCE.

Seed, H. B., Wong, R. T., Idriss, I. M. & Tokimatsu, K. (1984). *Dynamic Moduli and Damping Factors for Dynamic Analysis of Cohesionless Soils* (Report No. UCB/EERC-84/14). Berkeley CA: Earthquake Engineering Research Center.

Seed, H. B., Seed, R. B., Harder, L. F. & Jong, H.-L. (1988). Re-Evaluation of the Slide in the Lower San Fernando Dam in the Earthquake of Feb. 9, 1971 (Report No. UCB/EERC-88/04). Berkeley CA: Earthquake Engineering Research Center.

Seid-Karbasi, M. & Byrne, P. M. (2004). Embankment Dams and Earthquakes. *Hydropower and Dams, 2*, 96-102.

Seid-Karbasi, M. & Byrne, P. M. (2007). Seismic Liquefaction, Lateral Spreading, and Flow slides: A Numerical Investigation into Void Redistribution. *Canadian Geotechnical Journal, 44*, 873-890.

Sento, N., Kazami, M., Uzuoka, R., Ohmura, H. & Ishimaru, M. (2004). Possibility of Postliquefaction Flow Failure due to Seepage. *Journal of Geotechnical and Geoenvironmental Engineering, 130*(7), 707-716.

Shen, J. L., Herrman, L. R. & Sadigh, K. (1978). Analysis of Cyclic Simple Shear Test Data. *Proceedings of the Earthquake Engineering and Soil Dynamics Specialty Conference*, Pasadena CA, USA (pp. 864-874). New York: ASCE.

Sherard, J.L., Woodward, R. T., Gizienski, S. F. & Clevenger, W. A. (1963). *Earth and Earth-rock Dams. New* York : John Wiley & Sons, Inc.

Sherif, M. A., Tsuchiya, C., & Ishibashi, I. (1977). Saturation Effect on Initial Soil Liquefaction. *Journal of the Geotechnical Engineering Division*, ASCE. 103(8). 914–917.

Sigaran-Loria, C. & Hack, R. (2006). Two-dimensional Assessment of Topographical Site Effects on Earthquake Ground Response. *Proceedings of FLAC and Numerical Modeling in Geomechanics 2006, Madrid, Spain* (pp. 195-204). Minneapolis MN: Itasca Consulting Group, Inc.

Système d'information geominier de Québec (SIGEOM). (2000). 1:20,000 scale geologic and fault map of quadrant 32D07-200-0201.

Singh, S. (1994). Liquefaction Characteristics of Silts. *Proceedings of Ground Failures Under Seismic Conditions, Atlanta GA, USA (pp.* 105-116). New York: ASCE.

Singh, S. (1996). Liquefaction Characteristics of Silts. *Geotechnical and Geological Engineering, 14*, 1-19.

Sivathayalan, S. (1994). *Static, Cyclic and Post Liquefaction Simple Shear Response of Sands*. Ph.D. Thesis (unpublished), University of British Columbia, Vancouver BC, Canada.

Sonu, C. J., Ito, K. & Oishi, H. (1993). Harry Seed, Liquefaction and the Gravel Drain. *Civil Engineering Magazine, 63*(12), 58-60.

Sriskandakumar, S. (2004). *Cyclic Loading Response of Fraser River Sand for Validation of Numerical Models Simulating Centrifuge Tests*. Ph.D. Thesis, University of British Columbia, Vancouver BC, Canada.

Stark, T. D., Olson, S. M., Kramer, S. L. & Youd, T. L. (1998). Shear Strength of Liquefied Soil. *Proceedings of Geotechnical Earthquake Engineering and Soil Dynamics III, Seattle WA, USA* (pp. 313-324). New York: ASCE.

Steedman, R. S., Ledbetter, R. H., & Hynes, M. E. (2000). The Influence of High Confining Stress on the Cyclic Behavior of Saturated Sand. *Proceedings of Soil Dynamics and Liquefaction 2000, Denver CO, USA* (pp. 35-57). Rotterdam, The Netherlands: Balkema.

Stone, K. J. L., Randolph, M. F. & Sales, A. A. (1994). Evaluation of Consolidation Behavior of Mine Tailings. *Journal of Geotechnical Engineering, 120*(30), 473-490.

Taiebat, M., Jeremic, B. & Kaynia, A. M. (2009). Propagation of Seismic Waves through Liquefied Soils. *Proceedings of 2009 International Foundation Congress and Equipment Expo, Orlando FL, USA* (pp. 198-205). Reston VA: ASCE.

Terzaghi, K. & Peck, R. B. (1967). *Soil Mechanics in Engineering Practice* (2nd ed.). Toronto ON: John Wiley & Sons Inc.

Terzaghi, K., Peck, R. B., & Mesri, G. (1996). *Soil Mechanics in Engineering Practice* (3rd ed.). Toronto, ON: John Wiley & Sons Inc.

Thevanayagam, S. (1998). Effect of Fines and Confining Stress on Undrained Shear Strength of Silty Sands. *Journal of Geotechnical and Geoenvironmental Engineering, 124*(6), 479-491.

Thevanayagam, S. & Mohan, S. (1998). Intergranular Void Ratio - Steady State Strength Relations for Silty Sands. *Proceedings of Geotechnical Earthquake Engineering III, Seattle* WA, USA (pp. 349-360). New York: ASCE.

Thevanayagam, S., Fiorillo, M. & Liang, J. (2000). Effect of Non-plastic Fiens on Undrained Cyclic Strength of Silty Soils. *Soil Dynamics and Liquefaction 2000: Proceedings of sessions of Geo-Denver 2000, Denver CO, USA* (pp. 77-91). Reston VA: ASCE.

Toprak, S. & Holzer, T. L. (2003). Liquefaction Potential Index: Field Assessment. *Journal of Geotechnical and Geoenvironmental Engineering, 129*(4), 315-322.

Troncoso, J. H. (1986). Critical State of Tailing Silty Sands for Earthquake Loading. *Soil Dynamics and Earthquake Engineering, 5*(3), 248-252.

Troncoso, J. H. & Verdugo, R. (1985). Silt Content and Dynamic Behavior of Tailings Sands. *Proceedings of the 11th Intl Conf on Soil Mechanics and Foundation Engineering*, San Francisco CA, USA (Vol 3., pp. 1311-1314). New York: ASCE.

Tuttle, M., Such, R. & Seeber, L. (1989). Ground Failure Associated with the November 25, 1988 Saguenay Earthquake in Quebec Province, Canada. The Saguenay Earthquake of November 25, 1988, Quebec, Canada: Strong Ground Motion Data, *Ground Failure Observations, and Preliminary Interpretations – Preliminary Report,* (pp. 41-64). Buffalo NY: National Center for Earthquake Engineering Research.

Tuttle, M., Hough, S., Seeber, L., & Jacob, K. (1990a). The November 25, 1988 Saguenay, Quebec Earthquake and its Implications for Liquefaction Potential. *Proceedings of the Canadian Geotechnical Conference ,Quebec City, PQ, Canada* (pp. 183-187). Edmonton AB: Canadian Geotechnical Society.

Tuttle, M., Law, K. T., Seeber, L. & Jacob, K. (1990b). Liquefaction and Ground Failure Induced by the 1988 Saguenay, Quebec, Earthquake. *Canadian Geotechnical Journal, 27*(5), 580-589.

Ulrich, B. F. & Hughes, J. M. O. (1994). SPT/CPT correlations for Mine Tailings. *Proceedings of the International Conference on Tailings and Mine Waste '94, Fort Collins CO, USA* (pp. 215-223). Rotterdam: Balkema.

U. S. Environmental Protection Agency (US EPA). (1994). *Design and Evaluation of Tailings Dams* (Technical Report EPA530-R-94-038). Washington DC: U.S. Government Printing Office.

United Nations Environment Program (UNEP). (1996). *Tailings Dam Incidents 1980-1996.* Washington DC: United Nations Environmental Program.

Vaid, Y. P. (1994). Liquefaction of Silty Soils. *Proceedings of Ground Failures Under Seismic Conditions, Atlanta GA, USA* (pp. 1-16). New York: ASCE.

Vaid, Y. P. & Thomas, J. (1995). Liquefaction and Post-Liquefaction Behavior of Sand. *Journal of Geotechnical Engineering, 121*(2), 163-173.

Vaid, Y. P., Fisher, J. M., Kuerbis, R. H. & Negussey, D. (1990). Particle Gradation and Liquefaction. *Journal of Geotechnical Engineering, 116*(4), 698-703.

Vaid, Y. P. & Sivathayalan, S. (1999). Fundamental Factors Affecting Liquefaction Susceptibility of Sands, *Proceedings of Physics and Mechanics of Soil Liquefaction, Baltimore MD, USA. P.V. Lade and J. Yamamuro (eds.)* (pp. 105-120). Rotterdam: Balkema.

Vaid, Y. P., Stedman, J. D. & Sivathayalan, S. (2001). Confining Stress and Static Shear Effects in Cyclic Liquefaction. *Canadian Geotechnical Journal, 38*, 580-591.

Vaid, Y. P., Chen, J. C. & Tumi, H. (1985). Confining Pressure, Grain Angularity and Liquefaction. *Journal of Geotechnical Engineering, 111*(10), 1229-1235.

Van Laak, P. A., Taboada, V. M., Dobry, R., and Elgamal, A. W. (1994). Earthquake Centrifuge Modeling Using a Laminar Box. *Proceedings of Dynamic Geotechnical Testing II, San Francisco CA, USA* (pp. 370-384). Philadelphia PA: ASTM.

Vick, S. G. (1990). *Planning, Design and Analysis of Tailings Dams*. Vancouver, BC: BiTech Publishers Ltd.

Vick, S. G., Dorey, R., Finn, W. D. L. & Adams, R. C. (1993). Seismic Stabilization of St. Joe's Park Tailings Dams. *Proceedings of Geotechnical Practice in Dam Rehabilitation, Rayleigh NC, USA*. (pp. 402-415). New York: ASCE.

Wang, Z.-L. & Makdisi, F. I. (1998). Liquefaction Assessment Using a Bounding Surface Hypoplasticity Model for Sand. *Proceedings of Geotechnical Earthquake Engineering and Soil Dynamics III, Seattle WA, USA* (pp. 902-913). New York: ASCE.

Wang, Z.-L., Egan, J., Scheibel, L. & Makdisi, F. I. (2001). Simulation of Earthquake Performance of a Waterfront Slope Using Fully-coupled Effective Stress Approach. *Proceedings of the 2nd International FLAC Symposium, Lyon, France* (pp. 101-110). London: Taylor and Francis.

Wang, Z.-L., Makdisi, F. I., & Egan, J. (2006). Practical Applications of a Nonlinear Approach to Analysis of Earthquake-induced Liquefaction and Deformation of Earth Structures. *Soil Dynamics and Earthquake Engineering, 26*, 231-252.

Wang, Z.-L., Dafalias, Y., F., & Shen, C.-K. (1990). Bounding Surface Hypoplasticty Model for Sand. *Journal of Engineering Mechanics, 116*(5), 983-1001.

Weichert, D. H. (1980). Estimation of the Earthquake Recurrence Parameters for Unequal Observation Periods for Different Magnitudes. *Bulletin of the Seismological Society of America, 70*(4), 1337-1346.

Wieland, M & Malla, S. (2002). Seismic Evaluation of a 117 m High Embankment Dam Resting on a Thick Soil Layer. *Proceedings of the 12th European Conference on Earthquake Engineering, London, UK* (on CD-ROM). Oxford: Elsevier Science.

Wijewickreme, D., Sanin, M. V. & Greenaway, G. (2005a). Cyclic Shear Response of Fine-grained Mine Tailings. *Canadian Geotechnical Journal, 42*, 1408-1421.

Wijewickreme, D., Sriskandakumar, S. & Byrne, P. (2005b). Cyclic Loading Response of Loose Air-pluviated Fraser River Sand for Validation of Numerical Models Simulating Centrifuge Tests. *Canadian Geotechnical Journal, 42*, 550-561.

Wise Uranium Project (WISE). (2009). *Chronology of Major Tailings Dam Failures*. Consulted on February 15, 2009. http://www.antenna.nl/wise/uranium/mdaf.html.

Woeller, D. J., Boyd, T. J., Weemees, I. & Robertson, P. K. (1996). Seismic Cone Penetration Testing for Evaluating the Compressibility and Liquefaction Potential of Mine Tailings. *Proceedings of the 5th International Conference on Tailings and Mine Waste `96, Fort Collins CO, USA* (pp. 101-111). Rotterdam: Balkema.

Woods, R. D. (1994). Laboratory Measurement of Dynamic Soil Properties. *Proceedings of Dynamic Geotechnical Testing II, San Francisco CA, USA* (pp. 165-190). Philadelphia PA.

Wong, R. T., Seed, H. B. & Chan, C. (1975). Cyclic Loading Liquefaction of Gravelly Soils. *Journal of the Geotechnical Engineering Division, GT6*, 571-583.

Xia, H. & Hu, T. (1991). Effects of Saturation and Back Pressure on Sand Liquefaction. *Journal of Geotechnical Engineering, 117*, 1347-1362.

Yang, J., Savidis, S. & Roemer, M. (2004). Evaluating Liquefaction Strength of Partially Saturated Sand. *Journal of Geotechnical and Geoenvironmental Engineering, 130*(9), 975-979.

Yang, S. & Ling, H. I. (2005). Calibration of Generalized Plasticity Model and its Application to Liquefaction Analysis. *Proceedings of the Geo-Frontier 2005Conference, Austin TX*, USA (pp. 483-494). Reston VA: ASCE.

Yasuda, N., Matsumoto, N., Yoshioka, R.-I. & Takahashi, M. (1997). Undrained Monotonic and Cyclic Strength of Compacted Rockfill Material from Triaxial and Torsional Simple Shear Tests. *Canadian Geotechnical Journal, 34*, 357-367.

Yoshimi, Y., Tanaka, K., & Tokimatsu, K. (1989). Liquefaction Resistance of a Partially Saturated Sand.'' *Soils and Foundations.* 29, 157–162.

Yoshimine, M., Robertson, P. K. & Wride, C. E. (1999). Undrained Shear Strength of Clean Sands to Trigger Flow Liquefaction. *Canadian Geotechnical Journal, 36*, 891-906.

Youd, T. L., Idriss, I. M., Andrus, R. D., Arango, I., Castro, G., Christian, J. T. et al. (2001). Liquefaction Resistance of Soils: Summary Report from the 1996 NCEER and 1998 NCEER/NSF Workshops on Evaluation of Liquefaction Resistance of Soils. *Journal of Geotechnical and Geoenvironmental Engineering*, 127(10), 817-833.

Youd, T. L., and Noble, S. K. (1997a). Magnitude Scaling Factors. *Proceedings of the NCEER Workshop on Evaluation of Liquefaction Resistance of Soils, Buffalo NY, USA (*pp. 149–165). Buffalo NY: National Center for Earthquake Engineering Research.

Youd, T. L., and Noble, S. K. (1997b). Liquefaction Criteria Based on Statistical and Probabilistic Analyses. *Proceeding of the NCEER Workshop on Evaluation of Liquefaction Resistance of Soils*, Buffalo NY, USA (pp. 201–215). Buffalo NY: National Center for Earthquake Engineering Research.

Zhaoji, S. (1987). Study of Silt Liquefaction During Earthquakes. *Earthquake Research in China, 1*(3), 415-429.

Zhou, J., Lee, W. & Zhou, K. (1995). Dynamic Properties and Liquefaction Potential of Silts. *Proceedings of the 1st International Conference on Earthquake Geotechnical Engineering, Tokyo, Japan* (pp. 833-838). Rotterdam: Balkema.

Zhu, R. & Law, K. T. (1988). Liquefaction Potential of Silt. Proceeding of the Ninth World Conference on Earthquake Engineering, Tokyo-Kyoto, Japan, (Vol. III, pp. 237-242).

APPENDICES

(on CD-ROM)